

2

AD-A257 780

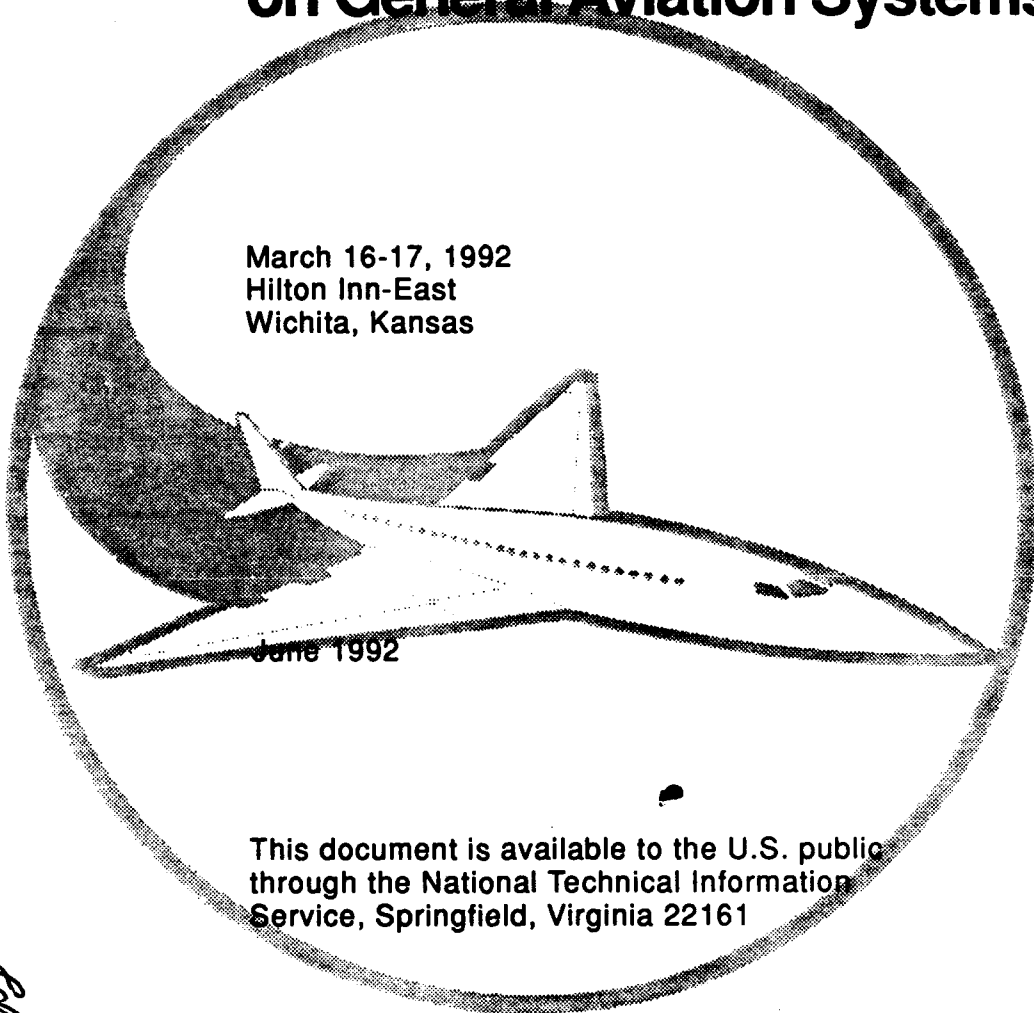


DOT/FAA/CT-92/17

FAA Technical Center
Atlantic City International Airport
N.J. 08405

Proceedings of the 1992 AIAA/FAA Joint Symposium on General Aviation Systems

March 16-17, 1992
Hilton Inn-East
Wichita, Kansas



This document is available to the U.S. public
through the National Technical Information
Service, Springfield, Virginia 22161

92-28975
51682



DISTRIBUTION STATEMENT A
Approved for public release
Distribution Unlimited

U.S. Department of Transportation
Federal Aviation Administration

DTIC
SELECTE
NOV 06 1992
S B D

92 11 05 026

NOTICE

This document is disseminated under the sponsorship of the U.S. Department of Transportation in the interest of information exchange. The United States Government assumes no liability for the contents or use thereof.

The United States Government does not endorse products or manufacturers. Trade or manufacturers' names appear herein solely because they are considered essential to the objective of this report.

Technical Report Documentation Page

1. Report No. DOT/FAA/CT-92/17		2. Government Accession No.		3. Recipient's Catalog No.	
4. Title and Subtitle PROCEEDINGS OF THE 1992 AIAA/FAA JOINT SYMPOSIUM ON GENERAL AVIATION SYSTEMS March 16-17, 1992				5. Report Date June 1992	
				6. Performing Organization Code	
7. Author(s) Compiled by Gus Ferrara and Karen Mason				8. Performing Organization Report No. DOT/FAA/CT-92/17	
9. Performing Organization Name and Address American Institute of Aeronautics and Astronautics General Aviation Systems Technical Committee Federal Aviation Administration Technical Center				10. Work Unit No. (TRAIS)	
				11. Contract or Grant No.	
12. Sponsoring Agency Name and Address U.S. Department of Transportation Federal Aviation Administration Technical Center Atlantic City International Airport, NJ 08405				13. Type of Report and Period Covered PROCEEDINGS March 16-17, 1992	
				14. Sponsoring Agency Code ACD-210	
15. Supplementary Notes Held at Hilton Inn-East, Wichita, Kansas					
16. Abstract The 1992 AIAA/FAA Joint Symposium on General Aviation Systems was the result of the combined efforts of the AIAA General Aviation Systems Technical Committee and the Federal Aviation Administration Technical Center. This symposium offered the opportunity to present and review the current state of the art in research that is being conducted in support of general aviation. All told, the papers presented covered the entire spectrum of research, and the participants had the opportunity to hear presentations on everything from alternate fuels to developments in air traffic control.					
17. Key Words Proceedings General Aviation Systems AIAA FAA			18. Distribution Statement Document is available to the public through the National Technical Information Service, Springfield, Virginia 22161		
19. Security Classif. (of this report) Unclassified		20. Security Classif. (of this page) Unclassified		21. No. of Pages 508	
				22. Price	

FOREWORD

The 1992 AIAA/FAA Joint Symposium on General Aviation Systems was the result of the combined efforts of the AIAA General Aviation Systems Technical Committee and the Federal Aviation Administration Technical Center. This symposium offered the opportunity to present and review the current state of the art in research that is being conducted in support of general aviation. All told, the papers presented covered a wide spectrum of research, and the participants had the opportunity to hear presentations on everything from alternate fuels to developments in air traffic control.

The Federal Aviation Administration Technical Center and the AIAA General Aviation Systems Technical Committee would like to thank the authors for investing the resources needed to prepare the papers which are contained in these proceedings and Mr. Bruce Holmes, NASA Langley, for giving the keynote address. We would also like to thank the individuals who acted as technical editors or session chairmen, since their efforts were instrumental in getting the symposium underway. They are as follows:

Mel Snyder, Wichita State University
Gus Ferrara, FAA Technical Center
David Ellis, CBAR, National Institute for Aviation Research
Andrew J. Craig, Wichita State University
W.H. Wentz, NIAR, Wichita State University
Dennis Dungan, Cessna, Wichita
David Bernstorff, Beech, Wichita
Randall Chambers, NIAR, Wichita State University
Ed Hooper, Beech, Wichita

DTIC QUALITY INSPECTED 4

Accession For	
NTIS GRA&I	<input checked="checked" type="checkbox"/>
DTIC TAB	<input type="checkbox"/>
Unannounced	<input type="checkbox"/>
Justification	
By _____	
Distribution/	
Availability Codes	
Dist	Avail and/or Special
A-1	

TABLE OF CONTENTS

<u>Title</u> Author/Co-Author	<u>Page</u>
<u>U.S. General Aviation: The Ingredients for a Renaissance</u> Bruce J. Holmes NASA Langley Research Center	1
<u>ATC 2000</u> John Turner NAS Development, FAA Development	29
<u>FAR/JAR, ARAC, & FAA/EAA/SAMA Programs</u> Dick Yotter FAA Central Region	31
<u>Pilot Weather Advisor</u> W.A. Kilgore ViGYAN Inc.	33
<u>Impact of Data Link on Cockpit Information</u> Raymond LaFrey / Jonathan Bernays / Robert Grappel MIT Lincoln Laboratory	73
<u>An Overview of Propulsion Systems for Small Civil Aircraft</u> Dave Ellis / Kenneth Foote Wichita State Univ. / AVORTEC Inc.	91
<u>Ethanol in Reciprocating Aircraft Engines</u> Max Shauck / M.G. Zanin Baylor University	109
<u>Combustion Properties of Ethanol Blended Turbine Fuels</u> Gary Eiff Southern Illinois University	119
<u>Rotor Alone Noise of Shrouded and Unshrouded Propellers</u> Walter Eversman University of Missouri-Rolla	185

<u>Title</u> Author/Co-Author	<u>Page</u>
<u>Two Leading-Edge Droop Modifications for Tailoring Stall Characteristics of a General Aviation Trainer Configuration</u> Holly M. Ross / Dr. John Perkins NASA Langley Research Center / N. Carolina State University	205
<u>A Simulation of a Display and Control System Requiring Reduced Training and Proficiency</u> Eric C. Stewart NASA Langley Research Center	219
<u>Sensitivity Study of a Single-Engine General Aviation Airplane</u> David W. Levy University of Michigan	259
<u>Aircraft Flight Test in an Academic Environment</u> Thomas N. Mouch / Jean M. Fernand / John Valasek / David R. Downing University of Kansas	279
<u>Results of a Parameter Identification Flight Test Program for General Aviation</u> John Valasek / Jean M. Fernand / Thomas N. Mouch / David R. Downing University of Kansas	293
<u>Doppler Global Velocimetry: A Potential Velocity Measurement Method for General Aviation Applications</u> L. Scott Miller / J.F. Meyers and J.W. Usry Wichita State Univ. / NASA Langley Research Center	325
<u>Experience With Computational Fluid Dynamics Codes</u> Michael Papadakis / Steve Klausmeyer / Xiaoxian Liu Wichita State University	337

<u>Title</u>	<u>Page</u>
Author/Co-Author	
<u>An Aerodynamic Comparison of G A Factory & Amateur Built Aircraft</u>	355
Shadid Siddiqi / Jeffery Viken Analytic Services and Material	
<u>Evaluation of Five Displays for Aircraft Guidance</u>	357
Saeid Mirsafian / M.G. Nagati Wichita State University	
<u>Effectiveness of Cockpit Display for Guidance</u>	373
Cheryl L. Fulton / M.G. Nagati Wichita State University	
<u>Technical Opportunities for Advancement of Human Factors by the Year 2000</u>	401
Charles W. Howard Raytheon	
<u>All Weather Landing--Man Over Automation</u>	403
Norris J. Krone University of Maryland	
<u>An Investigation into the Cumulative and Interactive Effects of Stressors on Pilot Performance</u>	405
Susan M. Murray Central Missouri State University	
<u>Aging Commercial Airframes</u>	449
Howard W. Smith University of Kansas	
<u>A Comparison of the V-G Method and the Root Locus Method for Flutter</u>	463
Walter Eversman / Brian Sibbitt Univ. of Missouri-Rolla / McDonnell Aircraft Company	
<u>Rotor Containment Issues in General Aviation</u>	491
J.A. Mathis Wichita State University	

<u>Title</u>	<u>Page</u>
Author/Co-Author	
<u>Wind Tunnel and Flight Testing of a Novel Aircraft Design</u>	503
Hugh Schmittle University of Maryland	

**U.S. GENERAL AVIATION:
THE INGREDIENTS FOR A RENAISSANCE**

by

**Bruce J. Holmes
NASA Langley Research Center
Hampton, VA 23665**

**For Presentation to the AIAA/FAA Joint Symposium on General
Aviation Systems at the Hilton Inn-East, Wichita, KS
on March 16-17, 1992**

**U.S. GENERAL AVIATION:
THE INGREDIENTS FOR A RENAISSANCE**

**Bruce J. Holmes
NASA Langley Research Center**

**American Institute of Aeronautics and Astronautics
Federal Aviation Administration
National Institute for Aviation Research**

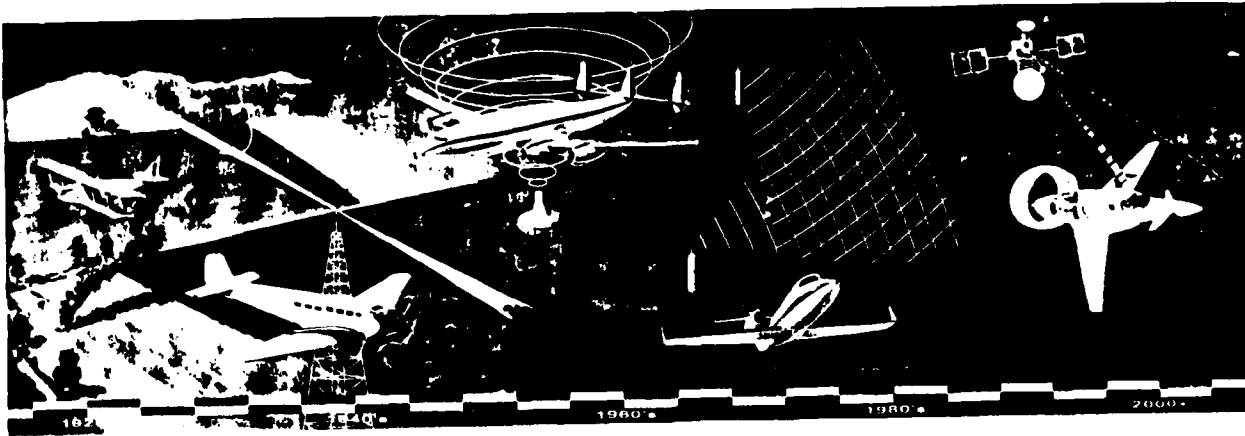
**SYMPOSIUM ON
GENERAL AVIATION SYSTEMS**

**March 16-17, 1992
Wichita, Kansas**

NASA Langley Research Center

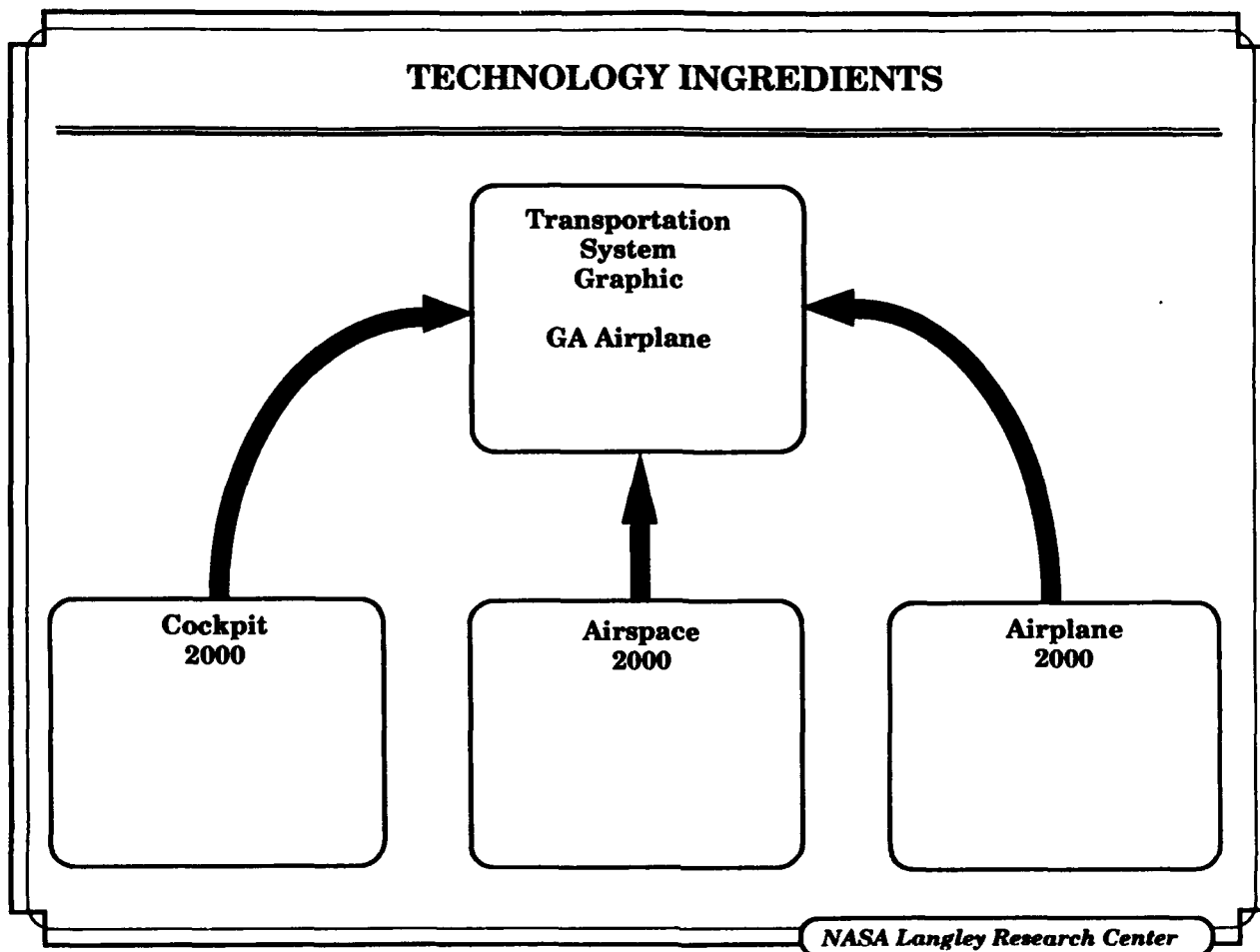
INTRODUCTION

- **U.S. has an amazing, unique air transportation system in which General Aviation aircraft play an integral role. The vital G.A. contribution to the infrastructure of that air transportation system appears threatened by inadequate aircraft production, dwindling supply of student pilots, outdated training aircraft, and a broad range of inhibitors to utility.**
- **In 1989, AIAA/GAMA Wkshp on Role of Technology in Revitalizing U.S. GA**
 - **Wkshop gathered industry, government, universities**
 - **Identified significant technology opportunities: C2000;A2000;A2000**
 - **Also clarified constraints on techn. progress imposed by product liability; certification and manufacturing costs**
- **This presentation builds on those workshop recommendations; and goes further:**
 - **identifies Technology Goals**
 - **recommends Technology Strategy**
- **Do we have the Ingredients for a Renaissance?; you be the judge .**



PANORAMA

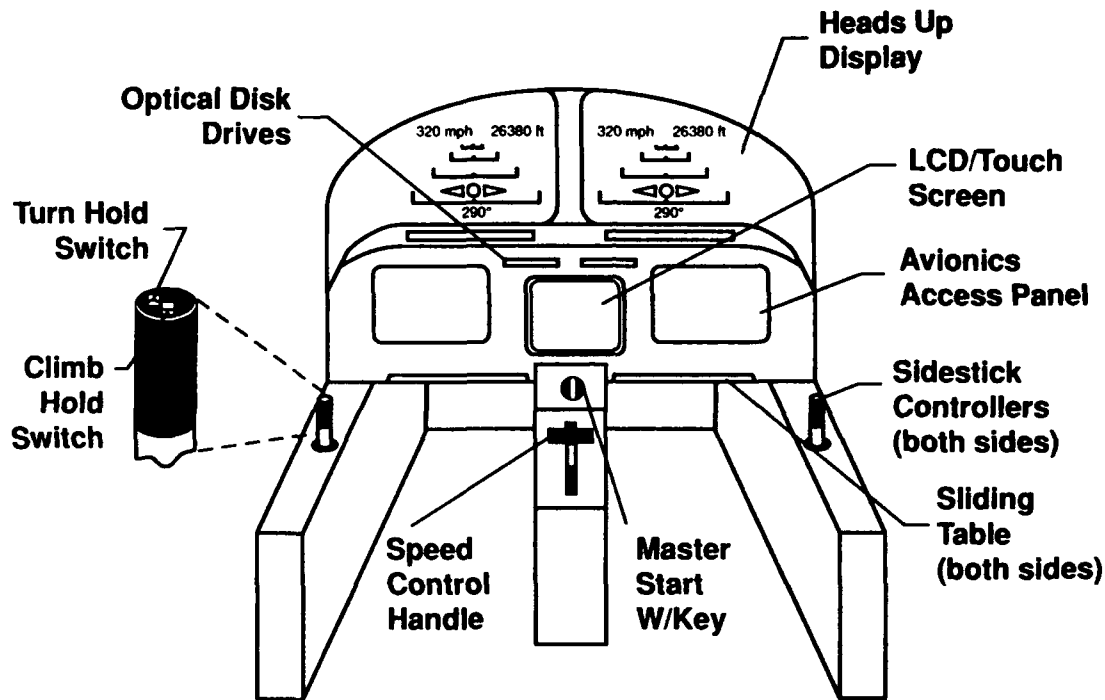
- **The earliest visions for general aviation included the notion of airplanes for the common man.**
- **1955, Daniel Zuck, "An Airplane in Every Garage"**
- **Then, technology would not support the vision**
- **General Aviation today has actually grown far beyond that dream:**
 - **Large business aircraft**
 - **Commuter aircraft**
- **The part of the vision concerning "an airplane in every garage" was never realized**
- **Today, technology could support that part of the vision**



TECHNOLOGY INGREDIENTS

- **Specifically, Cockpit/Airspace/Airplane Technologies which matured in 1980's and which will mature in the 1990's, enable the vision of airplanes for travelers as a new mode of personal and business air transportation**

COCKPIT 2000



Cockpit 2000

TECHNOLOGY

- **Information systems (voice, data, videoXMSN)**
- **Micro computers and advanced displays**
- **Advanced flight systems**

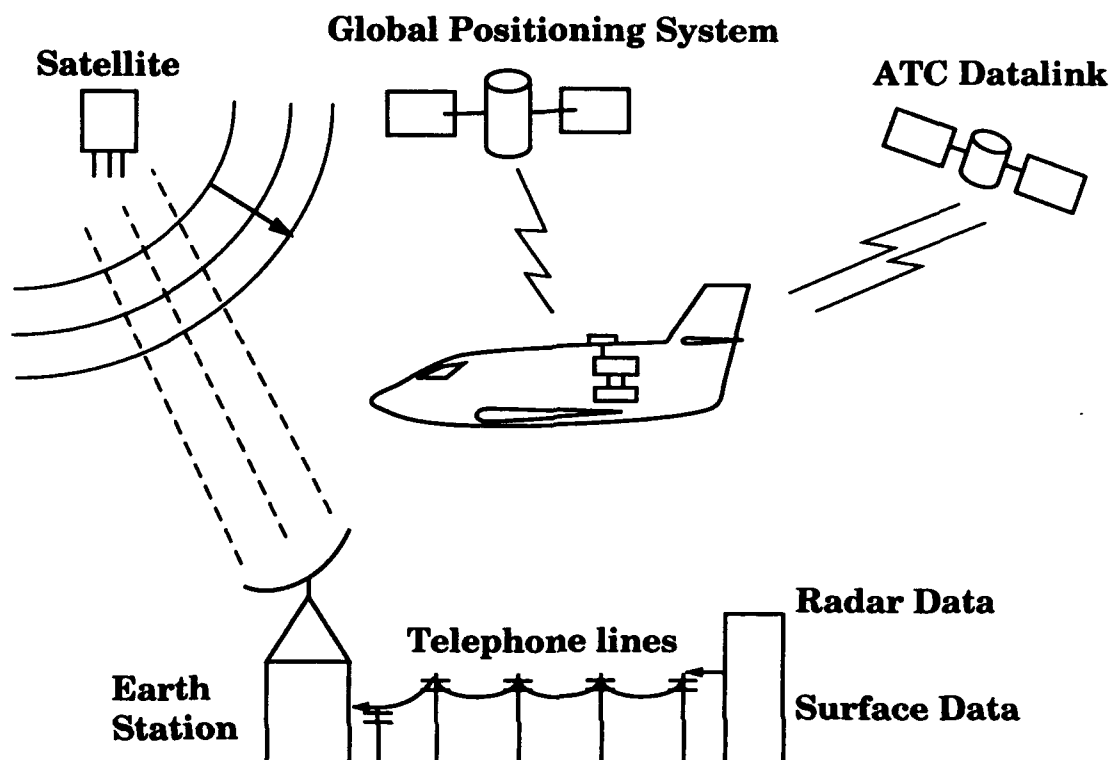
ENABLED OPPORTUNITY

High utility, safety.

"Paperless Cockpits," reduced training costs, autonomous collision avoid.

Intuitive, decoupled controls.

AIRSPACE 2000



Airspace 2000

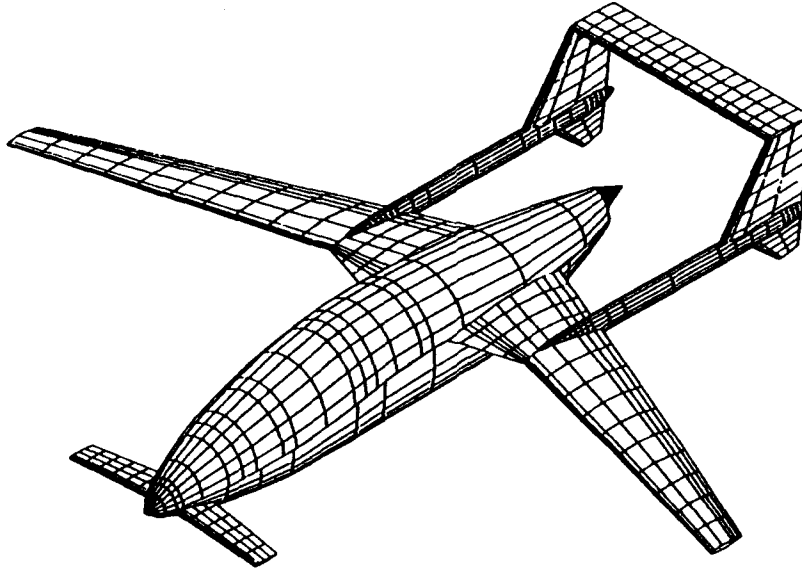
- **Satellite navigation and communications systems.**

Single-port nav/comm, very low cost, simple

- **Advanced National Airspace System and National Weather System**

Simplified airspace access and simplified operations.

AIRPLANE 2000



Airplane 2000

- **Advanced aerodynamics, structures, and materials** **Double speed, range, and payload.**
- **Advanced engines and propellers** **Double the thrust-to-weight ratios, low noise.**

- **Bottom Line: Airplanes for Travelers, vis-a-vis Enthusiasts**
Keep G.A. healthy as a vital segment of the U.S. Air Transportation System

- anonymous politico on hearing of
Alexander Graham Bell's success
with the telephone -

***"It is not hard to imagine the day
when every city will have one."***

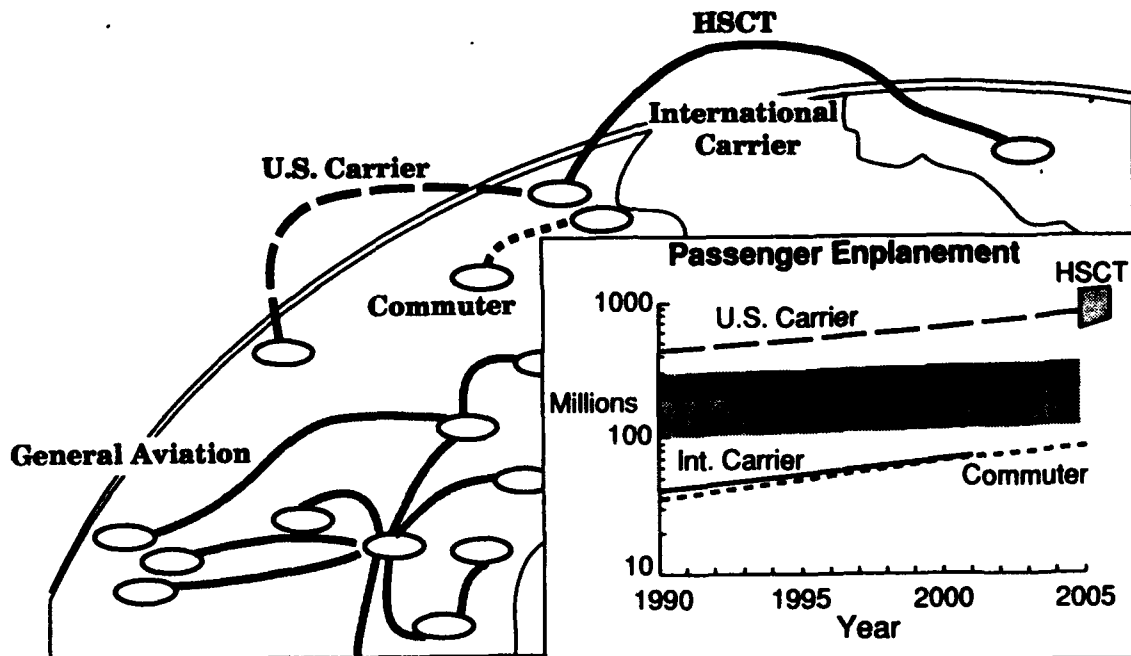
NASA Langley Research Center

QUOTE

- **The question is, "What's holding us back?"**
- **One man's vision is another man's novelty**
- **Point: Takes clarity of vision to develop GA Technology Goals and Strategy**

MARKET PRESSURES

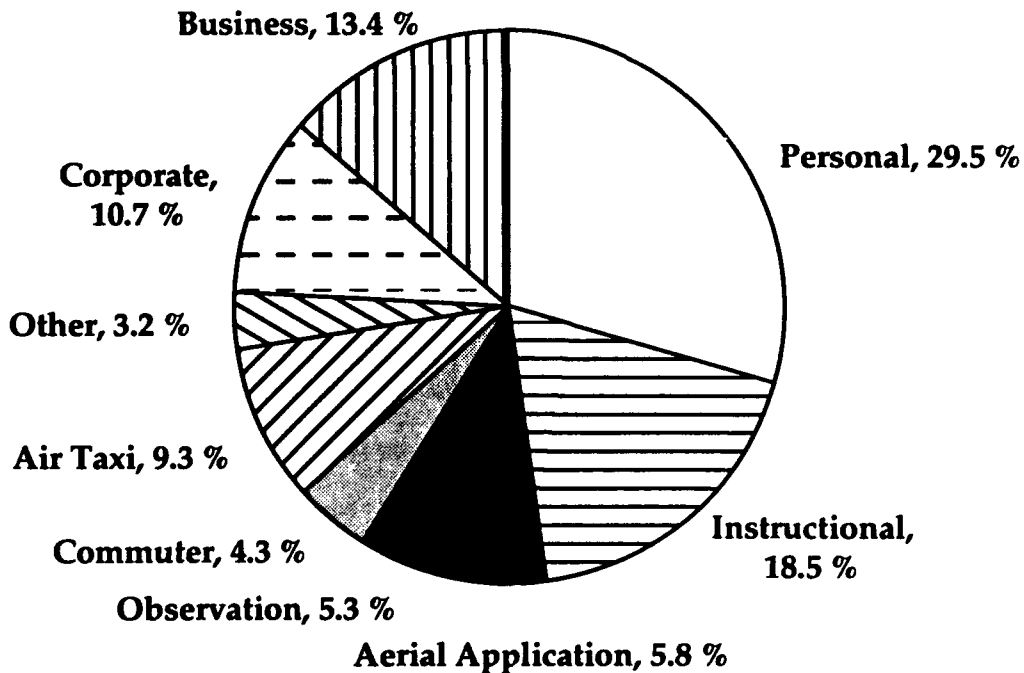
Air Transportation System Fleet Mix



MARKET PRESSURES

- Environment within which a technology strategy would be developed:
 - Economics; Operations; Accidents; Pilot Populations; Performance
- "The Pull" - Market Pressures and Opportunities
- History and Trends
- "The Push" - Technology Drivers and Impacts
- At the forecast 4% rates of air travel growth, there will be three times as much air travel in 2010 as there was in 1992. (Traffic has quadrupled since the Boeing 747 entered service in 1969) This growth could require three times as many aircraft as today. Presumably, general aviation could grow at similar rates.
- The cost of air traffic congestion is estimated today at \$10B annually in U.S. and Europe. These costs are forecast to double by 1997. The cost of U.S. ground traffic congestion is estimated at \$100B annually.
- To avoid aerial grid lock: 1) bigger, faster acft; 2) airports/airways-sm a/c
 - bigger airplanes: 1000 passenger mega-transports (>5000 miles)
 - faster airplanes: 300 passenger high speed civil transports (>7000 mi.)
 - tiltrotors to/from urban centers (<100 miles)
 - high-speed commuters overfly hubs (500 to 1000 miles)
 - mid-speed commuters (<250 miles)
 - personal/business air transportation to fill the gap for mid-speed/mid range (100 to 750 miles, at 150 to 350 mph, 4 to 8 passengers)

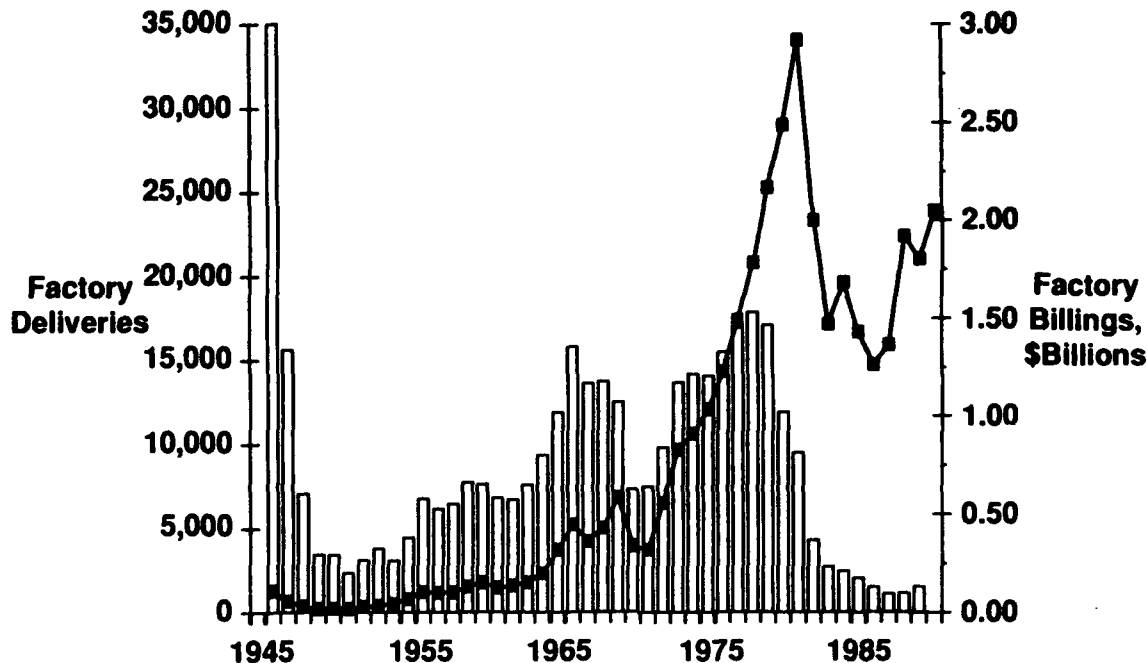
General Aviation Aircraft Use 1989 Total = 35,012,000 Hours



GENERAL AVIATION AIRCRAFT USE

- **Over 70% of General Aviation flying directly generates jobs and tax revenues**
- **30% Personal is the GA equivalent of tourist flying on the airlines**
- **By the measures of enplanements and value of useage, GA is clearly a key part of the U.S. Air Transportation System infrastructure; any solutions to the problems of that system should address the GA segment**

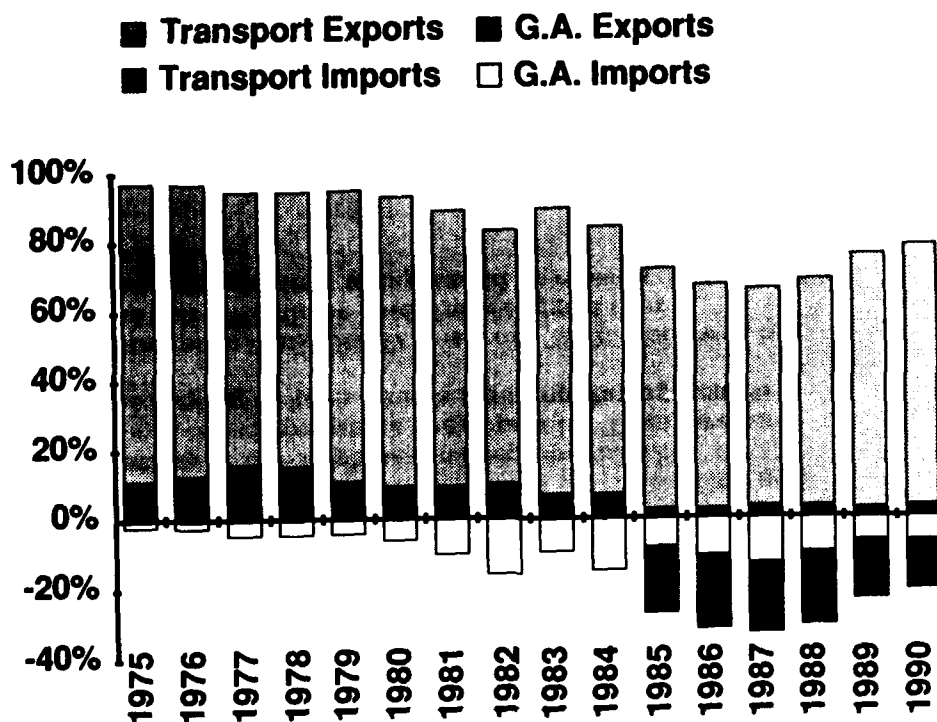
General Aviation Shipments and Billings



GENERAL AVIATION SHIPMENTS AND BILLINGS

- **Significant features:**
 - Shipments and billings used to follow the GNP until 1981; then uncoupled
 - \$2B is part of \$40B U.S. Civil aerospace (1st year to outpace military)
- **After peak of 1978, slide**
 - product liability
 - tax code
 - cheap used airplanes satisfy the need for "enthusiast" flying
 - Product liability has sapped the resources needed for innovation and R&D to expand the utility of the airplanes to keep up with the requirements of the system within which they operate. Today we have 1960's utility airplanes trying to keep up in a 1990's operating system
- **The last major investment in NASA R& D was from '70-'75, followed by peak deliveries in the late '70's; those lead times suggest that implementing a technology strategy today would be expected to pay off in the early 2000's time frame.**

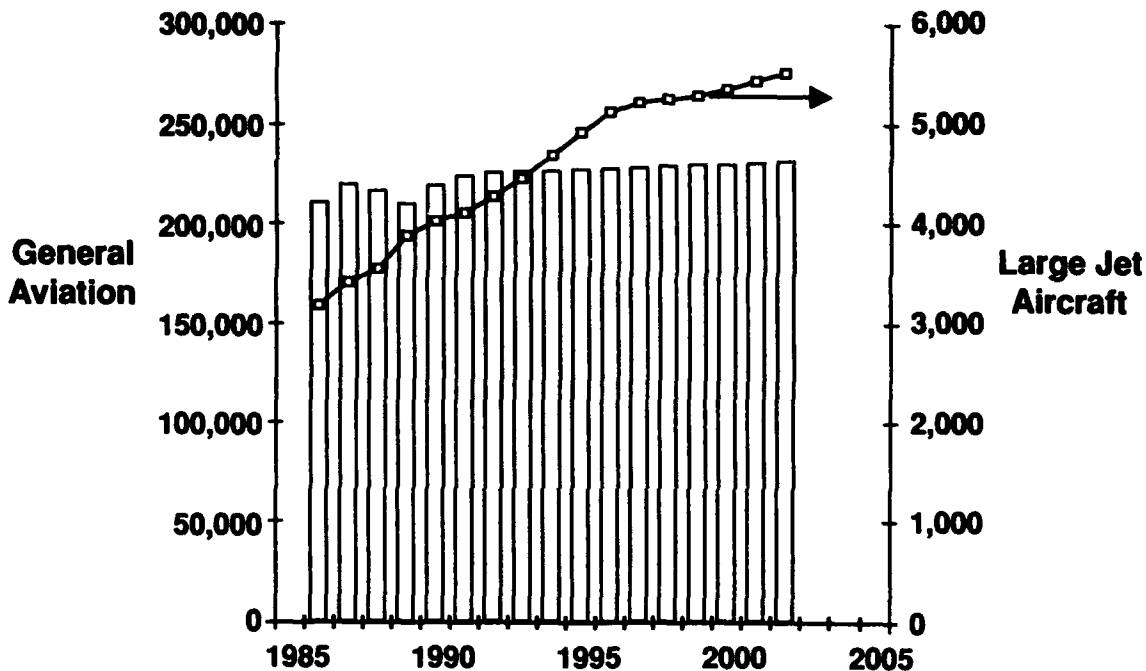
U.S. AIRCRAFT EXPORTS AND IMPORTS



U.S. AIRCRAFT EXPORTS AND IMPORTS

- The 1978 peak in GA factory billings corresponded to nearly 20% of U.S. balance of trade.
- 1981 - U.S. became a net General Aviation importer (red vs. green)
- Decline in General Aviation has hurt overall U.S. balance of trade
- 1985 - Airbus
- 1990: Total civil exports \$20B
- Message: GA could be a significant player in balance of trade:
 issue: if a new market of aircraft for travelers vs. enthusiast is created,
 the U.S. should be on the export side of this chart, not import side

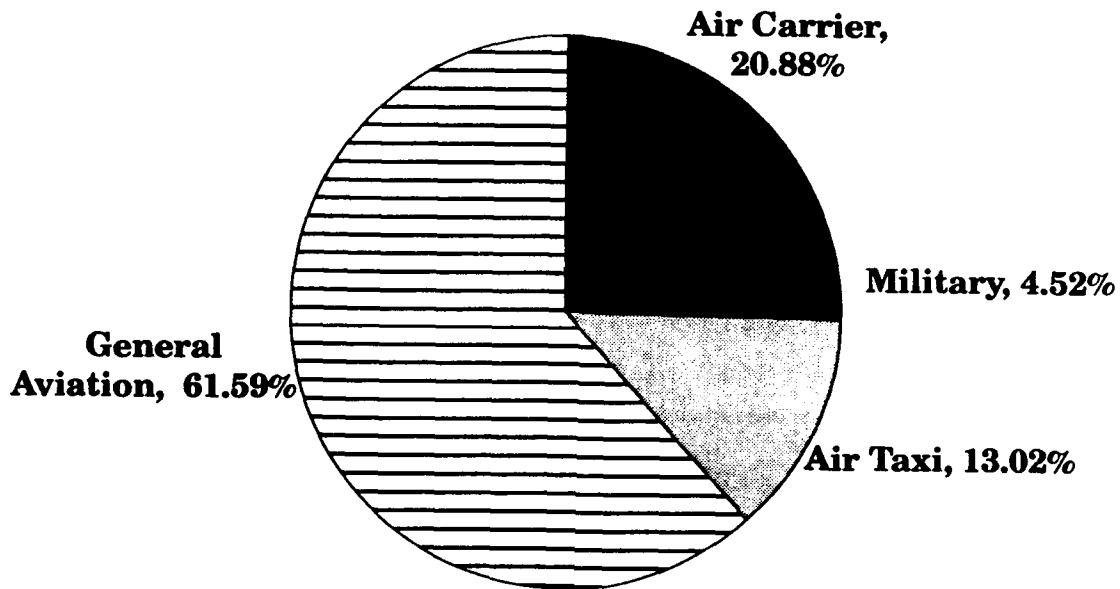
ACTIVE AIRCRAFT TRENDS AND FORECASTS



ACTIVE AIRCRAFT TRENDS AND FORECASTS

- Currently 220,000 active (46,000 inactive!)
- FAA forecasts 0.3% rate of growth in active G.A. aircraft; 10 times that rate is considered a healthy GDP growth rate (3-4%)
- Large jet aircraft past 6-7%; future growth predicted at 4-5%
- In "normal" times, G.A. could be expected to grow at similar rates
- This will be the future IF NOTHING CHANGES;
 - Need technology strategy
 - Need product liability resources for R&D

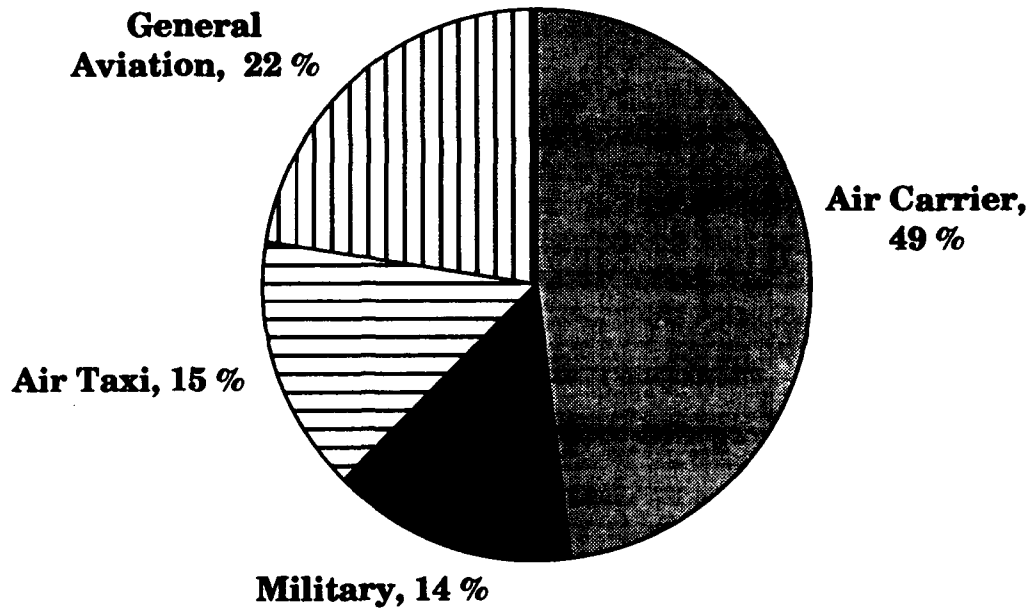
U.S. Total Annual Air Traffic Operations 1987 - 1989 Average



U.S. TOTAL ANNUAL AIR TRAFFIC OPERATIONS

- Operational aspects for a technology strategy
- 61% G.A. + 13% Air Taxi -- 75% G.A. Aircraft
- General Aviation component of research on airspace capacity and airplane utility
 - Technology Strategy should deal with numbers of operations

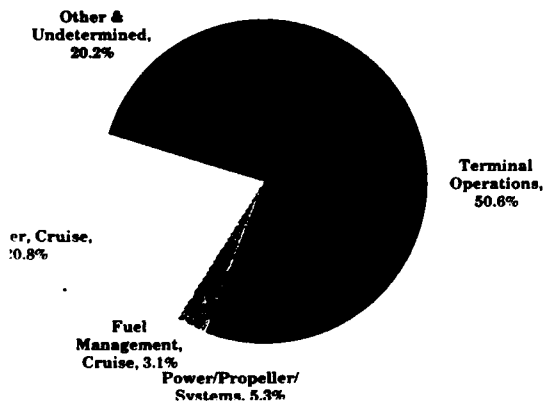
U.S. ANNUAL IFR AIR TRAFFIC OPERATIONS 1987 - 1989 AVERAGE



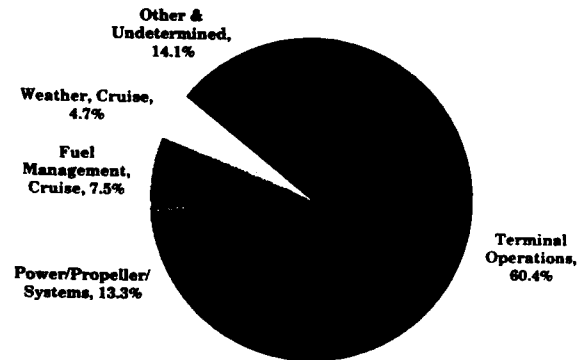
U.S. TOTAL ANNUAL AIR TRAFFIC OPERATIONS

- **Operational aspects for a technology strategy**
- **61% G.A. + 13% Air Taxi -- 75% G.A. Aircraft**
- **General Aviation component of research on airspace capacity and airplane utility**
 - **Technology Strategy should deal with numbers of operations**

**FATAL GENERAL AVIATION ACCIDENTS
BY CAUSE, 1982-1988**



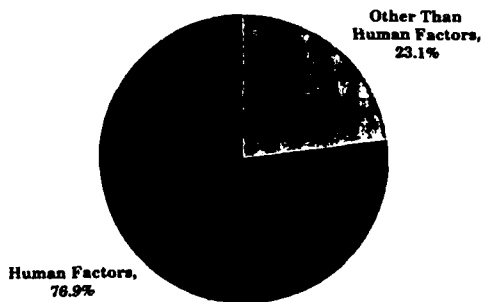
**ALL GENERAL AVIATION ACCIDENTS
BY CAUSE, 1982-1988**



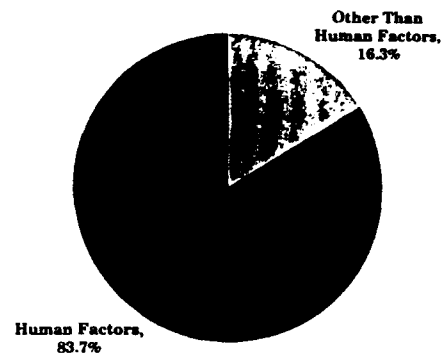
GENERAL AVIATION ACCIDENTS (1982-1988, ASF)

- **Enormous improvements over the past decades for G.A. accidents; current fatalities/100Khrs is 1/2 of 1975 rate; During past 4 years, G.A. acft flown by salaried crews had fewer accidents/100khrs that scheduled air carriers (one of the ironies of the current rates of product liability)**
- **Read Axes: Primary cause**
- **All Accidents - first**
- **Fatal Accidents - next**
- **Weather-related accidents represent a disproportionate rate of the total**
- **Takeoff/Landing/Low Maneuvering - more than fair share of the total**
- **Technology implications:**
 - **VFR flight into IFR conditions**
 - **Stall/Spin resistance technology**
 - **Fuel management systems: GPS**

**ALL GENERAL AVIATION PILOT-RELATED
ACCIDENTS
1982-1988**



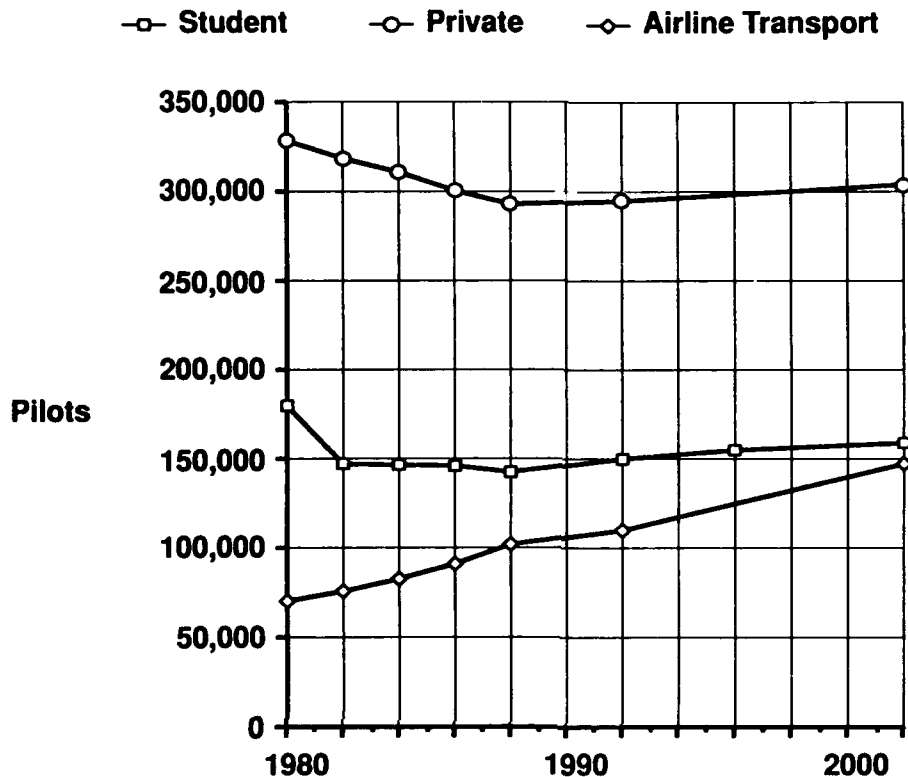
**FATAL GENERAL AVIATION
PILOT-RELATED ACCIDENTS, 1982-1988**



**GENERAL AVIATION PILOT- RELATED ACCIDENTS
(1982-1988, ASF)**

- **Overwhelming proportion: Human Factors**
- **Definition of "Human Factors" related accidents**
 - judgement
 - man-machine interface
- **Technology offers to greatly alleviate many "Human Factors" accidents**
- **Include GA in National Human Factors Research Program**
 - USAF Pilots' Associate Program

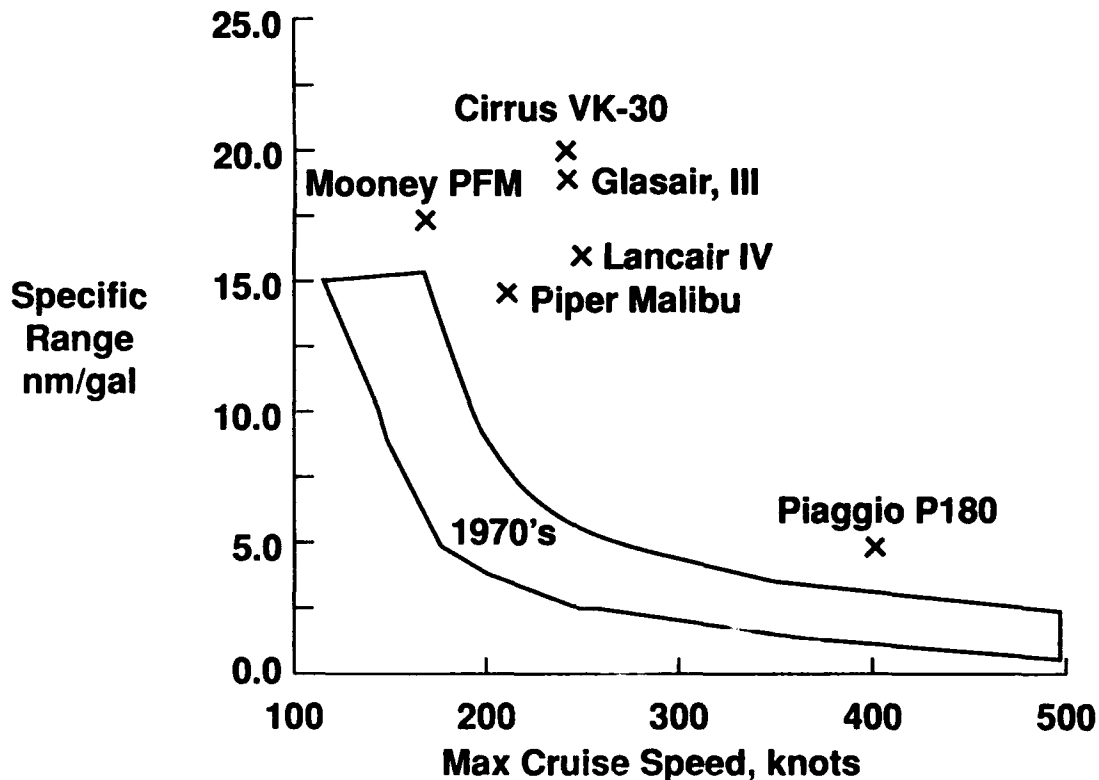
Pilot Population Trends & Forecasts



PILOT POPULATION TRENDS & FORECASTS

- General Aviation has historically provided a large percentage of the nation's civil pilot workforce
- It is fair to ask where the pilots will come from in the future
- Chart illustrates the small (0.3%) growth rate forecast by the FAA for Private Pilots and 4-6% rates for Airline Transport Pilots
- Technology implications for future training aircraft with "glass cockpits" and Fly-By-Wire based flight control systems such as decoupled controls

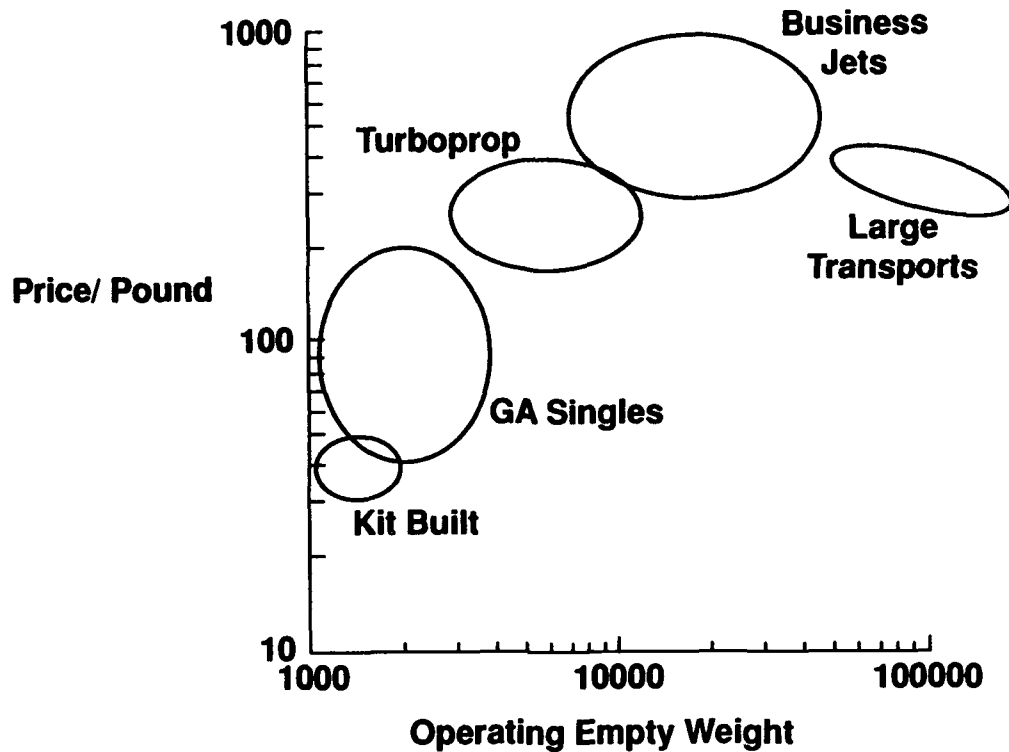
FUEL EFFICIENCY COMPARISONS



FUEL EFFICIENCY COMPARISONS

- 1970's technology studies illustrated the ability of technology to provide doubling the speed or fuel efficiency of airplanes with 1200 lb. payloads
- New aircraft today accomplish those performance opportunities identified in the late 70's
- I believe that new technologies can provide even more performance than the HIPS now being flown
 - Laminar flow can go much further than it has:
10-15%% drag reductions with 50% laminar wing go after 90% on wing; plus nacelles, tail surfaces
 - Engines with twice the P/W and 50% lower SFC (SCORE; Molded Phenolic Composite engines)
 - Twin-pac engines for efficiency, safety

AIRCRAFT PRICE PER POUND



AIRCRAFT PRICE PER POUND

- Technologies should pay their way onto the airplane
- Kit builders: performance at less cost
- Technology development chain: manufacturing / certification costs
- Kit builders = technology validators
- Technology validation is key element of strategy; requires industry and government to find new ways to work together

UTILITY INHIBITORS

- **Proficiency requirements**
- **Cost of ownership / operation**
- **Cabin comfort**
- **Performance**
- **Reliability**
- **Regulations / airspace access**
- **Airport Noise**

NASA Langley Research Center

UTILIZATION INHIBITORS

- **Utility definition: GA Not**
- **Proficiency requirements**
 - flying the airplane requires expensive proficiency time
 - access to the airspace system requires expensive equipment and proficiency time
- **Cost of ownership / operation**
 - product liability adds \$xx,000.00 to the purchase price
 - current production rates of 1500 aircraft do not command economy of scale
 - tax laws
 - airline competition
 - reliability
- **Cabin comfort**
 - gust response:
 - interior noise: without headphones;
 - features: air-conditioning; audio systems; flight phones; seat comfort
- **Performance**
 - speed, range, payload:
 - weather-flying limitations: lightning protection; ice protection;
- **Reliability**
 - maintainability: auto equivalent; self-maintenance;
 - redundancy: fail operational capabilities
- **Regulations and airspace access**
 - operations: restricted/controlled airspace avoidance;
 - certification: time/cost for licensing;
- **Airport noise: rate of closings; curfews**

PROGRESS IN TECHNOLOGY

NON-AERONAUTICAL

- **airbags**
- **anti-lock brakes (in 1.7 million 1992 cars)**
- **CD-ROM**
- **cellular telephones**
- **cruise control**
- **electronic ignition**
- **electronic moving maps**
- **infrared remote controls**
- **interior noise control**
- **displays**
- **micro computers**
- **radial tires**
- **reliable powered subsystems**
- **smart "idiot" lights**
- **smart subsystems**
- **smart suspension systems**

NASA Langley Research Center

PROGRESS IN TECHNOLOGY

- **Since the last applications of significant technical advancements in G.A. , numerous technologies have become a part of everyday life in mass markets and presumably could contribute to the development of new airplanes.**

PROGRESS IN TECHNOLOGY

AERONAUTICAL

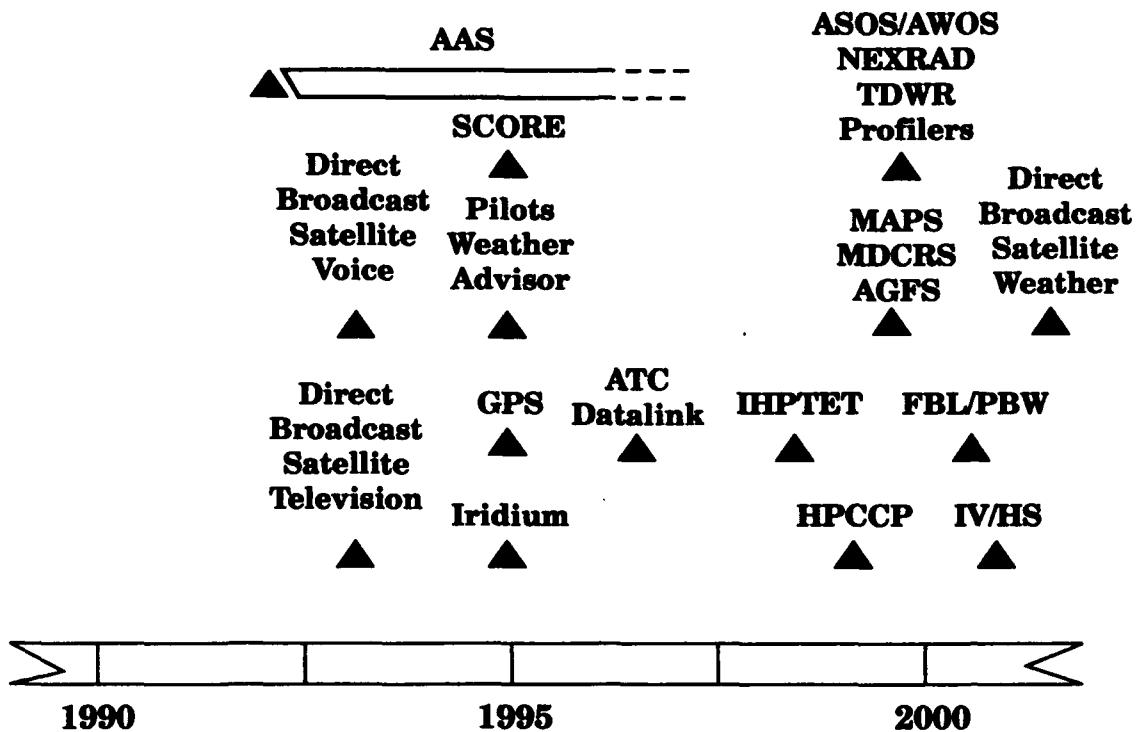
- ACARS
- Active Noise Control
- Advanced Metallics
- Artificial Intelligence
- Approach Image Generator (AIG)
- CAD/CAM
- Computational Fluid Dynamics (CFD)
- Lightning Protected Composites
- Crash-worthiness
- Computational Structural Mechanics (CSM)
- Engine Monitoring and Control System (EMACS)
- Enhanced Visual Systems (EVS)
- GPS
- LORAN
- NLF/HLFC
- Molded Phenolic Composite Engines
- Stratified Charge Rotary Combustion Engines
- Spin resistance
- Takeoff Monitoring and Performance System

NASA Langley Research Center

PROGRESS IN TECHNOLOGY

- During the past decade aeronautics technology has advanced as well
- Situation and outlook in NASA Aeronautics
 - investments do not support technology validation (flight)
 - risk losing key technology leads to foreign competition
 - facilities issues
 - infrastructure (R&T discretionary base; university support labs; research contracts)

FUTURE TECHNOLOGY DRIVERS



FUTURE TECHNOLOGY DRIVERS

ASOS: (NWS: 537 units 1992-1996)

AWOS: (FAA: 40 units 1992 - 1993)

NEXRAD (NWS: 113 sites 1993 - 1996?)

TDWR (FAA: 47 sites 1993 - 1995)

**Profilers (NWS: Block 1, mid U.S. today
Block 2, 200-300 units nationwide about 2000 a.d.)**

MAPS (NCAR/NWS: Aviation Gridded Forecast System 1998)

MDCRS (Airlines - ACARS now)

ATC Datalink (FAA 1998)

SCORE/MPC

HPCCP

IHPTET

FBL/PBW

Intelligent Vehicle/Highway System

STATUS

- **AIAA Workshop on the Role of Technology in Revitalizing U.S. General Aviation, 1989**
- **Congressional action on product liability**
- **EAA/Industry Team Small Airplane Certification Compliance Program**
- **Very Light Aircraft (VLA) Certification**
- **Primary Aircraft Certification Proposal**
- **Growth of amateur-built aircraft sector**
- **FAR/JAR Harmonization**
- **FAR 23 changes**
- **Recreational Pilot Certificate**
- **Civil-use of military airfields**

NASA Langley Research Center

STATUS

- **Signs of life**
- **1989 AIAA Workshop on the Role of Techn. in Revit. U.S. GA initiated the thinking process behind this presentation**

TECHNOLOGY GOALS

- **Universal VFR Equivalence**
- **Autonomous Flight Planning and Operations**
- **Paperless Cockpits**
- **Instructorless Flight Training**
- **Aircraft for new transportation mode**

NASA Langley Research Center

TECHNOLOGY STRATEGY

- **Establish viability of a new transportation mode:**
 - **Technical**
 - **Economic**
 - **Environmental**
- **Establish public constituency in support of a new air transportation mode**
 - **U.S. love affair with airplanes rivals that for automobiles**
 - **G.A. is today where the automobile was in the 1930's before I.Hwy.Syst.**
 - **Educate public about this future G.A. role**
- **Initiate research planning now**
 - **Because the entire U.S. industry is now working toward limitations on product liability, and because of R&D lead times, now is the time to initiate research planning and advocacy.**
- **Integrate research with certification processes for new technologies.**
 - **Predictable cost to certify**
 - **Predictable time to certify**
- **Establish avenues for tech. transfer involving cooperative-proprietary eff.**
 - **New ways for Industry/Government to collaborate for competitiveness**
 - **Strengthen weak link in the technology development chain: validation**
 - **NASA / FAA/ Universities/SBIR**
- **Do we have the Ingredients for a Renaissance? Yup:**
At very least it's not hard to imagine the day
"...when every city will have one."

ATC 2000

by

**John Turner
NAS Development
FAA Washington**

COPIES NOT AVAILABLE

**For Presentation to the AIAA/FAA Joint Symposium on General
Aviation Systems at the Hilton Inn-East, Wichita, KS
on March 16-17, 1992**

FAR/JAR-23, ARAC, & FAA/EAA/SAMA PROGRAMS

by

**Dick Yotter
FAA Central Reg.**

COPIES NOT AVAILABLE

**For Presentation to the AIAA/FAA Joint Symposium on General
Aviation Systems at the Hilton Inn-East, Wichita, KS
on March 16-17, 1992**

PILOT WEATHER ADVISOR

by

**W.A. Kilgore
S. Seth
ViGYAN Inc.
Hampton, VA**

**N.L. Crabill
Aero Space Consultants
Newport News, VA**

**S.T. Shipley
I. Graffman
Hughes-STX
Lanhan, Maryland**

**J. O'Niell
NIALl Enterprizes
Belmont, Wisconsin**

**D. Stauffacher
EXCELL Inns
Madison, Wisconsin**

**For Presentation to the AIAA/FAA Joint Symposium on General
Aviation Systems at the Hilton Inn-East, Wichita, KS
on March 16-17, 1992**

Abstract

This report gives the results of the work performed by ViGYAN, Inc. under contract to NASA to demonstrate the Pilot Weather Advisor cockpit weather data system using a broadcast satellite communication system.

The purpose of the Pilot Weather Advisor is to improve the safety and utility of aircraft operations by providing automatic updates of the weather situation to the in-flight pilot in a form that is easily understood in terms of the planned mission. Current weather detection and dissemination system for general aviation are not completely satisfactory. Airborne radar is expensive, often impractical for small single engine aircraft, has a relatively short range, and severe attenuation in heavy rain. Lightning detectors do not provide indications of precipitation and do not give accurate ranges for lightning activity. Radio contacts with ground sources to acquire weather data requires considerable effort; at times is impractical; and does not always provide an adequate representation to permit strategic flight planning. The Pilot Weather Advisor will overcome most of these disadvantages by automatically providing near real-time graphical depictions of weather information in the aircraft via satellite communications.

In Phase I the Pilot Weather Advisor collected NWS surface observations and WSI NOWRAD radar data four times each hour. These surface observations and radar data were encoded into a data stream by STX in Lanham, MD and then sent via telephone communications to the GTE satellite Earth Station in Grand Junction, CO for uplink to the GSTAR I communications satellite. The data stream was then broadcast covering the Continental United States area. This data stream was received by a Qualcomm satellite communications system provided by NIALL Enterprises of Belmont, WI on-board the aircraft. The data stream was processed and displayed on a PC/AT computer as a graphical depiction of the surface observations and radar data for a given geographical area using the software developed by STX in support of the FAA Pilot Advisor Weather Support System (PAWSS) program. These graphical depictions show the Visual Flight Rules/Instrument Flight Rules (VFR/IFR) status, the weather of reporting airports, and the current radar data for the area. The aircraft position is also displayed to enable the pilot to determine the best course of action in the presence of hazardous weather.

The Pilot Weather Advisor (developed under the NASA Langley Research Center Small Business Innovation Research Program 90-1, subtopic 03.02, Aircraft Severe Weather Environments) demonstrated that the technical problems involved with transmitting significant amounts of weather data to an aircraft in-flight or on-the-ground via satellite are solvable with today's technology. The Pilot Weather Advisor is an excellent solution for providing accurate and timely weather information for aircraft.

Introduction

This report gives the results of the work performed by ViGYAN, Inc. under contract NAS1-19250 as Phase I, of the NASA Langley Research Center Small Business Innovation Research (SBIR) program 90-1, subtopic 03.02, Aircraft Severe Weather Environment. This subtopic requested "Innovative concepts for an airborne weather monitoring and processing system that will accept data from various sensor units (airborne and ground based) to provide hazardous weather information to the pilot". In the response to this request, ViGYAN proposed to apply the results of the Pilot Automated Weather Support System to develop the Pilot Weather Advisor as a commercial. The Pilot Weather Advisor puts large amounts of weather data on-board aircraft using a satellite communications system and to display this data to the in-flight pilot in a suitable color graphic format.

The Phase I work was performed during January 1991 through September 1991 by ViGYAN and its subcontractors, and is reported herein. ViGYAN is now involved in the Phase II of the NASA SBIR program to develop and test a Pilot Weather Advisor system for commercial service.

PWxA System Description

The purpose of the Pilot Weather Advisor (PWxA) is to improve the safety and utility of aircraft operations. The PWxA system shown in figure 1 provides near real-time graphical depictions of weather information in the aircraft via satellite communications. The PWxA collects National Weather Service (NWS) Sequence Weather Reports (surface observations) and WSI NOWRAD radar data four times each hour. These surface observations and radar data are encoded into a broadcast data file and then sent via telephone communications to a satellite earth station for uplink to a communications satellite. The data file is then broadcast over the Continental United States. This data file is received by a satellite communications system on-board an aircraft. The data file is processed and displayed on a PC/AT computer as a graphical depiction of the surface observations and radar data for a given geographical area. These depictions show the VFR/IFR status and the weather elements of reporting stations and the current radar for the area. The aircraft position is also displayed to enable the pilot to determine the best course of action in the presence of hazardous weather.

The PWxA depictions are a subset of the depictions developed in the Pilot Automated Weather Support System (PAWSS) project. (Ref. 1) The depictions used by the PWxA included regional data for "Airport/Station Weather", (Airport Weather) and "Airport/Station Category", (Airport Category), a regional version of ground weather radar reflectivity "Mosaic Radar" (Radar), and Airport/Station Identification (Station ID). The Station ID depiction is a summary of the geographical region and is shown in figure 2. The Airport Category depiction shown in figure 3 is a graphical display of the VFR/IFR condition at specified observation stations. The Airport

Weather depiction shown in figure 4 is a graphical display of the weather elements at specified observation stations. The Radar depiction shown in figure 5 is a mosaic of the current precipitation radar for a given geographical region. All the displays use color to differentiate the different conditions of Airport Weather, Airport Category, and Radar conditions.

Ground Data Processing System

The weather data acquisition and ground processing system was constructed by ST Systems Corporation (STX) at its Lanham, MD facility using real-time weather data from the NWS and WSI. New concepts and designs for the real-time data processing software and broadcast data formats were developed for the PWxA, and operated in support of the SBIR Phase I effort.

Ground data processing was initiated to broadcast a final data file four times per hour on the quarter hour. The quarter hour intervals were defined as A, B, C, and D intervals with A being the first quarter hour. Processing for the Airport Weather and Airport Category during this SBIR Phase I effort was time consuming, and therefore started 10 minutes before the broadcast time.

Processing for the radar data was relatively rapid. However, the WSI NOWRAD radar for the quarter hour was not available to users until about 10 minutes after the time of observation, the delay in delivery ranged from 9 to 11 minutes.

An overall data flow diagram for the PWxA is shown in figure 6, identifying the major data stores at both the ground and aircraft processing segments.

Airport Weather and Airport Category Data

The PWxA Airport Weather and Airport Category data were obtained from the NWS Sequence Weather Reports (SA, SP, or RS) referred to as surface observations. The SA and RS reports are specific weather observations taken at designated reporting sites throughout the United States. These observations are usually made hourly at 50 minutes past the hour and are available within 15 minutes of the observation time. When the weather conditions are changing a special observation (SP) is made at any time during the hour.

The surface observations are available as ASCII data from the NWS data file and are acquired and stored "as is" in a file on an hourly basis, beginning ten minutes before broadcast time. The data is "frozen" temporarily four times per hour to transfer all surface observation reports to the ground data processor. The PWxA ground data processor deciphers these SA, SP, and RS into a broadcast file format.

For Airport Weather the given conditions are displayed in the PWxA depiction as the corresponding colors:

<u>Condition</u>	<u>Color</u>
no report	clear/clear
no weather, ceiling \geq 3000 ft. or visibility \geq 5 mi.	white/white
ceiling < 3000 ft.	green/green
rain or drizzle	blue/white
obstruction to vision	white/yellow
both rain or drizzle and obstruction to vision	blue/yellow
hazardous weather	red
winds > 20 kt.	white outline

For Airport Category the given conditions are displayed in the PWxA depiction as the corresponding colors:

<u>Condition</u>	<u>Color</u>
no report	clear/clear
ceiling > 3000 ft. or visibility \geq 5 mi. (VFR)	white
ceiling \leq 3000 ft. or visibility 5 mi. (MVFR)	green
ceiling < 1000 ft. or visibility < 3 mi. (IFR)	blue
ceiling < 500 ft. or visibility 1 mi. (LIFR)	yellow
ceiling < 200 ft. or visibility < 0.5 mi. (<CAT I)	red

Figure 7 shows the a typical SA for LSE (LaCrosse, WI) and how the PWxA ground processor deciphers an SA into Station ID, Airport Category, and Airport Weather. The colors for the PWxA depiction differentiate the flying conditions set by the FAA guideline. For the LSE SA shown in figure 7 the Airport Category (circle) color is white and the Airport Weather (diamond) color is all red. An additional feature not show in figure 7 is that if the winds are greater than 20 knots the weather symbol (diamond) is outlined in white instead of black.

Once the surface observations have been deciphered into Station ID, Airport Weather, and Airport Category, they are combined into a *.SFX file which will be merged with the Radar data file and then broadcast.

The Stations selected and used for the PWxA are set in the ground processing system for a given geographical region. The geographic regions for the PWxA SBIR Phase I was centered on Dubuque, IA (DBQ). The stations used for the DBQ geographical region are listed in Appendix A.

Radar Data

The PWxA Radar data is obtained from the WSI NOWRAD radar data. The radar data is acquired using the usual commercial access method support by the WX-VIEW software of Robertson Software, Inc. The user downloads a regional mosaic radar at 320 by 240 resolution in six reflectivity levels, in the cylindrical equidistant map projection centered on the desired station site (for Phase I Dubuque, IA). The data is then displayed on a PC/AT at the 640 by 480 resolution, and written to a flat image file. The flat image file is then processed to create a Radar broadcast file (*.RX). The Radar broadcast file provides the WSI NOWRAD radar data as an 80 by 60 line grid with four reflectivities.

The Radar reflectivity levels are assigned the following values based on the Video Integrated Processor (VIP) assessments of the precipitation intensities for the given conditions and displayed as the corresponding colors:

<u>Condition</u>	<u>Color</u>
zero reflectivity	Clear (not drawn)
non-zero reflectivity, VIP levels 1 and 2	green
non-zero reflectivity, VIP levels 3 and 4	yellow
non-zero reflectivity, VIP levels 5 and 6	red

Once the Radar (*.RX) and Airport Weather/Category (*.SFX) broadcast files are generated they are merged together to create a final PWxA broadcast file (*.BX). A sample PWxA broadcast file including Radar, Airport Weather, Airport Category, and Station ID is shown as Appendix B.

Satellite Communications System

Communications satellites are positioned 22,300 miles above the equator and travel in an orbit that is synchronized with the rotation speed of the earth. The satellites that broadcast to North America are positioned along the equator between 55° and 140° west longitude. From there they cast a signal over the entire Continental United States.

Current communication satellites are made up of 16/24 transponders that are roughly similar to TV channels when used for television or other broadband distribution services. These channels are readily divided into much narrower bandwidth segments for data uses called Single Channel Per Carrier applications (the technology used for the PWxA).

To reach the satellite requires a earth station that uses a large, highly directional antenna system to avoid interfering with adjacent satellites. These earth stations are used to format the information to be sent to various transponders on satellites and to exercise the quality control function over the entire process.

NIALL Enterprises, Inc., Belmont WI, was operating a Piper Malibu aircraft in a test mode with a Qualcomm satellite communications system on-board. NIALl has developed a satellite communications data link for its own proof-of-concept use to deliver air traffic controllers' radar data to the cockpit to generate a cockpit display for collision avoidance purposes. (Ref. 2) It was a relatively simple matter to deliver weather data on this data link instead of air traffic controllers' radar data. ViGYAN negotiated with NIALl to provide the use of this aircraft and satellite communications system for the PWxA test flights in the Wisconsin area. The PWxA test flights were successfully conducted using the satellite communications system described below.

For the series of test flights, the "satellite communications chain" of elements making up the communications system is shown in figure 8 and briefly described as follows:

1. The earth station and space segment were secured from GTE Spacenet on Ku band, (12 and 18 gigahertz), on the satellite GSTAR I located at 103° west longitude fed by a GTE Spacenet earth station at Grand Junction, CO.
2. The mobile satellite receive system mounted on the aircraft was a standard Qualcomm OMNITRACS system currently in use on over 14,000 semi-trailer trucks operating in North America. This system is a half duplex, two-way data (message) system using a patented mechanically steered antenna mounted on the mobile unit. The antenna tracks the satellite based on the received signal strength and internal software. The antenna was mounted on the nose of the aircraft as shown in figure 9.
3. The two-way OMNITRACS data system was modified to accommodate an additional satellite broadcast (one-way) data channel from transponder #12 on which the PWxA broadcast data file was carried at 9600 baud. Modulation and demodulation were accomplished with ComStream high speed VSAT data modems on each end of the satellite communications data link.
4. In the aircraft, the PWxA broadcast data was fed to the COM 1 port of an IBM PS/2 Model 30 computer for use by the PWxA airborne processing system.
5. PWxA broadcast data was delivered to the GTE Spacenet ground station at Grand Junction, CO from STX at Lanham, MD via dial up telephone modem at 2400 baud.

PWxA Airborne Processing System

The software for the airborne processing system of PWxA has been designed for the common PC/AT family of personal computers. This family of microprocessors provides a reliable and cost effective platform for the reception and display of the

PWxA depictions. A serial data stream of the broadcast file is provided to the standard COM port 1 of the PC/AT at a standard baud rate. The user control of the PWxA is provided through a standard keyboard. The depictions developed for the PWxA by the PAWSS project are designed for a standard VGA video, which supports 16 programmable colors in a 640 by 480 display resolution.

The PWxA broadcast data files are received and processed to generate data stores and depictions as shown in figure 6. A complete byte-for-byte copy of the received data stream is collected into a quarter hourly series of files with the extension *.PCK. This data is subsequently scanned by a decoder to identify valid (error free) packets. Decoded data for the Airport Weather and Airport Category depictions are stored in a quarter hourly series of files with the extension *.SFM. Decoded data for the Radar depictions are stored in a quarter hourly series of files with the extension *.RAD.

The *.PCK, *.SFM and *.RAD series of quarter hourly files are uniquely identified by filenames. All data received during each quarter hour segment is logged into the latest (open) *.PCK file and is overwritten to the latest *.SFM and *.RAD files.

The PWxA requires, at a minimum, the following personal computer characteristics:

- IBM PC/AT or compatible
- VGA display (640 x 480) with at least 256 kByte video memory
- 640 kByte RAM memory
- keyboard

The system disk is prepared for the PWxA by creation of a directory (directory path and name is user choice), plus two required subdirectories IMAGES and DATA with appropriate files.

The files in the ..\IMAGES subdirectory and define the geographical map projection and list of valid Station Identifiers, respectively.

The *.PCK, *.SFM, *.RAD files are the stored PWxA data which are stored for playback and trend assessment of the depictions in the \DATA subdirectory.

The PWxA system is then executed running the PWxA executable:

PWXA.EXE

Users must follow the on-screen prompts to provide information on the parameters desired for COM port 1 (baud rate, parity and number of START and STOP bits). The PWxA will initialize, open COM port 1 for data acquisition, and start operations

showing the initial PWxA introduction page. At this time, the PWxA is looking for valid user keypress or commands.

Test Aircraft

The aircraft utilized for the test flights was a Piper PA-46 Malibu, N711XL owned by Dave Stauffacher, President of EXCELL INNS, Inc. of Madison, WI. The aircraft was operated on all flights by Dave Stauffacher. A sketch of the aircraft showing the locations of the satellite communications equipment and the on-board PC is shown in figure 10. This equipment is not normally carried on the aircraft during usual flights.

Pertinent aircraft avionics include a Sperry Weather Radar, a Wx 1000 Storm Scope, an ARNAV 50i LORAN, a VOR/DME Area Navigation System, a VFIS Electronic Moving map, as well as the conventional VOR and NDB receivers.

Test Area

All test flight for the PWxA were conducted in the Wisconsin area as shown in figure 11. All test flights originated from Platteville, WI (PVB). Appendix A gives all the states and their stations included in the Wisconsin test area.

Preflight Test Scenario

Early in the day, available sources of weather information (commercial TV broadcast, Weather Channel, telephone FSS briefing) were utilized to formulate one or several flight test scenarios for the Wisconsin test area. The aircraft was then ferried from Madison to Grant County Airport near Platteville, WI (PVB). At PVB, the satellite communication equipment, PC, and display equipment were installed and checked out. The satellite communications were established and following execution of the PWxA software through the keyboard, the current PWxA depictions was displayed, reviewed, and compared with the previous knowledge of the weather situation. The flight test scenario for the day was then confirmed or modified, and the Decision-to-Go was made by the pilot.

Flight Test

Four complete test flights were flown with the PWxA system in June 1991. Each flight was documented with a video recorder, voice recorder, and the PWxA broadcast data and depictions. Because of the development nature of the PWxA system several changes were made to improve the PWxA system between flights. A detailed analysis was conducted for all the flights to determine the performance of the PWxA system. (Ref. 3) The June 25 and 26 flights were VFR; the June 27 flight was IFR, with the ATC Clearance obtained via telephone from PVB, and picked up in the air after a VFR takeoff. The last flight (June 27, 1991) is discussed in this report.

June 27, 1991 Flight

Summary: A morning IFR flight was conducted from Platteville, WI (PVB) to Minneapolis, MN (MSP) in Visual Meteorological Conditions with a landing at MSP, and a return flight later that afternoon. Takeoff from PVB was at 9:09 a.m. CDT, and landing at MSP at 10:39 a.m. CDT. The route of flight to MSP, takeoff, and landing times are shown in figure 11, along with a list of the PWxA depictions received during the flight. The aircraft path and position data shown herein were added after the flight.

Preflight: Information indicated a line of possibly severe convective weather was in the Wisconsin test area, stretching from southwestern through northern Minnesota. Cell movement was 25 to 35 kt along the line; the line itself was supposed to move slowly southeast. The MSP terminal forecast shown below, indicated a reasonable chance of success for the flight.

MSP FT 270808 C 80 BKN 1812. 11Z 25 SCT C 80 BKN 1810 CHC C 25 OVC
3TRW. 15Z 50 SCT 100 SCT C 250 BKN 1915 CHC C 40 OVC 5TRW AFT
21Z. 02Z VFR TRW

This situation was confirmed with the first depictions (13B) were received on the ground at about 1400Z, figure 12 and 13. VFR conditions existed along the route of flight with the line of convective activity positioned a little farther northwest than expected. It was decided to fly to MSP and land there if possible, using the PWxA system to monitor the development and movement of the convective weather line.

Enroute: After a VFR takeoff at 1409Z, the IFR clearance was received from Chicago Center to climb and maintain 8,000 feet via Rochester (RST) and then direct MSP. The Storm Scope showed lightning activity at about 80 and 100 miles at 11 to 12 o'clock positions, even though the aircraft was about 220 miles from the radar line.

The first depiction received in the air was 13C, figure 14, at about 1430Z. This 13C depiction showed a little bit further spread into northern WI, and a yellow (level 3 or 4) cell northwest of MSP. Some yellow appeared at the southwest end of the line. The line was between MSP and Alexandria (AXN), just east of Brainerd (BRD). Some low level radar activity was noted in central Wisconsin that did not appear on the NWS Radar Summary reviewed after the flight.

Several times the aircraft position was manually entered into the system and shown on the display. This greatly reduced the effort to interpret the depiction. The approximate aircraft positions were determined and plotted after the flight on the figures in this report.

Just before 1445Z, the Storm Scope indicated lightning activity at about 125 miles, at the 12 o'clock position. This appeared to correlate with the position of the line on the (13C) Radar depiction, figure 14.

When the 13D depiction, figure 15, arrived on-board it showed the line about 50 miles northwest of MSP had 3 yellow squares (levels 3 and 4) whereas at 13C it had one yellow square. It was decided to monitor this development closely. Subsequently the Storm Scope showed lightning activity 30°L to 20°R, 150 to 200 miles.

The 14A depiction, figure 16, showed the line directly behind MSP was thinning out, and was dividing into two parts, northeast and southwest of our line of flight, and had not come closer to MSP. No surface observations were shown with this depiction. (It was later found that STX ground processor for the surface observations had failed.) The Storm Scope showed at that time the same indications of lightning activity at 15°L at 160 miles and 25°R at 120 miles, with no activity indicated dead ahead.

During the flight, the cloud shield on the horizon ahead was rising steadily, and after 1500Z it rose to approximately 30° above the horizon. Soon after this at about 59 miles out and 12,000 feet altitude, MSP approach started vectoring the aircraft for descent into the MSP terminal area. At about 1516Z the aircraft was under a high overcast that extended to the horizon on the left, but above and out of the field of view to the right.

When the 14B depiction was received at about 1515Z, figure 17, it showed that the storm line was still 50 miles northwest of MSP, and that the yellow (levels 3 and 4) had moved northeast to a point directly north of MSP. Some yellow did appear down to the southwest end of the line in South Dakota. It appeared that the cells were moving along the line to the northeast, but the line was not moving toward MSP.

The 14B depiction continued to show the low level radar activity in central to eastern Wisconsin. The MSP ATIS Kilo obtained at this time indicated CONVECTIVE SIGMETS 19C and 20C were current. MSP 1453Z weather was 9500 scattered, 15000 scattered, estimated ceiling 20,000 broken, visibility 12 miles, temperature 84°, dew point 69°, wind 200° at 14 knots with the altimeter at 29.83. Because of the proximity to landing and the active vectoring of approach control there was little opportunity to contact Flight Service to determine the content of the SIGMET advisory. The aircraft landed at MSP on runway 11R at 1539Z in Visual Meteorological Conditions.

After landing, the PWxA system remained on, and 14D depiction was received, figure 18, at about 1545Z. This showed that no immediate threat existed at MSP, although some red (levels 5 and 6) had appeared down to the southwest end of the line. The next 15A was not sent by STX and therefore not received. The last depiction 15B, figure 19, was received on the ground at about 1615Z also without

surface observations. This confirmed the overall trend, that MSP was "safe" and our flight route home to PVB showed no convective activity.

System Performance, June 27, 1991 Flight

For a complete analysis of the system performance, the flight was broken down into a discrete set of events from which it was possible to determine the errors in the system. Below is the procedure required to obtain a depiction in the aircraft as described earlier. This procedure is repeated every 15 minutes.

1. NWS Sequence Weather Reports are processed to obtain desired surface observations.
2. Surface observations are then assembled into Airport Weather and Airport Category for specified stations. (*.SFX files)
3. WSI NOWRAD radar data is assembled into Radar for the specified test area. (*.RX files)
4. The Surface observations and Radar files are then combined into a Broadcast file and broadcast to the aircraft. (*.BX files)
5. The Broadcast files are then received by the satellite receiver and sent to the on-board PC for processing. These Broadcast files when received are saved. (*.PCK files)
6. The Received files are then processed and Displayed on the PC monitor.

By comparing each step of the procedure an estimation of the system performance can be determined. This analysis cannot separate the system errors and possible human errors associated with each step in the procedure. The system performance analysis was conducted for this flight by comparing what was the original surface observation with what was displayed in the aircraft. The analysis is broken into the following steps and deals only with the surface observations:

1. Surface observations -- Broadcast (Ground Processing)
2. Broadcast -- Receive (Satellite Communications)
3. Receive -- Display (Airborne Processing)
4. Surface observation -- Display (Overall Performance)

The above steps cover all the aspects of the system which are the ground processing, satellite communications, airborne processing, and an overall performance.

Because this analysis only dealt with the surface observations, the analysis was performed only with data sets (broadcast files) that were complete with the surface observations and the radar data as shown in Appendix B.

For the flight on 6-27-91, PWxA Software Version 5, the analysis results are given below:

<u>Display</u>		<u>Errors</u>	<u>%Errors</u>
JUN27_13B	Surface Obs. -- Broadcast	10/49	20.4%
	Broadcast -- Receive	0/49	0.0%
	Receive -- Display	2/49	4.1%
	Overall Set Performance	11/49	22.4%
JUN27_13C	Surface Obs. -- Broadcast	9/49	18.4%
	Broadcast -- Receive	0/49	0.0%
	Receive -- Display	6/49	12.2%
	Overall Set Performance	13/49	26.5%
JUN27_13D	Surface Obs. -- Broadcast	9/49	18.4%
	Broadcast -- Receive	0/49	0.0%
	Receive -- Display	6/49	12.2%
	Overall Set Performance	12/49	24.5%
JUN27_14A	Surface Obs. -- Broadcast	10/49	20.4%
	Broadcast -- Receive	0/49	0.0%
	Receive -- Display	49/49	100.0%
	Overall Set Performance	49/49	100.0%
JUN27_14B	Surface Obs. -- Broadcast	10/49	20.4%
	Broadcast -- Receive	0/49	0.0%
	Receive -- Display	0/49	0.0%
	Overall Set Performance	10/49	20.4%
Overall Flight Surface Obs. -- Broadcast		19.6%	
Overall Flight Broadcast -- Receive Error		0.0%	
Overall Flight Receive -- Display Error		25.7%	
Overall Flight Performance Error		<u>38.8%</u>	

Several conclusions were drawn from the above analysis. The ground processing had some problems creating an accurate broadcast file. The process appeared to have

specific problems with -X, -BKN, -OVC, double letters in the surface observations, problems with visibility at 5 miles, and stations reporting more than once during the hour.

The satellite communications were extremely reliable. The communications maintained a perfect score for these flight sets.

For this flight the airborne process experienced a complete software failure that caused a 100% error on the JUN27_14A display. This error could be attributed to several factors. The airborne software occasionally required a reboot of the on-board PC. This 100% error could have occurred during one of these reboots. If the 100% error is ignored from this analysis, the Overall Flight Receive -- Display Error is reduced to 7.1% and the Overall Flight Performance Error for this flight is 23.5%.

Overall performance of the PWxA system software for this flight was considered fair. This fair performance can be directly related to the ground processing software. The satellite and airborne processing software performed well if the 100% error of JUN27_14A is ignored as a possible human error. Automation of all the processes is required to avoid human errors and to provide a very low error system.

Flight Review and Data Comparison

This section contains available NWS weather data and maps pertinent to this flight. The maps were supplied by the FAA FSS at Patrick Henry Airport, VA (PHF), and the alphanumeric data were supplied by STX.

National Weather Depiction: The 16Z depiction, figure 20, indicated scattered to broken clouds along the route, with high bases (20,000 to 25,000 feet). West and north of MSP, there was overcast at 9,000 and 11,000 feet. The existence of the convective line northwest of MSP was not indicated. The 19Z depiction, figure 21, showed the route was VFR with scattered clouds at 4,000 feet visibility at DBQ. A stationary front was depicted northwest of MSP.

National Radar Summary: The 1335Z, 1435Z, 1535Z, and 1635Z data, figures 22, 23, 24, and 25, generally agree with the Radar depictions displayed on-board the aircraft. The location, intensity, and dynamic behavior as discussed earlier is well represented. However, the activity shown in the on-board depictions in central WI and southern IA are not shown on the National Radar Summaries.

Surface Observations: A complete listing of the surface observation for the flight are given in Appendix A. The performance of the PWxA system in depicting the surface observations was considered only fair because of software problems associated with the ground processing system as mentioned earlier in this report. The RWF and MSP observations are repeated below for 15Z, 16Z, and 17Z:

MSP SA 1453 95 SCT 150 SCT E200 BKN 12 095/84/69/1911/983/ 307 1078
RWF Missing

MSP SA 1553 100 SCT E200 BKN 12 098/83/70/1910/984/FEW ACCAS NW
RWF RS 1555 60 SCT E90 BKN 250 OVC 10 084/81/71/2212/980/TE40 MVD ENE OCNL
LTGIC N

MSP SA 1652 100 SCT E150 BKN 200 OVC 10 093/88/71/1717G22/983
RWF SA 1651 55 SCT E95 BKN 250 OVC 10T 080/80/71/1912/979/TB17 OVHD-N
MVG NE VIRGA W-N LTGICCG NW-NE

RWF SP 1730 55 SCT 95 SCT 250 -OVC 12 2309/982/TE15 MOVD NE DRK NE

The NWS Radar Summary supports the Radar depictions presented by the PWxA. The RWF SA 17Z indicates that thunder began at 1617Z overhead and to the north, and was moving northeast, with cloud-to-cloud and cloud-to-ground lightning to the northwest through the northeast. As noted from the other data types and the experience of the flight crew, the line of thunderstorms did not reach to MSP during this flight. For this flight the Airport Categories and Airport Weather depiction performance was considered only fair because of the errors associated with the ground processing as discussed earlier. In subsequent testing performed by the FAA PAWSS project in response to the errors found in using the PWxA system, several software changes were made by STX to improve the performance. These improvements reduce the performance error to less than 2% for the Airport Categories and Airport Weather depiction. If this performance capability for the PWxA system had existed during this flight, the overall performance error would have been about 2%. It is believed that this overall error can be reduced to significantly less than 1% in an operational system.

Pilot's Comments

The potential for the PWxA system became evident to the pilot, Dave Stauffacher. His comments included the following:

"...It's great. The limitations on what we're doing is the quality and quantity of the data. It's that simple. Quality is the real-timeliness of it and the accurateness of it, because the older it gets, the less important it is. The ability to get it into the airplane has been demonstrated. Software, we can do anything with, it's just a matter of how sophisticated you want to get. So it just boils down to what they're giving us on the other end, what the data stream looks like, and so its great what you're doing but we obviously have to refine that so they can turn data around very fast, because as we saw today, we had a tough time catching up with the weather sometimes..."

"When we get NEXRAD, I've been lead to believe we'll get it faster... Yeah...There's so much you can do! It was Good! OK. I'm just pleased, Good."

He indicated that the delay between getting the Radar depiction (approximately 15 minutes) was too long and he would like the option to see the actual surface observations in alphanumeric form.

He also indicated that the PWxA system set-up used in flight must be designed for minimum pilot workload and very reliable. He felt that if the display could be placed on the instrument panel, and possibly incorporated into the electronic moving map for navigation, it would reduce the overall workload and be very useful.

Conclusions

The PWxA system developed under the NASA SBIR program has demonstrated that the technical problems involved in transmitting significant amounts of weather data to a general aviation aircraft in-flight or on-the-ground via satellite are solvable with today's technology. The potential usefulness and need for the PWxA system concept was demonstrated to all those on-board the test flights. The Pilot Weather Advisor is an excellent solution for providing accurate and timely weather information for general aviation aircraft.

It must be noted that the usefulness of the Airport Category and Airport Weather depictions to flight management was not demonstrated due to the generally VFR weather encountered. Additional testing will be run under fall, winter, and spring conditions.

Future

ViGYAN Inc. has been awarded a Phase II SBIR from NASA to further develop the PWxA system into a commercial product. The future PWxA system will have many of the same feature with additional improvements and more information.

Some of the improvements are:

1. Aircraft position automatically plotted on all depictions with a history of the aircraft track.
2. Better resolution in the Radar data block size (smaller than the 8 x 8 pixels per block).
3. A fast acting "looping" technique to permit quick trend assessment.
4. Complete automation of the ground processing of the PWxA system to improve accuracy and speed of the PWxA system.
5. Simplified control system.

6. Improved graphical depictions.
7. Automatic NSSL "Watch Boxes" overlay on any depiction.
8. National/Regional geographical areas.
9. Improved aerodynamics and electronics of the satellite communications antenna.
10. Indication of Lightning activity on Radar depictions.
11. Trend assessment of specified airports.

This development will be a two year effort to provide a reliable and cost effective system of providing weather information to general aviation aircraft.

References

1. Dash, E.R., STX, and Norman L. Crabill, ViGYAN. The Pilot's Automated Support System Concept (PAWSS). Paper presented at the Seventh International Conference Interactive Information and Processing Systems for Meteorology, Oceanography, and Hydrology, AMS. January 1991, New Orleans.
2. J. O'Neill, NIALL Enterprises, Belmont, WI
3. Kilgore, W.A., Crabill, N.L., Shipley, S.T., O'Neill, J., Stauffacher, D., Graffman, I., and Seth, S. Pilot Weather Advisor, Final Report for NASA Langley Research Center, SBIR Phase I, Contract No. NAS1-19250, September 1991

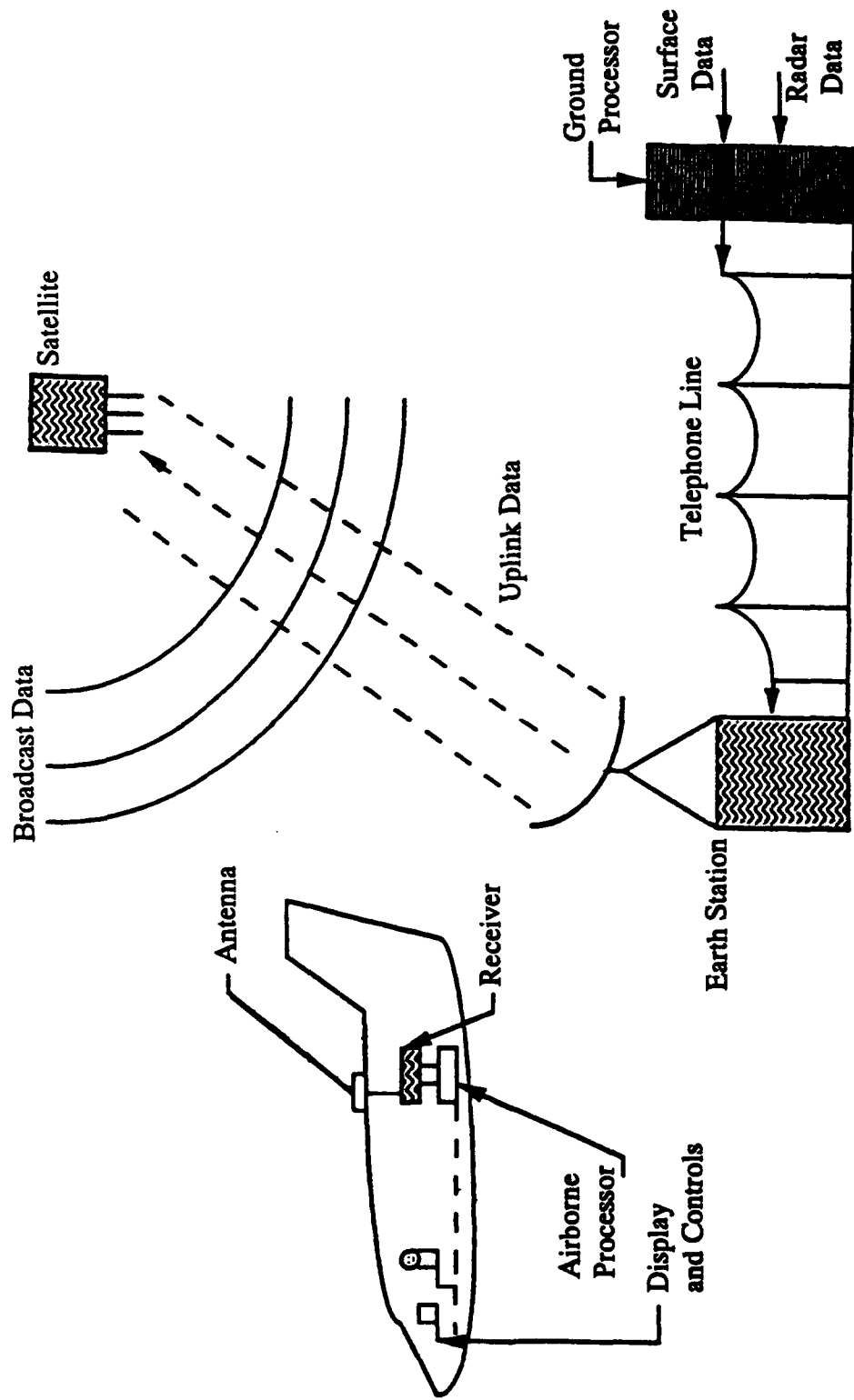


Figure 1. Pilot Weather Advisor System.

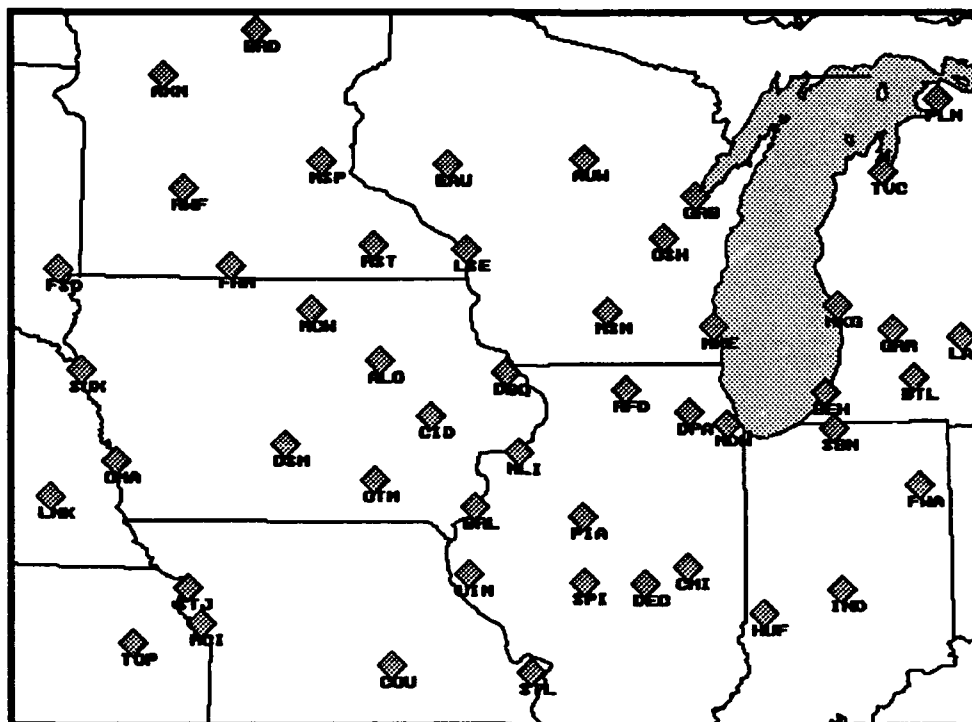


Figure 2. Airport/Station Identification Depiction.

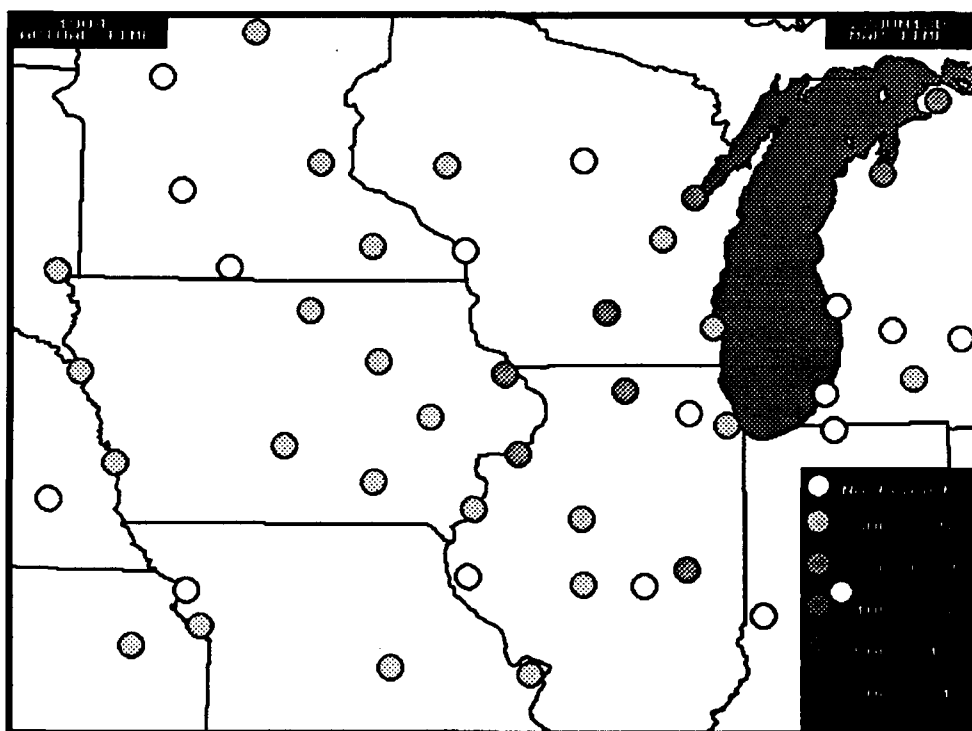


Figure 3. Airport Category Depiction.

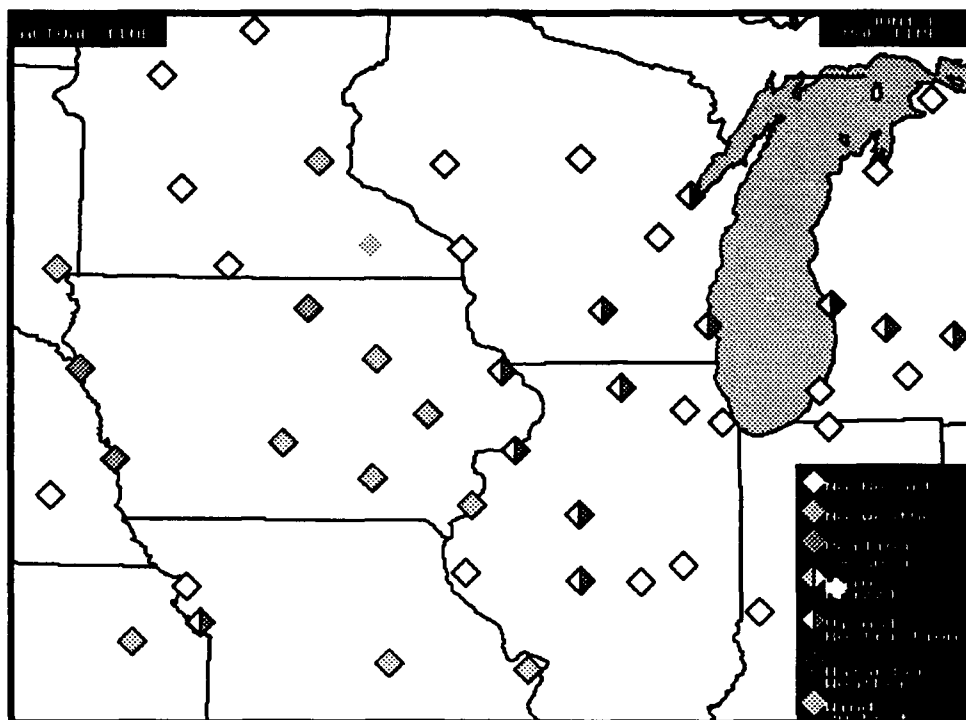


Figure 4. Airport Weather Depiction.

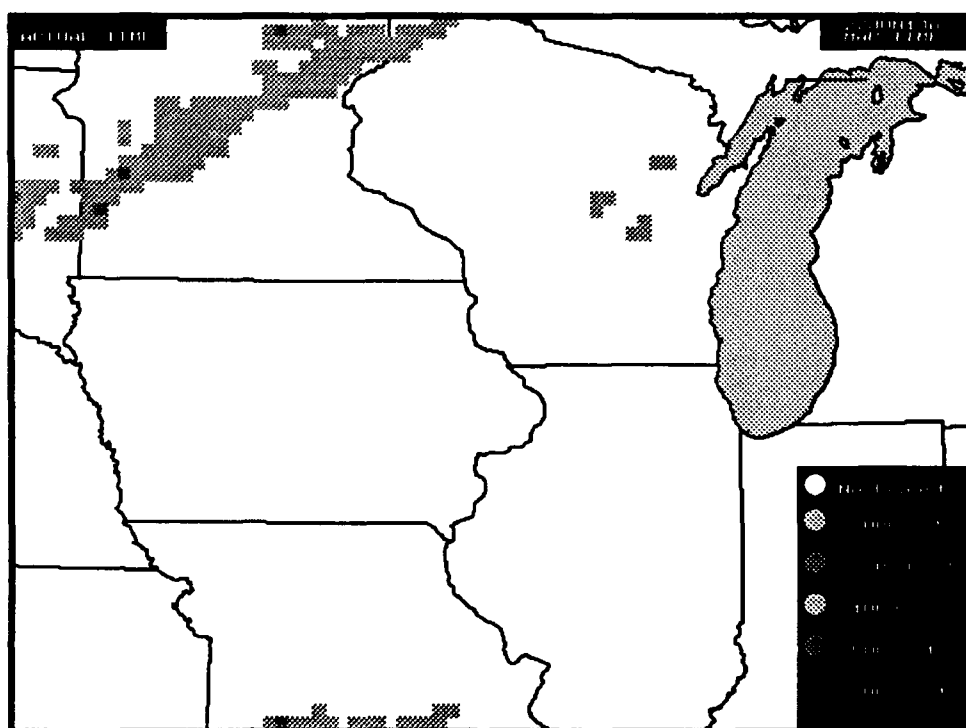


Figure 5. Radar Depiction.

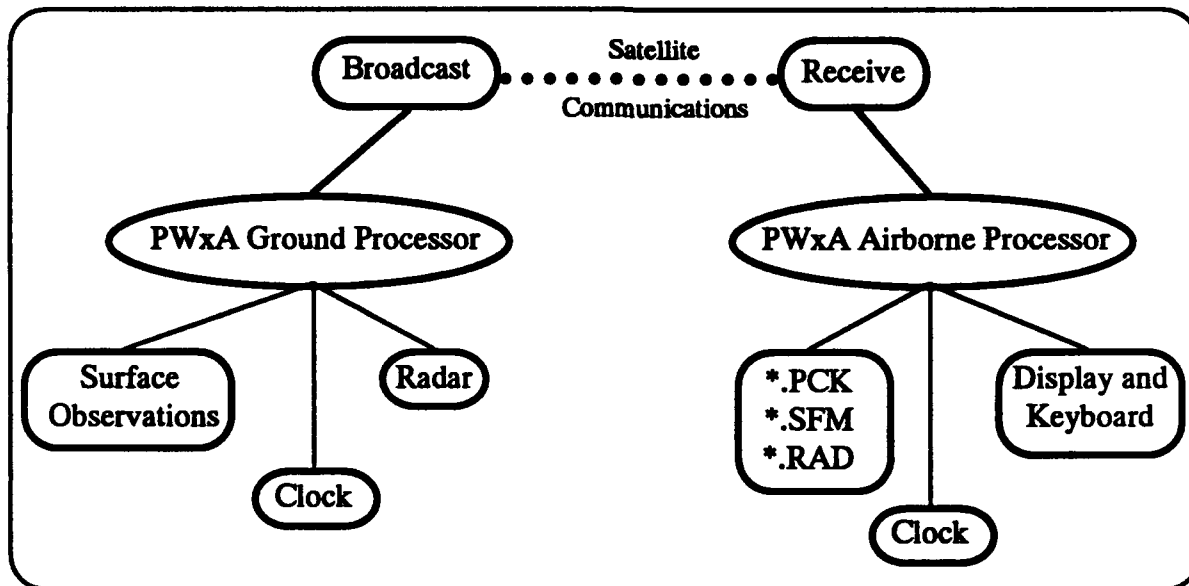


Figure 6. PWxA Data Flow Diagram

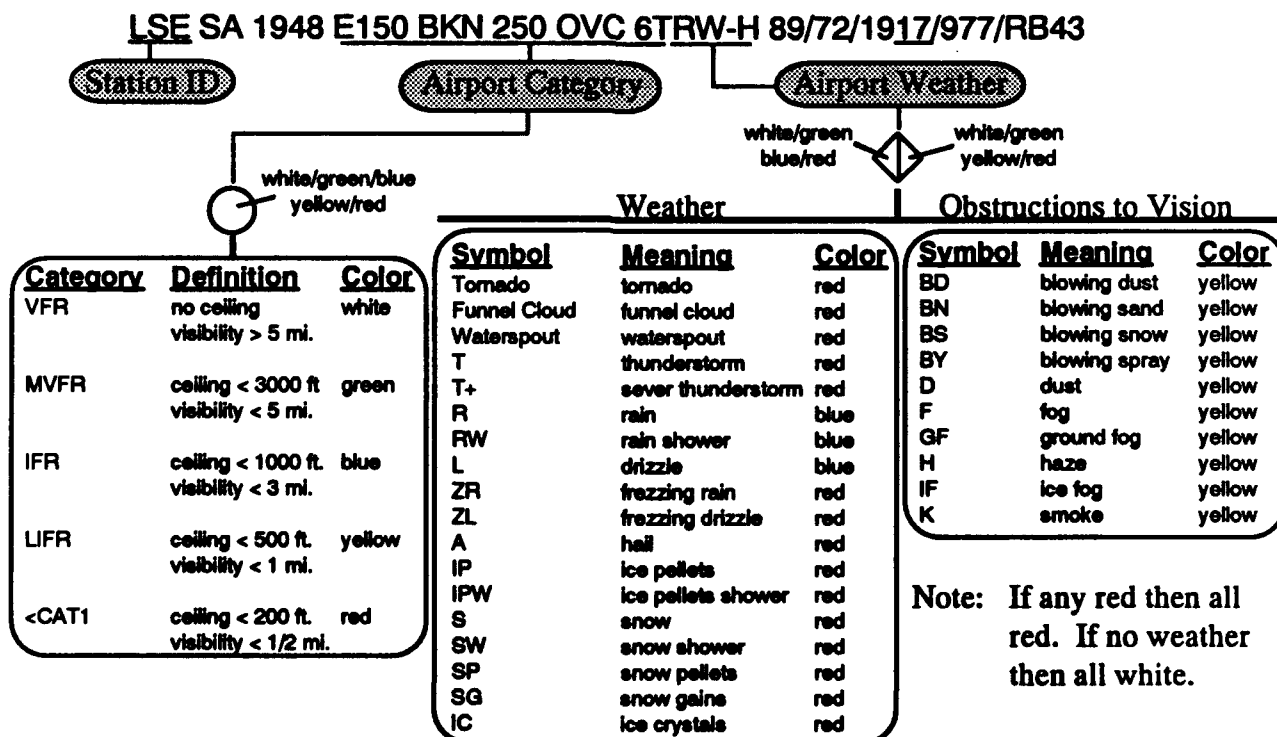


Figure 7. Analysis of Surface Observations

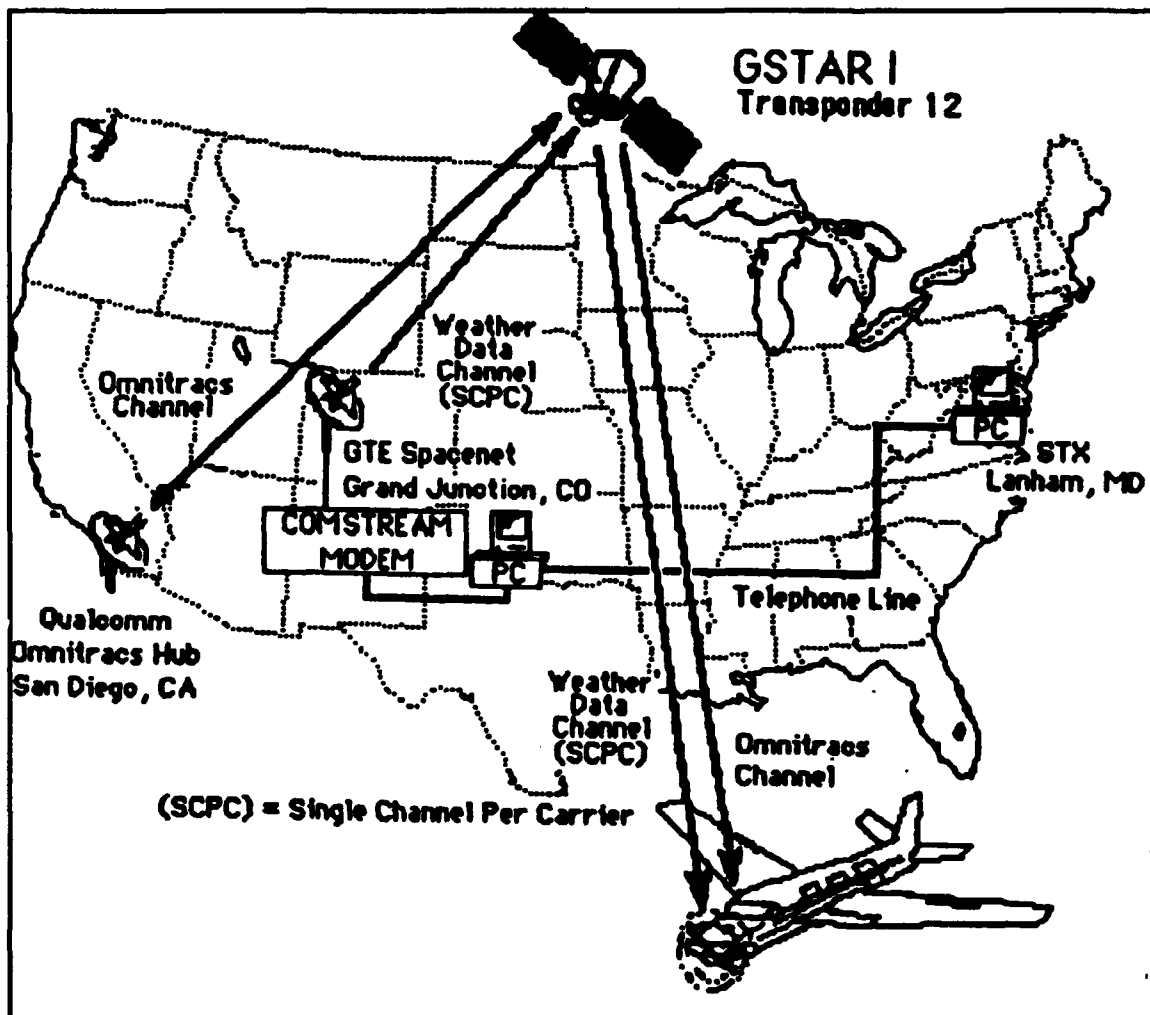


Figure 8. Satellite Communications System.

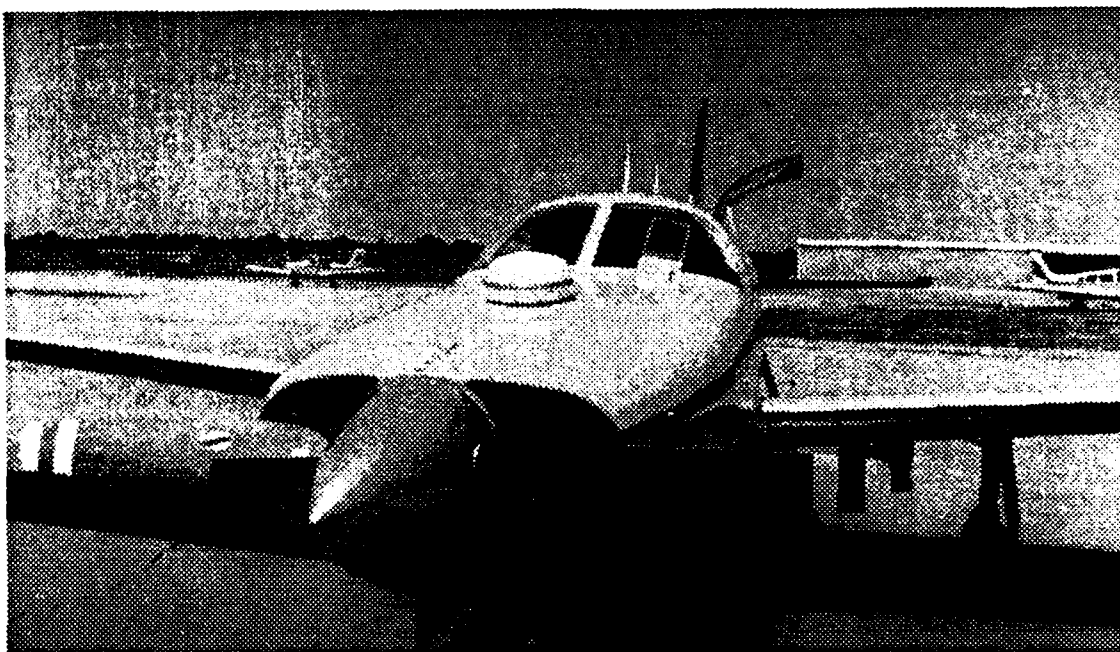


Figure 9. Piper Malibu Aircraft with Qualcomm Antenna Located on Nose.

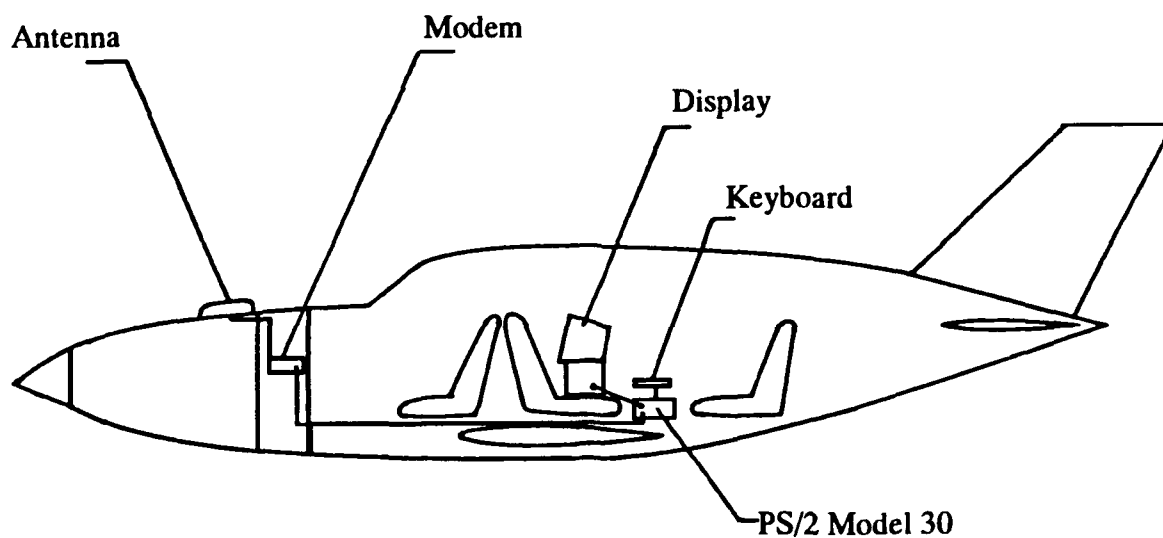
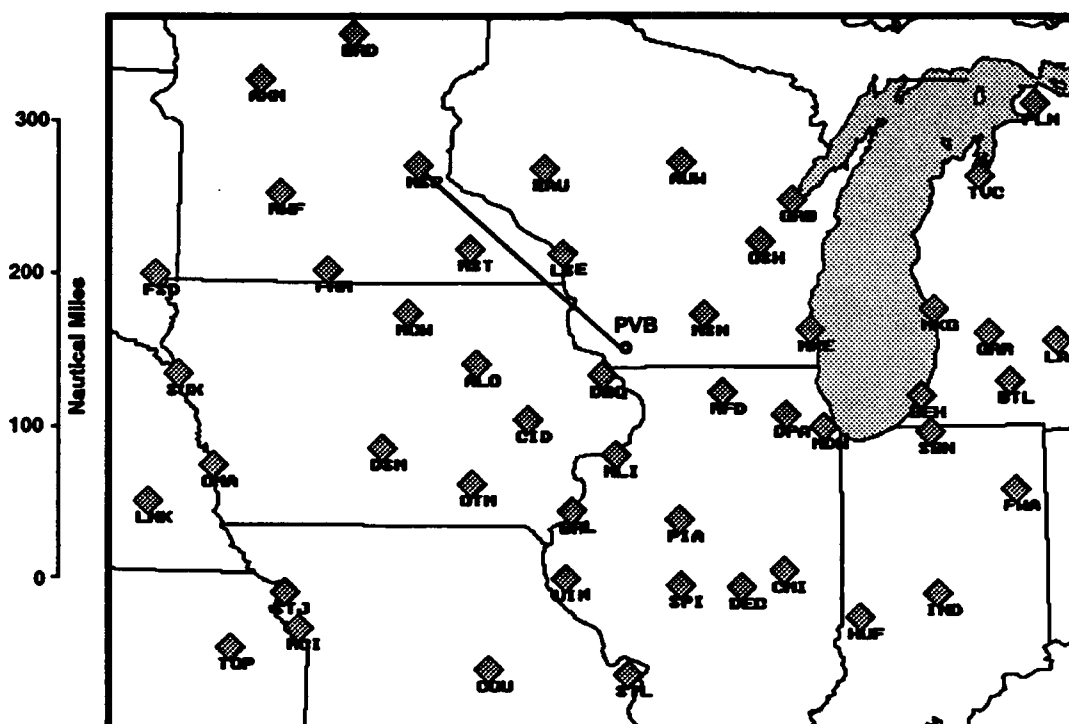


Figure 10. Schematic of Aircraft Showing Equipment Location.



Flight Times

Takeoff @ PVB

1409Z = 9:09CDT

Depictions Received

13B 1400Z

13C 1430Z

13D 1445Z

14A 1500Z

14B 1515Z

Landing @ MSP

1539Z = 10:39CDT

14C Not Received

14D 1545Z

15A Not recieved

15B 1615Z

Figure 11. Wisconsin Test Area, June 27, 1991 Flight.

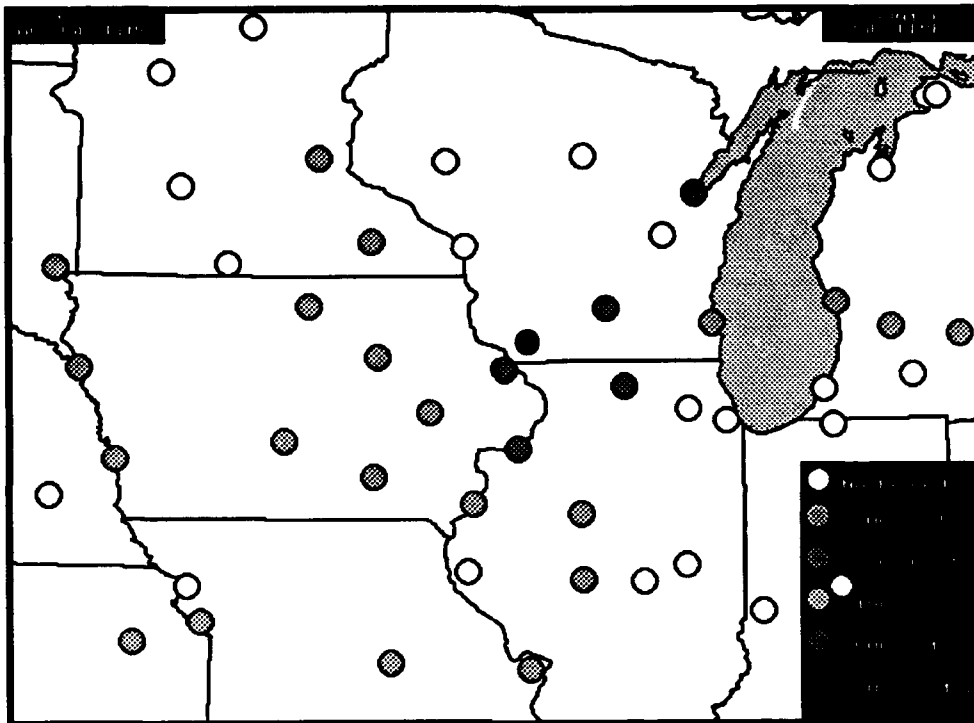


Figure 12. 27JUN13B, Category and Radar Depiction, 1400Z.

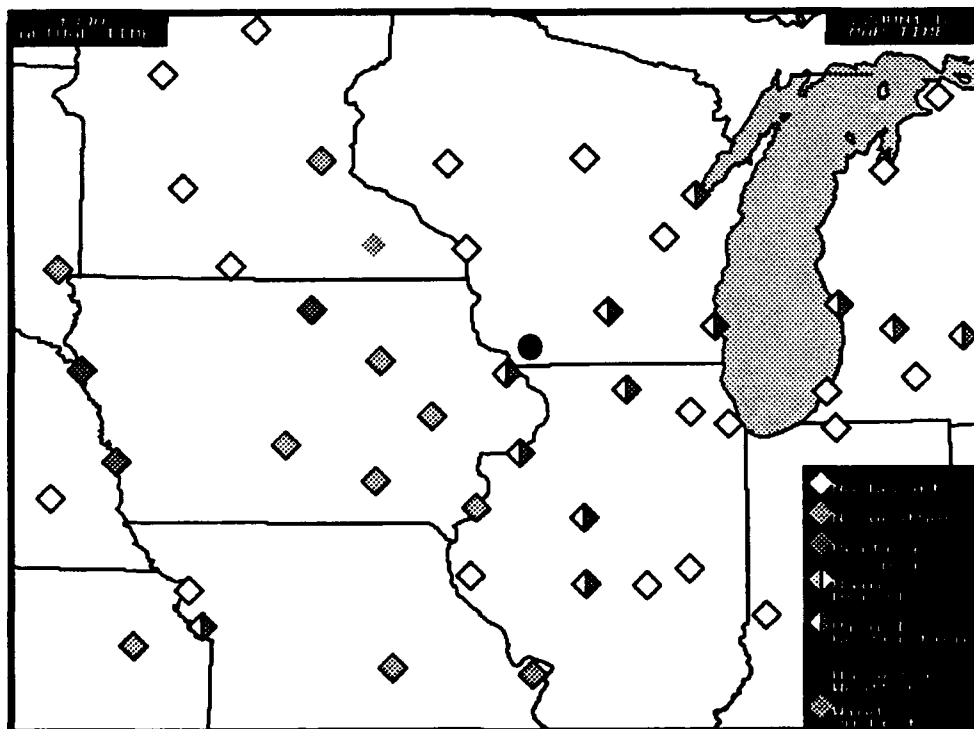


Figure 13. 27JUN13B, Category and Radar Depiction, 1400Z.

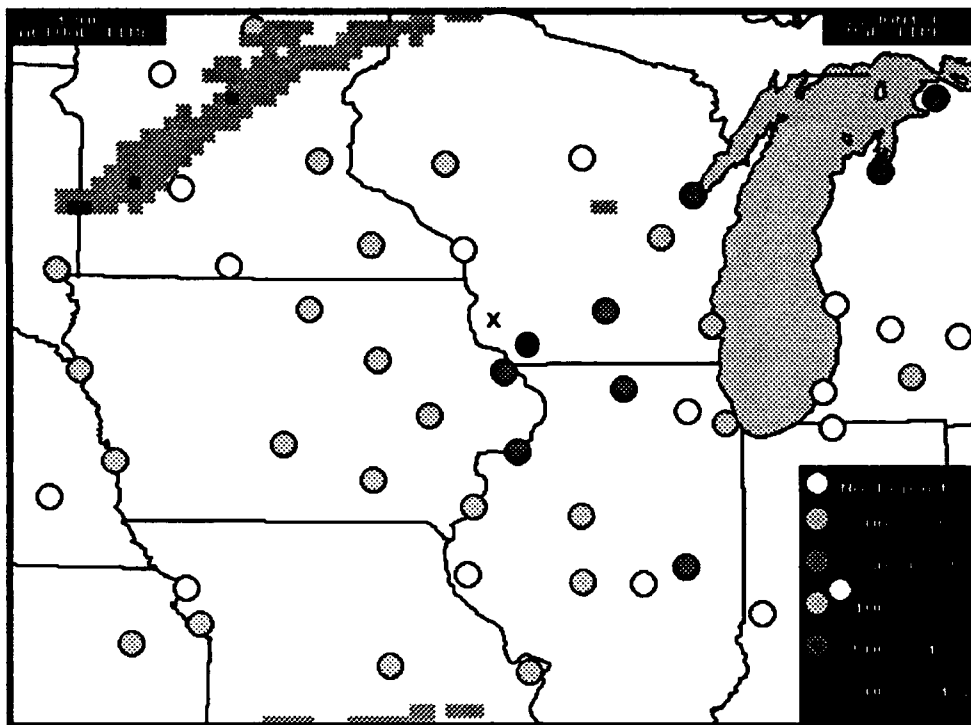


Figure 14. 27JUN13C, Category and Radar Depiction, 1430Z.

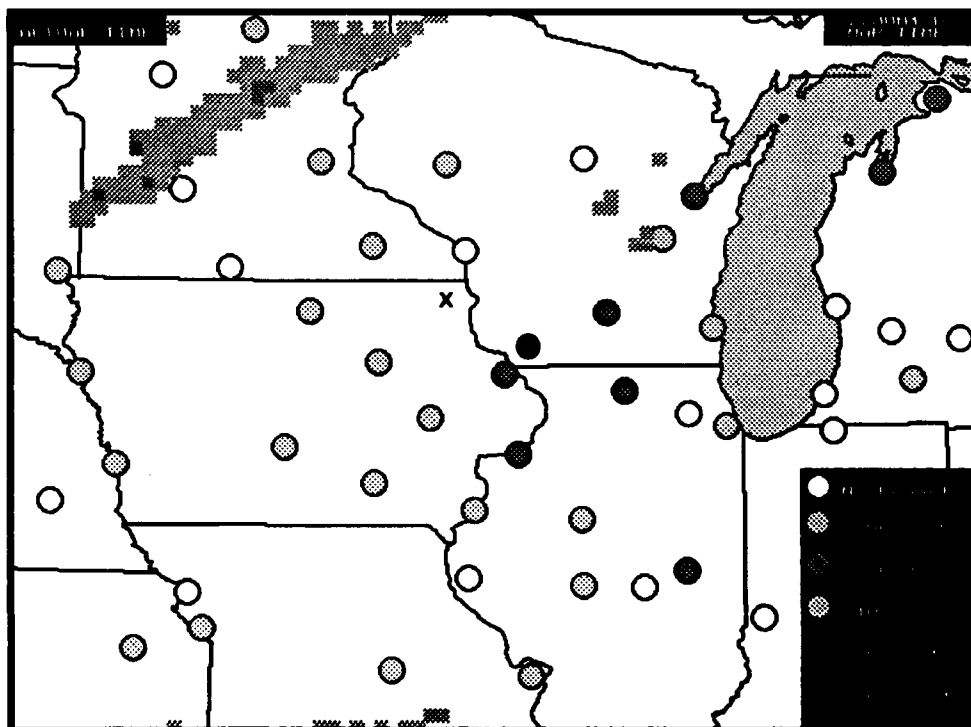


Figure 15. 27JUN13D, Category and Radar Depiction, 1445Z.

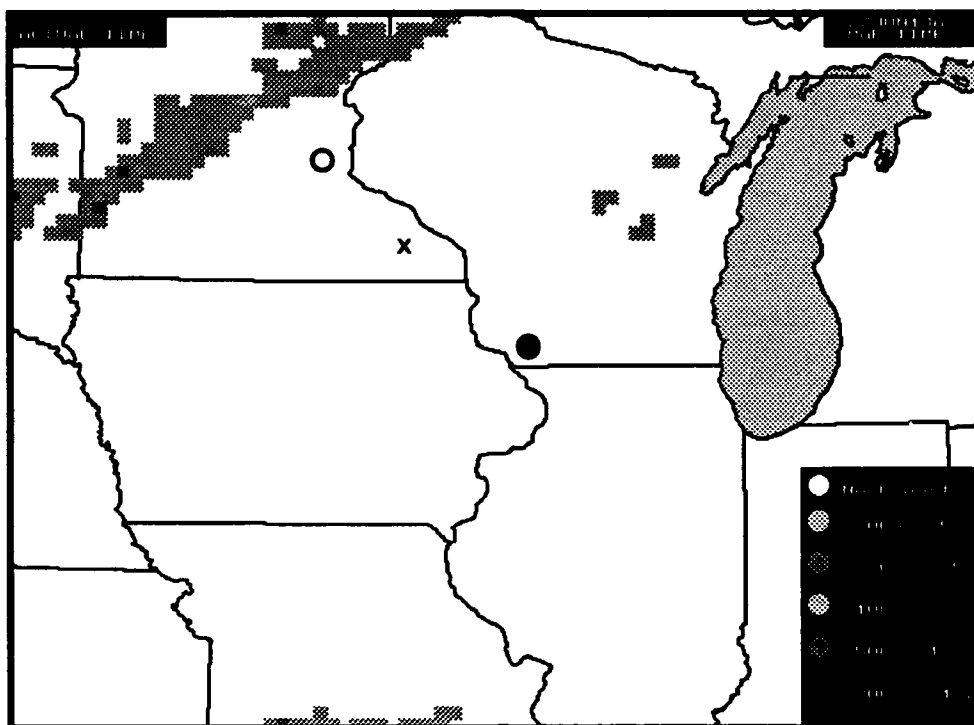


Figure 16. 27JUN14A, Category and Radar Depiction, 1500Z.

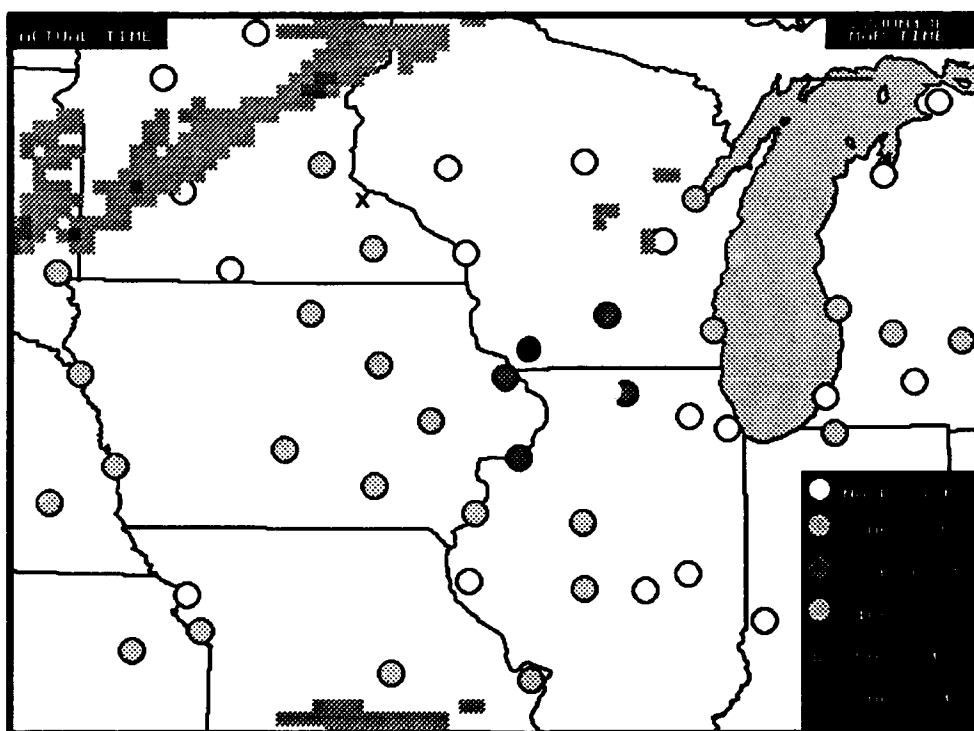


Figure 17. 27JUN14B, Category and Radar Depiction, 1515Z.

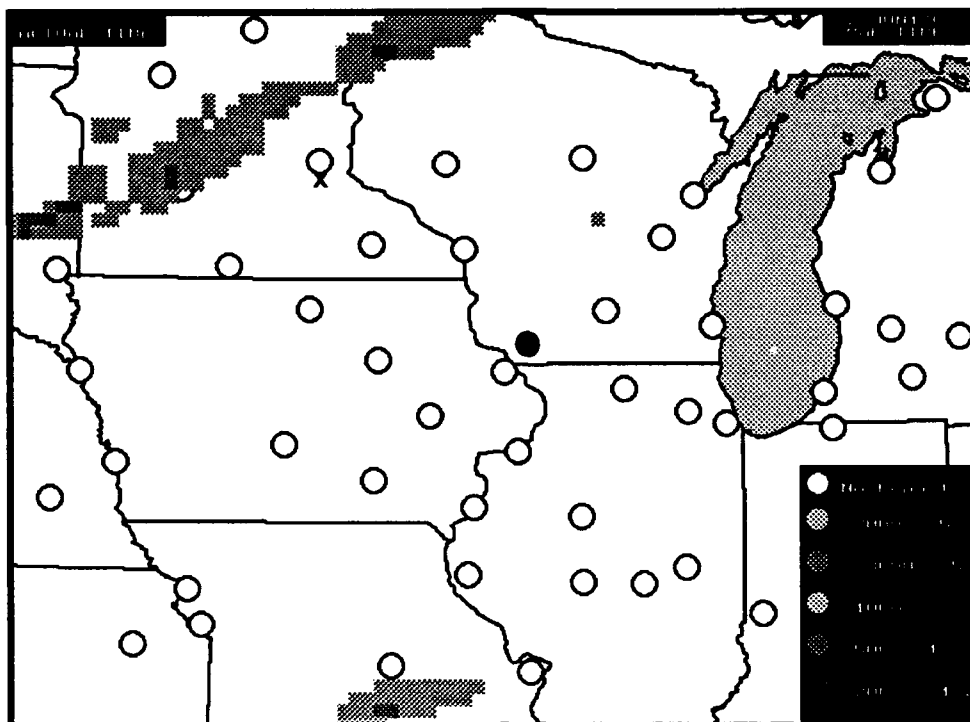


Figure 18. 27JUN14D, Category and Radar Depiction, 1545Z.

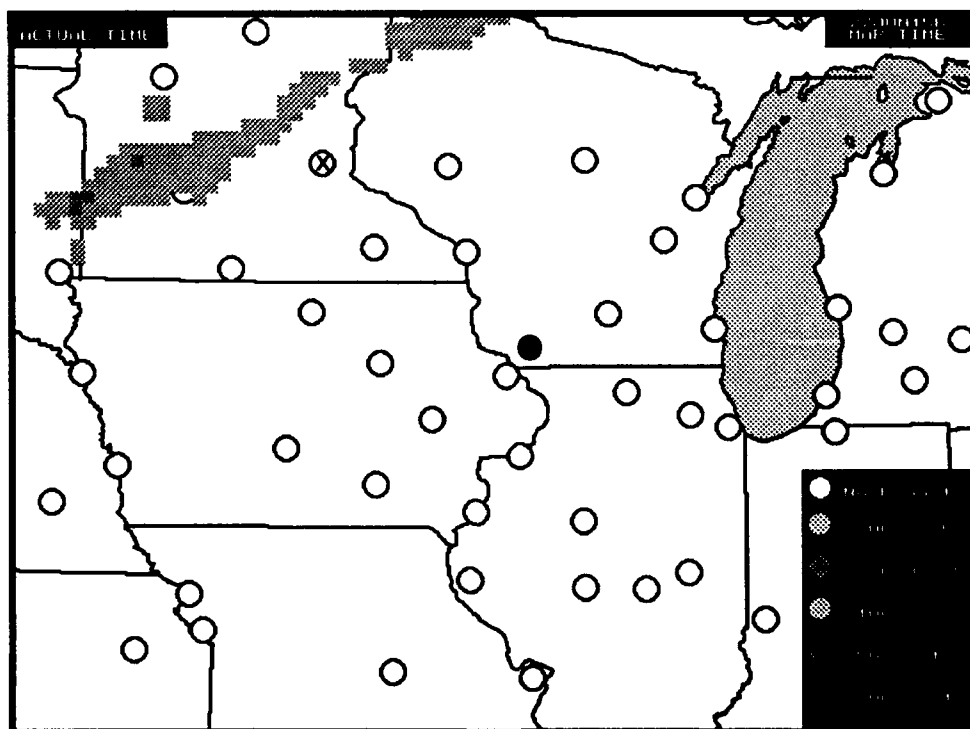


Figure 19. 27JUN15B, Category and Radar Depiction, 1615Z.

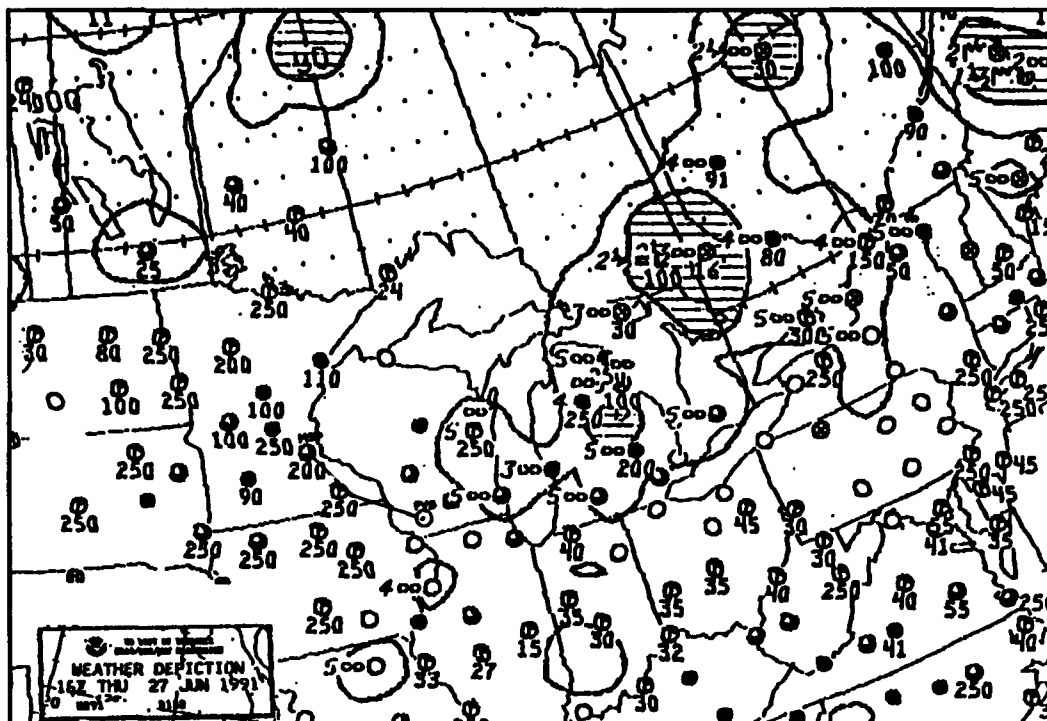


Figure 20. Weather Depiction 16Z 27 JUN 1991.

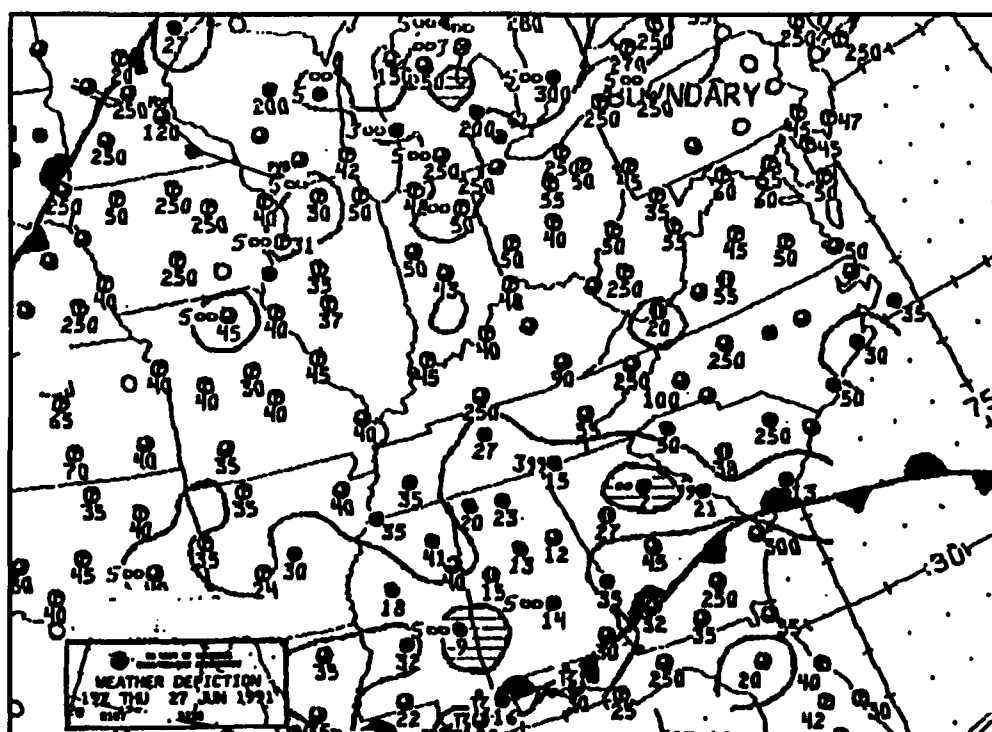


Figure 21. Weather Depiction 19Z 27 JUN 1991.

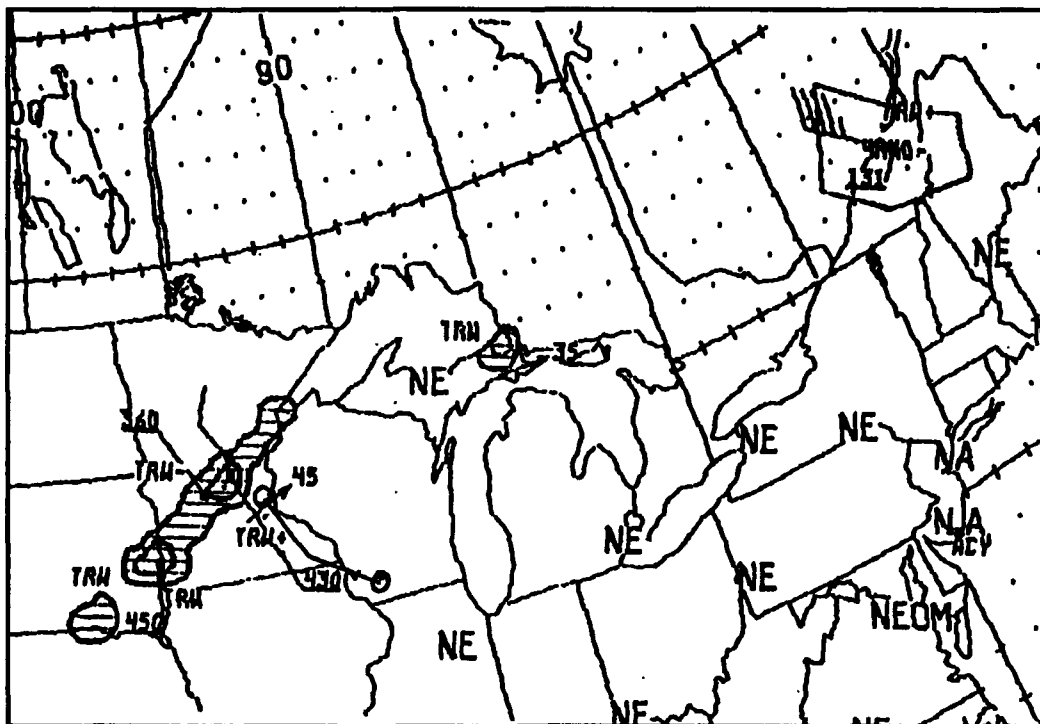


Figure 22. Radar Summary, 1335Z 27 JUN 1991.

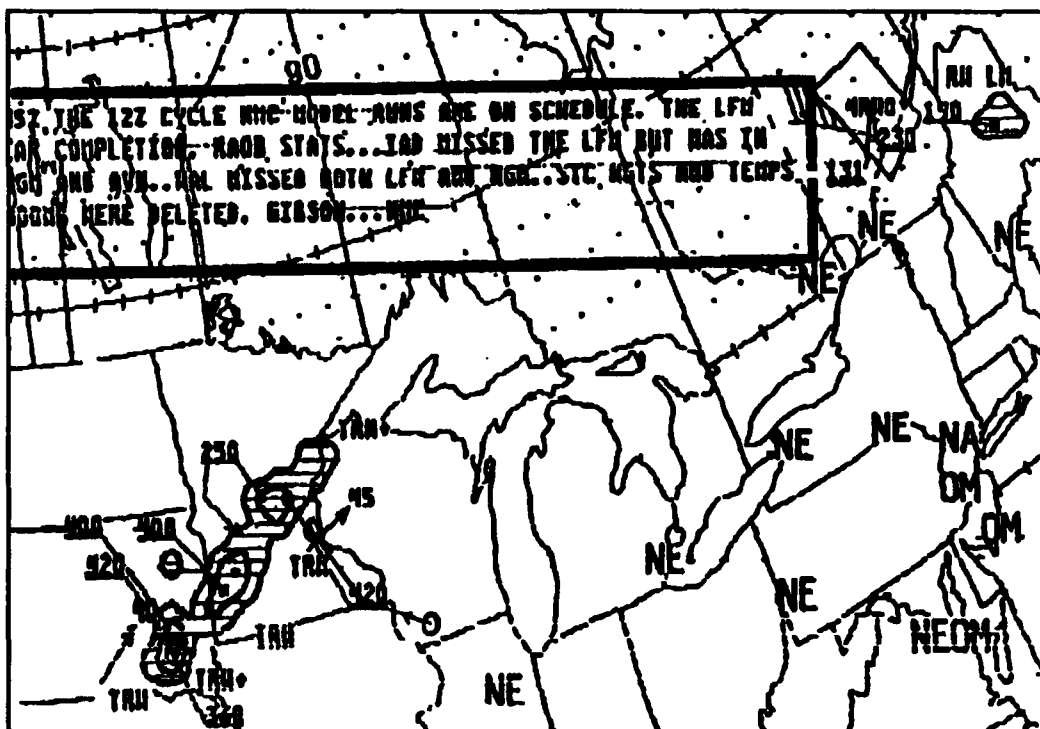
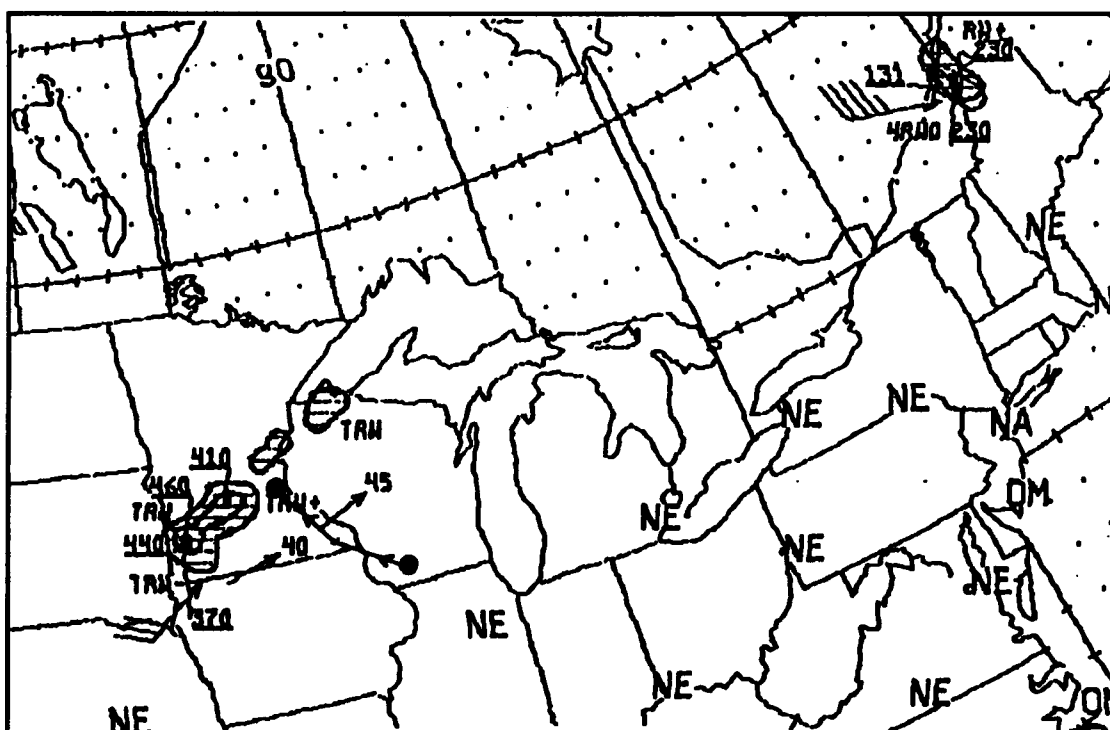
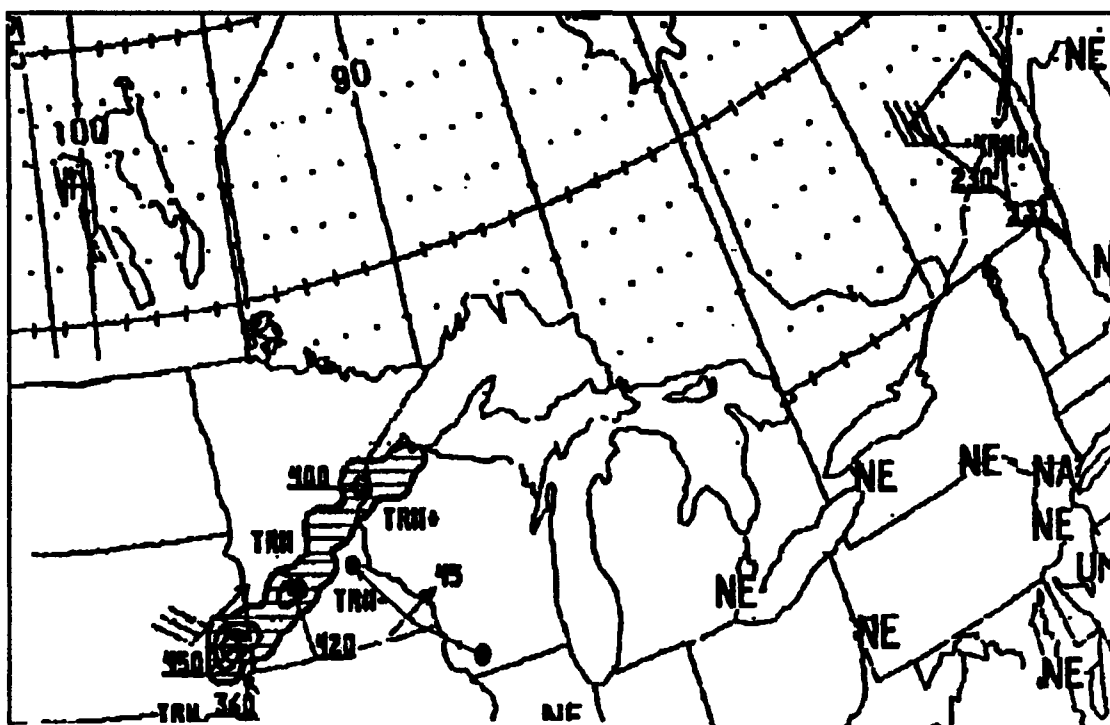


Figure 23. Radar Summary, 1435Z 27 JUN 1991.



Appendix A

Station Identifiers for those stations included in Wisconsin test area, centered on the Dubuque, Iowa radar site (DBQ).

Illinois

CMI=Champaign
DEC=Decatur
DPA=Dupage
MDW=Midway
MLI=Quad City
PIA=Peoria
RFD=Rockford
SPI=Springfield
UIN=Quincy

Nebraska

LNK=Lincoln
OMA=Omaha

South Dakota

FSD=Sioux Falls

Indiana

FWA=Ft. Wayne
HUF=Terre Haute
IND=Indianapolis
SBN=South Bend

Michigan

BEH=Benton Harbor
BTL=Battle Creek
GRR=Grand Rapids
LAN=Lansing
MKG=Muskegon
PLN=Pellston
TVC=Traverse City

Wisconsin

AWU=Wausaw
EAU=Eau Claire
GRB=Green Bay
LSE=LaCrosse
MKE=Milwaukee
MSN=Madsion
OSH=Oshkosh

Iowa

ALO=Waterloo
BRL=Burlington
CID=Ceder Rapids
DBQ=Dubuque
DSM=Des Moines
MCW=Mason City
OTM=Ottumwa
SUX=Sioux City

Minnesota

AXN=Alexandria
BRD=Brainerd
FRM=Fairmont
MSP=Minn./St. Paul
RST=Rochester
RWF=Red Wood Falls

Kansas

TOP=Topeka

Missouri

COU=Columbia
MCI=Kansas City
STJ=St. Joseph
STL=St. Louis

Appendix B

PWxA broadcast "062714C.BX" on 27 JUN 91.

s300340021440C8xs30113001111002101001101001101002146056xs302250081470D3xs3
03230091480D4xs304190021010081500F6xs305180091530D6xs306200021014031540F3x
s307190011024021560FDxs308160041014021570FExs309150061590DAxs310120071610
C9xs311100071630CAxs3121000140616305Fxs313110041380011260F6xs314090051660
D6xs315070041014011670FCxs3160600110140413700113001Exs317050031400021300F
1xs318050021730D1xs319520011270D2xs320510021270CAxs321800A1xs322800A2xs323
800A3xs324800A4xs325800A5xs326800A6xs327800A7xs328800A8xs329800A9xs330800A
1xs331800A2xs332800A3xs333800A4xs334800A5xs335800A6xs336800A7xs337800A8xs3
38800A9xs339800AAxs340800A2xs341800A3xs342800A4xs343800A5xs344800A6xs34580
0A7xs346800A8xs347800A9xs348800AAxs349800ABxs350800A3xs351800A4xs352800A5
xs353800A6xs354800A7xs355800A8xs356800A9xs357800AAxs358800ABxs359800ACxs2
ALO 011568xs2AUW 000072xs2AXN 00006Cxs2BEH 000054xs2BRD 011564xs2BRL
01156Cxs2BTL 041571xs2CID 01155Cxs2CMI 041669xs2COU 011573xs2DBQ
041667xs2DEC 000051xs2DPA 00005Axs2DSM 011570xs2EAU 011567xs2FRM
00006Axs2FSD 011569xs2FWA 000063xs2GRB 04166Bxs2GRR 041584xs2HUF
04167Exs2IND 04168Exs2LAN 041574xs2LNK 011578xs2LSE 000069xs2MCI
041568xs2MCW 021574xs2MDW 041577xs2MKE 04156Cxs2MKG 041578xs2MLJ
041672xs2MSN 04167Exs2MSP 01157Cxs2OMA 02156Axs2OSH 041579xs2OTM
01157Cxs2PIA 041569xs2PLN 0E168Bxs2RFD 04166Cxs2RST 0B1596xs2RWF
000074xs2SBN 000068xs2SPI 04157Bxs2STJ 000076xs2STL 01157Fxs2SUX
02158Dxs2TOP 01157Fxs2TVC 04167Dxs2UIN 000071x

Appendix C

Surface Observations collected for 1400Z, 6-27-91

ALO SA 1351 250 -SCT 12 141/81/72/2011G19/997
BRD SA 1350 20 SCT E100 BKN 250 BKN 10 70/64/0000/979
BRL SA 1350 100 SCT 250 -BKN 7 180/78/71/2108/008/HAZY
BTL SA 1345 250 -BKN 4H 80/68/2212/015
CID SA 1353 CLR 7 155/80/73/1812/001/HAZY
CMI SA 1345 CLR 5H 77/69/2010/014
COU SA 1350 30 -SCT 250 -SCT 7 180/77/69/1809/009
DBQ SA 1352 250 SCT 5H 164/79/72/2112/004
DSM SA 1351 CLR 7 143/80/71/1913/998/FEW STFR AND FEW CI
EAU SA 1352 200 SCT 15 104/83/69/1908/986
FSD SA 1350 110 SCT 250 -OVC 15 075/80/69/1915/979/ACCAS SW-NW-NE
GRB SA 1350 150 SCT 250 -OVC 4H 135/82/72/2116G21/994
GRR RS 1350 250 -OVC 5H 193/79/68/2211/012
HUF SA 1359 30 SCT 5FH 77/71/2307/019
IND SA 1352 CLR 5H 220/78/68/2003/020VSBY LWR E-SE
LAN SA 1352 250 -OVC 3H 201/79/69/2112/015
LNK SA 1350 150 SCT 250 -SCT 15 106/81/70/2015G24/988/WND 18V24
MCI SA 1350 CLR 6H 158/80/73/1814/003/FEW CU N
MCW SA 1350 250 -BKN 12 124/81/69/1920/993
MDW SA 1345 200 -BKN 6H 79/68/2311/013
MKE SA 1353 250 -OVC 4H 161/83/71/2012/002
MKG SA 1350 250 -OVC 3H 190/75/68/1711/010
MLI SA 1350 CLR 3H 175/80/72/2211G15/006/FEW CI SFC VSBY 5
MSN SA 1355 270 -SCT 4H 153/81/72/2216/000
MSP SA 1354 E150 BKN 250 OVC 12 084/83/69/2020/980/ACCAS FRMG W-NW
OMA SA 1350 250 -BKN 8 108/79/71/1916/988/HAZY
OSH SA 1355 200 -BKN 4H 83/71/2210/997
OTM SA 1350 CLR 8 164/81/71/1912/004
PIA RS 1350 250 -OVC 5H 197/77/71/1809/013
PLN SA 1350 120 SCT E180 OVC 4H 138/81/70/2322G30/994
RFD SA 1353 250 -SCT 3H 184/80/71/1913/009
RST SA 1352 250 -SCT 10 105/82/69/2121G31/987
SPI SA 1350 250 -SCT 6H 198/77/69/1810/013
STL SA 1351 250 -SCT 7 195/79/68/2010/012/FEW CU NE-S AND W
SUX SA 1350 250 -BKN 20 093/81/71/1814/983
TOP SA 1350 CLR 10 154/79/73/1910/001
TVC SA 1349 E150 OVC 4H 83/70/2515G21/998/BINOV

Surface Observations collected for 1500Z, 6-27-91

ALO SA 1450 250 -SCT 10 137/84/72/1912/996/FEW AC/ 803 1032
BRL SA 1450 250 -BKN 10 180/81/70/1910/008/ 110 1008
BTL SA 1445 250 -BKN 5H 82/68/2212/015
CID SA 1450 CLR 7 155/83/74/1913/001/HAZY FEW CI E/ 400 1001
CMI SA 1445 15 SCT 8 80/69/2108/015
COU SA 1450 55 SCT 10 183/80/68/1614/010/ 115 1500
DBQ SA 1451 250 SCT 5H 164/82/73/2110/004/ 003 1008
DSM SA 1452 250 -SCT 8 141/83/72/2014G20/997/ 002 1001
EAU SA 1450 150 SCT 15 101/86/69/2113/985/ 803
FSD SA 1450 110 SCT E250 OVC 15 077/81/69/2115/979/ACCAS ALQDS/ 107 1081
FWA SA 1450 CLR 7 221/82/65/2307/020/FEW CU/ 003 1100
GRB SA 1452 250 -BKN 4H 135/85/72/2216/994/FEW AC E/ 603 1037
GRR SA 1450 250 -OVC 5H 190/82/68/2212/011/ 003 1001
HUF SA 1445 E20 BKN 6H 79/72/2108/019
HUF SP 1530 M10 OVC 2F 3520/980/PHASE III TEST
IND SA 1451 CLR 6H 222/80/69/2407/020/CU FRMG E/ 114 1100
LAN SA 1453 250 -OVC 4H 200/81/69/2413/014/ 003 1007
LNK SA 1450 150 SCT 250 -SCT 15 107/85/71/2115G20/989/WND 18V24/ 207 1081
LSE SA 1446 250 -SCT 8 88/71/1922/990
MCI SA 1450 CLR 6H 158/82/73/1913G21/003/FEW CU/ 110 1100
MKE SA 1450 250 -OVC 5H 157/85/71/2313G18/001/ 000 1007
MKG SA 1450 250 -OVC 3H 187/77/68/1810/009/ 007 1007
MLI SA 1450 55 SCT 3H 173/81/72/1812G17/005/SFC VSBY 5/ 005 1500
MSN SA 1455 250 -SCT 5H 153/83/73/1812/000/ 603 1001
MSP SA 1453 95 SCT 150 SCT E200 BKN 12 095/84/69/1911/983/ 307 1078
OMA SA 1450 250 -BKN 8 112/83/72/1915/989/HAZY/ 207 1004
OTM SA 1450 CLR 8 164/83/71/1915/004/ 103
PIA SA 1450 250 -BKN 8 195/82/71/2010/012/ 108 1001
PLN SA 1450 40 SCT E150 OVC 4H 147/81/69/2711/997/ 314
RFD SA 1450 250 -SCT 5H 180/82/71/1914/008/ 000 1001
RST SA 1453 250 -SCT 10 112/85/69/2222G28/990/ 503 1008
SBN SA 1450 250 -SCT 6H 200/82/68/2314/014/FEW CU/ 803 1101
SPI SA 1450 250 -SCT 6H 198/79/70/1911/013/FEW CU/ 115 1106
STL SA 1453 250 -SCT 10 197/82/66/1807/013/CU NW-N/ 117 1101
SUX SA 1450 250 -BKN 15 092/84/71/1918G23/983/ 103 1006
TOP SA 1450 CLR 10 141/83/73/1915G23/997/ 203
TVC SA 1445 E150 BKN 5H 84/70/2515G24/998

Surface Observations collected for 1600Z, 6-27-91

ALO SA 1551 250 -SCT 12 137/86/72/2012G21/996
AUW SA 1550 250 -OVC 7 123/84/71/2212/992
AXN SA 1546 E100 BKN 250 BKN 15 080/75/67/2707/978
BEH SA 1559 40 SCT 6H 86/71/2310G16/012
BRD SA 1445 20 SCT E100 BKN 250 OVC 10 71/67/0000/979
BRL SA 1550 100 SCT 250 -OVC 10 180/83/71/1808/008/FEW CU
BTL SA 1545 100 SCT 250 -BKN 5H 84/67/2410/015
CID SA 1552 25 SCT 7 155/86/75/1910/001/HAZY
CMI SA 1545 15 SCT 10 82/68/2212/014
COU SA 1550 M60 BKN 10 183/81/69/1913/010
DBQ SA 1555 CLR 6H 162/85/72/2212/003
DEC SA 1545 50 SCT 6H 84/70/2010G15/015
DPA SA 1545 -X 250 SCT 4H M/M/2311G18/008/H2
DSM SA 1551 250 -SCT 8 141/85/72/1815G21/997/FEW CU E
FSD SA 1550 110 SCT E250 BKN 12 081/84/70/2115G22/981/ACCAS ALQDS
FWA SA 1550 CLR 7 218/83/65/2106/019/FEW CU HAZY
GRB SA 1551 250 -SCT 5H 133/88/73/2216/994
GRR SA 1550 50 SCT 250 -OVC 6H 188/84/69/2315/010
HUF SA 1545 M20 BKN 7 81/72/2010/018
IND SA 1554 30 SCT 6H 218/83/68/2306/019/TCU ALQDS
LAN SA 1550 250 -OVC 4H 196/83/69/2114/013
MCI SA 1550 CLR 6H 155/85/73/1915/002/FEW CU
MCW SA 1550 250 SCT 12 121/86/69/2018G26/992
MDW SA 1545 200 SCT 6H 85/68/2315/010
MKE SA 1551 120 SCT 250 -BKN 5H 156/88/72/2113/001
MKG SA 1550 250 -OVC 3H 187/79/69/1810/009
MLI SA 1550 CLR 4H 171/85/73/1909G14/005/FEW AC
MSN SA 1551 250 -BKN 6H 153/86/73/2013/000
MSP SA 1553 100 SCT E200 BKN 12 098/83/70/1910/984/FEW ACCAS NW
PIA SA 1550 250 -BKN 9 194/84/69/2010/012/FEW CU
RFD SA 1550 CLR 6H 176/84/73/2014/007/FEW CU
RST SA 1552 250 SCT 10 115/88/70/2319/990
RWF RS 1555 60 SCT E90 BKN 250 OVC 10 084/81/71/2212/980/TE40 MVD ENE OCNL L
TGIC N
SBN SA 1550 40 SCT 6H 199/85/67/1914/013
STJ SA 1555 35 SCT 7 86/72/1915/999
STL SA 1551 250 SCT 10 195/83/66/1608/012/FEW CU WND 12V18
SPI SA 1550 27 SCT 250 -SCT 8 196/81/69/1811/013/HAZY
SUX SA 1550 250 -OVC 15 092/86/72/2115/984/ACCAS DSNT N
TOP SA 1550 CLR 10 141/84/74/1914G22/997/FEW STFRA
UIN SA 1547 33 SCT 250 SCT 6H 184/82/67/1812G16/010
OMA SA 1550 250 -BKN 10 107/86/73/1815/988/SML CU E
OTM SA 1550 CLR 10 163/87/73/1913/004
OSH SA 1545 CLR 5H 88/72/2013/996

Surface Observations collected for 1700Z, 6-27-91

ALO SA 1650 CLR 12 137/88/71/1916G21/996/FEW CI
AUW SA 1650 250 -OVC 7 127/86/70/2310/993
AXN SA 1646 60 SCT E100 BKN 250 BKN 15 085/77/67/3107/980
BEH SA 1655 40 SCT 200 -BKN 6H 87/69/2208/012
BRD SA 1655 20 SCT E100 BKN 15 76/68/2703/980
BRL SA 1650 250 -OVC 10 177/84/72/2210/007/FEW CU
BTL SA 1645 40 SCT 250 -BKN 5H 87/68/2210/013
CID SA 1652 30 SCT 8 155/87/74/1913/001/HAZY
CMI SA 1645 E25 BKN 10 82/69/2108/012
COU SA 1650 33 -SCT 7 183/84/70/1412/010
DBQ SA 1652 CLR 7 162/86/73/2010/003/FEW SC AC
DEC SA 1645 50 SCT 7 87/71/2012/013
DPA SA 1645 250 -SCT 4H M/M/2511G18/008
DSM SA 1652 250 -SCT 8 140/87/72/2016G20/997/FEW CUFRA NW-N
EAU SA 1650 E150 BKN 15 106/90/71/2210/987
FSD SA 1650 110 SCT E250 BKN 12 084/86/70/2315G19/982/ACCAS W-NE
FWA SA 1650 40 SCT 7 214/87/65/2210/018
GRB SA 1650 250 -SCT 5H 133/89/72/2117G24/994
GRR SA 1650 50 SCT 250 -OVC 6H 187/87/67/2216/010
HUF SA 1646 -X 35 -SCT 150 -SCT 200 -BKN 300 -OVC 7 85/72/0000/002/TEST PHII I AB
HUF SA C05/069
HUF SA 1700 E20 BKN 7 84/73/1510/016
IND SA 1653 34 SCT 6H 215/85/69/2009/019/FEW MDT CU
LAN SA 1652 E250 OVC 5H 198/85/68/2313/014/FEW CU CIG PTLY THN
LNK SA 1650 250 -SCT 15 103/92/70/1917G25/988/WND 16V21=
LSE SA 1645 250 -SCT 8 93/71/1922/990
MCI SA 1650 45 SCT 6H 154/87/74/1915/002
MCW SA 1650 250 SCT 12 121/89/69/1922G28/992
MDW SA 1650 40 SCT 6H 88/67/2314/010
MKE SA 1651 120 SCT 250 -SCT 6H 156/89/71/2014G20/001/FEW CU
MKG SA 1650 250 -OVC 3H 187/79/68/2113/009
MLI SA 1653 27 SCT 4H 168/86/74/2207G16/004
MSN SA 1653 250 -BKN 7 153/88/73/2213/000
MSP SA 1652 100 SCT E150 BKN 200 OVC 10 093/88/71/1717G22/983
OMA SA 1650 250 -SCT 10 107/89/73/1916/988/SML CU OVR BLUFFS E
OSH SA 1645 200 SCT 5H 91/72/2115/996
OTM SA 1650 CLR 10 160/89/71/1914/003/CU ALQDS
PIA SA 1650 250 -SCT 9 190/85/69/2214/011/FEW CU
PLN SA 1653 E250 OVC 5H 141/87/70/2313/995
RFD SA 1650 50 SCT 5H 176/86/73/2116/007
RST SA 1655 250 -BKN 10 115/91/69/2219G25/990
RWF SA 1651 55 SCT E95 BKN 250 OVC 10T 080/80/71/1912/979/TB17 OVHD-N
MVG NE VIRGA W-N LTGICCG NW-NE
RWF SP 1730 55 SCT 95 SCT 250 -OVC 12 2309/982/TE15 MOVD NE DRK NE
SBN SA 1650 38 SCT 250 -SCT 6H 194/87/66/2414/012
SPI SA 1650 33 SCT 250 SCT 8 191/83/68/2013/011/HAZY
STJ SA 1645 35 SCT 7 88/73/1913/998
STL SA 1652 40 SCT 250 SCT 10 191/85/66/1513/011
SUX SA 1650 250 -OVC 15 092/90/72/2313G23/984
TOP SA 1650 CLR 10 140/86/75/1912G21/997/FEW SC
TVC SA 1645 E150 BKN 5H 91/70/2612G22/996
UIN SA 1650 35 SCT 55 SCT 220 SCT 6H 180/85/68/1711G17/008

IMPACT OF DATA LINK ON COCKPIT INFORMATION

by

**Raymond LaFrey
Jonathan Bernay
Robert Grappel
Massachusetts Institute of Technology
Lincoln Laboratory
P.O. Box 73
Lexington, Massachusetts 02173-0073**

**For Presentation to the AIAA/FAA Joint Symposium on General
Aviation Systems at the Hilton Inn-East, Wichita, KS
on March 16-17, 1992**

2nd SYMPOSIUM ON GENERAL AVIATION SYSTEMS

American Institute of Aeronautics and Astronautics

Wichita, Kansas

March 16 and 17, 1992

IMPACT OF DATA LINK ON COCKPIT INFORMATION*

MIT LINCOLN LABORATORY

Raymond R. LaFrey

D. Jonathan Bernays

Robert D. Grappel

* This work was sponsored by the Federal Aviation Administration under contract No. DTFA01-89-Z-02033.

ACKNOWLEDGEMENTS

The authors wish to thank Dr. Vincent Orlando, Katharine Krozel, and Patricia Doiron for their assistance in the preparation of this paper. We also are grateful for the support and encouragement of Ron Jones, Data Link Program Manager, and Hugh McLaurin, Data Link Cockpit Development Manager at the Federal Aviation Administration.

IMPACT OF DATA LINK ON COCKPIT INFORMATION

Introduction

Two continuing general aviation concerns are in-flight encounters with hazardous weather and with other aircraft. The AOPA Air Safety Foundation analyses, Table 1, show the effect of weather on accident and fatal accident rates [1]. A significant number of these accidents were the result of continuing the flight into deteriorating weather. General Aviation mid-air collision accidents during the same period are also shown in Table 1. It seems clear that a common factor for both classes of accidents is a lack of awareness by the pilot(s) of the hazard.

TABLE 1
General Aviation Accidents 1982 - 1988 [1]

	Weather-Related Accidents		Mid-Air Collisions	
	Accidents	Fatal Accidents	Accidents	Fatal Accidents
Cruise	760	629	72	44
Descent	1*	1*	5	3
Approach	69*	38*	72**	32**
Total	830	668	149	79

* Selected from descent and approach data that suggest a lack of weather awareness.

** All were approaches at uncontrolled airports.

During the development of the Mode S secondary surveillance system, several experimental Data Link services were developed, including a means to provide traffic information to aircraft within radar range. In the past several years, techniques to compress graphical weather maps for transmission over bandwidth limited air-ground data links, such as Mode S, were also developed. This paper describes the need for airborne displays of weather and traffic and how they can be provided over air-ground data links.

The Need For Graphical Weather

AOPA Air Safety Foundation Data, Figure 1 [2], show that significant percentages of general aviation accidents and fatal accidents are due to weather. Examination of these accidents suggests that a lack of awareness of the actual weather and mistrust of the forecast weather often leads pilots to make poor decisions that, in turn, lead to accidents. The desire to avoid those errors and increase the utility of their aircraft has led many mid- and high-end general aviation operators to install weather radars. Unfortunately, single engine aircraft owners typically do not have that option because of cost and space limitations. However, since aircraft owners have found graphical lightning (turbulence) detectors attractive, a real-time graphical portrayal of weather would also be popular if the cost was reasonable.

Weather As A Factor In General Aviation Accidents 1982-1988

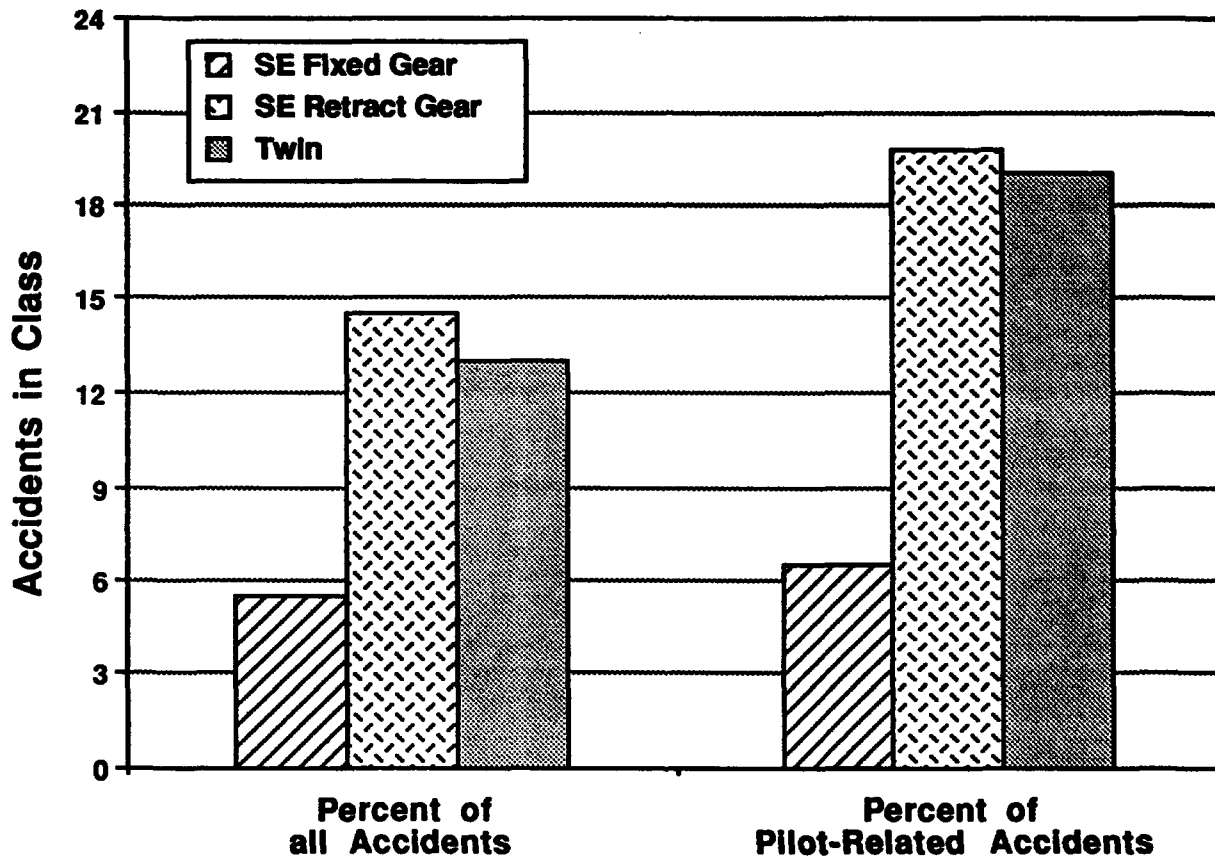


Figure 1. AOPA Air Safety Foundation Data

It is fortuitous that digital weather graphics are becoming more available. During the 1990s the Federal Aviation Administration (FAA) and others will be deploying several new weather radar systems. En route weather will be provided by WSR-88D, a new doppler weather radar that provides wind estimates as well as precipitation. Terminal Doppler Weather Radars and ASR-9s will provide wind-shear and gust-front alerts in terminal areas. The Integrated Terminal Weather System will combine the various terminal weather sensors into a composite product. The problem then is not whether graphical weather data is becoming available, but how to transfer the data to general aviation aircraft in an affordable manner.

The Need For Traffic Information

About 25 mid-air collisions involving general aviation aircraft occur each year in the United States. While not a large number in an absolute sense, the accident rates nevertheless continue to represent a major concern. As part of the development of Mode S and TCAS, several studies were conducted by MIT Lincoln Laboratory to (a) characterize the effectiveness of unalerted visual search ("see-and-avoid"), (b) develop a visual acquisition model to understand and predict pilot performance, and (c) quantify the benefit of providing automatic traffic advisories to pilots.

These studies [3, 4] showed that under certain visibility conditions, such as a very clear sky, it can be very difficult for pilots to see other aircraft until a small number of seconds prior the point of closest approach. They also showed that if a graphical portrayal of traffic is provided to the pilot(s), visual acquisition performance improved dramatically: one second of visual search based on information received from a traffic alert was shown to be equivalent to about eight seconds of normal vigilance.

The visual acquisition model developed by Lincoln Laboratory was used by the National Transportation Safety Board during their investigation of the 1986 Cerritos, California, mid-air collision between a DC-9 and a Piper Archer [3, 5]. The model showed that the probability of effective collision avoidance by the unalerted DC-9 pilots was 42% using a 12-s warning time as a criterion. If the DC-9 pilots had received a traffic advisory, the likelihood would have improved to 95%. The benefits of traffic advisories led the NTSB to recommend TCAS II be installed in all air carrier aircraft.¹

The options for providing traffic information to general aviation operators are, unfortunately, limited. Installed TCAS II Part 121 systems cost about \$150,000, and it is difficult to build and certify a low-cost unit that provides a range and bearing traffic advisory. However, FAA ground radars have all of the surveillance information needed to provide traffic information to cockpits if a means to transfer that data can be provided to the cockpit.

The Aeronautical Telecommunications Network

The FAA and states of the International Civil Aviation Organization (ICAO) are currently developing an Aeronautical Telecommunications Network (ATN). The ATN will provide a network of ground routers, communications media, and aircraft avionics that enable the transmission of data between any ground or airborne source to any ground or airborne destination. The ATN currently envisions three communications media: satellites, VHF data link, and Mode S data link. An overriding ATN design requirement is that Open Systems Interconnection (OSI) protocols be used, to insure inter-operability.

¹ The Traffic Alert and Collision Avoidance System II is now carried by more than 50% of commercial air carriers in the U.S. and will be on 100% of those aircraft by the end of 1993.

The Mode S data link may be the most useful link for the transmission of weather and traffic information to general aviation aircraft. Mode S has immediate access to the surveillance data needed for traffic information as well as access to the FAA and National Weather Service graphical weather. It has a small delivery delay (2.5-s average); it has the communications capacity; and it is likely to represent lower long-term costs than VHF or satellite alternatives. However, we have developed techniques for the transmission of graphical weather products that are compatible with the ATN. Therefore, the graphical weather messages can be delivered using any of the ATN data links provided that delivery time requirements can be met.

The Mode S Data Link

Mode S is a secondary surveillance radar (SSR)² and data link system. It is being implemented in the United States to provide improved surveillance data for air traffic control purposes and to improve air-ground communications. The first production Mode S sensor was delivered to the FAA last year, and the deployment of operational systems to 133 terminal and en route sites will begin in 1993. Most European countries will implement Mode S by the end of the 1990s. The Mode S data link is also used to coordinate TCAS II maneuvers.

The Mode S data link provides the means to send digital messages to each aircraft within radar coverage. The data is sent in packets, ranging from 56 bits to 1280 bits, one packet each 4.8-s antenna scan period. Air traffic control tactical messages that reduce the VHF frequency congestion, such as frequency handoffs and clearance amendments, and messages that provide textual weather similar to DUAT, will be early uses of the data link.

The following sections will describe a Graphical Weather Service (GWS) and a Traffic Information Service (TIS) and how they could be provided by the Mode S system.

The Graphical Weather Service

The initial objective of the Graphical Weather Service is to deliver National Weather Service radar observations, defined in terms of precipitation intensities. Table 2 defines the current 6 levels of severity and associated turbulence, hail, and lightning. Examples of 64-x 64 km radar observations from experimental weather radars at Denver Stapleton are shown in Figure 2.

The major challenge with using a data link to transmit weather pictures is the large number of bits required to specify a weather image. For example, if a weather map is defined to consist of an array of 64 x 64 (4096) pixels, and each pixel must indicate one of the seven National Weather Service weather levels (zero plus the six shown in Table 3), then a weather-map image will consist of 12,288 bits of information. Providing this much data to a realistic number of aircraft, even when updated every 5-10 minutes, will excessively load any of the proposed ATN data links. For the Mode S case, this equates to 9.6 Mode S ELMs (Extended Length Messages), not counting any data link overhead. Since the Mode S data link protocols can only guarantee the transmission of one ELM (1280 bits) per aircraft per antenna scan, it is necessary to compress the data ten-fold. Also, the algorithms used to perform the compression and decompression must be computationally efficient; the ground computer performing the compressions may have to handle many aircraft requests in a given scan, and the airborne computer doing the

² The term *secondary* means surveillance that is accomplished through the interrogation of airborne transponders. Primary surveillance sensors provide data based on radar reflections from the aircraft body.

SAMPLE WEATHER MAPS

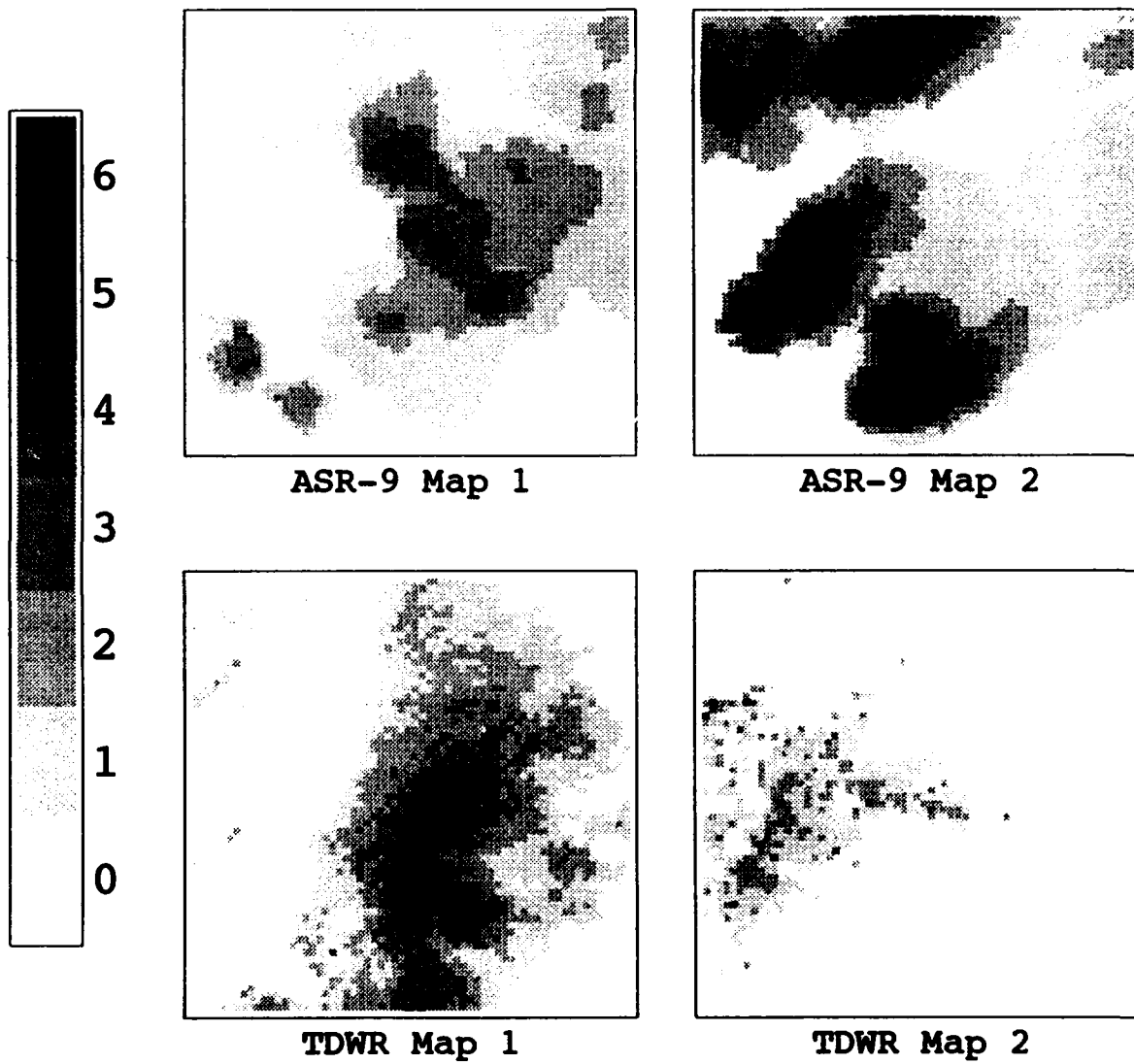


Figure 2. 64 x 64 km radar observation examples.

decompressions may not be particularly powerful or have extensive memory capacity. The following paragraphs discuss research performed to develop a solution to this challenge.

TABLE 2

National Weather Service Precipitation Levels

NWS Level	Precip. Intensity	Rainfall in/hr	Possible Turb.	Hail	Lightning
LEVEL 6	Extreme	≥ 7.1	Severe	Large	Yes
LEVEL 5	Intense	4.5-7.1	Severe	Likely	Yes
LEVEL 4	Very Strong	2.2-4.5	Severe	—	Yes
LEVEL 3	Strong	1.1-2.2	Severe	—	Yes
LEVEL 2	Moderate	0.2-1.1	Light/Moderate	—	No
LEVEL 1	Weak	< 0.2	Light/Moderate	—	No

Graphical Weather Compression Techniques

An extensive study of standard data compression techniques (runlength coding, Lempel-Ziv, select, Huffman, etc.) was made on sample weather map images. The best of these approaches achieved compressions in the range of 4 to 1. None could guarantee a minimum compression ratio independent of the input weather map. Also, the standard approaches could not trade off small amounts of map distortion for compression in a controlled way. A compression algorithm tailored for graphical weather maps was required to achieve the necessary data reduction of at least 10 to 1.

Weather maps exhibit a great deal of structure of which the compression algorithm can take advantage. Weather maps tend to form smooth, continuous regions. Regions of more intense weather tend to be wholly contained within regions of less-intense weather. Weather regions do not typically have sharp points, holes, etc. Also, for purposes of providing a useful rendition of the weather map to the pilot, certain small distortions of the map may be made. Isolated pixels may be eliminated or smoothed over. Weather regions may be rendered with less resolution. The graphical weather map compression algorithms make use of controlled distortion and smoothing when required to achieve the desired compression.

Huffman-Hilbert Algorithm

Two independent graphical weather compression algorithms have been developed. The first (termed the Huffman-Hilbert algorithm) is based on a modified runlength approach. A Huffman coding is used to minimize the number of bits required to specify the runlengths of each weather level. Special encoding techniques based on the typical ordering of weather regions (more-intense inside less-intense) are employed to reduce the number of bits necessary for specifying a weather level from 3 bits per runlength to an average of 1 bit. A separate Huffman encoding for each weather level, a set of default Huffman tables, and some novel encoding mechanisms which compress the actual Huffman table representations themselves all increase the performance of this compression algorithm. A major innovation in this algorithm is the use of a Hilbert scan pattern (see

Figure 3) instead of the more-usual raster scan. The effect of the Hilbert scan is to produce very long runlengths when the scanning curve stays within a weather region. It tends to produce many short runlengths when the scanning curve just "nicks" a weather region. Hence, instead of the more-or-less uniform runlength distribution of the raster-scan, the Hilbert scan tends to produce a bimodal runlength distribution with many very short and many very long runlengths. This distribution has two advantages: the very-short runlengths may be filtered out if required to meet the compression limit (their loss introduces minimal distortion), and the very-long runs lead to a more efficient Huffman encoding set.

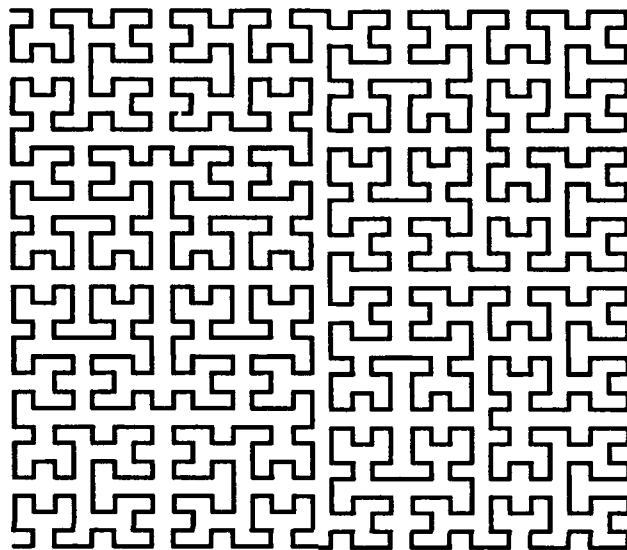


Figure 3. 32 x 32 Hilbert Scan Pattern

Polygon-Ellipse Algorithm

The second graphical weather compression algorithm (termed the polygon-ellipse algorithm) is based on the concept of shape-fitting. Weather regions can be modelled using a set of geometric shapes. As the algorithm's name implies, each weather region is modelled as either an ellipse or a polygon. The parameters of the shape form the actual message. Weather regions whose shape is well-approximated by an ellipse are encoded by the location of their two foci and the ellipse "distance" parameter. Non-elliptical weather regions are encoded as a set of vertices describing the enclosing polygon. Special algorithms are used in both shape-fitting regimes to increase compression by allowing incremental increases in map distortion. The "ellipticity" requirements can be reduced, and polygon vertices can be smoothed over. A number of special encoding "tricks" have been employed to reduce the average number of bits required for polygon and ellipse parameters. For example: assuming a 64 x 64 pixel weather map, it would require 6 bits to specify a point (polygon vertex or ellipse focus) coordinate. However, by specially ordering the vertex or foci list before encoding it, the range of possible coordinate values can be reduced – reducing the number of bits required for the coordinate value.

Figure 4 illustrates the results of applying these two weather compression algorithms to weather data gathered by the ASR-9 radar operating during especially severe weather at the Denver airport. Each pixel represents a square kilometer. The shading indicates the weather precipitation intensity level. The map in the upper-left shows the

ASR-9 MAP 1

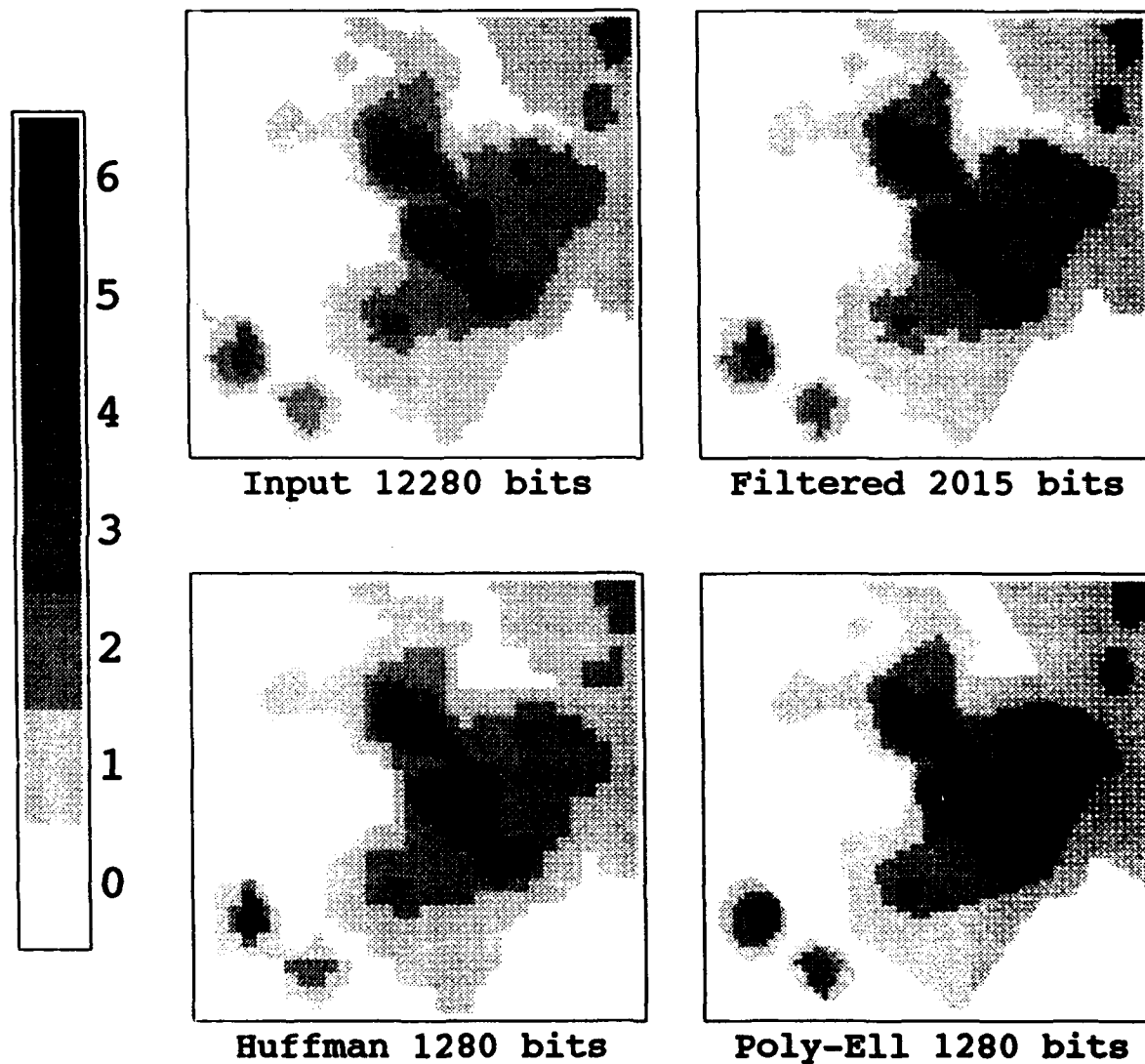


Figure 4. Weather graphics compression results.

input weather map received from the radar. The map in the upper-right shows the result of applying the Huffman-Hilbert algorithm and filtering isolated areas. The two lower maps show the results of each of the compression algorithms when the bit-limit was set to a single ELM (1280 bits). Note that each algorithm has introduced some distortion, but both have done a quite reasonable job of rendering the input map.

Graphical Weather Human Factors

An FAA-sponsored Mode S Graphical Weather Program at Lincoln Laboratory is currently beginning a multi-year activity to determine, through human-performance experiments, how pilots react to the various data compression algorithms and how pilot decisions are affected by the presentation of Mode S Data Link graphical weather. This effort will include experiments with desk-top simulators, flight simulators, and full-scale flight tests with real-time weather graphics in a C172 and C421. Human performance evaluations are also being planned in collaboration with the NASA Langley Research Center and the FAA Technical Center. We will be seeking participation by general aviation pilots and manufacturers during these studies, and will be supporting a broad NASA-FAA examination of weather requirements in the cockpit.

The objective of this work is to establish which compression algorithms are practical and effective, how often the map must be updated, how the service is initiated, and other practical issues.

The Traffic Information Service

The Traffic Information Service has been designed to provide automatic traffic information to all participating aircraft within radar coverage of Mode S sensors. In operation, TIS provides an indication of traffic that comes within 5 nautical miles (nmi) and 1200 feet in altitude of one's own aircraft. Displayed aircraft are categorized as proximate traffic (aircraft are within 5 nmi and 1200 feet) or threat traffic (aircraft are simultaneously within 52 s of horizontal closest approach or 0.8 nmi, and within 52 s of vertical closest approach or 1200 feet).

The Mode S uplink message structure is designed to provide the location of up to eight traffic aircraft. This is consistent with the efficient use of the 56-bit Mode S uplinks. TIS messages refresh the display each 4.8-s scan whenever proximate or threat traffic are present.

Each TIS 56-bit message is composed of four fields, broken down as follows:

Data Link Header	8 bits
Own-Aircraft Heading	6 bits
Traffic Block 1	21 bits
Traffic Block 2	21 bits

The Data Link Header identifies the message as originating from TIS and includes any data link message overhead. The Own-Aircraft Heading field gives the current heading of own-aircraft derived from its ground tracked x-y velocity and quantized to 6-degree units. It is used as the basis for calculating the bearing to the "proximate" or "threat" traffic. The own-aircraft course may be compared with an independent source of heading on the aircraft (a gyrocompass) to correct the airborne display for aircraft "crab angle" or turns in progress. Each Traffic Block contains bearing, range, altitude, altitude rate, and heading data for a given traffic aircraft.

The TIS message formatting algorithm orders the Traffic Blocks such that all "threat" data precedes "proximity" data. Within a category, blocks are ordered by increasing range separation. Hence, the highest-priority, shortest separation traffic appears first. This allows TIS displays to indicate the most important traffic information as their capacity permits.

The TIS Airborne Display

The basic layout of the airborne display used in the M.I.T. Lincoln Laboratory Data Link testbed is shown in Figure 5. The testbed display is implemented with a 3-inch square monochrome panel-mounted CRT.

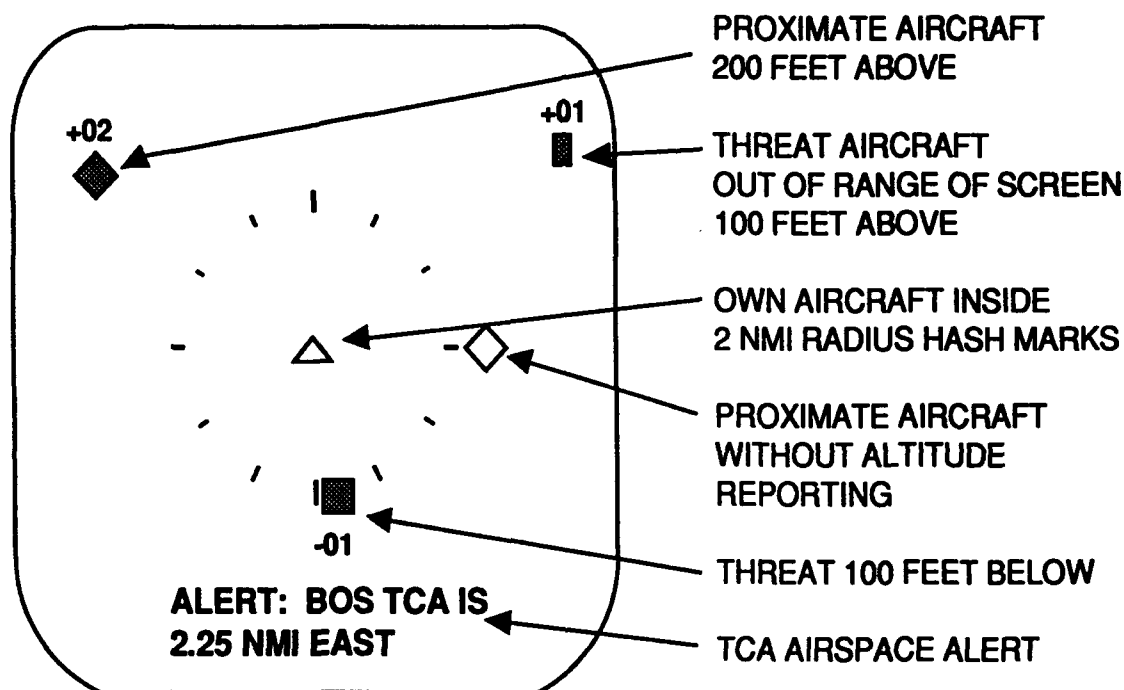


Figure 5. The TIS Airborne Display

The format of the TIS testbed display is designed to be similar to that of TCAS. The triangle at the center of the display indicates the position of own-aircraft. A set of hash marks form a 2-mile scale indicator at the "clock positions." Traffic which is "proximate" is indicated by a diamond symbol, while traffic which is a "threat" is indicated by a square symbol. Traffic which has a known altitude is indicated by a filled symbol – unfilled symbols indicate traffic at unknown altitude. For traffic with known altitude, the relative altitude is indicated in flight levels (100s of feet) above the symbol (if the traffic is co-altitude or above own-aircraft) or below the symbol (if the traffic is below own-aircraft). The sign of the relative altitude is displayed as well. Though not shown on the figure, Traffic Altitude Rate (if the traffic is climbing or descending) is indicated by the presence of an up-arrow or down-arrow at the side of the symbol. Traffic whose position places them off the display screen (the scale of the testbed display goes out to about 5 nmi) are indicated by half-symbols at the edge of the display.

The design of the testbed display does not make use of the Traffic Heading data. It was felt that adding this data would unnecessarily clutter the small available display area, and there is no display format for this type of information in the TCAS model. The design does permit the inclusion of textual messages such as the TCA alert.

Traffic Information Service Flight Evaluation

Shakedown flight testing of TIS was completed during 1990-1991 using a C172 and Collins Mode S Transponder. An Eventide Argus 5000 was used to display TIS to company and guest pilots. A limited set of encounters using local subject pilots suggests visual acquisition performance similar to that observed in previous studies. The pilots also stated that TIS improves safety and blends well with normal flight operations. Additional tests, done more formally with 20 pilots, will be conducted next year to quantify how TIS assists visual acquisition, to determine the effect of a 4.8-s update rate, delivery delay, impact on work-load, and other human factors issues.

Summary

The Aeronautical Telecommunications Network can provide two services that should enhance safety and improve aircraft utility. The Graphical Weather Service should provide valuable and timely weather information to assist the pilot in making informed route-of-flight decisions. The Traffic Information Service should reduce the threat of mid-air collisions and increase situational awareness with respect to other aircraft. Techniques have been developed to transmit this information to the cockpit over the Mode S data link. The methods developed also support the transmission of compressed graphical weather over other suitable ATN data links. Activities are currently underway to complete the development of these services in the next several years.

GLOSSARY

AOPA	Aircraft Owners and Pilots Association
ATN	Aeronautical Telecommunications Network
DUAT	Direct User Access Terminal
ELM	Extended Length Message
GWS	Graphical Weather Service
ICAO	International Civil Aviation Organization
nmi	nautical mile
NTSB	National Transportation Safety Board
OSI	Open Systems Interconnect
s	second(s)
SSR	secondary surveillance radar
TCAS	Traffic Alert and Collision Avoidance System
TSI	Traffic Information Service
WSR-88D	Weather Surveillance Radar-1988 Doppler

REFERENCES

1. AOPA Air Safety Foundation, General Aviation Accident Analysis Book, 1991, p. 20, and pp. 45-68.
2. *Ibid*, p. 20.
3. John W. Andrews, "Modeling of Air-to-Air Visual Acquisition," *The Lincoln Laboratory Journal*, Vol. 2, No. 3, 1989.
4. J. W. Andrews, "Air-to-Air Visual Acquisition Performance with TCAS II," 7 Nov. 1984, DOT/FAA/PM-84/17.
5. National Transportation Safety Board, "Aircraft Accident Report - Collision of Aeronaves de Mexico, S.A., McDonnell Douglas DC-9-32, XA-JED and Piper PA-28-181, N4891F, Cerritos, California, August 31, 1986," Washington, DC, NTSB/AAR-87/07.

**AN OVERVIEW OF PROPULSION SYSTEMS FOR
SMALL CIVIL AIRCRAFT**

by

**Dave Ellis
National Institute for Aviation Research
Wichita State University
and
Kenneth Foote
AVORTEC, Inc.
Hillsburo**

**For Presentation to the AIAA/FAA Joint Symposium on General
Aviation Systems at the Hilton Inn-East, Wichita, KS
on March 16-17, 1992**

AN OVERVIEW OF PROPULSION SYSTEMS FOR SMALL CIVIL AIRCRAFT

by Kenneth Foote, AVROTEC, Inc., Hillsboro, OR and Dave Ellis, National
Institute for Aviation Research, The Wichita State University

presented at:

The AIAA Second Annual Symposium on General Aviation, March 16-17,
1992, Wichita Kansas.

ABSTRACT

According to available sources there are over 40 companies worldwide devoted to production or development of piston, rotary, turbopropeller or turbojet powerplants for small (less than approximately 6,000 pounds GTOW) airplanes. Much of the production activity is focused on uncertified engines of less than 100 HP for use in ultralight or mircrolight category aircraft, while at the other extreme are the 400 - 600 HP turboprops found in many trainer and utility airplane applications. Because of the precipitous decline in piston powered single and twin engine aircraft in the mid-eighties, production of that class of engine is limited to little more than replacement needs. A few well-established manufacturers supply nearly all of the current production engines.

Despite the limited production needs, interest in the development of new powerplants remains high. The reasons for this are several: a continuing urge to adapt automotive engines to aircraft use, mainly for cost reasons, but also to take advantage of technologies not available in production aircraft piston engines; the opportunity to become independent of unreliable avgas supplies by utilizing multi-fuel (stratified charge rotary combustion engine) or diesel engine technology; opportunities in non-metallic materials, leading to use of ceramic and composite components; and, to some extent, the feeling that new and improved powerplants are a needed ingredient in the "revitalization" of general aviation.

Technical issue aside, possible changes in environmental rules, certification regulations, and product liability laws will have strong effects on the course of engine development.

GENERAL BACKGROUND

Relatively few small (for our purposes, less than 6,000 pounds maximum weight) civil aircraft are being produced at the present time. GAMA reports

that only slightly over 600 new fixed wing aircraft powered by piston engines were delivered in the U. S. during 1991. While no firm numbers are available, estimates put the worldwide production of certificated small (under 500 HP) engines at less than 2,000 units during the same period. In the face of such small production numbers, it is surprising to find a great deal of activity in the development of new engines and in the application of new technologies. The latest Jane's All the World's Aircraft indicates that there are over 40 engine manufacturers in this category world wide, although admittedly much of the activity is devoted to supplying engines to the non-certified homebuilt and ultra-light aircraft market.

Certified intermittent combustion engine production is dominated by the two U. S. piston engine manufacturers, Textron Lycoming and Teledyne Continental, producing a range of power outputs from 100 to 400 HP. Production of un-certified engines, mostly below 120 HP, is dominated by Rotax, the Austrian subsidiary of the Canadian conglomerate Bombardier. Other producers in this category include Mosler, Limbach, and Hirth. On the next tier are the one-off modifiers of automobile, motorcycle, GPU, and out of tolerance aircraft engines for non-certified applications.

New developments in the intermittent combustion engines fall in three areas: new engines designed specifically for aviation, engines based on production automotive powerplants modified for aviation, and engines based on alternative technologies (DynaCam, rotaries, etc.).

In the small turbine area, Allison of the U.S.A. and Turbomeca of France produce powerplants rated in excess of 400 HP used primarily in small utility helicopters. The turbine industry's elusive and as yet unreached goal is a 300 HP \$50,000 turbine engine. Even at \$100,000, such an engine would revolutionize the industry, but the high costs associated with manufacturing a turbine have not been overcome.

ENGINE PROGRAM REVIEW

Intermittent Combustion Engines.

Certified Production Engines

Textron Lycoming manufactures approximately 48 models of horizontally opposed air cooled piston engines ranging from 115 to 400 horsepower. They also actively support the existing fleet, offering three levels of overhaul. At overhaul time an owner can exchange for factory new, or buy a factory remanufactured engine, which meets the same criteria and carries the same warranty as new, or a factory overhaul unit, which has undergone a regular FAR 43 overhaul.

Lycoming is conducting ongoing research on electronic ignition and fuel injection, but to date has not developed systems that they are willing to certify and offer to the fleet. In response to the proposed elimination of leaded fuel, Lycoming is conducting extensive testing to determine the impact of relatively high octane fuels formulated without lead. To date they report that they have encountered no problems, and are guardedly optimistic that their engines will be able to operate with unleaded aviation fuel developed to a new ASTM specification.

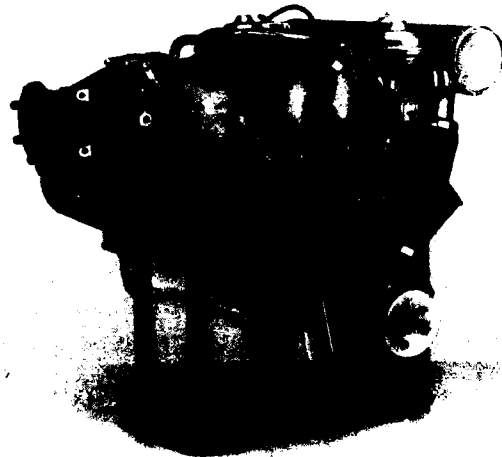
Teledyne Continental produces approximately 54 models of opposed air cooled piston engines ranging from 100 horsepower to 435 horsepower. They offer an overhaul program similar to Lycoming's. During 1991 Continental reports delivering approximately 3,800 engines including new, remanufactured and overhauled units.

Continental has certified liquid cooled versions of their 550 cubic inch engines, an outgrowth of their participation in military high altitude reconnaissance vehicles and the Voyager around the world aircraft. The TSIOL-550-A, producing 350 HP, has been retrofitted into Cessna 414's with impressive results. The TSIOL-550-B, has been certified in a Beech A-36 Bonanza. Continental is reportedly working on certifying an IO-240 engine, a four cylinder engine based on the IO-360 six cylinder engine. The engine produces 125 HP, is air-cooled, and has a solid crankshaft, precluding installation of a constant speed prop.

Poland's PZL purchased the rights to the Franklin line of opposed engines and Wright radial engines some years ago and, in addition to supplying spare parts to the aftermarket, is offering new production engines for sale. They manufacture 3 models of horizontally opposed engines from 60 to 220 horsepower. They also manufacture 2 models of radial engine at 256 and 600 HP.

Non-certified Production Engines

The acknowledged leading manufacturer of non-certified aviation engines is Rotax of Austria, a subsidiary of Bombardier of Canada. They manufacture a line of 2 and 4 stroke engines for ultralight and homebuilt aircraft and,

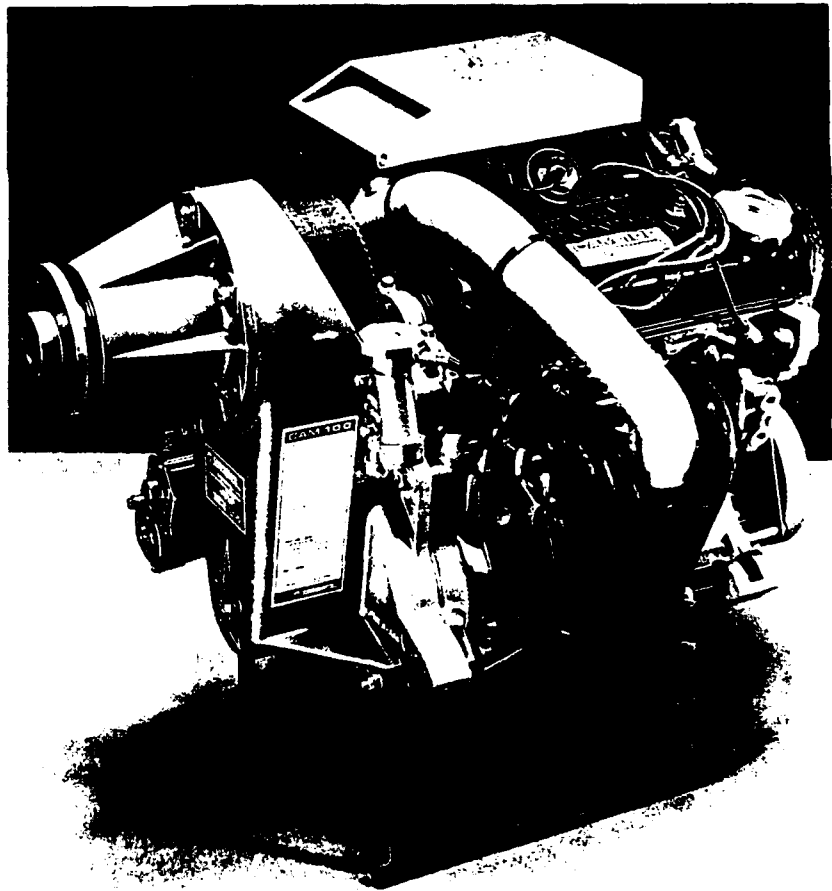


ROTAX 914

in addition, have recently introduced an opposed 4 cylinder water cooled engine producing 80 horsepower. They plan to produce a turbocharged version boasting 115 HP at sea level and 100 HP at 16,000 ft. Weighing over 100 pounds less than equivalent certified engines, these engines are built to comply with European JAR certification standards. Certification is reportedly unlikely under the current standards. Rotax manufactures some 50,000 snowmobile engines a year with over 1,000 employees at their same facility, and boasts the ability to ramp up immediately to any volume order they might receive. Rotax continues to produce a full line of two cycle engines for the homebuilt market.

In the U. S. the dominate manufacturer appears to be Mosler. It's line of engines, based originally on a Volkswagen, now offers a power range from 42 through 80 HP. The only stock Volkswagen parts remaining are a highly modified case and the valves, the rest being custom manufactured for the Mosler engine. Mosler does not plan to certify the engine, feeling that the cost and liability exposure exceed any possible return. Mosler anticipates being able to provide powerplants for the aircraft certified under the light aircraft simplified rules when they are issued.

Canadian Air Motive is producing a small engine based on the Honda Civic 1500 cc engine. It produces 100 HP, weighs 224 pounds, and uses a 4" cog belt for reduction of the engine speed of 6,000 RPM to the prop's 2,500 RPM. The engine is in production, costs \$5,895 US, and has been installed in a number of homebuilt aircraft.



CANADIAN AIRMOTIVE CAM 100

Other manufacturers supplying engines to the homebuilt market include Glob Hirth and Limbach, both of Germany. These engines have also found application in motor gliders certified under JAR 22. The Limbach engine is also used in the new American Lightship blimp.

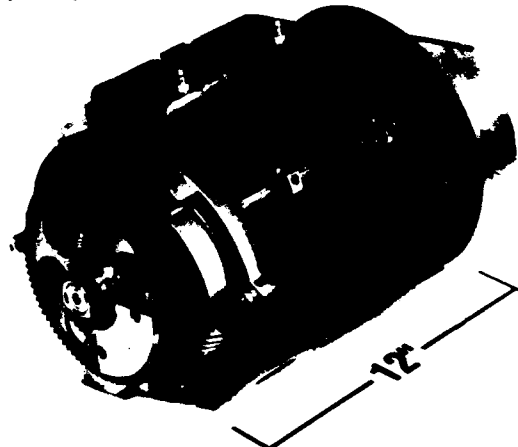
In addition to the companies supplying whole engines to the homebuilt market, there are also a number of companies offering to modify automotive engines for aviation use. The most popular engines appear to be the Subaru liquid cooled opposed 4 and the Mazda rotary. There are belt, chain, and gear reduction offerings with various torsional damping schemes included. These modifiers will work on an owner supplied engine, or will supply a complete powerplant ready to install. Lou Ross in Tucson, AZ and Alturdyne in San Diego, CA are examples of this type modifier.

Under Development - Candidates for Certification

Rotary Combustion Engines

Moller International, Davis California, is developing an extremely lightweight air cooled Wankel type rotary for use in their Volanter powered lift aircraft. Prior to certifying the Volanter, they will certify the powerplant. Their funding has been uncertain, and they have not done any development of the engine in the last 9 months. They have received a commercial contract to develop a non-aviation liquid cooled version of their engine for industrial applications, and that project is progressing very rapidly. They expect to have that engine running in another month.

The rotor, trochoid housing, fuel system, and engine controls are identical to what is proposed for the aircraft engine. At present Moller has no plans for a standard aircraft engine, but continues to evaluate the possibility of developing an engine for general aviation applications. The engine displaces 80 cu. inches and produces 150 HP. The target weight for the air cooled aviation engine is well under 100 pounds.



MOLLER PROTOTYPE ROTARY

Rotary Power International has purchased the interests and facilities of John Deere at Wood-Ridge, New Jersey and is continuing development of the stratified charge multi-fuel rotary engine. Working with Avrotec, Inc. in Hillsboro Oregon, R.P.I. proposes rapid development of an aviation version.

of the 80 cubic inch two rotor engine. Two of these 200 HP powerplants would be attached to a Soloy Dual Pac ® reduction gearbox and certified as a unit to be installed as a replacement powerplant for various high performance general aviation singles.

Norton Motors in England, most famous for motorcycles, has developed a 300 cc. per rotor two rotor liquid cooled rotary engine. It is offered in three versions, one without reduction drive and two with reduction drives and propeller hub. The engines develop 84-90 HP, weigh about 140 lb., and have a fuel consumption in the range of .5 LB/HP-hr. Norton has reached agreement whereby Mid-West Aeroengines Ltd. in Wilkshire, England will be the exclusive distributor of the engines for manned flight applications. They plan to certify the 90 HP engine under JAR-E and FAR 33 at some point in the future.

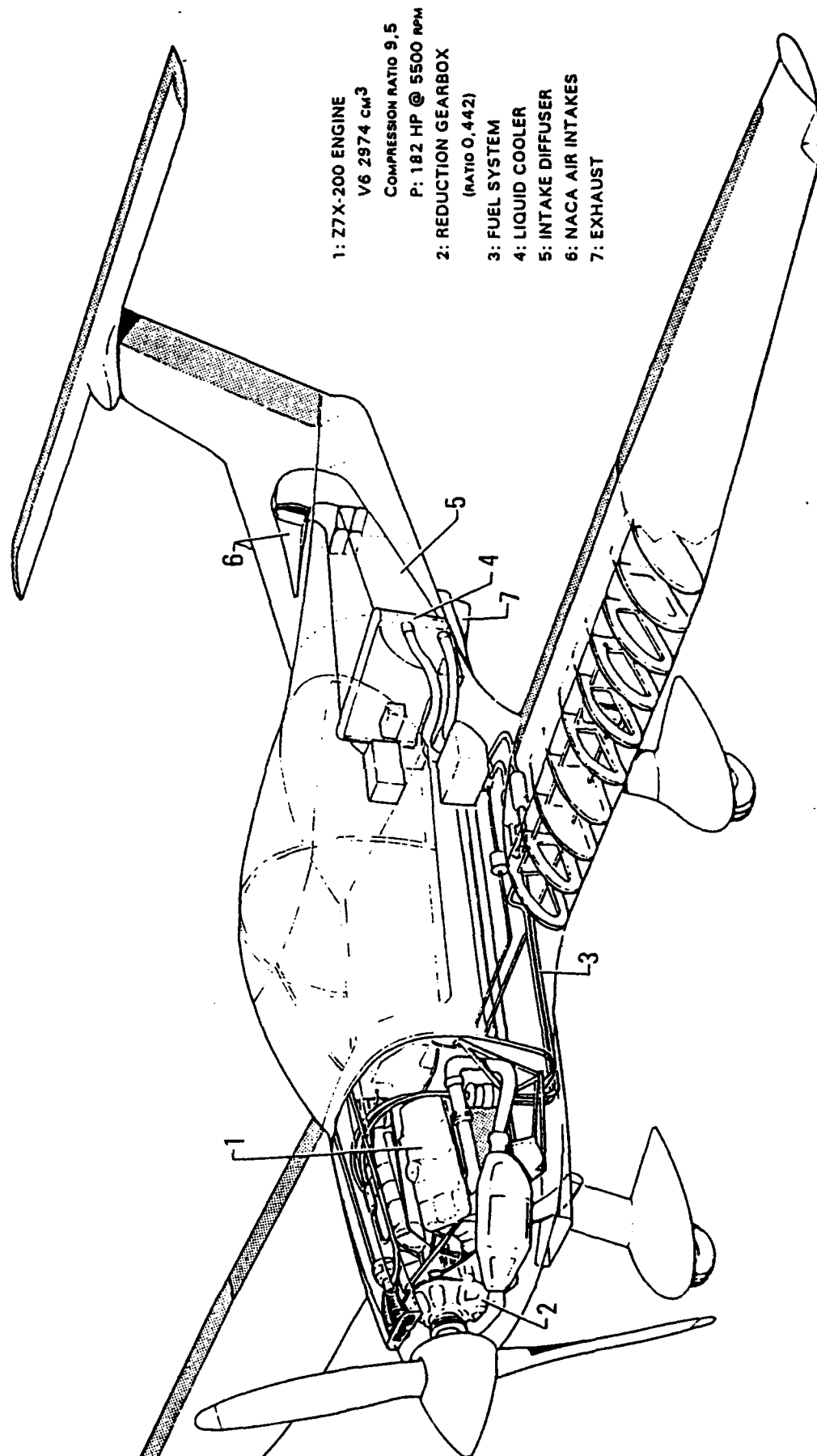
The Dynacam Engine

The Dynacam engine was certified many years ago and has never been certified into an aircraft. Dynacam has just completed an improved version of the engine with superior cooling and performance. The company is marketing the engine to the homebuilt community. When it has received orders for 100 engines, it will produce them. It has received 32 firm orders so far. They feel that until there are a substantial number of the engine flying successfully in homebuilt aircraft, they will not be able to obtain liability insurance, and without liability insurance will not be able to raise the kinds of capital necessary to get production under way. The engine produces 200 HP, weighs 300 lb. and at take-off turns 2,000 RPM with virtually no vibration.

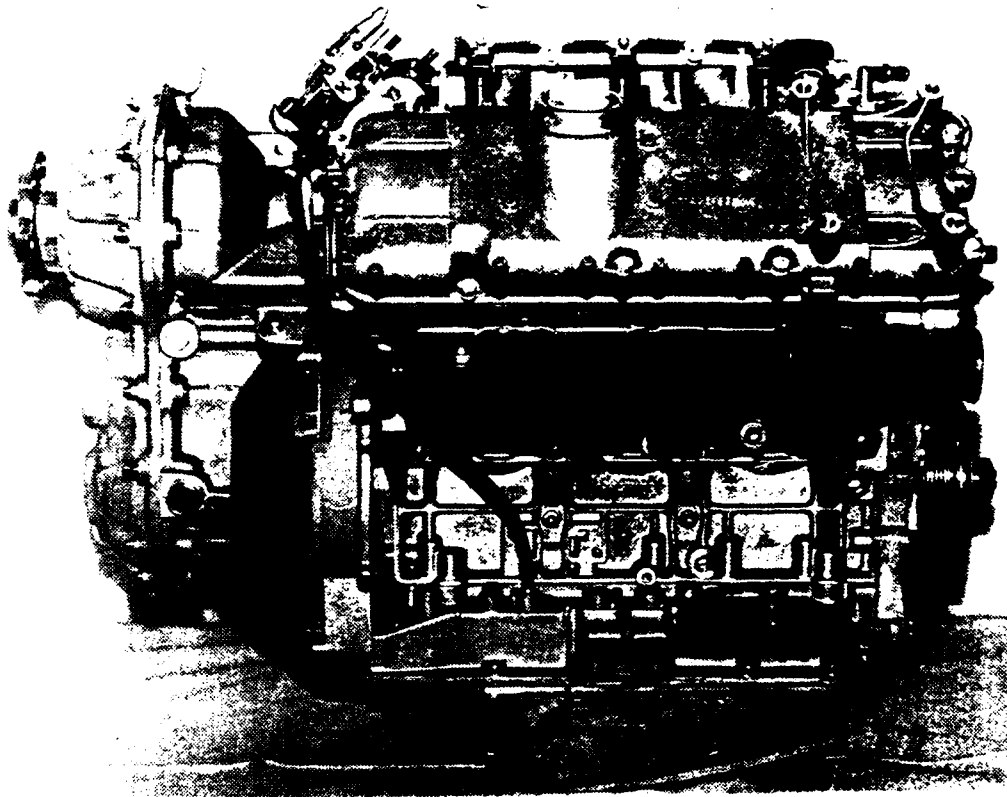
Derived from Automotive Engines

Avions Pierre Robins is in the process of certifying a liquid cooled V-6 engine based on the Peugeot, Renault, Volvo 3 liter V-6. They expect to have it certified under JAR-E by July 92. The engine has been flying in one of Robins singles for over a year.

It produces 185 HP, with the engine turning at 5,500 rpm and the propeller at 2430 through a Porsche reduction gearbox. It features Siemens electronic fuel injection and dual electronic ignition. The fuel injection and ignitions are similar to the ones used on the Porsche engine. Robins states that it has no plans to certify the engine under the FAR's, an approach consistent with their aircraft manufacturing.



Avions Pierre Robins Flying Testbed showing locations of components.

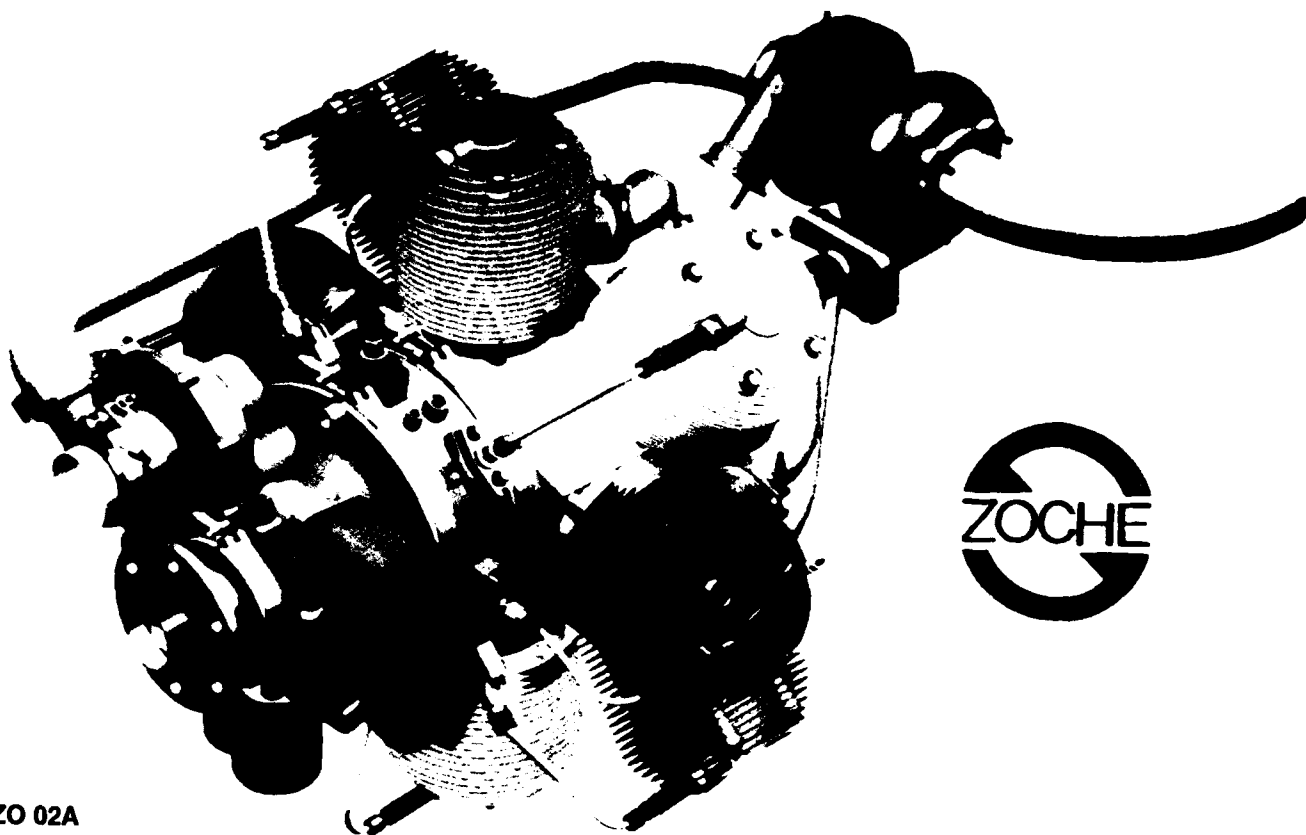


Robins R-3000 V-6 engine

Toyota has received substantial press about their apparent engine development efforts. They have been and continue to be very secretive, stating that they will tell the world when they actually have something to announce. They brought Lexus V-8 engines over from Japan and test flew them in a twin at Mojave. They put about 150 hours of flight time in, and boxed everything up and returned to Japan. Reportedly they are recruiting engine DER's, which would indicate increased activity toward certification. Details regarding the performance, output, or weights of the proposed engine remain unavailable.

Other Engines

Michael Zoche, of Munich Germany, has developed a radial air cooled two stroke Diesel on which he is starting the certification testing under both JAR-E and FAR 33. The engine produces 150 HP from 4 cylinders, or 300 HP from 8 cylinders. It runs at 87 In. manifold pressure, has a fuel consumption of less than .4 LB/HP-hr, and weighs less than 1 pound per horsepower. The engine has not been flown in an aircraft, but has received extensive testing fully accessorized and running a constant speed prop. Mr. Zoche anticipates a sales price competitive per horsepower with current certified engines.



ZO 02A

ZOCHÉ Diesel Aviation Engine

V M Motori of Italy have developed a line of turbocharged opposed liquid cooled reciprocating Diesel engines. Designed to meet JAR-E and FAR 33, these engines have received extensive ground testing but no flight testing. The engines, designed in 4, 6 and 8 cylinder versions, produce 210, 320, and 430 HP respectively. The engines are designed to install in place of existing Lycoming engines with little or no modification. The factory has discontinued development of the engines, citing excessive regulatory difficulties in Italy. They are actively looking for an aviation concern willing to purchase the program and continue its development and certification.

Development of the three cylinder Diesel Merlyn engine remains stalled. Intech of Spokane proposed to use the engine in an Army ground effect vehicle, but the program was canceled and further development became impossible. Intech reports that there would have to be substantial changes in the aviation market and the liability question before they would consider reactivating the project.

Polimotor's founder and president, Matty Holtzberg, has developed a plastic engine. It has a compression molded glass filled phenolic resin block with cast iron sleeve inserts and aluminum head. It's available in a 2.3 liter version and a 2.5 liter version. In a turbocharged version it produces 250 HP and weighs less than 1 pound per horsepower. Holtzberg is making a

concerted effort to approach the homebuilt aircraft market. He has sold two units, one each of the 2.3 liter versions and one of 2.5 liter versions. Lou Ross of Tucson will provide the reduction gearboxes and final drive. Current pricing of the engines is in the \$13,000 to \$17,000 range, but in production quantities could come down to \$10,000. Mr. Holtzberg indicates that he has no plans to certify the engine, given the regulatory environment and irrational liability picture.

Small Turbine Engines

Certified Production Engines

General Motors Allison Division's 250 series produces 420 HP and up. It is used in numerous helicopters and has been certified in a number of fixed wing single engine aircraft including more than 500 Beech Bonanzas. This is a mature design with a substantial installed base and current research centers on increased output outside the range under consideration here.

Pratt and Whitney of Canada's venerable PT-6A turbine engine series starts at 450 HP and goes up. While the engine has enjoyed phenomenal success overall, it has received limited application to smaller aircraft. The initial cost of the engine, exceeding the original cost of most small aircraft, makes the engine an unlikely candidate for wide application in general aviation aircraft.

Turbomeca of France has certified a new family of engine in the 400 HP range. The Arrius series engine, certified into Aerospatiale helicopters, and being developed for other helicopters produces 406 HP continuous with take-off power in the 500 HP range. A turboprop version (approximately 375 HP) of the powerplant is being flown in a SOCATA Omega aircraft for evaluation, but no certification program has been established for it.

Turbomeca indicates that its certification programs hinge on the development needs of airframe manufacturers.

Under Development Intended for Certification

Soloy Corporation in Olympia Washington has patented a dual input single output combining/reduction gearbox incorporating a dual freewheeling system, the Dual Pac ®. They are completing certification of a twin engine Bell Jet Ranger using two Allison 250-C20R's and the Dual Pac ®. Either engine alone can provide the rated capacity of the helicopter transmission, so that performance at sea level remains unchanged in the event of one engine's failure. Soloy is working with Pratt and Whitney of Canada to develop a Dual Pac for the PT-6A series of engines, targeting larger utility

aircraft like the Cessna Caravan and DeHaveland Otter. The FAA has indicated that the Dual Pac can be certified as a multi-engine installation thereby allowing passengers operations under FAR 135 in Instrument conditions. Soloy sees the potential for the PT-6A Dual Pac as an ideal follow-on powerplant for larger single propeller cabin class aircraft like the Aerospatiale TBM 700 and the Pilatus PC-12.

Regulatory Environment.

The current engine certification process does little to encourage new technologies. The industry could be stimulated by the FAA providing affirmative guidelines on how to incorporate the newer developments from the automotive world into aircraft powerplant applications. Examples would include closed loop electronic fuel injection that monitors exhaust to optimize the mixture, electronic ignition with non-linear advance curves, and multi-fuel capabilities. With industry support the FAA could develop and issue Advisory Circulars detailing the designs they would consider acceptable, the methods for showing compliance with the regulations and the related testing levels, and increased willingness to accept research results performed by non-aviation entities. It shouldn't be necessary to re-test technology that has received extensive competent testing and has performed well in other industries all over again as part of a certification program. The current production source control requirements are unrealistically demanding and serve to prevent the incorporation of significant parts of modern automotive technology to the certificated aviation engine. Both safety and promotion of aviation would be well served by a more pro-active approach to engine and production certification.

What Will the Future Bring?

Innovative engine development continues despite the absence of a large market. Assuming the industry is able to solve its problems and start selling airplanes in substantial numbers again, there will be a ready market for a superior powerplant. One would hope for a powerplant that combines the durability and ease of operation of a turbine with the lower cost and better fuel consumption of an intermittent combustion engine. The engine would burn a variety of fuels, all unleaded. From this one can project a liquid cooled, electronically controlled engine, burning jet fuel, diesel, unleaded av-gas, or auto gas. To achieve lighter weights, smaller engines turning at higher RPM, driving the propeller through reduction gearboxes would appear the favored choice. On the turbine side we see continued improvements in materials and specific fuel consumption. One remains

hopeful that the elusive \$50,000 300 HP small turbine engine will materialize.

There has been a lot of exciting development in engines. Some will develop into production engines, some will fall by the wayside. The next few years will prove exciting as the industry finds innovative solutions to its problems, or disappears completely. The one thing we can all agree on is that the status quo will not last.

APPENDIX I -Criteria for a new generation small aviation engine.

- Certified to operate on any readily available fuel, including: jet fuel, diesel, all grades of aviation and automobile gasoline, reformulated gasolines, gas alcohol blends, and methanol or ethanol.
- Weigh less than 1.5 pounds per horsepower with all accessories and have a specific fuel consumption lower than 0.4 lb/BHP-hr, or 20 gallons/hour at 300 HP output.
- Potential to operate for 3,000 hours prior to requiring overhaul, or any maintenance that would require removal of the engine from the aircraft.
- Have small physical dimensions and a configuration which will lend itself to low drag installations.
- Require minimal cyclic maintenance and not require any service between scheduled maintenance/inspection points.
- Tolerate large power changes without special considerations for rapid cooling.
- Operate with a single power lever over the whole operating range including: taxiing, take-off, cruise, descent, and reverse. This would include a high reliability solid state ignition and a closed loop fuel-injection/mixture/emission control system.
- Start easily and reliably in all normally encountered service conditions.
- Never fail catastrophically (an engine failure should only result in less and less power over a long enough interval to allow a safe landing. There should be no sudden complete loss of power).
- Have a cost competitive with currently available turbo-charged liquid-cooled intermittent combustion engines of equivalent output.

ABBREVIATIONS:

ASTM	American Society of Testing and Materials
FAR	Federal Air Regulations
GAMA	General Aviation Manufacturer's Association
GPU	Ground Power Unit
HP	Horse power
JAR	Joint Airworthiness Regulation - European equivalent to FAR.

REFERENCES:

1. THOUVENOT, J L, "Optimization of a Light Helicopter with Arrius Power Plants. presented May 1991 American Helicopter Society Forum in Phoenix AZ.
2. JONES, C., "Stratified Charge Rotary Engine Developments at JDTI from 1984 to 1991. SAE paper 920310 1992

CONVERSATIONS:

1. Aerotech Industries; Gould G.
2. Avions Pierre Robin: Mueller, D.
3. Canadian Airmotive, Inc.: Arney, D.
4. Dynacam: Palmer, D.
5. FAA; Smythe, T.; Parado, J.; Robinette, J;
6. Intech; Evans, H
7. International Aerospace Manufacturing; Belina, J.
8. Machen; Hoover, A.
9. Moller International; Griffith, M.
10. Mosler Motors; Kerns, T.
11. Polimotor; Holtzberg, M.
12. Ross Manufacturing; Ross, L.; Ross C.
13. Rotary Power International; Figart, W.
14. Rotax; Tucker, E.
15. Soloy Corporation; Baena, G.

16. Teledyne Continental; McClellan, C.
17. Textron Lycoming;
18. Turbomeca; McGraw, J.
19. V.M. Motori; Baretta, Mr.
20. Zoche Aero Diesel; Zoche, M.

ETHANOL IN RECIPROCATING AIRCRAFT ENGINES

by

**Max Shauck
M.G. Zanin
Baylor University
Waco, Texas**

**For Presentation to the AIAA/FAA Joint Symposium on General
Aviation Systems at the Hilton Inn-East, Wichita, KS
on March 16-17, 1992**

ETHANOL IN RECIPROCATING AIRCRAFT ENGINES

Shauck, M.E., Zanin, M. G.

Baylor University, Waco, Texas

I. INTRODUCTION

Research and development of ethanol as an aviation fuel has been conducted at Baylor over the past 11 years. The initial motivation was the possibility of fuel supply interruptions as a result of political instability in the Middle East. Six different aircraft were modified and flown on this fuel. These aircraft accumulated over 1300 hours of flying time during carefully planned test programs in which performance was recorded and analyzed. In addition to being renewable and domestically available, it was found that ethanol is economically competitive on a cost per mile basis with avgas, produces more power, burns cleaner and cooler and resists detonation better than avgas.

Once the feasibility, reliability and performance had been established, the next step was certification of the fuel with the FAA. Additionally, a program to increase public awareness about the advantages of ethanol as an aviation fuel was undertaken.

II. CHARACTERISTICS OF ETHANOL AS AN AVIATION FUEL.

Ethanol can be made from any substance containing starch or sugar. In the United States the most common feedstock is corn, in Europe sugar beets and in South America sugar cane. Most ethanol produced is intended for blending with unleaded automotive gasoline in a ratio of 90% gasoline, 10% ethanol. This is done to increase octane and decrease tailpipe emissions. In order to render the ethanol non-potable, it is denatured by the addition of 2-5% unleaded gasoline. Ethanol treated in this manner is referred to as E-95.

Since many industrial processes have waste streams which include starch or sugar, ethanol is also produced from these sources. The ethanol used in the initial stages of this project was produced from the waste from the M&M Mars candy factory in Waco, Texas. The development of a new process enabling ethanol to be processed from woody biomass will dramatically increase the amount of material which can be used to produce ethanol and reduce the cost. It is estimated the process will be commercially available within 5 years and the cost of ethanol will drop from the current price of \$1.30 to approximately \$0.65 per gallon.

Current annual production of ethanol in the United States is approximately 1 billion gallons and projected to reach 3 billion by the year 2000. The anticipated increase in production is due to the requirements of the Clean Air Act. This legislation mandates the removal of all lead from gasoline and the use of oxygenated fuels in a number of highly polluted urban areas. The removal of lead from fuel is a cause for concern in the aviation industry. Although aviation has been granted a waiver by the EPA, the general consensus is that EPA will keep the pressure on until lead is out of all fuels.

The main difficulty with all unleaded petroleum alternatives to 100 low lead aviation gasoline is the inability to obtain the minimum motor octane rating of 98 recommended by the General Aviation Manufacturers Association without the use of metallic additives. Attempts have been made to increase motor octane ratings by increasing concentrations of Toluene, Xylene or blending with MTBE or ETBE. While Toluene and Xylene both failed to produce significant octane enhancement, MTBE improved octane, but was still inadequate. Due to its inherent high motor octane rating, ETBE is considered superior to MTBE, but it is not yet economically feasible.

Another problem with these options is that the blending of components for octane enhancement adversely affects the distillation curve of the the final product. Reid vapor pressure (RVP) limits for avgas are between 5.5 and 7.0. The lower limit is set for ease of engine starting and to prevent introduction of liquid fuel into cylinders. This causes washdown of lubricants from the cylinders and dilution of crankcase oil. The upper limit of 7.0 psi controls excessive vapor formation under high density altitude conditions. If the volatility of the fuel is too high, fuel can vaporize in the tank causing undue venting losses. Rapid vaporization also produces a cooling effect which can cause ice formation in the carburetor under certain conditions of humidity and air temperature. The most serious effect from a safety standpoint is the tendency of fuels with a high RVP to vapor lock causing fuel starvation and engine shutdown.

These problems can be overcome by selective blending of pure iso-octane, iso-butane and MTBE. Phillips Petroleum reports that this fuel has a motor octane of 100.5, a rich octane of 115.8 and RVP of 5.8 psi. Unfortunately this fuel cannot be produced commercially due to prohibitive costs.

Octane ratings for ethanol exist only as blend octane ratings. The blend motor octane value for 10% ethanol and 90% unleaded gasoline is given as 96-99 and the blend research value is given as 128-135. Thus the R+M/2 is 112-116. This project has tested engines in flight on both 180 proof (10% water) and 200 proof ethanol (anhydrous). These engines had compression ratios ranging from 7.0:1 to 10.5:1. There was no evidence of detonation during any of these flight tests.

The following are five of the aircraft flight tested to date:

AIRCRAFT	ENGINE	COMPRESSION RATIO
1. Bellanca Decathlon	Lycoming IO-320	7.5:1
2. Pitts Special S1S	Lycoming IO-360	10:1(Modified)
3. Piper Aztec	Lycoming IO-540	8.5:1
4. SIAI-Marchetti SF-260	Lycoming AEIO-540	8.5:1
5. Velocity (prototype)	Lycoming HIO-360	10.5:1(Modified)

Tests were conducted to satisfy FAA requirements for certification of ethanol for a Lycoming IO-540 engine. These requirements are outlined in The Federal Air Regulations Part 33. One of the final tests for fuel certification is detonation testing. This is a very

rigorous test requiring operation of the engine at very high cylinder head temperatures and under mixture setting running from full rich to lean. The engine must perform at all power setting including full power under these conditions. Detonation testing equipment could detect no detonation or loss of power. The designated engineering representative (DER) wrote in his final report that the use of ethanol extends the limits of detonation over avgas. This characteristic of ethanol combined with the lower cylinder head temperatures will increase engine life.

The RVP of ethanol at 100 degrees Fahrenheit is 3.0. This results in starting difficulties at temperatures below 65 degrees Fahrenheit. This problem has been solved by the addition of a small (1/2-1 gallon) tank of unleaded auto gas. The fuel lines are charged with unleaded gas and the ethanol tank is then turned on. The engine starts on gasoline using the small amount in the lines and immediately after that it runs on ethanol. This procedure has caused no difficulties and has been used in 100% ethanol powered automobiles in Brazil for over 12 years. Since the RVP of ethanol is considerably less than that of avgas, the possibility of vapor lock is significantly diminished.

In all of the aircraft tested on ethanol an increase in available power was observed. The FAA requirements for fuel certification using the 150 hour endurance test on an engine test stand calls for a pre and post endurance test to insure that the engine tested develops rated power before and after the test. The power output was determined by a calibrated dynamometer. In both cases the rated power of the engine was exceeded. It should be noted that this engine was not modified to take advantage of the increased ability of ethanol over avgas to resist detonation. As noted above, the Pitts and Velocity engines were modified to increase the compression ratio and take advantage of this characteristic of ethanol. This modification further increased the power available when using ethanol.

The single drawback encountered in the use of ethanol is its reduced heating value which results in a reduction in miles per gallon. Gasoline has 125,000 BTUs per gallon versus 75,000 BTUs per gallon for ethanol. If the thermodynamic efficiencies of ethanol and avgas were the same, a range reduction of 40% would be experienced using ethanol. The higher thermodynamic efficiency of ethanol reduces the loss of range to between 15% to 20%. This figure is the result of extensive flight test data taken using a variety of aircraft. This does not include the results observed with the Velocity, which has the highest compression ratio. Preliminary results have indicated a considerable improvement in efficiency with this engine. The experience of the Brazilian automobile industry has been a decrease in mpg of only 11% with a compression ratio of 11.2:1 using hydrous ethanol (containing approximately 10% water). Since the changes to the aircraft engines to date have been minimal, considerable increase in efficiency is expected with more extensive modifications.

Other key properties of the fuel were tested during the project. The FAA certification provided documented data supplementing the information previously obtained during flight tests. To obtain independent, authoritative characterizations, the Fuels and Lubricants Research Division of Southwest Research Institute (SWRI) was engaged to conduct tests and data analysis on E-95. A brief summary of their findings is reported:

1. Lubricity: Using the widely accepted Ball-on Ring Evaluator (BORLE), SWRI found that E-95 has slightly better lubricity than gasoline and is within the range considered acceptable for aeronautical systems. This result was corroborated by the post endurance test engine inspection. Prior to the endurance test the engine was disassembled and all

parts subject to wear as a result of the fuel were measured under FAA surveillance. The engine was then reassembled and installed on the test stand. After the endurance test the engine was removed from the test stand and the measurements were repeated. The wear measurements indicated that all components were within service limits. The wear exhibited during this test on all components was less than or equal to that experienced in the same test using avgas.

2. Oil Analysis and consumption: FAA requires periodic fuel and oil analysis during the test. All results of these tests were satisfactory. Additionally, the report of the DER stated that oil consumption during the test was almost nil.

3. Luminosity: Flame luminosity was measured by a United Detector Technology Model 40X Optimeter System. Luminosity of E-95 was adequate to insure safety.

4. Samples of fuel wetted materials were subjected to soak tests to determine material compatibility. SWRI concluded that no materials compatibility problems existed with E-95.

III. FLIGHT TESTING AND DEMONSTRATIONS

1. Bellanca 8KCAB Decathlon.

This was the first aircraft modified and flown on ethanol in this project. The Decathlon is a single engine, high wing, two place aerobatic trainer. The engine is a Lycoming AEIO-320-E2B. It has four cylinders and is a direct drive, fuel injected, horizontally opposed aerobatic engine with a rated maximum continuous horsepower of 150 at 2700 RPM. The compression ratio of this engine is 7:1.

Using hydrous ethanol which contains 10% water, this aircraft consumed 12 gallons per hour at 120 miles per hour versus 9 gallons per hour of avgas at the same airspeed. This is a 25% increase in consumption which would result in the same percentage reduction in range. These figures were obtained in a very low compression engine using ethanol with 67,500 BTU's per gallon as opposed to anhydrous ethanol which contains 75,000 BTU's per gallon. Using a Lebow torque sensor and manifold pressure and RPM gauges (calibrated and certified), the engine produced 4% more power at full power and 7% more power at normal cruise power settings on hydrous ethanol than on avgas. Detonation testing was conducted and there was no evidence of detonation on ethanol.

Over 600 hours of flying time on ethanol has been logged on this aircraft. Aerobatic demonstrations have been flown on ethanol with this airplane in numerous airshows in the United States, including the EAA airshow in Oskosh. Aerobatic demonstrations have also been performed in a number of cities in Brazil including Sao Paulo and Rio de Janeiro. In 1982, this Decathlon made the first transcontinental flight on ethanol. Subsequently a total of 3 National Aeronautic Association records were established by ethanol-powered flights in this airplane.

Although this aircraft successfully demonstrated that ethanol is a viable aviation fuel, the relatively low compression of the Lycoming IO-320-E2B engine was not ideally suited for this project from the standpoint of efficiency.

2. Pitts Special S1S

The Pitts Special used in this portion of the ethanol project was in the experimental category. It was a single engine, single seat aerobatic biplane powered by a modified Lycoming IO-360 A4A. The compression ratio was increased from 8.5:1 to 10:1. Aircraft instrumentation included a digital fuel flow meter, EGT and CHT gauges and a portable thermistor to measure cockpit temperatures.

Performance data taken while flying at 2000 ft. AGL, 2700 RPM and 155 MPH indicated airspeed shows a fuel consumption of 8.8 GPH on avgas and 10.4 GPH on ethanol. This would result in a 15.4% decrease in range on ethanol. The CHT decreased from 380 on avgas to 358 on ethanol.

Since the aircraft had a fixed pitch propellor, a reliable indication of the power available on avgas versus ethanol was obtained by flying the aircraft at full throttle on both fuels at 2000 ft. AGL and 3000 ft. AGL. These flight were conducted on the same date within an hour time to reduce the possibility of changes in density altitude. At full throttle on avgas at 3000 ft. the engine RPM was 3150, and on ethanol showed 3275. The limiting RPM for Lycoming engines is given as 2700, consequently the curves indicating power output at a given RPM do not include these values. Thus it not possible to translate these figures into a percentages of power increase. It can be concluded that the use of ethanol increased the power available.

This Pitts was flown in numerous airshows in the United States and Italy on alcohol. During portions of these airshows the engine was run at speeds in excess of 3400 RPM with high outside air temperatures, high oil temperatures and cylinder head temperatures. Despite these extreme conditions, the engine performed very well with no indication of pre-ignition or detonation.

Another Pitts (same model) was modified in Paris, France, and flown to demonstrate ethanol performance.

3. SIAI Marchetti SF-260

This aircraft is a single engine, cantilever low wing monoplane of metal construction equipped with retractable landing gear. The powerplant is a Lycoming AEIO-540-D4A5 fuel injected engine rated at 260 HP at 2700 RPM. The compression ratio of this engine is 8.5:1.

Modification of the engine and aircraft was accomplished at the SIAI Marchetti factory in Italy and ground tests on ethanol were performed on the factory grounds. The aircraft was shipped to the United States where flight testing on ethanol was completed.

Inflight data indicated that at an altitude of 9000 ft. MSL and 75% power, the MPG on ethanol was 10.7. Under these conditions, the aircraft will realizes 13 MPG. This results in a reduction in range of 18% on ethanol. The aircraft was flown approximately 100 hours on ethanol. At this point, the engine was removed to undergo certification tests. The certification tests were successfully completed and the Supplemental Type Certificate to operate the Lycoming series of IO-540 parallel valve engines was granted on March 12, 1990.

4. Velocity

This is a single engine, all fiberglass, canard type aircraft. The Velocity used in this project is the prototype built by the designer. It was chosen for the purpose of making the first transatlantic flight on ethanol. Experience with the other aircraft in the project demonstrated that miles per gallon on ethanol increased as the compression was increased. Accordingly, the engine modifications included raising the compression ratio from 7.5:1 to 10.5:1 in the aircraft's Lycoming HIO-360.

In addition to modifying the aircraft to use ethanol as a fuel, it was necessary to install additional fuel tanks for the transatlantic flight. The large cabin space permitted the installation of tanks capable of increasing the total capacity to 160 gallons. A special long range communication radio and survival equipment was added.

An extensive flight test program was carried out to determine engine performance as well as the best altitudes and power settings to achieve maximum range. During this period it was observed that the difference between range on ethanol and avgas in this configuration was much less than in the previous tests on other aircraft.

The aircraft was flown from Waco, Texas to Paris, France on ethanol. No problems related to the fuel were encountered either during the preparation or the flight itself. The fuel consumed flying from St. Johns, Newfoundland to Lisbon Portugal was 123 gallons, for a cost of \$160 at the current price of \$1.30 per gallon. This flight was undertaken to provide dramatic proof of the reliability of ethanol as an aviation fuel.

IV. CURRENT PROJECTS

As an outgrowth of the results of this project and as a response to the evolving situation concerning aviation fuel, a Research and Development Center for Ethanol Fuel in Aviation has been established at Baylor University.

The initial undertaking of the center is the certification of three aircraft on ethanol. These aircraft are a Cessna 152, a Piper Pawnee and a Pitts S2B. After certification, the Cessna and the Pitts will be used in the flight training portion of the Aviation Sciences at Baylor University and the Pawnee will be used in agricultural spray operations in South Dakota. The collection and analysis of performance and economic data will be carried out while these aircraft are flying in commercial operations.

The center will also pursue certification of additional engine-airframe combinations and conduct research to improve the efficiency of ethanol powered aircraft engines. A current statewide aviation demonstration program will be expanded to a national program and further educational material on ethanol as an aviation fuel will be produced.

V. CONCLUSION

Ethanol has met and exceeded the FAA requirements for certification in a series of Lycoming aircraft engines. It has been successfully flight tested in a number of general aviation aircraft in a variety of demanding circumstances and has proven its reliability by powering a single engine aircraft in a flight across the Atlantic Ocean. Ethanol produces more power, burns cleaner and cooler, has less tendency than avgas to pre-ignite and detonate and resists vapor lock better than avgas. Ethanol is now economically competitive

with avgas and will improve its economic position in the future. It is a renewable fuel which can be produced domestically in sufficient quantities to satisfy current and future demands for piston engine aircraft.

It is not only the Clean Air Act and its potential consequences which call into question the future of petroleum fuels in general aviation. We now import 50% of our petroleum and a substantial amount of that is from regions of the world which have proven their instability. During the first Arab oil embargo in 1972, the United States Congress considered either cutting off all fuel to general aviation or rationing the amount each pilot could use. Our continued dependence on petroleum as our only liquid transportation fuel threatens our economy and domestic security. Ethanol can be the solution, a superior performing, economically competitive fuel for which continued availability is assured.

In demonstrations around the United States the response of pilots has been overwhelmingly favorable towards the use of ethanol. Most of them ask two questions: "Why is it taking so long to move ethanol into aviation?" - and- "Is it possible to convert my airplane now to use ethanol?". It is hoped that soon the first question will be unnecessary and the answer to the second question will be "yes".

**COMBUSTION PROPERTIES OF ETHANOL BLENDED
TURBINE FUELS**

by

Gary Eiff
Susan Putz
Aviation Technologies Division
College of Technical Careers
Southern Illinois University
Carbondale, Illinois
and
Clifford Moses
Division of Engines, Fuel, and Vehicle Research
Southwest Research Institute
San Antonio, Texas

**For Presentation to the AIAA/FAA Joint Symposium on General
Aviation Systems at the Hilton Inn-East, Wichita, KS
on March 16-17, 1992**

COMBUSTION PROPERTIES OF ETHANOL BLENDED TURBINE FUELS

by

Gary Eiff
Susan Putz
Aviation Technologies Division
Southern Illinois University
Carbondale, Illinois

and

Clifford Moses
Engine, Fuel, and Vehicle Research Division
Southwest Research Institute
San Antonio, Texas

ABSTRACT

The principal objectives of this research project were to establish baseline data for ethanol blended turbine fuels, measure combustion byproducts of blended fuels, and identify any changes in exhaust temperature distribution and combustor linear temperatures between Jet-A and blended test fuels. Other factors evaluated in the research included the test fuel's effect on soot formation and flame stability limits. Ten test fuels of varying ethanol concentrations were evaluated in a test apparatus utilizing Allison T-63 combustor assembly components. The research suggested the potential viability of using ethanol blended turbine fuels in unmodified aviation jet engines. Although combustion efficiency was reduced by the increasing concentrations of ethanol in the test fuel blends, no significant loss in power was noted if fuel flow rates were adjusted to compensate for the lower BTU content of the fuels. While the study did not support the dramatic reduction of hydrocarbon and carbon monoxide emissions alleged in a previous study, significant reductions in oxides of nitrogen and soot emissions were noted. Significant increases in aldehyde emissions were found with increasing concentrations of ethanol especially at idle and low power conditions.

INTRODUCTION

BACKGROUND OF THE STUDY

Several research studies over the past decade have explored the use of ethanol as an alternative fuel for the aviation turbine engines. Pilot projects conducted by the Alabama Aviation Technical Institute, the Federal Aviation

Administration, Southwest Research Institute, and the United States Navy generally supported the feasibility of using ethanol blended fuels in current technology aviation turbine engines [1,4,5,7,8,&20]. Unmodified aircraft turbine engines have been successfully run on fuel blends containing as much as 15% ethanol for periods up to one hundred seventy-five hours with no apparent ill effects [20]. These tests generally suggested that the use of ethanol blended fuels did not significantly effect engine performance [1,4,7,8,&20]. One study also declared that ethanol blending of jet fuel dramatically reduced engine emission pollutants [5].

While several research efforts performed by Southwest Research Institute and others during the early 1970's utilized ethanol fuel variants while testing various turbine engine combustion performance parameters, the first significant effort to focus specifically on the use of ethanol as a jet fuel extender was conducted by Edmund L. "Skip" Eveleth at Alabama Aviation and Technical College during 1984 and 1985. As a result of these efforts, Mr. Eveleth reported in 1986 that the addition of ethanol to aircraft turbine fuels dramatically reduced exhaust emissions while causing no degradation in engine performance [5]. In a series of what he called "probe tests" using a Pratt & Whitney PT-6 aircraft turbine engine under ground, static test conditions, Mr. Eveleth evaluated the effects of adding increasingly greater concentrations of ethanol to the engine's Jet-A. Among the findings reported by Mr. Eveleth were [5]:

- * No pungent exhaust odor was apparent with ethanol blended fuels.
- * With a blend of 10% ethanol / 90% Jet-A, exhaust analysis was reported to show hydrocarbon concentrations of zero parts per million at rated power and cruise.
- * The same 10% / 90% fuel blend was also reported to have carbon monoxide concentrations of 0% at rated power and cruise.
- * There was no apparent loss of power with the blended fuels despite the disparity of BTU content between the ethanol blended test fuel and the Jet-A base fuel.
- * All engine temperatures were reported to be within normal ranges.

Mr. Eveleth was sufficiently encouraged by the research results to seek support for a series of tests which would

lead to the issuance of a Supplemental Type Certificate (STC) by the Federal Aviation Administration (FAA) for the use of ethanol blended fuels in the PT-6 powerplant. In preparation for evaluation of the ethanol blended fuel alternative, the FAA initiated a series of tests at its Technical Center in New Jersey exploring the use of ethanol fuels in turbine aircraft powerplants [1,2,3,4,7,8,&9]. An additional project was performed by the United States Navy [20]. The purpose of these tests was to evaluate some of the fuel and engine performance parameters which dictate the general viability of fuels for aviation use. Although these tests did not evaluate the emissions for the test fuels, they did indicate the potential viability of ethanol/Jet-A fuels at low blending rates.

There existed, however, a lack of linearity among the tests. Research findings from the various studies suggested a degree of inconsistency and even contradictions among the various test results. Indications of dramatically reduced emissions by one research project were untested by subsequent research. Several of the projects indicated that the turbines under test exhibited nominal or only slightly reduced engine performance while other research indicated that engine performance was slightly improved with the addition of ethanol. Of considerable concern was the fact that several of the turbines used in the tests experienced minor turbine damage over the length of the experiments [5,&9]. Although several hypotheses were offered by the researchers involved, the cause of this damage was never empirically determined.

NEED FOR THE STUDY

Before contemplating the practicability and tenability of engine certification with ethanol blended turbine fuel alternatives, variations among previous research observations had to be reconciled. Although a general agreement existed among the previous projects concerning the potential feasibility of ethanol blended jet fuels, there were several important discrepancies among these research efforts which require clarification. Further testing was needed to clarify discrepancies among previous research and to explore additional combustion parameters before meaningful certification efforts could be pursued.

In order for the aviation community to embrace a new or reformulated fuel, there must be a distinct advantage for adopting the new fuel as compared to fuels in current use. The Alabama research gave evidence of just such a motivator [5]. Current emphasis on cleaner air has generated considerable negative feelings by the general public with

regard to the pollution caused by jet aircraft [13,14,19,&21]. The Alabama research suggested that pollution from jet emissions was greatly reduced with the addition of ethanol to the jet fuel. Such a finding could provide the justification necessary for the adoption and use of ethanol blended fuels. Unfortunately, subsequent research made no attempt to verify these emissions findings. Further clarification of the alleged significant reduction of engine emissions was, therefore, a necessary precursor to certification testing to support the marketability of the fuel.

RESEARCH OBJECTIVES

Through this research effort, researchers hoped to contribute to the body of knowledge concerning ethanol fuels and to help add definition to baseline data for ethanol blended turbine fuels. Of principle concern was the measurement of combustion byproducts of Jet-A/ethanol blended fuels at increasing ethanol concentrations. Measurement of the combustion exhaust temperature distribution and combustor liner temperatures for Jet-A and blended fuels was also an important parameter in order to ascertain whether turbine damage might have been the result of blended fuel combustion anomalies. Other factors evaluated in the research included the test fuel's effect on soot formation, flame radiation, and ignition and flame stability limits. Specifically, this project sought to establish baseline data concerning:

- * Combustion byproducts (emissions) of pure Jet-A fuel.
- * Combustion byproducts of Jet-A/ethanol blended fuels at increasing ethanol blending ratios.
- * The combustion exhaust temperature distribution of pure Jet-A fuel.
- * The changes, if any, in the combustion exhaust temperature distribution of blended fuels as ethanol blending rates are increased.
- * The effects of ethanol blending of Jet-A fuels on soot formation.
- * The effects of ethanol blending of Jet-A fuels on ignition and flame stability limits.

RESEARCH DESIGN

EXPERIMENTAL METHODOLOGY

This experimentation program was conducted in a pressurized combustion rig based on Allison T-63 turbine engine hardware. The fuels test profile began by testing samples of the 100% Jet-A and pure 200 proof neat ethanol base fuels in order to establish a baseline of their physical properties. Each base fuel was then tested in the combustor apparatus at emulated power levels of idle, descent, cruise, and climb power conditions. It was originally intended to measure take-off power as well, but combustor apparatus safety concerns and fuel pump limitations precluded measurements at this simulated power condition.

Once this referent datum was established, observations were collected for each of the various ethanol blended Jet-A fuels at each simulated engine performance level. Turbine fuel blends were evaluated by incrementally changing the ethanol concentration of the fuel and measuring the resulting parameters of combustion at each of the power levels. In addition, the procedure was performed at both nominal fuel flow rates for the engine and at a fuel flow rate which compensated for the energy (BTU) difference between the Jet-A base fuel and the blended fuel. This procedure continued until a definitive correlation between ethanol blending rates and combustion parameters was established.

In an effort to determine the propensity of the blended fuels to cause turbine engine starting problems ("hung starts"), the researchers performed several tests on ignition and stability (lean blow-out) limits for each of the various ethanol blended fuels. These tests helped identify any proclivity of the fuels to cause engine ignition problems which could damage the turbine section of the engine.

EXPERIMENTAL FACILITIES AND PROCEDURES

Combustion Test Facilities - The experiments were performed at the United States Army's Belvoir Fuels and Lubricants Research Facility (BFLRF) located on the research campus of Southwest Research Institute (SwRI) at San Antonio, Texas. The test cell facility utilized for this research project was specifically designed for combustion research on gas turbine fuels. An air supply system provided a clean, smooth (pulsation free), temperature controlled source of air flow for the combustor rig

assembly. The air supply system used in this study is capable of delivering filtered air at mass flow rates of 1.1 kg/s (2.5 lbm/s) and pressures to 1620 kPa (16 atm). Air flow was passed through an indirect heating chamber capable of providing unvitiated temperature controlled air to 1100K (1500°F). Turbine flow meters and strain-gage pressure transducers were used to measure flow properties for both air and fuel systems. Thermocouples were referenced to a 339K (150°F) oven. Test fuel was delivered to the combustor rig assembly by way of an aircraft-type gear pump driven by a variable speed motor.

Combustor Test Fixture - The combustor test assembly used for this study is based on engine hardware from the Allison T-63 turbine engine (used on the Navy's TH-57A and other military helicopters). The T-63 assembly is a single can combustor with a dual orifice pressure atomizer centrally located in the dome. The Allison T-63 combustor system was fitted into a test apparatus which allowed for the emulation of turbine engine air flow and temperature conditions representing various T-63 power conditions. Table 1 lists the air and fuel flow conditions for the nominal power conditions tested.

The combustion liner assembly was instrumented with five thermocouples along its length to measure burner can temperatures (Figure 1). At the exit of the burner can is a centerbody which diverts the flow of exhaust gases into the annulus where the nozzles and turbine blades are normally located. Gas sampling probes, pressure probes, and fifteen thermocouples arranged circumferentially in the plane of this annulus at various radial positions (Figure 2). The purpose of the thermocouples was to measure exhaust gas temperatures in order to measure the uniformity of the exhaust temperature profile. These measurements were considered important since changes in fuel spray pattern and other variables can affect the combustion patterns. This, in turn, can precipitate changes in the exhaust temperature profile, termed the exhaust temperature distribution, which can lead to reduced life of the turbine blades. This was of principle concern since previous research had noted turbine blade damage during testing. Finally, gas sampling probes were inserted into the exhaust stream aft of the thermocouples in order to extract gases for analysis according to standard procedures.

Instrumentation and Data Acquisition - Data acquisition, recording, and reduction was performed on-line by a Hewlett-Packard 3497 data acquisition system coupled to a Hewlett-Packard 9000 computer. Operational parameters and test observations were polled from transducers and displayed on a

monitor screen and recorded on a printer. Data acquisition was performed and displays up-dated on a ten second cyclic rate over the period of the test. Combustor air and fuel flow rates were measured with turbine flow meters. Pressure measurements were sensed by strain gage pressure transducers activated by filtered and regulated power supplies. Chromel-alumel thermocouples, referenced to a 339K (150°F) regulated oven, were utilized to measure all temperatures. At the completion of the experimental run, the data were reduced and presented on a printed report by the data acquisition system.

Exhaust Gas Analysis Instrumentation - Exhaust emission gases were measured on-line using the following instrumentation in accordance with SAE-Aerospace Recommended Practice (ARP) 1256, "Procedures for the Continuous Sampling and Measurement of Gaseous Emissions from Aircraft Turbine Engines". This was done for all emission gases with the exception of NO and NO_x gases which were measured by chemiluminescence.

Test Parameter	Instrument	Sensitivity
Carbon Monoxide	Beckman Model 315B NDIR	50 ppm to 16%
Carbon Dioxide	Beckman Model 315B NDIR	300 ppm to 16%
Unburned Hydrocarbons	Beckman Model 402 FID Hydrocarbon Analyzer	0.5 ppm to 10% (CH ₄)
Nitric Oxide	Thermo-Electron 10A Chemiluminescence Analyzer	3 ppm to 10K ppm
Total Oxides of Nitrogen	Thermo-Electron 10A Chemiluminescence Analyzer with NO _x Converter	3 ppm to 10K ppm
Oxygen	Beckman Fieldlab Oxygen Analyzer	0.1 ppm to 100%

Exhaust samples were routed to emission gas analysis carts through a stainless steel tube heated to 177°C (350°F) and then appropriately distributed. A steady flow of exhaust emission gas was maintained by applying a pressure differential to the analysis instrumentation end of the sample tube.

Smoke Analysis - Particulate emissions were evaluated by measuring exhaust smoke levels according to the requirements and procedures established in SAE-ARP 1179. Briefly, this procedure passes a volumetrically metered exhaust sample through a strip of filter paper where particulate emissions from the exhaust are trapped on the surface of the filter. The resulting "spot" is measured for "grayness" against a scale ranging from white to black, dependent on the sample size and particulate content of the exhaust. The spot is then evaluated using a reflectometer. The smoke number (SN) of each spot is calculated according to the formula:

$$SN = 100 \cdot \left[1 - \frac{R_S}{R_W} \right]$$

where R_S and R_W are the diffuse reflectance ratio between the sample spot and the clean filter paper. Exhaust samples were taken over a range of sample sizes around $W/A = 0.023$ pounds of sample per square inch of filter area. The resulting smoke numbers were then plotted against the function $\log(W/A)$. These values were least-squares fitted with a straight line. The interpolated value of the smoke number at $W/A = 0.023$ is the reported smoke number for the experimental engine operation condition.

Acids and Aldehydes Analysis - In an effort to determine the levels of aldehydes in the exhaust of the various test fuels, a portion of the exhaust stream was diverted through a set of impingers filled with an acetonitrile solution of dinitrophenylhydrazine. The aldehydes reacted with this solution to form derivatives which were analyzed by High Performance Liquid Chromatography (HPLC) to yield both quantitative and qualitative results. The HPLC analysis gave specific concentrations for C_1 - C_6 aldehydes as well as total aldehydes.

The evaluation of acids in the exhaust for each of the test fuels was performed by diverting a portion of the exhaust stream through a set of impingers filled with specially purified water. After the gas samples were bubbled through the impingers, the resulting solution was analyzed by Ion Chromatography (IC) resulting in both qualitative and quantitative measures of the combustion acids present. Specific concentrations of acetic and formic acids were measured as well as for total acids.

Combustion Efficiency - Combustion efficiency was determined from exhaust gas analysis according to the relationship developed by Hardin: [11,&12]

$$\eta_b = \left[1 - \frac{-A \cdot f(\text{UBH}) - 121745 \cdot f(\text{CO}) - 38880 \cdot F(\text{NO}) - 14654 \cdot F(\text{NO}_2)}{-A \cdot [f(\text{CO}_2) + F(\text{CO}) + f(\text{UBH})]} \right] \times 100\%$$

where $f(i)$ is the concentration of "i" in the exhaust and A is a constant based on the heat of combustion and hydrogen/carbon ratio of the fuel, and UBH is unburned hydrocarbons.

Ignition and Stability Limits Test - Ignition and stability limits were evaluated for each ethanol blended fuel and for the 200 proof ethanol base fuel. Test results were compared to the Jet-A base fuel in an effort to identify any trend resulting from the blending of ethanol to the base fuel which might cause potential ignition or lean blow-out problems. In each test, the fuel flow transition gradient was adjusted using a constant speed motor to manipulate the motor speed control for the fuel pump in order to provide a uniform and gradual increase or decrease in fuel flow.

Ignition performance was evaluated by determining the minimum fuel-air ratio at which the test fuel would "light off" in the combustor. This test was performed by establishing air flow conditions of 0.23 kg/s (0.5 lbm/s) at ambient temperature and a burner inlet pressure slightly above ambient. The igniter was activated and fuel flow rates gradually increased until ignition occurred at which point the fuel flow rate was recorded. After the ignition point was determined, the fuel was turned off allowing the flame to extinguish. The procedure was repeated several times for each fuel, allowing the combustor to cool to ambient temperatures between trials.

The measurement of flame stabilization is the lean limit for flame-out, that is, the minimum fuel-air ratio limit. Flame stabilization was determined by essentially the inverse procedure for determining the lean ignition point. Combustor conditions were stabilized at an idle power condition and then the fuel flow was gradually reduced until the flame was extinguished. The fuel flow rate was noted at the point of flame-out.

EXPERIMENTAL FUELS

Ten test fuels were used in this research design. The two base fuels used in the experimental fuel blending process were Jet-A aircraft turbine fuel and 200 proof neat ethanol. Fuels were blended by weight and the resulting test fuels were stored in clean fifty-five gallon drums until used for testing. Incremental changes of five percent ethanol were used at low blending rates since previous research suggested that this was the most viable range of fuels for unmodified aircraft turbine engines. Additional data points were recorded for forty and fifty percent blends to further delineate any trends which might result from the blending. Blends above fifty percent ethanol were not sampled since it is generally agreed that blending rates of this magnitude would not produce viable fuels for unmodified aircraft turbine use. A complete list of fuels used in the study are listed in the table below.

EXPERIMENTAL FUELS TESTED

Test Fuel Number	% Concentration By Weight Jet-A	ethanol
1	100%	0%
2	95%	5%
3	90%	10%
4	85%	15%
5	80%	20%
6	75%	25%
7	70%	30%
8	60%	40%
9	50%	50%
10	0%	100%

In order to establish baseline data for the study, several empirical measurements were made of a number of the base fuels' physical properties. These values were important for determining the energy compensated fuel flow rates used in the research.

PHYSICAL PROPERTIES OF FUELS

Fuel	Heat of Combustion -Gross-	Heat of Combustion -Net-	Specific Gravity	Kinematic Viscosity	Percent Carbon	Percent Hydrogen	Oxygen by Diff.
Jet-A	19721.2	18452.5	0.8154	2.13	86.14	13.78	-
ETOH	12687.4	11461.3	0.7938	1.51	51.55	13.44	35.01
10% ETOH	19427.4	18328.8	0.8112	1.92	-	-	-
20% ETOH	18420.1	17163.0	0.8086	1.89	-	-	-

SUMMARY OF RESULTS

FUEL IGNITION AND STABILITY LIMITS

Ignition Point Test - Figure 3 presents the effects of ethanol on the minimum fuel flow rate necessary to cause ignition. As the level of ethanol concentration in the test fuel blend was increased, a gradual reduction in the fuel flow necessary to cause ignition was observed. A first order regression line was added to the data in Figure 3 to help illustrate this tendency.

Flame Stabilization (Lean Blow-Out) Test - As depicted in Figure 4, increasing concentrations of ethanol in the blended test fuels resulted in combustion flame-out at increasingly higher fuel flow rates. This tendency suggests that as ethanol concentrations in the fuel are increased, the stability of the flame is decreased. The reduction in flame stability was probably due to the lower BTU content of the fuel. Again, a line representing the first order regression model helps illustrate this tendency.

A post study evaluation of the ignition and stability limits testing procedures raised concerns that the data acquisition rate used in the tests, one cycle every ten seconds, may have been too coarse. A shorter acquisition cycle might have provided greater repeatability of the data and, therefore, better definition of the test fuel's ignition and flame stabilization limits.

SMOKE NUMBER

Because of the length of time required for this test, exhaust gases were sampled and SAE smoke numbers determined for each base fuel and blended test fuel only at energy compensated fuel flow rates. Repeated samples were taken for the various fuels at each power setting to insure the repeatability of the data. The data presented in Figure 5 illustrates the relationship between levels of ethanol in blended fuels and the formation of particulate emissions. Observations were repeated for each operating condition and the values presented are average values.

Figure 5 shows that experimental results indicated that the addition of ethanol to Jet-A fuel caused a dramatic reduction in soot formation. This trend was pronounced throughout the range of fuels tested (0% to 50% ethanol). Samples taken for 200 proof ethanol produced no measurable smoke number. These findings are similar to observations recorded in a previous research study into the effects of ethanol microemulsions on soot formation of JP-4 and JP-8 turbine fuels [16,&18].

AVERAGE SAE SMOKE NUMBERS
(Energy Compensated Fuel Flow Rates)

% Ethanol in Fuel	- 10%	Emulated Power Setting 40%	55%	- 75%
Jet-A	19.60	32.30	37.10	37.60
5% ETOH	16.30	28.40	35.30	34.80
10% ETOH	13.90	24.00	30.20	30.30
15% ETOH	11.10	20.80	27.10	26.60
20% ETOH	9.00	17.00	22.20	22.30
25% ETOH	5.50	13.70	17.40	19.50
30% ETOH	4.80	10.70	15.00	*
40% ETOH	1.60	4.90	8.10	*
50% ETOH	0.00	1.60	3.20	*
100% ETOH	0.00	0.00	0.00	*

* Missing data due to the inability of the fuel pump to supply adequate fuel flow.

EMISSION GASES

Hydrocarbon Emissions - Hydrocarbon emissions were sampled and analyzed for all test fuels at both nominal and energy compensated fuel flow rates; these results are presented in Figures 6 and 7 respectively. The blending of ethanol to the Jet-A base fuel caused an immediate and unabated increase in the level of hydrocarbon emissions over the entire range of blended fuels tested. As expected, increases in hydrocarbon emissions were highest at the lower power settings, adding to already existing high levels of emissions.

The increasing levels of hydrocarbon emissions were somewhat less pronounced with energy compensated fuel flow rates but remained quite apparent especially at low power settings. The rate of increase in the hydrocarbon emission level moderated as power settings were increased until the rate at 75% power was considerably less pronounced. Blending levels above 50% ethanol were not tested except for the 100% ethanol base fuel. The line projected on the data plots in Figures 6 and 7 represents a second order regression model of best fit for all of the data points at each power setting. Previous research findings that hydrocarbon emissions were reduced to zero (0) parts per million with low levels of ethanol blended into jet turbine fuels [5] were unsupported by this research. The results of this research study suggest that ethanol blends will increase hydrocarbon emissions. This is especially true at idle and low power conditions used by aircraft during ground operations.

Carbon Dioxide - Figures 8 and 9 present the analysis of emission gases for levels of carbon dioxide at nominal and energy compensated fuel flow rates. Results suggest that the addition of ethanol to the Jet-A base fuel caused a noticeable decline in the levels of carbon dioxide present in the exhaust. This tendency was more apparent in evaluations of test fuels at nominal fuel flow values. Energy compensated fuel flow rates resulted in considerably less dramatic declines in the carbon dioxide concentrations. The reduced levels of carbon dioxide were most likely due to reductions in flame temperature and lower combustion efficiency.

Carbon Monoxide - Figures 10 and 11 present the analysis of emission gases for levels of carbon monoxide at both nominal and energy compensated fuel flow rates. Experimental results demonstrated that the addition of ethanol to the base turbine fuel caused a marked increase in the concentrations of carbon monoxide. Changes in the

levels of carbon monoxide were more pronounced for energy compensated fuel flow rates than for nominal rates. Although lower power settings caused less pronounced increases in carbon monoxide levels, as anticipated, carbon monoxide concentrations remained highest at the lower power settings for all of the blended fuels. A previous research report's suggestion that the addition of ethanol to Jet-A turbine fuel caused carbon monoxide concentrations to drop to zero percent [5] was not supported by this research.

Oxides of Nitrogen - Figures 12 and 13 present the relationship between concentrations of ethanol in the fuel and detected levels of total oxides of nitrogen for nominal and compensated fuel flows. Figures 14 and 15 further define these concentrations by specifically present concentrations of nitric oxide at the two fuel flow rates. Contrary to hydrocarbon and carbon monoxide, oxides of nitrogen were expected to be greatest at higher power settings due to the higher combustion temperatures.

Assessment of combustion gases for oxides of nitrogen indicated that blending turbine fuel with ethanol produced dramatically lower concentrations of these gases in engine emissions. Both total oxides of nitrogen (Figures 12 & 13) and nitric oxide (Figures 14 & 15) were substantially reduced with increasing concentrations of ethanol in the blended test fuel. This trend was true for both nominal and energy compensated fuel rates and for all power settings tested. This finding may be significant in light of the recent identification of NO and NO_x as the polluting emission of principal concern for turbine powered aircraft [10,13,14,19,&21].

Oxygen - Combustion exhaust was also evaluated to establish the level of oxygen (O₂) present in the engine exhaust for the various test fuels. Figure 16 presents oxygen concentrations for nominal fuel flow conditions. Under these conditions there was a marked increase in oxygen levels as ethanol concentrations were increased. Figure 17 illustrates results for energy compensated fuel flow conditions and suggests that very little change was realized in the levels of oxygen in the exhaust under compensated conditions. Increased levels of oxygen were most likely due to lower combustion temperatures.

ACID AND ALDEHYDES

An evaluation of acids and aldehydes for the various test fuels was undertaken to explore any relationship between ethanol concentrations and levels of acids and aldehydes

realized as combustion by-products. Only a few select points were analyzed due to the high cost for these tests. A greater number of points were chosen at lower power conditions since it was anticipated that this would represent the worst case conditions. Compensated fuel flow rates were used to maintain a constant energy condition.

Acetic Acid - Figure 18 presents the resulting levels of acetic acid in the emission for the various test conditions. Despite the scatter of the data, results seemed to suggest that the concentration of acetic acids was generally higher at idle conditions, which is consistent with the higher hydrocarbon concentrations previously described. Specific relationships concerning the effect of ethanol on acetic acid concentrations remained unclear because of the excessive scatter in the data.

Formic Acid - Figure 19 presents the effect of ethanol concentration on the level of formic acid in the exhaust. As in the test for acetic acid, the data collected for formic acid concentrations contained more scatter than desired. The data seem to suggest a slight trend of higher levels of formic acid with comparable increases in the blending rates of ethanol in the test fuel. The effect of ethanol on formic acid concentrations in the exhaust was not clear, however, due to the excessive scatter in the data.

Total Acids - Figure 20 presents the level of total acids realized with increasing concentrations of ethanol in the fuel. Although the data were less scattered, results did not produce a clear relationship between the concentration of ethanol and levels of total acids in the exhaust. The data for the 10% power setting was the most suggestive of a trend of any of the power settings. The research design for the acids test was predicated on the hypothesis that the greatest acid formation would be at lower power levels. This "worst case" premise lead the researchers to design the experiment in such a way as to collect more numerous samples at lower power settings. The suggestion of a trend established by the limited number of 75% power points indicated that greater numbers of samples at high power conditions may have been warranted. As in the data for formic and acetic acids, the data on the formation of combustion acids was not as definitive as anticipated by the researchers. Results in each case did not yield any clear relationship between ethanol concentrations and acid levels in the exhaust.

Acetaldehyde - Figure 21 presents the effects of increasing ethanol concentrations on the levels of

acetaldehydes in the exhaust. A concern associated with the use of alcohol fuels is the production of aldehydes as combustion by-products. In an effort to determine if the production of aldehydes might be problematic when blending ethanol with Jet-A fuels, the research evaluated two of the principal aldehydes associated with alcohol fuel combustion, acetaldehyde and formaldehyde. Again, it was hypothesized that the production of aldehydes would be greater at lower power settings. Therefore, greater numbers of samples were taken at these levels. Samples taken for simulated power settings of 10% and 40% demonstrated a marked propensity to produce higher levels of acetaldehyde as ethanol levels in the test fuels were increased. A considerable diminished tendency was noted for 55% and 75% power levels. In fact, acetaldehyde levels for the 75% power setting showed no significant change from the Jet-A baseline for the limited samples taken.

Formaldehyde - Figure 22 presents the levels of formaldehyde produced at varying concentrations of ethanol. Tendencies to produce formaldehyde were less apparent due to widely scattered data. Results appear to indicate a significant increase in the formation of formaldehyde at idle power conditions. Relationships for other power settings are not clear. The limited data points sampled for the 75% power setting seems to suggested that formaldehyde levels may, in fact, be reduced as compared to the Jet-A fuel baseline. Widely scattered or limited results made it impossible to draw any clear relationships between formaldehyde levels in the exhaust and ethanol concentrations.

COMBUSTION EFFICIENCY

Combustion efficiency was calculated according to Hardin's equation presented earlier and data points plotted in an effort to delineate any relationship between the blending rates of ethanol in the test fuels and changes in combustion efficiency. Figure 23 presents the calculated combustion efficiencies for nominal fuel flow conditions. Results indicated a dramatic decline in combustion efficiency as ethanol concentrations were increased. This reduction in combustion efficiency was more pronounced for lower power conditions than for cruise or climb power. Figure 24 represents the results for compensated fuel flow conditions. Testing at energy compensated fuel flow values produced somewhat lower rates of degradation in the combustion efficiency but the trend was still quite noticeable. Generally, the results suggested that as concentrations of ethanol increased in the test fuel, a marked deterioration occurred in combustion efficiency. This effect was greatest at lower power settings.

COMBUSTOR LINER TEMPERATURE

Figures 25 through 32 present the thermocouple readings for each of the power conditions for both nominal and energy compensated fuel flow rates. Data represents thermocouples placed in each of the burner's principal combustion zones (Figure 1) commencing with one on the assembly's dome (TC #16), one in the primary zone (TC #17), one in the secondary zone (TC #18), one in the quench zone (TC #19), and one in the exhaust region (TC #20). Of specific interest in evaluating the temperature plots were converging or diverging projection lines indicative of changes in the heating pattern of the liner. Any alteration in this pattern could indicate that the position of the flame front was changing. Such a change could affect the viability of the fuel since it could result in reduced engine life or damage.

Nominal Fuel Flow Conditions - Figures 25 through 28 present the thermocouple measurements for each power condition under nominal fuel flow rates. Results for each of the blended fuels showed a slight reduction in combustor liner temperatures over the range of ethanol concentrations. Erratic readings were recorded for thermocouple #19 approximately midway through the fuel testing sequence. The data plot for TC #19 beginning on Figure 24 represents the widely varied readings realized from this probe. Experienced test cell technicians working on the study indicated that the observations were consistent with thermocouple readings from probes which had separated from their welded positions on the liner. These data points were, therefore, regarded as unreliable and not representative of actual liner readings.

Energy Compensated Fuel Flow Conditions - Figures 29 through 32 present the data for each of the power settings under energy compensated fuel flow conditions. Results from these tests also showed a trend of slightly reduced liner temperatures. The degree of variation, however, between the Jet-A baseline values and those over the range of test fuels was not nearly as pronounced as those under nominal fuel flow conditions. Again, the readings for thermocouple number 19 were deemed unreliable in Figures 30, 31, and 32.

EXHAUST TEMPERATURE DISTRIBUTION

Turbine damage noted in previous studies raised concerns among the researchers that ethanol blending of turbine fuels may have caused a change in flame structure. One of the most plausible explanations for the turbine wheel erosion experienced in previous research studies was that turbine

inlet temperatures or the exhaust temperature distribution of the engine may have been adversely affected when ethanol was added to the fuel. This facet of the study was performed to evaluate the effects of increasing ethanol concentrations on turbine inlet temperatures and exhaust temperature distribution.

Nominal Fuel Flow Conditions - Figures 33 through 36 present the exhaust distribution for each power condition under nominal fuel flow rates. Exhaust temperatures were dramatically reduced as ethanol concentrations in the test fuel increased under nominal fuel flow conditions. This trend was anticipated since, as ethanol blending rates increased, the BTU content of the fuel was greatly diminished from that of Jet-A. This trend was replicated across all four simulated power conditions and resulted in changes in exhaust temperatures which approached five hundred degrees Fahrenheit. The lack of convergence or divergence in the temperature plots indicates no apparent change in the exhaust temperature distribution across the range of fuels tested. No adverse effects were noted for the increasing concentrations of ethanol in the test fuel except for the dramatic reduction in exhaust temperature. This condition would result in less energy being available to the turbine section which should produce a correlative loss in engine power.

Energy Compensated Fuel Flow Conditions - Figures 37 through 40 present the exhaust temperatures for each power condition under energy compensated fuel flow rates. The figures clearly indicate that a much less conspicuous decline in exhaust temperatures was observed under energy compensated fuel flow conditions. Since the fuel had, theoretically, the same energy content as the Jet-A base fuel, no reduction in temperatures was anticipated. Although a reduction in temperature was observed, the gradient of change in temperature was much less pronounced than for the nominal fuel flow conditions. Of greatest importance was the fact that the experiment gave no evidence that increasing concentrations of ethanol caused significant changes in the exhaust temperature distribution or gave indication of dangerous increases in temperature. The empirical data suggests that turbine damage sustained during earlier research was not caused by changes in flame propagation as a result of increasing concentrations of ethanol in the test fuels.

CONCLUSIONS

Results of the research generally supported implications by previous research as to the general viability of ethanol blended turbine fuel for use in unmodified aircraft turbine engines. Combustor lining temperature measurements suggested that there was little change in the propagation of the flame front within the combustor when tested over the range of the various fuel blends. Combustion exhaust distribution demonstrated little change over the range of fuels. Exhaust temperatures were proportionately lower for increasing ethanol blends at lower power settings, but remained nominal at higher power settings. Turbine inlet temperatures remained within nominal ranges and gave no indication of a propensity to cause turbine blade damage.

Fuel ignition points demonstrated a gradual decrease in the fuel flow necessary to cause ignition, while an increase in flow rate was noted for lean blow-out as ethanol concentrations were increased. These trends suggest easier starting but a slight decrease in flame stability as blending levels of ethanol increased. Although combustion efficiency was slightly affected by the increasing concentrations of ethanol in the test fuels, no significant loss in power was noted if fuel flow rates were adjusted to compensate for the lower BTU content of the fuels.

Particulate emission (smoke) was dramatically reduced with increased blending rates of ethanol. While the study did indicate marked reductions in carbon dioxide, oxides of nitrogen, and soot formation, unsupported were the Alabama study's claims of dramatically reduced carbon monoxide and hydrocarbon emissions. Also, adding ethanol to the jet fuel resulted in significant increases in exhaust aldehydes. The effects of ethanol concentrations on hydrocarbon, carbon monoxide, and aldehydes was greatest at low power settings, conditions typical of idle and taxi power conditions. This suggests that levels of hydrocarbons, carbon monoxide, and aldehydes would increase at airport locations if ethanol were to be blended into jet fuel. However, the dramatic reduction in oxides of nitrogen resulting from the addition of ethanol to jet fuel may prove to be of considerable importance in light of the recent identification of these pollutants as the most significant environmental turbine emission problem.

REFERENCES

1. Biehl, K. J., & Demko, P. S. (1990, May). Flight testing with ethanol in turboprop engines. In Proceedings of the 1990 AIAA/FAA Joint Symposium on General Aviation Systems (pp. 56-65). Ocean City, NJ: AIAA/FAA. (NTIS Report No. DOT/FAA/CT-90/11)
2. Block, M. S. (1988, September). ASTM Tests of Alcohols in Turbine Fuel. Atlantic City, NJ: Federal Aviation Administration Technical Center. Report No. DOT/FAA/CT-TN88/36.
3. Corp, P. K. (1988, July). Laboratory Investigations into the Effects of Adding Alcohol to Turbine Fuel. Atlantic City, NJ: Federal Aviation Administration Technical Center. Report No. DOT/FAA/CT-TN88/25.
4. Demko, P. S., & Biehl, K. J. Flight Testing With Ethanol in Turboprop Engines. Atlantic City, NJ: Federal Aviation Administration Technical Center. Flight Test Branch, ACN-360.
5. Eveleth, E. L. (1989). Ethanol and Methanol in Intermittent Combustion Engines. Philadelphia, PA: American Society for Testing and Materials. ASTM STP 1048.
6. Ferrara, A. M. (1988, June). Alternate Fuels for General Aviation Aircraft with Spark Ignition Engines. Atlantic City, NJ: Federal Aviation Administration Technical Center. Report No. DOT/FAA/CT-88/05.
7. Ferrara, A. M., & Rea, C. (1990, February). In-Flight Evaluations of Turbine Fuel Extenders. Atlantic City, NJ: Federal Aviation Administration Technical Center. NTIS Report No. DOT/FAA/CT-89/33.
8. Ferrara, A. M. (1989, October). Turbine Fuel Alternatives (Near Term). Atlantic City, NJ: Federal Aviation Administration Technical Center. (NTIS Report No. DOT/FAA/CT-89/23)
9. Glaeser, J. S. (1990, August). Analysis of the T63-A-700 Engine used in Alcohol Turbine Fuel Extender Test. Atlantic City, NJ: Federal Aviation Administration Technical Center. Report No. DOT/FAA/CT-TN90/18.
10. Gupta, A., Kink, M. K., Daily, J., & Sabla, P. (1990, July). Combustion faces environmental challenges. Aerospace America, pp. 52-55.

11. Hardin, M. C. (1972, January 25). Addendum to Calculation of Combustion Efficiency and Fuel-Air Ratio from Exhaust Gas Analysis (Report No. 71-28). Detroit Diesel Allison Division/General Motors Corporation, Indianapolis, IN.
12. Hardin, M. C. (1973, July). Calculation of Combustion Efficiency and air-Fuel Ratio from Exhaust Gas Analyses (Report No. 73-48). Detroit Diesel Allison Division/General Motors Corporation, Indianapolis, IN.
13. Kandebo, S. W. (1991, November 25). Advanced combustors under development to cut emissions in conventional engines. Aviation Week & Space Technology, 135(21), 51-54.
14. Kandebo, S. W. (1991, November 25). NASA-industry propulsion team addressing HSCT environmental issues. Aviation Week & Space Technology, 135(21), 58-59.
15. Moses, C. A. (1973, December). Installation of Turbine-Fuels Research Combustor Laboratory. Report No. 27. San Antonio, TX: U. S. Army Fuels and Lubricants Research Laboratory, Southwest Research Institute.
16. Moses, C. A., Coon, C. W. (1976, September). Reduction of Exhaust Smoke from Gas-Turbine Engines by Using Fuel Emulsions. Report AFLRL No. 84. San Antonio, TX: U. S. Army Fuels and Lubricants Research Laboratory, Southwest Research Institute.
17. Moses, C. A. (1975). Studies of Fuel Volatility Effects on Turbine Combustor Performance. San Antonio, TX: U. S. Army Fuels and Lubricants Research Laboratory, Southwest Research Institute. Presentation at the 1975 Joint Spring Meeting of Western and Central States Sections of the Combustion Institute, San Antonio, TX.
18. Naegeli, D. W., & Moses, C. A. (1983). Fuel microemulsions for jet engine smoke reduction. Journal of Engineering for Power, 105(1), 18-23.
19. Ott, J. (1991, November 25). Future of global environment dictates airlines' agenda. Aviation Week & Space Technology, 135(21), 48-50.
20. Romano, R. (1989, June 8). T63-A-5A Engine Modified Fuel Evaluation. Final Report. Trenton, NJ: Department of the Navy, Naval Air Propulsion Center. Report No. NAPC-LR-89-12.
21. Wyman, V. (1990, May 31). Aircraft engines join thrust for lower emission levels. The Engineer, p. 50.

TABLE 1. T-63 Combustor Rig Nominal Operating Conditions

Mode	% Power	BIP kpa (psia)	BIT °C (°F)	w_a kg/s (lb/s)	w_f kg/m (lb/m)	F/A	BOT °C (°F)
Ground Idle	10%	252 (36.6)	149 (300)	0.699 (1.54)	0.46 (1.01)	.0109	561 (1042)
Descent	40%	363 (52.6)	204 (400)	0.948 (2.09)	0.74 (1.64)	.0131	699 (1290)
Cruise	55%	417 (60.5)	221 (430)	1.03 (2.27)	0.89 (1.97)	.0145	759 (1399)
Climb/Hover	75%	461 (66.9)	244 (472)	1.12 (2.46)	1.11 (2.45)	.0166	848 (1559)
Takeoff	100%	525 (76.2)	273 (524)	1.21 (2.66)	1.43 (3.16)	.0198	971 (1780)

Nomenclature

BIP: Burner Inlet Air Pressure
 BIT: Burner Inlet Air Temperature
 w_a : Air Flow Rate
 w_f : Fuel Flow Rate
 F/A: Fuel/Air Ratio
 BOT: Typical Burner Outlet Temperature

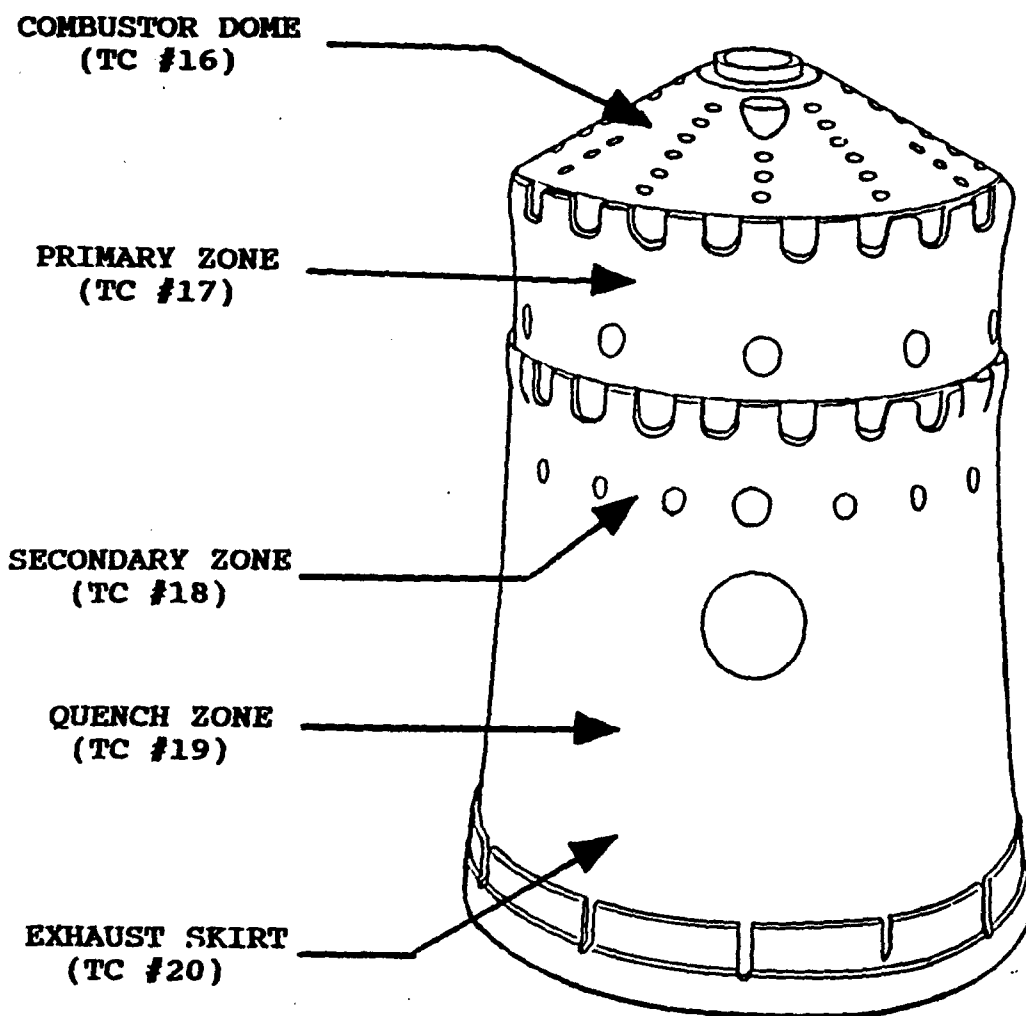


FIGURE 1. T-63 Combustor with Thermocouple Locations

EXHAUST TEMPERATURE Thermocouple Placement

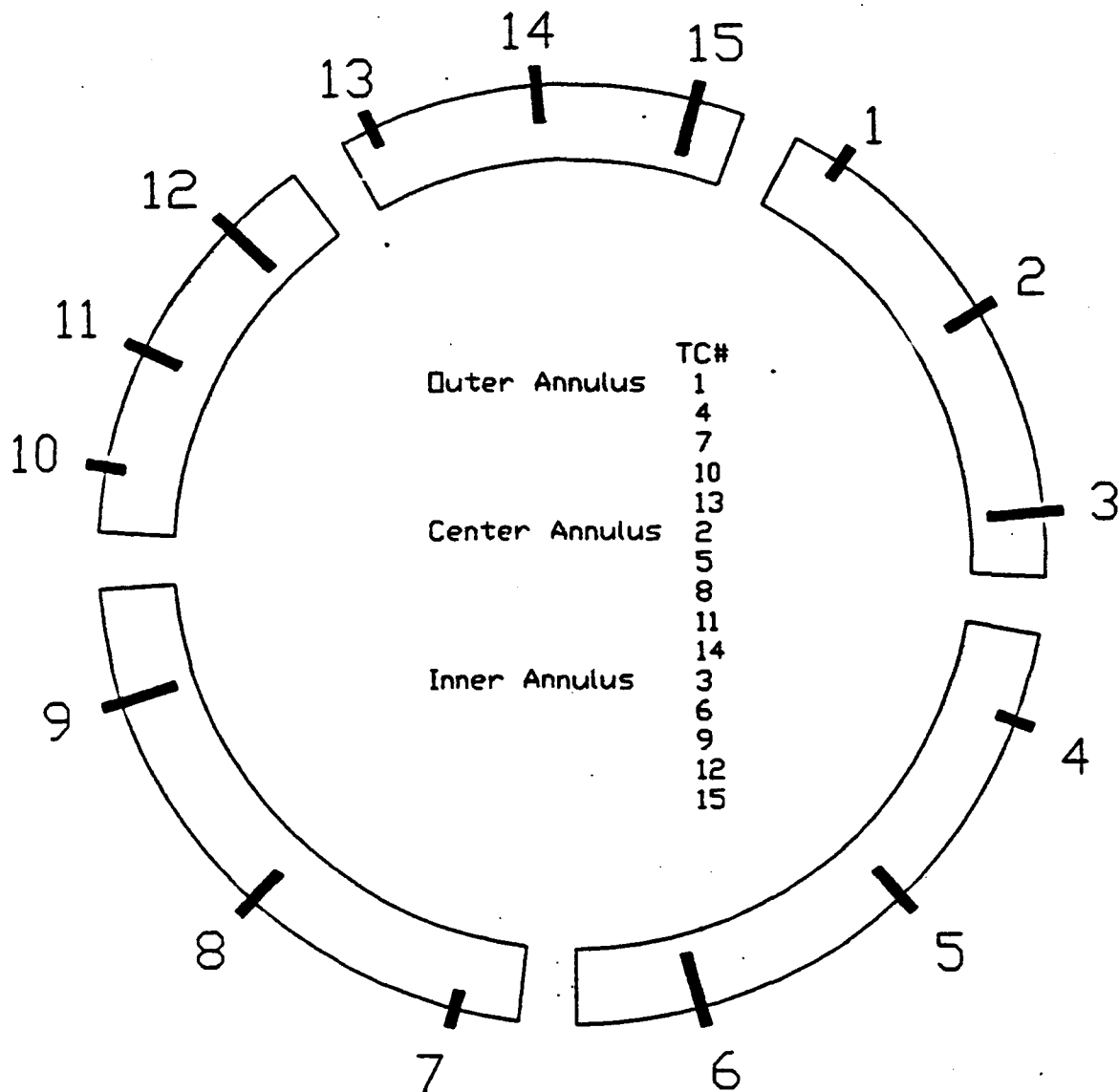


FIGURE 2. Exhaust temperature distribution test thermocouple probe placement in the exhaust annulus of the flame diverter at the combustor can exit. Probes were placed at varying depths to measure differences between exhaust temperatures at the outer, middle, and inner levels of the exhaust stream into the turbine section.

IGNITION POINT

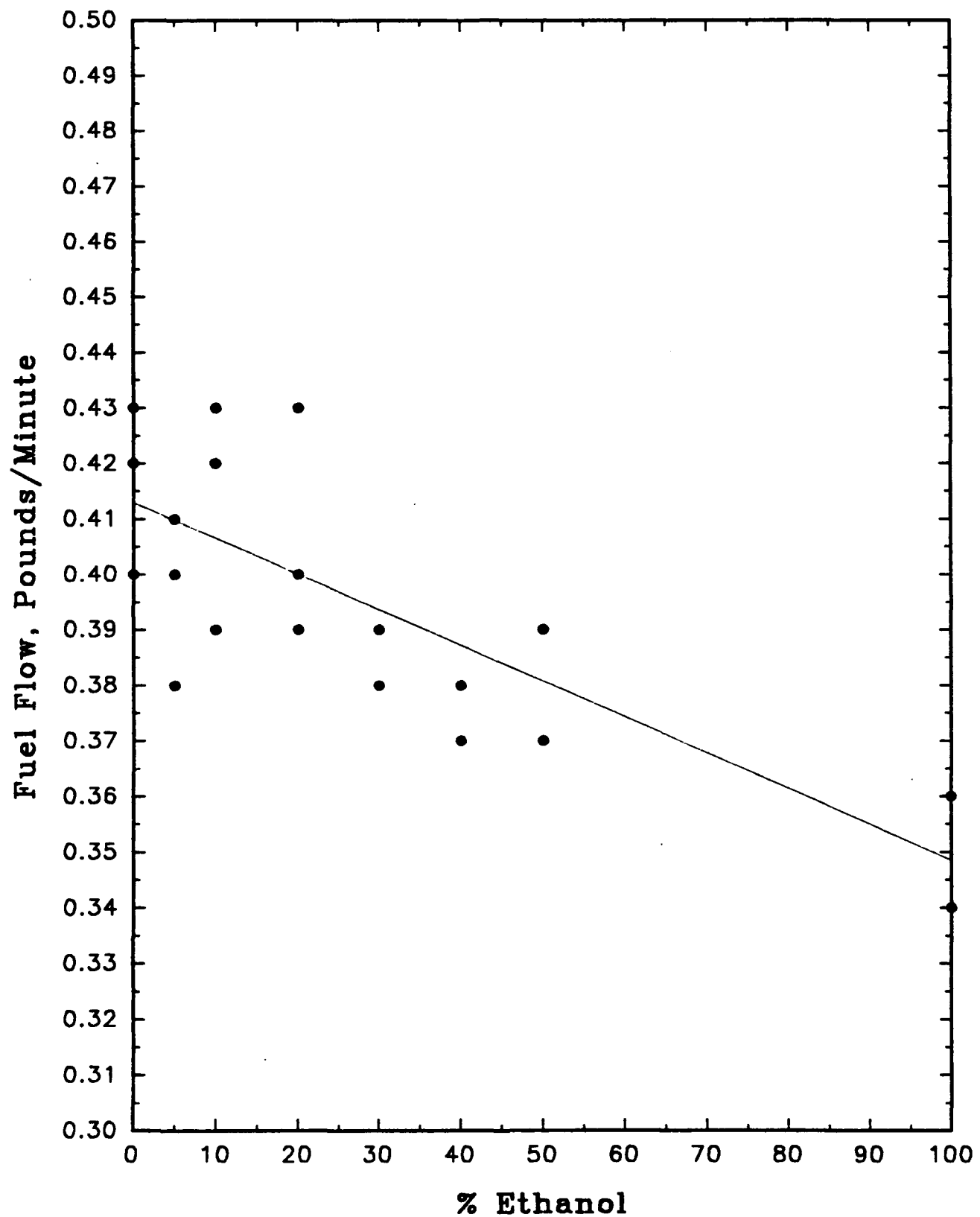


FIGURE 3. Effect of Ethanol Concentration on Minimum Fuel Flow Rate for Ignition

FLAME-OUT POINT

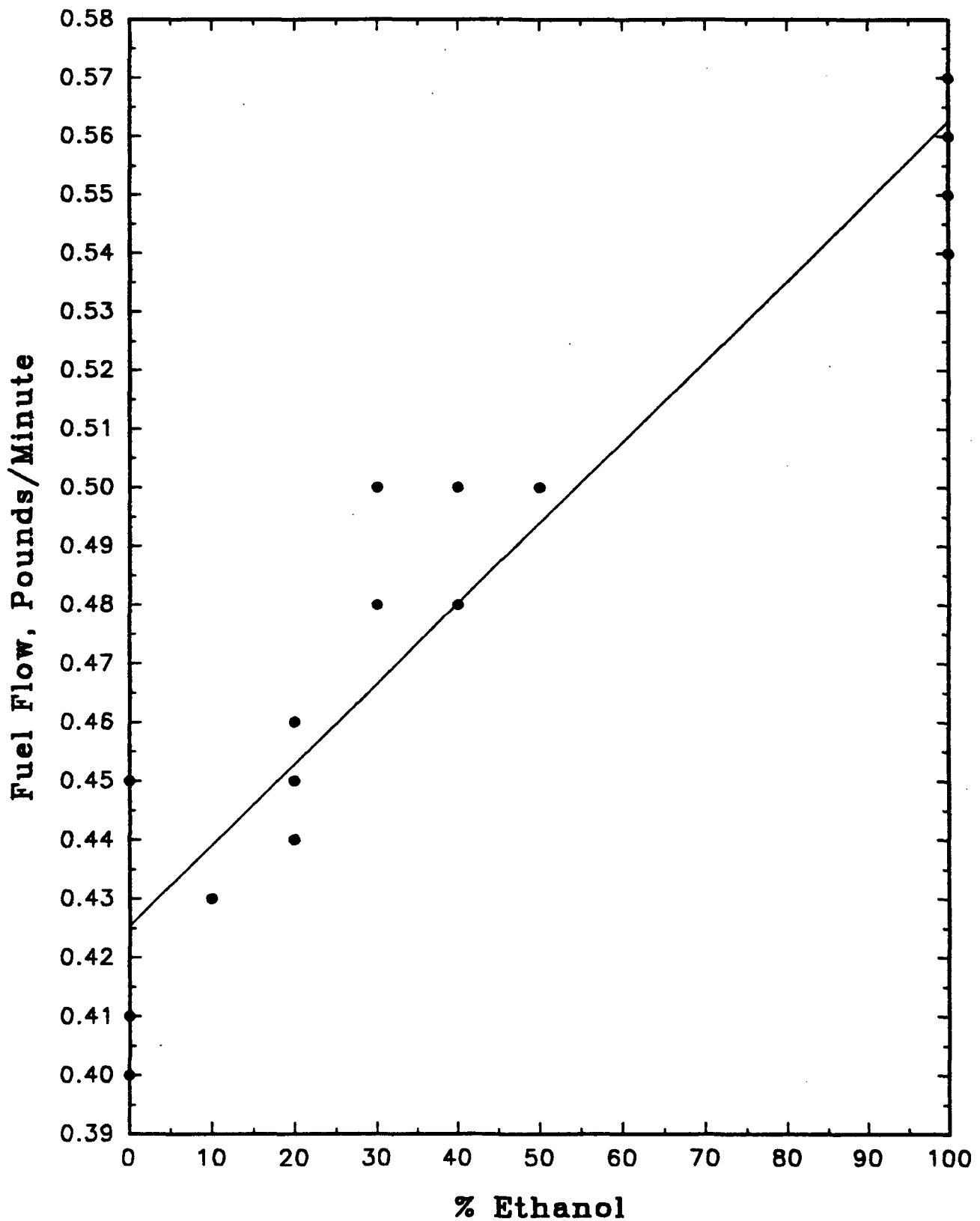


FIGURE 4. Effect of Ethanol Concentration on Lean Blow-out Limit

SMOKE NUMBER

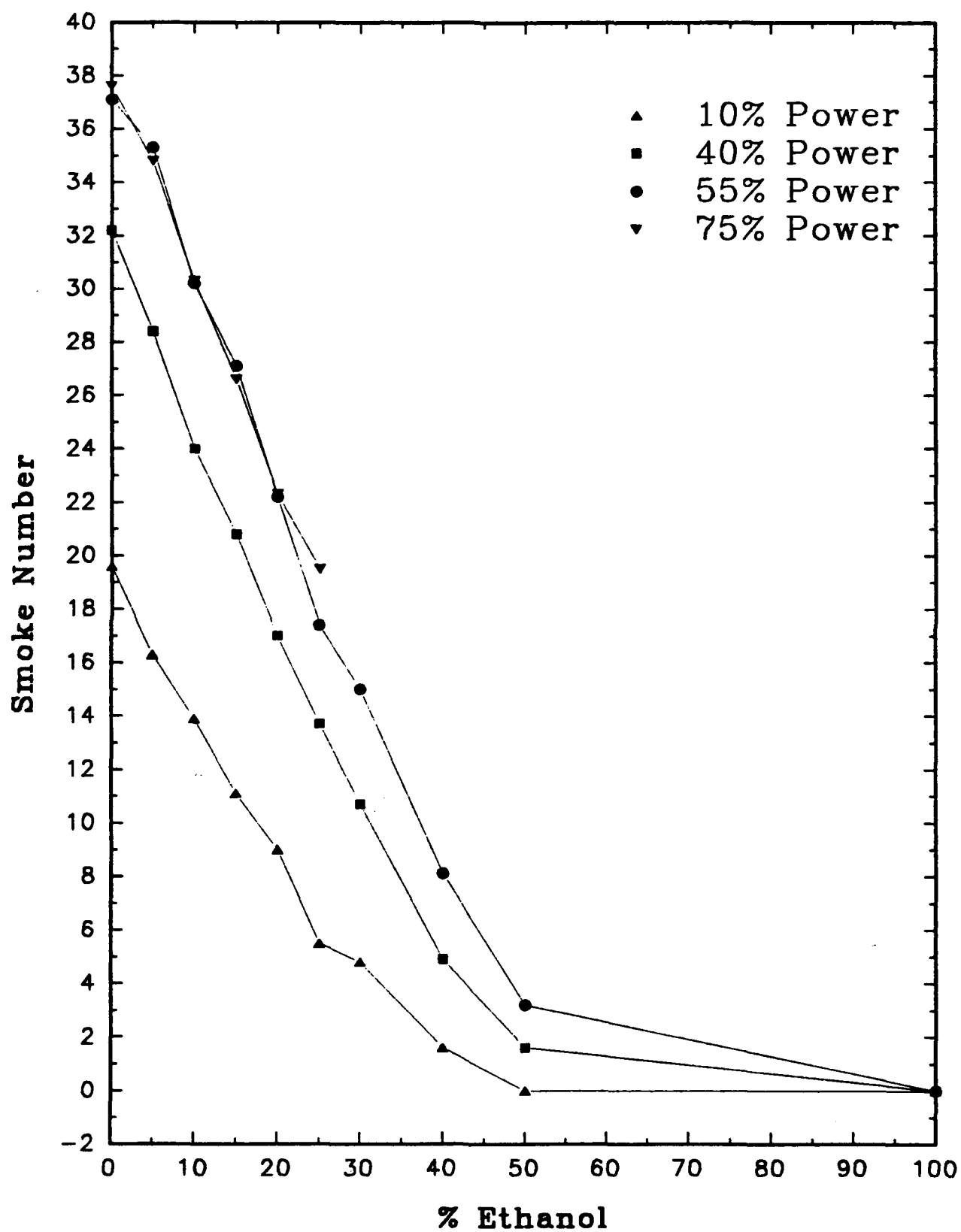


FIGURE 5. Effect of Ethanol Concentration on Exhaust Smoke

TOTAL HYDROCARBONS – NOMINAL

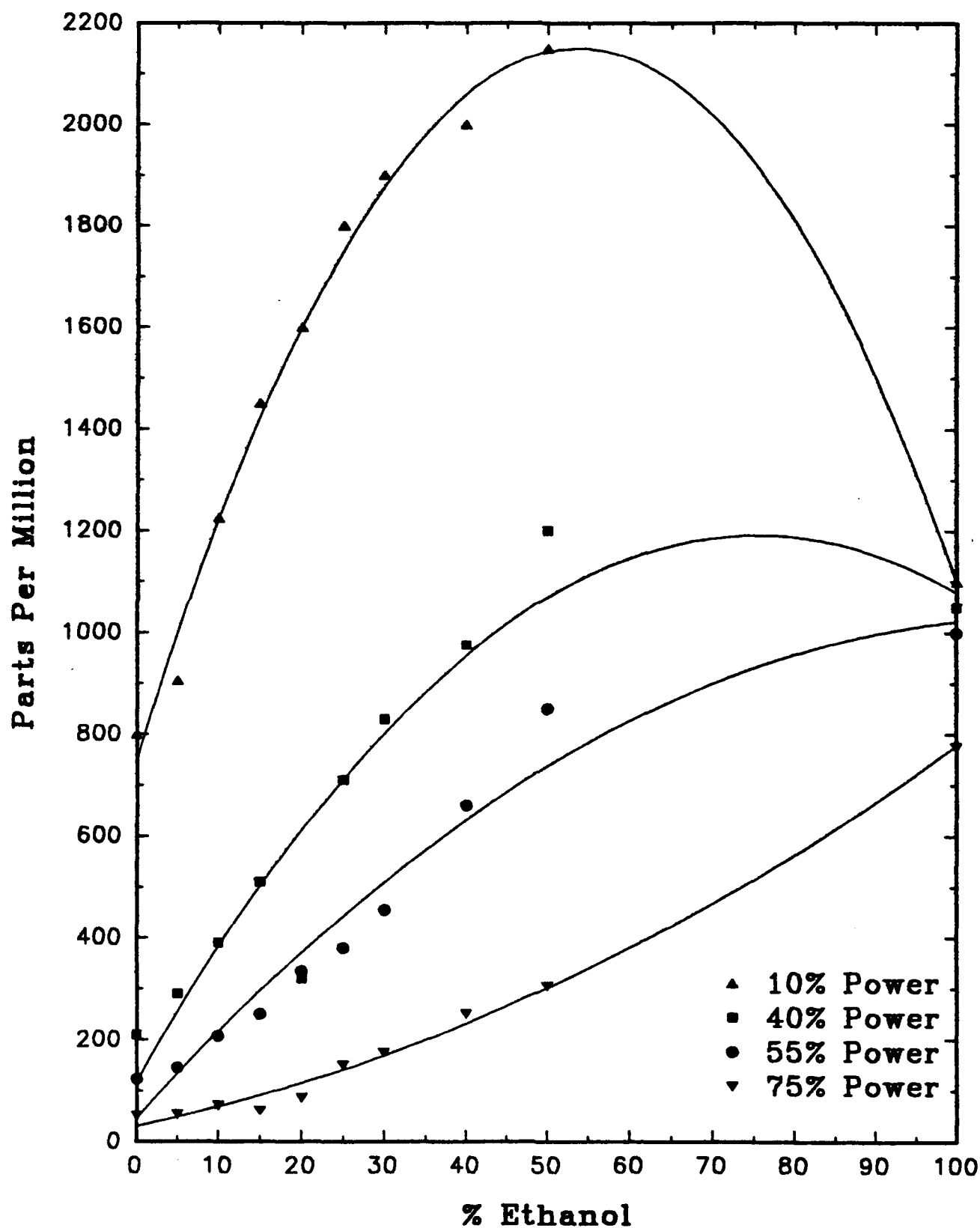


FIGURE 6. Effect of Ethanol Concentration on Exhaust Hydrocarbons at Constant Fuel Flow Rate

TOTAL HYDROCARBONS—COMPENSATED

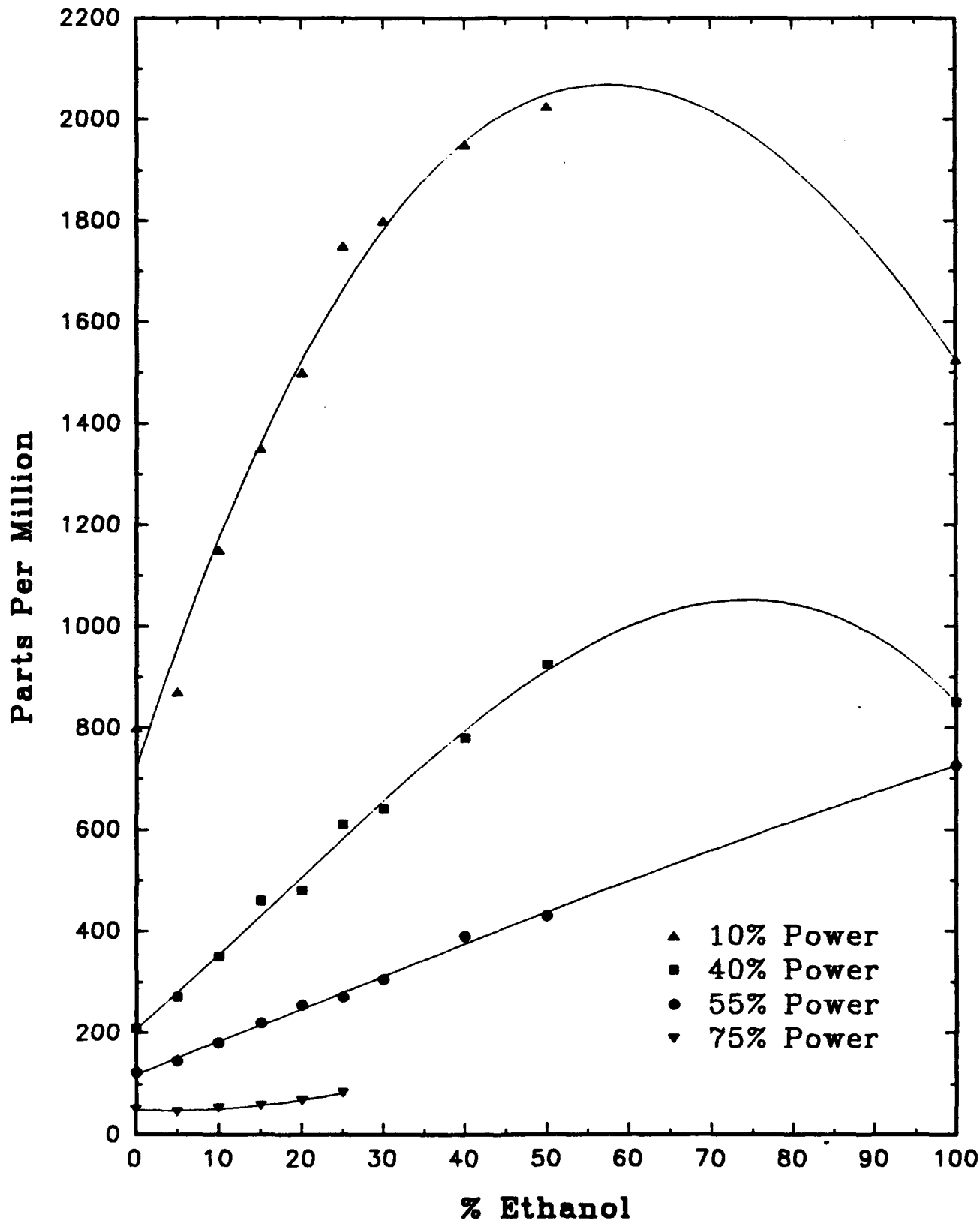


FIGURE 7. Effect of Ethanol Concentration on Exhaust Hydrocarbons at Constant Energy Input

CARBON DIOXIDE - NOMINAL

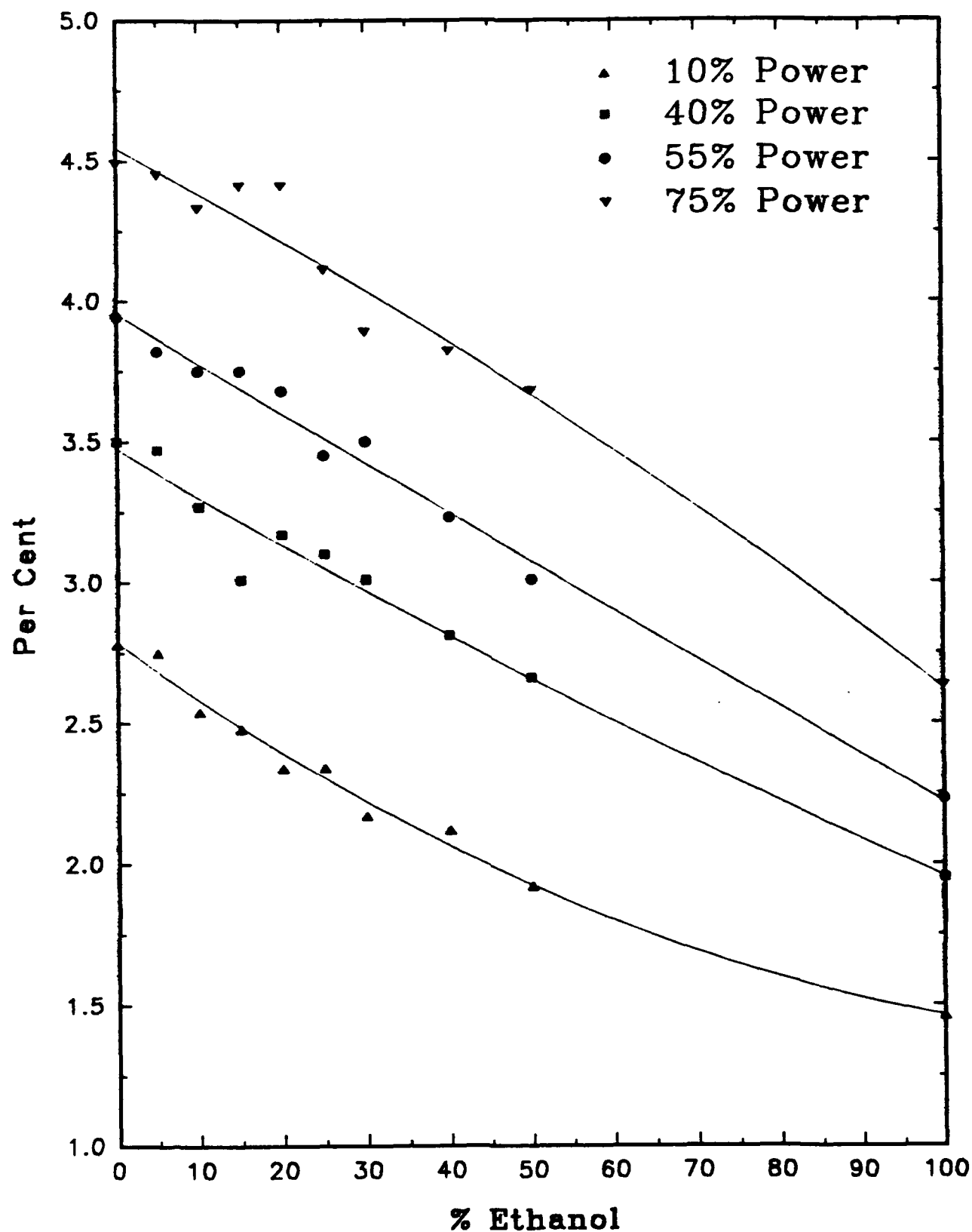


FIGURE 8. Effect of Ethanol Concentration on Carbon Dioxide at Constant Fuel Flow Rate

CARBON DIOXIDE - COMPENSATED

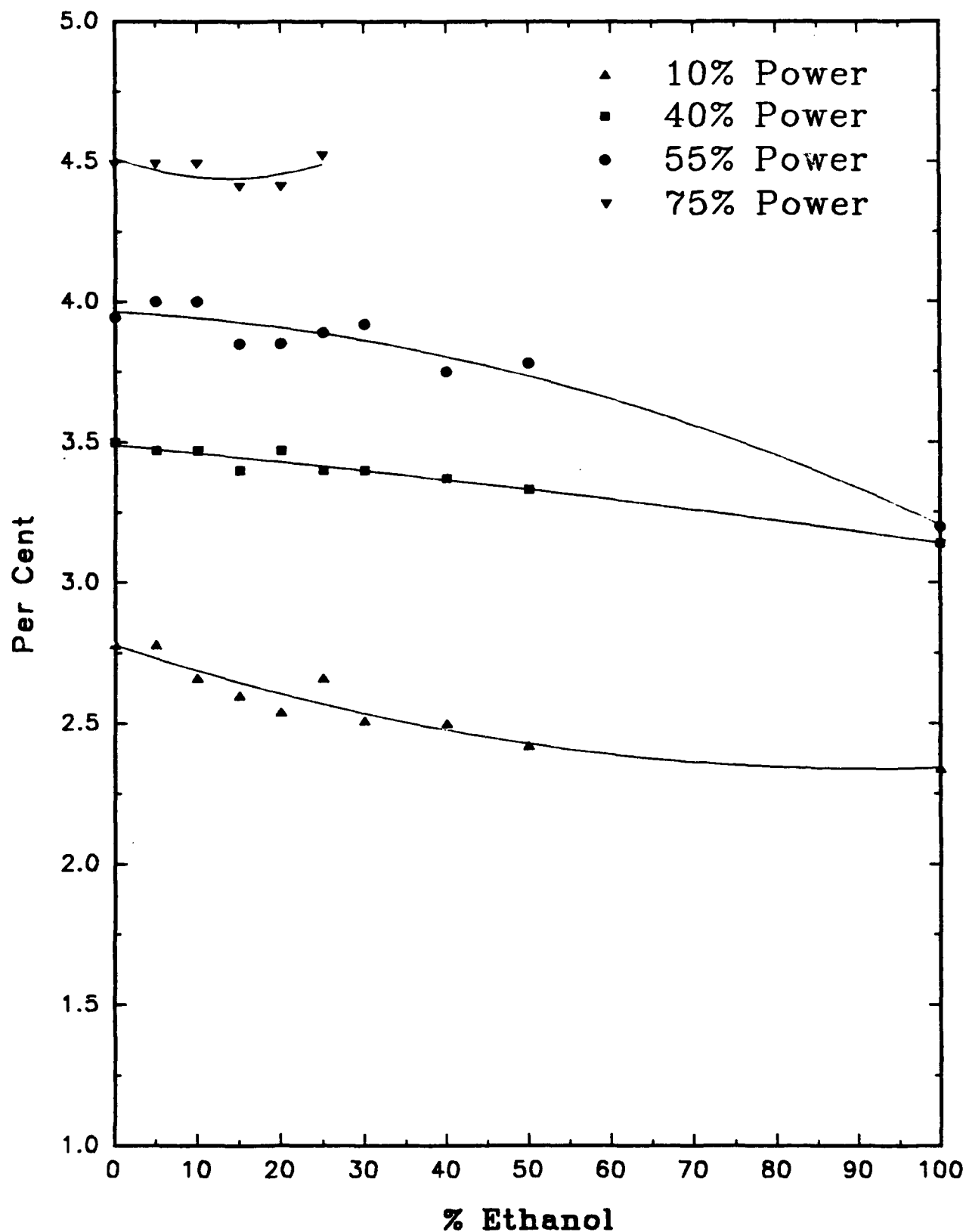


FIGURE 9. Effect of Ethanol Concentration on Carbon Dioxide at Constant Energy Input

CARBON MONOXIDE – NOMINAL

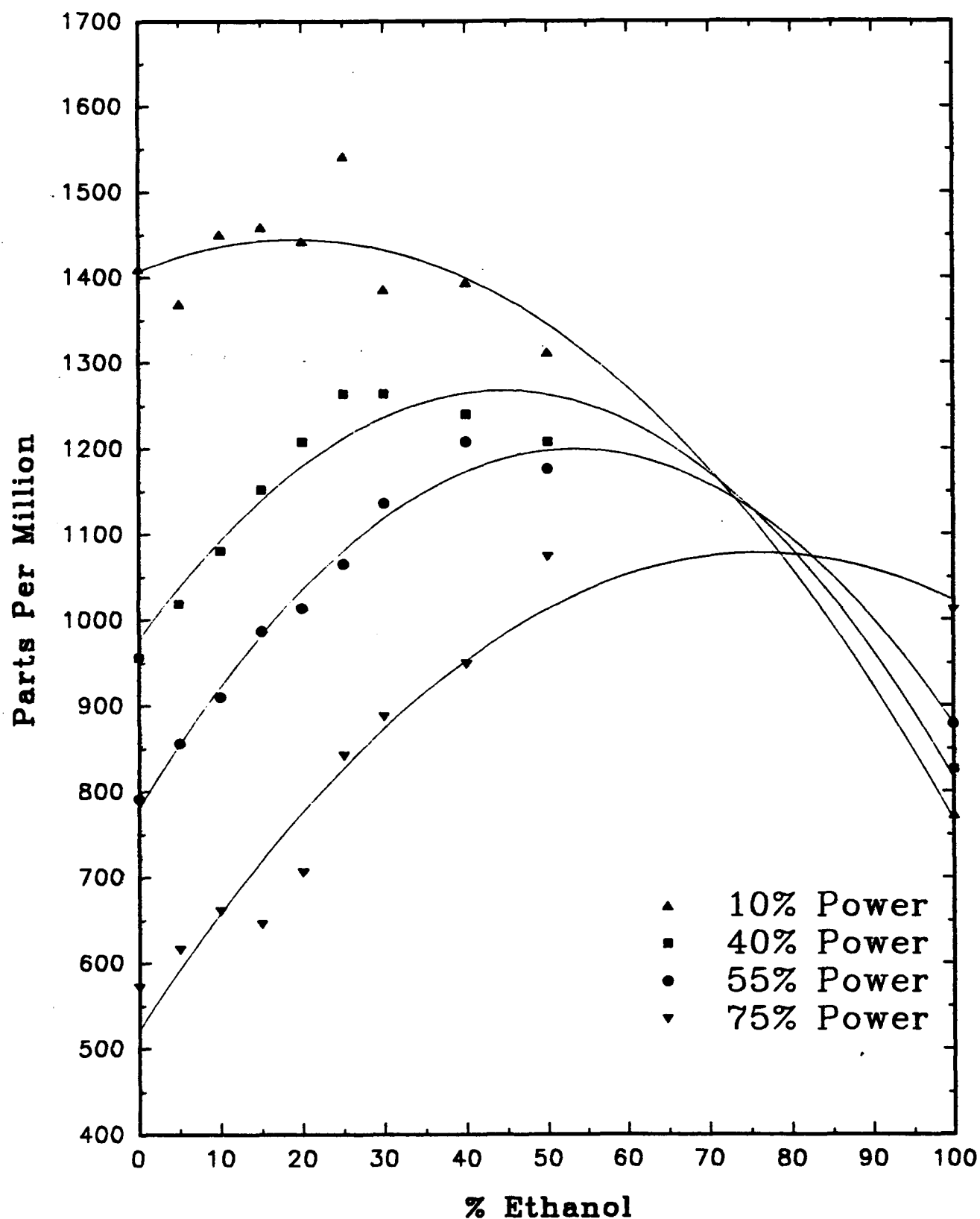


FIGURE 10. Effect of Ethanol Concentration on Carbon Monoxide at Constant Fuel Flow Rate

CARBON MONOXIDE-COMPENSATED

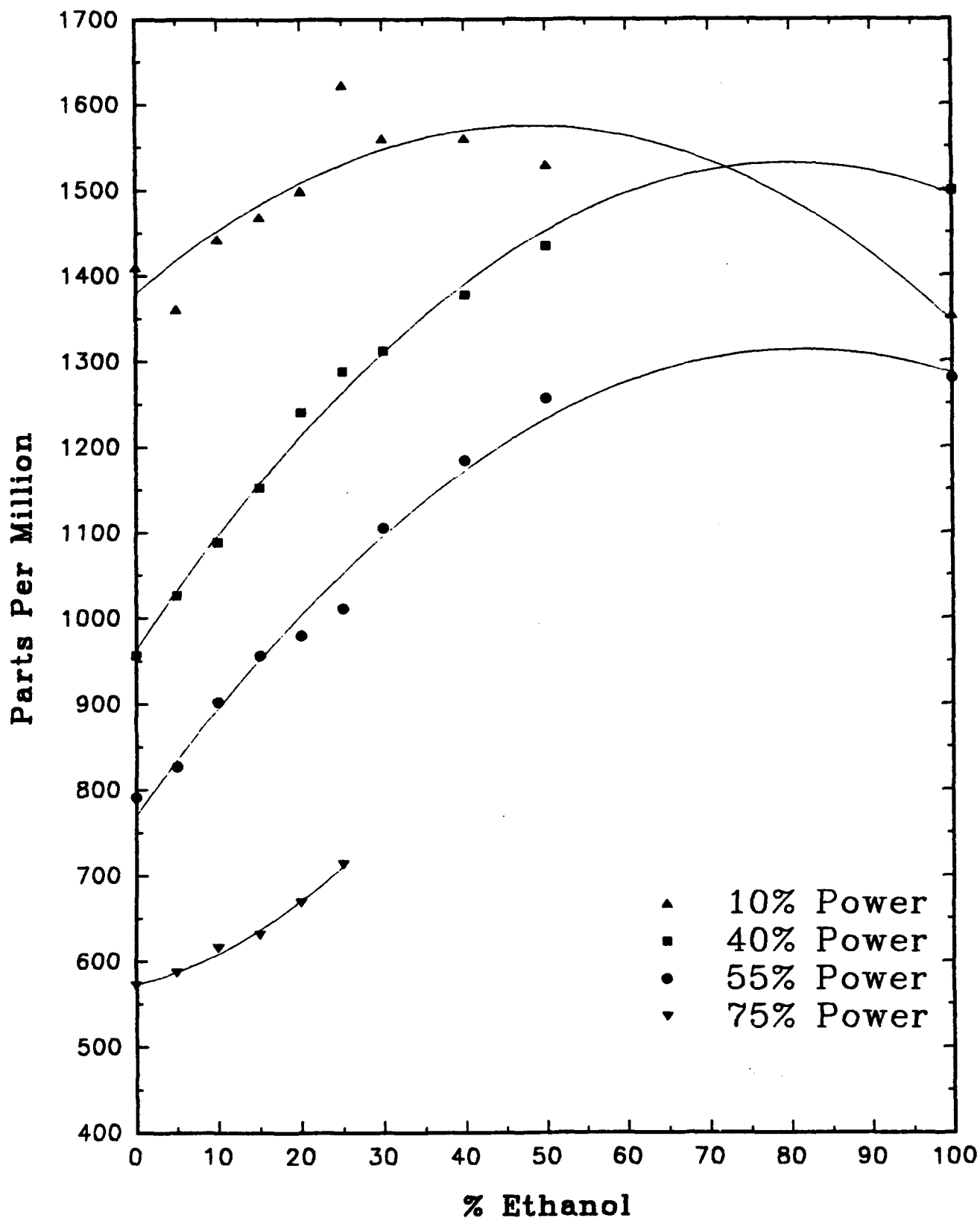


FIGURE 11. Effect of Ethanol Concentration on Carbon Monoxide at Constant Energy Input

OXIDES of NITROGEN—NOMINAL

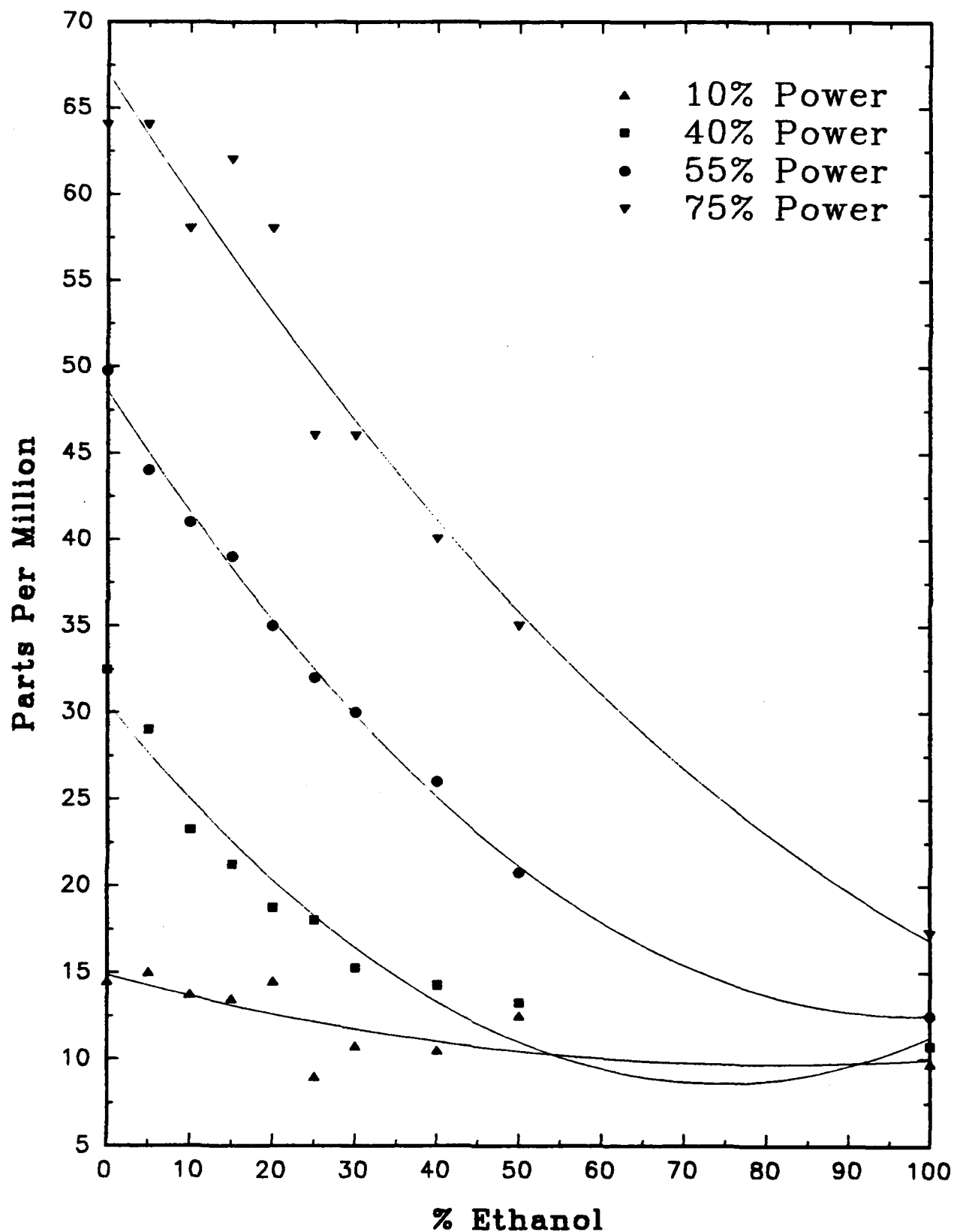


FIGURE 12. Effect of Ethanol Concentration on Oxides of Nitrogen at Constant Fuel Flow Rate

OXIDES of NITROGEN-COMPENSATED

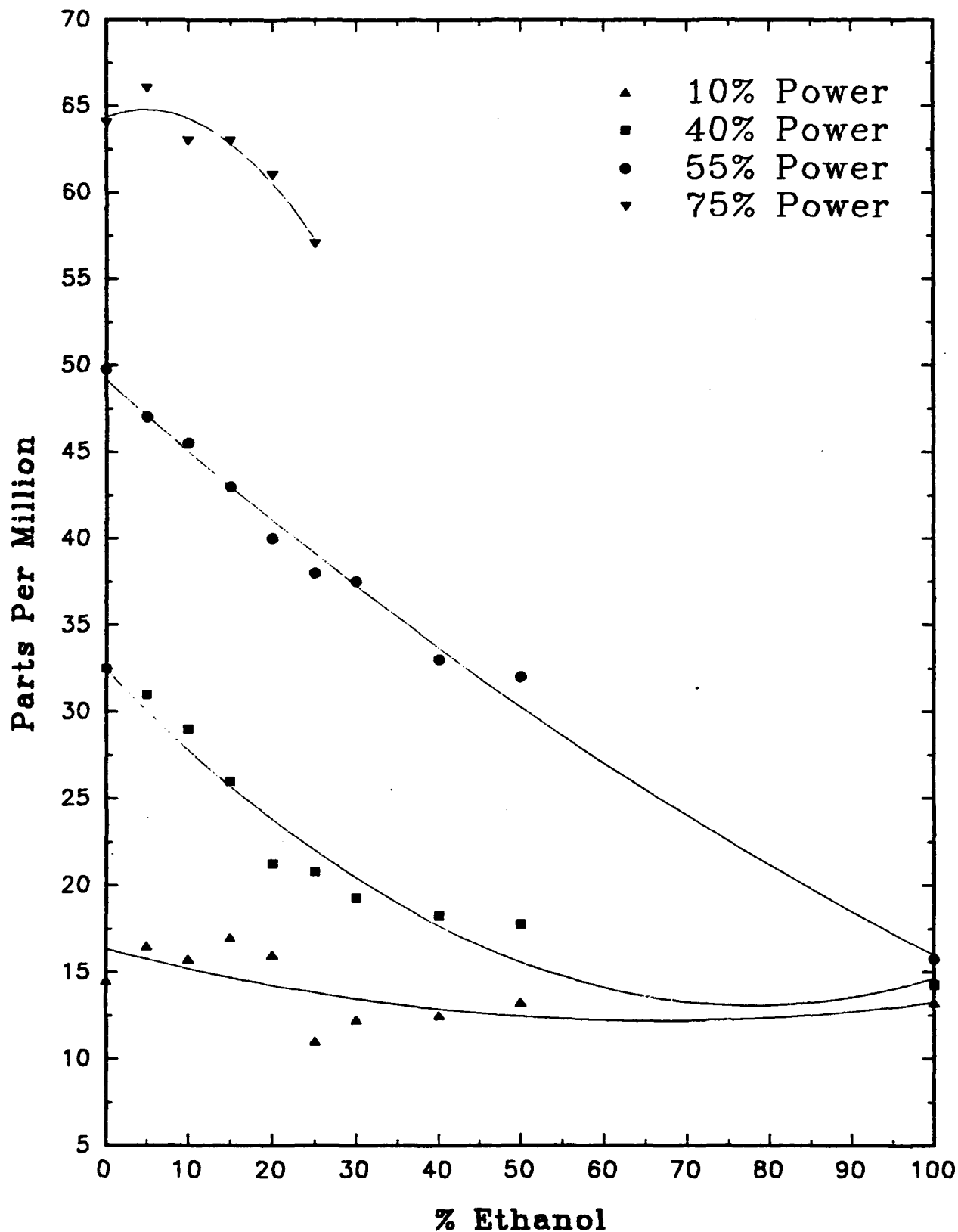


FIGURE 13. Effect of Ethanol Concentration on Oxides of Nitrogen at Constant Energy Input

NITRIC OXIDE - NOMINAL

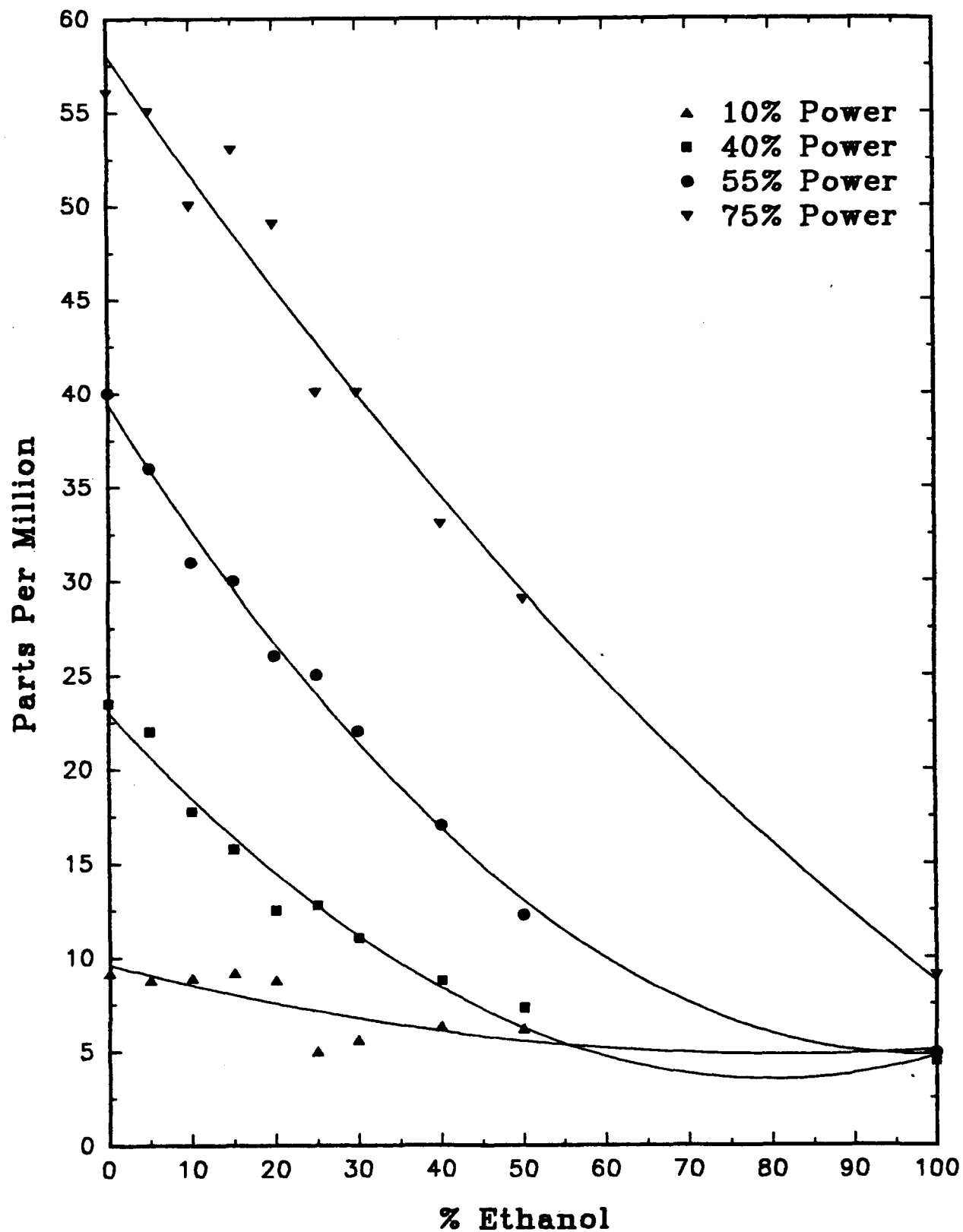


FIGURE 14. Effect of Ethanol Concentration on Nitric Oxide at Constant Fuel Flow Rate

NITRIC OXIDE - COMPENSATED

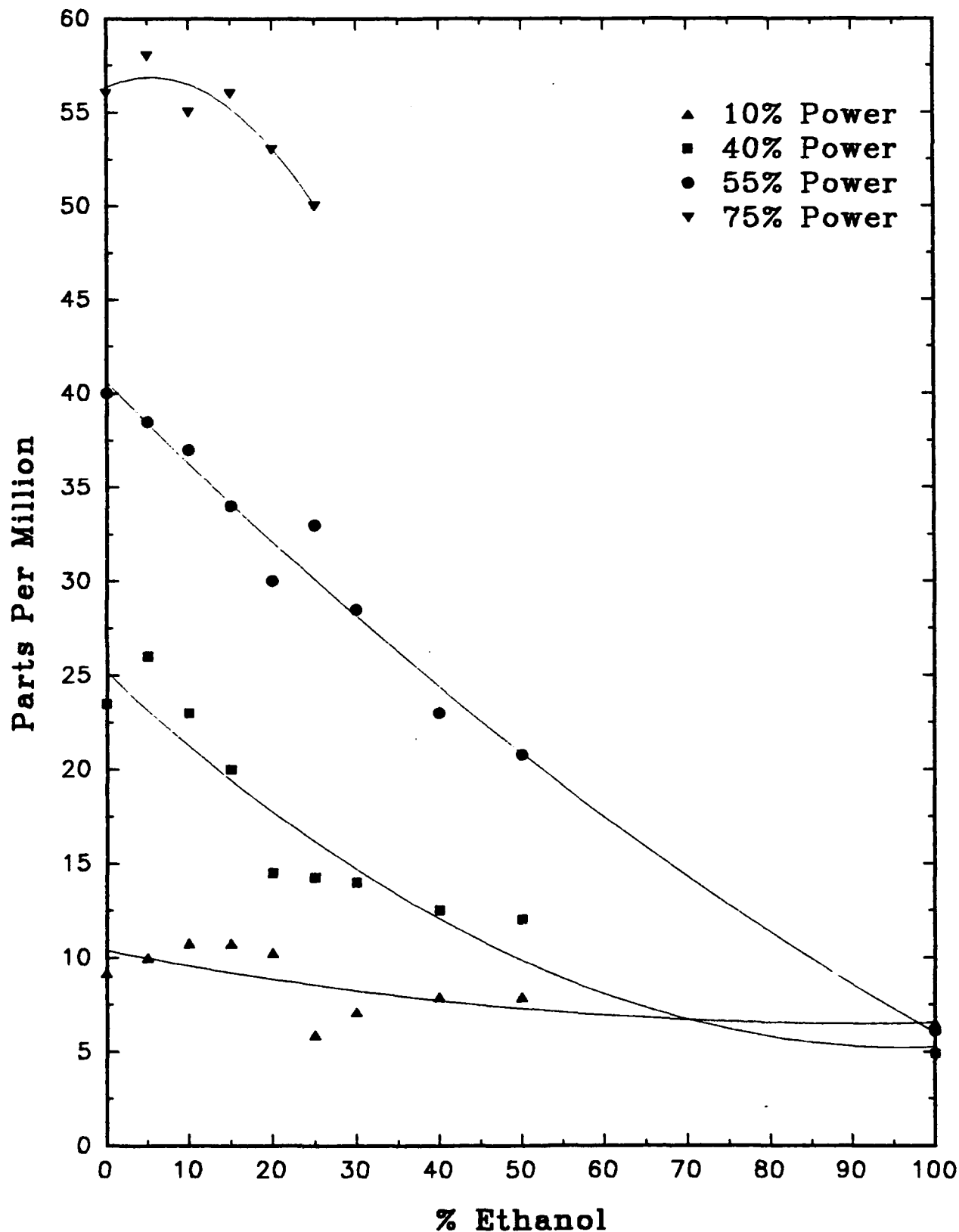


FIGURE 15. Effect of Ethanol Concentration on Nitric Oxide at Constant Energy Input

OXYGEN - NOMINAL

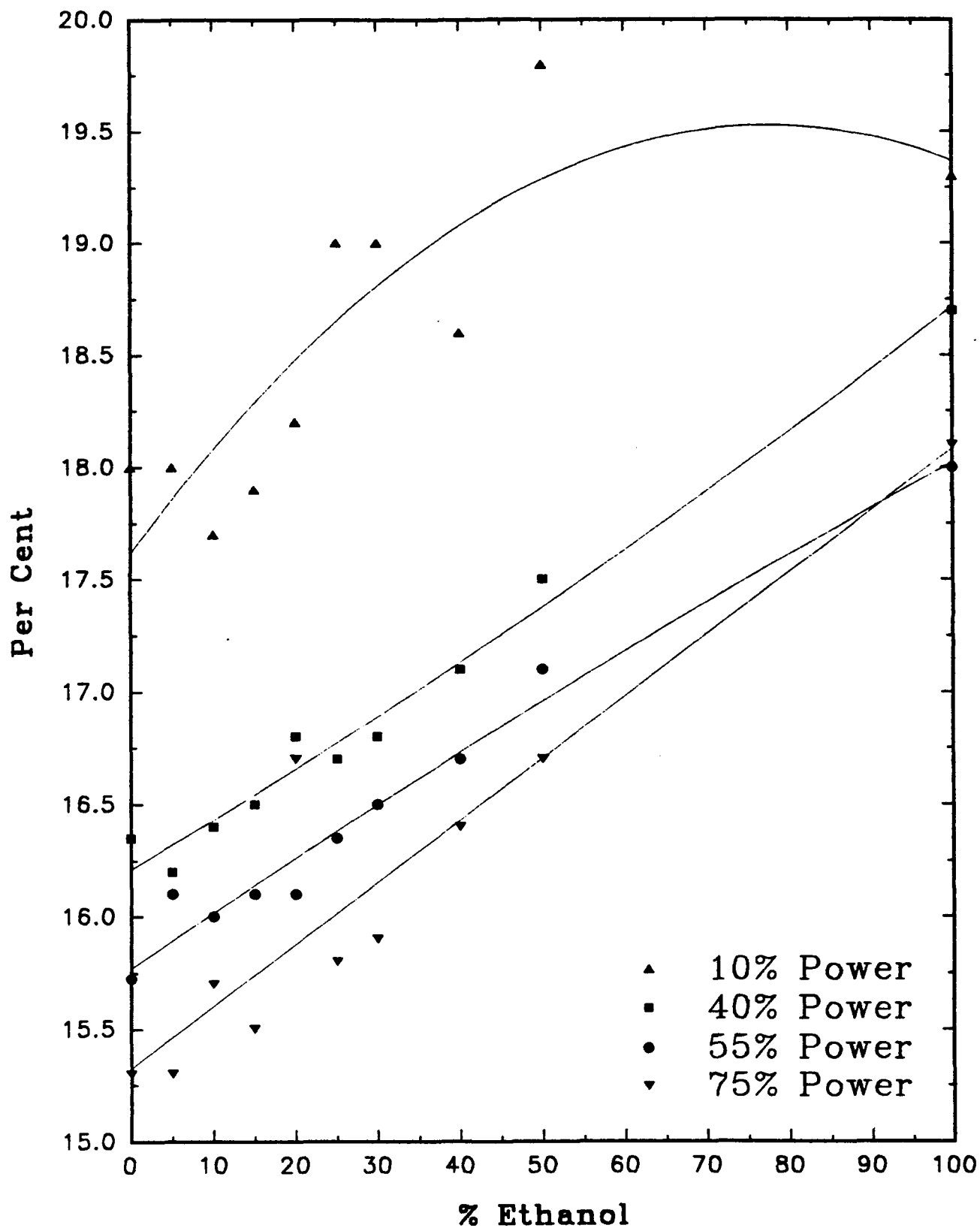


FIGURE 16. Effect of Ethanol Concentration on Oxygen in the Exhaust at Constant Fuel Flow Rate

OXYGEN - COMPENSATED

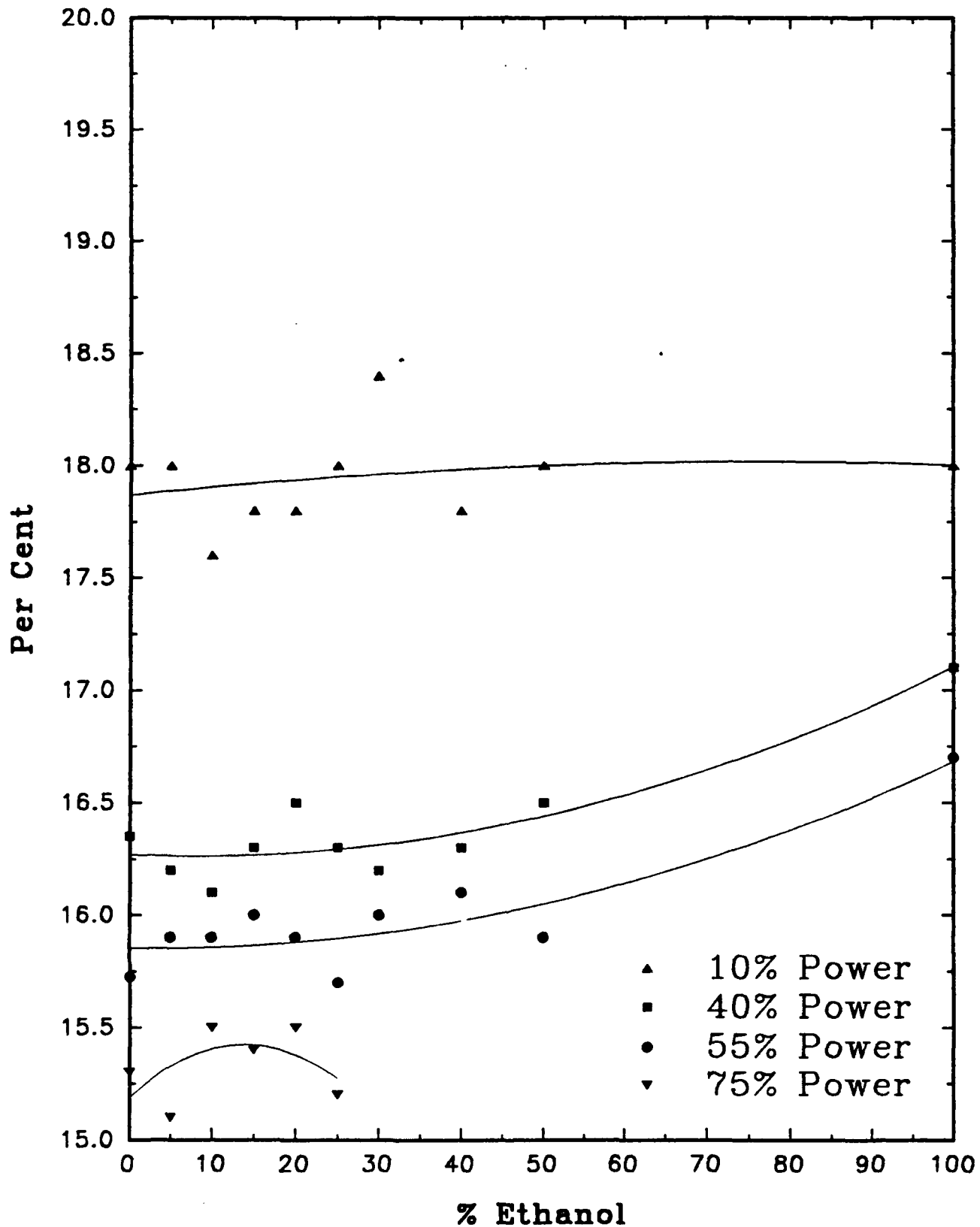


FIGURE 17. Effect of Ethanol Concentration on Oxygen in the Exhaust at Constant Energy Input

ACETIC ACID

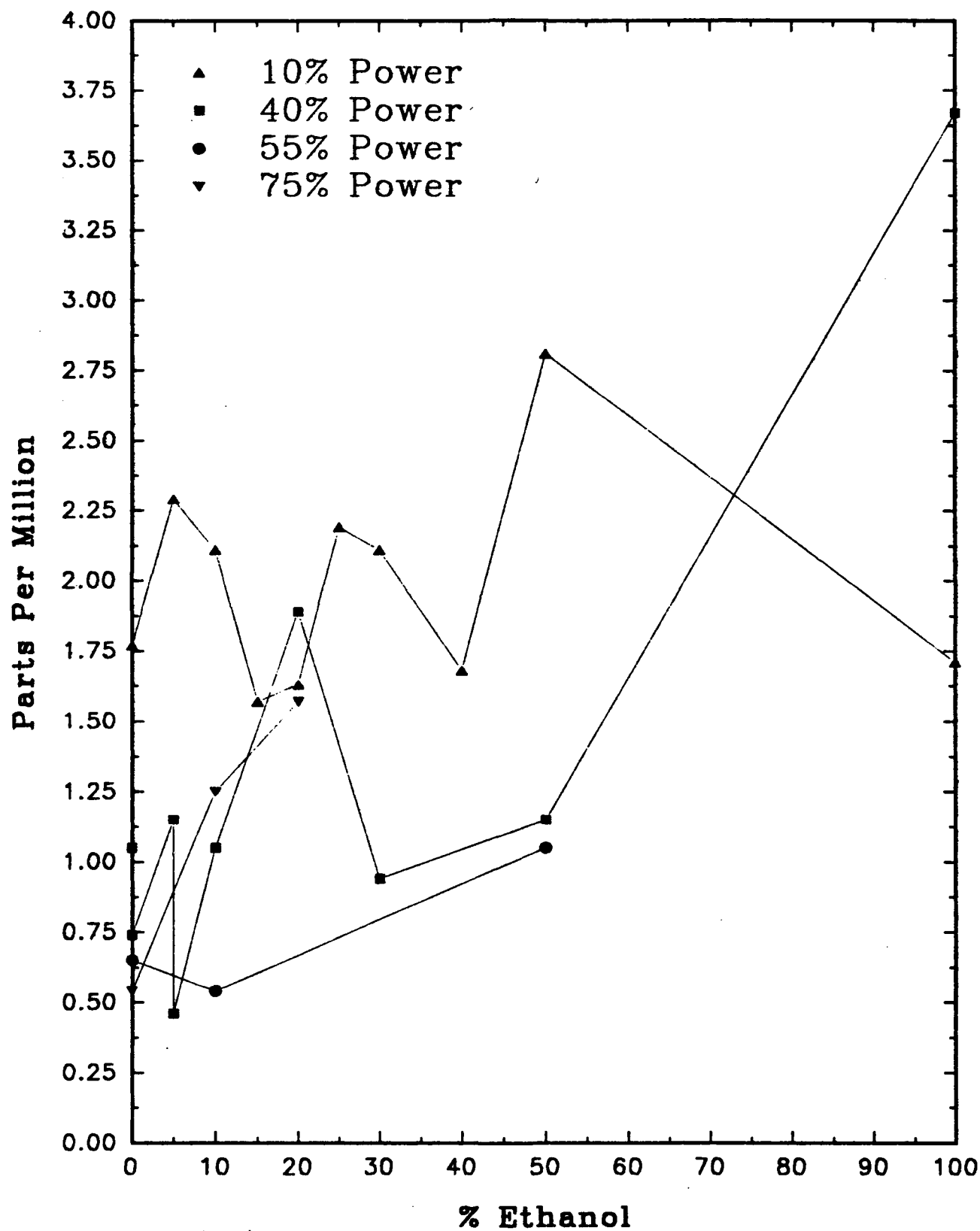


FIGURE 18. Effect of Ethanol Concentration on Acetic Acid in the Exhaust

FORMIC ACID

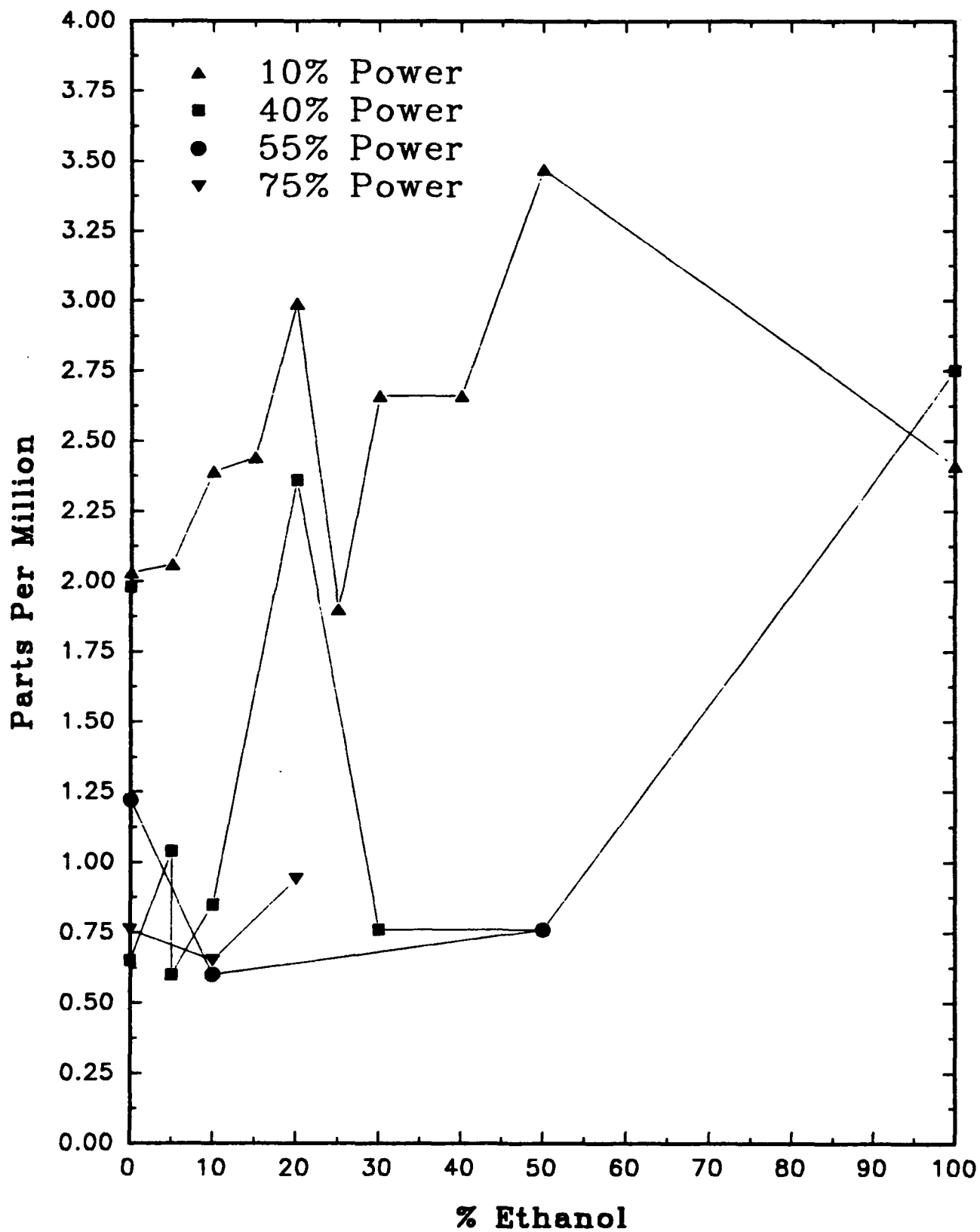


FIGURE 19. Effect of Ethanol Concentration on Formic Acid in the Exhaust

TOTAL ACIDS

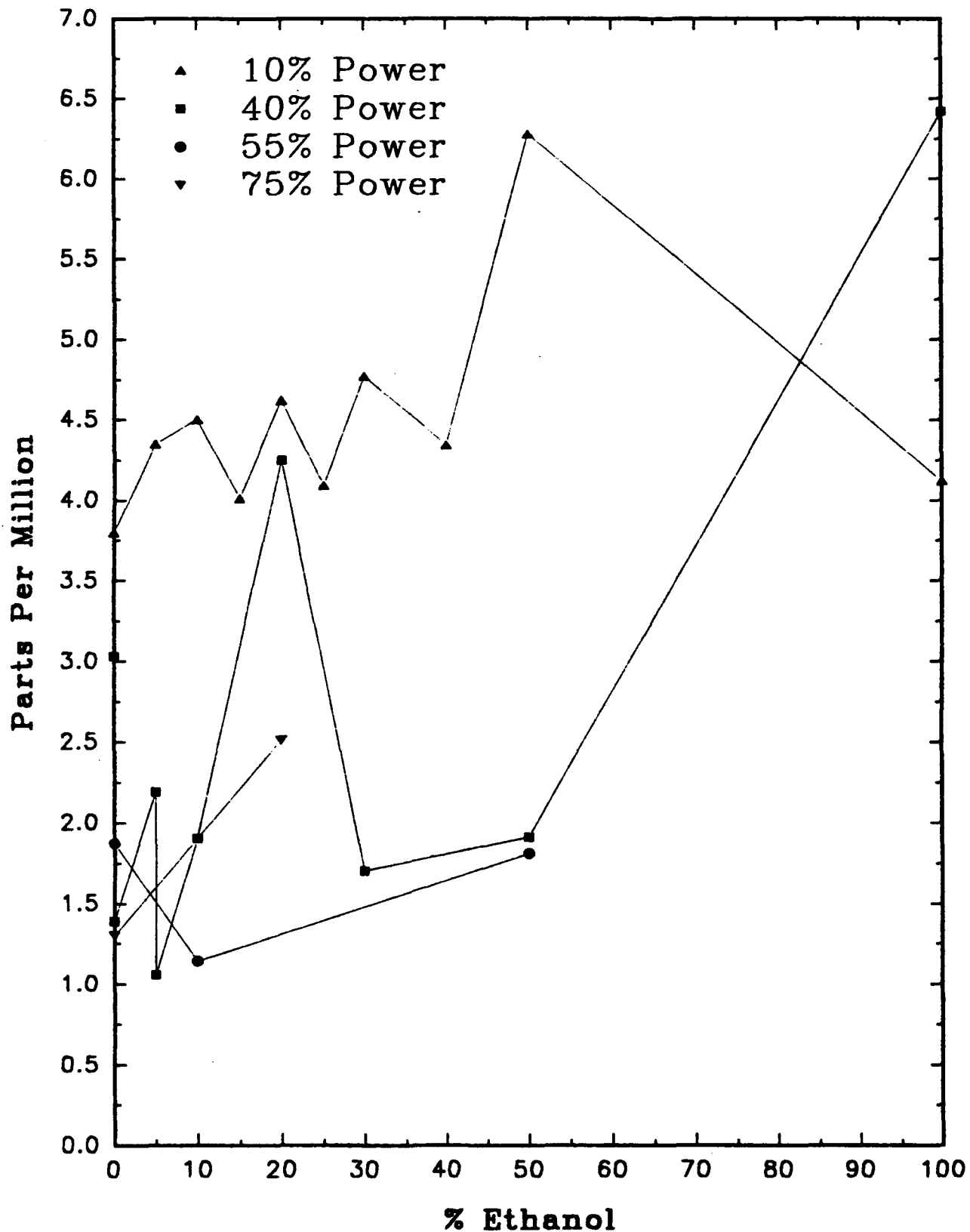


FIGURE 20. Effect of Ethanol Concentration on Total Acids in the Exhaust

ACETALDEHYDES

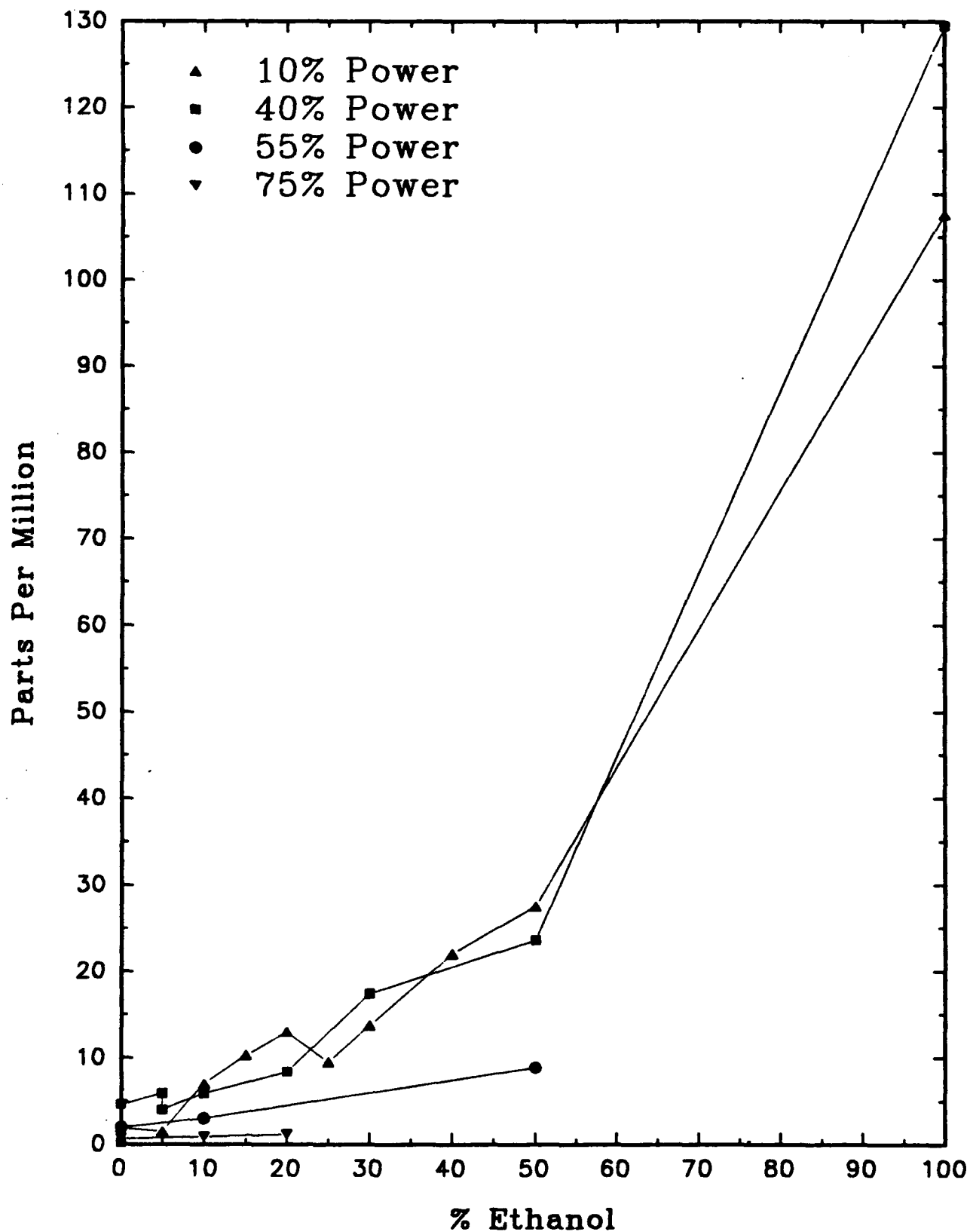


FIGURE 21. Effect of Ethanol Concentration on Acetaldehydes in the Exhaust

FORMALDEHYDES

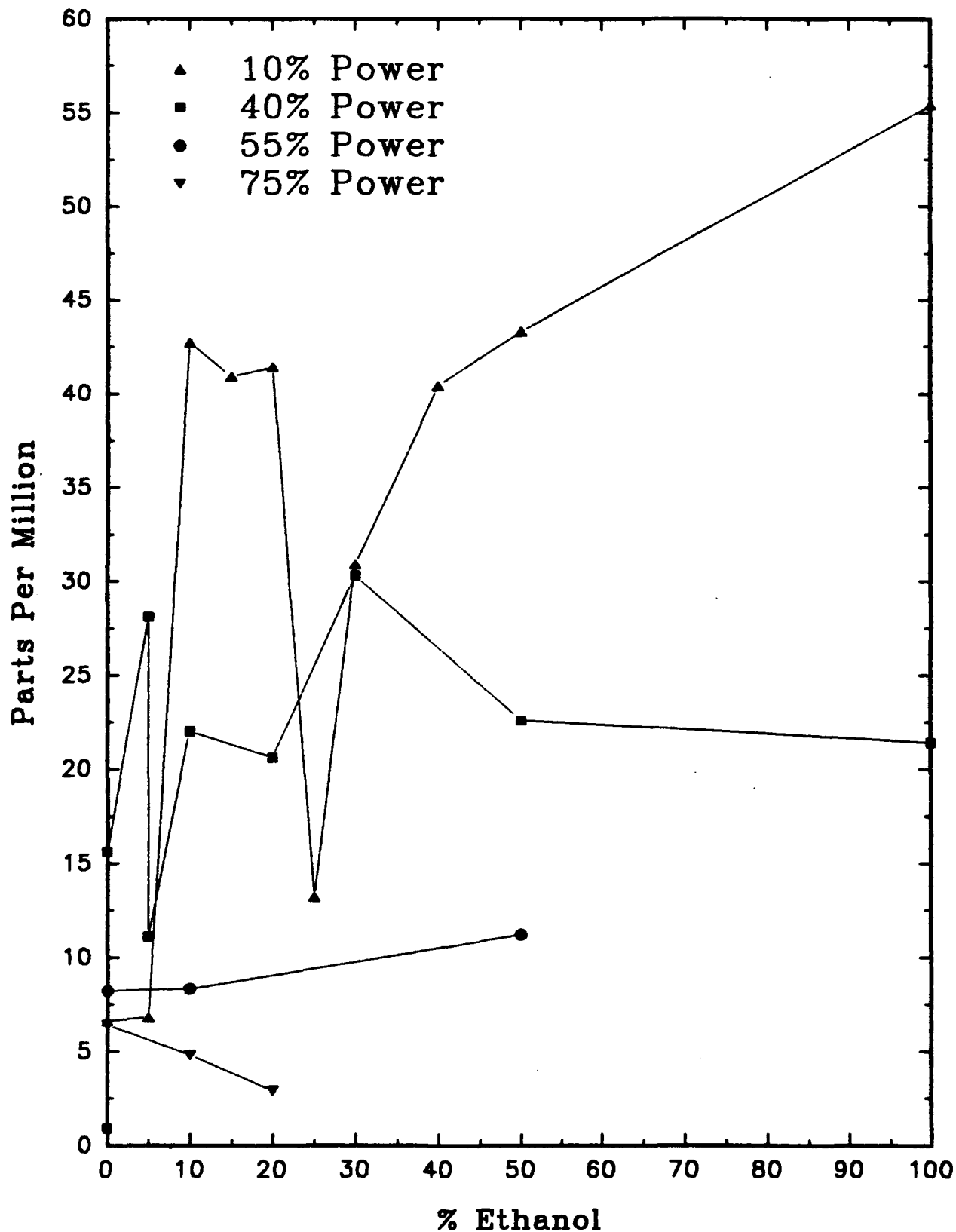


FIGURE 22. Effect of Ethanol Concentration on Formaldehydes in the Exhaust

COMBUSTION EFFICIENCY

Nominal Fuel Flow

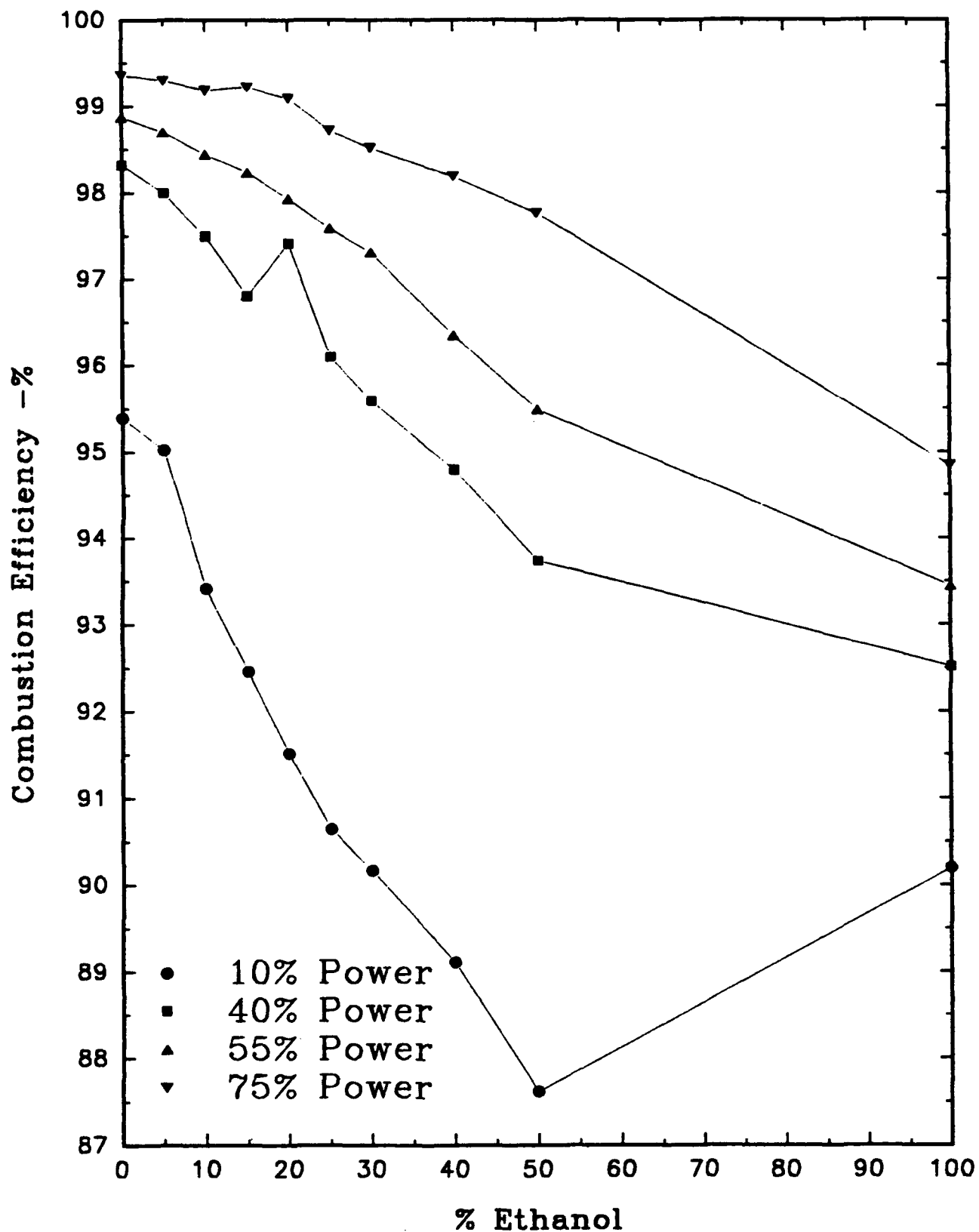


FIGURE 23. Effect of Ethanol Concentration on Combustion Efficiency at Constant Fuel Flow Rate

COMBUSTION EFFICIENCY

Compensated Fuel Flow

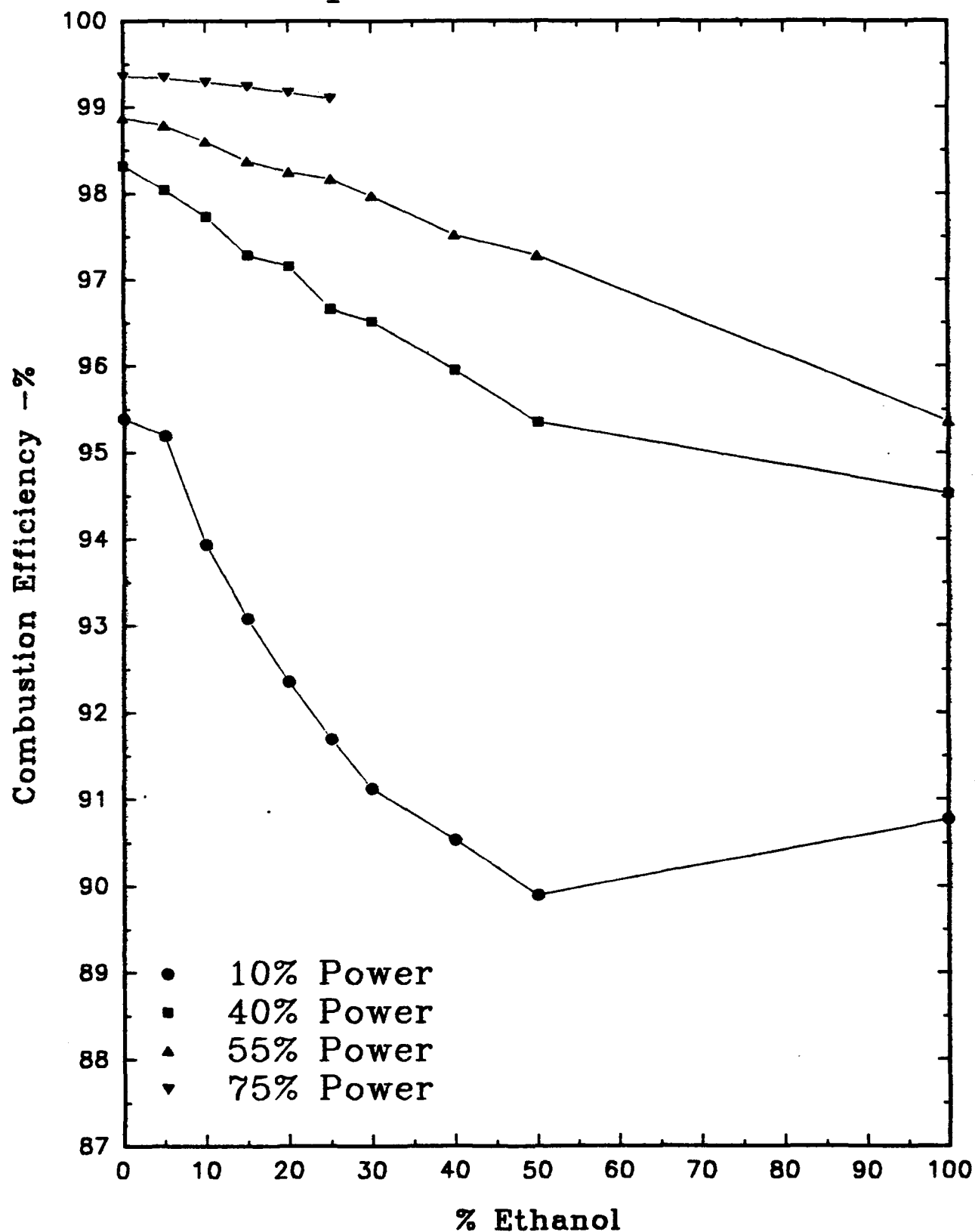


FIGURE 24. Effect of Ethanol Concentration on Combustion Efficiency at Constant Energy Input

COMBUSTOR CAN THERMOCOUPLES

10% Power - Nominal

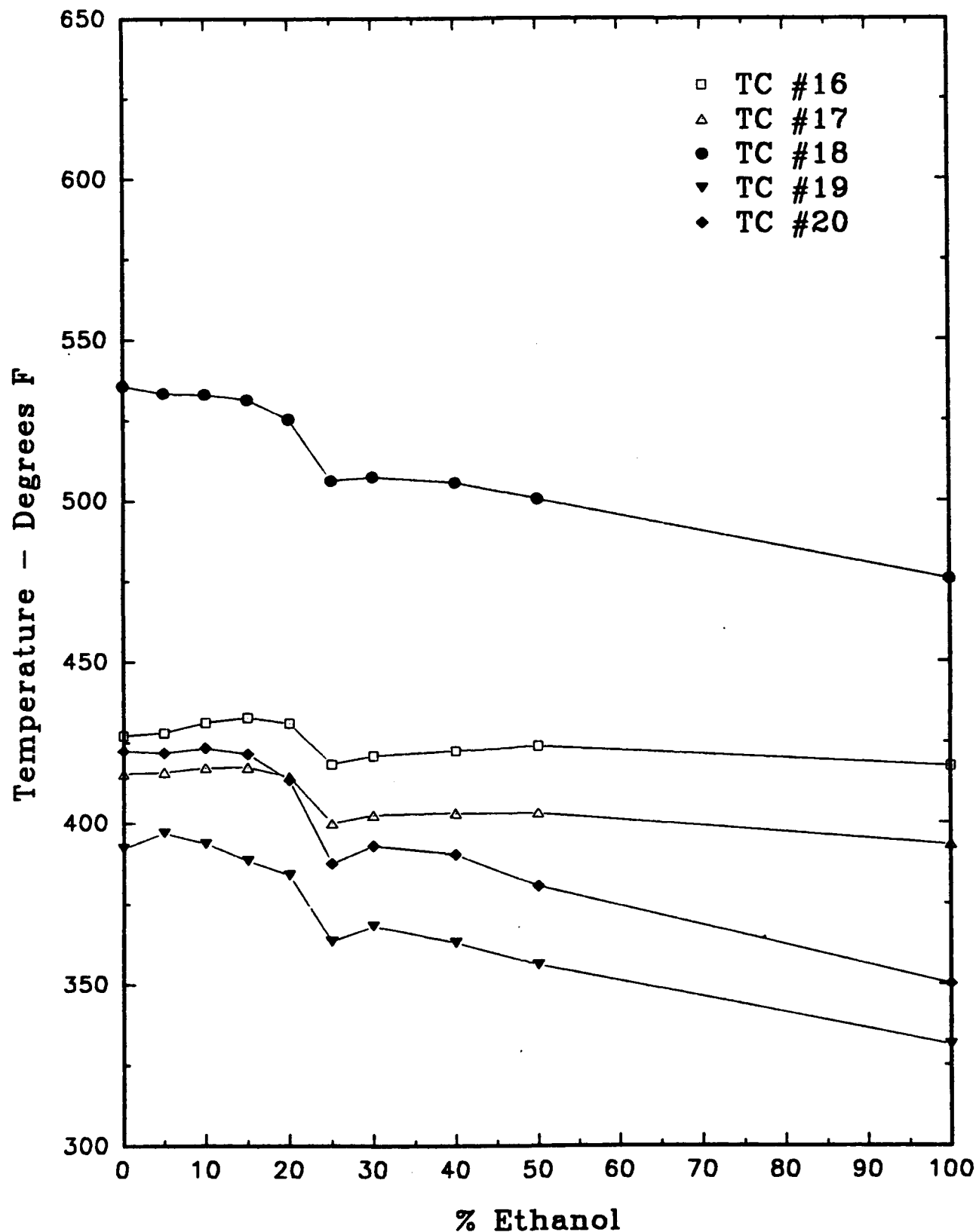


FIGURE 25. Effect of Ethanol Concentration on Liner Temperatures at 10% Power Condition with Constant Fuel Flow Rate

COMBUSTOR CAN THERMOCOUPLES

40% Power - Nominal

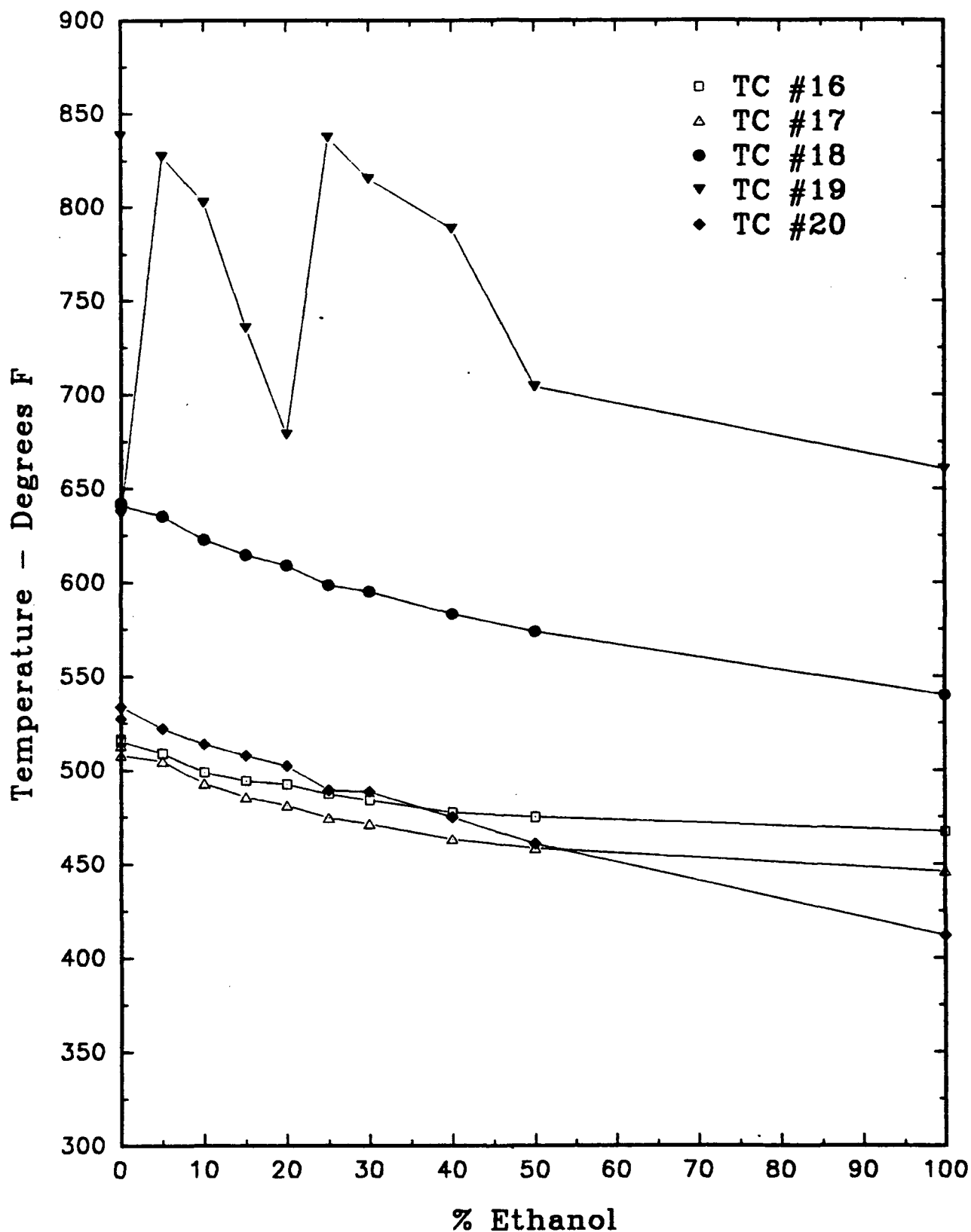


FIGURE 26. Effect of Ethanol Concentration on Liner Temperatures at 40% Power Condition with Constant Fuel Flow Rate

COMBUSTOR CAN THERMOCOUPLES

55% Power – Nominal

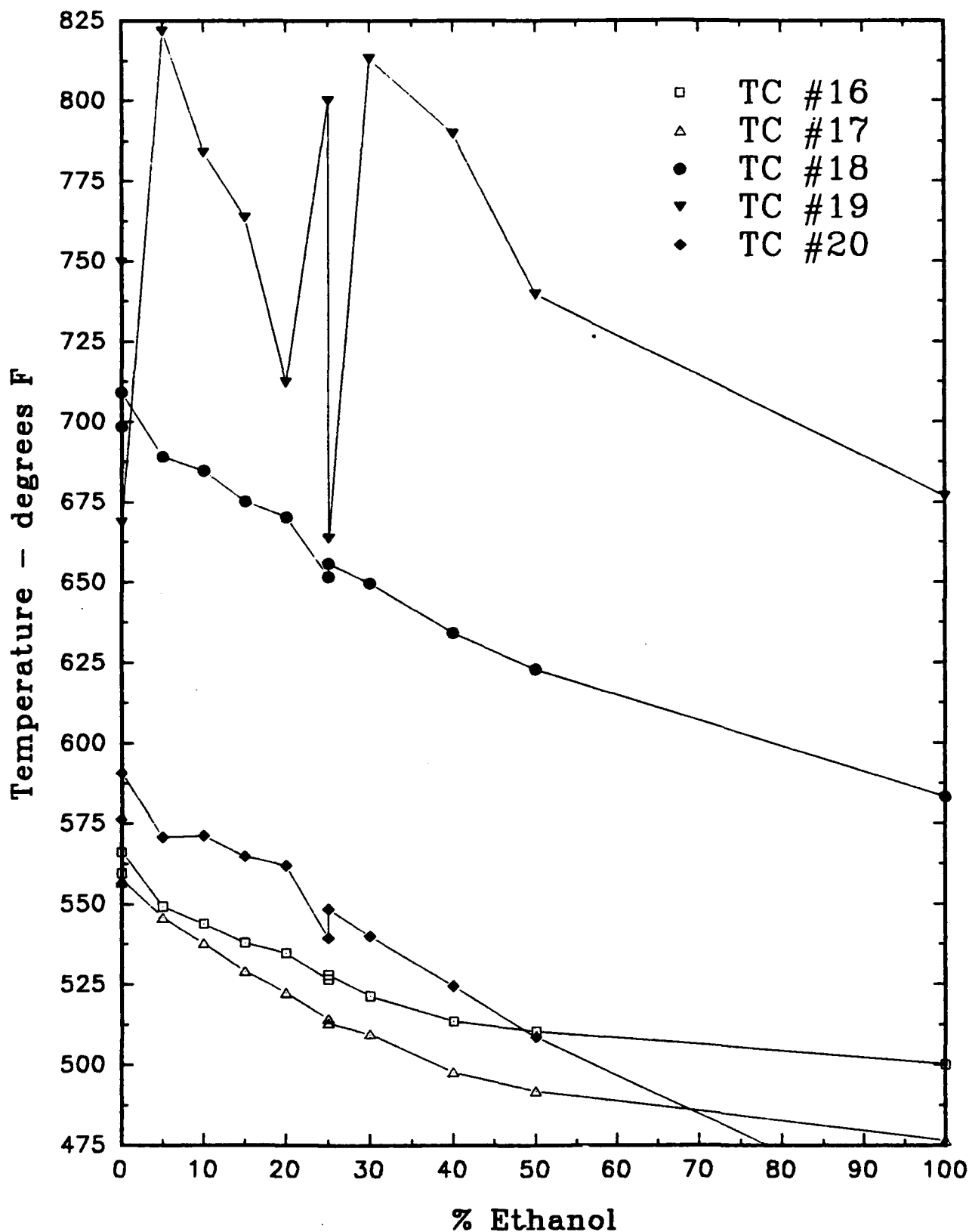


FIGURE 27. Effect of Ethanol Concentration on Liner Temperatures at 55% Power Condition with Constant Fuel Flow Rate

COMBUSTOR CAN THERMOCOUPLES

75% Power - Nominal

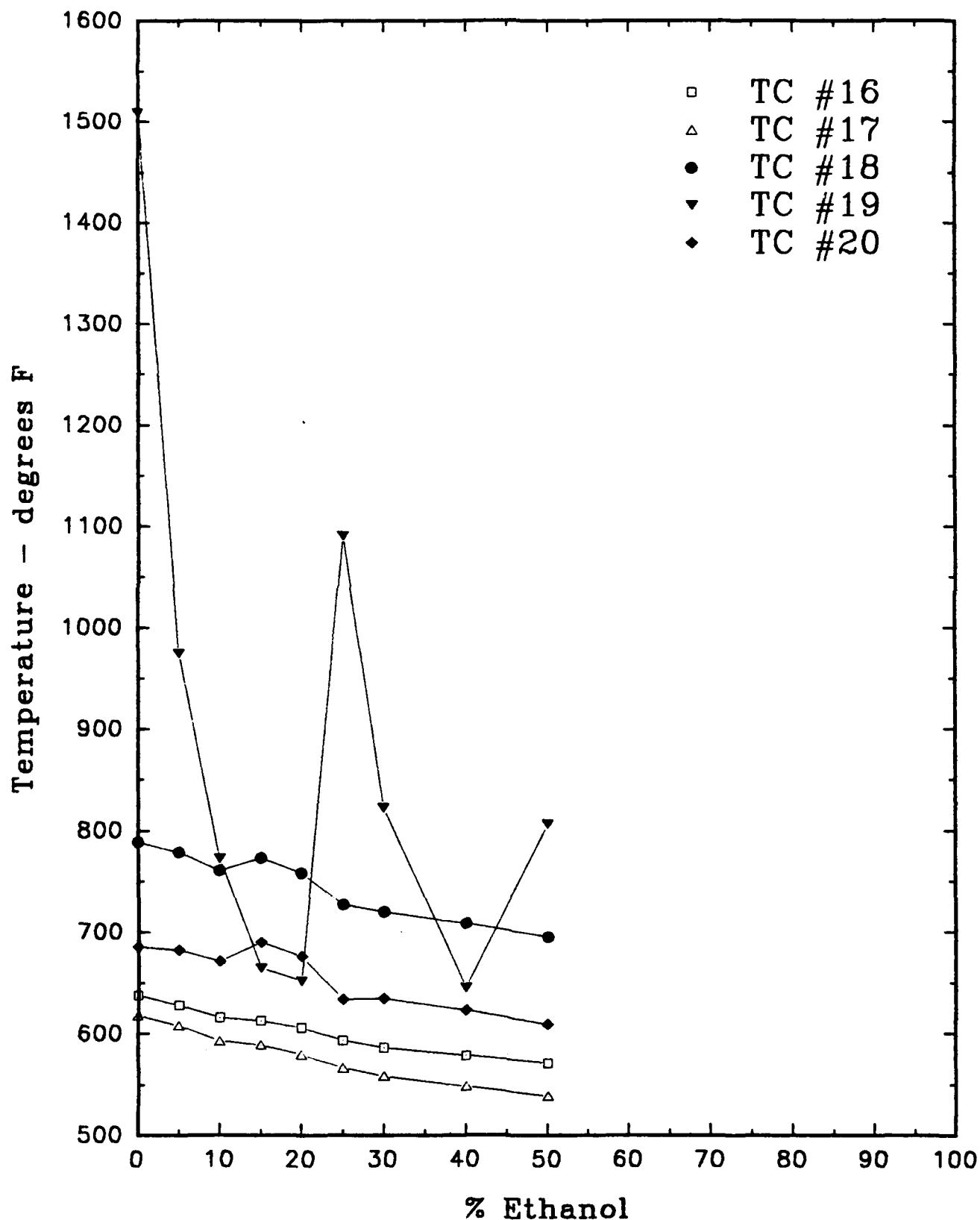


FIGURE 28. Effect of Ethanol Concentration on Liner Temperatures at 75% Power Condition with Constant Fuel Flow Rate

COMBUSTOR CAN THERMOCOUPLES

10% Power – Compensated

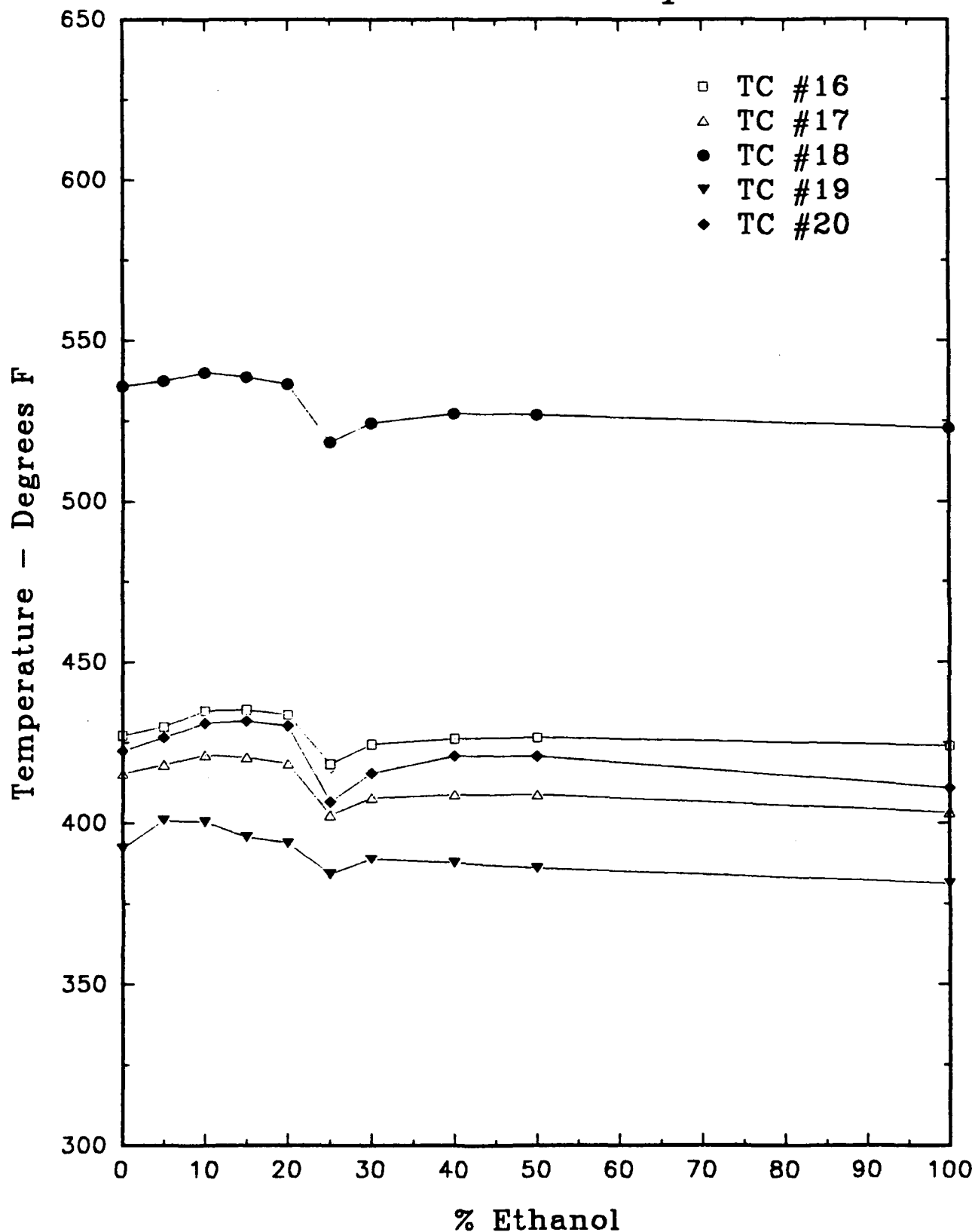


FIGURE 29. Effect of Ethanol Concentration on Liner Temperatures at 10% Power Condition with Constant Energy Input

COMBUSTOR CAN THERMOCOUPLES

40% Power - Compensated

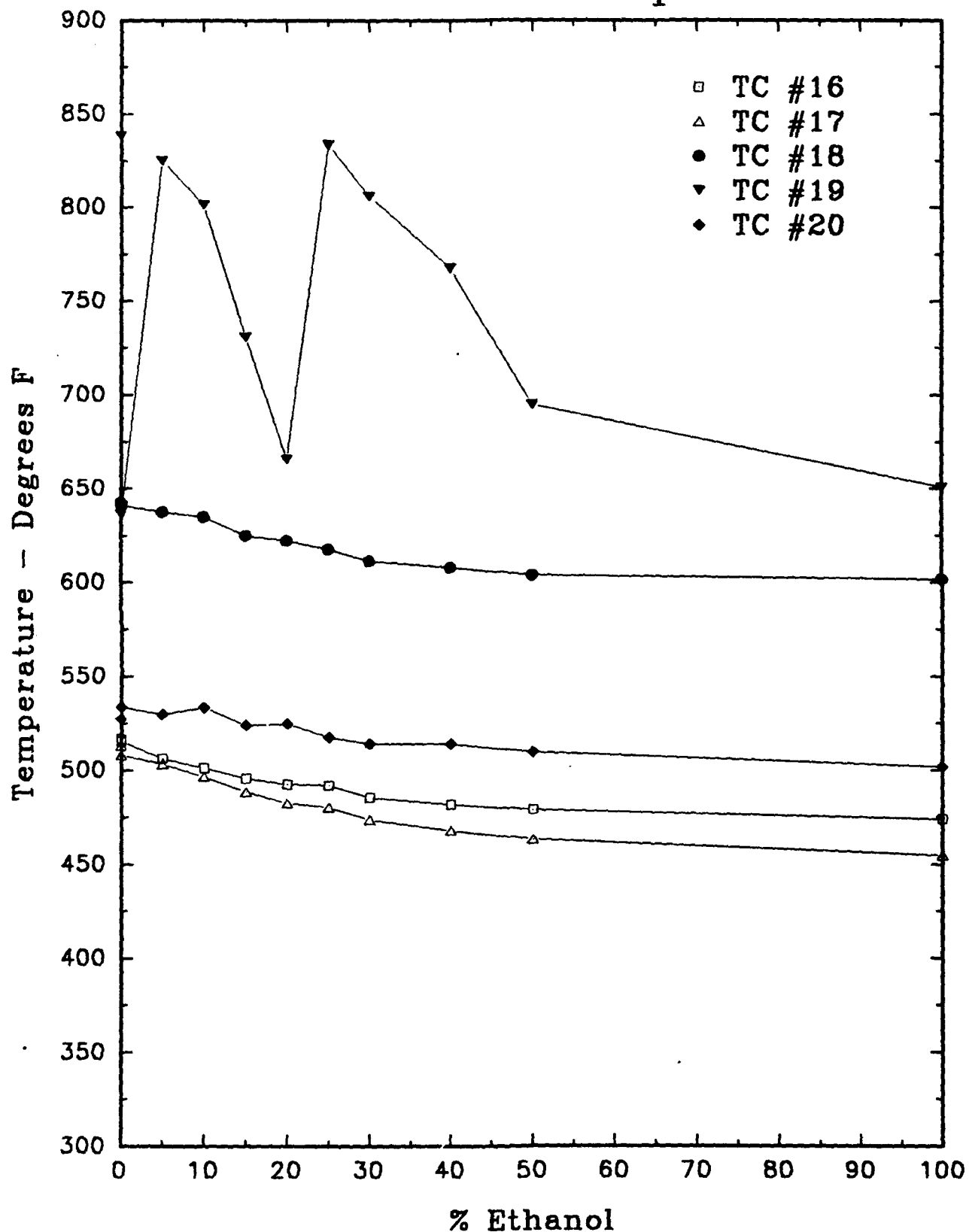


FIGURE 30. Effect of Ethanol Concentration on Liner Temperatures at 40% Power Condition with Constant Energy Input

COMBUSTOR CAN THERMOCOUPLES

55% Power - Compensated

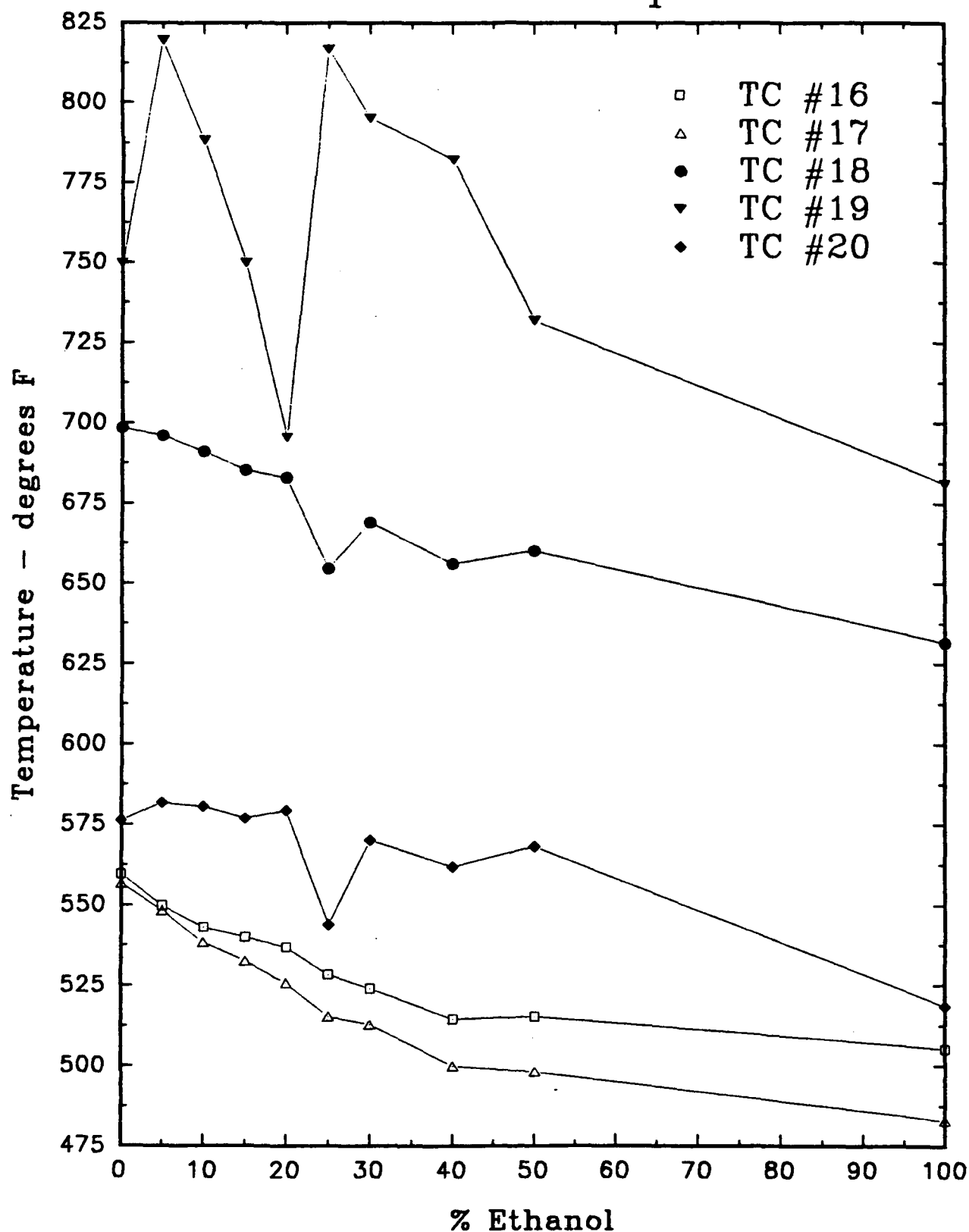


FIGURE 31. Effect of Ethanol Concentration on Liner Temperatures at 55% Power Condition with Constant Energy Input

COMBUSTOR CAN THERMOCOUPLES

75% Power - Compensated

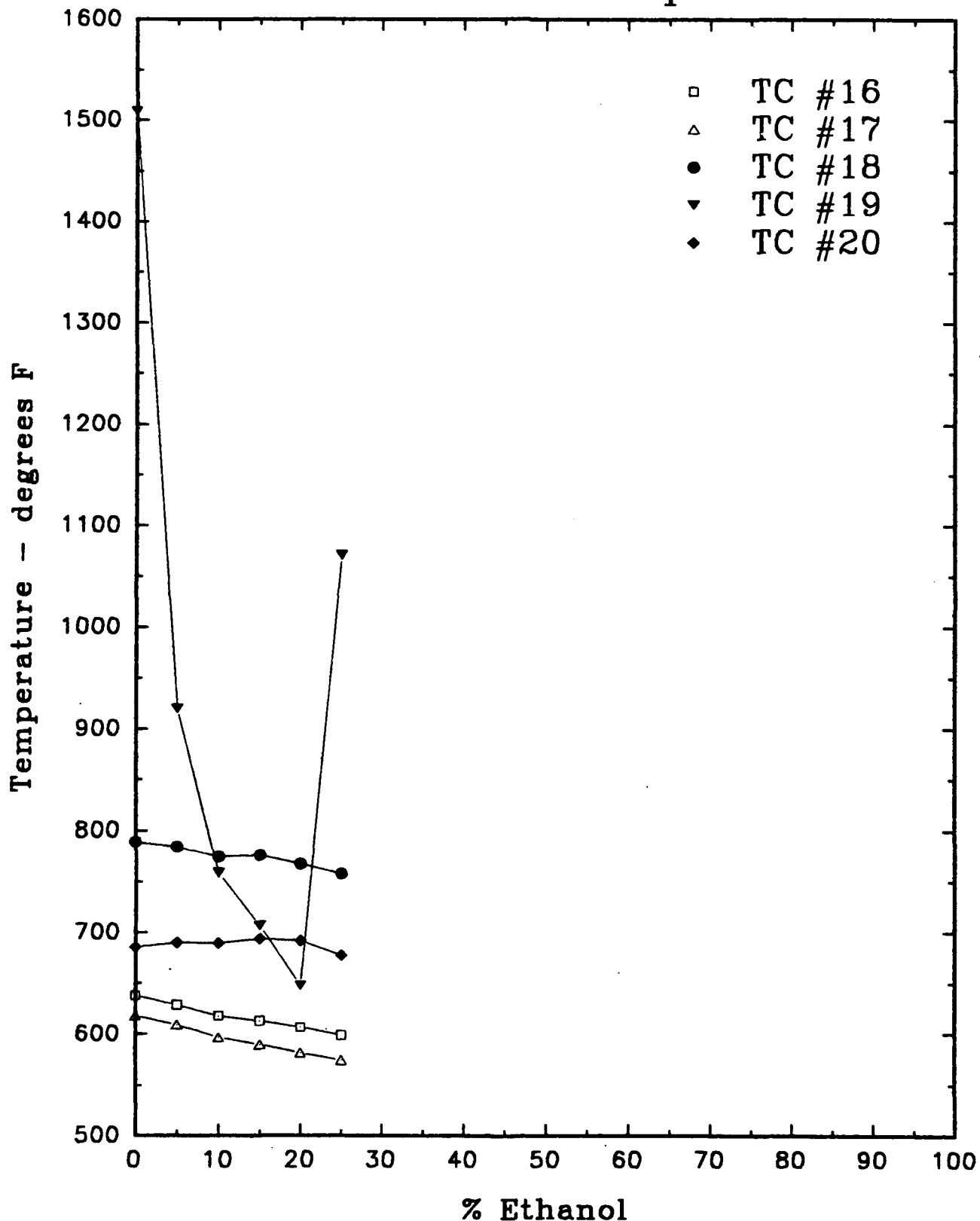


FIGURE 32. Effect of Ethanol Concentration on Liner Temperatures at 75% Power Condition with Constant Energy Input

EXHAUST TEMPERATURES

10% Power – Nominal

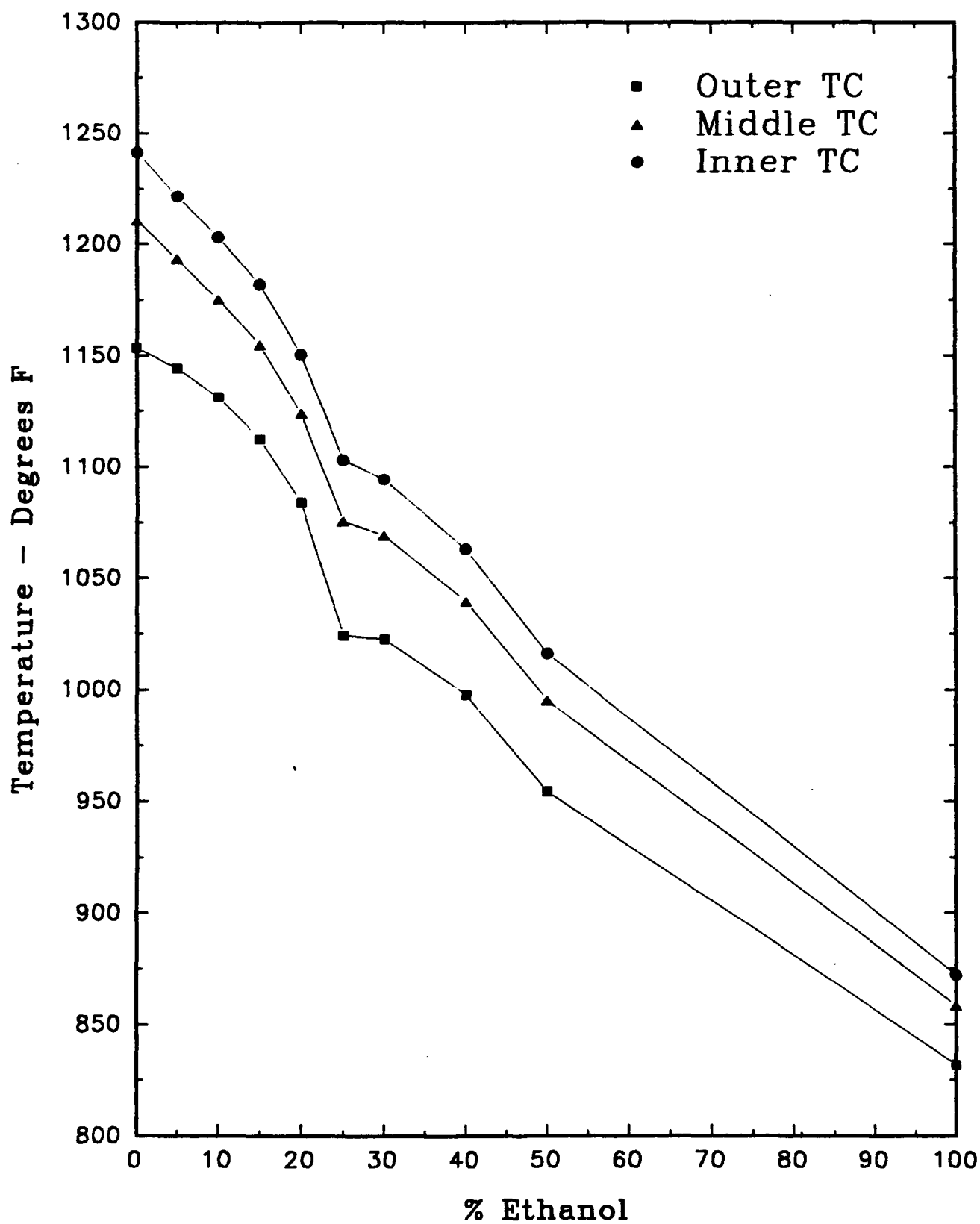


FIGURE 33. Effect of Ethanol Concentration on Average Circumferential Exhaust Temperatures at 10% Power Condition with Constant Fuel Flow Rate

EXHAUST TEMPERATURES

40% Power – Nominal

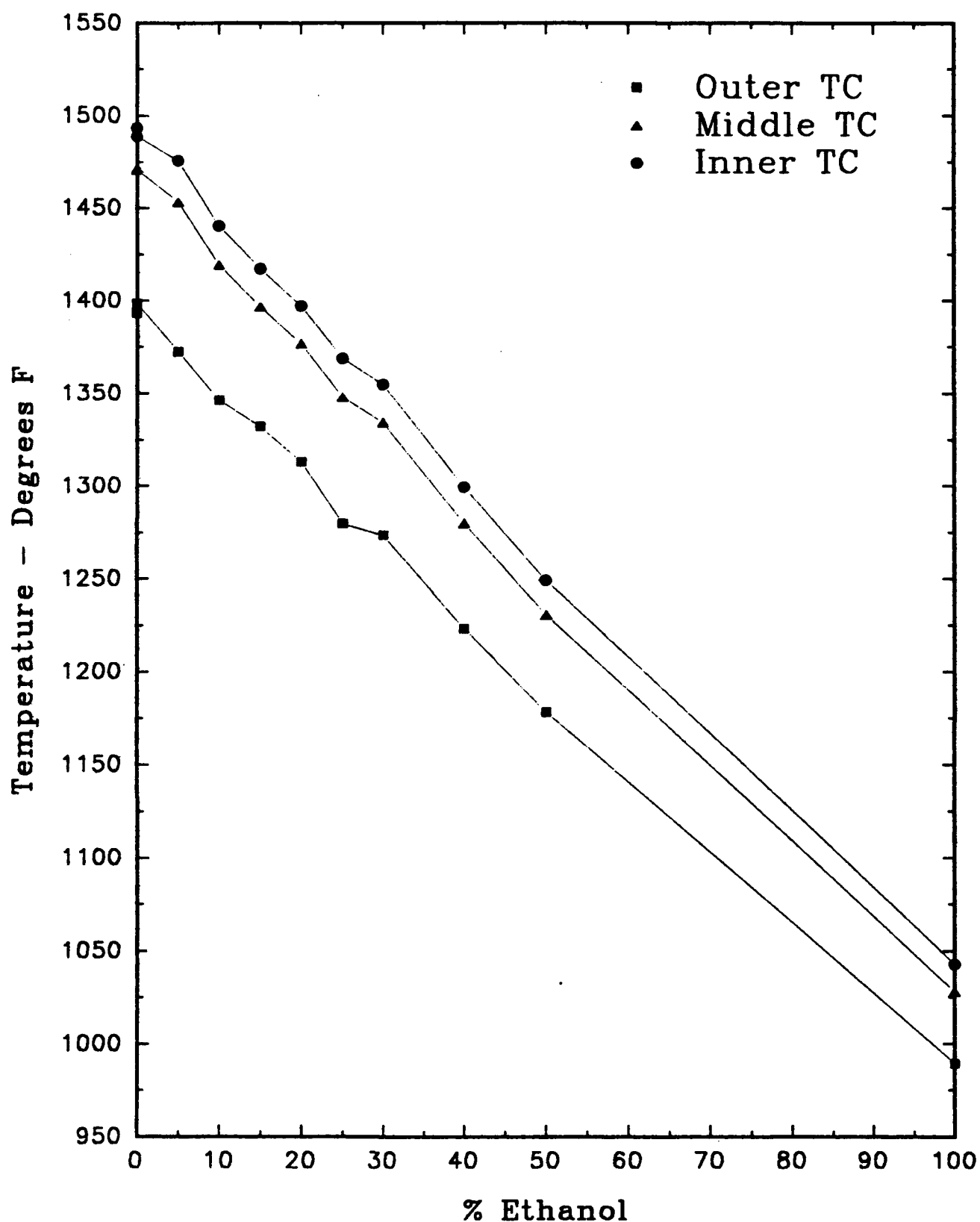


FIGURE 34. Effect of Ethanol Concentration on Average Circumferential Exhaust Temperatures at 40% Power Condition with Constant Fuel Flow Rate

EXHAUST TEMPERATURES 55% Power – Nominal

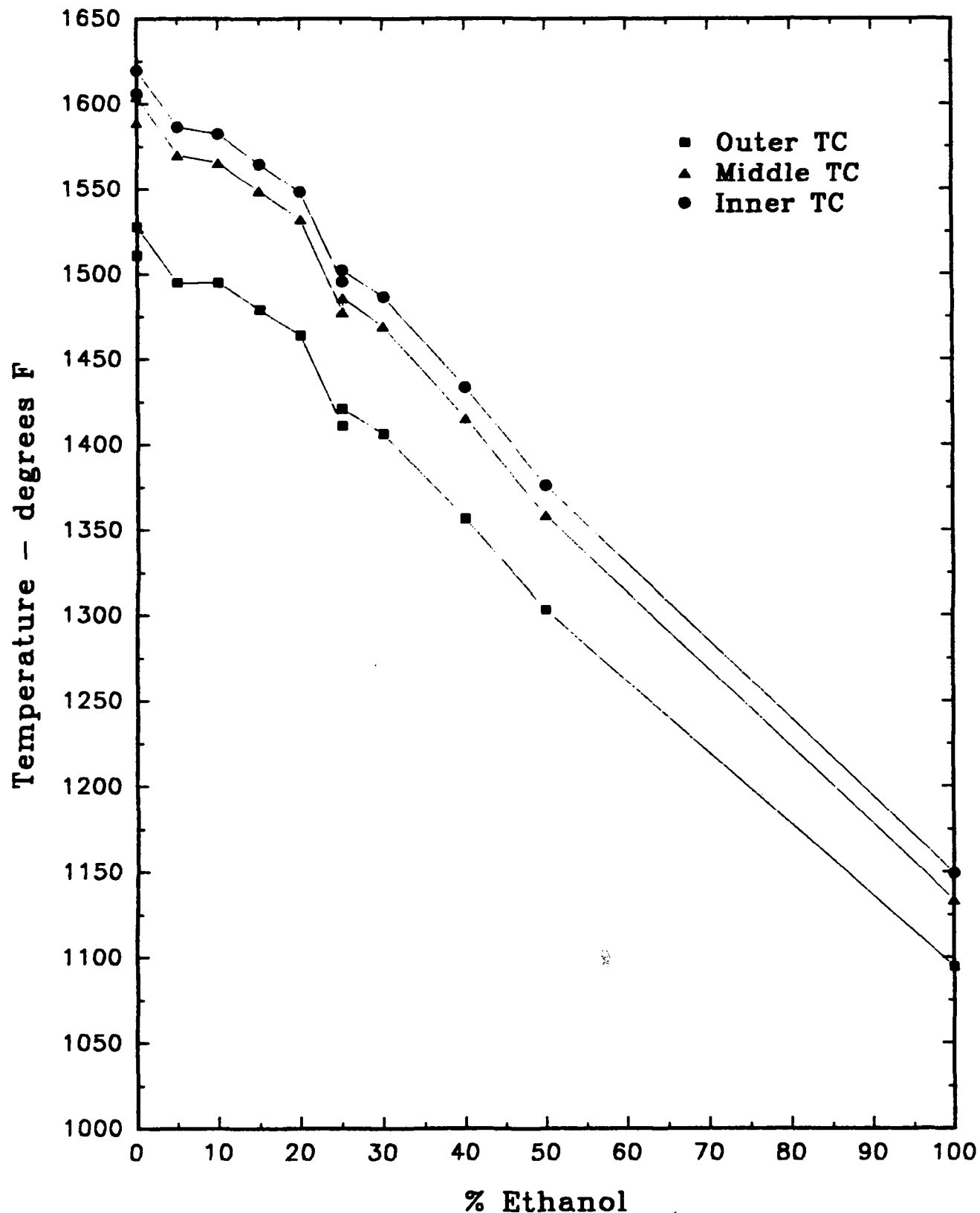


FIGURE 35. Effect of Ethanol Concentration on Average Circumferential Exhaust Temperatures at 55% Power Condition with Constant Fuel Flow Rate

EXHAUST TEMPERATURES

75% Power – Nominal

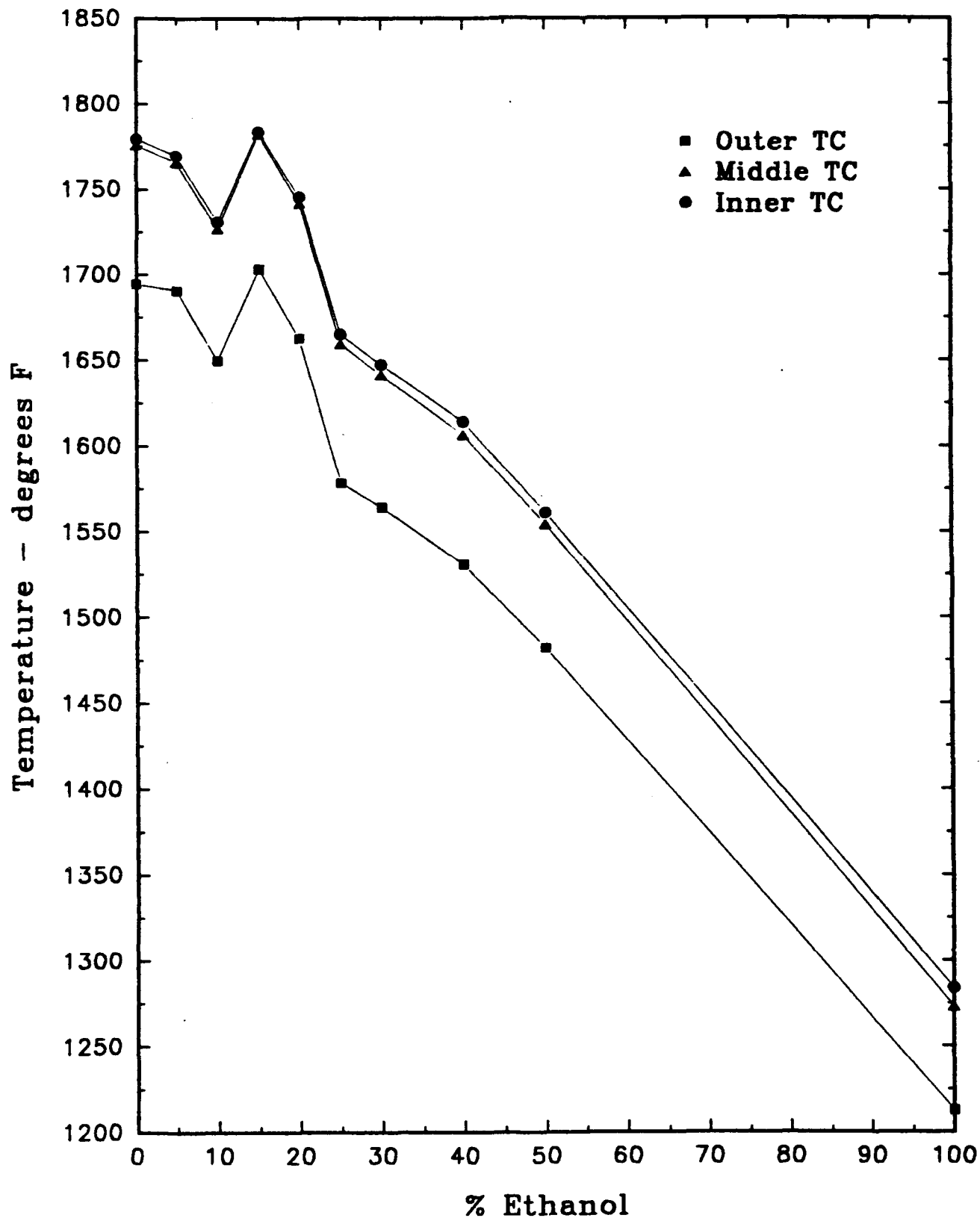


FIGURE 36. Effect of Ethanol Concentration on Average Circumferential Exhaust Temperatures at 75% Power Condition with Constant Fuel Flow Rate

EXHAUST TEMPERATURES

10% Power - Compensated

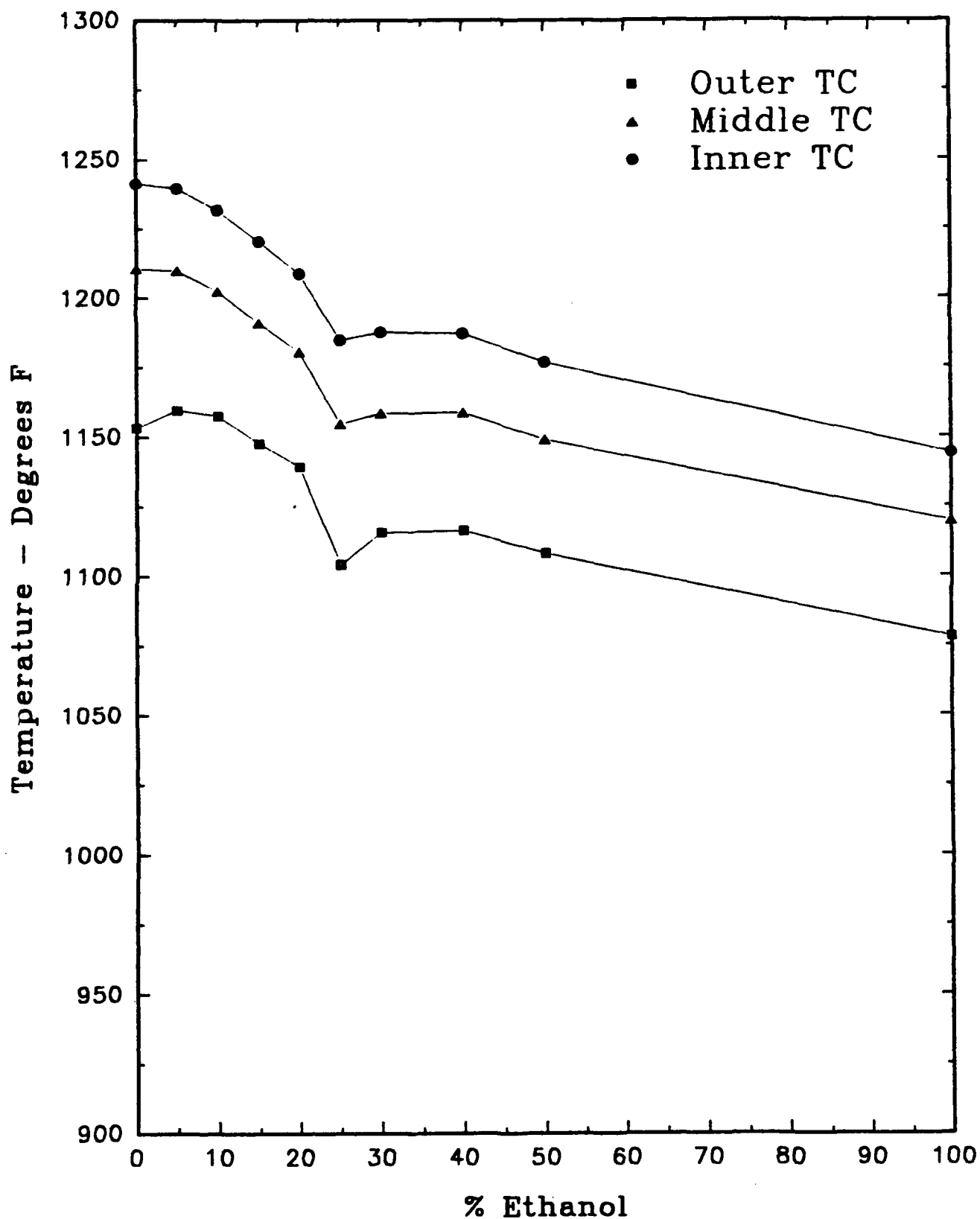


FIGURE 37. Effect of Ethanol Concentration on Average Circumferential Exhaust Temperatures at 10% Power Condition with Constant Energy Input

EXHAUST TEMPERATURES

40% Power – Compensated

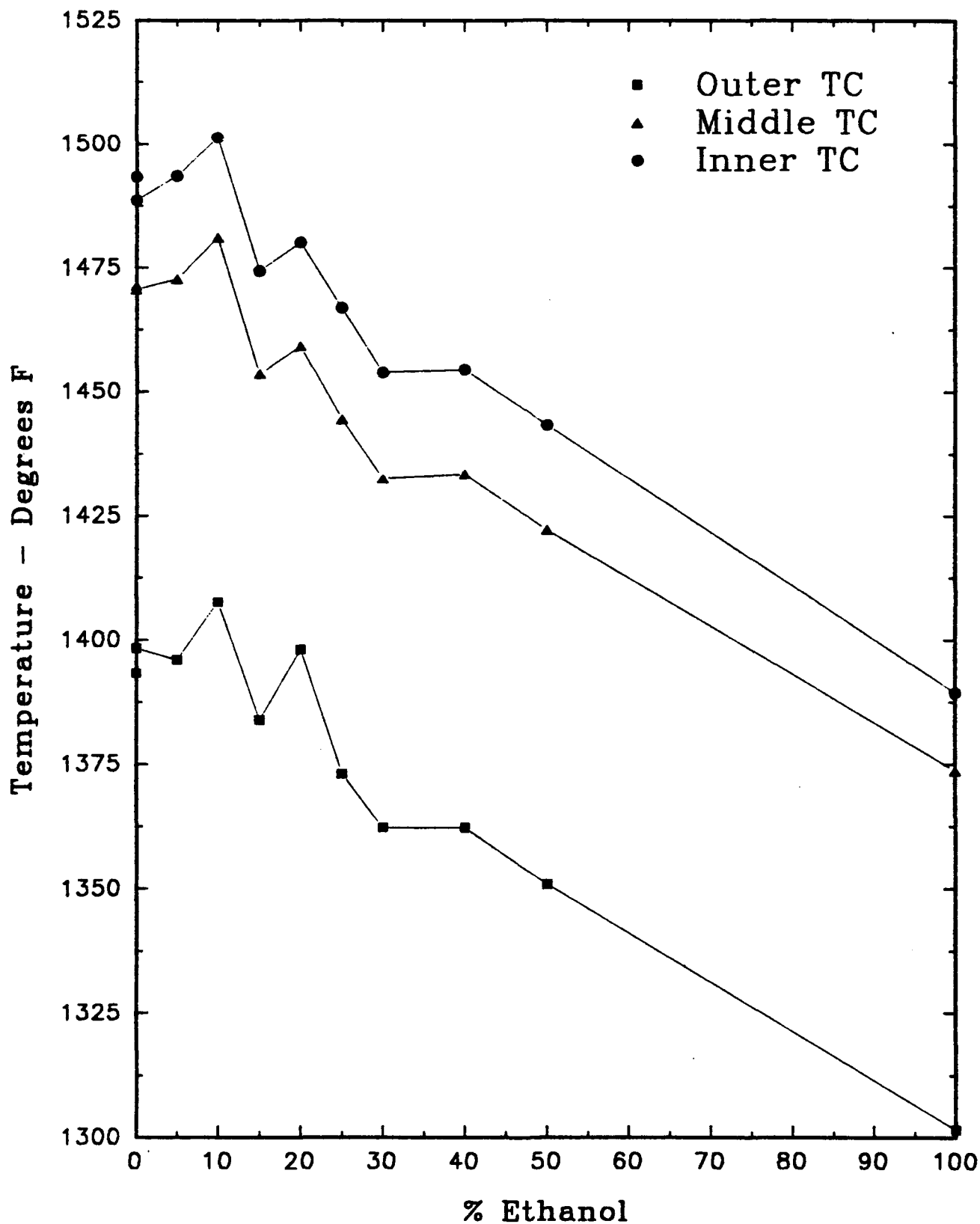


FIGURE 38. Effect of Ethanol Concentration on Average Circumferential Exhaust Temperatures at 40% Power Condition with Constant Energy Input

EXHAUST TEMPERATURES 55% Power – Compensated

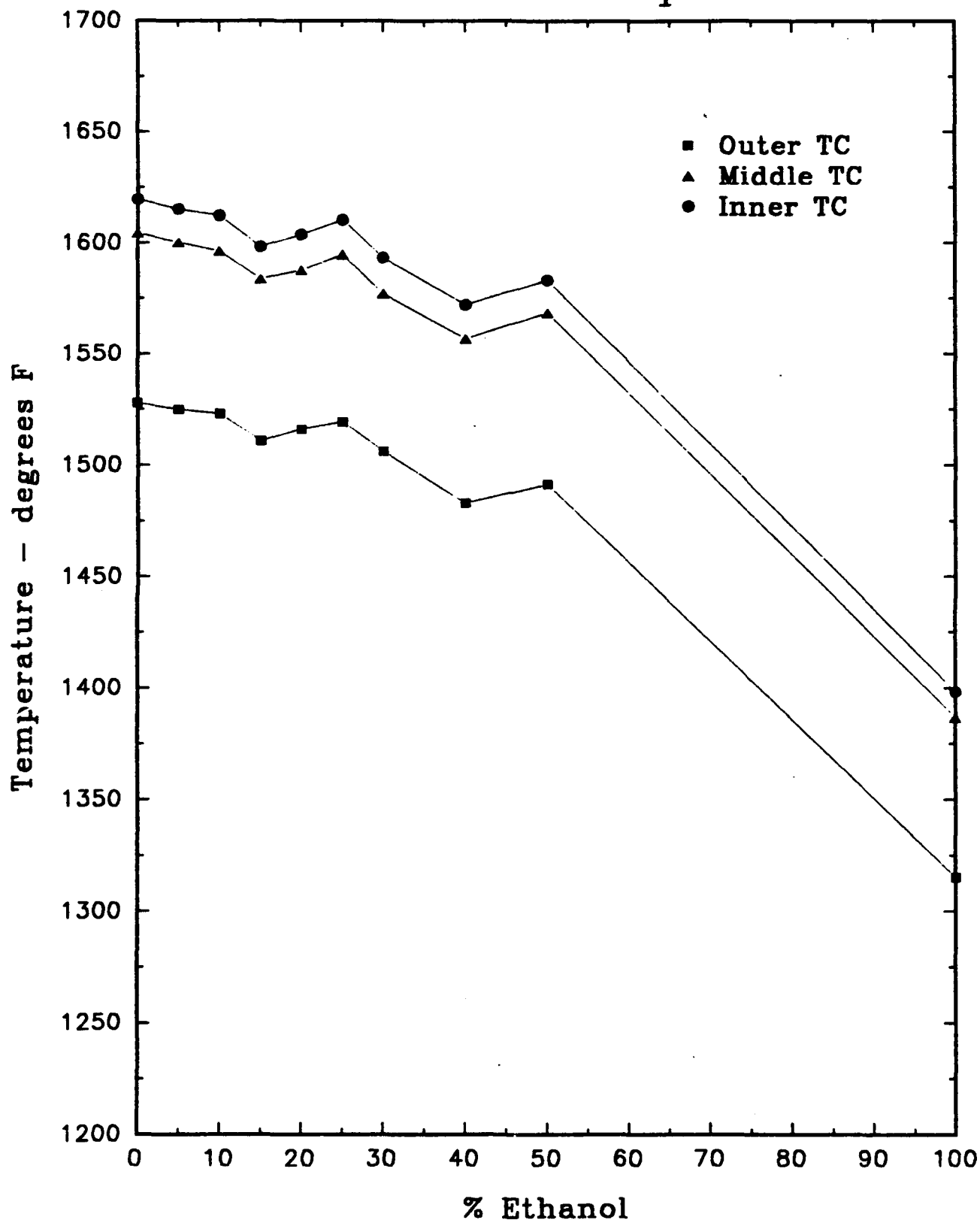


FIGURE 39. Effect of Ethanol Concentration on Average Circumferential Exhaust Temperatures at 55% Power Condition with Constant Energy Input

EXHAUST TEMPERATURES 75% Power – Compensated

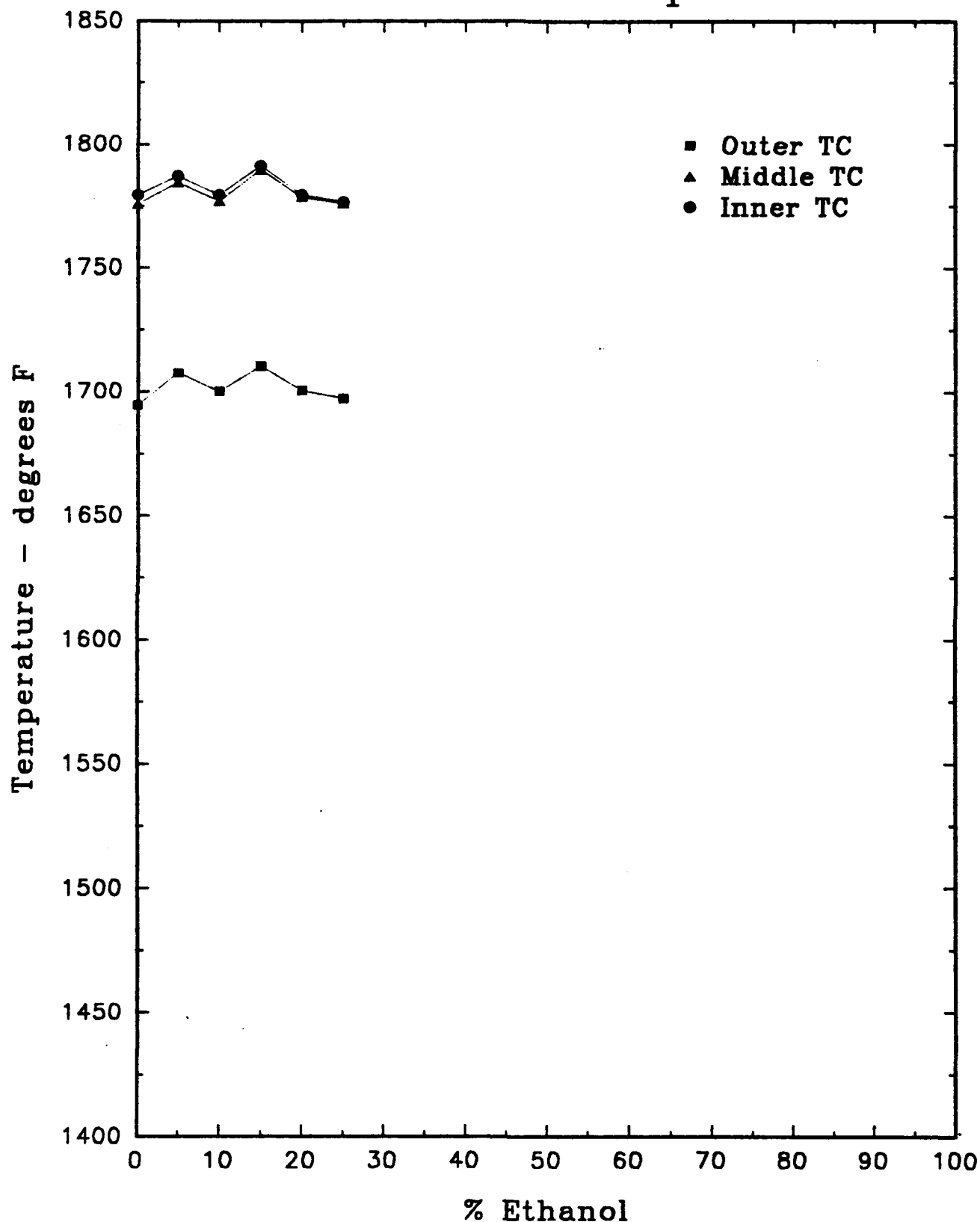


FIGURE 40. Effect of Ethanol Concentration on Average Circumferential Exhaust Temperatures at 75% Power Condition with Constant Energy Input

**ROTOR ALONE NOISE OF SHROUDED AND
UNSHROUDED PROPELLERS**

by

**Walter Eversman
Mechanical and Aerospace Engineering
and Engineering Mechanics
University of Missouri-Rolla
Rolla, Missouri 65401**

**For Presentation to the AIAA/FAA Joint Symposium on General
Aviation Systems at the Hilton Inn-East, Wichita, KS
on March 16-17, 1992**

ROTOR ALONE NOISE OF SHROUDED AND UNSHROUDED PROPELLERS

Walter Eversman
Mechanical and Aerospace Engineering
and Engineering Mechanics
University of Missouri-Rolla
Rolla, Missouri 65401

ABSTRACT

A finite element model is created for the generation, propagation, and radiation of steady, rotor alone noise of shrouded propellers. In the case of rotor alone noise the acoustic source is represented by a rotating lifting line of thrust and torque dipoles distributed radially on the blade. For a specified number of blades, angular mode harmonic, and rotor angular velocity, the acoustic field is described in a cylindrical coordinate system reduced to only the axial and radial directions. The blade loading is imposed on a radial line at the axial location of the fan. The blade loading is assumed to vary linearly from the hub to the tip. The blade tip loading is determined by a specified thrust requirement and the inflow velocity. In the configurations considered in the present study, emphasis is on ducted fans or ducted propellers for which the by-pass ratio is very large. In this case the usual assumption is made that the fan, or propeller, is operating in a mean flow environment which is uniform and the same as the forward flight velocity. The flow acceleration in the inlet, acceleration in the fan duct, and jet free shear layer are not accounted for in the present model. The model accounts for the noise generation process, the propagation through the inlet and fan duct, and the radiation to the near and far field. The major issue addressed in the computational examples is the relationship between the far field radiated Sound Pressure Level (SPL) and directivity and fan tip speed.

INTRODUCTION

Ultra high by-pass ratio turbo-fan engines and ducted or shrouded propellers are attractive from the standpoint of propulsive efficiency. In addition there are possible advantages to be gained in radiated noise levels due to the imbedding of the propeller or fan acoustic source within the nacelle or shroud. An unducted propeller generates an acoustic field which tends to produce high levels on the sideline, and therefore may create unacceptable noise levels in the interior of the aircraft. A ducted propeller is restricted in the way in which it can radiate to the near and far field. It is known that steady, rotor alone noise, created by blade loading, is a principle source mechanism for unducted propellers. It is generally assumed that in the case of a ducted propeller the rotor alone noise is not propagated to the far field if the tip speed does not exceed the speed of sound. This result, due to pioneering work of Tyler and Sofrin [1], is true for rotor generated noise in a thin annulus with the absence of duct mean flow.

The purpose of the work presented here is to investigate the differences in the radiated acoustic fields of ducted and unducted propellers of the same thrust operating under similar conditions. Hanson [2] has created a comprehensive acoustic model for unducted propellers which accounts for spanwise and chordwise details of the blade loading. It is not the intent in the present study to focus on such a refined model. Instead, the approach is to generate a very simple source model, similar to the classic lifting line theory suggested by Gutin [3], to concentrate on the propagation and radiation effects introduced by the duct, and to compare the acoustic performance of similar ducted and unducted propellers based on the same source model.

The finite element method (FEM) has been used in previous studies to model the wind tunnel acoustic testing of propellers and the free field acoustic radiation of propellers [4-7]. In the present study the FEM is used to model the ducted propeller in the free field. This combines the propeller modeling previously reported and some aspects of earlier work on the prediction of the radiated acoustic field from turbofan engine inlets [8-9].

The generation, propagation, and radiation of sound from a ducted fan is described in this study by the convected wave equation with volumetric body forces. Body forces are used to introduce the blade loading for rotating blades and stationary exit guide vanes (EGV). For an axisymmetric nacelle or shroud, the problem is formulated in cylindrical coordinates. For a specified angular harmonic the angular coordinate is eliminated and a two dimensional representation results. A finite element discretization based on nine node quadratic isoparametric elements is used. The nacelle and center body or core engine are defined as rigid surfaces. The assumption is made that the bypass ratio is large enough so that the entire flow field is uniform, consistent with the usual model in propeller acoustic analyses. Features not modeled are the nonuniform flow in the inlet and fan duct, and the free shear layer in the fan duct exhaust jet.

Geometry and Coordinate System

In this investigation the acoustic field is conveniently represented in a cylindrical geometry with the axis of the propeller or rotor/nacelle designated as the x axis. It is assumed that the nacelle/centerbody combination is axially symmetric and that the inlet flow field is axially symmetric. Specifically excluded by this restriction are drooped inlets and nacelles for which the inlet duct is not circular. The acoustic field is not required to be axially symmetric, and it would be unlikely that it is. The acoustic field is periodic in the angular coordinate of the cylindrical system. It is represented as the components of a Fourier Series in the angular coordinate θ . The acoustic field for each angular component, or "angular mode," is represented by a field equation in only the axial and radial components x , r of the cylindrical system.

Figure 1 shows an idealized geometry for a rotor/nacelle arrangement. Noise sources related to the rotating blades and the interaction of the blades with stationary exit guide vanes can be modeled.

The steady velocity field in and around the nacelle is assumed to be uniform. For many applications, notably the case of the ultra high bypass fan or the ducted propeller this is probably satisfactory. For other cases it may be necessary to model the flow in and around the nacelle. It may also be required to consider the effects of the shear layer in the interface between the fan exhaust and the surrounding steady flow.

Mathematical Model

The acoustic field is described by the convected wave equation with body forces

$$\nabla^2 p^* - \frac{1}{c^2} \frac{D^2 p^*}{Dt^{*2}} = \rho_o \nabla \cdot \bar{f}^* \quad (1)$$

where p^* is the acoustic pressure, ρ_o is the ambient density, c is the ambient speed of sound, and \bar{f}^* represents the body force per unit mass acting on the fluid. $\rho_o \bar{f}^*$ is the body force per unit volume. Equation (1) is in dimensional form. In the development which follows a nondimensional form of equation (1) is used with the following scaling

$$x = \frac{x^*}{L}, \quad p = \frac{p^*}{\rho_o c_o^2}, \quad t = \frac{ct^*}{L}, \quad \bar{f} = \frac{L}{c_o^2} \bar{f}^*$$

t^* is the dimensional time and x^* is any of the linear spatial coordinates. The reference length L is the propeller radius R . The nondimensional form of the acoustic field equation is

$$\nabla \cdot (\nabla p - M^2 \frac{\partial p}{\partial x} \bar{i} - \bar{f}) - 2M \frac{\partial^2 p}{\partial x \partial t} - \frac{\partial^2 p}{\partial t^2} = 0 \quad (2)$$

The body force per unit mass \bar{f} is related to the force exerted on the fluid by the rotating blade or stationary vane.

The major deficiency in this model is the assumption that the interior flow and external flow are uniform and at the flight Mach number. This is required because a pressure formulation has been chosen to introduce the acoustic source model for the rotor or EGV via equivalent body forces acting on the fluid. This is consistent with previous models of propellers [4-7]. In the pressure formulation it is required that the flow field be uniform in order that the acoustic field equations can be reduced to the convected wave equation.

By modeling the acoustic field using the pressure formulation some liberties have been taken. Even though for ducted propellers or high by-pass ratio ducted fan types of flow fields the internal and external flows over most of the region may be approximated as being uniform and tangent to the nacelle, a region will exist near the inlet lip where the flow is clearly not uniform. The formulation of the problem using the convected wave equation

does not account for this. Although the primary convective effect of the mean flow is modeled, effects due to localized flow gradients will not be included.

In addition to the requirement that the flow be uniform there is a more subtle restriction that is introduced by the natural boundary condition for the convected wave equation that would require

$$(\nabla p - M^2 \frac{\partial p}{\partial x} \vec{i}) \cdot \vec{n} = 0 \quad (3)$$

if no forced boundary condition exists. \vec{n} is the outward normal on the nacelle surface. On the nacelle surface the rigid wall boundary condition requires that

$$\nabla p \cdot \vec{n} = 0$$

which is equivalent to specifying that the acoustic particle velocity normal to the surface vanishes. Equation (3) does not reduce to this condition except where $\vec{i} \cdot \vec{n} = 0$. This is clearly violated where the surface normal is not perpendicular to the duct axis, and particularly near the inlet lip. The natural boundary condition (3) is used here with the argument that its apparent failure where $\vec{i} \cdot \vec{n} \neq 0$ is an artifact of the assumption of uniform flow. No apparent effect of this approximation can be seen in the computational results.

A second modeling option has been used in previous studies of acoustic radiation from turbofan inlets [8,9]. The assumption is made that the mean flow and acoustic field are irrotational. The acoustic source is introduced through the specification of acoustic modal amplitudes at the fan face. This is accomplished by including suitable boundary terms. It is therefore not required to include the body forces in the momentum equation. This allows a first integral of the linearized momentum equation to be obtained, which can be interpreted as an acoustic Bernoulli equation. The combination of the continuity equation and the acoustic Bernoulli equation written in terms of the acoustic velocity potential provides the basis of the mathematical model in [8,9].

The velocity potential formulation does not seem to be appropriate if the source model is to be introduced through equivalent body forces. The critical feature which is lost is the first integral of the momentum equation leading to the acoustic Bernoulli equation. This integral is not possible unless the body force is derivable from a potential. This does not appear to be the case for the types of body forces required to represent a propeller, rotor, or EGV.

The finite element formulation of the convected wave equation (2), is the same as described in previous work related to propeller acoustic radiation [4-7]. Nine node quadratic isoparametric elements are used with special attention given to the elements spanning the propeller and containing the source terms. A frontal solver is used and models with as many as 18000 degrees of freedom have been handled routinely.

The models used for the propeller or rotor and exit guide vane acoustic sources are discussed in the following sections.

Blade Loading

The blade loading of the propeller or rotor will be considered as the only source of rotor alone noise. No effects of blade thickness will be modeled in this investigation. Blade loading will be based on isolated lifting surface theory using a strip analysis. The discussion of Dommasch, Sherby and Connolly [10] is directly relevant to the following development.

Figure 2 shows an airfoil section at the radius r from the hub. The local angle of attack of the section at radius r depends on the inflow velocity, U , the relative velocity due to rotation $r\Omega/U$, where Ω is the angular velocity of the rotor or propeller, and the blade twist ϕ . The velocity seen by the section is

$$V = U \sqrt{1 + \left(\frac{1}{j}\right)^2}, \quad j(r) = \frac{U}{r\Omega} \quad (4)$$

The angle β defining the direction of the velocity seen by the section and the angle of attack α are given by

$$\cos\beta = \frac{\frac{1}{j}}{\sqrt{1 + \left(\frac{1}{j}\right)^2}}, \quad \sin\beta = \frac{1}{\sqrt{1 + \left(\frac{1}{j}\right)^2}}, \quad \alpha = \phi - \beta \quad (5)$$

The lift per unit span at the tip is

$$l_{tip} = \frac{1}{2} \rho U^2 \left[1 + \left(\frac{1}{J}\right)^2\right] c_{tip} c_{l_\alpha} \alpha_{tip}, \quad J = \frac{U}{R\Omega} \quad (6)$$

$c(r)$ is the local blade chord and c_{l_α} is the section lift coefficient taken as constant in the present study. The lift per unit span as a function of radius is

$$l(r) = l_{tip} \frac{\left[1 + \left(\frac{1}{j}\right)^2\right]}{\left[1 + \left(\frac{1}{J}\right)^2\right]} \bar{c}(r) \bar{\alpha}(r) \quad (7)$$

For the present investigation it is assumed that the blade loading is linearly distributed from root to tip, that is

$$l(r) = l_{tip} \left(\frac{r}{R} \right) \quad (8)$$

The thrust on N_B blades is given by

$$T = N_B \int_{R_i}^R l(r) \cos \beta dr = N_B l_{tip} \int_{R_i}^R \left(\frac{r}{R} \right) \frac{\left(\frac{1}{j} \right)}{\sqrt{1 + \left(\frac{1}{j} \right)^2}} dr \quad (9)$$

or

$$T = N_B l_{tip} R J^2 D(J) \quad (10)$$

where

$$D(J) = \left[\frac{\left(\frac{1}{j} \right)}{2} \sqrt{1 + \left(\frac{1}{j} \right)^2} - \frac{1}{2} \ln \left(\frac{1}{j} + \sqrt{1 + \left(\frac{1}{j} \right)^2} \right) \right]_{R_i}^R \quad (11)$$

R_i is the inner radius of the propeller or rotor. The required tip loading for a given thrust can now be determined from equation (10)

$$l_{tip} = \frac{T}{N_B R J^2 D(J)} \quad (12)$$

The thrust and torque loading are

$$l_t = l_{tip} \cos \beta \left(\frac{r}{R} \right), \quad l_m = l_{tip} \sin \beta \left(\frac{r}{R} \right) \quad (13)$$

Other types of loading can be considered by reformulating equation (8) and the subsequent analysis. Since the investigation reported here centers primarily on comparisons of unshrouded and shrouded propellers, it is not deemed critical to precisely specify the loading.

The lift distribution discussed here is dimensional, and thus based on full scale parameters.

Rotor Alone Noise

Rotor alone noise generation is viewed from the perspective of a volumetric force fixed in space which is active during the passage of a blade with its associated lift

distribution. It is assumed that the duration of passage of the blade past a fixed point is $\tau = \frac{a}{\Omega r}$ where $a(r)$ is the projection of the blade chord on the rotor plane. The strength of the volumetric force representing the blade passage is taken as the negative of the lifting pressure differential across the blade, approximated by $l(r)/c(r)$ where $c(r)$ is the local chord.

The strength is

$$\rho_o \bar{f} = - \frac{l(r)}{c(r)} \delta(y^*) \bar{e}_n \quad (14)$$

where y^* is a dimensional coordinate normal to the blade. The lift per unit span here is taken to act normal to the blade chord, which is oriented by the twist angle ϕ . The unit vector \bar{e}_n is taken normal to the blade. The relationship between x^* , the dimensional axial coordinate, and y^* , the normal to the blade chord, for $\theta = \text{constant}$, is

$$y^* = x^* \cos \phi$$

By making use of the property of the Dirac delta function that $\delta(ax) = a^{-1} \delta(x)$, equation (14) can be written

$$\rho_o \bar{f} = - \frac{l(r)}{c(r) \cos \phi} \delta(x^*) \bar{e}_n \quad (15)$$

$c(r) \cos \phi$ is the projection of the blade chord on the rotor plane so that

$$\rho_o \bar{f} = - \frac{l(r)}{a} \delta(x^*) \bar{e}_n \quad (16)$$

At a fixed angular position $\theta = 0$, for the successive passage of N_B blades

$$\begin{aligned} \rho_o \bar{f} &= - \frac{l(r)}{a} \delta(x^*) \bar{e}_n & 0 \leq t \leq \tau \\ &= 0 & \tau \leq t \leq \frac{2\pi}{N_B \Omega} \end{aligned} \quad (17)$$

The body force per unit volume is periodic with period

$$T = \frac{2\pi}{N_B \Omega}$$

and can be expressed in the Fourier Series

$$\rho_o \bar{f} = - \frac{l(r)}{a} \delta(x) \sum_{m=-\infty}^{\infty} C_m e^{imN_B \eta t} \quad (18)$$

where $\eta = \frac{\Omega R}{c}$ and

$$C_m = \frac{\sin mN_B \Omega \tau + i(\cos mN_B \Omega \tau - 1)}{2\pi m} \quad (19)$$

The body force per unit volume can be resolved into thrust and torque components on the basis of the angle which orients the velocity seen by the blade. The components are

$$\rho_o f_t = - \frac{l(r)}{a} \cos \beta \delta(x) \sum_{m=-\infty}^{\infty} C_m e^{imN_B \eta t} \quad (20)$$

$$\rho_o f_m = \frac{l(r)}{a} \sin \beta \delta(x) \sum_{m=-\infty}^{\infty} C_m e^{imN_B \eta t} \quad (21)$$

Note that these body forces are on the fluid and are therefore opposite to the corresponding forces on the blade. The thrust component is rearward and the torque component is in the direction of blade rotation.

The development to this point is for the reference location $\theta = 0$. At any other location the same temporal event occurs with the phase lag $\Delta t = \theta/\Omega$. Hence at any angle, in non-dimensional form

$$f_t = - \frac{1}{\rho c_o^2} \left(\frac{l(r)}{a} \right) \cos \beta \delta(x) \sum_{m=-\infty}^{\infty} C_m e^{imN_B \eta t} e^{-imN_B \theta} \quad (22)$$

$$f_m = \frac{1}{\rho c_o^2} \left(\frac{l(r)}{a} \right) \sin \beta \delta(x) \sum_{m=-\infty}^{\infty} C_m e^{imN_B \eta t} e^{-imN_B \theta} \quad (23)$$

The body force per unit volume has frequencies which are integer multiples of the blade passage frequency $N_B \Omega$. The nondimensional form is obtained by noting that the nondimensional body force per unit volume is obtained from the dimensional form by dividing by c_o^2/R . Furthermore, the dimensional Dirac delta function with the dimensional argument is nondimensionalized by division by R .

FINITE ELEMENT FORMULATION

Equation (2) is the field equation which governs the radiated sound field generated by the distribution of body forces \vec{f} which are defined by equations (22) and (23). References (4-9) give details of the finite element discretization of equation (2). Here the important features are reiterated.

A Galerkin weighted residual formulation seeks a solution for the acoustic pressure p among the class of functions C^1 with continuous first derivatives which satisfy the weighted residual statement

$$\begin{aligned} & \iiint_V W_i \left[\nabla \cdot (\nabla p - M^2 \frac{\partial p}{\partial x} \vec{i} - \vec{f}) - 2i\eta M \frac{\partial p}{\partial x} + \eta^2 p \right] dV \\ & - \iint_S W_i \left[(\nabla p - M^2 \frac{\partial p}{\partial x} \vec{i}) \cdot \vec{n} - (\nabla \bar{p} - M^2 \frac{\partial \bar{p}}{\partial x} \vec{i}) \cdot \vec{n} \right] dS \\ & = 0 \end{aligned} \quad (24)$$

for piecewise continuous weighting functions W_i . Equation (24) is the combination of the volume weighted residual of the field equation and the surface area weighted residual of a combination of terms which turns out to be the natural boundary condition. The overbar on \bar{p} signifies that it is to be designated on S . The weak form of equation (24) is obtained by using the divergence theorem to reduce the level of continuity required of the solution p . In this form a solution p is sought in the class of continuous functions C^* , with piecewise continuous first derivatives such that

$$\begin{aligned} & \iiint_V \left[\nabla W_i \cdot \left(\nabla p - M^2 \frac{\partial p}{\partial x} \vec{i} \right) + 2i\eta M W_i - \eta^2 W_i p \right] dV \\ & = \iint_S \nabla W_i \cdot \vec{f} dV + \iint_S W_i \left(\nabla \bar{p} - M^2 \frac{\partial \bar{p}}{\partial x} \vec{i} \right) \cdot \vec{n} dS \end{aligned} \quad (25)$$

for all weighting functions W_i in C^* . Use is made of the fact that \vec{f} , the body force, vanishes on the boundary S of the domain V . The body forces are distributed over the volume V_f . \vec{n} is the unit normal vector out of the volume V .

Because of the axial symmetry of the geometry of the nacelle, equation (25) is implemented in cylindrical coordinates. Figure 3 shows the bounding surfaces of the computational domain in a $\theta = \text{constant}$ slice. The surfaces of the center body S_c and the nacelle S_N are rigid so that $\nabla p \cdot \vec{n} = 0$. On these surfaces the natural boundary condition is given by the surface integral in equation (25), which if it were to vanish on S_c and S_N would require that

$$(\nabla p - M^2 \frac{\partial p}{\partial x} \bar{i}) \cdot \bar{n} = 0 \quad (26)$$

on S_c and S_N . As noted previously, the pressure formulation used here does not allow the specification of the details of the mean flow in the neighborhood of the nacelle lip and the centerbody tip due to the restriction of a uniform axially directed flow inside and outside the nacelle. The important features that are missing are the tangency of the mean flow in the vicinity of the nacelle lip and centerbody tip and the flow gradients which exist there. The flow gradients exist over a length scale which is short compared to a wave length and can reasonably be neglected. The boundary condition of equation (26) is derived on the basis of the restriction of uniform axial flow and hence that the normal \bar{n} is perpendicular to the x axis so that $\bar{i} \cdot \bar{n} = 0$. Just as the flow is not tangent to the surface of the nacelle near the nacelle lip and centerbody tip, $\bar{i} \cdot \bar{n}$ does not vanish. In the pressure formulation described here, equation (26) is taken as the natural boundary condition for all rigid surfaces with the argument that in a more exact formulation, for example, the velocity potential formulation of References [8,9], the equivalent boundary condition would be based on the tangential component of mean flow, and would therefore vanish. The validity of these assumptions can only be tested by checking the computational results and looking for anomalies in the radiated acoustic field near the nacelle lip and centerbody tip.

In the case when the propeller is unshrouded, the surface integral on S_c and S_N does not exist (in the present study the center body does not exist if the propeller is unshrouded). For the unshrouded case the uniform axial flow assumption is also not rigorously true because of flow gradients which must exist to account for the momentum increase which creates the thrust. No known propeller acoustic model accounts for this. In this context, the formulation for the shrouded case is viewed as equivalent. With these arguments, equation (25) is taken as the weak form with the surface integral existing only on S_∞ , the reflection free outer boundary. The important features of the finite element mesh used in the discretization of equation (25) are discussed in [4,8,9].

The volume integral over the distribution of body forces representing rotor alone noise generation requires some special treatment because of the nature of the loading in the form of a Dirac delta function. Details are discussed in Reference [4].

The large set of algebraic equations created by the FEM discretization of equation (25) is solved by using a frontal solution routine. The resulting nodal pressures are postprocessed to create an acoustic directivity pattern, which is a contour of equal sound pressure level (SPL) on an x-r plane sliced out of the cartesian system, side line SPL, which is a plot of SPL on a line parallel to the axis and at a specified distance, and polar SPL, which is a plot of SPL at a fixed polar radius centered on the nacelle. Polar SPL results for several cases can be superposed on a summary polar SPL plot. Only polar SPL results are shown here.

COMPUTATIONAL RESULTS

In this study rotor alone noise for a shrouded propeller will be compared to unshrouded propeller noise for a fixed thrust. Computations were made using the finite element procedures implemented in two codes, one specifically for the shrouded case, and the other for the unshrouded case.

A. Nacelle and Propeller Configuration

A model scale propeller and nacelle is considered here. The propeller has four or eight blades and is of dimensional radius 0.311 m (1.02 ft). The blade chord is taken to be uniform at 0.052 m (0.17 ft). The non-dimensional propeller angular velocity is taken as $\eta = 0.8$ and $\eta = 0.9$ in the subsonic case and $\eta = 1.2$ in the supersonic case. For a speed of sound of 1125 ft/sec, this corresponds to angular speeds $\Omega = 8426$ RPM and $\Omega = 9479$ RPM for the subsonic case and $\Omega = 12639$ RPM for the supersonic case. The nacelle geometry is shown in Figure 4. In the unshrouded propeller case no centerbody is present. This has only a slight effect on the propeller loading. The source location, whether rotor alone or EGV interaction, is just ahead of the center of the nacelle. The flow velocity inside and outside of the nacelle is $M = 0.4$.

B. Rotor Alone Noise

Figures 5 and 6 are summaries of the polar radiation directivity for four and eight blade shrouded propellers with comparisons to similar unshrouded propellers. Both supersonic and subsonic tip speeds are shown. Figure 5 is the four blade case. For supersonic tip speed, $\eta = 1.2$, the (4,1) mode (fourth angular, first radial) is cut off with cutoff ratio $\xi_{41}(1.2) = 0.988$ while at subsonic tip speeds it is cut off with cut off ratios $\xi_{41}(0.9) = 0.74$ and $\xi_{41}(0.8) = 0.66$. The corresponding attenuations based on the cut off ratio in the duct length of 1.3R are 10 dB, 44 dB, and 49 dB. It is seen that the peak radiated noise at a distance of ten duct radii is 120 dB created by the unshrouded propeller (this sets the scale level for the plot). The shrouded supersonic propeller has a peak level of about 109. The unshrouded subsonic propeller with $\eta = 0.9$ peaks at 114 dB and the case with $\eta = 0.8$ peaks at 112 dB. The corresponding shrouded propellers peak at 80 dB and 74 dB. The relationship of the SPL levels of the shrouded propellers below those of the unshrouded propellers is consistent with the projected attenuations due to the cutoff phenomenon, though not numerically equivalent. The comparison of the SPL levels of the two subsonic shrouded propellers with the supersonic shrouded propeller shows additional attenuations for the subsonic cases which are also consistent.

For the eight blade propeller a somewhat different picture emerges, as shown in Figure 6. For supersonic tip speed the (8,1) mode is propagating with $\xi_{81}(1.2) = 1.085$, but for the subsonic tip speeds it is cut off with $\xi_{81}(0.9) = 0.81$ and $\xi_{81}(0.8) = 0.72$ with calculated attenuations of 70 dB and 83 dB. Reference to Figure 6 shows that the shrouded propeller at supersonic tip speed creates the highest SPL and sets the scale level at 130 dB. The corresponding unshrouded propeller has a peak level about 10 dB lower. The unshrouded

subsonic propeller at $\eta = 0.9$ peaks at about 112 dB and the corresponding shrouded case is heavily attenuated at only about 74 dB. This attenuation of 56 dB with respect to the shrouded supersonic propeller is consistent with the cutoff phenomenon. A similar result applies when $\eta = 0.8$. The unshrouded propeller peaks at 108 dB while its shrouded counterpart peaks at 39 dB (hardly visible on the figure). This attenuation of 91 dB with respect to the shrouded supersonic propeller is also consistent with the cutoff phenomenon. The interesting feature here is the high peak SPL of the shrouded propeller. The (8,1) mode for the supersonic case is cut on, as opposed to the (4,1) mode being slightly cut off for the four blade propeller. It appears that the mechanics of wave propagation in the duct enhances the radiation of the ducted propeller noise when the mode is cut on.

SUMMARY

Several important observations can be made. 1) Contrary to the usual understanding of the Tyler and Sofrin result [1], supersonic tip speed rotor noise can be cut off if the tip Mach number is only slightly in excess of unity and if the number of blades is relatively small. If there are many blades, the fundamental angular mode number is large, and the Tyler and Sofrin result for thin annuli becomes more relevant. 2) Shrouding of subsonic tip speed propellers is a very effective means of controlling rotor alone noise. 3) There appears to be no benefit in terms of the peak radiated SPL for shrouded supersonic propellers when the fundamental mode is propagating.

ACKNOWLEDGEMENT

The investigation described here was carried out with the support of NASA Langley Research Center.

REFERENCES

1. Tyler, J. M. and Sofrin, T. G., "Axial Flow Compressor Noise Studies," Society of Automotive Engineers Transactions 70, pp. 309-332, 1962.
2. Hanson, D.B., "Near Field Frequency Domain Theory of Propeller Noise," AIAA Paper 83-0688, 1983.
3. Gutin, L., "On the Sound Field of a Rotating Propeller," NACA TM 1195, 1948 (originally in Russian 1936).
4. Eversman, W. and Steck, J. E., "Finite Element Modeling of Acoustic Singularities with Application to Propeller Noise," Journal of Aircraft, Vol. 23, No. 4, April 1986, pp.275-282.
5. Eversman, W. and Baumeister, K. J., "Modeling of Wind Tunnel Wall Effects on the Radiation Characteristics of Acoustic Sources," Journal of Aircraft, Vol. 23, No. 6, June 1986, pp. 455-463.
6. Baumeister, K. J. and Eversman, W., "Effects of Wind Tunnel Wall Absorption on Acoustic Radiation of Propellers," Journal of Propulsion and Power, Vol. 5, No. 1, January-February 1989, pp.56-63.
7. Eversman, W., "Analytical Study of Wind Tunnel Acoustic Testing of Propellers," Journal of Aircraft, Vol. 27, No. 10, October, 1990, pp.851-858.

8. Eversman, W., Parrett, A. V., Preisser, J.S., and Silcox, R. J., "Contributions to the Finite Element Solution of the Fan Noise Radiation Problem," ASME Journal of Vibration, Acoustics, Stress, and Reliability in Design, Vol. 107, No. 2, February 1985, pp. 216-223.
9. Preisser, J. S., Silcox, R. H., Eversman, W. and Parrett, A. V., "A Flight Study of Tone Radiation Patterns Generated by Inlet Rods in a Small Turbofan Engine," Journal of Aircraft, Vol. 22, No. 1, January 1985, pp. 57-62.
10. Dommasch, D. O., Sherby, S. S. and Connally, T. F., Airplane Aerodynamics, Pitman, New York, 1967, pp. 219-233.
11. Vincent, E. T., The Theory and Design of Gas Turbines and Jet Engines, McGraw-Hill, New York, 1950, pp.324-335.

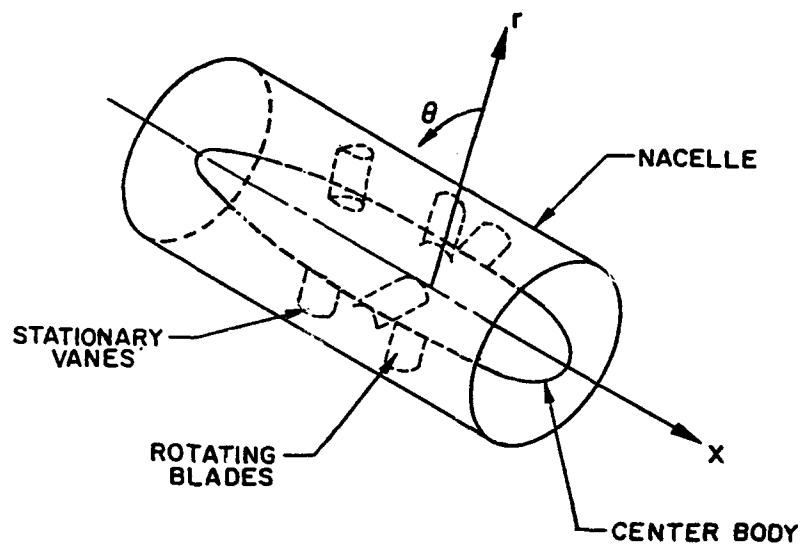


Figure 1. Geometry of Shrouded Propeller or Rotor.

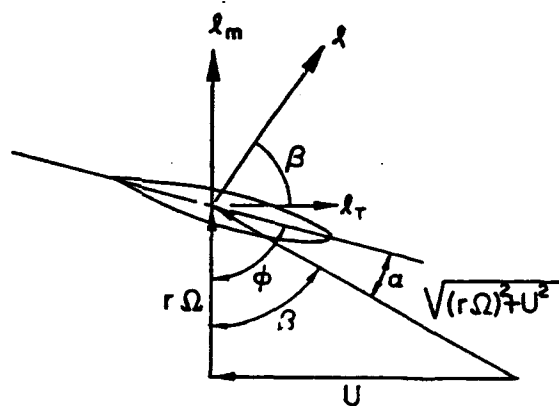


Figure 2. Velocities and Inflow Angles Experienced by a Blade Element.

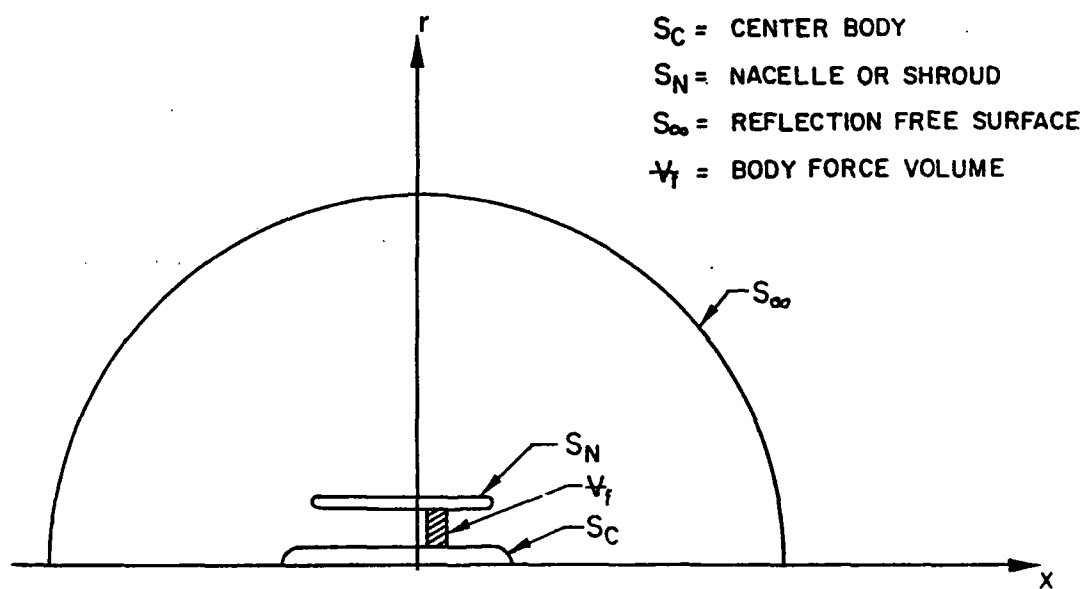


Figure 3. The Computational Domain.

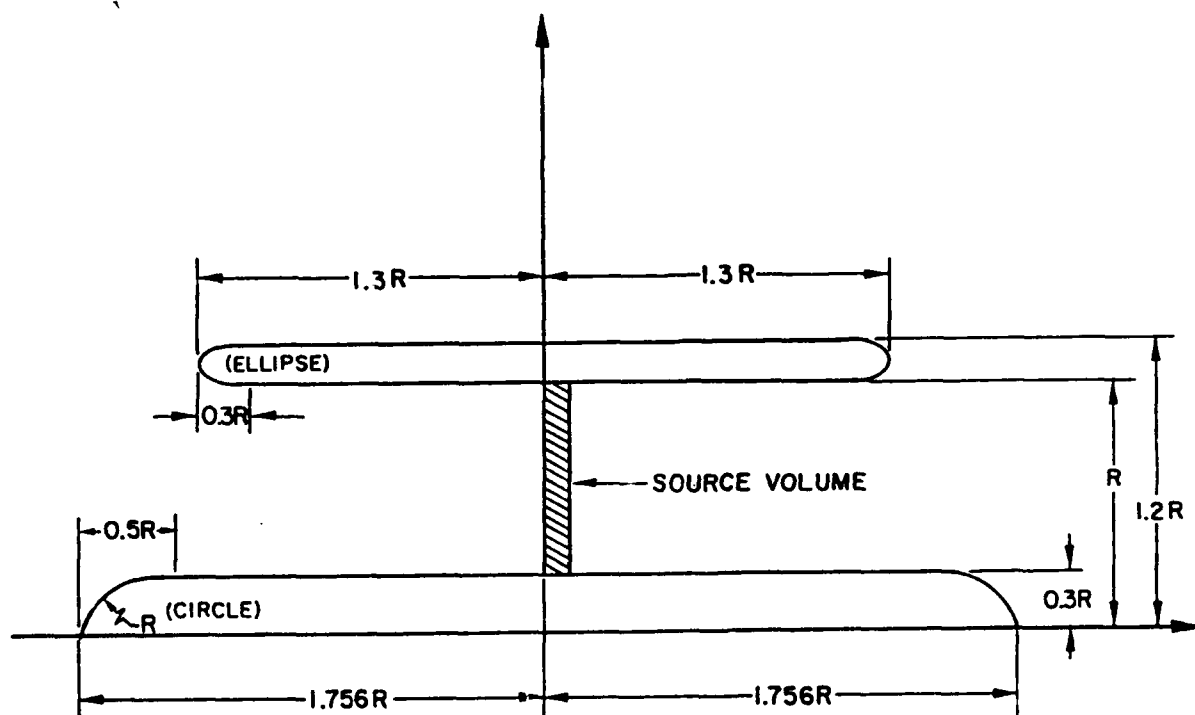


Figure 4. Idealized Shrouded Rotor for Example Cases.

SCALE LEVEL 120.14
 FLOW MACH NO. -0.40
 INLET MACH NO. -0.40
 ANGULAR MODE NO. 4

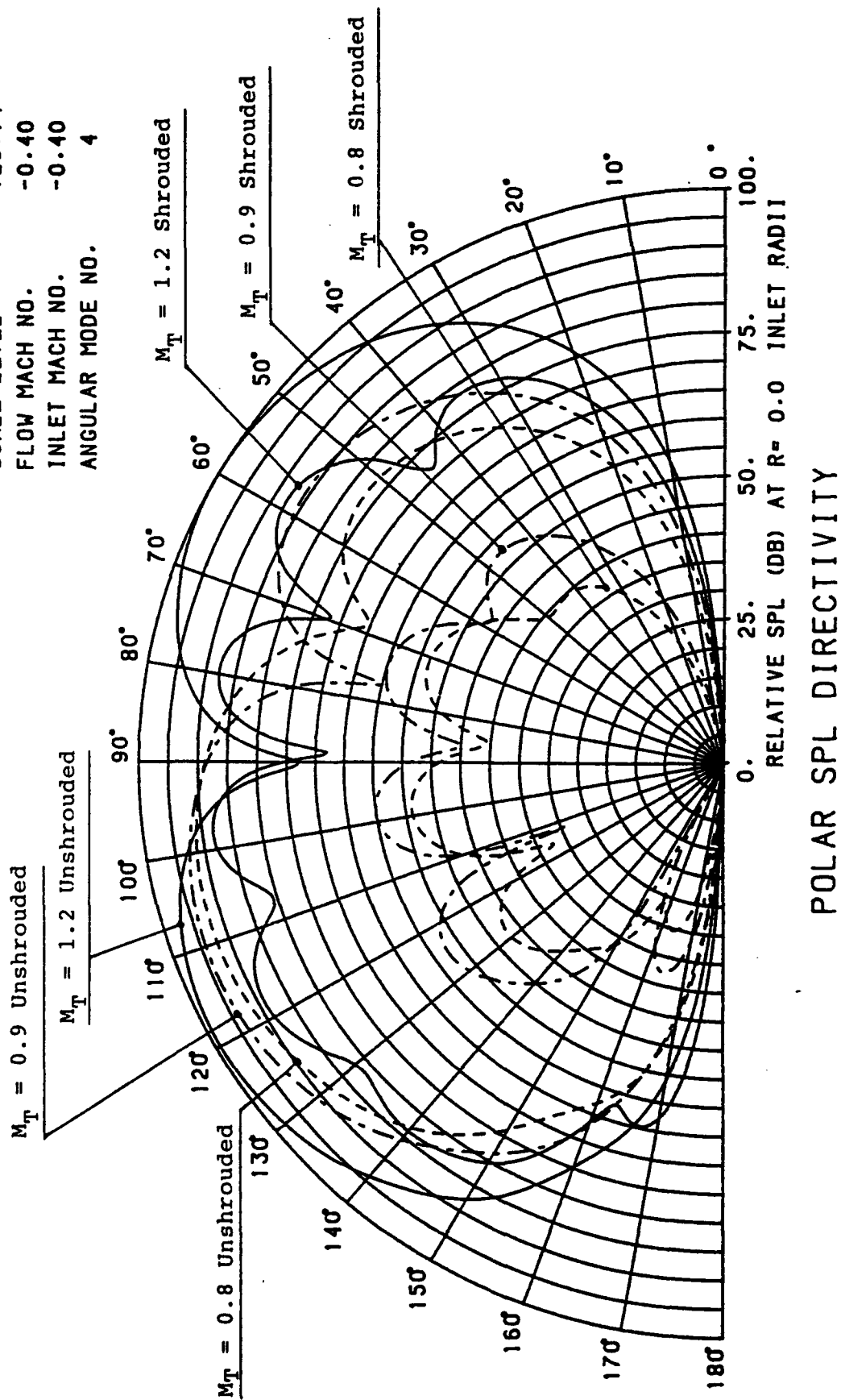


Figure 5. Radiated Acoustic Field for a Four Blade Propeller, Rotor Alone.
 Actual SPL is Relative SPL + 20.14 dB.

SCALE LEVEL 130.50
 FLOW MACH NO. -0.40
 INLET MACH NO. -0.40
 ANGULAR MODE NO. 8

$M_T = 1.2$ Shrouded

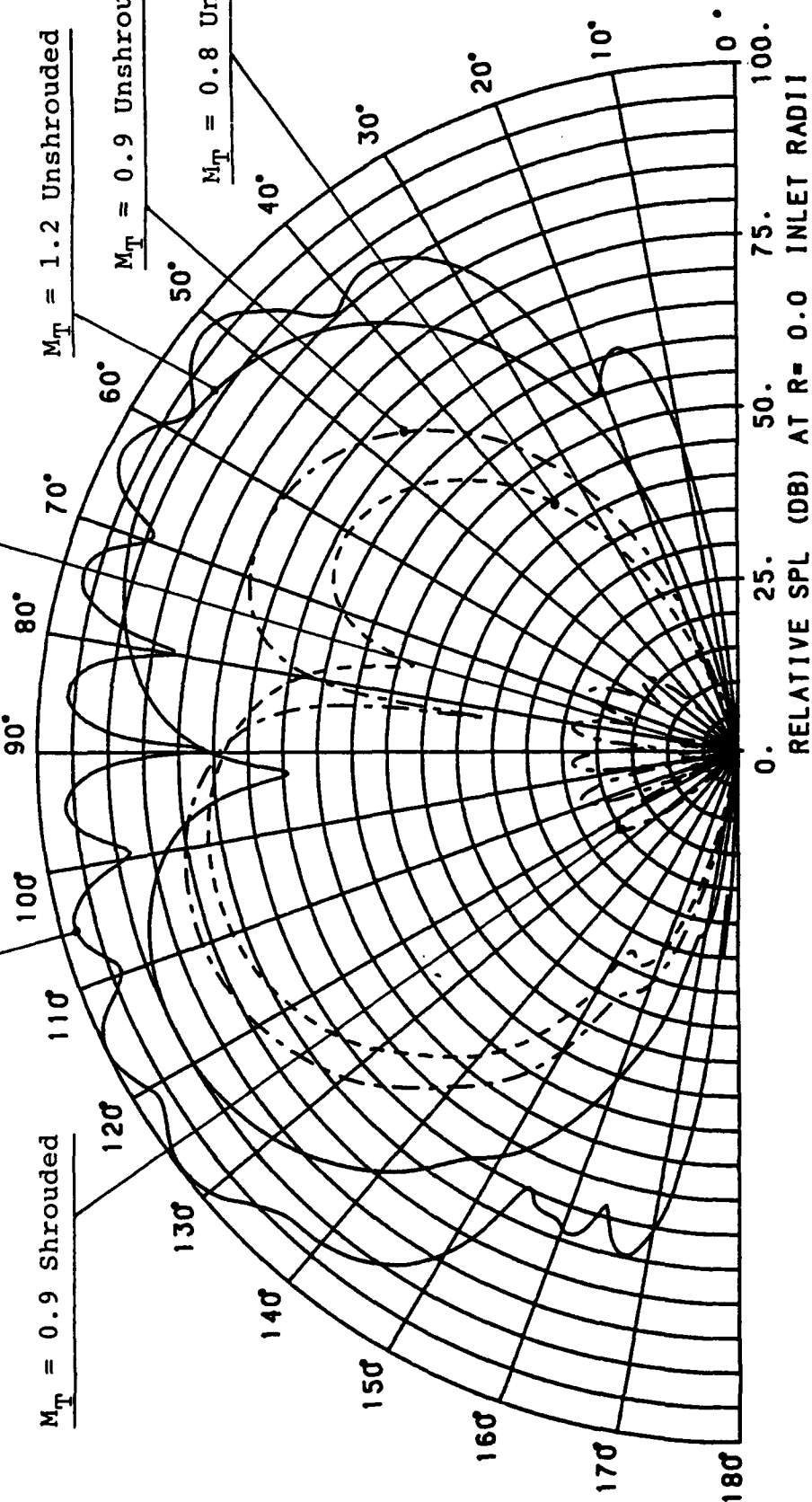
$M_T = 0.8$ Shrouded

$M_T = 0.9$ Shrouded

$M_T = 1.2$ Unshrouded

$M_T = 0.9$ Unshrouded

$M_T = 0.8$ Unshrouded



POLAR SPL DIRECTIVITY

Figure 6. Radiated Acoustic Field for Eight Blade Propeller,
 Rotor Alone. Actual SPL is Relative SPL + 30.5 dB.

**TWO LEADING-EDGE DROOP MODIFICATIONS FOR TAILORING
STALL CHARACTERISTICS OF A GENERAL AVIATION
TRAINER CONFIGURATION**

by

Holly M. Ross
NASA Langley Research Center
Hampton, VA
and
Dr. John N. Perkins
North Carolina State University
Raleigh, NC

For Presentation to the AIAA/FAA Joint Symposium on General
Aviation Systems at the Hilton Inn-East, Wichita, KS
on March 16-17, 1992

TWO LEADING-EDGE DROOP MODIFICATIONS FOR TAILORING STALL CHARACTERISTICS OF A GENERAL AVIATION TRAINER CONFIGURATION

by

**Holly M. Ross
NASA Langley Research Center
Hampton, Virginia**

**Dr. John N. Perkins
North Carolina State University
Raleigh, North Carolina**

Summary

As part of a cooperative research program between NASA Langley Research Center and the Smith Aircraft Corporation, wind-tunnel tests were performed on a 1/6-scale model of a general aviation trainer configuration in the Langley 12-Foot Low-Speed Tunnel. The purpose of these tests was to investigate the configuration's low-speed stability and control characteristics and its high-angle-of-attack characteristics. The focus of the high-angle-of-attack testing was to develop leading-edge modifications that would tailor the stall characteristics of the model.

Two different leading-edge modifications were determined. A small profile leading-edge droop on the outboard 24-percent of the wing was developed which kept the outboard wing flow attached to high angles of attack, resulting in increased roll damping and added aileron authority. The second leading-edge modification developed was a large profile leading-edge droop on the outboard 50-percent of the wing. This large droop kept the outboard wing flow attached to very high angles of attack which greatly improved the roll damping characteristics and stall/departure resistance as well as provided large increases in aileron authority.

The longitudinal stability for the baseline and both modified configurations were good for low angles of attack, but the modified configurations demonstrated neutral longitudinal stability just prior to stall. The baseline and both modified configurations exhibited good lateral stability characteristics for low angles of attack, but all configurations were directionally unstable at high angles of attack.

Introduction

Most general aviation stall/spin accidents occur at low-speed flight conditions, such as take off and landing. In these situations the aircraft is generally at a low altitude and thus the pilot has little time to recover control. The problem is magnified when the aircraft is a trainer with a student pilot flying. The use of wing leading-edge modifications, such as leading-edge droops, leading-edge slots, and vortex generators, has been the subject of many studies at NASA Langley Research Center. These studies have shown that these leading-edge modifications can be used successfully to improve the stall/departure characteristics of general aviation configurations and have demonstrated applications of these concepts to make several configurations spin resistant (references 1-5). In many cases the leading-edge modifications that provided the large improvements did so without significantly degrading cruise performance. Improvements such as these can be achieved through comprehensive testing including low-speed wind-tunnel tests and full-scale stall and spin tests.

Leading-edge droops have primarily been used on the outboard wing to keep the flow attached to higher angles of attack and have been applied successfully on many configurations. Leading-edge droop profiles are shaped so that the maximum negative pressure peak is greatly reduced at the leading edge of the airfoil, thus decreasing or alleviating the steep adverse pressure gradient that often exists. This characteristic allows achievement of higher angles of attack without flow separation. The sharp, discontinuous edges of leading-edge droops adds to the effectiveness by creating vortical flow which energizes the local boundary layer as well as

acts as an aerodynamic fence to keep the stalled inboard flow from spreading to the outboard wing, as illustrated in figure 1. The result of achieving more attached flow over the outboard portion of the wing is to increase roll damping at the stall and provide stall/departure resistance. Also, by keeping the outboard wing flow attached, the aileron effectiveness is generally maintained to higher angles of attack.

The configuration that was the subject of this investigation was a trainer aircraft that was designed by the Smith Aircraft Corporation. This aircraft was to have two different training roles. The first role was to provide a spinnable aircraft in which a student pilot could learn spin entry and spin recovery techniques. The second training role was to provide a spin-resistant aircraft that could be safely flown by student pilots without fear of inadvertent spins. It was thought that the two very different types of training could be accomplished with one aircraft design by modifying the wing leading edges in order to alter the high-angle-of-attack characteristics. General aviation wing designs usually incorporate some washout which improves the stall characteristics. Because the Smith design included a wing with no twist, a leading-edge modification would have to be used for both the spinnable and the spin resistant configurations to ensure good stall behavior. The leading-edge modification for the spinnable version would be used to provide a more gentle, controllable stall while still allowing the aircraft to enter a spin. Thus, the leading-edge modification would need to be relatively small and kept on the outboard wing only. In contrast, the spin resistant configuration should have a leading-edge modification that maintains attached flow on the outboard wing to very high angles of attack in order to provide good roll damping past the stall. This would require a relatively large leading-edge droop with enough chord extension and added camber to provide the needed attached flow.

The study reported on in this paper investigated the high angle of attack characteristics of the configurations using flow visualization, free-to-roll testing, and static force testing in a low-speed wind tunnel. These tests focused on stall characteristics and were not aimed at determining spin entry, developed spin, or spin recovery characteristics. It was the purpose of this investigation to define leading-edge modifications that could improve the stall characteristics of the spinnable configuration and greatly improve the stall/departure characteristics of the spin resistant configuration.

Nomenclature

b	wing span, ft
C_L	lift coefficient, $Lift/q_\infty S$
C_l	rolling moment coefficient, Rolling Moment/ $q_\infty S b$
ΔC_l	incremental rolling moment coefficient, $C_l \text{ deflected} - C_l \text{ undeflected}$
$C_{l\beta}$	lateral stability derivative, $\delta C_l / \delta \beta$
C_m	pitching moment coefficient, Pitching Moment/ $q_\infty S \bar{c}$
$C_{n\beta}$	directional stability derivative, $\delta C_n / \delta \beta$
C_n	yawing moment coefficient, Yawing Moment/ $q_\infty S b$
c	local wing chord, ft
\bar{c}	mean aerodynamic chord, ft
i	horizontal tail incidence, deg
q_∞	free-stream dynamic pressure, lb/ft ²
S	wing reference area, ft ²
α	angle of attack, deg
β	angle of sideslip, deg
δ_a	aileron deflection, deg
δ_e	elevator deflection, deg
δ_f	flap deflection, deg
δ_r	rudder deflection, deg

Abbreviations:

mac	mean aerodynamic chord
NLF	natural laminar flow

Description of Model and Test Techniques

A 1/6-scale model of the Smith Aircraft trainer configuration was used for the wind tunnel tests. The tests were performed at NASA Langley Research Center in the 12-Foot Low-Speed Tunnel at a free-stream dynamic pressure of 4 psf which corresponded to a free-stream tunnel velocity of 58 ft/sec. Based on the mean aerodynamic chord, the test Reynolds number was 269,400. Data were measured over an angle of attack range of -5° to 40° and an angle of sideslip range of -15° to 15° .

A three-view sketch of the model is shown in figure 2, and a photo of the model mounted in the tunnel is shown in figure 3. A summary of the model geometric characteristics is presented in Table I. The wing airfoil used was an NLF(1)-0414F which is designed to promote natural laminar flow. The fuselage

was constructed as a fiberglass shell, while the wings and tails were made of solid balsa wood. The spinner was the type used on radio-controlled models, but no propeller was installed. The model incorporated a conventional elevator, ailerons, and rudder and had slotted trailing-edge flaps. The control surface deflection ranges were as follows: $\delta_e = -20^\circ$ to $+8^\circ$, $\delta_f = 0^\circ$ to $+20^\circ$, $\delta_a = -20^\circ$ to $+20^\circ$, and $\delta_r = -35^\circ$ to $+35^\circ$, where positive values indicate trailing-edge down or trailing-edge left deflections. Radio-controlled model type servo-actuators were used to remotely deflect all of the control surfaces except for the flaps which were set with brackets. The horizontal stabilizer incidence was adjustable up and down by 2° .

Two different leading-edge droop profiles were tested and are shown in figure 4. Figure 4a shows the small droop, the profile selected to provide gentle stall characteristics for the spinnable configuration, and figure 4b shows the large droop, the profile selected to provide stall departure resistance for the spin resistant configuration. The small droop has the same leading-edge droop profile as tested on the Cessna T-210 outfitted with an NLF wing (reference 6). This droop was designed using the leading-edge contour of an NLF(1)-0215 airfoil faired into the NLF(1)-0414 original airfoil. The derived airfoil shape was intended to keep laminar flow over the upper and lower surfaces. The large droop was designed using a 2-dimensional droop design computer code which iterated on many input parameters, trying to decrease or alleviate the large negative pressure peak that occurred at the leading edge of the NLF(1)-0414F airfoil while keeping within prescribed limits on several other design values. This droop profile was not predicted to maintain laminar flow, and thus a drag penalty would be expected.

Free-to-roll tests were performed in order to determine suitable lengths for the leading-edge droops. This type of testing involves mounting the model on a special rig that allows the model to move freely about the roll axis. The free-to-roll technique was used because it gives a good indication of roll damping and stall/departure resistance. For this study, data gathered by this form of testing were purely qualitative. The runs were video taped, and observations were made regarding the angle of attack at which wing rock occurred and the relative magnitude. A great number of runs were made this way, and a large test matrix of leading-edge droop sizes and locations could be completed quickly.

Free-to-roll testing was used to determine desired lengths of the droops. The procedure followed was to

first test a droop with a span of 50-percent $b/2$. Then 1-inch was cut from the inboard side of the droops and the resulting configuration was tested. This procedure was followed until a trend developed relating the droop span to roll damping characteristics as determined from the wing rock displayed. From this information, the final droop spans were decided.

After the free-to-roll testing was completed, static force tests were performed to quantify the effects of the leading-edge droops on force and moment characteristics. Longitudinal and lateral-directional stability characteristics was the investigated as was the control effectiveness.

Very thin mylar tufts were used for flow visualization on the upper surface of the wing for all of the configurations tested. The tufts were on the model for the free-to-roll tests and the static force tests. Flow visualization results from the static force testing were used to chart the wing stall progression of the various configurations.

Results and Discussion

Free-To-Roll and Flow Visualization Results

Baseline Configuration. A stall map showing the stalled flow progression of the unmodified wing was made from the tuft patterns and is shown in figure 5. Separation first occurred at the wing-fuselage juncture near the trailing edge of the wing at $\alpha = 8^\circ$. This area of separated flow then began to spread outboard with increased angle of attack. At $\alpha = 12^\circ$, a stall cell began to form on the flap trailing edge, and by $\alpha = 14^\circ$, 75-percent of the wing had stalled. Large amplitude roll oscillations began at $\alpha = 16^\circ$ due to the loss of roll damping and continued until $\alpha = 23^\circ$, at which point the wing flow was completely separated.

Small Leading-Edge Droop Configuration. The flow visualization results for all of the small droop spans tested showed that the wing area behind the droop span maintained attached flow up to high angles of attack. Thus, the amount of attached flow could be increased by simply increasing the droop span. The free-to-roll tests showed that a droop span of 50-percent $b/2$ provided enough roll damping to prevent wing rock. It was shown that a shortened droop span maintained less attached flow, but still demonstrated good roll damping characteristics. The smallest droop span tested was 7-inches (24-percent $b/2$). This droop length kept attached flow over the ailerons and over the outboard section of the wing. It also provided enough roll

damping to prevent all but a slight wing drop at $\alpha = 16^\circ$. Because the results were so predictable with changing droop span, an optimized span could easily be determined in flight tests. It was believed that this droop would not inhibit a spin entry; however, free-to-roll testing could not provide such information. Free-to-roll tests were also performed with flap deflections of 10° and 20° which showed only slight degradations in the roll damping characteristics.

Figure 6 shows the stall map for the 7-inch small droop configuration. As expected, the inboard section of the wing was generally unaffected by the outboard droop. Up to $\alpha = 20^\circ$, the flow directly behind the droop remained attached, whereas the unmodified wing flow was completely separated except at the very tip. This improvement in the outboard flow provided the increased roll damping observed in the free-to-roll testing. Figure 6 also shows that the ailerons had attached flow up to $\alpha = 18^\circ$ or 20° which improved the lateral control capability at high angles of attack.

Large Leading-Edge Droop Configuration. The large leading-edge droop results were similar to those for the small droop. The large droop promoted attached flow on the wing directly behind the droop span up to high angles of attack and thus increased the roll damping. The span determined to be the best was 14.69-inches (50-percent $b/2$). At this span, the droop provided attached flow over nearly half of the wing up to $\alpha = 27^\circ$, as shown in figure 7, and provided enough roll damping to prevent wing rock for all the angles of attack tested. The ailerons had attached flow until $\alpha = 27^\circ$ indicating good aileron control. The large droop configuration was deemed stall departure resistant and possibly spin resistant; however, spin resistance could not be determined by the tests conducted in this study.

Static Force Test Results

Baseline Configuration. Presented in figure 8 are the lift and pitching moment characteristics of the baseline configuration. The lift curve shows the maximum lift occurred between $\alpha = 12^\circ$ and 14° . The lift curve dropped sharply after that point, indicating an abrupt stall. The pitching moment data, reduced using a center-of-gravity location of 25-percent \bar{c} , showed good longitudinal stability at low angles of attack. The stability was reduced somewhat at $\alpha = 6^\circ$, but the stability was improved after the stall. Flow visualization showed that the increased pitch-down that occurred after $\alpha = 12^\circ$ was due to the separation of flow

on the wing while the attached flow was maintained on the horizontal tail.

The lateral-directional stability characteristics of the baseline configuration are presented in figure 9. The derivatives $C_{n\beta}$ and $C_{l\beta}$ were obtained from tests conducted at sideslip angles of 5° and -5° . The directional stability, as shown in the $C_{n\beta}$ vs α plot, was good at low angles of attack, but at $\alpha = 18^\circ$, the directional stability approached neutral and became unstable at $\alpha = 22^\circ$. This was due to the vertical tail becoming immersed in the stalled wake of the wing at these higher angles of attack and thus losing its effectiveness. The lateral stability, as shown in the $C_{l\beta}$ vs α plot, shows negative values of $C_{l\beta}$ for the entire angle of attack range tested indicating stable effective dihedral.

Small Leading-Edge Droop Configuration. The lift and pitching moment characteristics which compare the small droop profile with a 7-inch span to the unmodified wing are shown in figure 10. The unmodified wing data shown in figure 10 were taken with a horizontal tail incidence of $i = 0^\circ$. The tail incidence was later changed to $i = 1^\circ$, trailing-edge up, in order to better represent the design trim specifications. The data shown for the small droop configuration was taken with $i = 1^\circ$. Comparison of lift curves for the two configurations show that the small droop configuration closely resembled the unmodified wing at low angles of attack but had a slightly higher value of C_{Lmax} . Most notable was the effect of the small droop above C_{Lmax} . The small droop configuration showed an increment in lift which made the stall more gradual. The added lift came from the attached flow that the droop provided at angles of attack where the unmodified wing had separated flow. Thus, the small droop was able to improve the stall characteristics. The longitudinal stability of the small droop configuration decreased between $\alpha = 8^\circ$ and 10° but broke stable after the stall. The pitching moment trim change was due to the difference in tail incidences as previously discussed.

Figure 11 shows the lateral-directional characteristics of the small droop configuration compared to the unmodified wing. The directional stability is essentially unchanged with the small droop for the low angles of attack, but a slight improvement occurred between $\alpha = 20^\circ$ and 28° . In this region, the unmodified configuration was unstable, but the small droop configuration was stable. The lateral stability showed only negligible changes due to the modification.

Figure 12 shows a comparison of maximum aileron effectiveness for the unmodified wing and the small droop configuration. The control power for low angles of attack differed insignificantly for the two configurations. However, at $\alpha = 10^\circ$, the unmodified wing started to lose aileron authority abruptly while the small droop configuration was able to maintain good authority until about $\alpha = 25^\circ$. This was due to the attached flow on the outboard wing that the small droop modification provided. The additional lateral control gained at the stall and beyond would improve the pilot's ability to counteract any roll-off that might occur at high angles of attack.

Large Leading-Edge Droop Configuration. The lift and pitching moment characteristics for the large leading-edge droop modification are presented in figure 13. The lift curve showed no major changes compared to the unmodified wing at low angles of attack and only a slight increase in the stall C_L . As with the small droop, the real benefit of the large droop was the increment in lift above stall that resulted in a more gradual stall. The lift curve reflects the stall pattern seen in the tuft flow visualization (figure 7). After the initial separation that occurred on the inboard wing, the outboard wing flow remained attached until between $\alpha = 27^\circ$ and 33° , which is reflected in the additional lift at these high angles of attack. The longitudinal stability for the large droop configuration decreased before stall and was neutrally stable between $\alpha = 10^\circ$ and 12° . Similar behavior was also seen for the small droop configuration.

Presented in figure 14 are the lateral-directional stability characteristics for the large droop configuration. The directional stability was degraded from the unmodified wing configuration after $\alpha = 12^\circ$ and became unstable at $\alpha = 18^\circ$. Because this configuration was designed to be spin resistant, directional instability would be an undesirable characteristic. Although it was not pursued in this study, the addition of a ventral fin or added vertical tail area could improve this situation. The spike in the data that occurred at $\alpha = 30^\circ$ is believed to be due to an asymmetric separation of flow behind the droop at that angle of attack. Only insignificant changes were seen in lateral stability compared to the unmodified configuration.

The effect of the large droop on the maximum lateral control authority is shown in figure 15. These data show that the large droop maintained a very high level of roll control up to $\alpha = 30^\circ$ due to the attached flow on the outboard wing sections. Except for a small

loss around $\alpha = 14^\circ$, the aileron control authority remained nearly constant from $\alpha = 0^\circ$ to 30° . In the $15^\circ \leq \alpha \leq 30^\circ$ region, the control authority was close to twice the authority of the unmodified wing. The added control gained by the droops would enable a pilot to maintain near full lateral control up to and beyond stall.

Summary of Results

A wind tunnel investigation was performed on a general aviation trainer configuration in order to define two different leading-edge modifications that could tailor the aircraft's high-angle-of-attack characteristics. Also, static stability and control characteristics were evaluated. The major results of this test are summarized below:

1. The baseline configuration had an abrupt stall as shown by flow visualization and static force data. The free-to-roll tests showed large amplitude roll oscillations between $\alpha = 16^\circ$ and $\alpha = 23^\circ$ due to the loss in roll damping caused by outboard wing flow separation.
2. A small, outboard leading-edge droop with a 7-inch span (24-percent $b/2$) was found to be effective in keeping the outboard wing flow attached to high angles of attack, making the stall less abrupt and providing an improvement in roll damping. This modified configuration showed minimal wing rock in the free-to-roll tests. Also, aileron authority was improved for angles of attack past stall due to the increase in attached flow over the ailerons.
3. A large, outboard leading-edge droop with a span of 50% $b/2$ was found to be effective in keeping the outboard wing flow attached to very high angles of attack, making the stall less abrupt and greatly improving the roll damping. This modified configuration showed no wing rock in the free-to-roll tests. Also, aileron authority was maintained up to very high angles of attack due to the increase in attached flow over the ailerons.
4. The longitudinal stability of the baseline and both modified configurations was good at low angles of attack but degraded as stall was approached. Both the small droop and large droop configurations showed a decrease in longitudinal stability near the stall but had good stability characteristics the stall break.
5. The lateral-directional stability characteristics of the baseline configuration were good except for the high angle of attack region where the configuration became directionally unstable. The small droop configuration showed a slight increase in directional stability for high angles of attack, but showed no appreciable change in lateral stability. The large droop configuration showed

degraded directional stability at high angle of attack compared to the unmodified configuration, but no appreciable change in lateral stability.

Acknowledgements

The authors wish to thank Messrs. Joseph Stickle, Paul Stough, and David Robelen of NASA Langley Research Center for their inputs and help on this research project, and Messrs. Mike Smith and Bob Stewart of Smith Aircraft Corp. for their involvement.

References

1. Staff of Langley Research Center: *Exploratory Study of the Effects of Wing Leading-Edge Modifications on the Stall/Spin Behavior of a Light General Aviation Airplane*, NASA TP-1589, 1979.
2. Newsome, William A.; Satran, Dale R.; and Johnson, Joseph L., Jr.: *Effect of Wing Leading-Edge Modifications of a Full-Scale, Low-Wing General Aviation Airplane*, NASA TP-2011, 1982.
3. Stough, H. Paul, III; DiCarlo, Daniel J.; and Stewart, Eric C.: *Wing Modification for Increased Spin Resistance*, SAE Paper No. 830720, April 1983.
4. Stough, H. Paul III; DiCarlo, Daniel J.; and Patton, James M., Jr.: *Flight Investigation of the Effects of an Outboard Wing Leading-Edge Modification on Stall/Spin Characteristics of a Low-Wing, Single-Engine, T-Tail Light Airplane*, NASA TP-2691, 1987.
5. Ross, Holly M.; Yip, Long P.; Perkins, John N.; Vess, Robert J.; and Owens, D. Bruce: *Wing Leading-Edge Droop/Slot Modification for Stall Departure Resistance*, *Journal of Aircraft*, Vol. 28, No. 27, July 1991, pp.436-442.
6. Murri, Daniel G.; and Jordan, Frank L., Jr.: *Wind Tunnel Investigation of a Full-Scale General Aviation Airplane Equipped with an Advanced Natural Laminar Flow Wing*, NASA TP-2772, November 1987.

Table I - Model Geometric Characteristics

Wing:

Area, ft ²	4.44
Span, ft.....	6.14
Mean aerodynamic chord, ft.....	0.73
Root chord, ft.....	0.86
Tip chord, ft.....	0.58
Aspect ratio.....	8.48
Taper ratio	0.68

Wing incidence (root).....	0°
Dihedral angle.....	3°
Twist.....	0°
Leading edge sweep angle.....	1.3°
Trailing edge sweep angle	3.88°
Airfoil.....	NLF(1)-0414F

Split flap:

Area (one), ft ²	0.30
Inboard wing station	4.42
Outboard wing station.....	23.72
Span (per side), ft.....	1.61
Chord, percent c.....	25

Aileron:

Area (one), ft ²	0.13
Inboard wing station	23.72
Outboard wing station.....	33.11
Span, ft.....	0.78
Chord, percent c.....	25

Horizontal tail:

Area, ft ²	0.81
Span, ft.....	1.92
Root chord, ft.....	0.52
Tip chord, ft.....	0.35
Incidence (adjustable).....	-2° to 2°
Elevator area, ft ²	0.32
Airfoil.....	NACA 66-009

Vertical tail (including rudder):

Area (reference), ft ²	0.43
Span (reference), ft.....	0.84
Root chord (reference), ft.....	0.68
Tip chord, ft.....	0.39
Rudder area, ft ²	0.26
Airfoil.....	NACA 66-009

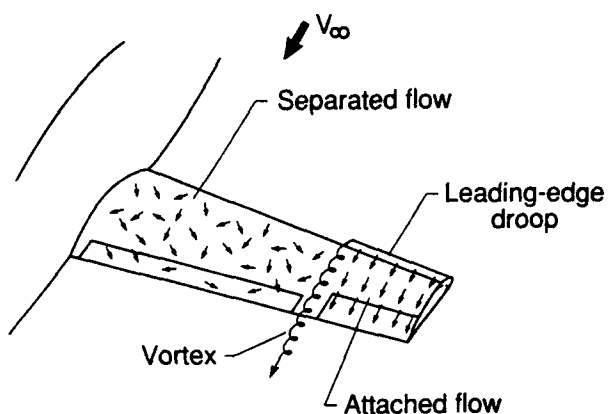


Figure 1. Leading-edge droop aerodynamics.

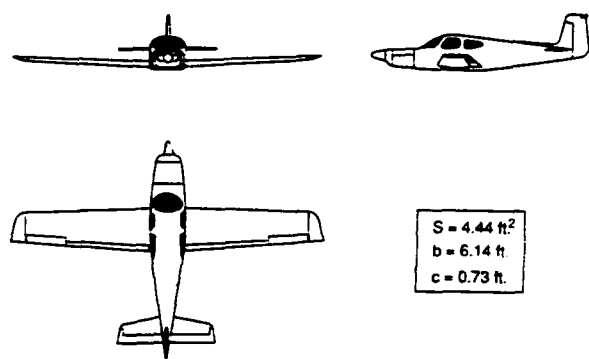


Figure 2. Three view sketch of model.

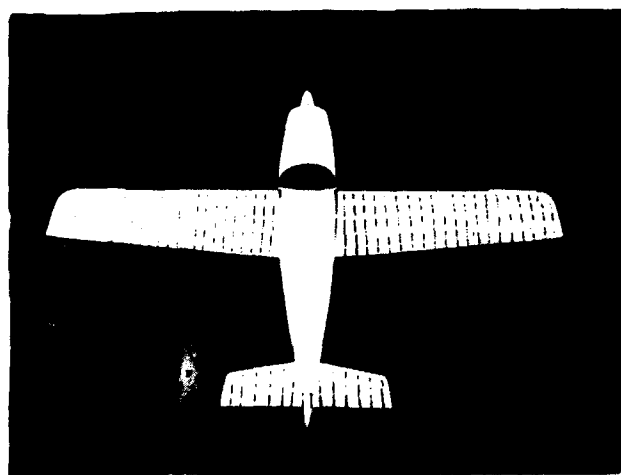


Figure 3. Photo of model mounted in the wind tunnel.

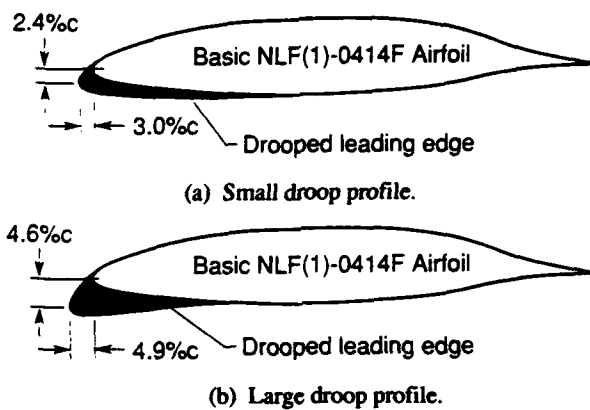


Figure 4. Leading-edge droop modifications.

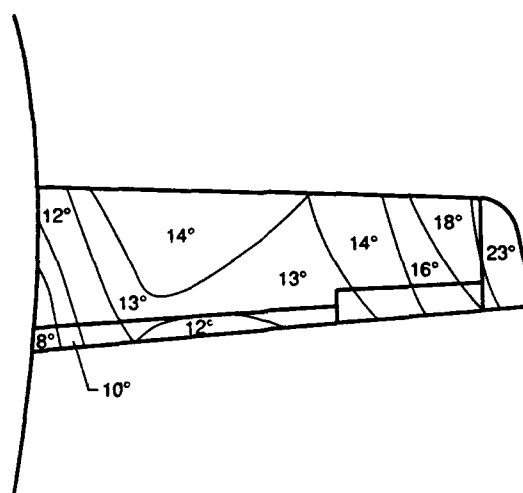


Figure 5. Baseline wing stall pattern. Numbers indicate the angle of attack at which separated flow first occurred.

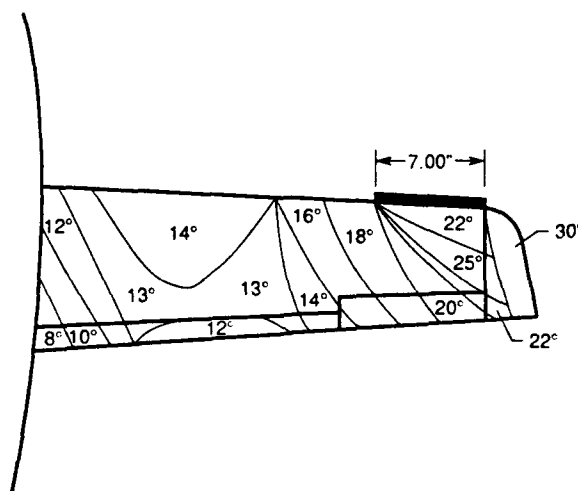


Figure 6. Small droop configuration stall pattern.

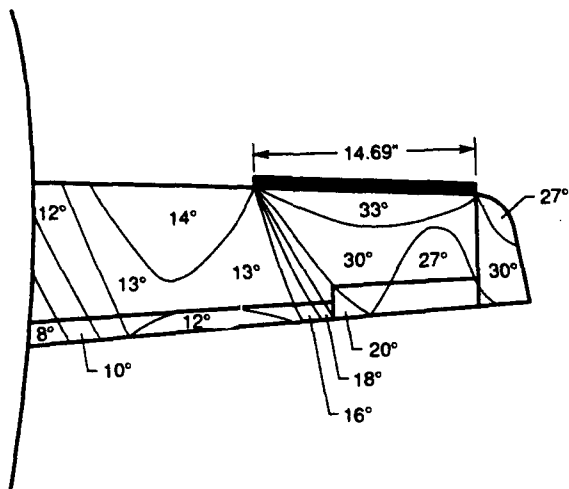


Figure 7. Large droop configuration stall pattern.

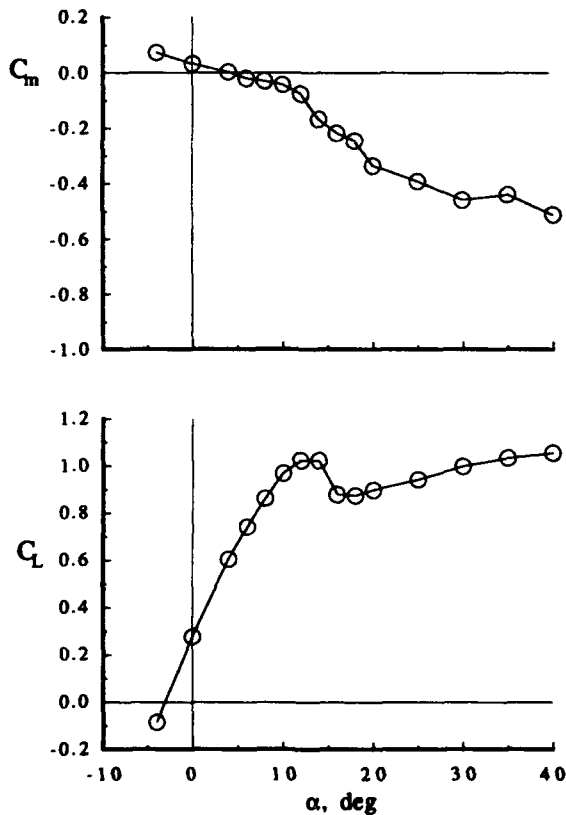


Figure 8. Longitudinal characteristics, baseline configuration.

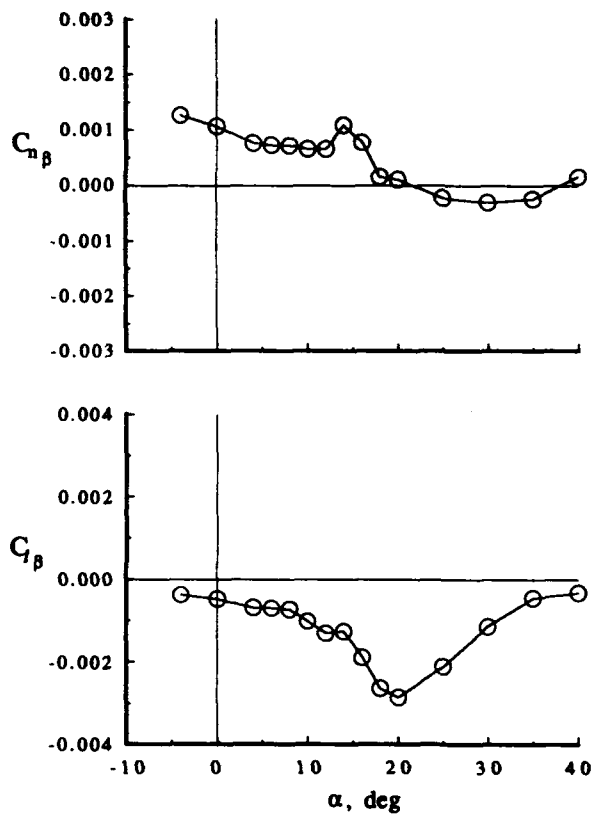


Figure 9. Lateral-directional stability characteristics, baseline configuration.

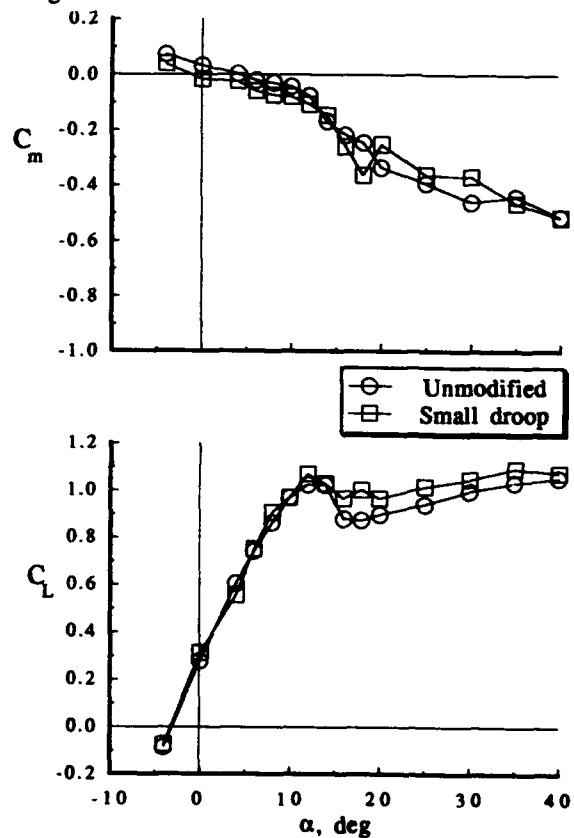


Figure 10. Longitudinal characteristics, small droop configuration.

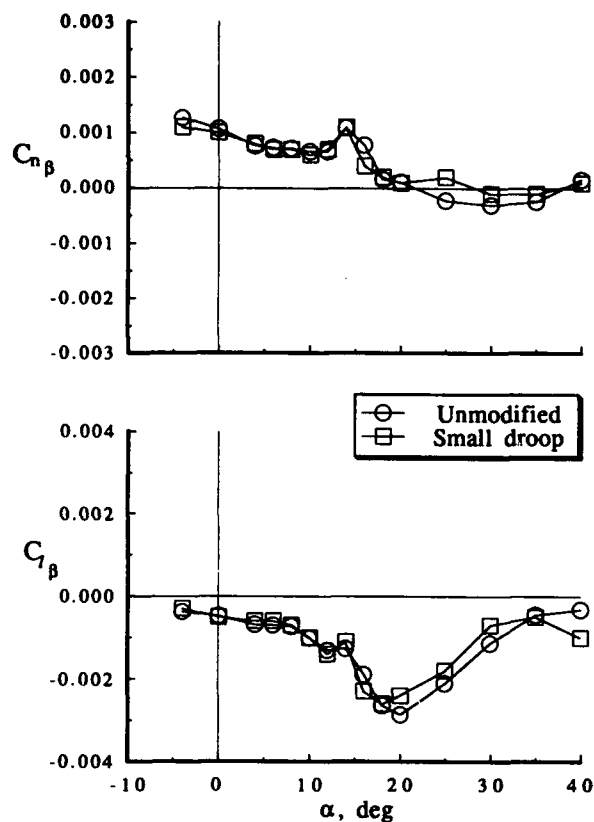


Figure 11. Lateral-directional stability characteristics, small droop configuration.

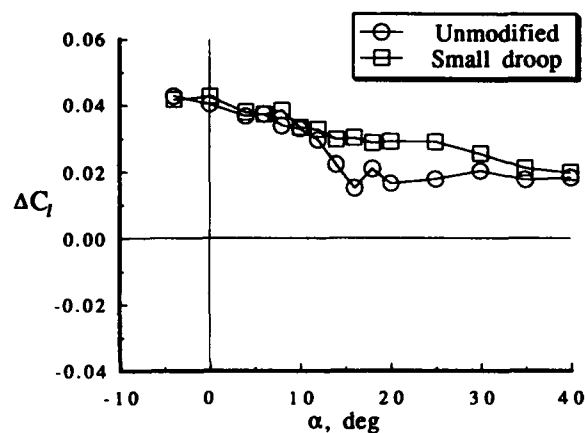


Figure 12. Effect of the small droop modification on the maximum lateral control authority.

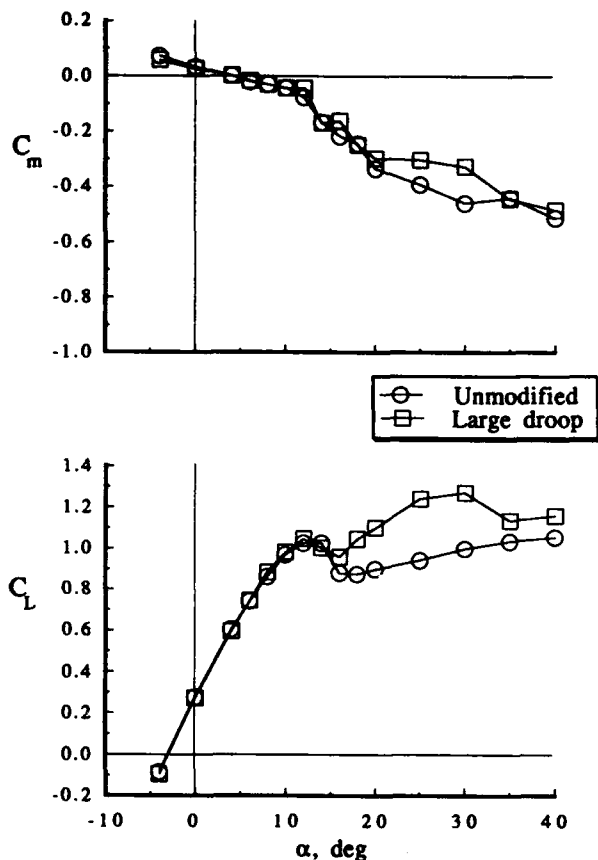


Figure 13. Longitudinal characteristics, large droop configuration.

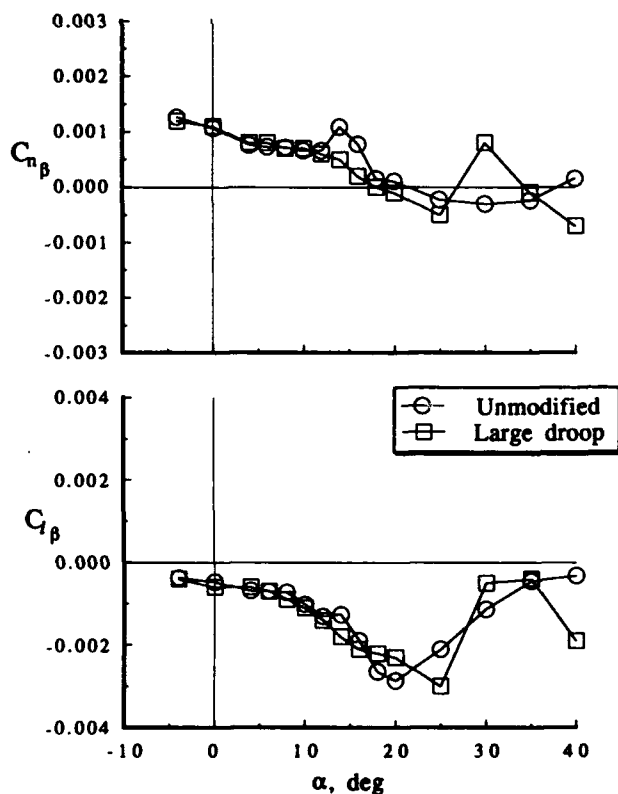


Figure 14. Lateral-directional stability characteristics, large droop configuration.

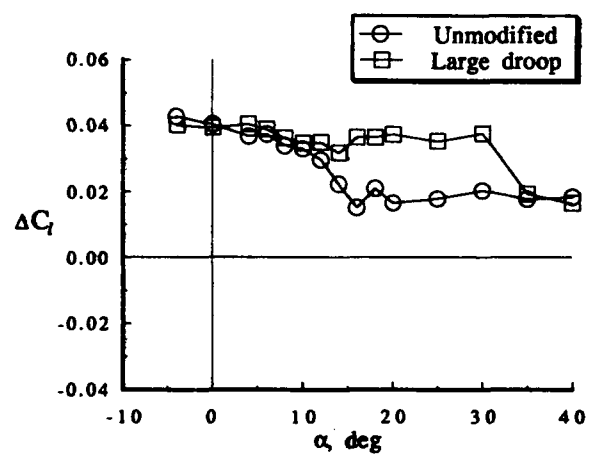


Figure 15. Effect of the large droop modification on the maximum lateral control authority.

**A SIMULATION OF A DISPLAY AND CONTROL SYSTEM
REQUIRING REDUCED TRAINING AND PROFICIENCY**

by

**Eric C. Stewart
Flight Applications Division
NASA Langley Research Center
Hampton, Virginia 23665**

**For Presentation to the AIAA/FAA Joint Symposium on General
Aviation Systems at the Hilton Inn-East, Wichita, KS
on March 16-17, 1992**

A Simulation Study of a Display and Control System Requiring Reduced Pilot Training and Proficiency

**by
Eric C. Stewart**

Abstract

A simulation study of a decoupled, fly-by-wire control system combined with a pictorial head-up display has been conducted. The test subjects were primarily non-pilots who were given no training or practice before the data runs. Despite their lack of experience and training, the test subjects were generally able to complete a complex piloting task on their very first run. The piloting task was performed in reduced visibility conditions and consisted of a continuous series of common maneuvers beginning with a takeoff and ending with a landing. Variations of the pictorial display format as well as a head-down configuration were also studied. Quantitative and qualitative data are presented to illustrate the vast superiority of the advanced controls and displays over conventional controls and instruments.

Introduction

The time and cost of becoming a private pilot has always been a deterrent to widespread use of general aviation airplanes for personal transportation. Many people who begin to take flying lessons drop out of the process before they get their license because of the time and costs involved. And many more quit flying in a few years after they get their license due to the recurring proficiency requirements. Unfortunately, these training and proficiency requirements are well justified by the complexity of safely operating an airplane. What is needed is new technology that would reduce the complexity of safely operating an airplane. This new technology, which is probably as important as technology for increasing fuel efficiency or performance, could reduce the need for extensive pilot training.

Such new technology is currently being developed and used in other fields of aviation; however, it could be of tremendous benefit to both beginning and veteran general aviation pilots. For example, the fly-by-wire technology which has been developed for military and commercial aviation probably would be of much greater benefit to a novice pilot than it has been to full-time pilots. The full-time pilot who regularly accumulates many hours of flying time is very comfortable with the control characteristics of an airplane and really doesn't have a great need for an airplane which is easier to fly. The beginning pilot, on the other hand, often finds the control characteristics of an airplane strange and hard to understand. Other new technologies which could be used to simplify personal air transportation are the microprocessors and their huge memory devices as well as the Global Positioning System. These technologies will eventually make three dimensional navigation possible without maps and charts or the costs of inertial navigation systems.

Over the years the NASA has developed technology aimed at increasing the efficiency and safety of general aviation airplanes. For example, NASA has explored ways to reduce the possibility of stalls and spins, reference 1, which historically have been responsible for many accidents and which have reinforced the continued requirement for rigorous pilot training. The present work grew out of these stall/spin studies when the program began to expand from single-engine airplanes into twin-engine airplanes. A simulation study of the engine-out characteristics of light twins, reference 2, highlighted the need for improved control. Although a simple automatic trim system was developed which could aid the pilot in coping with an engine failure, the pilot still had to make the same basic control inputs, reference 3.

It soon became apparent that the only way to eliminate the effects of the majority of pilot mistakes was to use digital fly-by-wire control systems such as those in many military fighter designs. However, once these control systems are installed on an airplane for safety purposes, relatively simple software changes can tailor them to provide benign, intuitive control characteristics which were not previously possible, reference 4. Although these control characteristics were very easy for a novice to learn to fly, the problem of navigation and situational awareness in low visibility conditions was still far beyond the capabilities of the novice using conventional cockpit instruments. Therefore, a head-up pictorial display was developed which was compatible with the intuitive fly-by-wire control system, reference 5.

The present paper describes and presents the most-recent refinements of the control system (designated as Ez-Fly) and the pictorial display (designated as the Highway in the Sky or HITS). The control system has been modified with a feed-forward path that reduces engine throttle activity while maintaining the fundamental decoupling of the primary state variables. The pictorial display has been modified to provide enhanced vertical situation awareness and future flight path information. The landing-flare flight director has been improved to provide more consistent touchdown performance. Finally, a head-down display and cross-wind maneuvers have been studied.

As in the previous studies, the system was evaluated using a combination of non-pilots and pilots. None of the test subjects was given any training or practice before the data runs were started. The piloting task was performed in reduced visibility conditions and consisted of a continuous series of common maneuvers beginning with a takeoff and ending with a landing. The task lasted slightly less than 10 minutes. The results were consistent with the earlier studies in that a substantial majority of the novice pilots was generally able to complete the entire maneuver without prior training when both the fly-by-wire control system and pictorial display were used. When the pictorial display was used by itself without the fly-by-wire control system, some of the novice test subjects were still able to complete the entire maneuver. Although not specifically demonstrated again in these tests, without the pictorial display, the test subjects would wander around the skies hopelessly lost in the clouds. The latest modifications of the pictorial display were shown to be improvements both quantitatively and qualitatively over the previous versions.

Symbols

alt	altitude, feet
a	vertical acceleration (positive upward), ft/sec ²
F _{col}	force applied to longitudinal control by pilot, lb
h	vertical speed, ft/sec
h _{dspl}	vertical speed displayed on flight director arrow, ft/sec
h _{flare}	vertical speed required to perform ideal flare, ft/sec
h _{max}	maximum vertical speed which airplane can sustain, ft/sec
K _{FD}	flight director gain, non-dimensional
lat	lateral displacement from centerline of HITS display, feet
Δp	deadband around feed-forward throttle position, equal to .2 (20% of throttle travel)
q	pitching rate, deg/sec
$\overline{q_\infty}$	dynamic pressure, lb/ft ²
r _{coord}	yaw rate in a coordinated turn, deg/sec
s	Laplace operator, sec ⁻¹
V	airspeed, knots or ft/sec
V _c	commanded airspeed, knots
x ₀	zero-force control position, inch
α	angle of attack, deg
β	angle of sideslip, deg
δ _a	aileron position, deg
δ _{col}	longitudinal column (wheel) position, inch
δ _e	elevator position, deg
δ _{e,trim}	trim elevator position, deg
δ _f	flap position, deg
δ _g	landing gear position, [0 or 1.0]
δ _{pedal}	rudder pedal position, deg
δ _{prop}	propeller speed control position, [0,1.0]
δ _r	rudder position, deg
δ _{th}	throttle lever position in cockpit or engine throttle position, [0,1.0]
δ' _{th}	throttle position parameter in control law, [0,1.0]
δ _{th,a}	effective throttle position in control law, [0,1.0]
δ _{th,ff}	feed-forward throttle position, [0,1.0]
δ _{wheel}	wheel position (lateral cockpit control), deg

ϕ	roll attitude, deg
θ	pitch attitude, deg
τ	time constant, seconds

Subscripts:

c	commanded
r	right
l	left
error	error

Abbreviations:

Ez-Fly	easy-to-fly, fly-by-wire, decoupled control system
HITS	highway in the sky pictorial display
HUD	head-up display
PI	proportional plus integral (control law)
ref	reference
RMS	root-mean-squared
s	seconds

Description of System

The overriding principle for the design of the total system was to have, as far as the pilot was concerned, one mode of operation which could be used for all phases of flight. This mode of operation would require the pilot to continuously and actively "close the loop" on the control of airplane. The pilot is thus forced to be aware of the airplane's state at all times and is not merely a monitor for automatic systems which fly the airplane. It is believed that such an approach would produce a higher level of acceptance by the potential users because of the feeling of control over the situation. Complete automatic control would probably lead to anxiety in certain situations when the passenger-monitor would have to passively observe certain maneuvers. This manual mode of operation could be used in all phases of flight and ordinarily would be used everywhere except during long periods of cross-country flight when a completely automatic system could be used to track a desired path.

Although the system was designed to appear to the pilot to have only one mode of operation, the gains and logic for the control system and display change for different phases of flight. However, these changes are nearly transparent to the pilot and he operates the airplane in essentially the same manner at all times. Thus, so-called "mode errors" (errors in which the pilot makes an inappropriate input because he forgot which mode the airplane was operating in) are eliminated. Mode errors are probably more likely in highly automated systems than in simpler systems, and they are usually more serious than other types of errors.

Control System

The primary control-response relationships for the advanced decoupled control system (designated the Ez-Fly control system) are shown in figure 1. The three main cockpit controls (Longitudinal Wheel, Throttle, and Lateral Wheel) individually and uniquely determine the three primary response parameters (Vertical Speed, Airspeed, and Heading Rate). The rudder pedals control the sideslip angle but this control is not a factor except in crosswind landings. The primary control-response relationships are very intuitive and contrast sharply with conventional airplane responses. In a conventional airplane moving one cockpit control causes two or three of the primary response parameters to change. The pilot through training has to learn to suppress these responses by simultaneously moving the other controls to get the desired (single) response, reference 4. It is possible for the pilot to command combinations of vertical speed and airspeed with the Ez-Fly control system which the airplane could not maintain indefinitely. In this case the vertical speed has the priority.

Block diagrams of the control laws used in the simulation are given in figure 2. The elevator and throttle control laws are basically proportional plus integral (PI) control laws although the throttle also incorporates a feed-forward term.

Vertical Speed-Elevator: The elevator is driven by the longitudinal wheel position which, as shown in figure 2a, closes the loop on the vertical speed. The commanded vertical velocity is limited to maximum and minimum values as a function of the flap deflection and bank angle so that the pilot cannot command vertical velocities which the airplane cannot sustain. Gain scheduling as a function of airspeed and dynamic pressure is provided. Proper damping of the system is accomplished by feeding back pitch attitude and pitch rate. Although the limits placed on the commanded vertical velocity eliminate unsafe conditions such as stall, a stall prevention system using angle of attack is added for a back-up.

An automatic trim system for the longitudinal control force was incorporated in the Ez-Fly control system. Although, a wheel-mounted, spring-loaded switch controlled a simulated electric trim system, an automatic system was used in conjunction with the electric trim. The automatic system slowly drove the zero-force position of the longitudinal wheel in the direction to relieve any control force. The rate at which the zero-force position changed was so slow that it took several seconds to reduce the control force to near-zero after a substantial change in the commanded airspeed. This automatic trim system would run until the force was within the range of plus or minus 2 lbs.

Another feature of the elevator control system was that the gain on the longitudinal control (commanded vertical speed/longitudinal control deflection) was reduced on final approach to provide finer control. The gain (K_{FD} in figure 2a) was reduced as a function of distance from the runway threshold starting after roll-out to the final heading at a distance of 23,000 feet. The final gain during the flare maneuver was one third that used for the rest of the test circuit.

Airspeed-Throttle: The engine throttle is driven by the cockpit throttle lever position which, as shown in figure 2b, closes the loop on the airspeed. Since a twin-engine airplane was used as the simulation platform there were actually two throttle levers. The first step in the control law is to compare the two throttle lever positions to make sure the pilot is not intentionally commanding an asymmetric power setting. If he is, the automatic system is by-passed. If he is not, the two throttle commands are equalized and then shaped to provide finer control at low airspeeds. The commanded velocities are then limited to reasonable maximums and minimums depending on the flight condition and airplane configuration. A feed-forward term is then computed as a function of the commanded airspeed, airplane configuration, and maneuvering condition using an empirically determined function. This function usually provides an output which is within 10-20% of the actual throttle position required to produce the desired airspeed. The additional increments needed to reduce the airspeed error to zero are produced by the PI paths shown. The sum of the feed-forward and PI terms are next limited to a value which is within the feed-forward term plus or minus 0.2 (20% of the throttle travel). This limiting is provided to reduce throttle overshoots when large airspeed changes are commanded. As with the elevator system, the limits set on the commanded airspeed usually prevent the pilot from commanding any unsafe conditions. However, as a back-up, stall prevention is assured by adding a final term if the angle of attack gets too large. The final computed throttle position is sent to the engine model and propeller pitch laws. The propeller pitch laws are provided to prevent over-boosting the simulated turbo-charged engines.

Ailerons and Rudder: The ailerons were driven by the cockpit lateral wheel position and closed the loop on bank angle, figure 2c. The commanded roll attitude was limited to plus or minus 40 degrees to prevent unsafe conditions. Since a constant bank angle produces a constant heading rate, the lateral wheel is essentially commanding a heading rate as shown in figure 1. As was the case with the longitudinal control, the gain of the lateral wheel was reduced to one-third its initial value on final approach.

The rudder was driven by the cockpit rudder pedal position and closed the loop on the sideslip angle. Yaw damping was provided by a yaw rate feedback as shown in the diagram, figure 2d.

Display

A display called the Highway in the Sky (HITS) was used in these tests. The majority of the simulation runs was conducted with a wide-angle (40° by 23°) head-up display (HUD) configuration. However, limited evaluations were conducted of a 5-inch diagonal head-down display configuration for comparison.

Pictorial Highway: The basic concept of the HITS display was to reproduce a highway which the pilot would follow through the sky. The HITS display produced fixed features which the airplane flew over and through. Lane stripes on each side of the "road" were fixed in inertial space along the desired path and were always 150 feet long with a gap of 100 feet between stripes. Rectangular boxes were placed on top of the "roadway" at every fifth "lane stripe," figure 3. The lane stripes and boxes extended 6250 feet ahead of the airplane. As the airplane flew along, new lane

stripes and boxes were continually being added to the far end of the pictorial highway in order to maintain the 6250 foot length. The combination of lane stripes and boxes provided readily-recognizable shapes whose changing perspective gave intuitive position guidance information, figure 4, and attitude information, figure 5.

The lane stripes and boxes were always oriented with the local vertical--that is, they were not banked with the turns. The distance between the lane stripes and the dimensions of the boxes varied for different phases of flight. However, the distance and dimensions were always scaled proportionally so that the display always appeared as shown in figure 3. The width of the boxes always equalled 1.2 times the lateral separation of the lane stripes and the height of the boxes was always equal to .6 times the separation of the lane stripes. The lane stripes began at the takeoff end of the runway with the same separation as the width of the runway (150 ft). As the altitude increased, the separation of the lane stripes and the dimensions of the boxes were steadily increased until at a distance of 10,000 feet from the end of the runway and an altitude of 875 feet, the lane stripes were separated by 1000 feet. This 1000-foot separation was maintained until the last two segments of the approach to the landing. Over the last 23,000 feet of the approach, the separation of the lane stripes was linearly decreased from 1000 feet to 150 feet in order to precisely guide the pilot to the center of the runway for landing. At the runway threshold the center of the boxes was at an altitude of 62.7 feet above the ground. This height was calculated to produce a touchdown 1000 feet down the runway provided the test subject performed a perfect flare maneuver.

A special class of features was the small trend marks on the sides of the boxes. These marks were calculated from the flight path angle and ground track angle. They indicated the vertical and horizontal positions the airplane would have when it reached the plane of each box provided the airplane continued on its present trajectory. Thus, the trend marks gave the pilot advance information about the trajectory of the airplane. The perspective of the lane stripes and boxes gave information about the linear position of the airplane, figure 4, whereas the trend marks gave information about the linear rates of the airplane, figure 6.

Sign/Flight Director: In addition to the basic pictorial format of the lane stripes and boxes, the HTS display contained other complementary information. As shown in figure 3, a square area in the top center of the display was reserved for messages and flight director arrows which will be described later. Unlike, the lane stripes and boxes, these messages did not appear to be stationary with the airplane flying by them. Instead, whenever they were displayed, they remained fixed in the field of view.

The flight director arrows usually provide some of the same information as the perspective of the boxes and the trend marks as shown in figure 6. The arrows indicate the direction the pilot should make an input in order to follow the correct trajectory or get back to the correct trajectory. The length of the arrows indicate the size of the input required. Block diagrams of the code used to calculate the arrow lengths are shown in figure 7. Both the lateral arrow length and the vertical arrow length are basically proportional to the sum of the respective position error and the rate error. The position error for both arrows is the distance from the center of the desired trajectory through the boxes. In the case of the lateral arrow the rate error is generated by differentiating the position error. In the case of the vertical arrow

the rate error is the difference between the vertical rate required to follow the desired trajectory and the actual vertical velocity.

The flight director arrows were turned off whenever the pilot was stabilized on the correct trajectory and had the pictorial portion of the HITS display in view. This required that both the position error and the rate error be small. The logic which switched the arrows on and off is presented in the lower portion of figure 7. A hysteresis was built into the logic so that once the arrows were turned off the position error had to be twice as large as the error required to turn the arrows off previously. This hysteresis eliminated the arrows flickering on and off for small variations in position around the threshold values.

The arrows were turned on during certain portions of the maneuver regardless of whether the pilot was stabilized on the correct trajectory. For example, in the takeoff roll and the final approach the usual hysteresis logic was by-passed. During the takeoff roll, the arrows directed the pilot down the center of the runway until the rotation speed of 90 knots was attained; then the vertical arrow gave a full up command and the normal logic was followed. On the final approach, the hysteresis logic was also by-passed so that the arrows stayed on all the time. The length of the arrows on the display for a given physical error was increased on final approach in order to make it possible for the pilot to control the trajectory near the runway. This was accomplished with a multiplier K_{FD} which increased from a value of 1.0 to a value of 3.0 over the last 23,000 feet of the final approach. As mentioned in the control law sections, this same gain K_{FD} was also used to decrease the pilot's control sensitivity.

A special calculation was used for the vertical arrow length during the landing flare maneuver. The logic and calculations are shown in figure 8. The flare calculations were triggered when the actual vertical descent rate exceeded a critical vertical descent rate called the flare rate, h_{flare} . This flare rate was the vertical descent rate which would be achieved if a constant upward acceleration of 1 ft/sec/sec was maintained to a touchdown with a target touchdown velocity of -1 ft/sec. Once the flare calculations started, the reference vertical velocity in figure 7 was set equal to the flare rate. If the pilot had been exactly on the -3° glideslope at the approach speed of 90 knots, the flare arrow would be triggered at an altitude of 41 feet.

Alphanumeric information was also presented to the pilot in the square box ordinarily containing the flight director arrows. Examples of the types of information given are shown in figure 9. Whenever one of these messages appeared, the flight director arrows temporarily disappeared. When these messages first appeared they were accompanied by a short audio tone to alert the pilot. When the pilot "answered" the message by performing the correct action, the alphanumeric message disappeared or was replaced by the flight director arrows depending on the current situation.

Description of Simulation and Tests

Simulation Model and Equipment

An existing simulation package, reference 2, of a twin-engine, light airplane was used in these studies. The simulated airplane had a weight of 6200 lbs and a wing span of 40 feet. The simulated propulsion system consisted of two 300 Hp turbo-charged engines with constant-speed propeller systems. Although the simulated airplane had two engines, asymmetric power conditions were not investigated.

The simulation cockpit was mounted on hydraulic actuators to provide a very limited amount of motion cues, figure 10. This motion-base system was capable of small pitch, roll and heave motions. The interior of the simulation cockpit was similar to that of a typical twin-engine light airplane with side by side seating for two, figure 11. Conventional mechanical instruments were simulated, but rarely used, especially by the novice test subjects. The forces on the longitudinal wheel, lateral wheel, and rudder pedals were simulated with hydraulic loaders driven from the main computer. A visual scene from a color monitor was projected through a virtual image system to produce a visual scene with a field of view of about 40° horizontally by 23° vertically. The visual scene was a Computer Generated Image (CGI) of a typical airport runway (10,000 feet long and 150 feet wide) at a major city. In order to evaluate a head-down version of the HITS display, a 5 inch television monitor was mounted in the top center of the instrument panel, figure 12. Although the 5-inch monitor had a much smaller physical field of view than the head-up virtual image system, the field of view of the scaled image was actually larger--approximately 43° by 36°. Thus, more of the HITS display could be seen with the head-down version than with the head-up version. The cockpit also had a sound system to simulate the sounds of the engines and the airstream.

The equations of motion and all other calculations except those associated with pictorial display were solved on a Cyber 175A computer every .03 seconds. The pictorial display was generated on an Terabit Eagle 1000 graphics computer running in step with the Cyber computer. Data for analysis of pilot control activity and performance were calculated on the Cyber computer.

Piloting Task

The task given to the test subjects was intended to exercise the skills necessary to execute a typical trip from takeoff to a landing with a 200-foot ceiling. However, in order to limit the time required to complete the maneuver, a racetrack pattern was flown about a single runway, see figure 13. The maneuver included a takeoff, straight climbs, a turning climb, a level downwind section, a descending turn, and a two-segment straight-in approach to a flare and landing. A total of seven different segments were included, each with a different target airspeed from the previous

segment. The retractable landing gear and flap systems were also exercised at the appropriate places.

Test Subjects

A total of 16 test subjects were used in the evaluation of the various combinations of configurations and conditions. Each test subject completed 4 to 6 or more runs. Four test subjects had some pilot training and the other 12 test subjects had no previous piloting experience. Both male and female test subjects were used. Although most of the test subjects were either engineers or engineering students, there were 5 non-technical professionals in the group of test subjects.

Research Variables and Procedure

There were four primary research variables: the Ez-Fly control system, the trend marks, the HITS display location, and crosswinds. A typical test sequence to evaluate the research variables was as follows:

- Run 1: Ez-Fly control system (with the default HITS display)
- Run 2: Basic control system (with the default HITS display)
- Run 3: HITS trend marks off (with the Ez-Fly control system)
- Run 4: HITS head-down configuration (with the Ez-Fly control system)
- Run 5: Crosswind condition (with the Ez-Fly control system and HITS display)

Not all test subjects evaluated each of the variables, and the test sequence was not always in the order presented. In addition, the head-down configuration and the crosswind condition evaluations were sometimes made with slightly different trend mark configurations, depending on the personal preference of the test subject.

The first two runs were made to evaluate and demonstrate the effectiveness of the Ez-Fly control system when used with the HITS display. The test subjects received no training or practice before the data runs presented herein. They were given a short explanation of the cockpit controls and the display they would be using. After the first run with the Ez-Fly control system, the non-pilot test subjects were given a few minutes of additional instruction on the control characteristics of the basic control system (Ez-Fly off).

The second test variable, the trend marks, was evaluated in the next run(s). The default HITS display consisted of four boxes in the visible field of view. There were flight path (vertical control) trend marks on both sides of all four of the boxes, but there were track angle (lateral control) trend marks on the top and bottom of only the two nearest boxes. This default HITS display was compared with an identical display but without any trend marks at all. Occasionally, other combinations of trend marks were evaluated depending on the personal preference of the test subject. For example, a single type of mark (either flight path or track angle) or track marks on all four boxes was evaluated.

The third test variable was the location of the HITS display: either head-up or head-down. The head-up location was the default configuration.

The final test variable was the level of the simulated winds. The default value of the wind speed was zero. During the runs with wind, a 20 knot wind from 45° to the right of the runway heading was used. This produced a crosswind component on final approach of 14 knots.

Results

Baseline Ez-Fly and HITS Systems

The effectiveness of both the Ez-Fly control system and the head-up HITS display is perhaps best shown by reference to the following table:

	Control System			
	Ez-Fly		Basic (Ez-Fly Off)	
	No. of runs	No. of landings	No. of runs	No. of landings
Non-pilots	12	11	12	3
Pilots	4	4	4	4

(HITS Display on)

For non-pilots the piloting task was almost always completed successfully when the Ez-Fly decoupled control system was combined with HITS display. This result is very significant considering the fact that no training or practice was allowed before the Ez-Fly runs and that most of task was flown in reduced visibility without reference to any ground features. The one run that did not end with a successful landing was really just a hard, but controlled landing, 13 feet short of the runway threshold. The overall success rate of 92% (11 runs out of 12) for the non-pilots is a substantial improvement over the already impressive 50% success rate of the previous version of Ez-Fly and HITS, reference 5. The test subjects generally commented that this combined system made the maneuver almost as easy to fly as a car is to drive.

For the four test subjects who had some pilot training, all runs were successfully completed to a landing as can be seen in the table. The Ez-Fly control system and the HITS display were compatible with the pilots' previous training and required very little adaptation. All the pilots preferred the Ez-Fly control system and the HITS display to a conventional control system and instruments.

The effectiveness of the HITS display by itself (with Ez-Fly Off) was also clearly demonstrated by the data in the table. That is, for this piloting task which would be nearly impossible with convention displays, 3 out of 12 of the runs flown by the non-pilots were successful. And of the other 9 runs, the HITS display enabled most of non-pilots to successfully fly a majority of the reduced-visibility task. Again, it should be emphasized that no training or practice (except for the immediately preceding run with the Ez-Fly control system) was allowed. Without the Ez-Fly control system, airspeed control on final approach was usually too difficult for these novices. The most common mistake was a failure to add power quickly enough to compensate for the increased drag of the flap deployment. As the non-pilots attempted to maintain the correct flight path by following the HITS display, the airspeed decreased until the airplane stalled and "crashed."

Ez-Fly Control System

Time histories of two runs for a non-pilot are shown in figure 14. The first maneuver with the Ez-Fly control system shows good control of the airplane and a successful landing. The airspeed, V , followed the pilot's throttle control inputs, $\delta_{th,r}$, despite the simultaneous changes in the vertical speed, \dot{h} . The pilot's longitudinal control position, δ_{col} , and lateral control position, δ_{wheel} , have higher frequency components than the throttle control, $\delta_{th,r}$, due to the small corrections the pilot made to track the HITS display.

The second run for this test subject, figure 14b, with the basic control system instead of Ez-Fly, was not as successful as many for the other test subjects. This run lasted only about 2 minutes, ending with the simulated airplane spiralling into the ground during the first turn. Before the final spiral, control of the airspeed and vertical speed was erratic. The test subject finally lost visual contact with the pictorial portion of the HITS display and went into a highly banked turn while still in the clouds at a low altitude. By the time the test subject could see the ground, the descent rate was too great to arrest before impact.

Summaries of the all the test subjects' performance with and without the Ez-Fly control system also show the superiority of the Ez-Fly control system, figure 15. Each of the three parameters shown is the average RMS error from a perfect trajectory. The altitude and lateral errors appear to be relatively large because most of the maneuver was at altitude where the highway in the sky was 1000 feet wide and great precision was not required. The pilots' performance was about twice as precise when the Ez-Fly control system was on as when it was off. The airspeed error with the Ez-Fly control system on also appears to be large even though it is about one-half the value achieved with the Ez-Fly control system off. The reason for the large value with the Ez-Fly control system on was the seven different airspeed changes made during the maneuver. The engines were just not powerful enough to make the airspeed changes quickly. Once the airspeed was achieved, the Ez-Fly control system generally maintained the airspeed within 1 or 2 knots of the commanded airspeed.

Summaries of the pilots' control activity also show the superiority of the Ez-Fly control system, figure 16. The control activity of all three of the primary cockpit controls was substantially less than that with the basic control system (Ez-Fly off). Thus, the improved performance noted in the previous figure was achieved with less pilot control activity.

Summaries of the pilot's landing performance are presented in figure 17. Only maneuvers in which landings were actually made are included in the figure. The average descent rate at touchdown with the Ez-Fly control system was about one-half that of with the Ez-Fly control system off. As mentioned earlier, the vertical flight director arrow was programmed to produce a touchdown with a descent rate of 1 ft/sec. Even with the Ez-Fly control system, the test subjects were landing with higher descent rates. The descent rates are probably higher than they would have been if peripheral visual cues had been simulated. In fact, the flare arrow was originally conceived as a means to compensate for the (simulation's) lack of peripheral cues. The X touchdown position with the Ez-Fly control system was very nearly equal to the targeted value of 1000 feet (from the runway threshold). However, the test subjects generally landed about 400 feet long with the Ez-Fly system off. The Y touchdown position was practically the same with either control system and was satisfactory.

Head-down Configuration

Although a very limited number of runs were made with the head-down display, it appears there was relatively little difference in either the performance or the pilot control activity as a function of display location, figures 18 and 19. Although not shown here, the performance parameters showed very little difference also. This result is both surprising and encouraging. It is surprising in that the head-down display was much smaller and had relatively poor picture quality and resolution. However, its image represented a larger field of view as explained earlier. The test subjects definitely preferred the head-up display and objected to having to look back and forth between the instrument panel and the forward scene when using the head-down display. The small differences shown in the figures are encouraging because a head-down display would be much less costly to implement than the wide-angle head-up display.

Trend Marks

The trend marks had a very significant effect on the test subjects' performance as shown in figure 20. Both the altitude error and the lateral error were significantly reduced when the trend marks were turned on. The trend marks gave the test subjects a very positive indication of the rate of change of error and helped them anticipate their future trajectory. Almost all the test subjects preferred the trend marks to the flight director arrows even though they contained much of the same basic information most of the time.

The track angle trend marks were much more sensitive to pilot inputs than were the flight path trend marks. Eliminating the trend marks on the two most-distant boxes reduced this apparent sensitivity, but also reduced some of the information in the display. The test subjects were about equally divided on whether they preferred having track marks on all the boxes or just two of them. However, all the test subjects preferred having trend marks over having none at all.

The trend marks had a relatively small effect on the test subjects' control activity, figure 21. The control activity on the lateral wheel appears to be less with trend marks on, but there was considerable variation in the individual numbers.

Flight Director Arrows

Although the flight director arrows were not a research variable, an apparent flaw in their use should be mentioned. A few of the test subjects were observed making reversed control inputs when they focused on the flight director arrows. Usually they realized their error quickly, but when an arrow reached its full length the error was not readily apparent. As a result the test subject could hold an incorrect input in for a long period of time. A pursuit-type flight director was developed and briefly evaluated, but it was not satisfactory. The change in sensitivity needed for control on final approach and the limited area available on the display for the flight director appeared to make a pursuit flight director impractical when used in conjunction with the pictorial portion of the HITS display.

Crosswinds

The winds had relatively little effect on the task except for the final approach and landing. The airspeed was generally high enough that the test subjects could just detect that they were drifting relative to the highway in the sky. On final approach where the airspeed was 90 knots, the 20 knot wind was more noticeable. Despite a short explanation on the control of sideslip, few of the test subjects used (rudder) pedal inputs to align the longitudinal axis of the airplane with the pictorial highway and the runway. Instead they continued to fly as they had been without winds and accepted the fact that the nose of the airplane was pointed to the side of their ground track. This resulted in touchdown yaw attitudes which were not aligned with the ground velocity. However, the yawing moment introduced by the main landing gear at touchdown quickly aligned the airplane with its ground velocity.

The effect of the crosswind on the landing performance is summarized in figure 22. As might be expected the only significant effect was on the Y touchdown position. The crosswind component tended to blow the simulated airplane away from the centerline of the runway. The test subjects were constantly compensating for this drift but evidently were not able to precisely control their position.

Concluding Remarks

A fly-by-wire, decoupled control system (Ez-Fly) and a pictorial head-up display (Highway in the Sky or HITS) have been evaluated on the Langley General Aviation Simulator using untrained test subjects who were predominantly non-pilots. The piloting task was performed in reduced visibility conditions and consisted of a continuous series of common maneuvers beginning with a takeoff and ending with a landing. Quantitative and qualitative evaluations of task difficulty were made.

The results showed that with this advanced control system and display, approximately 92% of the novice test subjects successfully completed the entire piloting task without prior training or practice. In addition, 25% of the novice test subjects were able to successfully complete the piloting task using only the advanced pictorial display and a conventional mechanical control system.

The Ez-Fly control system was clearly superior to the conventional mechanical control system. All the test subjects preferred the Ez-Fly control system and practically every quantitative measure of pilot performance and control activity was better with the Ez-Fly control system. Without the Ez-Fly control system, the novice test subjects often lost control of airspeed on final approach, stalled the airplane, and "crashed."

A head-down display using the same HITS pictorial format was also evaluated. Although the test subject universally preferred the head-up display, there was very little difference in most measures of pilot performance and control activity.

"Trend marks" on the pictorial display were very useful in providing the test subjects with advanced information on their future trajectories. All the test subjects preferred the display with these trend marks over an identical display without the trend marks. The quantitative data showed that the trend marks also increased the precision with which the test subjects tracked the desired trajectory.

The novice test subjects were able to successfully complete the piloting task with steady winds of 20 knots. For most of the task the test subjects barely noticed the effects of the winds. However, on the final approach at an airspeed of 90 knots, the crosswind component of the wind (14 knots) caused considerable sideways drift which slightly degraded the lateral touchdown performance.

References

1. Chambers, Joseph R.: Overview of Stall/Spin Technology. AIAA Paper 80-1580. August, 1980.
2. Stewart, Eric C.; Moul, Thomas M.; and Brown, Philip W.: A Simulation Study of the Low-Speed Characteristics of a Light Twin with an Engine-out. AIAA Paper No. 83-2128.
3. Stewart, Eric C.; Brown, Philip W.; and Yenni, Kenneth R.: Piloted Simulation Study of the Effects of an Automatic Trim System on Flight Characteristics of a Light Twin-Engine Airplane with One Engine Inoperative. NASA TP-2633, November, 1986.
4. Stewart, Eric C.; Ragsdale, William A.; and Wunschel, Alfred J.: An Evaluation of Automatic Control System Concepts for General Aviation Airplanes. AIAA Paper No. 88-4364, August, 1988.
5. Stewart, Eric C.: Simulation Study of Easy-to-Fly General Aviation Airplanes: AIAA/FAA Joint Symposium on General Aviation Systems. Ocean City, New Jersey, April 11-12, 1990.

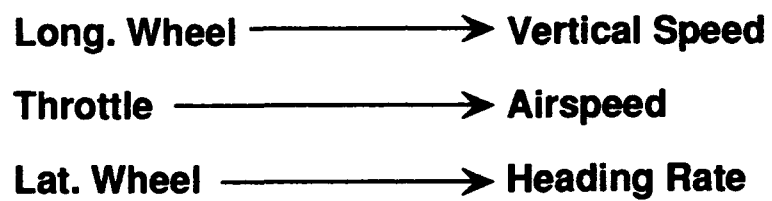
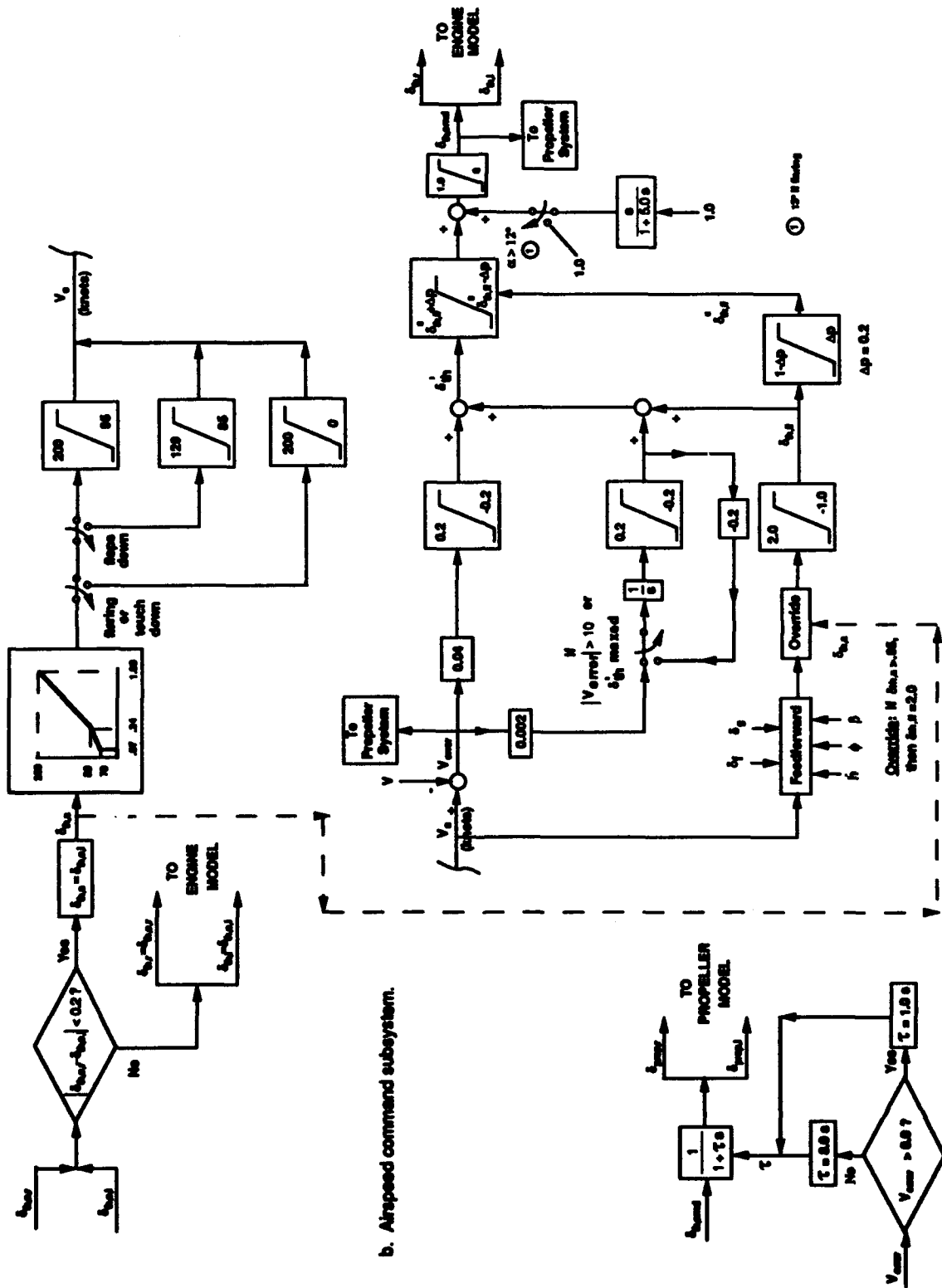


Figure 1. Functional control for Ez - Fly decoupled control system.



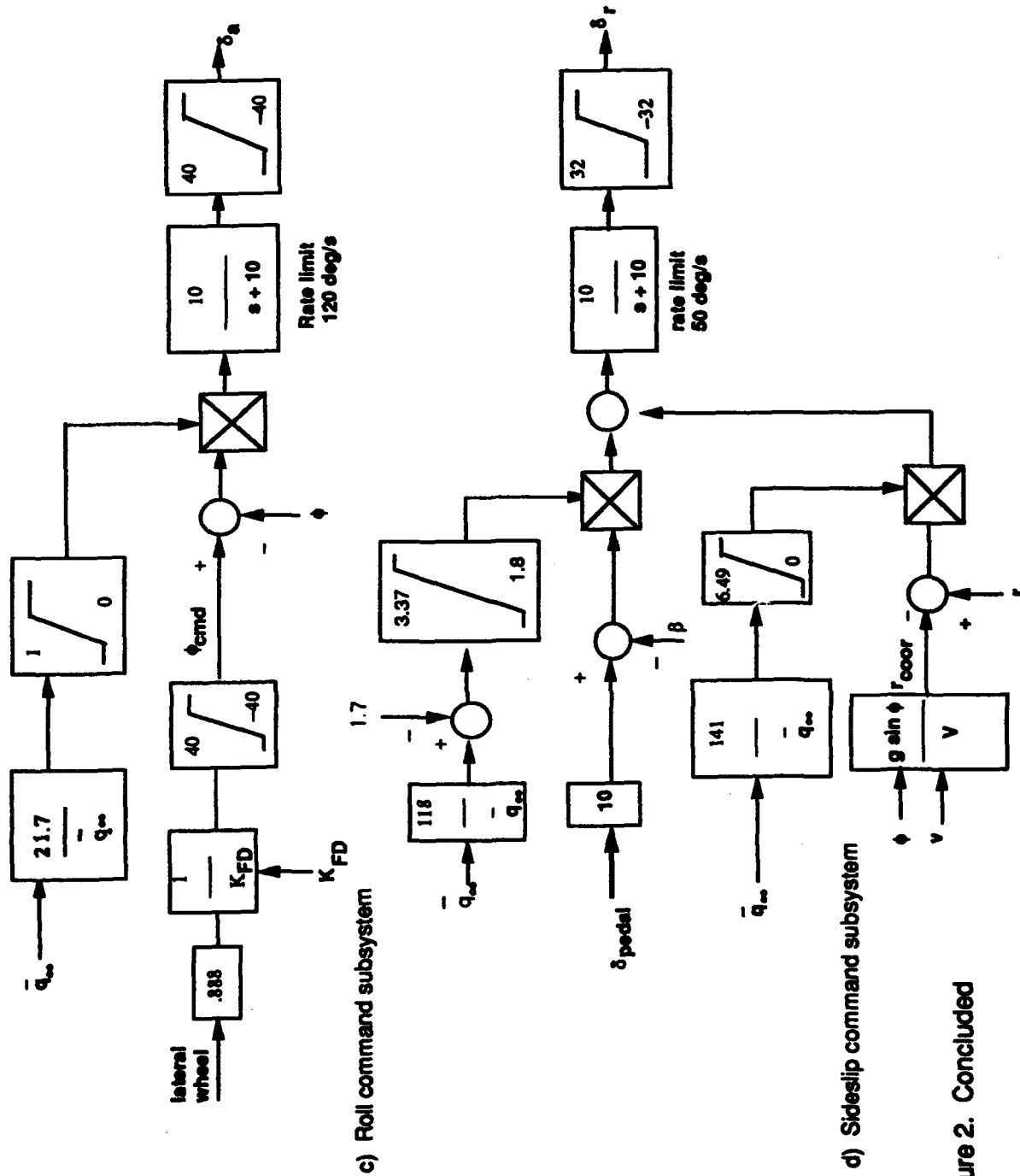


Figure 2. Concluded

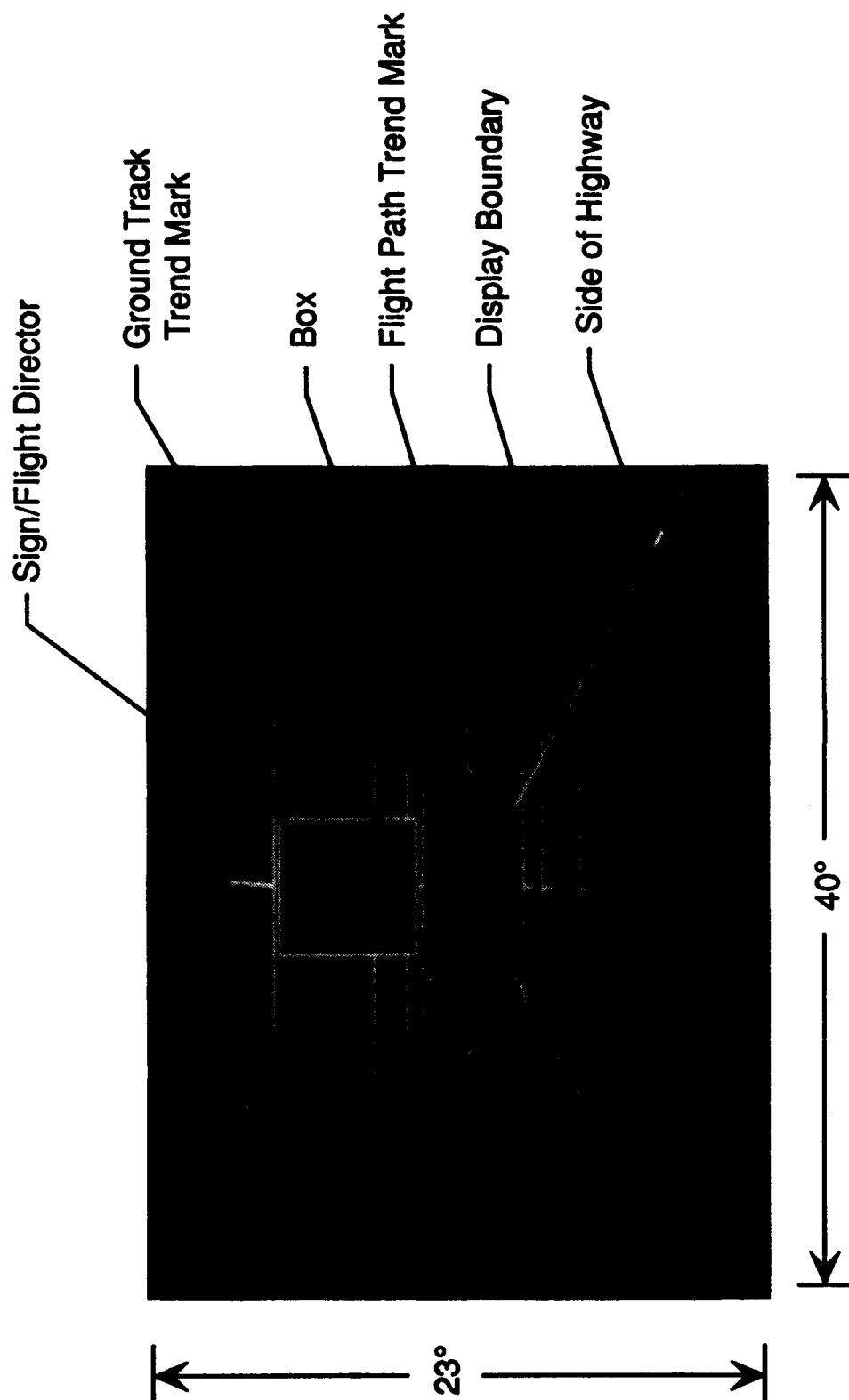


Figure 3. Format of Highway In The Sky (HITS) pictorial display.

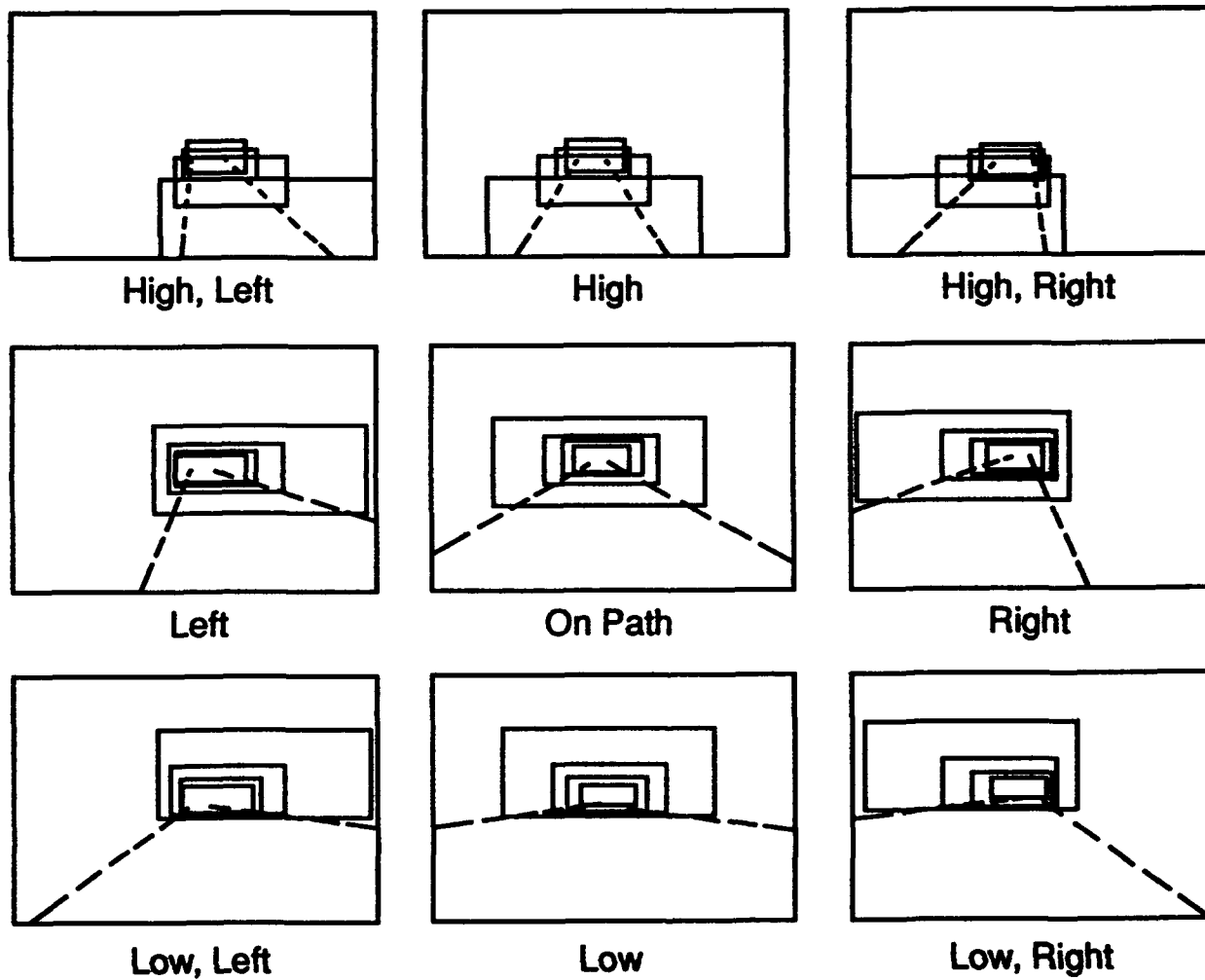


Figure 4. Highway In The Sky (HITS) position guidance

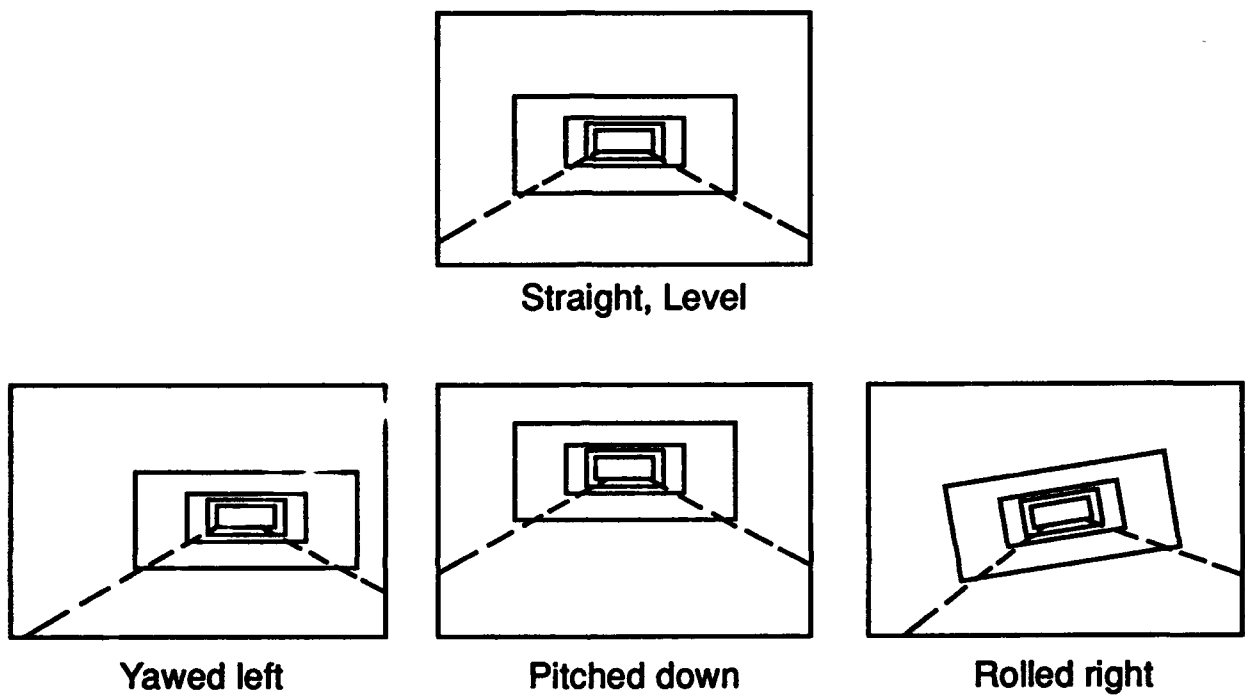
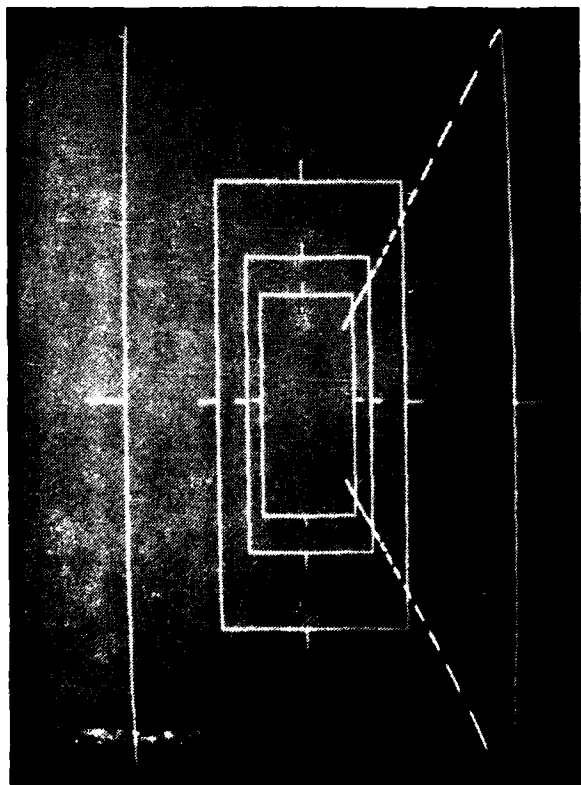
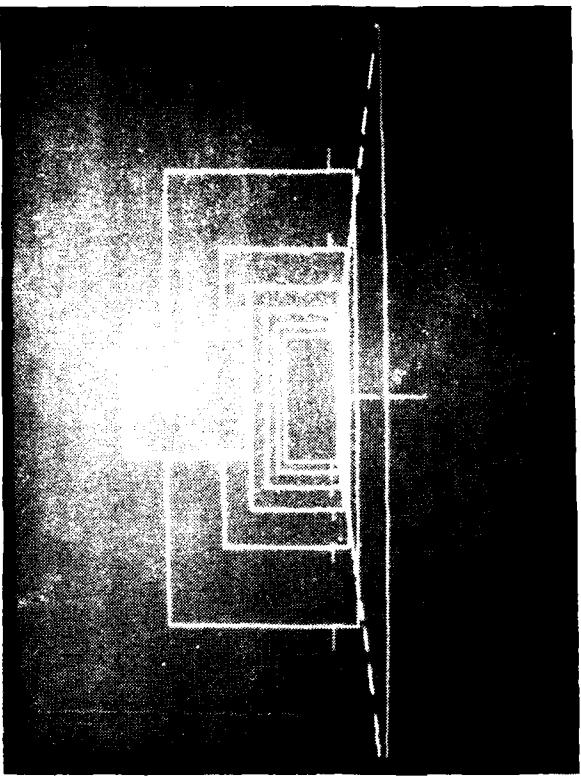


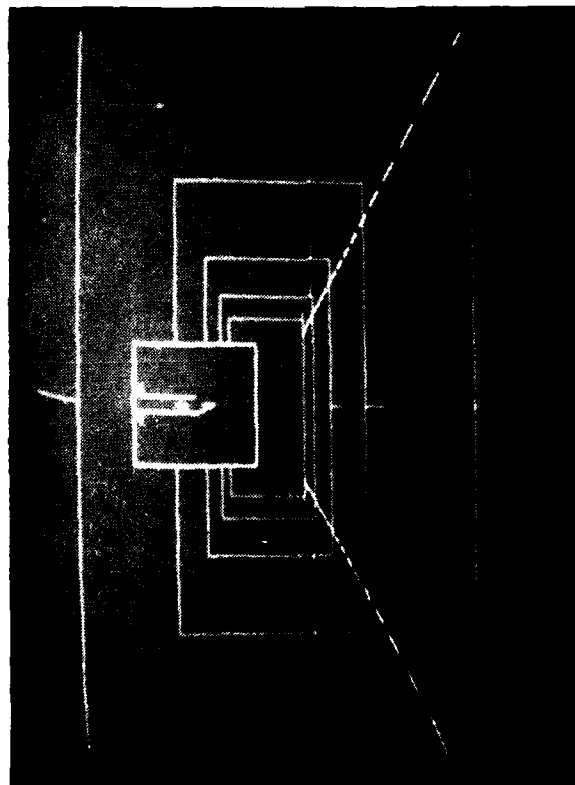
Figure 5. Highway In The Sky (HITS) attitude guidance



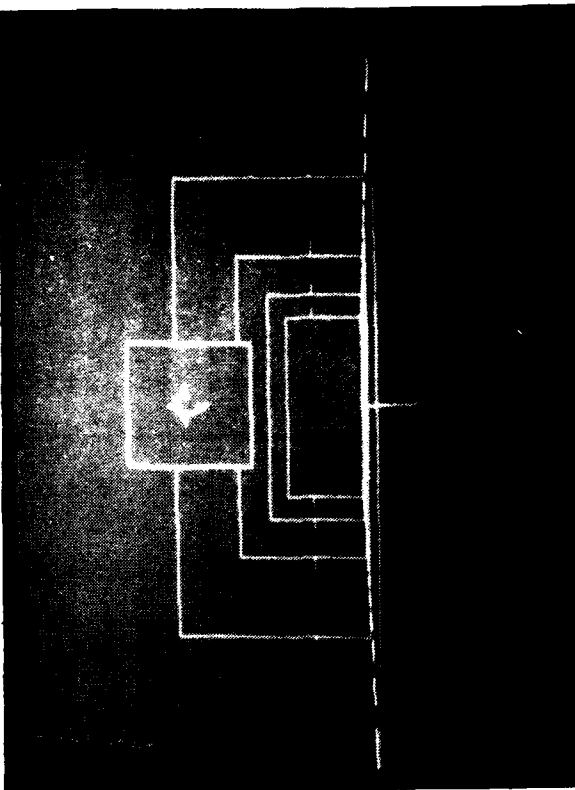
Correct Position
Correct Vertical Speed



Low Position
Zero Vertical Speed



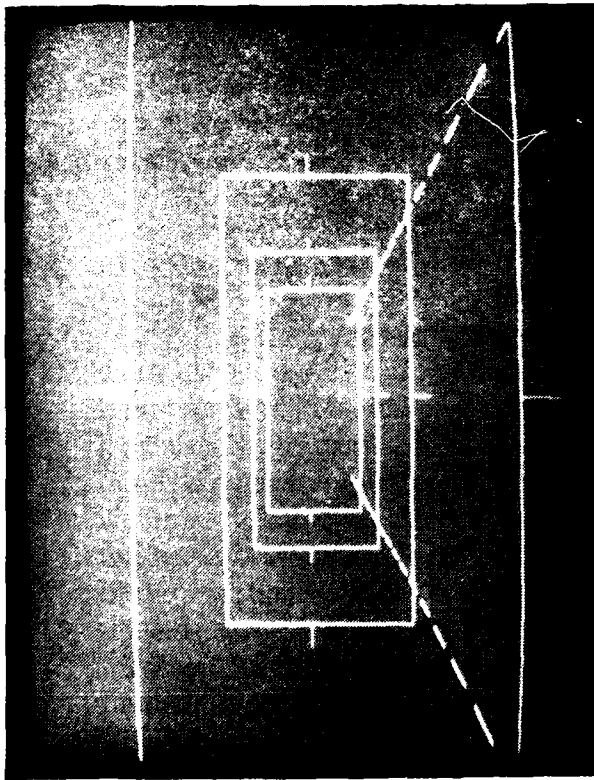
Correct Position
Downward Vertical Speed



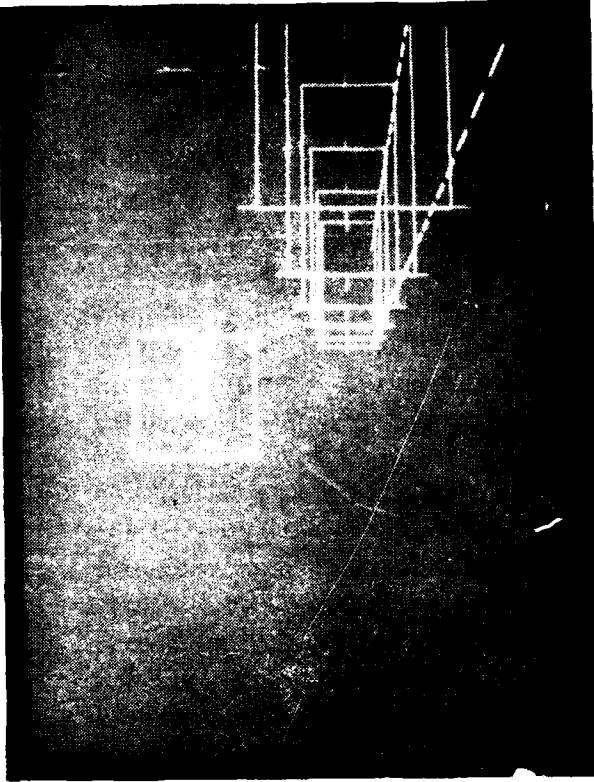
Low Position
Upward Vertical Speed

a) Vertical information

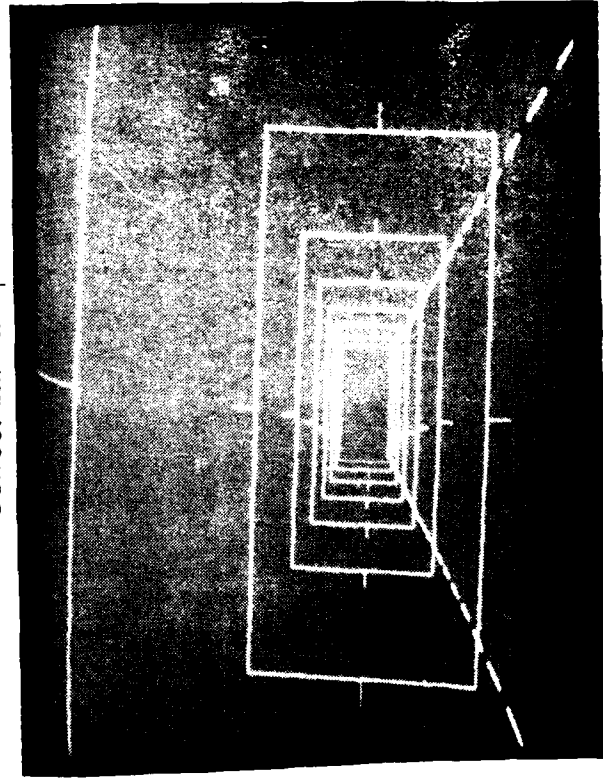
Figure 6. Illustrations of trend marks and flight director arrows for various flight conditions



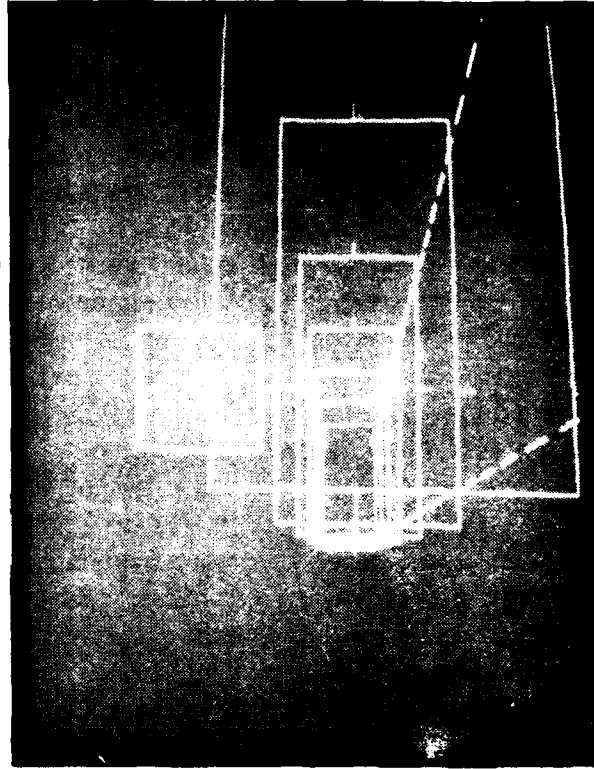
Correct Position
Correct Lateral Speed



Left Position Error
Lateral Rate Straight Ahead



Correct Position
Lateral Rate to Left



Left Position Error
Lateral Rate to Right

b) Lateral information

Figure 6. Concluded.

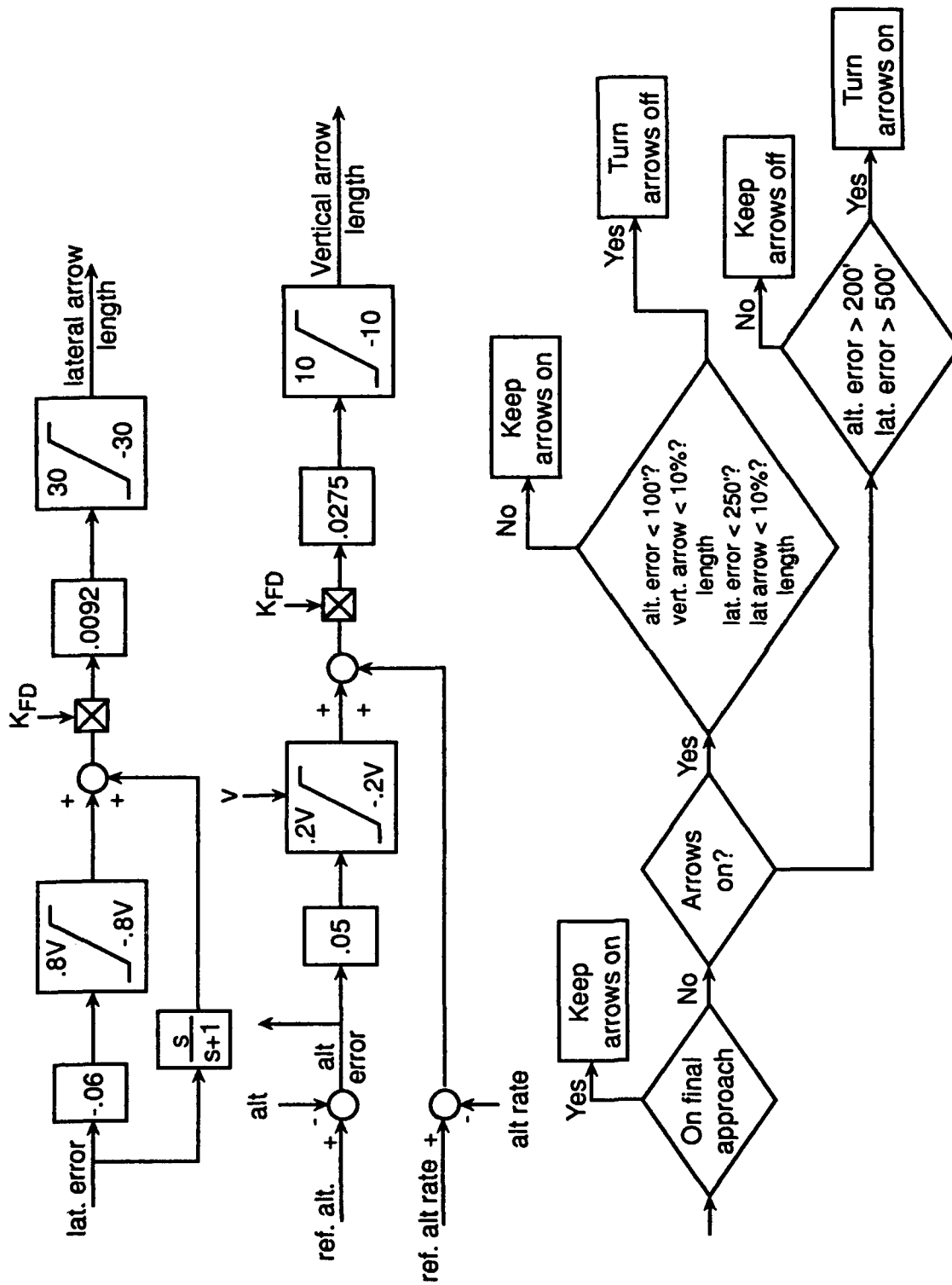
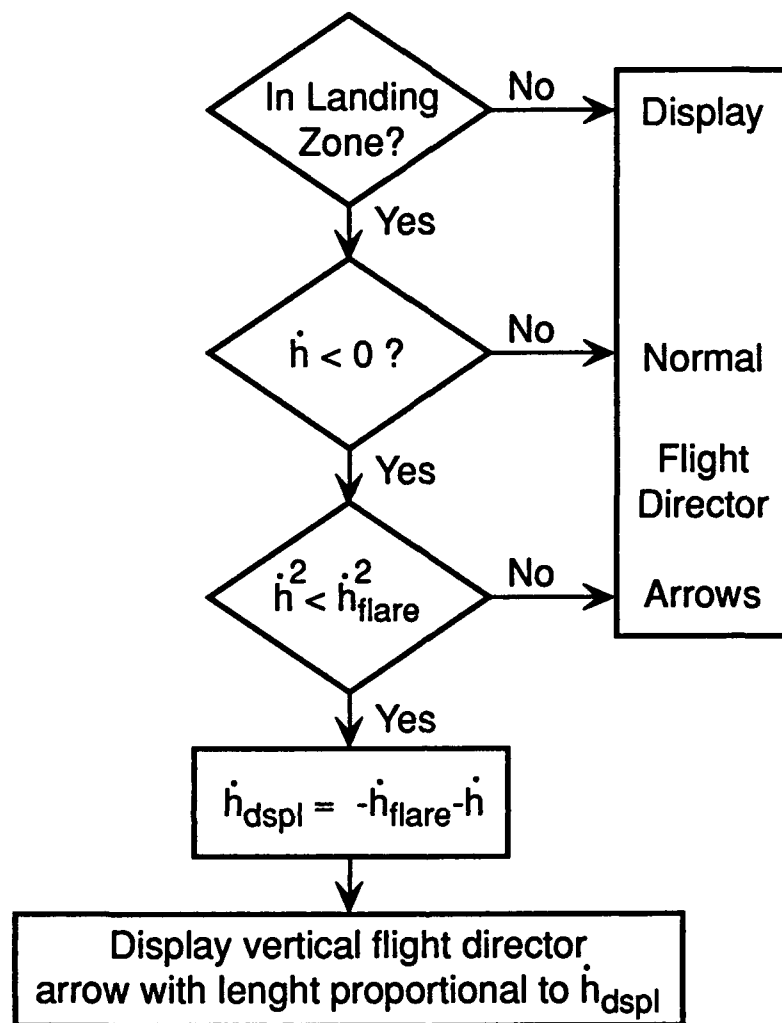


Figure 7. Flight director arrow calculations and display logic



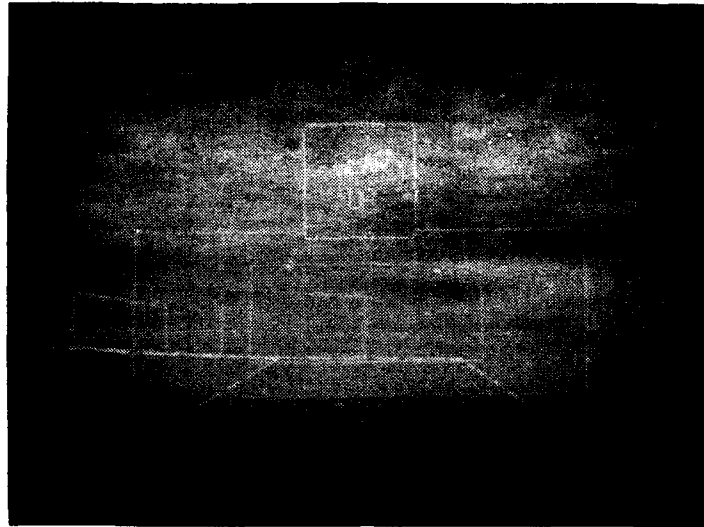
where

$$\dot{h}_{flare} = +\sqrt{2a(h - 5) + \dot{h}_{final}^2}$$

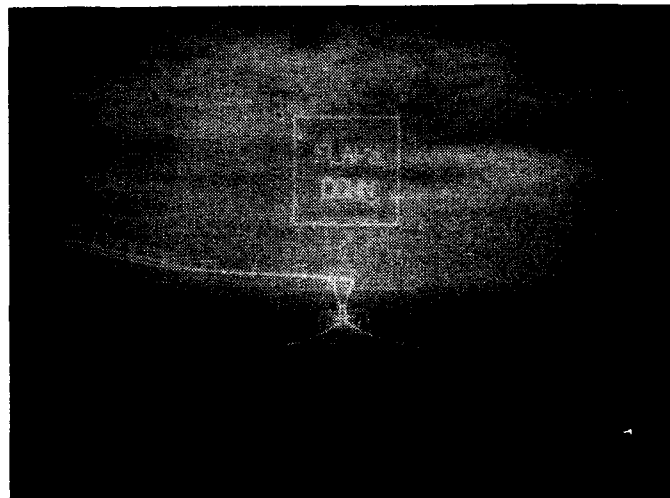
$$a = 1.0 \text{ ft/sec}^2$$

$$\dot{h}_{final} = -1 \text{ ft/sec}$$

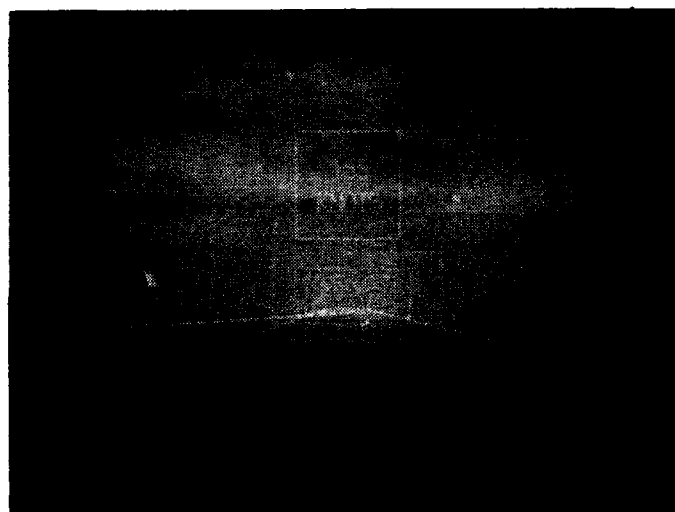
Figure 8. Logic for turning flare arrow on and determining arrow length.



Gear
Up



Flaps
Down



155
Knots

Figure 9. Typical messages in sign/flight director box

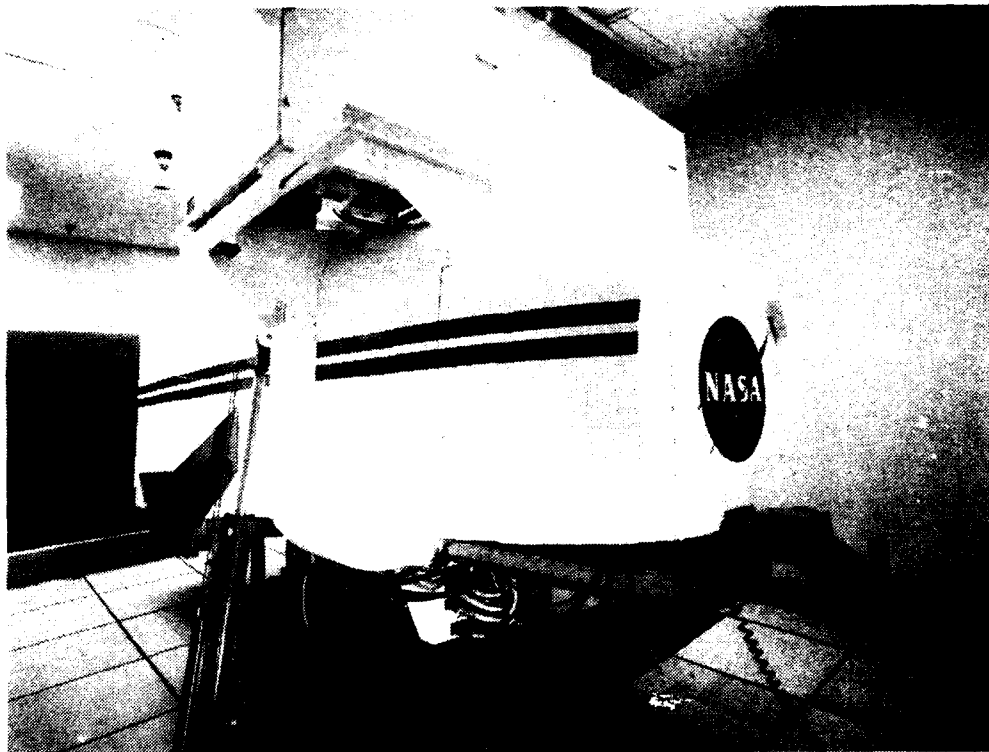


Figure 10. Exterior of simulation cockpit.



Figure 11. Interior of simulation cockpit.

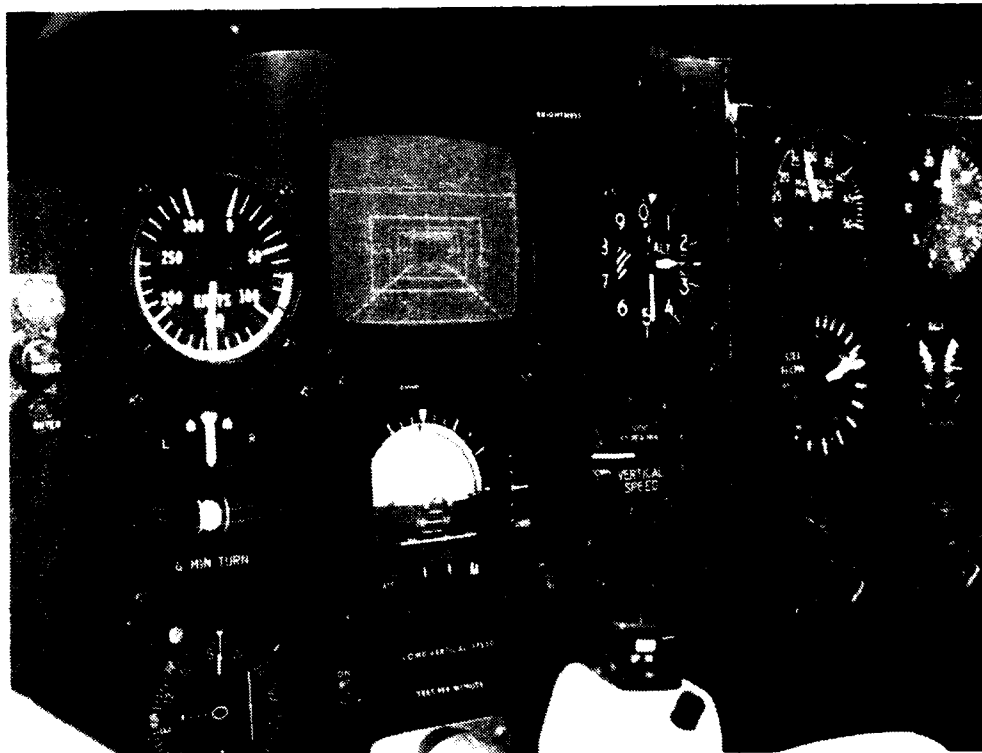


Figure 12. Instrument panel showing centrally-mounted 5-inch head-down display.

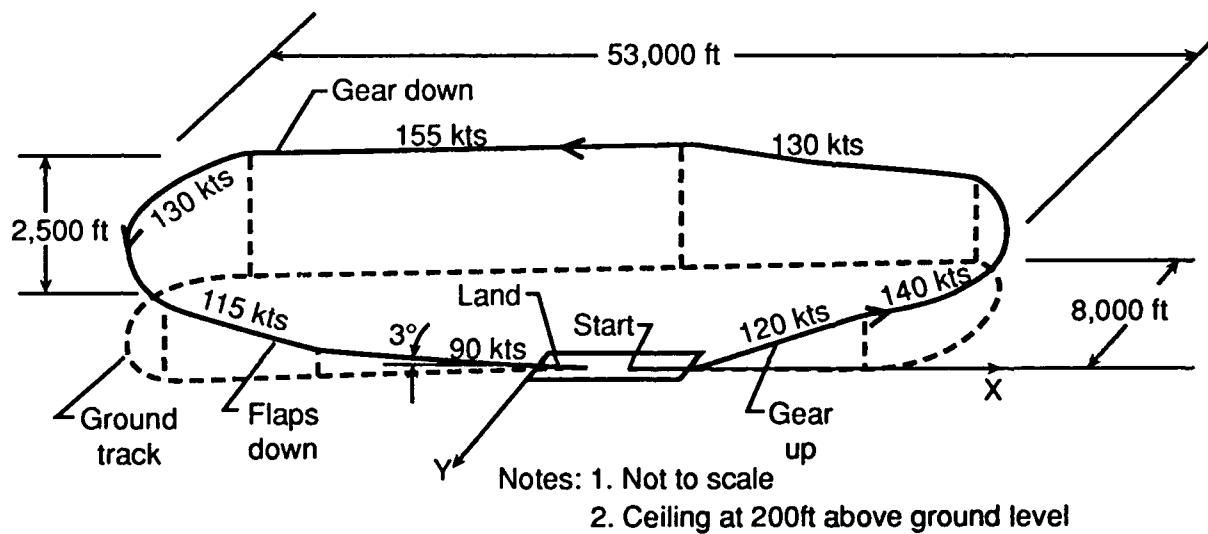
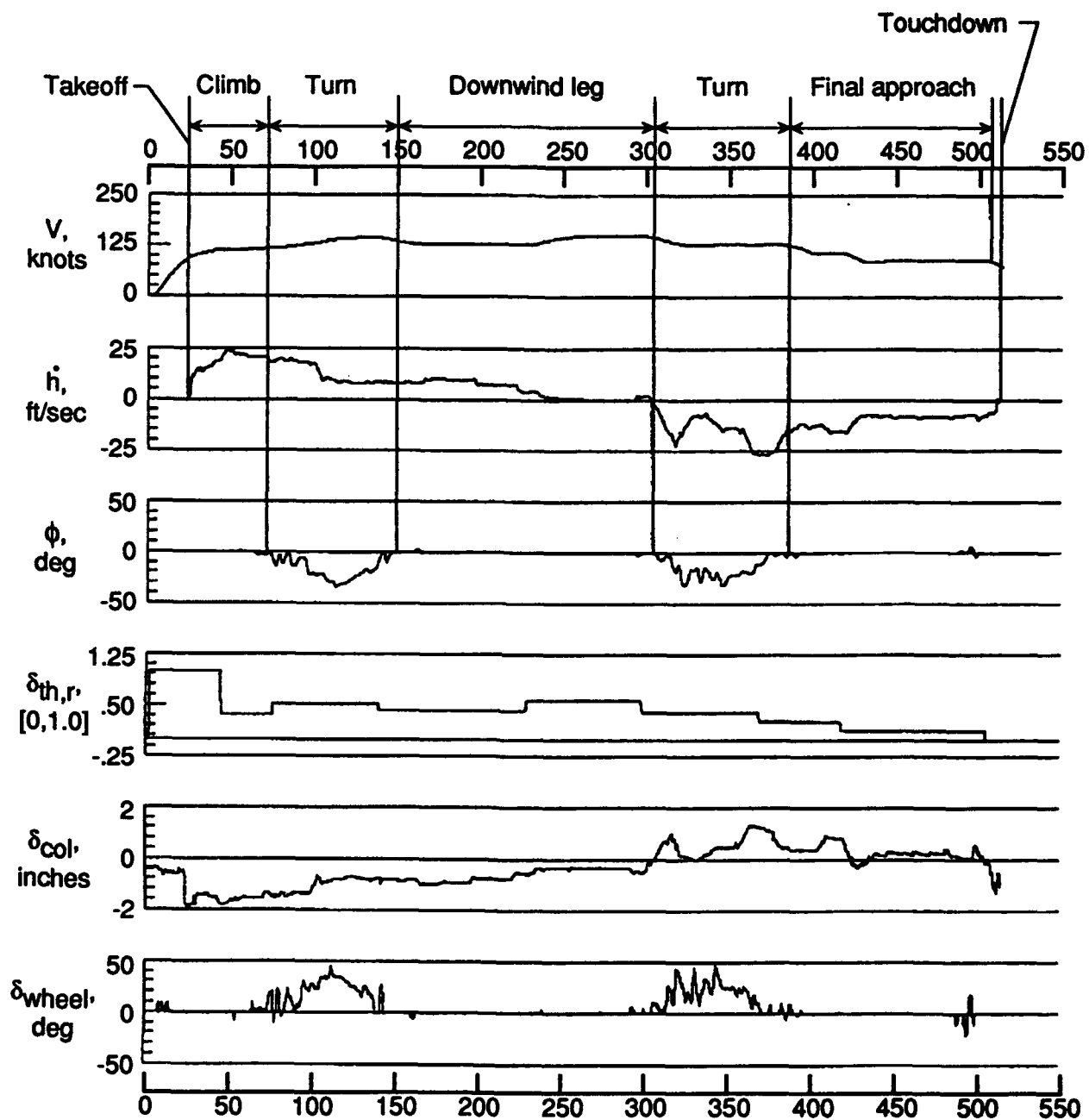
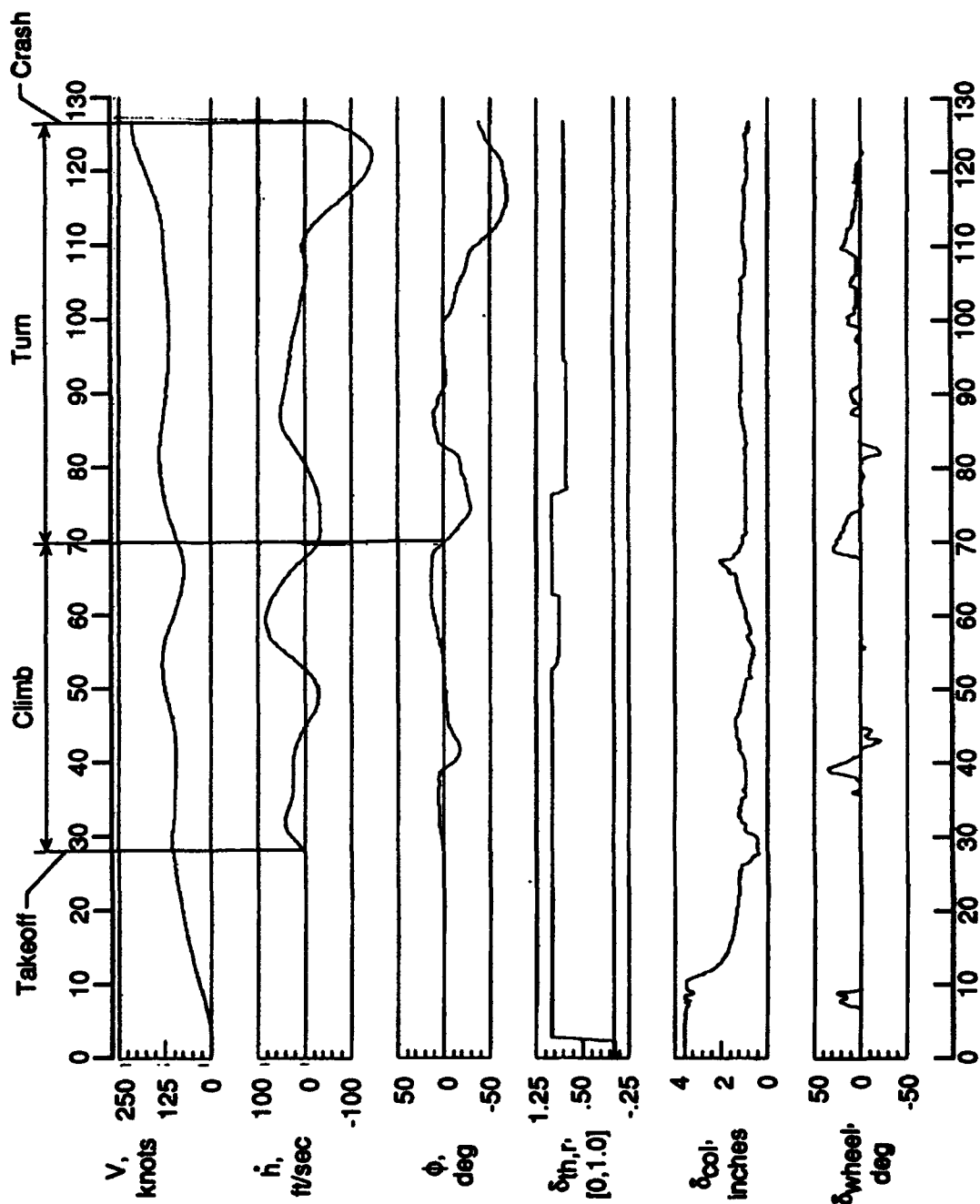


Figure 13. Trajectory flow to evaluate control system and display.



a) Combined Ez-Fly control system and HITS display in HUD configuration

Figure 14. Typical flight state and control positions for a non-pilot in reduced visibility.



b) Basic control system and HITS display in HUD configuration.

Figure 14. Concluded

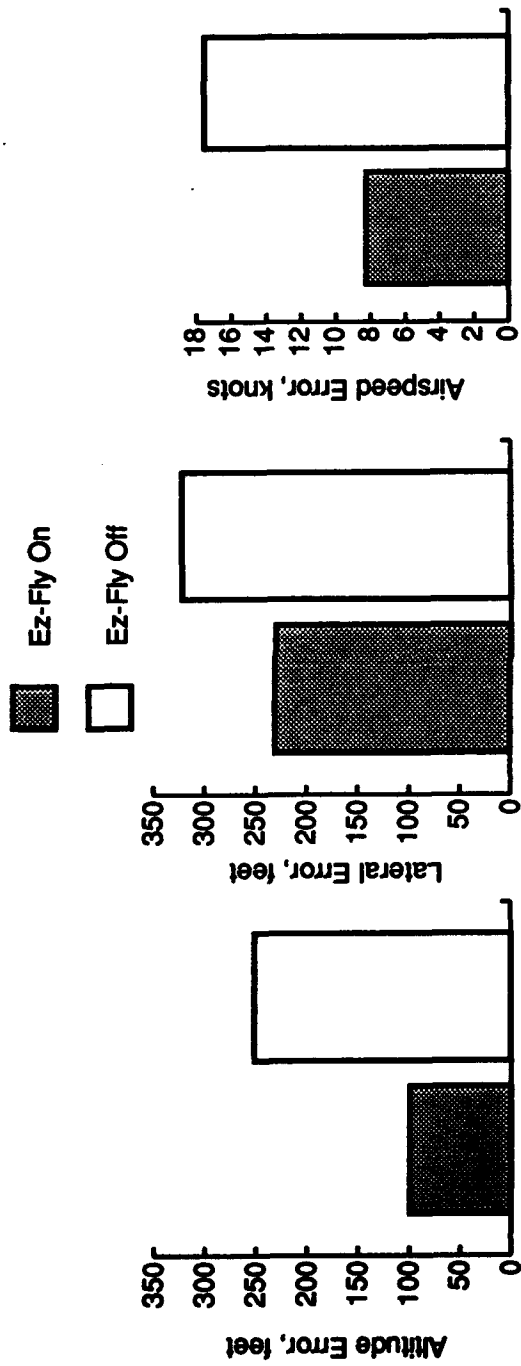


Figure 15. Effect of Ez-Fly decoupled control system on pilot performance, (Sixteen runs are contained in each category)

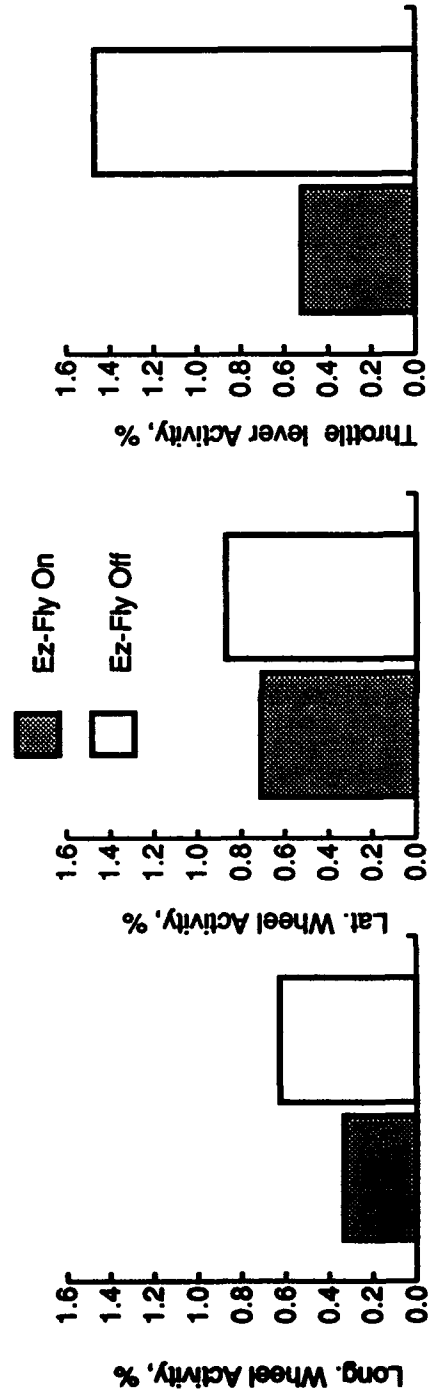


Figure 16. Effect of Ez-Fly decoupled control system on pilot's control activity, (Sixteen runs are contained in each category)

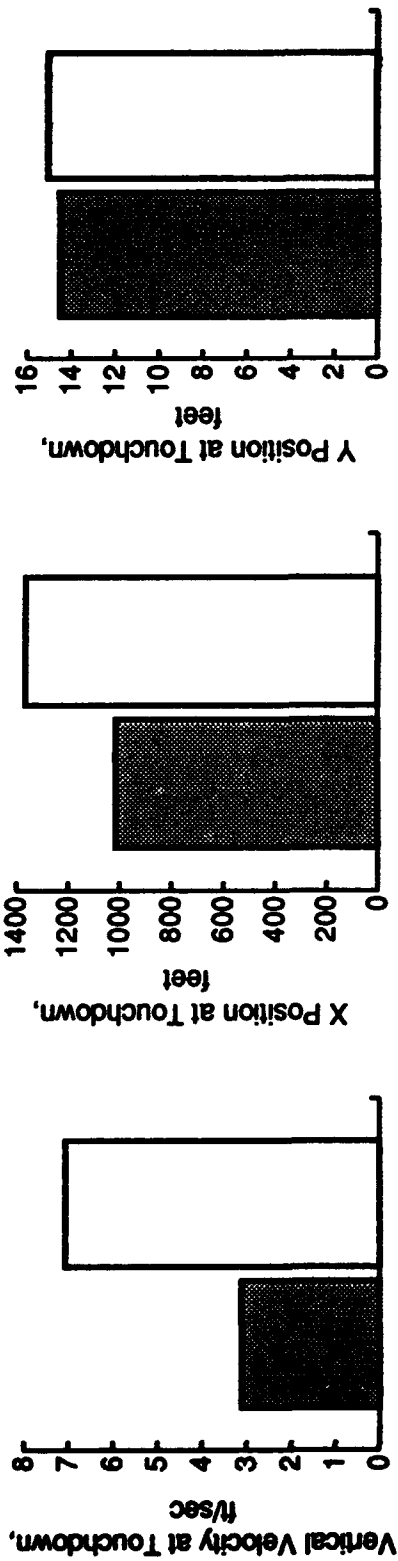


Figure 17. Effect of Ez-Fly decoupled control system on landing performance.
(Sixteen runs are contained in each category)

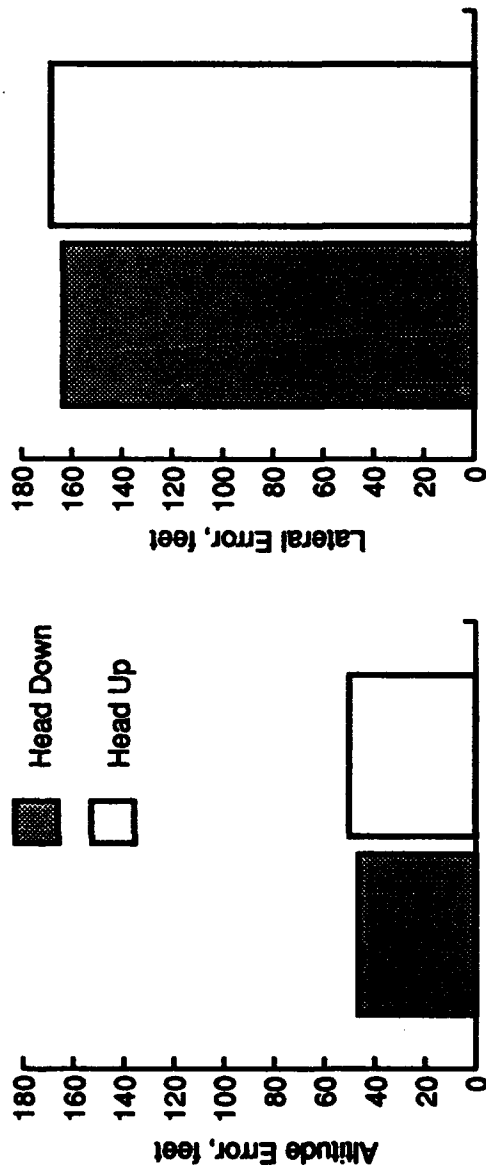


Figure 18. Comparison of pilot performance for head-up and head-down displays.
(Four runs are contained in each category)

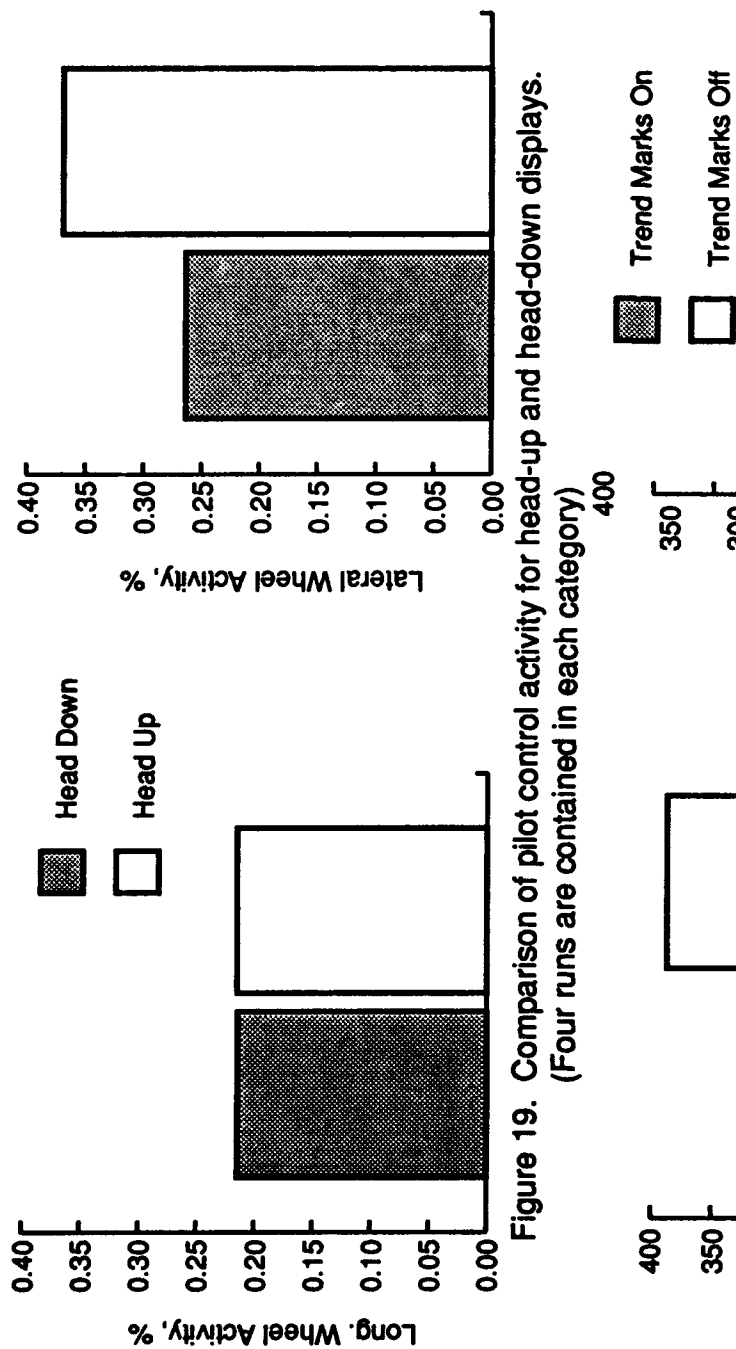


Figure 19. Comparison of pilot control activity for head-up and head-down displays.
(Four runs are contained in each category)

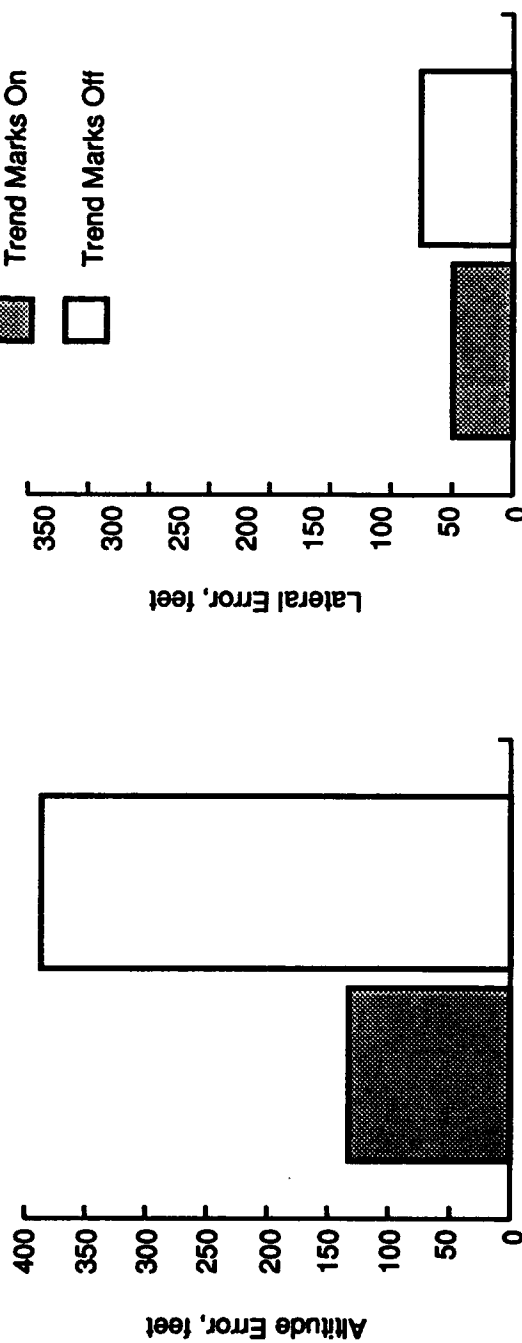


Figure 20. Effect of trend marks on pilot performance.
(Six runs are contained in each category)

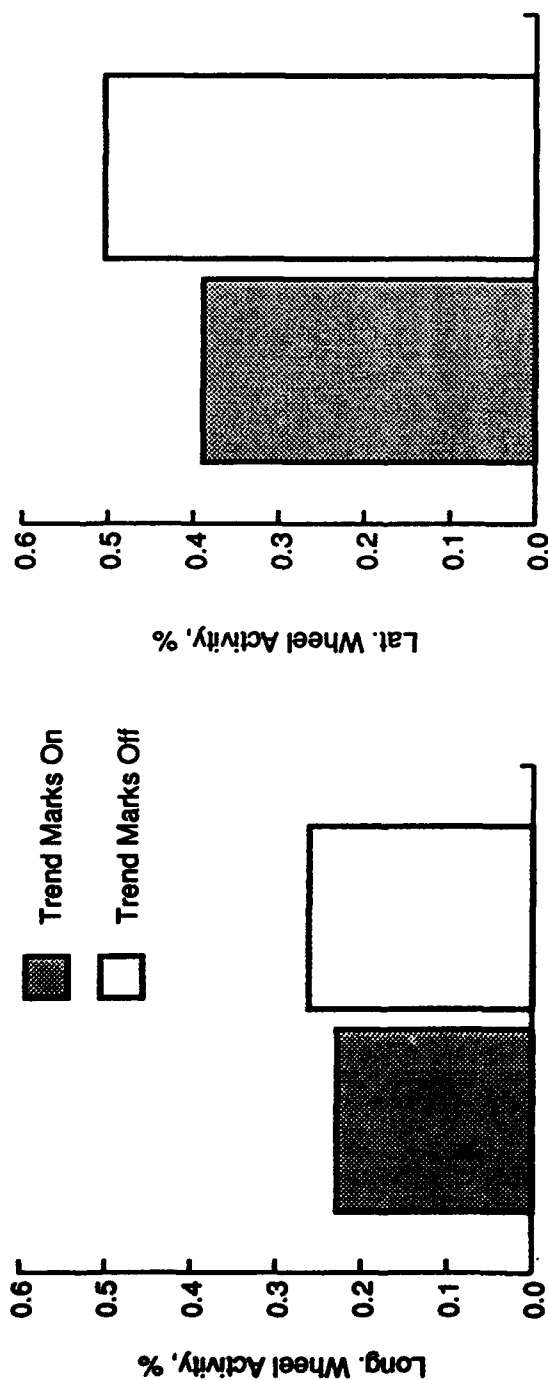


Figure 21. Effect of trend marks on pilot control activity.
(Six data points in each category)

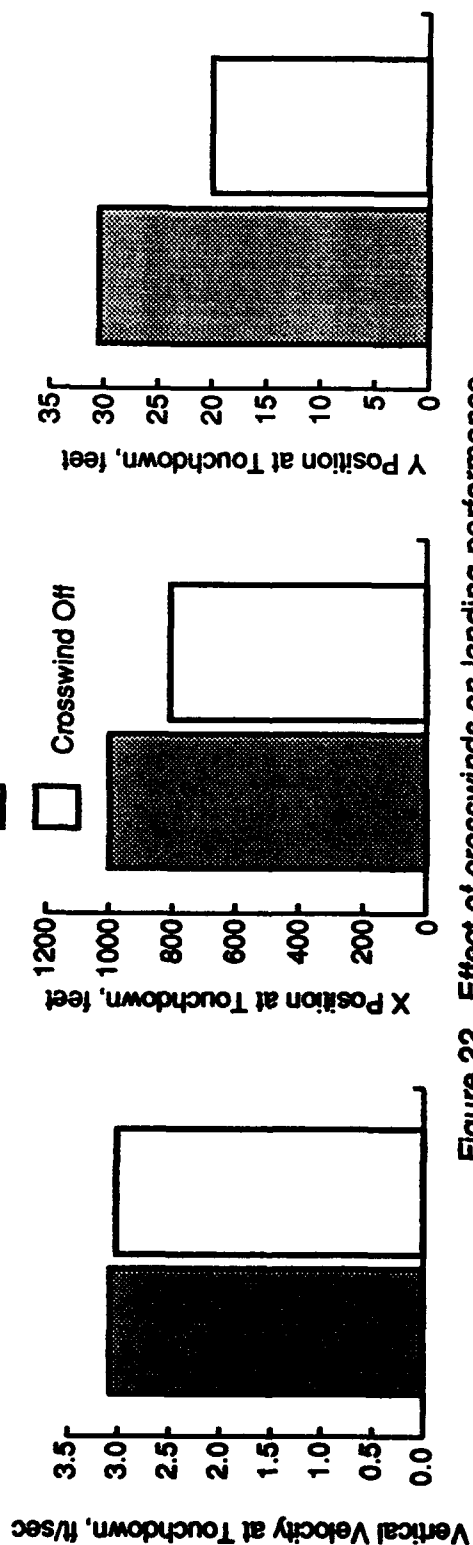


Figure 22. Effect of crosswinds on landing performance.
(Eleven runs are contained in each category)

**SENSITIVITY STUDY OF A SINGLE-ENGINE
GENERAL AVIATION AIRPLANE**

by

**David W. Levy
The University of Michigan
Department of Aerospace Engineering
Ann Arbor, MI**

**For Presentation to the AIAA/FAA Joint Symposium on General
Aviation Systems at the Hilton Inn-East, Wichita, KS
on March 16-17, 1992**

Sensitivity Study of a Single-Engine General Aviation Airplane

David W. Levy *

The University of Michigan
Department of Aerospace Engineering

Abstract

Simple sizing methods are applied to two existing single-engine general aviation airplanes. The methods are used in the conceptual design phase to estimate weight, wing area, and engine power required. The input parameters are calibrated to match the takeoff, empty, and fuel weight and to match key performance capabilities for the two baseline airplanes. The weight estimation method results in a closed form expression for the takeoff gross weight, from which global sensitivity coefficients may be derived. Potential weight reductions due to the application of current state of the art technology are then calculated. The increase in cruise speed possible due to the use of natural laminar flow airfoils and reduced wing area is estimated. The wing area is reduced by increasing the maximum lift coefficient with advanced high lift devices estimated while maintaining the same takeoff and landing field length requirements. A more general treatment is then presented which incorporates a statistical wing weight formula to improve the takeoff weight estimate. For this class of airplane, the optimal wing loading is approximately 30 lbs/ft², at which the baseline takeoff and landing field lengths are retained. Increases in cruise speed of up to 16 knots are predicted. Reductions in the takeoff weight and fuel weight are also possible.

Introduction

In the conceptual phase of the design of a new airplane, it is always necessary to determine how sensitive the airplane weight and cost are to certain design parameters. For example, the effects of a reduction in empty weight or an increase in cruise efficiency may be determined in terms of airplane gross takeoff weight, fuel required for the design mission, or some other measure of interest. One may then choose the areas of technology in which to concentrate development efforts so that the most benefit will result.

It is possible, using a very basic mission specification and statistical relations between empty weight and takeoff weight, to estimate the required takeoff weight for a given payload and mission. The sizing method, described in Reference [1], results in a closed-form

*Lecturer; Senior Member, AIAA

expression for the takeoff weight. This expression may then be differentiated to determine several sensitivity factors.

A second step in the conceptual design process is to determine required wing and engine sizes based on performance constraints. These constraints may include stall or approach speeds, takeoff and landing distances, and climb rate and cruise speed requirements. A performance matching diagram, which shows power loading and wing loading limits, may be used for this purpose.

This paper applies the sizing methods to two existing airplanes, and determines the sensitivity of airplane weight and performance to advanced technology. The baseline airplanes are in the single engine, propeller driven category and have capacities of four and six passengers. The airplanes were designed and certified in the late 1940's and 1950's. A derivative of one airplane is still in production, while the other had production suspended in 1987.

The sizing methodology is briefly described and then candidate technologies are discussed in a qualitative manner. The sizing methods are then "calibrated" to the published weight and performance data for each airplane and the sensitivity of the takeoff weight to several important parameters is determined. Then the effect of two candidate technologies on the cruise speed of the baseline airplanes is determined. In this analysis, the takeoff and landing field lengths are held constant. As a final study, the effects of wing area and aspect ratio on the empty weight is included in the takeoff weight estimation method. Then the effects of varying aspect ratio and wing loading on the cruise speed, takeoff weight, and fuel weight are determined.

The goal of this paper is to evaluate the potential of candidate technologies using very basic mission performance analysis techniques. Provided the simplified analysis techniques are reasonably accurate, then the changes in performance which are estimated will reflect the gains possible in the context of the mission the baseline airplanes are designed to perform. It should then be possible to make recommendations for or against certain technologies based on the inherent characteristics of the design mission.

Takeoff Weight Estimation Method

The takeoff weight of the airplane is broken down into three components:

$$W_{TO} = W_E + W_F + W_P \quad (1)$$

where:

W_{TO} is the takeoff weight
 W_E is the empty weight
 W_F is the mission fuel weight
 W_P is the payload weight.

In this analysis, the empty weight includes trapped fuel and oil and the weight of the crew is included in the payload. The total payload weight is assumed to be specified for the mission.

It is shown in Reference [1] that the following relationship exists between W_E and W_{TO} :

$$\log_{10} W_E = [(\log_{10} W_{TO}) - A] / B, \quad (2)$$

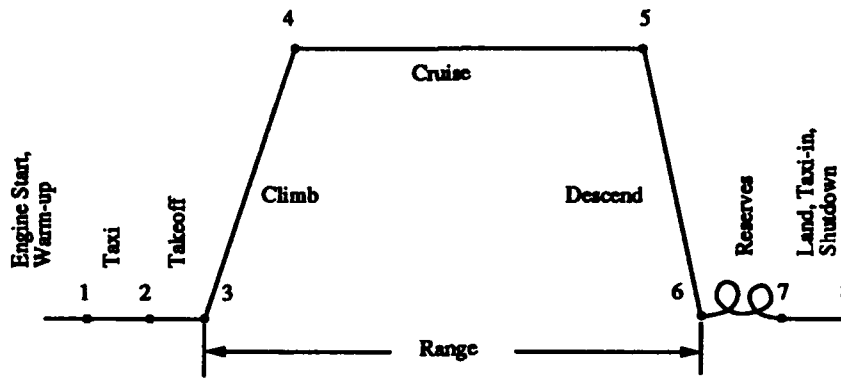


Figure 1: Typical Mission Profile for a General Aviation Transport

where A and B are constants which are specific to certain types of airplanes. This expression can be rewritten in the form:

$$W_E = 10^{-A/B} W_{TO}^{1/B} . \quad (3)$$

In other words, the takeoff and empty weights are related by a simple power law, with the power and constant of proportionality found by statistical regression. For single engine, piston propeller driven airplanes, Reference [1] recommends:

$$A = -0.1440, \quad B = 1.1162 . \quad (4)$$

For a given mission specification, the fuel weight may be related to the takeoff weight via the weight fraction method. A typical mission for the baseline airplanes is shown in Figure 1. Using data from [1, 2], the following weight fractions are estimated for the portions of the mission which are not fuel intensive:

$$\frac{W_4}{W_{TO}} = 0.992, \quad \frac{W_6}{W_5} = 0.995, \quad \frac{W_8}{W_7} = 0.996 . \quad (5)$$

The weight fractions for the cruise and reserves portions of the mission are calculated from the Breguet equations for range and endurance:

$$R = 326 \frac{\eta_p L}{c_p D} \ln \left(\frac{W_4}{W_5} \right) \quad (6)$$

$$E = \frac{326 \eta_p L}{V c_p D} \ln \left(\frac{W_6}{W_7} \right) . \quad (7)$$

Where:

- R is the design range in n.m.
- η_p is the propeller efficiency
- c_p is the brake specific fuel consumption in lb/hp/hr
- L/D is the lift to drag ratio
- E is the required endurance in hours
- V is the loiter speed in knots.

It should be pointed out that L/D , η_p , and c_p will have different values during the cruise and reserves (loiter) portions of the mission. It is now possible to compute the mission fuel

fraction, M_f for the mission:

$$M_f = \frac{W_1}{W_{TO}} \prod_{i=1}^7 \frac{W_{i+1}}{W_i} . \quad (8)$$

The three components of the takeoff weight have now all been specified, and when substituted into Equation 1, the following expression results:

$$\log_{10}(W_{TO}) = A + B \log_{10}(M_f W_{TO} - W_P) . \quad (9)$$

The takeoff weight is implicitly specified, and a numerical solution can be obtained by one of several methods.

Takeoff Weight Sensitivity

The sensitivity of the takeoff weight to a change in empty weight is found by differentiating Equation 2:

$$\frac{\partial W_{TO}}{\partial W_E} = B W_{TO} 10^{-(\log_{10} W_{TO} - A)/B} \quad (10)$$

The sensitivity of the takeoff weight to a performance parameter, y , is found by implicitly differentiating Equation 1, and solving for $\partial W_{TO}/\partial y$:

$$\frac{\partial W_{TO}}{\partial y} = \frac{B W_{TO} \left(W_{TO} \frac{\partial M_f}{\partial y} - \frac{\partial W_P}{\partial y} \right)}{M_f (1 - B) W_{TO} - W_P} \quad (11)$$

In this manner, the sensitivity of the takeoff weight to parameters such as lift to drag ratio or engine/propeller efficiency.

Wing and Engine Sizing Methodology

Once the takeoff weight is known, the wing and engine sizes may be determined by specification of performance constraints. These may include the takeoff and landing distances and the cruise speed. Other requirements such as climb performance can play a role but are not included in this study. The methods used are taken from Reference [1]. They involve statistical correlation of the performance parameter with certain combinations of wing loading, power loading, and other variables.

Takeoff Distance: It is possible to correlate the takeoff distance over a 50 ft obstacle, S_{TO} , with the "Takeoff Parameter,"

$$TOP = \frac{(W/S)(W/P)}{\sigma C_{LMAX TO}} , \quad (12)$$

where:

- W/S is the wing loading in lb/ft²
- W/P is the power loading in lb/hp
- σ is the density ratio
- $C_{LMAX TO}$ is the maximum lift coefficient in the takeoff configuration.

Statistical correlation of takeoff distances (in feet) with the *TOP* gives

$$S_{TO} = 8.134 TOP + 0.0149 TOP^2 . \quad (13)$$

Landing Distance: The landing distance from a 50 ft obstacle, S_L , is correlated with the stall speed in the landing configuration:

$$S_L = 0.5136 V_{S_L}^2 \quad (14)$$

with the landing distance in feet and the speed in knots. In this way, it is seen that the landing distance constraint is essentially a stall speed constraint.

Cruise Speed: The cruise speed correlation in [1] uses the same method taken from Reference [3] which is used to derive the zero lift drag coefficient. It is found that the cruise speed is proportional to the "Power Index:"

$$V_{CR} \propto I_p , \quad (15)$$

where:

$$I_p = \left[\frac{W/S}{\sigma W/P} \right]^{1/3} . \quad (16)$$

This proportional relation between cruise speed and power index is derived by assuming that the induced drag for most airplanes in this class is a small, fixed percentage of the zero-lift drag. Since a primary goal of this paper is an evaluation of the effects of relatively large changes in wing loading on cruise speed, it is probable that *this assumption will break down*. Since one of the results of the calibration process will be a drag polar, it is possible to derive a more precise form for the cruise speed relation.

The shaft power required can be expressed as:

$$P = \frac{DV}{\eta_p} = \frac{1}{\eta_p} \left[C_{D_o} q V S + \frac{C_L^2 q V S}{\pi A Re} \right] . \quad (17)$$

Introducing $C_L = \frac{W}{qS}$ and the density ratio:

$$\frac{1}{W/P} = 1.041 \times 10^{-5} \frac{\sigma V^3 C_{D_o}}{\eta_p W/S} + 0.9058 \frac{W/S}{\eta_p \sigma V \pi A Re} \quad (18)$$

where the power is in hp and the speed is in knots.

To compare this result with the takeoff and landing constraints, it must be recognized that the power here is *cruise* power, and the weight is the *cruise* weight. In this case, the power is corrected to reflect that a 75% cruise power setting is used. Similarly, the weight is adjusted to correspond to a mid-cruise value. In this way, the wing and power loadings may be compared directly with the value required to meet the takeoff and landing distances.

Discussion of Candidate Technologies

Since the baseline airplanes were designed and certified, substantial research has been made in all of the basic areas: structures, aerodynamics, controls, and propulsion. However, not

all should be applied to this class of airplane. For example, use of fly-by-wire flight control technology would be inappropriate for this class of airplane. It would be prohibitively expensive (these airplanes cost under \$200,000) and the improvements in performance and weight would be small. It is recognized, however, that significant improvements in safety could be realized with a fully automatic control system.

The author believes that a new model airplane in this class would be more competitive if it offers a substantial increase in cruise speed. There are a large number of used airplanes in this class available for approximately 30-40% of the price of a new model. There is no realistic way to reduce the price of a new airplane to a level which could compete with the used models, especially since approximately half the price is the cost of the engine and avionics. These are items over which the airframe manufacturer has no control. A new airplane must offer something which is not available in a used airplane, and at a cost not much higher than current new models.

A candidate technology should not be so new that significant development is required by the manufacturer. Such a development program would be a significant risk to the health of the company and would probably not be worthwhile. The technologies should be fairly well established and therefore low-risk.

Another very important consideration is the current product liability climate as it relates to the general aviation industry. The costs associated with liability can be high enough to make any new development program uneconomical. This topic, however, is beyond the scope of this study.

With these comments in mind, four technologies are chosen. These are: composite materials, high lift devices, modern airfoils, and engine/propeller technology. There are certainly others which could be considered.

Composite Materials: Approximately half of the empty weight of this class of airplane is the weight of the structure, the rest is due to the engine, avionics, and other systems. Therefore, if the weight of the structure could be reduced by 20% through the use of composites, the empty weight would be 10% less. However, this is more easily said than done. Issues of fatigue life, damage tolerance, inspectability, repairability, corrosion and a host of other considerations all tend to reduce the weight savings. Plus, the result is often a significantly more expensive airframe. More research is required to develop manufacturing methods which reduce the cost of composite structures. While the effects of a reduction in empty weight are determined, the investigation is not detailed.

Engine/Propeller Technology Earlier research, such as that in [4], indicates the potential for significant increases in efficiency through the use of stratified charge rotary engines along with reduced weight and volume requirements. This technology has failed to materialize. However, incremental improvements have been made in conventional powerplants. The specific fuel consumption of the Voyager series engine is reported to be 0.37 lb/hp/hr in [5]. The propeller efficiency of the propellers used in the Voyager around the world flight has also been reputed to be in excess of 0.90. However, there exist practical efficiency limits. The potential reduction in weight due to improvements in these parameters is determined. The use of turbine powerplants is not considered to be viable for this class of airplane due to the large increase in cost.

Modern Airfoils: Since the baseline airplanes were certified, two important types of airfoils have been developed. The NASA Low Speed, or GA(W) series is a high lift, relatively low drag airfoil. The Natural Laminar Flow series promotes laminar flow to a similar degree as the NACA 6-series, but develops higher maximum lift. The GAW and NLF airfoils are somewhat more difficult to manufacture because of their aft camber and the requirement for strict tolerances on the surface definition to achieve the advertised performance. Also, the NLF airfoils require a smooth surface to preserve the laminar flow. Either thick skins or composite construction would be necessary. For these reasons, the manufacturing cost of a wing with either of these airfoils would be higher than with a conventional airfoil. When laminar flow is desired, the necessity of a clean surface must be considered from an operational standpoint as well. Also, the performance and handling qualities must be evaluated both with and without laminar flow. Recent research [6] has shown negligible differences in stall speed and stability for an airplane equipped with an NLF airfoil when the boundary layer is turbulent.

High Lift Devices: The use of advanced high lift devices is well established in other categories of aircraft, such as jet transports. Their use in general aviation however is not as prevalent, partly due to manufacturing and maintenance cost considerations. Also, since the maximum lift is dependent on Reynolds number, it is unclear whether the potential is the same for this class of airplane. If the costs could be held to a reasonable limit and the performance improvements are significant then the cost/benefit trade may be worthwhile. The performance improvement due to the use of double-slotted Fowler flaps and part span leading edge slats is investigated. It is recognized that a good, clean installation of leading edge slats is no easy task, and that it may not be possible to maintain laminar flow past the slat trailing edge during cruise. It is assumed here that the desired laminar flow can be maintained, and that the associated increase in manufacturing costs are not excessive.

Calibration of Sizing Methods to Baseline Aircraft

From References [7, 2], the following characteristics of the baseline airplanes are obtained:

Airplane:	B	C	
Maximum takeoff weight	3400	3800	lb
Standard empty weight	2106	2139	lb
Maximum usable fuel	434	522	lb
Payload with full fuel	860	1139	lb
Cruise speed at 75% power	172	168	kt
Range at 75% power	716	765	n.m.
Reserves at 45% power	45	45	min
Wing Area	181	175	ft ²
Aspect Ratio	6.2	7.66	

To determine the lift to drag ratios in the cruise and loiter mission phases, one may use a drag polar for the airplane:

$$C_D = C_{D_0} + \frac{C_L^2}{\pi A R e}, \quad (19)$$

Parameter	Airplane B	Airplane C	Reference
C_{D_o}	.0192	.0200	.0192/.0200
e	.70	.60	.75
$\eta_{p_{cr}}$.85	.83	0.8
$\eta_{p_{ltr}}$.82	.79	0.7
$c_{p_{cr}}$ (lb/hp/hr)	.420	.466	.5-.7
$c_{p_{ltr}}$ (lb/hp/hr)	.450	.496	.5-.7
$(L/D)_{cr}$	9.4 ¹	10.5 ²	8-10
$(L/D)_{ltr}$	11.5 ³	11.6 ³	10-12
R (n.m.)	690	739	716/765
A	-.1782	-.1374	-.1440

¹ At $W = .942W_{TO}$, $h=6000$ ft, $V=172$ kt.

² At $W = .937W_{TO}$, $h=6500$ ft, $V=168$ kt.

³ At speed for maximum $C_L^{3/2}/C_D$.

Table 1: Calibrated Performance Parameters for Baseline Airplanes

where AR is the aspect ratio and e is Oswald's Efficiency factor. In Reference [3], cruise speed and power data are used to derive a zero lift drag coefficient of $C_{D_o} = .0192$. This derivation assumes that the induced drag is equal to 10% of the total drag during cruise.

There are still several parameters remaining to be specified, and a discussion of the final values assumed for some of them is warranted. It is observed that W_{TO} and W_E do not satisfy the statistical relationship in Equation 2, so the coefficients A and/or B must be adjusted. For this study, it is arbitrarily chosen to shift A , although substantially the same results are obtained if B is adjusted. For the cruise segment of the mission, the lift to drag ratio is calculated at the cruise speed and altitude, and at the mid-cruise weight. To calibrate the sizing method, the parameters C_{D_o} , e , η_p , and c_p may be adjusted in many combinations. As an additional specification, the power required at the cruise condition is computed and required to match the 75% maximum continuous rating. Still, there is considerable leeway in choosing the final values. For the baseline airplanes, the C_{D_o} values suggested in [1] are used directly. The reserve fuel is calculated for a speed corresponding to the minimum power required. Also, a credit is taken of 26 nautical miles for distance traveled during the climb and descent phases of the mission. The final, calibrated, values are listed in Table 1.

Notice that rather aggressive values for the performance parameters are required, by the standards of the values recommended by Reference [1] — especially for the propeller efficiency and the specific fuel consumption.

The sensitivity of the takeoff weight due to changes in empty weight and performance parameters are shown in Table 2, along with suggestions for a "reasonable" change due to advanced technology. The values suggested as reasonable do not yet reflect the application of any specific technology. They are given more to put matters into perspective, so that the potential gains can be realistically evaluated. The partial derivatives are to be interpreted as local slopes, but they are *global* in nature. For example, the sensitivity to a change in empty

	Airplane B:			Airplane C:			
y	$\frac{\partial W_{TO}}{\partial y}$	Change	ΔW_{TO}	$\frac{\partial W_{TO}}{\partial y}$	Change	ΔW_{TO}	
W_E	1.802 lb/lb	-210	-378 lb	1.983 lb/lb	-214	-424 lb	
L/D	$-110.8 \frac{\text{lb}}{\text{unit } L/D}$	+1	-111 lb	$-105.8 \frac{\text{lb}}{\text{unit } L/D}$	+1	-106 lb	
c_p	$2478 \frac{\text{lb}}{\text{lb/hp/hr}}$	-.05	-124 lb	$2382 \frac{\text{lb}}{\text{lb/hp/hr}}$	-.05	-119 lb	
η_p	$-1224 \frac{\text{lb}}{\text{unit } \eta_p}$	+.05	-61 lb	$-1337 \frac{\text{lb}}{\text{unit } \eta_p}$	+.05	-67 lb	
Total:			-674 lb	Total:			-716 lb

Table 2: Potential Savings in Takeoff Weight due to Advanced Technology

weight includes the resulting change in mission fuel weight. The statistical nature of the empty weight equation also reflects the changes in wing size, engine size, etc., which would be a result of a change in takeoff gross weight. However, specific applications of technology, e.g. an improvement in the high lift system which may allow a smaller wing, cannot be accurately determined by this method. Also, it should be noted that the sensitivities for the performance parameters reflect gains only in the cruise mission segment. Small additional gains are made during the reserves portion as well.

It is seen that the potential reductions are substantial. The total weight reductions listed in Table 2 assume linear superposition. It is possible to check this by adjusting A , L/D , c_p , and η_p in the weight estimation procedure. The weight reductions then predicted are 766 lbs for Airplane B and 734 lbs for Airplane C, so the linear approximation is fairly accurate. These total weight reductions are approximately 20% of the gross takeoff weight!

The wing and engine sizing formulas are now calibrated to agree with the following performance data obtained from References [7, 2, 8]:

Airplane:	B	C	
Takeoff distance to 50 ft	1769	1960	ft
Landing distance from 50 ft	1324	1611	ft
Cruise speed at 75% pwr	172	168	kt
Stall speed, clean	64	65	kt
C_{LMAX}	1.35	1.52	
Stall speed, landing	53	56	kt
C_{LMAXL}	1.97	2.04	
Takeoff wing loading	18.78	21.71	lb/ft ²
Takeoff power loading	11.93	12.67	lb/hp

The resulting clean and landing C_{LMAX} values obtained are used to calibrate the takeoff and landing formulas. The calibrated matching diagrams are shown in Figure 2.

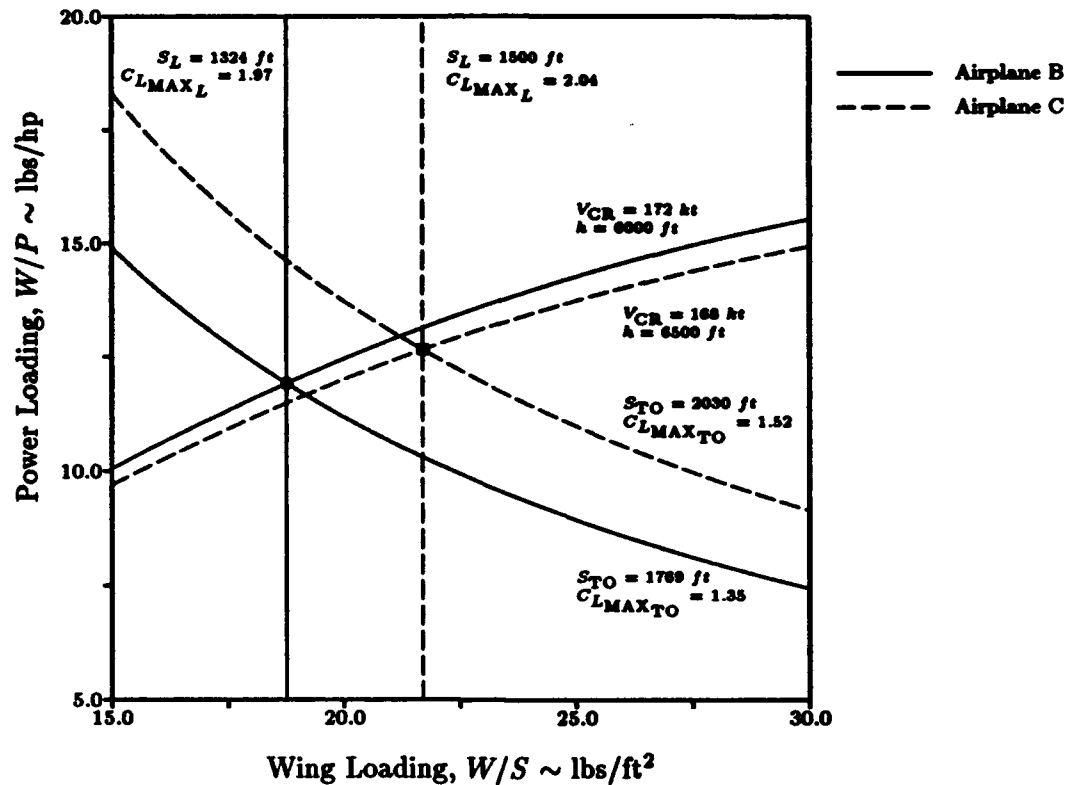


Figure 2: Performance Matching Diagram for Baseline Airplanes

Implementation of Advanced Technology

Once the performance boundaries are calibrated to the baseline field lengths and cruise speeds, it is possible to determine the effects of advanced technology on the cruise speed. New (higher) values of CL_{MAXL} are predicted based on new airfoil/high lift device combinations. To maintain the same landing distance, the stall speed is held constant which allows an increase in wing loading. At the same time, the wing profile drag coefficient is reduced, taking into account the effects of laminar flow and reduced wing area. The new cruise speed can be calculated for the case where power loading is held constant.

To calculate the new CL_{MAXL} , the characteristics of the airfoils must be known. These are obtained from experimental data for those currently used on the baseline airplanes and for the candidate airfoils and shown in Table 3. The first four airfoils listed are the airfoils for Airplanes A and B, respectively, as obtained from [7].

In the Class I method described in [1], the airplane maximum lift coefficient may be written in the form

$$C_{LMAX} = \frac{k_1}{2} (C_{lMAX_r} + C_{lMAX_t}) \quad (20)$$

where the factor k_1 accounts for the effects of wing sweep angle and taper ratio, plus the effects of the tail down-load required for longitudinal trim.

It would seem reasonable to calibrate the factor k_1 for each airplane to the clean CL_{MAX} and then use that k_1 to compute the new value of CL_{MAX} with the advanced airfoil. This results in values for k_1 of 0.882 and 1.052 for Airplane B and C respectively. It is not

Airfoil	$C_{l_{MAX}}$	Reference
NACA 23016.5 (Root)	1.45	[9]
NACA 23012 (Tip)	1.61	[9]
NACA 64 ₂ A215 (Root)	1.34	[9]
NACA 64 ₁ A412, $\alpha=0.5$ (Tip)	1.55	[9]
NASA NLF(1)-0416	1.69	[10]
NASA GA(W)-2	1.81	[11]

Reynolds number $\approx 3 \times 10^6$.

Table 3: Section Maximum Lift Coefficient, $C_{l_{MAX}}$, for Baseline and Candidate Airfoils

Type	Roskam [1], Class:		Hoerner [12]	Raymer [13]	Average
	I	II			
Slotted	1.38	1.01	1.18	1.30	1.22
Semi-Fowler	1.78	N/A	N/A	1.50	1.64
Full Fowler	2.01	1.43	1.67	1.69	1.70
Two-Slot Full Fowler	1.38	1.01	1.18	1.30	1.95
Leading Edge Slat	0.50	0.82	0.93	0.46	0.68

Table 4: Incremental Section Maximum Lift Coefficient, $\Delta C_{l_{MAX}}$, due to High Lift Devices

reasonable to believe a value greater than one, so it must be concluded that the theory is inadequate or that perhaps the airfoil has been modified in some respect for Airplane C.

A similar procedure is used to calculate the performance of an advanced high lift system. The current installation on Airplane B is a single-slotted trailing edge flap, while Airplane C uses a semi-aft translating Fowler flap arrangement. Neither aircraft uses leading edge devices. Several methods and sources are available to compute the maximum section lift increment. Values for the baseline installations and for advanced systems are listed in Table 4. For lack of better information, the average values are used in this study.

The incremental maximum lift coefficient for the airplane may be related to the section value with

$$\Delta C_{L_{MAX}} = k_2 \frac{S_{WF}}{S} \Delta C_{l_{MAX}} . \quad (21)$$

As with the clean maximum lift case, the factor k_2 accounts for planform and trim effects. The parameter S_{WF} is the flapped wing area, which is simply the planform area of the wing section bounded by the inboard and outboard edges of the flaps. Using the average $\Delta C_{l_{MAX}}$ values and the flapped area for the baseline aircraft, values for k_2 of 1.14 and 0.576 are obtained. As before, a value greater than one is not reasonable, and such a low value for Airplane C is rather disheartening.

Because of the poor correlation with the theory, it is not very clear how to proceed. The baseline $C_{L_{MAX}}$ for each airplane must be used directly, as should the $C_{l_{MAX}}$ value for

the advanced airfoil. Rather than use a calibration factor which is suspected as incorrect, a value of $k_1 = 0.95$ is used to calculate the new C_{LMAX} . This is a value within the range suggested by Roskam [1]. By similar logic, $k_2 = 0.95$ is used to calculate ΔC_{LMAX} for the new flap systems.

It is apparent from Table 3 that C_{LMAX} for the GA(W) airfoil is not significantly greater than that for the NLF airfoil. Indeed, a design goal for the NLF airfoil was to obtain maximum lift coefficients close to those for the GA(W) airfoil and preserve laminar flow at cruise lift coefficients. If the GA(W) airfoil is chosen, then the wing area would be somewhat smaller than if the NLF airfoil is used and would have less wetted area. But, this reduction in drag would not be as great as that due to laminar flow. Therefore the NLF airfoil is chosen for further study.

For the advanced flap system, three changes are proposed to be made to the baseline installation. The existing type of flap is upgraded to a double-slotted, fully aft translating Fowler flap system. Next, the flapped area is increased by extending the outboard edge of the flap to 85% span. To maintain adequate roll control authority, spoilers will be required. However, small "feeler" ailerons will remain, which should give adequate authority in cruise flight and will help to maintain good control feel characteristics. Finally, leading edge slats will also be employed. A part-span slat is used which extends from 55% to 95% span. This should help reduce manufacturing costs required for a good installation.

After the new clean and landing maximum lift coefficients are calculated, the wings are re-sized to maintain the same landing stall speeds. The wing aspect ratio is held constant. The result is that the inboard edge of the flap, as a percentage of the span, increases slightly and this effect is accounted for in the determination of the flapped area, S_{WF} . It also increases the span loading, which may degrade cruise performance somewhat from the value achievable if span loading is held constant. At this time, no change in wing weight is calculated. While the wing weight will probably decrease because of the large reduction in area, the reduction will be offset somewhat by the increased weight of the high lift systems and the addition of spoilers for roll control. This is discussed further below.

To calculate the drag coefficient for the existing wing and for the new wing, an approximate form of the Class II method in [1] is used:

$$C_{D_{ow}} = C_{f_w} \left\{ 1 + L' \left(\frac{t}{c} \right) + 100 \left(\frac{t}{c} \right)^4 \right\} \frac{S_{wet}}{S} . \quad (22)$$

The wing skin friction coefficient, C_{f_w} , is usually the value for turbulent boundary layers. When laminar flow is present, an area weighted average of laminar and turbulent values is used:

$$C_{f_w} = C_{f_{w_{turb}}} \frac{S_{wet_{turb}}}{S_{wet}} + C_{f_{w_{lam}}} \frac{S_{wet_{lam}}}{S_{wet}} . \quad (23)$$

Before proceeding further, it is noted that the baseline airfoil used in Airplane C is a NACA 6-series airfoil which is designed for laminar flow. The wing on Airplane C is constructed using conventional thin-skin aluminum, but it is assumed that laminar flow could exist at most to approximately 25% chord. As a second possibility, the new cruise speed is also calculated with no laminar flow on the baseline airplane. The term in the {}'s in Equation 22 accounts for thickness effects. Also note that both the wetted area and the reference planform area will change. The calibrated zero lift drag coefficient is then adjusted as follows:

$$C_{D_{onew}} = \left\{ C_{D_{old}} - C_{D_{owold}} \right\} \frac{S_{old}}{S_{new}} + C_{D_{ownew}} . \quad (24)$$

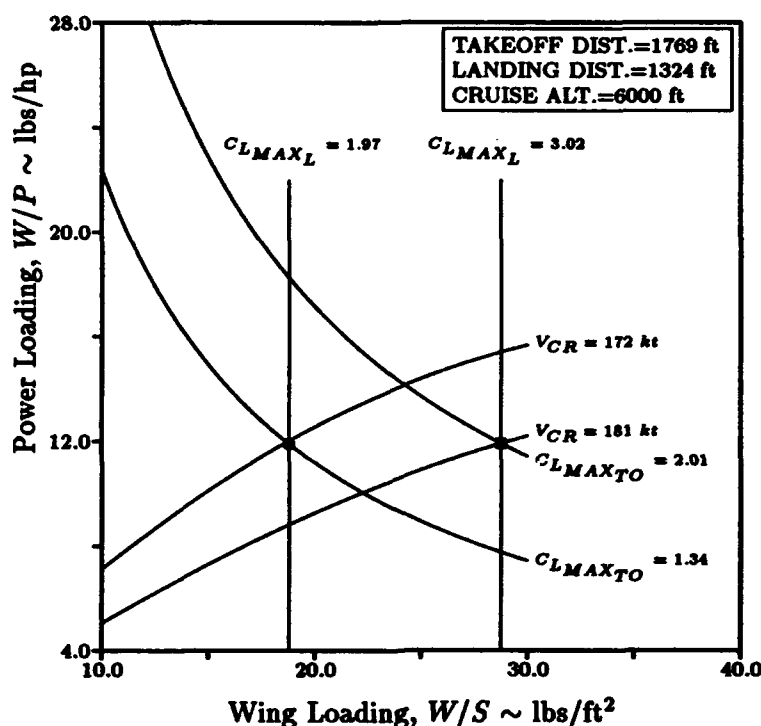


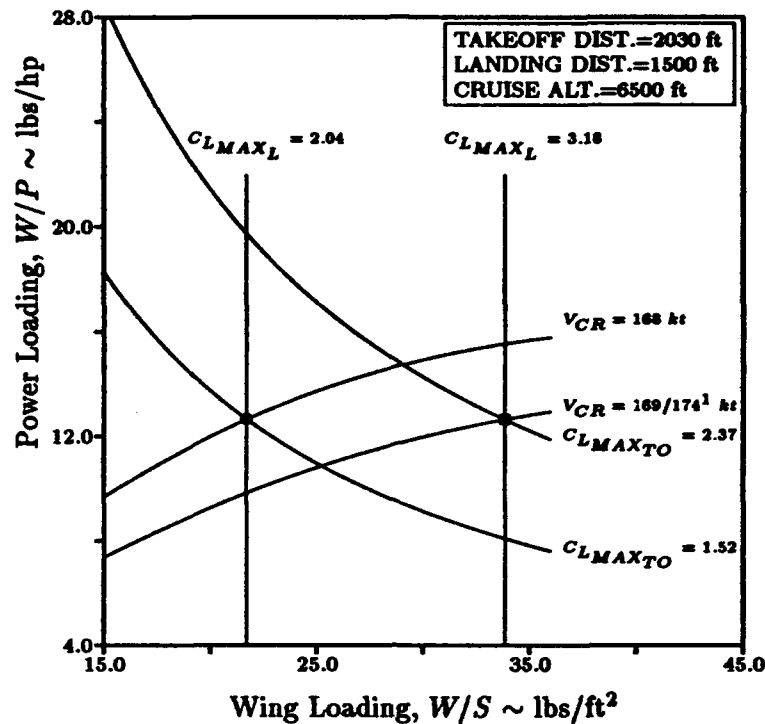
Figure 3: Performance Matching Diagram for Baseline Airplane B with Advanced Airfoil and Flap System

The incorporation of the new airfoil and high lift devices result in the following new parameter values:

Airplane:	B	C
C_{LMAX}	1.49	1.61
C_{LMAXL}	3.02	3.18
$S \text{ (ft}^2\text{)}$	118.2	112.4
$W/S \text{ (lb/ft}^2\text{)}$	28.8	33.8
C_{D0}	.0234	.0288

A new performance matching diagram may now be created for each airplane. As stated before, the wing loading is set to maintain the landing stall speed (and therefore the landing distance). At this point, the power loading is held constant. Then the new takeoff line can be calibrated by adjusting the value for C_{LMAXTO} . No effort is made to determine the flap deflection angle required. It is also assumed that takeoff and landing climb performance will still meet FAR Part 23 requirements. Finally, a new cruise speed can be calculated to match the wing and power loadings. These new matching diagrams are shown in Figures 3 and 4.

There is an increase in the cruise speed of nine knots for Airplane C, but only up to six knots for Airplane C. If 25% laminar flow is assumed for the wing of Airplane C, the improvement is only one knot! The marginal improvements for Airplane C results in more questions than answers. Is the assumption of constant wing weight reasonable? Has the wing loading been increased *too* much? To answer these and other questions, a simple trade



¹ Cruise speed for: 25%/0% laminar flow on wing of baseline airplane

Figure 4: Performance Matching Diagram for Baseline Airplane C with Advanced Airfoil and Flap System

study is needed.

Wing Sizing Trade Study

To study the effects of changing wing loading more precisely, the changes in wing weight, W_w , must be accounted for. At this analysis stage, statistical wing weight prediction formulas are appropriate for use. Several are available, such as the following from [1]:

$$W_w \propto AR^{0.566} S^{0.606} \quad (25)$$

The formula is calibrated to agree with wing weights for the baseline airplanes listed in [1]. The effects of changes in aspect ratio are easily included at this time. It should be noted that results will be different for different statistical forms for the wing weight equation. For example, if the exponent for the aspect ratio dependence were higher, then the weight penalty for an increase in aspect ratio would increase. The weight penalty associated with the improved high lift devices is difficult to estimate. Roskam [1] suggests an addition of two percent of the wing weight for Fowler flap systems. For this study, a six percent penalty is used to account for the double-slotted trailing edge Fowler flaps, leading edge slats, and roll control spoilers. The penalty is assumed to be a linear function of wing loading, varying from zero for the baseline to the six percent value at the wing loadings used in the previous section.

The changes in wing weight are incorporated into the sizing process by adjusting the coefficient A in the empty weight regression formula of Equation 2. First, a new empty weight is calculated

$$W_{E_{new}} = W_{E_{old}} - W_{w_{old}} + W_{w_{new}} \quad (26)$$

and then the regression coefficient is adjusted by

$$A_{new} = A_{old} - B \log_{10} (W_{E_{new}} / W_{E_{old}}) \quad (27)$$

as suggest in [1]. It is not clear at this time if there is any "double counting" of wing weight by using this process. A more detailed study is needed of what portion of the coefficient A (or B for that matter) is due to wing weight and how it may be affected by changes in wing geometry. The sizing process is automated on a computer and iterated until the takeoff weight and cruise speed both converge. The cruise speed is computed holding cruise power constant at the baseline value.

The effects of varying wing loading and aspect ratio on the cruise speed, takeoff weight and mission fuel required are shown in Figure 5. The improvements due to laminar flow over the wing are also shown.

The trends for both airplanes are very similar. Cruise speed increases with wing loading until an optimal value is reached. The optimal wing loading increases with aspect ratio. With laminar flow, however, the optimal wing loading is slightly lower. In general, the optimal wing loadings are from 5 to 20 lb/ft² higher than the baseline values, although in some cases the optimal values would result in increased landing distances with the proposed high lift lift systems. If a turbulent flow airfoil is used increases in cruise speed of nine knots at the maximum aspect ratio for both airplanes at their target wing loadings. A further six to seven knot increase is possible if the NLF airfoil is used.

Note that for Airplane C, if the aspect ratio remains at the baseline value of 7.66, then the wing loading of 33.8 lb/ft² possible with the improved high lift system is above the optimal value for the laminar flow case. It must be realized, however, that the cruise speed predicted by the performance matching process assumed that the takeoff weight remained constant. Direct comparisons to those results should be made with caution.

It is apparent from Figure 5 that the variation in takeoff weight with wing loading is much greater for Airplane B than for Airplane C. This is due to the higher values for the wing weight and the regression coefficient A for that airplane. If the aspect ratio is held fixed at the baseline value, it is seen that the takeoff weight could be reduced by 230 to 160 lbs for Airplane B and C, respectively. The reduction in wing weight due to the reduced area could be used to increase aspect ratio. With this wing weight model, the aspect ratio could be increased to the maximum value shown and the baseline takeoff weight would be retained. At the same time, a reduction in mission fuel required would decrease by approximately 20 lbs.

In this analysis, there is no explicit weight penalty associated with the use of the NLF airfoil. Their use results in a fuel weight reduction of approximately 20 lbs and an associated takeoff weight reduction of over 100 lbs.

Conclusions

Simple sizing methods are calibrated to two single-engine general aviation airplanes. The reduction in the takeoff weight and increase cruise speed is then determined due to the

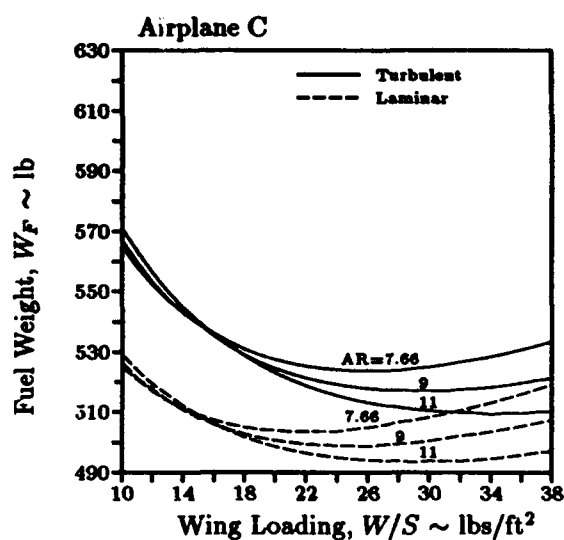
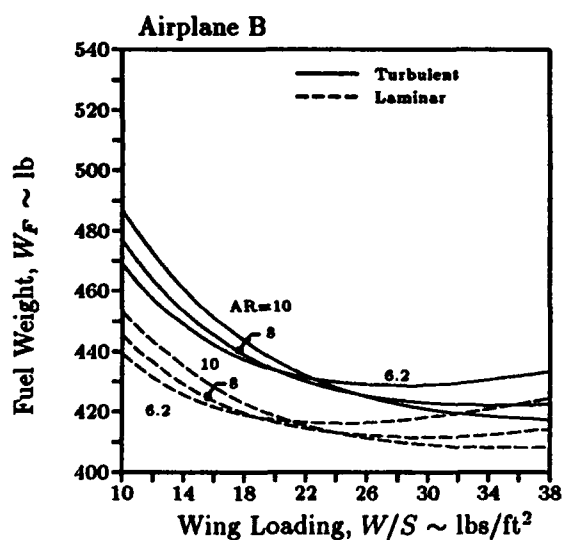
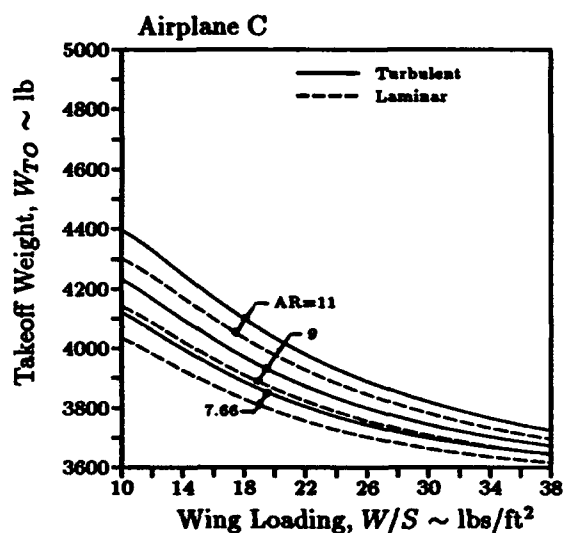
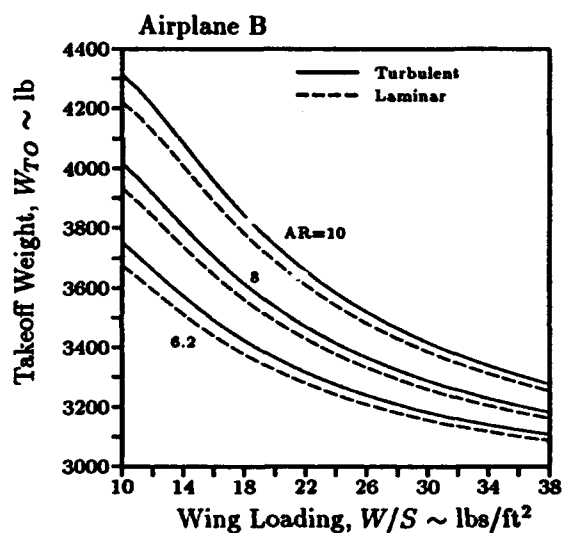
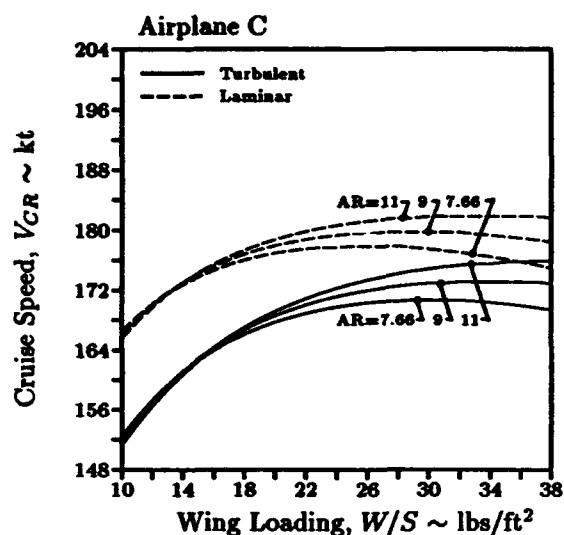
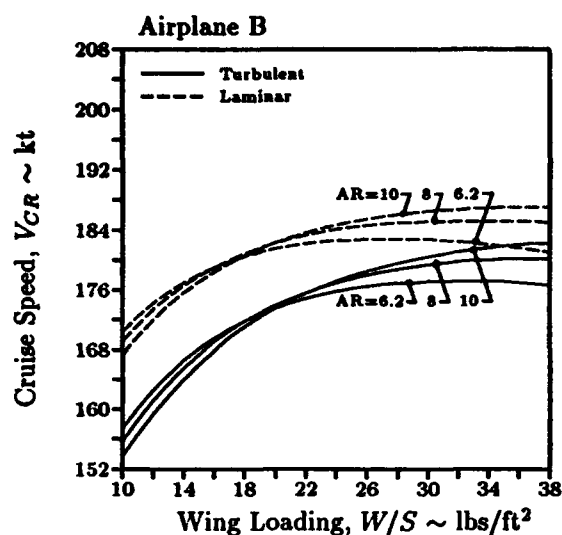


Figure 5: Wing Loading Trade Studies

use of state of the art natural laminar flow airfoils and high lift devices while holding takeoff/landing field length and payload weight fixed. Further improvements are possible through the use of advanced composites, although the associated manufacturing costs may be too great. Improvements in engine and propeller efficiency will also result in reduced takeoff gross weight and fuel required. This method predicts takeoff weight reductions of up to 20% with the use of these technologies.

The method is then augmented with empirical wing weight and drag prediction methods. Trade studies of wing loading and aspect ratio are performed. It is found that cruise speed may be increased by up to 16 knots for fixed cruise power by increasing the wing loading and aspect ratio and using natural laminar flow airfoils. It is predicted that the takeoff weight will not increase and the fuel weight will be reduced by over 5%. The takeoff weight may be reduced if aspect ratio is held constant, resulting in a smaller cruise speed increase. In all cases, the optimum wing loading is found to be somewhat higher than the baseline values, generally above 30 lb/ft².

References

- [1] J. Roskam, *Airplane Design*. Roskam Aviation and Engineering Corporation, Ottawa, Kansas, 1989.
- [2] Cessna Aircraft Company, *Cessna 210N Centurion Information Manual*, 1983.
- [3] L. Loftin Jr., "Subsonic aircraft: Evolution and the matching of size to performance," NASA Reference Publication 1060, 1980.
- [4] D. L. Kohman *et al.*, "A feasibility study for advanced technology integration for general aviation," NASA Contractor Report 159381, 1980.
- [5] M. Lambert, *Jane's All the World's Aircraft, 1990-91*. Jane's Information Group, London, 1990.
- [6] G. S. Manuel and W. A. Doty, "Flight-test investigation of certification requirements for laminar-flow general aviation airplanes," *Journal of Aircraft*, October 1991.
- [7] J. W. Taylor, *Jane's All the World's Aircraft, 1981-82*. Jane's Publishing Company, London, 1981.
- [8] Beech Aircraft Corporation, *Beech F33A Bonanza Pilot's Operating Handbook*, 1976 Rev. 1990.
- [9] I. H. Abbott and A. E. V. Doenhoff, *Theory of Wing Sections*. Dover, 1959.
- [10] D. M. Somers, "Design and experimental results for a natural-laminar-flow airfoil for general aviation applications," NASA Technical Paper 1861, 1981.
- [11] R. J. McGhee, W. D. Beasley, and D. M. Somers, "Low-speed aerodynamic characteristics of a 13-percent-thick airfoil section designed for general aviation applications," NASA TM-X-72697, 1977.
- [12] S. F. Hoerner and H. V. Eorst, *Fluid Dynamic Lift*. Hoerner Fluid Dynamics, P.O. Box 342, Bricktown, NJ 08723, 1975.
- [13] D. P. Raymer, *Aircraft Design: A Conceptual Approach*. American Institute of Aeronautics and Astronautics, 1989.

AIRCRAFT FLIGHT TEST IN AN ACADEMIC ENVIRONMENT

by

**Thomas N. Mouch
Jean M. Fernand
John Valasek
David R. Downing
University of Kansas
Lawrence, Kansas**

**For Presentation to the AIAA/FAA Joint Symposium on General
Aviation Systems at the Hilton Inn-East, Wichita, KS
on March 16-17, 1992**

Aircraft Flight Test in an Academic Environment

Thomas N. Mouch*, Jean M. Fernand*, John Valasek*, David R. Downing†

**University of Kansas
Lawrence, Kansas**

Abstract

A feel for how an aircraft performs and how to determine an aircraft's performance is important to the education of a student aerospace engineer. Through AE 642 "Flight Test Principles and Practice," a graduate-level course in introductory flight test techniques offered at the University of Kansas, the student aerospace engineer learns basic techniques in flight test. The flight test vehicle is a Cessna 172M. Data acquisition tools include the pitot-static and engine performance instruments standard to the test vehicle, a manifold pressure gauge, a stopwatch, a ruler and a fish scale. Through the analysis of data collected in flight by the student flight test engineer, aircraft performance, stability and control can be compared to flight manual data and the requirements of certifying documents.

Introduction

"Flight Test Practices and Principles" is intended for graduate students and qualified undergraduates. As such, students come into the course with a firm knowledge of the atmosphere, internal combustion engines, propeller aerodynamics, rigid body aircraft equations of motion, static performance and static stability and control. Because of the flight test vehicle available, the scope of the course is limited to propeller-driven aircraft with piston engines. (This includes the performance testing of a "homebuilt" aircraft.)

* Graduate Research Assistant, Flight Research Laboratory, University of Kansas Center for Research, Inc., Member AIAA

† Professor and Chair, Aerospace Engineering Department, University of Kansas, Associate Fellow AIAA

The principles of the course apply to any flight test vehicle using proper Flight Test Techniques (FTT).

Course Overview

The course contains 4 main sections: an introduction to flight test and one section for each of three flights, which involves the FTT's used on that flight. The next four sections of this paper will describe each of these sections of the course.

Introduction to Flight Test

The introduction previews, for the engineer familiar with testing on the ground, the basics of testing in an airborne vehicle. This preview includes a heavy emphasis on safety in and around the aircraft. Many of the students are not familiar with an airport and airplane environment. Thus safety must be stressed in the classroom, when discussing the test flight, and on the flightline, while preparing for and performing the test flight.

The introduction also reviews the background knowledge that the students bring to the course. Through this review, the students (1) become familiar with the flight test environment, and (2) develop a common background (as graduate students will have varied backgrounds). The review includes: the standard atmosphere, which makes up the assumed "wind tunnel" for the flight tests; pitot-statics, one of the main ways to collect data; the propulsion system, since knowledge of engine and propeller performance gives one way to determine total drag.

The standard atmosphere is a "defined"¹ profile of temperature, density and pressure in which flight test is very rarely accomplished. This is the standard for all data comparisons. The review includes methods to correct data taken in non-standard conditions to the standard.

The pitot-static system provides the basic information to determine an aircraft's performance during a FTT, but there are errors² involved with this system. Accounting for these errors (e.g., instrument, position and compressibility errors for the airspeed indicator³) improves the accuracy of the data collected. The review includes techniques to account for these errors. Depending on test

vehicle availability, a separate test flight to determine the test vehicle's error is flown or the flight manual data is used, assuming a "standard" test vehicle.

The propulsion system, propeller and engine, complete the performance measurement picture. Given engine power and propeller efficiency charts for the test vehicle, the power required can be calculated for a steady level flight condition. Besides a review of the required charts to determine power required, the review includes correcting actual conditions to standard.

Thus armed with a standard atmosphere in which to conduct the flight test and accurate methods to calculate the test vehicle's performance, the course moves into its next section, the first flight test.

Flight One

This flight emphasizes takeoff performance, cruise performance and turn performance. Figure 1 provides a summary of this flight's profile.

Takeoff performance measurement involves many variables, some of which are hard to determine accurately. This FTT gives the student some feel for the validity of the assumptions usually made in performance classes when predicting takeoff performance. The FTT involves using a known power setting, performing a "flight manual" takeoff, and measuring the time and distance from break release to liftoff speed. Uncertainty is introduced in the accurate measurement of the surface winds at the liftoff point and determining the airspeed, distance and time at which actual liftoff occurs. Thus takeoff performance is determined on each of the three flights and "reduced to standard conditions."¹ Then an average can be made from the three data points. The flight manual charts are verified by comparing the computed takeoff performance to the predicted takeoff performance. How valid were they? Reference 2 recommends computing takeoff distance at " $0.707 V_{to}$ " to represent the "average acceleration" during the takeoff run. Experience in this course bears truth in this recommendation.

Cruise performance measurement involves recording performance data at the test altitude and manifold pressure. This FTT allows the

student to determine the aircraft drag polar (assuming the classic quadratic relationship between C_D and C_L) as well as the airspeed for maximum range and endurance. (This FTT modifies the techniques of References 1 and 4, making manifold pressure the independent variable, due to the fixed pitch propeller of this test vehicle.) Non-standard aircraft weight or non-standard temperature at the test pressure altitude introduces errors in this technique. Both of these deviations would have to be corrected to the standard prior to inclusion in the data set. The airspeeds for maximum range and maximum endurance can be compared to the values given in the flight manual for the given altitude.

The turn performance FTT gives the students a feel for the effect of g-loading and airspeed on turn rate and radius. The test vehicle is stabilized at the desired bank angle and full power. Airspeed and time to turn 360° are recorded. This testing determines the airspeed for optimum sustained turn performance. For those students not familiar with flying, this is the first time they have had to work at 2 g's and the problems involved. Due to FAA restrictions, this is the highest g-loading they can experience but it does provide a feel for what the g-loadings mean.

Flight Two

This flight emphasizes specific excess power, climb and descent performance⁴. Figure 2 provides a summary of this flight's profile. If flight time permits, a demonstration of test vehicle stall characteristics is included.

Specific excess power is determined by starting an acceleration run at minimum flying airspeed with full power and concluding the run at maximum airspeed at that power setting while holding constant altitude. (Remember, P_s (weight specific excess power) = $\frac{dh}{dt} + \frac{V}{g} \frac{dV}{dt}$,

where "h" is altitude, "V" is velocity, "g" is the gravitational constant, and "t" is time¹.) This is a fairly quick test. Repeatability is easily demonstrated. These tests determine the best climb speed at a given altitude. This climb speed can be compared to the flight manual climb speed, and the results of the following climb performance tests.

Climb and descent performance involves constant airspeed climbs and descents through the test altitude. This test demonstrates to the student the different rates at which the test vehicle climbs or descends with varying airspeed. This test determines the airspeeds for the best rate and angle of climb and the airspeeds for power-on best glide and minimum sink. Depending on the test matrix (number of airspeeds evaluated at the test altitude), this FTT can be time consuming. This is usually time well spent, as the quality of the data is usually good.

For the student not familiar with stall characteristics, this demonstration brings everything talked about in the classroom together. The test involves smoothly slowing the test vehicle approaching the stall. Demonstrations approaching the stall include: control effectiveness, stall warning horn, buffet and g-break. The stall is not violent, but the wing definitely is not providing lift. Hysteresis during flow reattachment is evident.

Flight Three

This flight emphasizes longitudinal static stability, maneuvering flight and lateral-directional stability and control⁴. Figure 3 provides a summary of this flight's profile. This flight is the most technically demanding of the pilot. He has to make many of the measurements while flying the maneuver. As two different center of gravity (C.G.) locations are required to analyze the data, this flight can be broken into two short flights with the position of the students changing the C.G. location. This flight uses the yardstick (or a flexible tape measure) to determine yoke and rudder pedal deflections and fish scale to measure forces required to position the yoke. If flight time permits, the flight profile can include demonstrations of the phugoid, Dutch roll, and spiral dynamics.

The longitudinal static stability FTT requires determining the yoke deflection and control force required to effect a certain speed change ($\pm 15\%$ of V_{trim}) at a given C.G. location, trim condition and throttle position. This test emphasizes the difference between stick fixed and stick free neutral points. The pilot brings about the speed change by flying the aircraft using the fish scale and measures the yoke deflection with the yardstick (or a tailor's cloth tape measure). The yoke deflection leads to the calculation of the stick fixed neutral

point and the force required to cause the deflection leads to calculation of the stick free neutral point.¹ The effects of the friction band (How much force is required to cause the yoke to move?) and breakout forces (How much force is required to cause the aircraft to move?) become evident in the analysis of the data.

The maneuvering flight FTT requires the measurement of yoke deflection and control force while maintaining a constant airspeed and g-loading. This test emphasizes the difference between stick fixed and stick free maneuver points plus the relationship between the neutral point and its respective maneuver point. To maintain the constant airspeed while at a g-loading greater than one the aircraft will have to descend. The FAA restriction is 60° of bank that gives a g-loading of two. The yoke deflection leads to the calculation of the stick fixed maneuver point and the force required to cause the deflection leads to calculation of the stick free maneuver point.¹

The lateral-directional static stability test involves testing at only one C.G. location. This is a fairly quick test in which the student becomes familiar with the certifying documents. A steady straight sideslip is flown to collect the data¹--rudder deflection and force, aileron deflection and force, elevator force, bank and sideslip angle. Throughout these tests, the test vehicle is in a "cross-controlled" situation where the roll control is deflected in one direction and the yaw control opposed. Each of the measured values (except bank angle) is plotted versus sideslip angle plus the aileron deflection and force is plotted versus bank angle. Many of the values have to be estimated by the pilot (e.g., rudder force and yoke roll deflection). Specific modifications to the test vehicle to measure these values seem impractical for a limited increase in accuracy and might lead to certification problems. The certifying regulations only require linearity of these plots in a certain range of sideslip angle and the proper control motion for the control deflection.¹

For the student not familiar with an aircraft's dynamic characteristics, the phugoid, Dutch roll and spiral demonstrations quickly bring home the points from their dynamics class. The phugoid demonstration starts with the test vehicle established in straight and level, trimmed. It is disturbed in pitch. The student can observe the oscillations. The Dutch roll demonstration takes a little more input from the pilot. He needs to alternate left and right

rudder at the approximate frequency of the Dutch roll to get the aircraft to show a Dutch roll response. From these inputs, the student can see the combined roll and yaw response by observing the "egg" or "oval" shape drawn by the wingtip in relation to the horizon. The spiral demonstration involves establishing a 20 ° bank then release all controls. The student observes the motion of the test vehicle, noting whether the bank angle increases or decreases. Thus, the student can determine if the spiral is stable or not.

Summary

Flight testing brings a new perspective to an engineering education. The student becomes part of the experiment. He feels the forces he might design an aircraft to handle and can better imagine the performance capabilities of an aircraft. The flight tests present the basics of an aerospace engineering education for observation and analysis. This experimentation makes the certifying regulations more than just numbers to be met. Overall, the course provides motivation for the student to better understand the motions of an aircraft.

References

1. Payne, J.P., Flight Test Handbook, 3rd edition, JP Aviation, USAFA, CO 80840-0003, 1990.
2. Smith, H. C., Introduction to Aircraft Flight Test Engineering, IAP, Inc., Riverton, WY, 1981.
3. Lan, C.E. and Roskam, J., Airplane Aerodynamics and Performance, Roskam Aviation and Engineering Corp., Ottawa, Kansas, 1980.
4. Anon., Aero Engr 456 T-41 Test Plan, United States Air Force Academy, CO 80840-5701, Spring 1991.
5. Neate, R.E., Performance and Stability Flight Testing, 3rd Revision, Embry-Riddle Aeronautical University, Daytona Beach, FL, August, 1985.

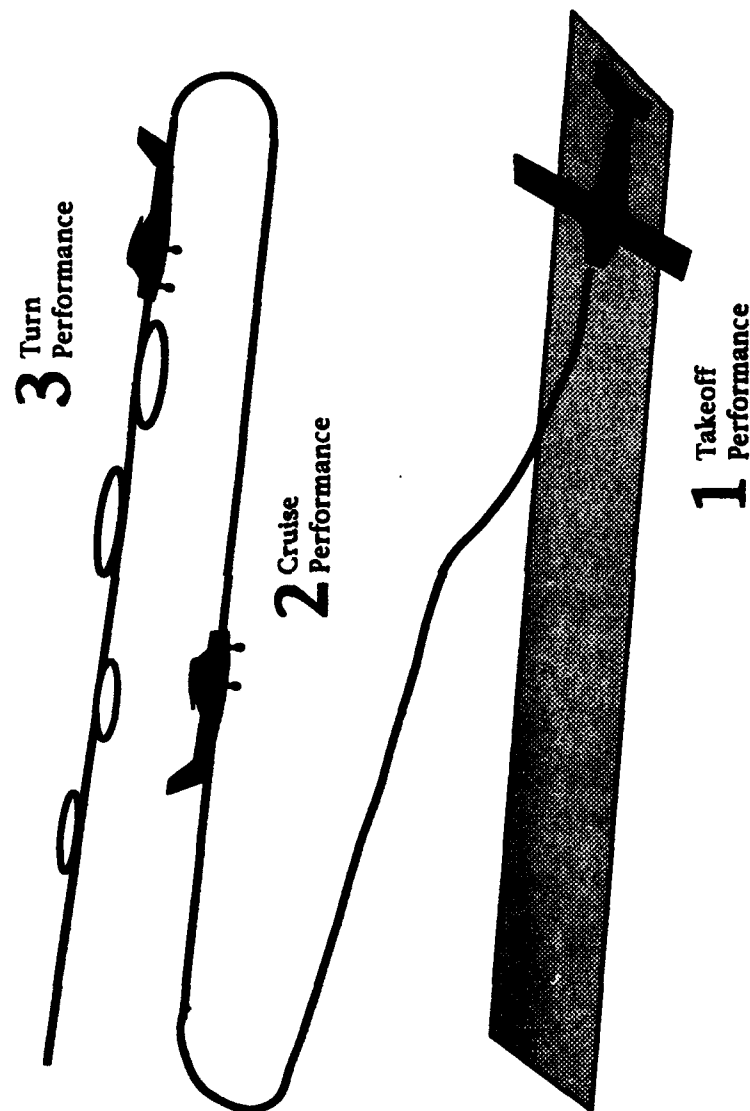


Figure 1. Flight 1 Profile

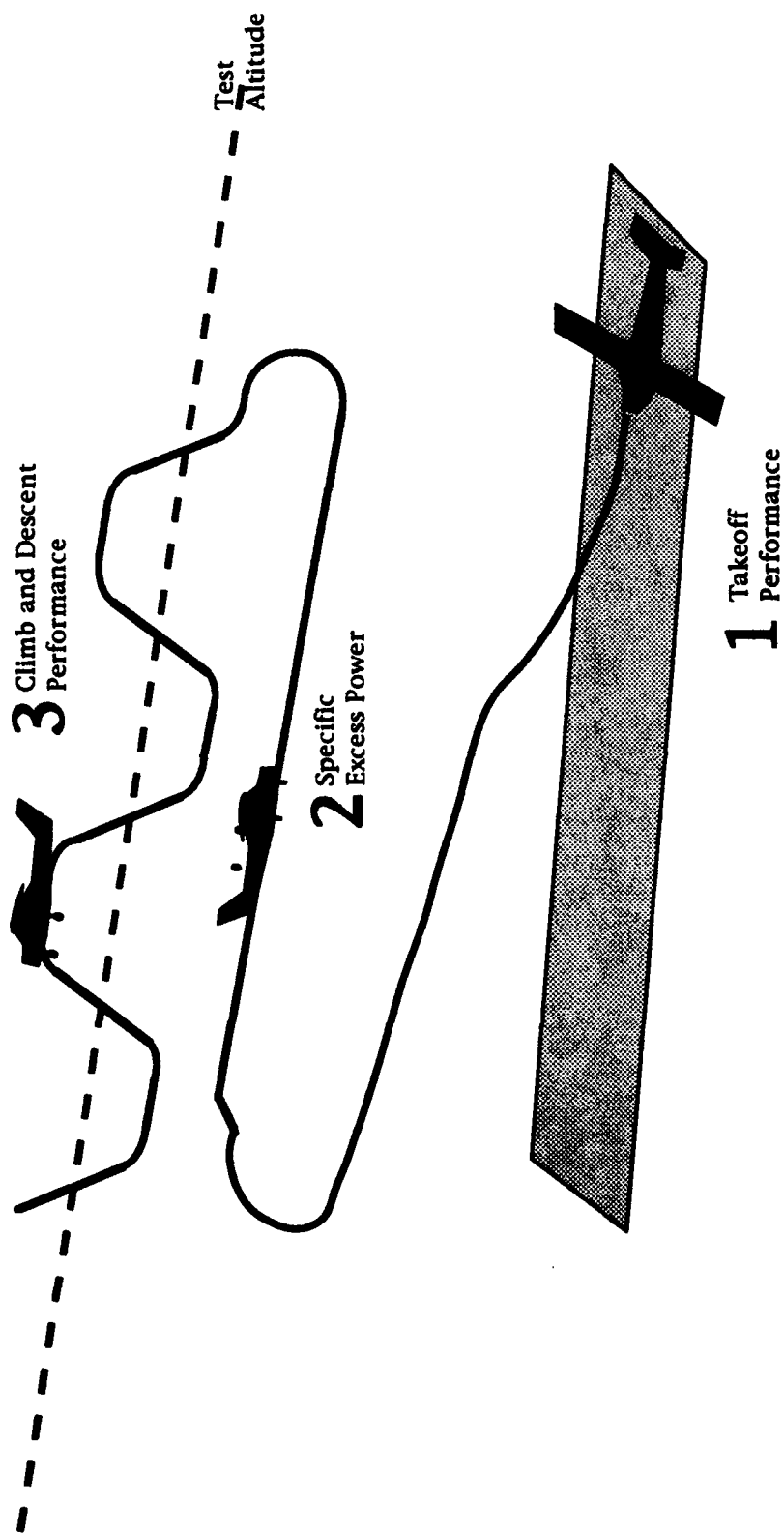


Figure 2. Flight 2 Profile

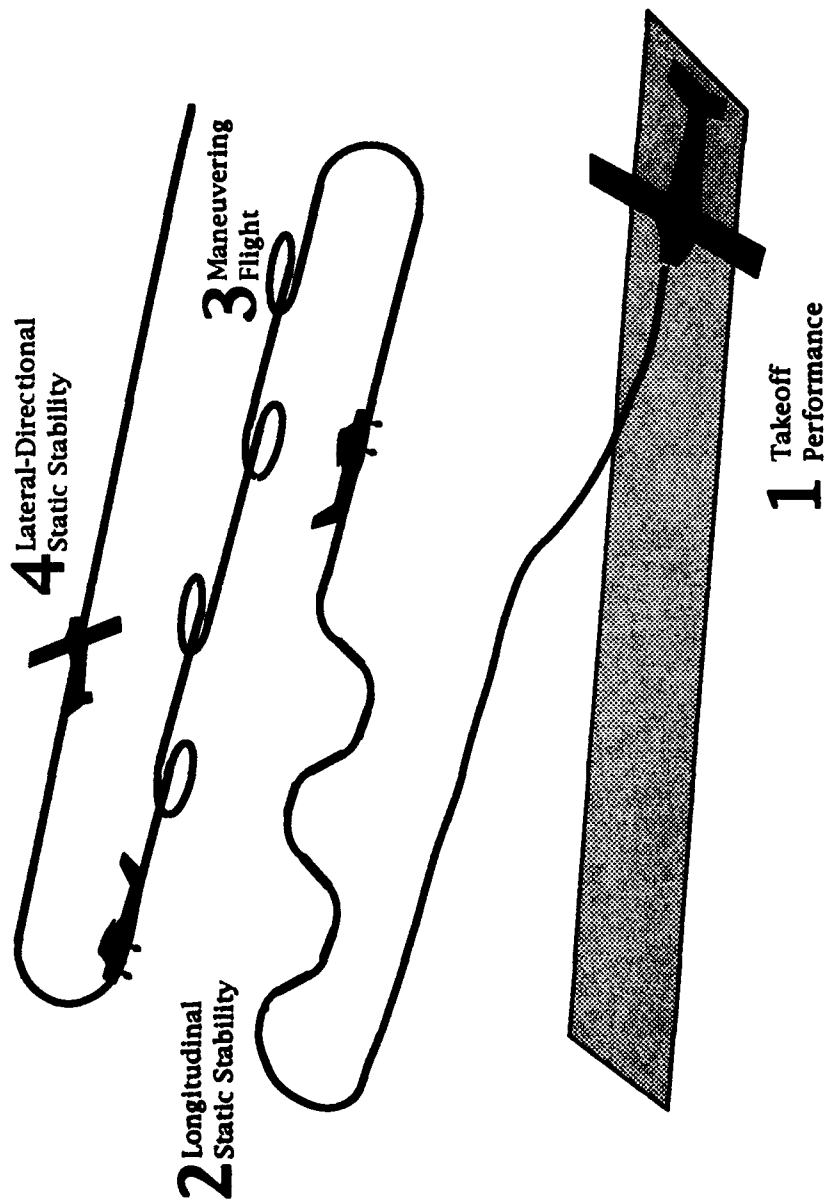


Figure 3. Flight 3 Profile

**RESULTS OF A PARAMETER IDENTIFICATION FLIGHT TEST
PROGRAM FOR GENERAL AVIATION AIRCRAFT**

by

**John Valasek
Jean M. Fernand
Thomas N. Mouch
David R. Downing
University of Kansas
Lawrence, Kansas**

**For Presentation to the AIAA/FAA Joint Symposium on General
Aviation Systems at the Hilton Inn-East, Wichita, KS
on March 16-17, 1992**

RESULTS OF A PARAMETER IDENTIFICATION FLIGHT TEST PROGRAM FOR GENERAL AVIATION AIRCRAFT

by

John Valasek*, Jean Michel Fernand*, Thomas N. Mouch*, and David R. Downing†
University of Kansas, Lawrence, Kansas

Second Joint Symposium on General Aviation Systems, Wichita, Kansas, March 16-17, 1992

Abstract

A limited parameter identification flight test program is conducted on a prototype Cessna TR 182 RG Skylane aircraft for the purpose of estimating non-dimensional stability and control derivatives. The test plan is carefully designed to be economical yet thorough in order to extract useful results from a minimum number of data points and flights. Test points consist of four different airspeeds, each evaluated at two altitudes, and for two aircraft configurations: dirty (gear down, flaps down) and clean (cruise). Longitudinal and lateral/directional maneuvers designed to excite the vehicle modes are repeated a minimum of eight times each, at each test point, for a total of 70 data points collected during the course of two flights. Flight data consisting of time histories of aircraft rates, accelerations, attitudes, pressures, and temperatures are recorded during flight by an onboard digital data acquisition system. Scatter plots of estimated non-dimensional stability and control derivatives are generated by a modified maximum likelihood estimate (MMLE) computer program. Estimated values of the non-dimensional stability and control derivatives are compared to corresponding published values for a similar aircraft. Differences between the clean and dirty configurations is quantified by differences in the estimated non-dimensional stability and control derivatives for each configuration. Results demonstrate that compared to a clean cruise configuration, extending the flaps and landing gear on the test aircraft reduces static lateral stability approximately 70%, while static weathercock stability increases approximately 50%. Rudder effectiveness increases approximately 70%, but cross coupling of the lateral and directional axes due to deflection of the rudder and ailerons is reduced. No significant change in static longitudinal stability is observed. Values of non-dimensional stability derivatives obtained from this testing compared well with published values for the similar aircraft. It is concluded that the limited scope and methods applied to this test program are sufficient for obtaining useful results for most general aviation aircraft.

* Graduate Research Assistant, Flight Research Laboratory,
University of Kansas Center for Research Inc. Member AIAA.

† Professor and Chair, Department of Aerospace Engineering.
Associate Fellow AIAA.

Nomenclature

$C_{l\beta}$	variation in rolling moment coefficient due to sideslip
$C_{l\delta_a}$	variation in rolling moment coefficient due to aileron deflection
$C_{l\delta_r}$	variation in rolling moment coefficient due to rudder deflection
C_{lp}	variation in rolling moment coefficient due to roll rate
C_{lr}	variation in rolling moment coefficient due to yaw rate
$C_{m\alpha}$	variation in pitching moment coefficient due to angle of attack
$C_{m\delta_e}$	variation in pitching moment coefficient due to elevator deflection
C_{mq}	variation in pitching moment coefficient due to pitch rate
$C_{n\beta}$	variation in yawing moment coefficient due to sideslip
$C_{n\delta_a}$	variation in yawing moment coefficient due to aileron deflection
$C_{n\delta_r}$	variation in yawing moment coefficient due to rudder deflection
C_{np}	variation in yawing moment coefficient due to roll rate
C_{nr}	variation in yawing moment coefficient due to yaw rate
$C_{y\beta}$	variation in sideforce coefficient due to sideslip
$C_{y\delta_a}$	variation in sideforce coefficient due to aileron deflection
$C_{y\delta_r}$	variation in sideforce coefficient due to rudder deflection
C_{yp}	variation in sideforce coefficient due to roll rate
C_{yr}	variation in sideforce coefficient due to yaw rate
CLB	variation in rolling moment coefficient due to sideslip
CMA	variation in pitching moment coefficient due to angle of attack
CMQ	variation in pitching moment coefficient due to pitch rate
CNB	variation in yawing moment coefficient due to sideslip
DAS	Data Acquisition System
FTE	Flight Test Engineer
FTT	Flight Test Technique
KEAS	equivalent airspeed (knots)
KIAS	indicated airspeed (knots)
KSR	Kohlman Systems Research, Inc.
KTAS	true airspeed (knots)
MMLE	Modified Maximum Likelihood Estimate

Introduction

Aircraft flight testing can be a costly and time consuming endeavor. By devising a test matrix with as much overlap as possible between competing tasks, reductions in the number of test flights and costs can be realized. All test instrumentation and data reduction services were on loan to the authors for only a short period of time, necessitating careful planning for maximum utilization of resources.

The objective of this experiment is to obtain non-dimensional stability and control derivatives for a general aviation aircraft using parameter identification techniques. To highlight variations in stability and control characteristics for the same aircraft in different configurations, flight data is obtained for both "clean" and "dirty" configurations. The "clean" configuration is defined as a landing gear retracted, flaps retracted configuration. The "dirty" configuration is defined as a landing gear extended, flaps extended configuration. Flight data consisting of aircraft accelerations, rates, attitudes, temperatures, and pressures are measured and recorded onboard the test aircraft using a digital DAS operated from the cabin by the flight test engineer. The raw flight data is then reduced on the ground post-flight and used to generate time histories of the aircraft states. These time histories are then used by an MMLE computer program (REF. 1) to obtain estimates of the non-dimensional stability and control derivatives. An estimated value for each of the desired non-dimensional stability and control derivatives is generated for each test point. A scatter plot for each non-dimensional derivative is constructed, from which the final estimated value can be determined by any desired statistical or graphical method. The values thus obtained are compared to published values for a similar type of aircraft (REF. 2). Estimates of the following non-dimensional stability and control derivatives for the clean configuration are used for comparison.

$$\begin{array}{c} C_{m_{\alpha}}, C_{m_q}, C_{m_{\delta_e}} \\ C_{l_{\beta}}, C_{l_p}, C_{l_r}, C_{l_{\delta_a}}, C_{l_{\delta_r}} \\ C_{n_{\beta}}, C_{n_p}, C_{n_r}, C_{n_{\delta_a}}, C_{n_{\delta_r}} \\ C_{y_{\beta}}, C_{y_{\delta_a}}, C_{y_{\delta_r}} \end{array}$$

Modified Maximum Likelihood Estimation

The MMLE computer program seeks to replicate recorded flight test time histories of output variables by varying the coefficients in a linearized model of the aircraft. The math model is linearized about the aircraft trim condition in steady level flight. The equations are decoupled into longitudinal and lateral-directional sets, and the coefficients are assumed to be constant but unknown.

The MMLE uses a modified Newton-Raphson numerical method to find the minimum of a cost function, J . J is the integral weighted sum of the squared error

between the actual flight test time history and a predicted time history using the actual control deflection time histories as inputs. Starting (a priori) values for the coefficients are provided from other external sources (e.g., analytical predictions, wind tunnel data, previous flight test results) to help stabilize the numerical method.

The weighting matrix, Q , is varied to reflect the engineer's confidence in the quality of the flight test data. As an example, the rolling moment due to aileron deflection would be difficult to estimate if no significant aileron deflections occurred in the time history. If the time history consisted of a rudder doublet and the subsequent transient response, then MMLE could be instructed not to estimate certain coefficients.

Experience with this program indicates that a high quality time history is characterized by all dynamic modes being excited, but with magnitudes of the motions not exceeding the linear assumptions intrinsic to the linear model (REF. 3). Also, disturbances and measurement noise must be kept to a minimum since they are not modeled.

Pilot Flight Test Technique

The basis of the FTT for performing parameter identification testing is the KSR Triplet. The KSR Triplet is similar to the standard doublet input, but differs in that constant magnitude portions of the input are not of equal duration but are instead in the ratio "2-3-1". The KSR Triplet has the same effect as a doublet, except that (ideally) more than just one vehicle mode is excited. The magnitudes used are selected by the pilot, and should be symmetrical about the trim point.

The KSR Triplet is executed by deflecting the pilot control and counting to two, followed immediately by a reversal of the input and a count to three, followed immediately by a return to the initial deflection and a count of one, then returning the control to neutral or trim (Figure 1). The control remains in the neutral or trim position until aircraft motions settle out to some satisfactory level. The test inputs should be practiced by varying magnitudes of deflections and durations of each constant portion until a combination that sufficiently excites the vehicle modes but remains in the linear range is determined. The desired input is the *smallest* input which excites the vehicle modes but is not so small as to be imperceptible to the DAS. A more responsive aircraft requires a quicker count, while a slower responding or larger aircraft requires a slower count; the deflection should be sharp. When exciting the lateral-directional vehicle modes, the first control input can be either the aileron or rudder. This is followed in the next input portion by the remaining unused lateral-directional control (aileron or rudder). Figure 2 demonstrates this technique. Note that one control can be used to keep the aircraft flying "straight", i.e. if the aileron input produces a large bank angle, use the rudder input to correct this "residual".

Experiment Design

In order to enhance the validity of the estimates it is desirable to obtain as many data points as is practical (REF. 4). In addition, acquiring data points at different

combinations of altitude and airspeed (dynamic pressures) will indicate trends of the non-dimensional derivatives if any exist. The instrumentation, data reduction, and manpower on loan from KSR was available for a total period of seven working days. Since the time constraints ensured that only two test flights could be accomplished, the test matrix is designed to obtain as much useful data as possible in each flight.

The test matrix consists of three airspeeds (75, 90, and 120 MPH indicated), two altitudes (5,000 and 10,000 feet pressure altitude), and two aircraft configurations (clean and dirty). Two test flights were flown in order to collect the raw flight data, with both longitudinal and lateral-directional data collection runs performed during each flight. Each test point is repeated eight times. Rather than having separate flights for longitudinal and lateral-directional data points, this policy ensured that data points for both types are obtained in the unforeseen event that only one flight is conducted. The flight test matrix for the first and second flights is indicated in Tables 1 and 2. Detailed descriptions of the test articles and equipment required to perform the experiment are contained in Reference 5.

As shown in Figure 3, the integrated flight test system used for the experiment is comprised of a microprocessor based data acquisition system (DAS), and a data analysis system. Special software prepares the instrument calibrations, transfers the raw flight data from the airborne system, converts digital data to engineering units, and plots time history information. This software is integrated into a single flight test data processing system capable of producing a data base which is corrected for flight conditions. Angle of attack and sideslip angle are not measured.

Figure 4 shows the acquisition computer, auxiliary tape drive, and display for remote operation as installed in the test aircraft. The view is from the FTE station, looking aft. The FTE operates and controls all DAS functions in flight by turning in his seat as required.

Results

The time histories of recorded flight data for run number 019 of test flight II, a typical longitudinal maneuver, are shown in Figure 5. The pilot generated pitch command is excellent and generates a desirable pitch attitude response. A small but undesirable roll rate is present, but is small enough to not significantly affect the results.

Figure 6 shows the matching of the time histories for this same run by the MMLE program. The predicted values shown in the time histories are determined using the estimated non-dimensional derivatives from the MMLE program. The tabular data in Figure 6 shows both the elements of the weighting matrix Q , and the values of the estimated non-dimensional derivatives for each of the 11 iterations required (for this particular case) to obtain a solution. Note the large magnitude of the axial acceleration element in the Q matrix as compared to the other elements. A large magnitude for this element instructs the MMLE program to consider the data for this parameter as being essentially very accurate; as a result the MMLE program will rely more heavily upon the values of this parameter than the others when making estimates. The weight on angle

of attack in the Q matrix is zero since angle of attack was not measured during flight.

A typical lateral-directional case, run number 014 of flight II, is shown in Figure 7. Note that the pilot generated KSR Triplet inputs are effective in perturbing both the roll rate and yaw rate and thus the Dutch roll mode. The time history of pitch rate shows that a small amount of coupling is present. Figure 8 contains the time history matches of the flight data and MMLE predicted values. The agreement is excellent, and representative of the majority of test cases. The tabular data demonstrates convergence to a solution in six iterations. The large magnitude of the lateral acceleration element in the Q matrix is required since sideslip angle was not measured and is not available for use in estimating the derivatives.

Figure 9 shows typical estimated longitudinal non-dimensional derivative scatter plots for the clean configuration. The value for each estimated derivative is obtained graphically by interpreting trends in the data visually (if any occur) and fitting a straight line. For most derivatives, such as $C_{m_{\dot{q}}}$, little to no variation with respect to airspeed is observed, and so a line with zero slope is fitted. Others, such as $C_{m_{\dot{\alpha}}}$, are fitted with a non-zero slope line at the engineer's discretion. The airspeed at which the value of this derivative is read is 130 KTAS. This is the airspeed at which the values of the non-dimensional derivatives reported in Reference 2 were obtained. In general the data for each longitudinal non-dimensional derivative does not contain much scatter except for the $C_{m_{\dot{\alpha}}}$ plot. This is probably due to the difficulty in estimating an angle of attack derivative when angle of attack data is not available.

The data for the longitudinal non-dimensional derivatives of the dirty configuration is obtained at approximately 80 KTAS only, since the 130 KTAS of the clean configuration is above the 140 KIAS maximum airspeed for flight with flap extensions of greater than ten degrees. The fewer number of data points and the inherent scatter makes fitting a straight line to the data difficult. Although there is some scatter in the $C_{m_{\dot{\alpha}}}$ estimate for the clean configuration at 80 KTAS, there is little scatter in the data for the dirty configuration at this airspeed, and the estimate is basically invariant with airspeed. However, better estimates of the non-dimensional derivatives might be obtained by applying statistical methods to the data.

Figure 10 shows typical estimated lateral-directional non-dimensional derivative scatter plots for the clean configuration. Most of the lateral-directional derivatives such as $C_{l_{\dot{\beta}}}$ are basically invariant with respect to airspeed. However, several of the lateral-directional derivatives such as $C_{n_{\dot{\beta}}}$ are not. Although the variation with respect to airspeed is generally small, definite trends exist. Lateral-directional derivative scatter plots which are fitted with nonzero slopes are evaluated at an airspeed of 130 KTAS. All of the lateral-directional derivative data points tend to be tightly grouped, with the exception of the yawing moment derivatives (C_{n_r} , $C_{n_{\dot{\beta}}}$, $C_{n_{\dot{\alpha}}}$). This is due to the difficulty in estimating these derivatives without sideslip angle measurements. This situation is completely analogous to that of the longitudinal pitching moment derivatives, which are also loosely grouped because of the lack of angle of attack measurements. All of the data points for the dirty configuration lateral-directional derivatives are obtained at an airspeed of approximately 80 KTAS. All of these scatter plots are fitted with zero slope lines since the airspeed for these data sets is essentially constant.

A comparison of the estimated and published values of the non-dimensional clean configuration derivatives is presented in Table 3. The flight condition is 120 KIAS at 5,000 feet pressure altitude. Although the similar aircraft of Reference 2 has fixed landing gear, the clean configuration of the test aircraft is used for comparison. This is because the flight test pilots determined before testing that flying with the landing gear extended had a negligible effect on flying qualities and airspeed for this particular aircraft. However, flying with the flaps extended noticeably effects the flying qualities and airspeed. Comparing the two sets of data, the agreement is in general excellent even though the payload, mass distribution, and landing gear position of the test aircraft is different than the similar aircraft of Reference 2. All of the estimated derivatives are of the correct sign, and of approximately the correct magnitude. Note that C_{y_p} and C_{y_r} are not presented since the version of the MMLE program used for this analysis does not estimate them.

The estimated non-dimensional derivatives for the dirty configuration are displayed in Table 4. The flight condition is 75 KIAS at an altitude of 5,000 feet pressure altitude. Reference 2 does not contain data for the dirty configuration (flaps extended), so no direct comparisons are possible. However, comparing the estimated dirty derivatives with the estimated clean derivatives in Table 3, it is seen that significant (defined here as greater than 25%) differences exist:

$C_{l\beta}$	reduced	72%
$C_{l\delta_r}$	reduced	68%
$C_{n\delta_r}$	increased	50%
$C_{n\beta}$	increased	48%
C_{n_p}	increased	43%
C_{l_r}	increased	40%
$C_{n\delta_a}$	reduced	32%

The greatest difference occurs $C_{l\beta}$, in indicating that the static lateral stability ($C_{l\beta} < 0$) of the test aircraft is reduced by extending the flaps and landing gear. The effect due to the reduction in speed is not as great as that due to the configuration changes. The control effectiveness of the rudder is increased, as is the static weathercock stability ($C_{n\beta} > 0$). Although C_{n_p} and C_{l_r} increase, they do not strongly influence the static stability characteristics of the aircraft. Additionally, the aileron is less effective in generating yawing moments. The only noteworthy result in the pitch axis is that there is no significant change in static longitudinal stability ($C_{m\alpha}$).

In summary, as a result of extending the flaps and landing gear, the static lateral stability is seen to decrease, while the static weathercock stability increases. Although the rudder effectiveness is increased, the cross coupling between the lateral and directional axes due to aileron and rudder deflections is reduced significantly. Static longitudinal stability remains essentially unchanged. In no instance during any of the test flights was safety compromised due to pilot FTT or aircraft configuration changes.

Conclusions

This paper presents the results of a limited parameter identification flight test program for a prototype Cessna TR 182 RG aircraft. The flight data was collected and recorded during two flights using an onboard digital data acquisition system. Parameter identification was performed post flight using a Modified Maximum Likelihood Estimate program. Values of the estimated non-dimensional stability and control derivatives to be reported were selected from scatter plots, and compared with published data for a similar aircraft. Based upon the results, the following conclusions are made:

1. The scope and methods for this investigation are adequate for obtaining reasonable estimates of non-dimensional stability and control derivatives of general aviation aircraft.
2. Compared to the clean configuration, extension of the flaps and landing gear produced the following effects on the static stability and control characteristics of the Cessna TR 182:
 - a. Static lateral stability is reduced approximately 70%, while static weathercock stability increases approximately 50%.
 - b. Rudder effectiveness increases approximately 70%, but cross coupling due to deflection of the rudder and ailerons is reduced.
 - c. Cross coupling of the lateral and directional axes due to perturbations in roll rate and yaw rate increases.
 - d. There is no significant change in static longitudinal stability.

These effects are quantified by differences between the estimated non-dimensional stability and control derivatives for the clean and dirty configurations.

Acknowledgement

The authors gratefully appreciate the instrumentation, equipment, manpower, and expertise provided by Kohlman Systems Research Inc., without whose assistance this investigation would not have been possible.

References

1. Maine, Richard E., and Iliff, K.W., "User's Manual for MMLE3, a General FORTRAN Program for Maximum Likelihood Parameter Estimation," NASA Technical Paper 1563, 1980.
2. Roskam, Jan, Airplane Flight Dynamics and Automatic Flight Controls, Part I, Roskam Aviation and Engineering Corporation, Ottawa, Kansas, 1979.
3. Fernand, Jean Michel, "Determination of the Stability and Control Derivatives for the Variable-Response Research Aircraft Using a Modified Maximum Likelihood Estimator," MS Thesis, Mechanical and Aerospace Engineering Department, Princeton University, 1978.
4. Payne, James P., Flight Test Handbook, Third Edition, JP Aviation, USAF Academy, Colorado Springs, Colorado, 1990.
5. Valasek, John, Fernand, J.M., Mouch T.N., and Downing, D.R., "Parameter Identification Flight Test for a General Aviation Aircraft," KU-FRL-831-5, University of Kansas Flight Research Laboratory, October 1991.
6. Brahney, James H., "Simplifying Flight Test," SAE Aerospace Engineering, January 1988.

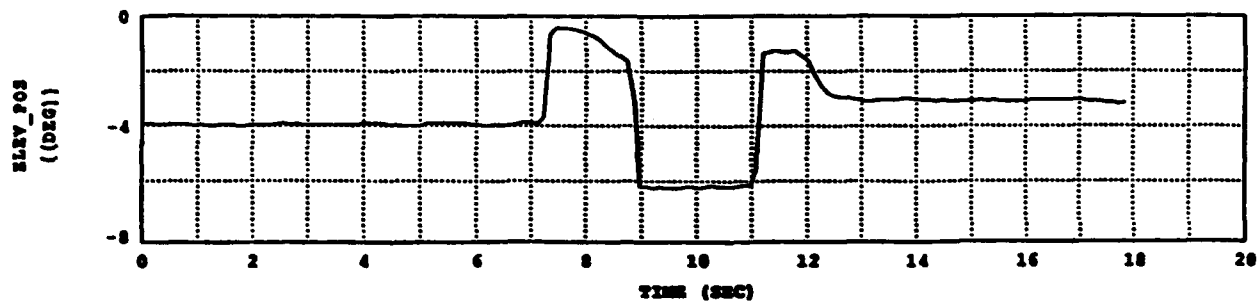


Figure 1 Typical KSR Triplet Sequence For Longitudinal Excitations

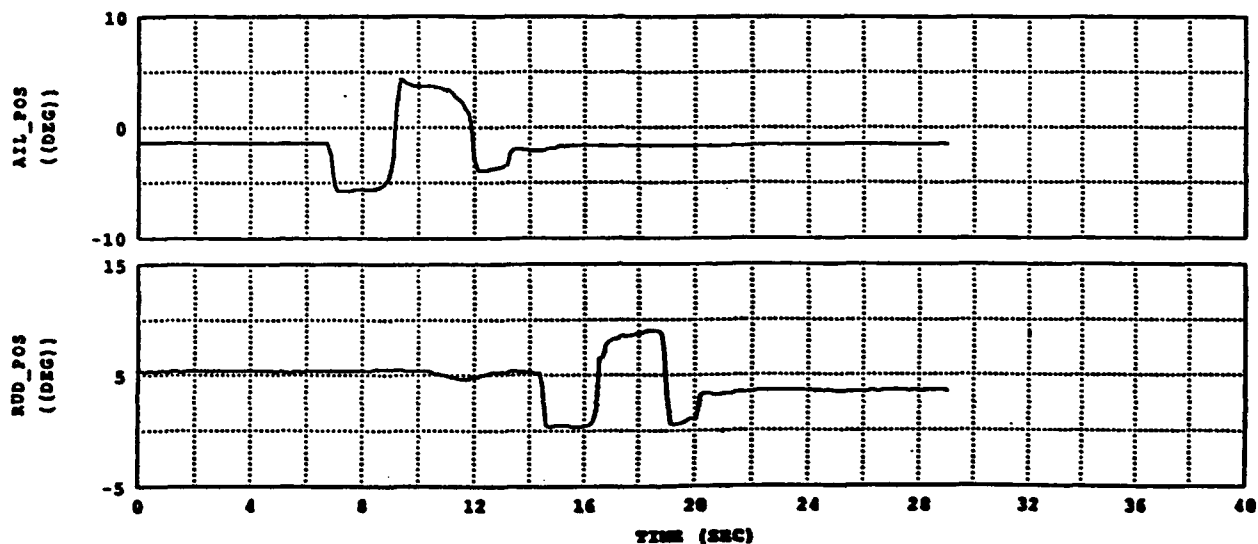


Figure 2 Typical KSR Triplet Sequence For Lateral-Directional Excitations

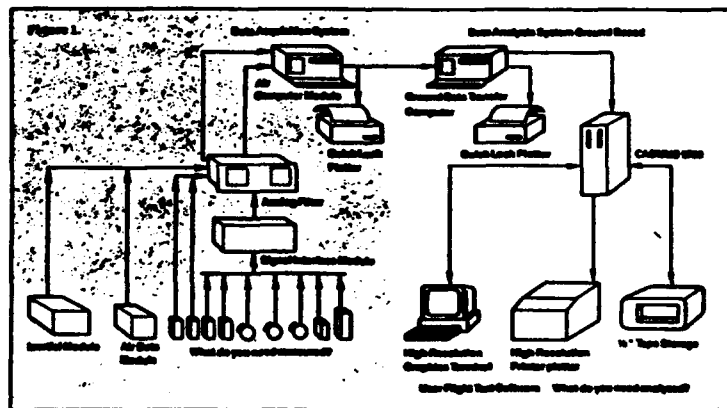


Figure 3 Layout Of Integrated Flight Test System (REF. 6)



Figure 4 Installation Of Acquisition Computer In The Test Aircraft

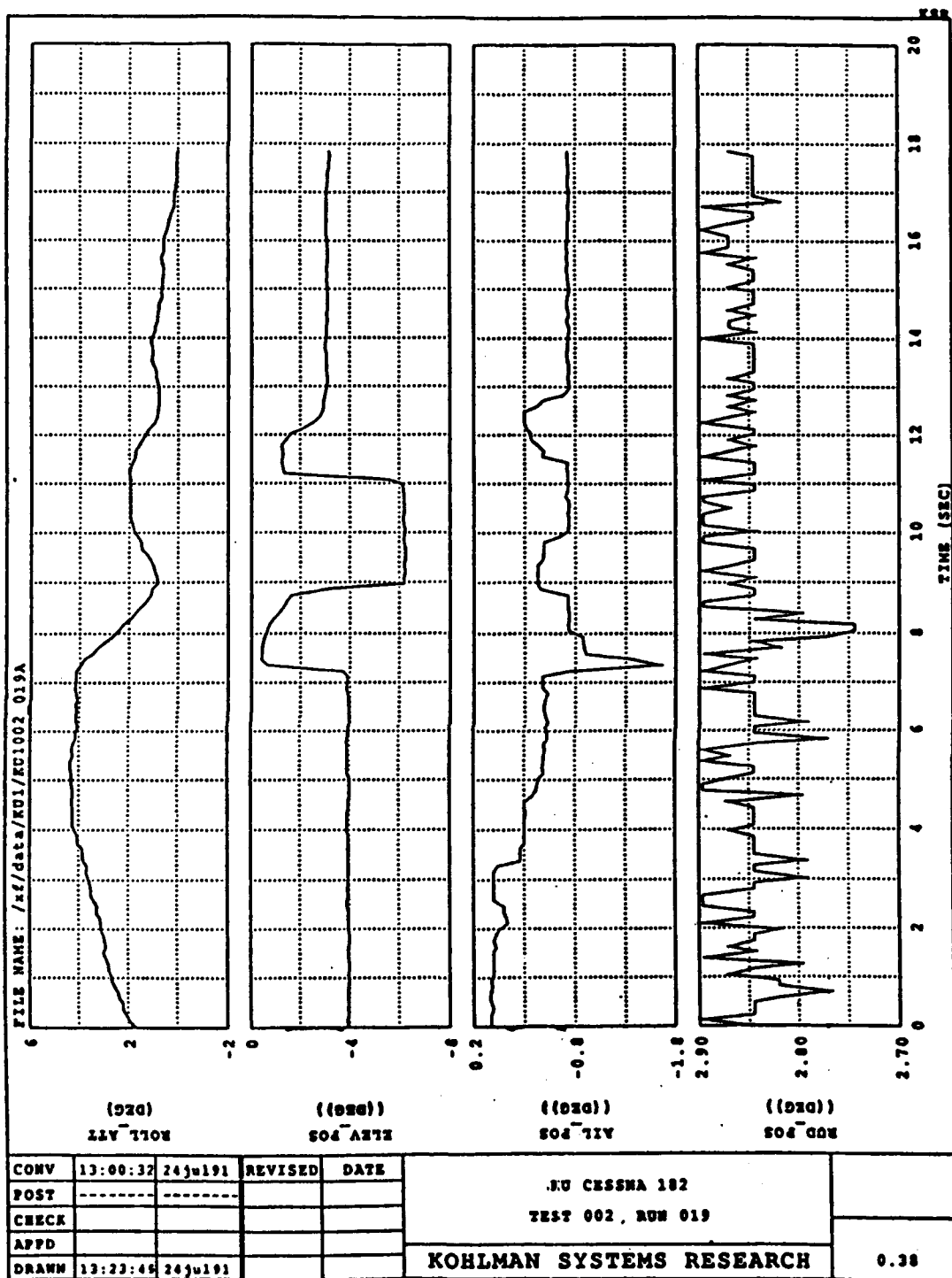


Figure 5 Typical Time Histories of Flight Data, Longitudinal Maneuver

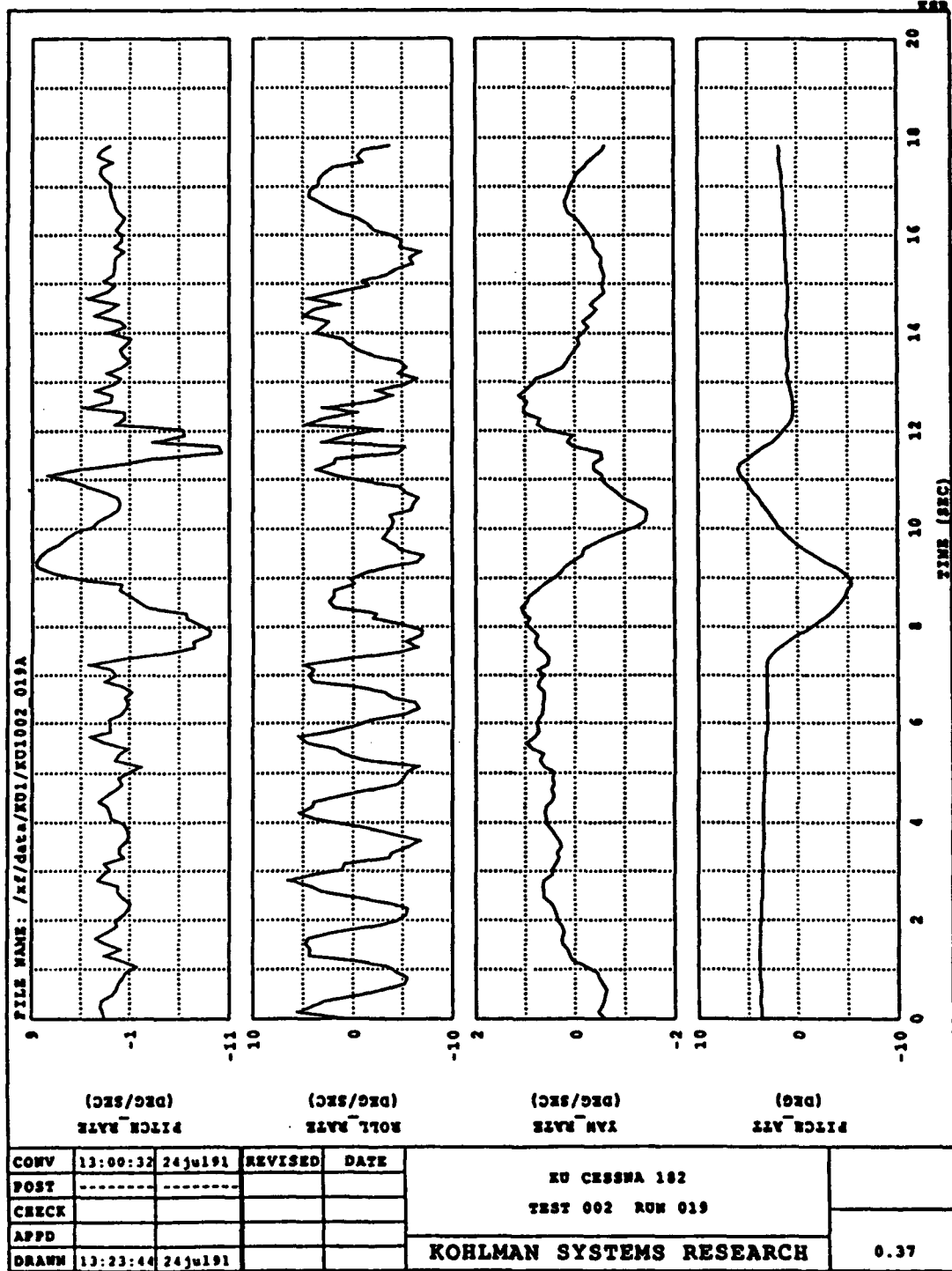


Figure 5 Continued

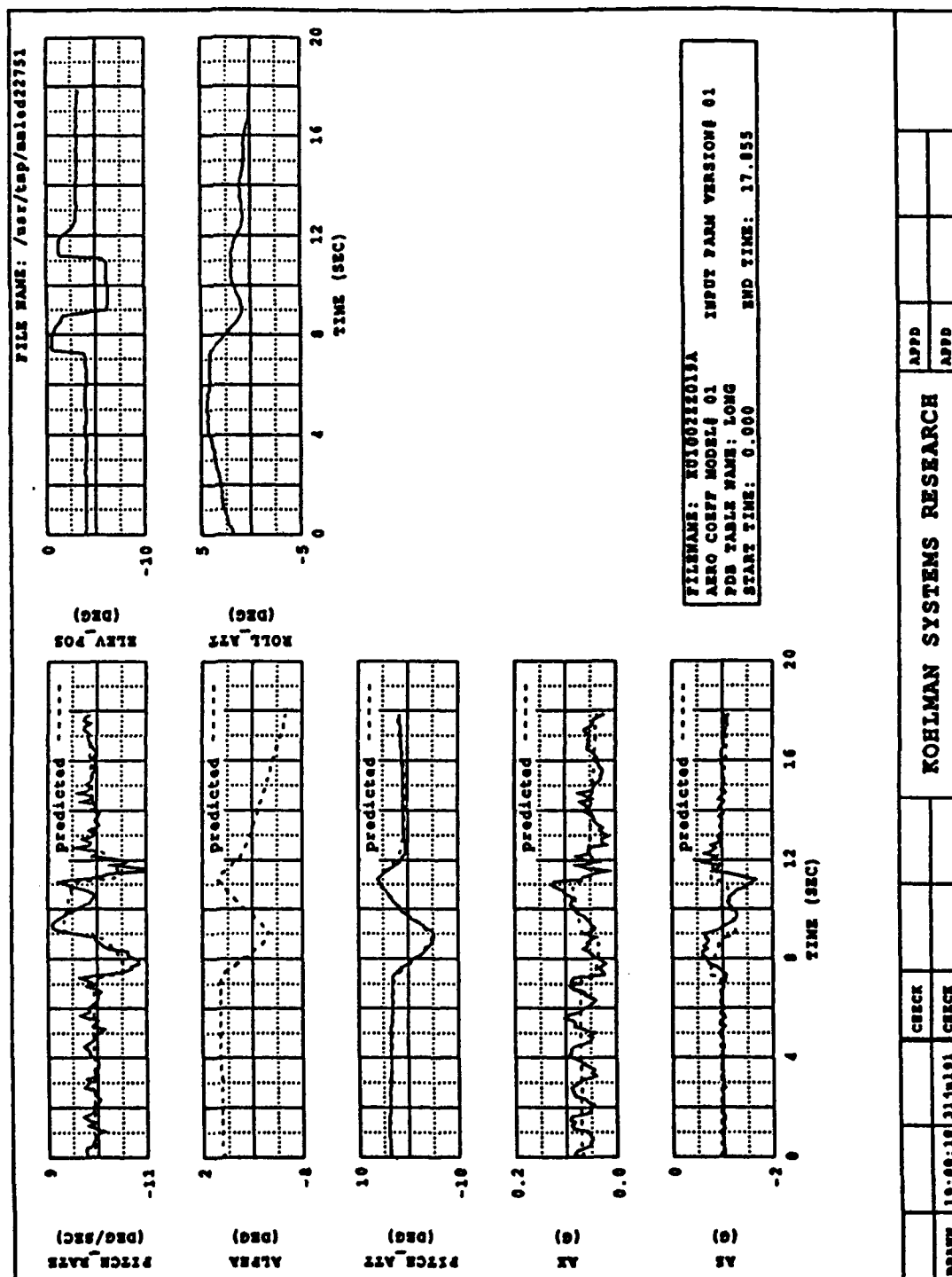


Figure 6 Time History Matches By MMLE Program, Longitudinal Maneuver

Maximum Likelihood Estimation program (MMLE)
Version 5, Fortran 5
1 Jan 1981
Richard E Maine

MMLE5 NEW CASE FTDB FILE NAME :KU1002ZZ019A
longitudinal case.

Flight condition and vehicle characteristics
(0 means value from time history on qbar, v, or mach)
(999 means this on alpha, theta, or phi)
metric units? F
dynamic pressure = 0.0 velocity = 0.0
mach = 0.000 alpha = 999.00
theta = 999.00 phi = 999.00
center of gravity = 0.250 other parameter = 0.000E+00
wing area = 174.0 span = 35.80 chord = 4.90
ix = 948.0 iy = 1346.0 iz = 1967.0
ixz = 0.0
weight = 2723.0 engine ix = 0.000

beginning gauss-newton iteration

weighted error sum = 9606.6

alpha	q	theta	an	ax
0.0000	1.000	4.700	48.70	339.0
0.0000	27.90	9569.	7.160	2.166

Stability and Control Derivatives (Body Axes)
CMA --0.155300E-01 CZA --0.803000E-01 CXA --0.227000E-02
CMQ = -12.4000 CZQ = -3.90000 CXQ = 0.000000
CMDE--0.212734E-01 CZDE--0.411867E-01 CXDE--0.105000E-02
CMAD= -5.20000

iteration 1 completed.

weighted error sum = 13.151

alpha	q	theta	an	ax
0.0000	1.000	4.700	48.70	339.0
0.0000	2.833	8.873	0.4119	1.032

Stability and Control Derivatives (Body Axes)
CMA --0.192427E-02 CZA --0.366938E-01 CXA = 0.455060E-02
CMQ = -8.83100 CZQ = -3.90000 CXQ = 0.000000
CMDE--0.106222E-01 CZDE--0.427426E-01 CXDE--0.307170E-02
CMAD= -5.20000

iteration 2 completed.

weighted error sum = 70.918

alpha	q	theta	an	ax
0.0000	1.000	4.700	48.70	339.0
0.0000	5.168	64.23	1.414	0.1085

Stability and Control Derivatives (Body Axes)
CMA --0.341426E-02 CZA --0.106812E-01 CXA = 0.429289E-02
CMQ = -29.2126 CZQ = -3.90000 CXQ = 0.000000
CMDE--0.141615E-01 CZDE= 0.983683E-02 CXDE--0.475089E-02
CMAD= -5.20000

iteration 3 completed.

weighted error sum = 19.248

alpha	q	theta	an	ax
0.0000	1.000	4.700	48.70	339.0

Figure 6 Continued

0.0000 3.453 14.71 0.9849 0.1013

Stability and Control Derivatives (Body Axes)
 CMA --0.463700E-02 CZA = 0.313060E-01 CXA = 0.212813E-02
 CMQ = -48.4069 CZQ = -3.90000 CXQ = 0.000000
 CMDE--0.293270E-01 CZDE= 0.139029E-01 CXDE--0.625106E-02
 CMAD= -5.20000

iteration 4 completed.

weighted error sum = 29907.

alpha	q	theta	an	ax
0.0000	1.000	4.700	48.70	339.0
0.0000	307.1	0.2938E+05	211.0	6.620

Stability and Control Derivatives (Body Axes)
 CMA --0.891225E-02 CZA = 0.311710E-01 CXA = 0.203409E-02
 CMQ = -93.5562 CZQ = -3.90000 CXQ = 0.000000
 CMDE--0.544056E-01 CZDE= 0.522690E-01 CXDE--0.614562E-02
 CMAD= -5.20000

iteration 5 completed.

weighted error sum = 11.784

alpha	q	theta	an	ax
0.0000	1.000	4.700	48.70	339.0
0.0000	3.530	5.844	2.297	0.1145

Stability and Control Derivatives (Body Axes)
 CMA --0.123197E-01 CZA = 0.275284E-01 CXA = 0.281968E-02
 CMQ = -96.1219 CZQ = -3.90000 CXQ = 0.000000
 CMDE--0.565455E-01 CZDE= 0.525927E-01 CXDE--0.614740E-02
 CMAD= -5.20000

iteration 6 completed.

weighted error sum = 6.5828

alpha	q	theta	an	ax
0.0000	1.000	4.700	48.70	339.0
0.0000	3.170	1.998	1.310	0.1051

Stability and Control Derivatives (Body Axes)
 CMA --0.111809E-01 CZA = 0.267669E-01 CXA = 0.332484E-02
 CMQ = -73.4139 CZQ = -3.90000 CXQ = 0.000000
 CMDE--0.443135E-01 CZDE= 0.512216E-01 CXDE--0.608381E-02
 CMAD= -5.20000

iteration 7 completed.

weighted error sum = 5.3224

alpha	q	theta	an	ax
0.0000	1.000	4.700	48.70	339.0
0.0000	3.111	0.8281	1.280	0.1033

Stability and Control Derivatives (Body Axes)
 CMA --0.998752E-02 CZA = 0.240869E-01 CXA = 0.304516E-02
 CMQ = -76.9632 CZQ = -3.90000 CXQ = 0.000000
 CMDE--0.465230E-01 CZDE= 0.465164E-01 CXDE--0.600955E-02
 CMAD= -5.20000

iteration 8 completed.

weighted error sum = 5.2611

alpha	q	theta	an	ax
0.0000	1.000	4.700	48.70	339.0
0.0000	3.130	0.7530	1.274	0.1037

Figure 6 Continued

```

      Stability and Control Derivatives (Body Axes)
CMA --0.102982E-01    CZA = 0.251312E-01    CXA = 0.310378E-02
CMQ = -76.0528        CZQ = -3.90000        CXQ = 0.000000
CMDE--0.458909E-01    CZDE= 0.480675E-01    CXDE--0.603834E-02
CMAD= -5.20000

iteration 9 completed.

weighted error sum = 5.2351
      alpha      q      theta      an      ax
0.0000      1.000      4.700      48.70      339.0
0.0000      3.127      0.7221      1.282      0.1037

      Stability and Control Derivatives (Body Axes)
CMA --0.103037E-01    CZA = 0.250820E-01    CXA = 0.309307E-02
CMQ = -76.5585        CZQ = -3.90000        CXQ = 0.000000
CMDE--0.461889E-01    CZDE= 0.480881E-01    CXDE--0.603398E-02
CMAD= -5.20000

iteration 10 completed.

weighted error sum = 5.2347
      alpha      q      theta      an      ax
0.0000      1.000      4.700      48.70      339.0
0.0000      3.129      0.7198      1.282      0.1037

      Stability and Control Derivatives (Body Axes)
CMA --0.103226E-01    CZA = 0.251368E-01    CXA = 0.309584E-02
CMQ = -76.5199        CZQ = -3.90000        CXQ = 0.000000
CMDE--0.461597E-01    CZDE= 0.481935E-01    CXDE--0.603623E-02
CMAD= -5.20000

iteration 11 completed.

cost function converged within bound.
weighted error sum = 5.2347
      alpha      q      theta      an      ax
0.0000      1.000      4.700      48.70      339.0
0.0000      3.129      0.7199      1.282      0.1037
case completed.

```

Writing output to the Processed Database

Starting time history plots

Figure 6 Continued

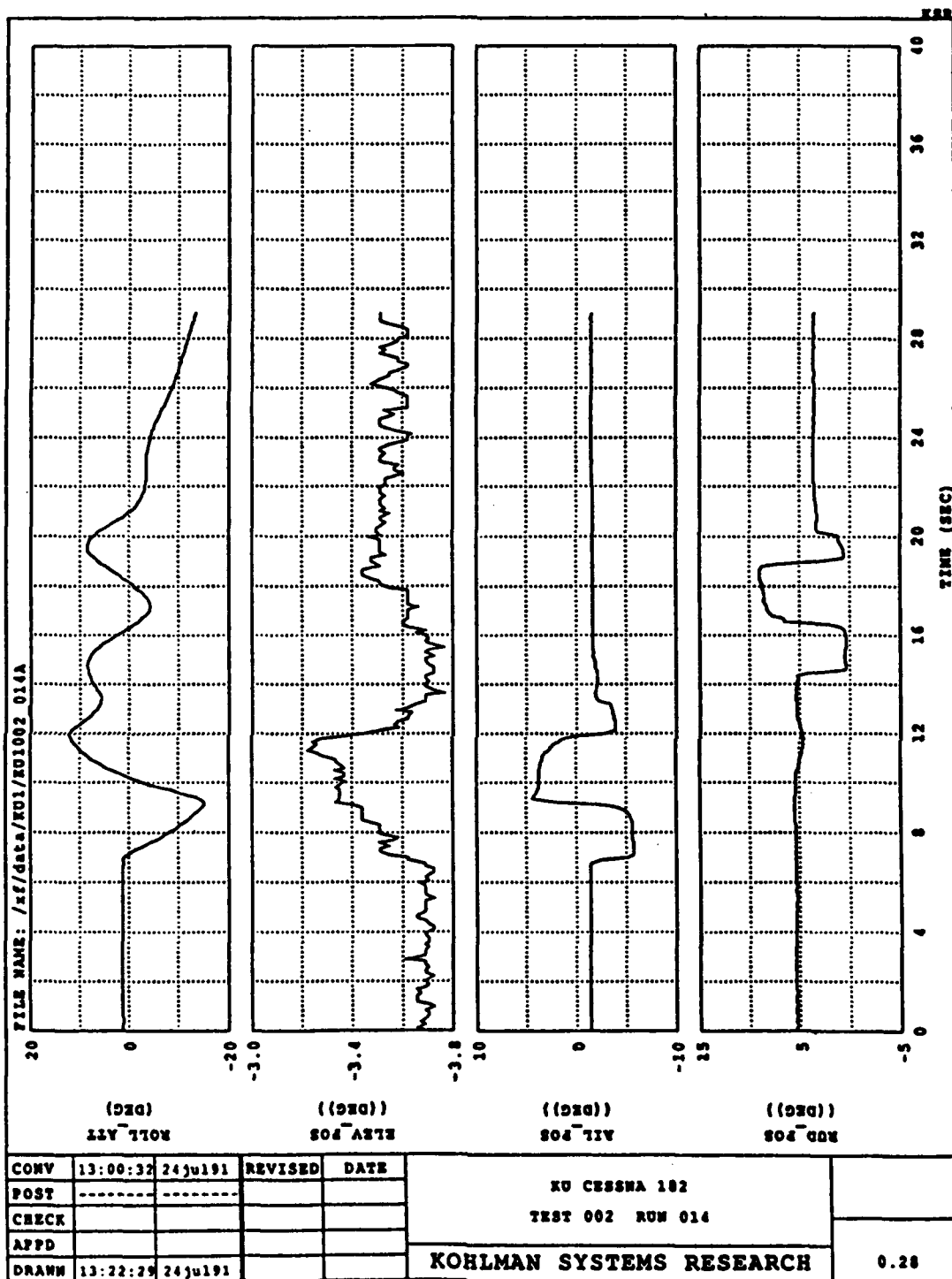


Figure 7 Typical Time Histories of Flight Data, Lateral/Directional Maneuver

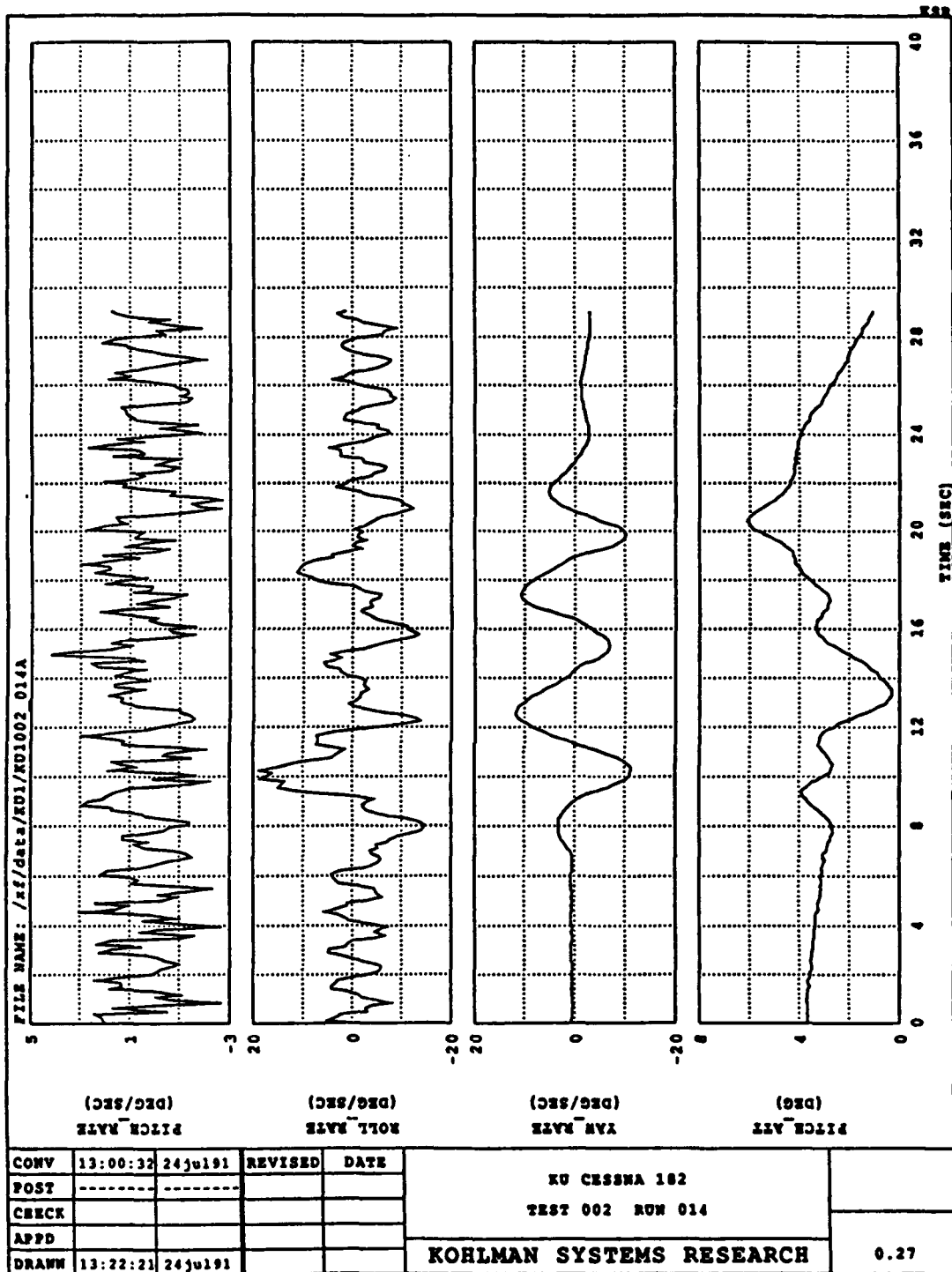


Figure 7 Continued

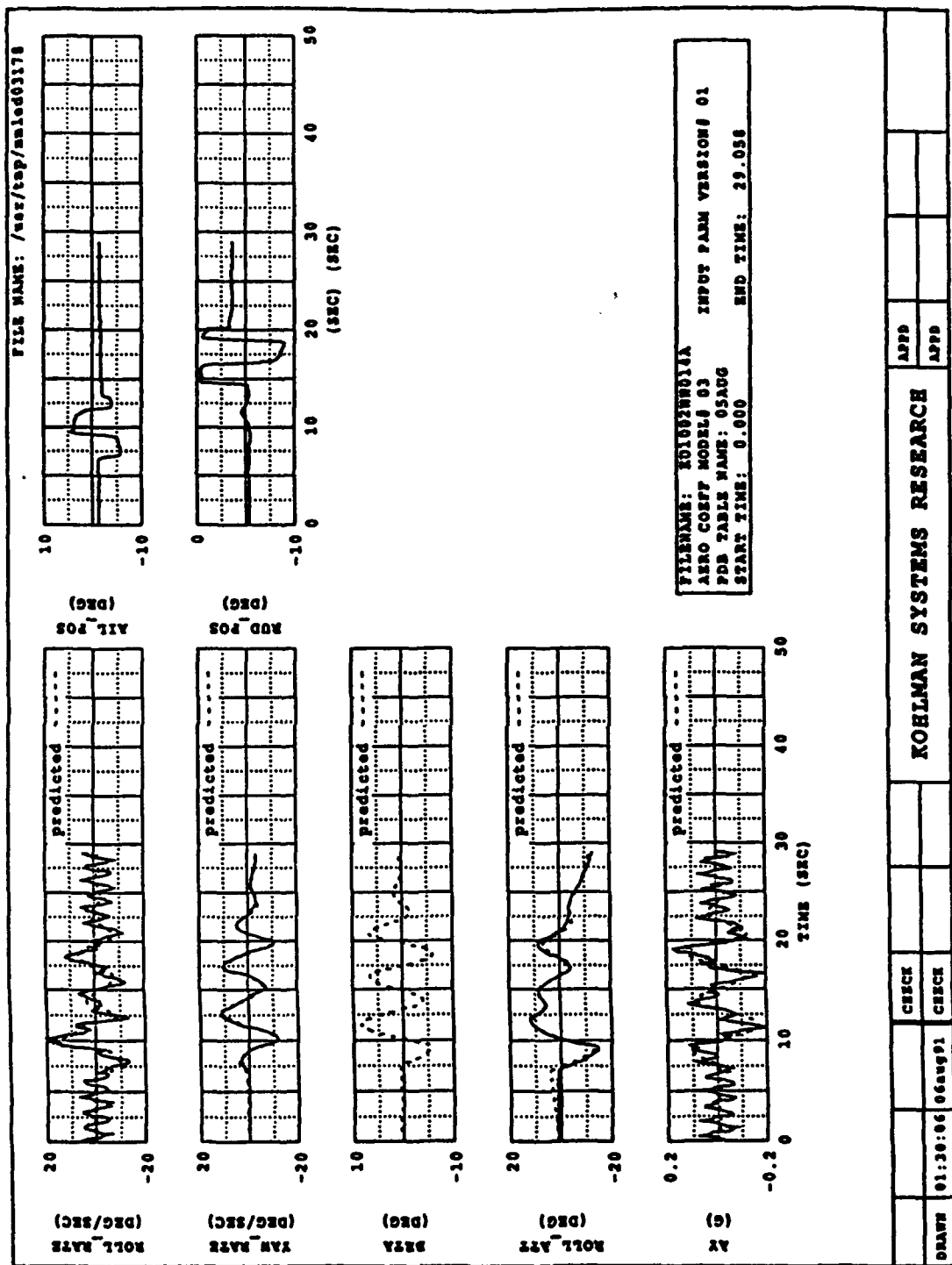


Figure 8 Time History Matches By MMLE Program, Lateral/Directional Maneuver

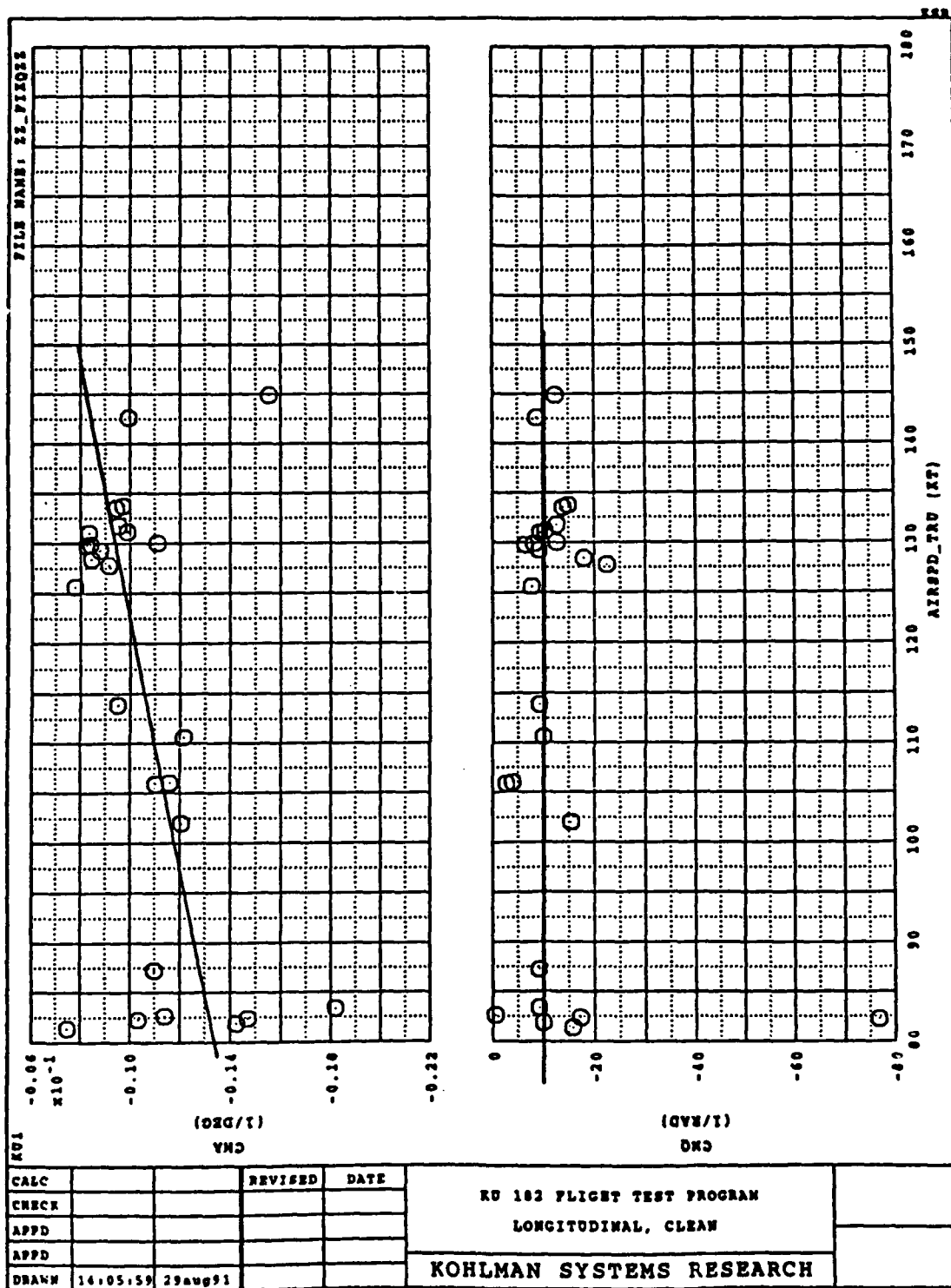


Figure 9 Scatter Plot Of Longitudinal Non-Dimensional Derivatives, Clean Configuration

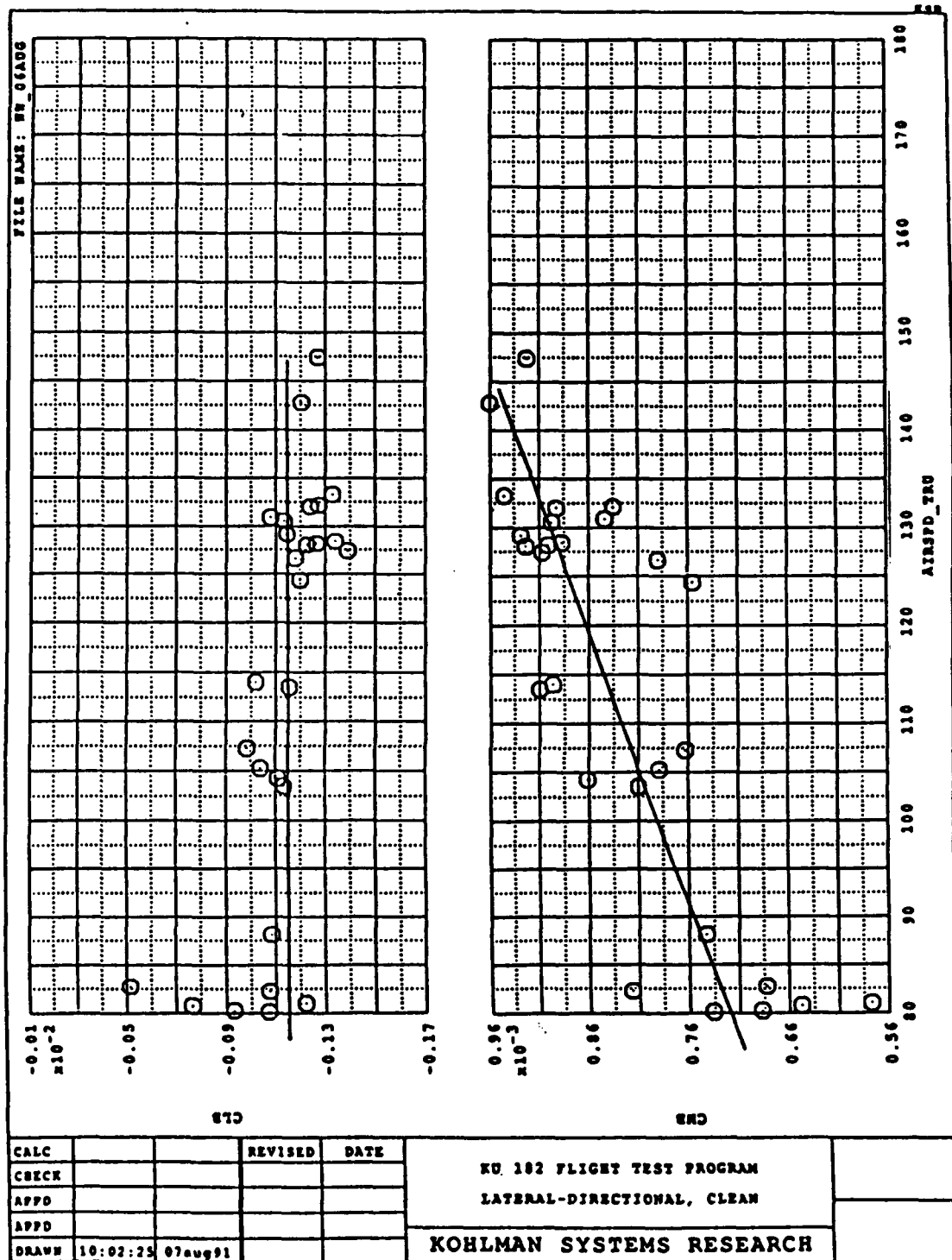


Figure 10 Scatter Plot Of Lateral-Directional Derivatives, Clean Configuration

Table 1 Test Matrix For Flight No. 1 (19 July 1991)

Flight	Run	Airspeed	Altitude	Gear	Flaps	Comments
1	1	power	loss	new	tape	zero speed check
2	2					climbing right turn
3	3					diving left turn
4	4					control sweep
5	5					zero speed cal
6	6	119	5000	up	up	lat/dir
7	7	120	5000			lat/dir
8	8	120	5000			long
9	9	120	5000			long
10	10	120	5000			long
11	11	120	5000			lat/dir
12	12	105	5000			long
13	13	105	5100			lat/dir
14	14	106	5080			long
15	15	106	5080			lat/dir
16	16	90	5000			long
17	17	90	5000			lat/d, stable spiral
18	18	90	5000			lon, phugoid
19	19	90	5000			lat/dir, ball no cntr
20	20	75	5000			long
21	21	75	5000			lat/dir
22	22	75	4940			long
23	23	75	4860			lat/dir
24	24	75	5000	down	down	long, flaps 40°
25	25	70	5000	down	down	lat/dir, elevator
26	26	74	5000	down	down	long
27	27	75	5000	down	down	lat/dir
28	28	121.369	10000	up	up	long
29	29	121.369	10000			lat/dir
30	30	121.369	10000			long
31	31	121.369	10000			lat/dir
32	32	90	10000			long
33	33	90	10000			lat/dir
34	34	90	10000			long

35	35	90	10000			lat/dir
36	36	74	5000	down	down	long
37	37	75	5000	down	down	lat/dir
38	38	75	5140	down	down	long
39	39	75	5020	down	down	lat/dir
40	40	121.369	5010	up	up	long, burble
41	41	121.369	5020			lat/dir
42	42	121.369	4980			long, turbulence
43	43	121.369	5000			lat/dir
44	44					control sweep
45	45					diving left turn
46	46					climbing right turn
47	47					climbing right
48	48					zero speed check
49	49					

Flight I Placard

Date: 19 July 1991
 Aircraft: Cessna TR 182 RG, N7188C
 Engine Start: 0905
 Engine Stop: 1210
 Pilot: T. Mouch
 Flight Test Engineer: J.M. Fernand
 Weight: 2848 lbs
 C.G.: 40.98" aft of firewall
 Fuel State: full

Table 2 Test Matrix For Flight No. 2 (24 July 1991)

Flight	Run	Airspeed	Altitude	Gear	Flaps	Comments
	1					zero speed check
	2					control sweep
	3					climbing left turn
	4					diving right turn
1	5	120	5000	up	up	long
2	6	120	5000			lat/dir
3	7	120	5000			long
4	8	120	5000			lat/dir
5	9	120	5000			long
6	10	B	A	D		lat/dir
7	11	B	A	D		
8	1	120	5000	up	up	long
9	2	120	5000			lat/dir
10	3	120	5000			long
11	4	120	5000			lat/dir
12	5	120	5000			long
13	6	120	5000			lat/dir
14	7	120	5000			long
15	8	120	5000			lat/dir
16	9	120	5000			long
17	10	120	5000			lat/dir
18	11	75	5000			long
19	12	75	5000			lat/dir
20	13	75	5000			long
21	14	75	5000			lat/dir
22	15	75	5000			long
23	16	75	5000			lat/dir
24	17	75	5000			long
25	18	75	5000			lat/dir
26	19	75	5000			long
27	20	75	5000			lat/dir
28	21	75	5000	down	down	lat/dir
29	22	75	5000	down	down	long

30	23	75	5000	down	down	lat/dir
31	24	75	5000	down	down	long
32	25	75	5000	down	down	lat/dir, β recoil
33	26	75	5000	down	down	long
34	27	75	5000	down	down	long
35	28	75	5000	down	down	lat/dir, spiral mode
36	29	75	5000	down	down	long
37	30	75	5000	down	down	lat/dir
38	31	120	5000	up	up	60° - 60° reversal
39	32	120	5000			"
40	33	120	5000			"
41	34					zero run
42	35					control sweep
43	36					climbing right turn
44	37					diving left turn

Flight II Placard

Date: 24 July 1991
 Aircraft: Cessna TR 182 RG, N7188C
 Engine Start: 0855
 Engine Stop: 1105
 Pilot: T. Mouch
 Flight Test Engineer: J. Valasek
 Weight: 2843 lbs
 C.G.: 40.97 " aft of firewall
 Fuel State: full

**Table 3 Comparison Of Non-Dimensional Stability And Control Derivatives,
Clean Configuration, 120 KEAS, 5,000 feet**

<u>derivative</u>	<u>estimated</u>	<u>reference 2</u>
C_{m_α}	-0.54	-0.89
C_{m_q}	-10.0	-12.4
$C_{m_{\delta_e}}$	-1.07	-1.28
C_{l_β}	-0.066	-0.089
C_{l_p}	-0.33	-0.47
C_{l_r}	0.107	0.096
$C_{l_{\delta_a}}$	0.129	0.178
$C_{l_{\delta_r}}$	0.0072	0.0147
C_{n_β}	0.052	0.065
C_{n_p}	-0.023	-0.030
C_{n_r}	-0.070	-0.099
$C_{n_{\delta_a}}$	-0.0063	-0.053
$C_{n_{\delta_r}}$	-0.0355	-0.0657
C_{y_β}	-0.80	-0.31
$C_{y_{\delta_a}}$	0.0	0.0
$C_{y_{\delta_r}}$	0.4298	0.187

C.G.: 40.97" aft of firewall
weight (lbs): 2,843

0.25 X_{cg}
2,645

**Table 4 Non-Dimensional Stability And Control Derivatives,
Cessna TR 182 RG, Dirty Configuration, 75 KEAS, 5,000 feet**

<u>derivative</u>	<u>estimated</u>
C_{m_α}	-0.573
$C_{m_{\dot{\alpha}}}$	-5.2
C_{m_q}	-8.0
$C_{m_{\delta_e}}$	-1.03
C_{l_β}	-0.018
C_{l_p}	-0.357
C_{l_r}	0.15
$C_{l_{\delta_a}}$	0.163
$C_{l_{\delta_r}}$	0.0023
C_{n_β}	0.077
C_{n_p}	-0.033
C_{n_r}	-0.085
$C_{n_{\delta_a}}$	-0.0043
$C_{n_{\delta_r}}$	-0.0533
C_{y_β}	-1.003
C_{y_p}	-2.5
C_{y_r}	-3.3
$C_{y_{\delta_a}}$	-1.89
$C_{y_{\delta_r}}$	0.516

C.G.: 40.97" aft of firewall

weight: 2,843 (lbs)

**DOPPLER GLOBAL VELOCIMETRY:
A POTENTIAL VELOCITY MEASUREMENT METHOD FOR
GENERAL AVIATION APPLICATIONS**

by

**L. Scott Miller
The Wichita State University
Department of Aerospace Engineering
and
J.F. Meyers and J.W. Usry
NASA Langley Research Center**

**For Presentation to the AIAA/FAA Joint Symposium on General
Aviation Systems at the Hilton Inn-East, Wichita, KS
on March 16-17, 1992**

Doppler Global Velocimetry: A Potential Velocity Measurement Method for General Aviation Applications

**L. Scott Miller
The Wichita State University
Department of Aerospace Engineering**

**J.F. Meyers and J.W. Usry
NASA Langley Research Center**

Abstract

A basic overview of Doppler Global Velocimetry (DGV), a new flow field velocity measurement method, is provided with respect to potential general aviation applications. DGV is currently undergoing evaluation at NASA, Northrop, and WSU. A discussion of present DGV theory, system specifications, measurement capabilities, and program development activities is provided. At this point, it appears likely that DGV systems will see increased application in wind tunnels. Flight test measurements will be much more difficult to obtain, however, due to flow seeding requirements and constraints.

Introduction

A wide range of flow field velocity measurement techniques currently exist and are available to the aerodynamic investigator. 5-Hole probes, Constant Temperature Anemometers (CTA's), and Laser Doppler Anemometers (LDA's) are perhaps the most commonly applied velocimetry methods in wind tunnel and flight test applications. Each of these techniques offer unique advantages for a particular need or test environment. Unfortunately, however, each of these methods also share a common weakness.

The 5-Hole, CTA, and Laser Doppler Anemometers are all point measurement techniques. Physical movement, or traversing, of the probe/measuring volume is required to identify multi-component velocity data over a large flow area. Data acquisition is, as a result, typically time consuming and simultaneous identification of global velocity data is essentially impossible. In most cases, global simultaneous data acquisition is preferred. This measurement capability can improve testing time, costs, and provide the ability to resolve unsteady flow features.

Northrop Research and Technology Center (NRTC) recently invented a velocimetry method which offers the potential for making simultaneous, global, multi-component velocity measurements. The method, called Doppler Global Velocimetry (DGV), is currently undergoing advanced development and evaluation at the NASA Langley Research Center (LaRC), the NRTC, and the Wichita State University (WSU). DGV is particularly attractive for application in both wind tunnel and flight testing environments due to its potential simplicity and global simultaneous measurement capabilities.

The present paper will discuss current DGV theory, capabilities, limitations, and the status of DGV development activities. Particular effort will be aimed at addressing potential General Aviation applications.

DGV Theory

The following provides a review of basic DGV theory. Further, much more detailed, information on the DGV method is provided in references 1-4.

Mie Scattering

In simple terms, the DGV makes velocity measurements by identifying the Doppler frequency of scattered laser light from sub-micron sized particles present and moving within a flow. The exact frequency of the scattered light is determined through the Doppler Effect and specifically by the following equation,

$$f = \nu_o + [\nu_o (\mathbf{O} - \mathbf{I}) \cdot \mathbf{V}] / c, \quad \text{Eq. 1}$$

Where f is the scattered light frequency, ν_o is the illuminating laser frequency, c is the speed of light, and \mathbf{O} and \mathbf{I} are the scattered light and laser illumination vector directions respectively. If one can identify or measure the scattered light frequency (f) a component of the total flow velocity vector \mathbf{V} can be calculated, since all other variables will be known. Figure 1 shows a schematic diagram illustrating the relationship between the scattered light, laser illumination, and measured velocity vectors. Since a global measurement is desired, a sheet of laser light is used to illuminate the flow field. The above equation will hold at all points within the light sheet where particles are present and illuminated. As can be seen, the measured component of the total velocity vector (\mathbf{V}) is approximately perpendicular to a line bisecting the viewing (\mathbf{O}) and illuminating (\mathbf{I}) vectors.

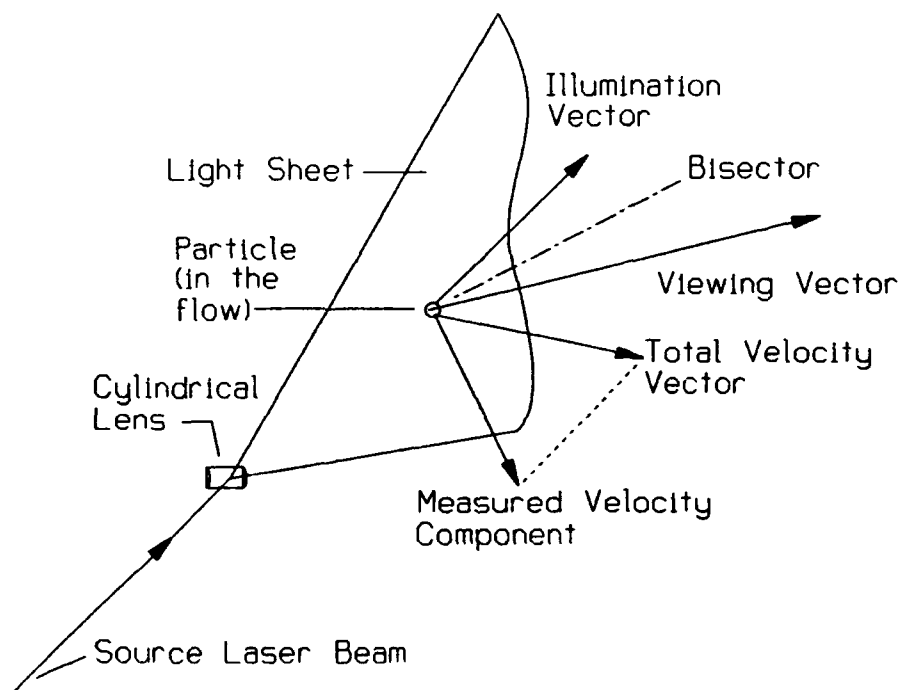


Figure 1. A schematic diagram showing the relationship between the observation (\mathbf{O}), illuminating (\mathbf{I}), and measured velocity (\mathbf{V}) vectors.

Frequency Discrimination

As was mentioned above, to measure flow velocity values the scattered light frequency must be identified. The DGV accomplishes this task by using a unique and key component known as an Absorption Line Filter or ALF. An ALF is essentially an optical filter assembly which has a transmission or absorption behavior similar to that shown in Figure 2. As can be seen, the amount of light passing through the filter will depend on the frequency of the input light. The DGV illumination laser is carefully tuned to a frequency which intersects the ALF transfer function at approximately the 50 percent transmission or absorption location. The flow field of interest is then directly viewed through the ALF. The unique Doppler interaction of the moving particles, illuminating laser light, and viewing vectors determines the scattered light frequency. Scattered light from the illuminated flow field will pass through an ALF with an output intensity level proportional to the frequency, or most importantly to the particle velocity. The ALF thus performs a linear frequency-to-intensity conversion over approximately 500 Mhz. A normally difficult Doppler frequency measurement has been reduced to a relatively simple intensity measurement task, as a result of using an ALF.

Wide area, or global, intensity measurements are typically performed using Charge Coupled Device (CCD) based video cameras. The recorded intensity data, for a large flow field region viewed through the ALF, can be related to the flow velocity once the ALF transfer function has been identified through a calibration.

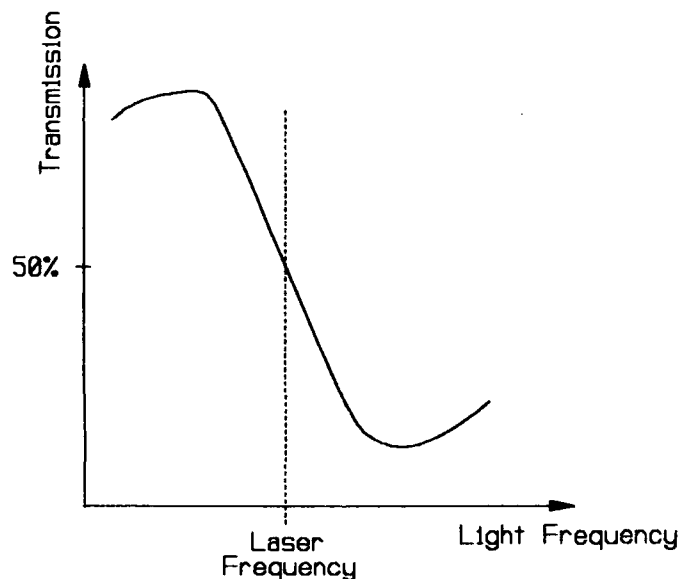


Figure 2. A typical ALF transfer function. (The vertical axis represents normalized transmission and the horizontal axis represents laser frequency in terms of mode number.)

Seeding Considerations

DGV, much like other laser based methods, requires the presence of particles within the flow to make measurements. Direct injection of particles, known as seeds, into the flow is often necessary since a sufficient number and size of particles may not naturally exist. The seed size, number, and distribution

must be carefully considered in order to assure good DGV measurements. Particle size and mass will effect both the scattered light intensity and the ability of the seeds to "follow the flow" accurately. Particle number and distribution throughout the flow will effect the data acquisition rate and the completeness of the global measurements. In general, seeding guidelines utilized for LDA flow measurements apply.

Illumination and Seeding Nonuniformities

Unfortunately, practical factors prevent perfectly uniform flow field illumination and seeding. These nonuniformities produce varying scattered light intensities. DGV measurement errors would result if these intensity variations, as measured by a CCD camera, were assumed to represent velocity information. To avoid potential problems of this nature, a second camera is used to measure the simple intensity variations in the flow field. These recorded intensities are then used to normalize the output from the other CCD camera and ALF. The normalized ratio of camera outputs thus contains only velocity information.

Data Acquisition and Analysis

DGV data, obtained from the CCD cameras, can be collected and analyzed in a number of different ways. The output from each camera can be simply recorded using standard video tape or optical disk recorders. This approach is attractive since a large amount of data can be stored quite simply and analyzed as is convenient later. If real-time (or near real-time) measurement and display capabilities are desired, a number of different approaches are possible. Specific techniques are outlined in reference 4. Each method typically relies on the use of one, or more, Frame-Grabber boards (usually installed in a Personal-Computer) to capture DGV camera images for detailed analysis.

Multiple-Component Measurements

To make multiple component velocity measurements using a DGV system a number of general approaches are possible. Equation 1, shown and discussed previously, indicates that only one component of the total velocity vector (V) can be measured for a given viewing (O) and illumination (I) direction. To identify other velocity components the viewing or illumination vectors must be adjusted. In one multi-component measurement DGV method, three velocity components can be measured simultaneously by viewing the flow region from three different and orthogonal directions. This approach requires three sets of CCD cameras, ALF's, and data acquisition equipment. Other multi-component measurement methods exist and are discussed in greater detail in references 1-4.

Typical DGV System Configuration

Figure 3 shows a schematic diagram of a basic one-component DGV system. Primary parts include a laser, two CCD video cameras, an Absorption Line Filter (ALF), and image acquisition and processing electronics. A number of different laser and ALF combinations are possible, but argon-ion lasers and iodine gas filled ALF's are currently in greatest use. Commonly available CCD cameras, of 512 X 512 CCD array size and 30 frame/second scan rate, are sufficient for recording DGV intensity data. Assorted instruments are necessary to acquire and analyze measured data. Efficient data storage is provided by commercially available video recorders. PC-based frame grabber boards can be utilized to acquire images from the cameras and to generate files suitable for detailed analysis by a computer. To improve data interpretation and presentation, velocity maps of the measured flow field can be produced by applying false colors to the captured computer images.

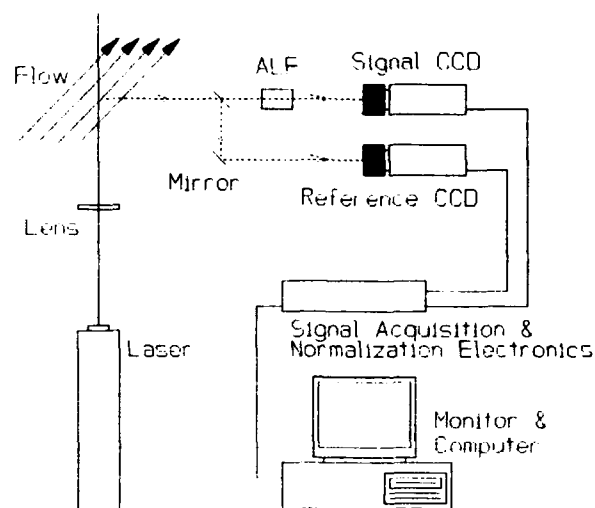


Figure 3. Simple one-component DGV system schematic.

Basic DGV Specifications

The full measurement capability of the DGV has, to this point in development, not been fully established. However, some basic DGV system specifications can be offered at this time and are summarized in Table 1 below.

Velocity Component Resolution	* One-, two-, or three-component coincident (simultaneous) measurements are possible.
Temporal Resolution	* Determined by the frame rate of the camera (Typical CCD cameras operate at 30 frames per second.)
Spatial Resolution	* Determined by CCD array size and lens selection (variable).
Data Rate	* Determined by camera frame rate.

Table 1 A summary of current DGV system measurement specifications.

Velocity Component Resolution Comments

Multiple component velocity measurements, as executed in the most common DGV configurations, require multiple camera and ALF components. This means system cost and complexity is increased by a factor roughly proportional to the desired number of measured components. Use of multiple camera and ALF sets does not assure simultaneous velocity measurements will be obtained under all circumstances however. Unfortunately, light is scattered more in some directions than others. Due to the complex nature of light scattering physics, a given camera and ALF set may not receive enough light to

register a good measurement. Careful illumination, particle sizing, and camera positioning can minimize the potential for problems however.

Temporal Resolution Comments

DGV temporal resolution can be further improved by using high frame rate CCD cameras. These cameras are however more expensive and typically less sensitive. Increasing the frame rate allows for the identification of short period flow phenomena. A continuous introduction of seeds, within the viewed flow region, will assure full advantage of the available frame rate is exploited. High frame rates and good seeding assures the best possible DGV temporal resolution.

Spatial Resolution Comments

DGV spatial resolution is variable and controllable through CCD array size and lens selection. For a given array size, the minimum resolvable feature is determined by the physical size of the field of view. Conversely, for a given field of view, the resolution can be improved by increasing the number of CCD pixels. Camera position and lens selection controls the field of view size. Additionally, seeding can also effect DGV spatial resolution. A sparse seed distribution minimizes the ability of the DGV system to resolve small features.

Data Rate Comments

Much like temporal and spatial resolution, the data rate capability of a DGV is determined by camera frame rate and flow seeding. The presence of seeds, to scatter light, is mandatory for DGV measurements. In essence, data can be recorded at the camera frame rate only if seeds are presence.

Potential DGV Measurement Capabilities

The following section will discuss the potential of DGV's for making specific types of measurements, typically of particular interest to theoretical, experimental and computational aerodynamics researchers. It should be noted that these discussions are very basic in nature. The complete DGV capability has yet to be defined, but Table 2 summarizes likely measurement capabilities.

Average Velocities	* Can be obtained by averaging pixel values from multiple images or frames.
Turbulent Velocity Fluctuations	* Can be obtained, after average velocities are identified.
Velocity Correlations	* Difficult, but not impossible, to identify.
Spectral Content	* Extremely difficult, if not impossible, to obtain.

Table 2 Summary of DGV application considerations.

Measurement Capability Comments

Proper determination of statistically valid average, turbulent fluctuation, and correlation velocity terms requires a large set of data. In addition, each velocity component measurement must be coincident or simultaneous. Velocity spectra calculations requires extremely high sample rates which may be difficult to generate at present. As has been mentioned previously, good flow seeding will enhance the ability of a DGV to make measurements.

DGV Development Status

As was mentioned earlier, DGV systems are currently undergoing development and evaluation at the NRTC, NASA LaRC, and Wichita State University. A number of basic flow field and wind tunnel measurements have been undertaken. Results of these initial experiments have been encouraging.^{5,6} Preliminary evaluations of these investigations have however identified some critical points of interest in implementing the DGV method.

Proper signal and reference camera alignment and laser frequency adjustment are of significant importance. Simple camera misalignment or image distortions are exaggerated as a result of the normalization process, thus corrupting the velocity measurements. Great care must be exercised to assure that both the signal and reference camera images overlap exactly. In addition, the illumination laser frequency, relative to the ALF transfer function, must be known exactly in order to assure linear DGV operation. This problem can be minimized or eliminated through calibration and laser frequency monitoring.

More wind tunnel tests are planned for the spring and summer of 1992. If results are favorable, development of systems for various wind tunnels and flight test applications (on board the NASA/Ames-Dryden F-18 High Alpha Research Vehicle) are planned. In light of this additional possibility, simple experiments have been performed using a Lear Jet and a solid state laser to study the possibility for making DGV measurements utilizing naturally occurring atmospheric particulates for light scattering. Initial results suggest that flow seeding will be necessary for DGV flight test applications.

Conclusions

A review of current DGV theory, system specifications, measurement capabilities, and program development activities has been provided. The following conclusions are offered in light of the discussions.

- 1) Doppler Global Velocimetry (DGV) is a global simultaneous multi-component flow field velocity measurement method.
- 2) The DGV is capable of making measurements at video frame rates assuming excellent seeding and light scattering conditions exist. Reasonable temporal and spatial measurement resolutions can be obtained if one can gather and store the DGV data fast enough.
- 3) DGV, like other laser based velocimetry techniques, requires the presence of a sufficient number and density of particles or seeds. In addition, a sufficient amount of light must be scattered from these particles for measurement purposes.
- 4) A less than ideal seed density, number, and scattered light intensity will reduce the available DGV data sample distribution, rate, and quantity. As a result, average multi-component velocity measurements will

be easier to obtain than the more data demanding (ie. high data rate required) quantities such as turbulent fluctuations, velocity correlations, and velocity spectrums.

5) DGV will likely see greater application in wind tunnels. Flight test applications will be more difficult due to seeding complexities associated with a flight environment.

References

- 1) Komine, H., Brosnan, S.J., Litton, A.H. and Stappaerts, E.A., "Real-Time Doppler Global Velocimetry," AIAA 29th Aerospace Sciences Meeting, AIAA-91-0337, Reno, NV., Jan. 1991.
- 2) Meyers, J.F. and Komine, H., "Doppler Global Velocimetry A New Way to Look at Velocity," ASME Fourth International Conference on Laser Anemometry, Cleveland, Ohio, Aug. 1991.
- 3) Komine, H. and Brosnan, S.J., "Instantaneous Three-Component Doppler Global Velocimetry," ASME Fourth International Conference on Laser Anemometry, Cleveland, Ohio, Aug. 1991.
- 4) Meyers, J.F., Lee, J.W. and Cavone, A.A., "Signal Processing Schemes for Doppler Global Velocimetry," IEEE 14th International Congress on Instrumentation in Aerospace Simulation Facilities, Rockville, Maryland, Oct. 1991.
- 5) Usry, J.W., Meyers, J.F. and Miller, L.S., "Doppler Global Velocimetry Measurements of the Vortical Flow Above a Thin Delta Wing," AIAA 30th Aerospace Sciences Meeting, AIAA-92-0005, Reno, NV., Jan. 1992.
- 6) Usry, J.W., Meyers, J.F., and Miller, L.S., "Assessing the Capabiltiy of Doppler Global Velocimetry to Measure Vortical Flow Fields," Optical Methods and Data Processing in Heat and Fluid Flow, City University, London, England, April, 1992.

EXPERIENCE WITH COMPUTATIONAL FLUID DYNAMICS CODES

by

**Michael Papadakis
Steve Klausmeyer
Xiaoxian Liu
Department of Aerospace Engineering
Wichita State University
Wichita, Kansas 67208**

**For Presentation to the AIAA/FAA Joint Symposium on General
Aviation Systems at the Hilton Inn-East, Wichita, KS
on March 16-17, 1992**

Experience with Computational Fluid Dynamics Codes

*Michael Papadakis * Steve Klausmeyer † and Xiaozian Liu ‡*
Department of Aerospace Engineering
Wichita State University, Wichita, Kansas 67208

Abstract

A number of aerodynamic configurations have been studied at the department of Aerospace Engineering of the Wichita State University using various Euler and Navier-Stokes solvers. Computer codes obtained from NASA Ames research center such as ARC2D and ARC3D and codes developed in the department are briefly described in this paper.

Solutions for several configurations including single and multi-element airfoils and a missile body are presented. Experience with these codes shows that the quality of numerical solutions depends on several factors. These factors include grid size, grid density, time-step, boundary conditions, artificial dissipation, turbulence models and numerical schemes used to integrate the differential equations in time.

Computational fluid dynamics codes, particularly those capable of three-dimensional flow analysis, require significant computer resources. Computer requirements such as CPU time, random access memory and disk storage capacity are discussed in this paper.

Introduction

A number of Euler and Navier-Stokes computer codes have been developed by government research centers, industry and universities. These computer codes can be used to solve a wide variety of aerodynamic flows. In many cases computer codes have been written for specific applications such as airfoil or wing analysis. In other cases more general codes have been developed which for example can analyze complete aircraft configurations. Due to the complexity of the physical phenomena and the wide range of geometries encountered in fluid dynamics the development of a universal code has not been possible. Users of Computational Fluid Dynamics (CFD) codes must choose codes which best fit the specific problem in hand or modify existing codes for the required application. In general CFD codes are complex tools and users must have substantial experience and training to use these computer tools.

There are several facets to a CFD code which influence the solution process. These include the following:

- The system of equations being solved, i.e., Euler, Thin Layer Navier-Stokes (TLNS), Parabolized Navier-Stokes (PNS), etc.
- The numerical scheme for integrating the equations in time or space has a strong influence on the stability and convergence characteristics of the solution.
- The type of artificial dissipation used to reduce numerical oscillations and improve shock capturing characteristics.
- The boundary conditions specified at the free stream, inflow, outflow, surface and wake boundaries.
- The turbulence model used for viscous flow analysis.
- The computational grid, grid clustering and grid quality have a significant impact on computational results.
- The numerical algorithm for solving the large system of equations resulting from implicit schemes has a direct effect in the efficiency of the numerical solution.

The majority of CFD computer codes require that the user understands how to choose and adjust the various code parameters depending on the configuration studied. In addition, the user must be familiar with

* Assistant Professor, member AIAA.

† Research Assistant, member AIAA.

‡ Research Assistant, member AIAA.

grid generation and post processing tools for analyzing the results. Definition of boundary conditions is in many cases a difficult task and its influence on the solution must be considered.

The complexities associated with the use of CFD codes and the extensive computational resources needed to solve practical aerodynamic configurations has limited the use of CFD in industry. However, as experience is gained with CFD computer codes and more robust numerical schemes are developed, CFD codes will be designed which reduce the demands on the user. In addition, it is expected that as massively parallel computers become more readily available the time required to obtain a solution will be significantly reduced. User friendly CFD codes and faster computers will expand usage of CFD to a wide range of industrial applications.

In this paper both qualitative and quantitative results obtained from the application of CFD computer codes to a variety of aerodynamic configurations are presented. Computer codes and configurations studied are briefly described.

Computer Tools

Software packages and computer systems used in the study of the the aerodynamic configurations presented in this paper are described in this section. Computer software include grid generation codes, flow solvers and flow visualization programs. Computer systems include a Cray 2 supercomputer, two IBM mainframes, and several workstations.

Grid Generation

Grid generation is usually the first step of the solution process and it tends to be time consuming for most but the simplest configurations. Grids maybe structured or unstructured, single or multi-block, fixed or adaptive. In many cases sections of a grid must be allowed to move with respect to other sections. There are a number of grid generators available such as 2DGRAPE (Ref.1), 3DGRAPE (Ref. 2), EAGLE (Ref. 3), GRIDGEN (Ref. 4), PLUTO (Ref. 5), RAMBO-4G (Ref. 6), etc. Application of these codes to generate grids about complex configurations requires substantial experience on the part of the user.

After a grid has been constructed the user must assess the quality of the grid before a flow solution is attempted. Grid orthogonality, cell aspect ratio, grid clustering and metrics are some of the parameters that determine grid quality.

In this work elliptic structured grids were generated using the 2DGRAPE code which is relatively easy to use with single element airfoils and other simple geometries. In some cases hyperbolic grids were used. For multi-element airfoils structured grids are much more difficult to generate and typically blocking techniques must be applied. In this paper unstructured grids were used with all multi-element configurations.

Flow Solvers

Flow solvers are computer codes designed to solve the governing equations of the fluid motion. Typically the Euler equations or some form of the Navier-Stokes equations are used in most CFD codes. These equations are solved numerically by a finite difference, a finite volume or a finite element method. Finite volume and finite element codes can be applied to structured and unstructured grids while finite difference methods are typically restricted to structured (body fitted) grids. Unstructured grids provide higher flexibility in discretizing complex geometries and offer the possibility of resolving localized flow phenomena through the use of adaptive meshing. Currently considerable efforts are being made to develop computer codes which use unstructured grids with finite volume or finite element schemes to solve the equations of fluid motion. Attempts are also being made to automate the grid generation process in these new flow solvers. Finite volume and finite element codes require significant book keeping which complicates the programing aspects of these methods. In addition storage requirements are greater. Turbulent flow calculations which are based on mixing length turbulence models are more difficult to implement in unstructured codes.

The time integration of the governing equations is usually performed with implicit or explicit schemes. Explicit schemes are easier to program but they are limited to small time steps, particularly in the case of viscous flows, due to stability requirements. Storage requirements with explicit schemes, however, are significantly lower because there is no need to store the coefficients of the large system of equations resulting from the use of implicit schemes. Implicit schemes have the main advantage of being numerically stable even when the integration time step is large. For example to obtain a converged solution of the steady two-dimensional viscous flow about a single element airfoil the time step of an implicit scheme can be an order of magnitude higher than that required for an explicit scheme. The numerical schemes for solving the

very large system of equations resulting from the use of implicit schemes must be chosen carefully so as to keep numerical operations and storage requirements to a minimum while maximizing numerical accuracy.

Another important aspect of many numerical formulations is the use of artificial viscosity (damping terms) for reducing or eliminating numerical oscillations in regions where large flow gradients are present. There are several types of numerical dissipation varying from simple constant dissipation schemes to variable non-linear dissipation schemes. Most of these schemes require user inputs to choose the type of dissipation and to adjust the level of dissipation. Various symmetric and upwind schemes have also been developed which use Total Variation Diminishing (TVD) principles to eliminate numerical oscillations and improve the shock capturing capabilities of flow solvers. The effect of dissipation terms on the convergence and stability of the flow solver must be considered carefully.

Study of turbulent flows requires the use of turbulence models. A number of turbulence models are now available varying from simple algebraic to two-equation models (Ref. 7-11). Typically turbulence models are calibrated for certain type of flows and therefore some fine tuning is always necessary whenever these models are applied beyond the range of their calibration. The addition of one or two-equation turbulence models to a flow solver may have adverse effects on the convergence of the code. This is because differential equations used in turbulence models have convergence characteristics which are considerably different than those of the governing differential equations.

Specification of boundary conditions is perhaps one of the most challenging aspects of computational fluid dynamics. In most cases it is possible to specify conditions at the boundaries of the flow and obtain a numerical solution. However, the conditions specified at the flow boundaries may not represent the physical problem being simulated. Guidelines for specifying boundary conditions have been developed for certain types of aerodynamic flows. For most flows, however, boundary conditions are difficult to specify. Furthermore, when CFD results are compared with experimental data the boundary conditions specified in the CFD code must represent those of the experimental configuration.

The computer codes used in this investigation were MTVD, RTVD, ARC2D, ARC3D and NS72. Brief descriptions of these computer codes are given in the following.

- MTVD is a two dimensional full Navier-Stokes finite difference code designed for structured grids. The solution is advanced in time with the explicit MacCormack Method (Ref. 12). Constant, non-linear, and TVD dissipation schemes are used in this code. Boundary conditions for free and impinging jets and for airfoil flows have been implemented in this program. The algebraic turbulence model of Baldwin-Lomax (Ref. 7) and the one-equation turbulence model of Baldwin and Barth (Ref. 9) have been implemented in this program. Steady state and time accurate solutions are possible with this code. Low subsonic to high supersonic flows can be simulated with MTVD which was developed in-house. Details of this code are given in Ref. 13.
- RTVD (Ref. 14) was also developed in-house and is similar to MTVD with the exception that the second order Runge-Kutta scheme is used to integrate the Navier-Stokes equations. Euler solutions can be obtained by setting the viscous terms to zero.
- ARC2D is an implicit finite difference code developed at NASA Ames (Ref. 15). This code can be used with structured grids only. The thin layer Navier-Stokes equations are integrated using the Beam and Warming implicit scheme. Various types of numerical dissipation models are available in this code. The Baldwin-Lomax algebraic model is used for turbulent flow calculations. Boundary conditions for flow about a flat plate and for airfoils are implemented. Steady (scaled time step) and time accurate (constant time step) solutions for subsonic to high supersonic flows are possible with this program. Steady state flows can be made to converge in 4 to 6 thousand iterations by choosing large time steps.
- ARC3D (Ref. 15) is the three dimensional version of ARC2D. This code was also developed at NASA Ames. Several modifications were made to this code by the present investigators. These include the addition of a simple grid generator for axisymmetric flows, TVD numerical dissipation, modifications to the boundary conditions and the addition of the one-equation turbulence model of Baldwin and Barth.
- NS72 is a two-dimensional finite element code (Ref 16) used for multi- element airfoil analysis. The code solves the Navier-Stokes or Euler equations using a Runge-Kutta method on an unstructured triangular grid. Convergence is accelerated using a multi-grid method

along with enthalpy damping and residual averaging. The code incorporates the algebraic turbulence model of Baldwin and Lomax. Second and fourth order damping are used to control numerical oscillations.

Visualization Software

A number of commercial graphics packages designed for CFD applications are currently available. Examples include FIELDVIEW (Ref. 17), TECPLOT, etc. Research scientists at NASA Ames have also developed a number of flow visualization software such as PLOT3D, GAS, FAST (Ref. 18-19) etc. Most of the NASA Ames graphics software are available thru COSMIC (Ref. 20). The graphics package used to visualize the majority of the computational results presented in this paper was PLOT3D. PLOT3D works only with structured grids and is available on a number of workstation platforms.

Computer Systems

Computer systems used in this investigation include an Apollo DN 10000 workstation, a Silicon Graphics 4D/240GTX workstation, an IBM Risc 6000/520 Workstation, an IBM 370/3081 mainframe, an IBM ES 9000/400 mainframe and a CRAY 2 supercomputer. The Apollo and Silicon Graphics workstations had three processors each so it was possible to run codes in parallel mode. The IBM ES 9000 and the CRAY 2 are vector machines. Use of vectors reduced run times significantly in most cases.

Results and Discussion

Geometries, flow conditions, grid topologies, and selected results are discussed in this section. The configurations presented are limited to external flows.

Single Element Airfoils

Subsonic and transonic flows about single element airfoils have been analyzed with the codes discussed in this paper. The results presented in this section are for the configurations given in Table 1. The transonic cases are more challenging computationally because they involve regions of subsonic and supersonic flow with embedded shocks. Shock location and shock boundary layer interaction are important aspects of transonic flow about airfoils which are difficult to predict accurately.

Table 1: Test Configurations

Airfoil Section	Mach No	α Deg.	Re
NACA 0011	0.130	5.00	2.2×10^6
RAE 2822	0.750	2.80	6.2×10^6
NACA 0012	0.752	3.02	9.0×10^6

Details of the test cases given in Table 1 can be found in Ref. 13,14 and 21.

Figure 1 shows the inner, outer and wake boundaries for a C-mesh. The curvilinear coordinate ξ varies clockwise around the airfoil while the curvilinear coordinate η varies along the normal to the airfoil surface. Typical elliptic and hyperbolic C-grids are shown in Fig. 2 and 3 respectively. Elliptic grids are more difficult to construct but allow greater flexibility in the specification of outer boundary geometry. They also allow the user to control the angles of intersection between the ξ and η lines at the inner and outer boundaries. Hyperbolic grids allow only one boundary to be specified. When constructing hyperbolic grids about airfoils, the inner boundary (airfoil) is specified. The outer boundary is obtained during the solution. Hyperbolic grids are easier to generate and can be used when the precise location of the computational outer boundary is not important.

Experimental and computational results for the test cases of Table 1 are given in Fig. 4-7. Figure 4 compares experimental and computational results for a NACA 0011 airfoil in subsonic flow. Results for angles of attack of 0, 5 and 10 degrees are presented. The Mach number was 0.13 and the Reynolds number 2.2×10^6 . The experimental data were taken from Ref. 21. Two numerical solutions are presented in Fig. 4. In one case conventional type (CON. BC) boundary conditions are applied at the outer boundary. In the second case (EXP. BC) the conditions at the outer boundary were set based on experimental measurements

(see Ref. 21). It is important to note that when the experimental boundary conditions are correctly specified in the CFD code the agreement between experimental and computational pressure distributions is improved. All computations presented in Fig. 4 were performed with the ARC2D code.

Figure 5 shows pressure distributions about a RAE 2822 airfoil at 2.8 degrees angle of attack in transonic flow $M = 0.75$ obtained with the RTVD and MTVD codes. The grid size was 249×56 and the outer boundary was set 16 chords from the airfoil surface. Experimental data from Ref. 22 are also presented for comparison. The Baldwin-Lomax algebraic turbulence model and the one-equation model of Baldwin and Barth were used in the computations presented. The best correlation with the experimental data is obtained with the Runge-Kutta upwind TVD scheme and with the one-equation model (Run id: TORU). In this case the predicted shock location is approximately at $x/c = 0.6$ and is close to the location given by the experimental results. Boundary layer velocity profiles for the RAE 2822 test case are shown in Fig. 6. The one-equation turbulence model of Baldwin and Barth outperformed the Baldwin-Lomax algebraic model for all locations on the airfoil surface ($x/c=0.319, 0.75$ and 0.9). Note that the one-equation model predicts boundary layer separation behind the shock ($x/c=0.75$). The Baldwin-Lomax algebraic model does not predict separation in this case. The results of Fig. 6 indicate that both models performed poorly in the wake region ($x/c=1.025$).

In Fig. 7 experimental and computational pressure distributions about a NACA 0012 airfoil at $\alpha = 3.02^\circ$ in transonic flow, $M = 0.752$ are presented. The computations were performed with the MTVD code. The grid size was 262×70 and the outer boundary was 12 chords from the airfoil. The experimental results are from Ref. 22. Results obtained with non-linear dissipation are shown in Fig. 7A. Computations with upwind TVD dissipation are given in Fig. 7B. Note that in both cases the shock location and the overall shape of the pressure distribution are in good agreement with the experimental data.

Some guidelines regarding the application of the CFD codes described above to single element airfoils are given in the following.

- For viscous flow calculations C-grids work well. Grid densities of 300×90 points are sufficient for most single element configurations (Ref. 23). Typically 240 points should be placed on the airfoil and 60 on the wake giving a total of 300 points. These points should be clustered in regions of large flow gradients. In the normal direction the points should be clustered near the airfoil surface for predicting boundary layer properties. The first grid point along the normal to the airfoil surface should be 0.00002 to 0.00005 chord lengths. For most computations the outer boundary should be placed 12 to 16 chord lengths from the airfoil surface. The location of the outer boundary however, also depends on the type of boundary conditions used as explained below. Maintaining grid orthogonality is very important particularly near the airfoil surface. In the wake region near the airfoil trailing edge the size of grid cells along the x-direction must vary smoothly and must be of similar size to those on the airfoil. The guidelines regarding grid construction have been arrived at from subsonic and transonic flow computations with Reynolds numbers varying from 2 to 10 million and with Mach numbers from 0.13 to 0.8. Grids with lower point density such as 250×50 points can be used in preliminary computations of viscous flows. Lift coefficient and pressure distributions obtained from computations with lower point density grids are in general accurate however, the drag coefficient is not. For inviscid flow computations grids with 190×35 points are sufficient for capturing shocks and predicting pressure distributions. Smaller grids reduce computation times significantly.
- For viscous steady state computations, with the Beam and Warming implicit scheme used in ARC2D, time steps of the order of 1 to 10 times the time step based on the CFL condition (condition for numerically stable solutions see Ref. 12) can be used in most cases. With explicit schemes the time steps should be 0.3 to 2.0 the time step based on the CFL condition depending on the configuration studied and numerical scheme used. The second order Runge-Kutta scheme allows the use of larger time steps than the MacCormack scheme. TVD methods impose greater restrictions on time step size than non-linear dissipation. Typically 4000 to 6000 iterations are required for a steady state computation to converge with implicit schemes. With explicit schemes 15000 to 20000 iterations are typically required for convergence. The user must carefully evaluate C_l , C_d and pressure data before a decision is made to terminate the solution. Inviscid computations converge in substantially fewer iterations and allow larger time steps than viscous flows. This is true for explicit and implicit schemes.

- For inviscid flows with embedded shocks upwind TVD dissipation models provide better shock resolution than non-linear dissipation. For viscous flows TVD and non-linear dissipation have very similar shock resolution properties. In all cases, however, non-linear dissipation requires user inputs to adjust the level of dissipation. TVD schemes do not require such inputs. Generally, non-linear dissipation is computationally more efficient than upwind TVD schemes.
- The boundary conditions used at the outer (far field) flow boundary have a direct effect on the distance of this boundary from the airfoil surface. For lifting airfoils in subsonic flow the outer boundary should be placed 90 to 100 chords from the airfoil for accurate C_l calculations. This restriction in the placement of the outer boundary results in large grids and increases computational times. By imposing a compressible potential vortex solution at the far field boundary (Ref. 15), the outer boundary can be placed at 12 to 16 chords from the airfoil surface, reducing the grid size significantly.
- When comparing computational results with wind tunnel data it is important that the wind tunnel boundary conditions are modelled accurately (Ref. 21). In many cases disagreement between experimental and computational results is attributed to factors related to the numerical schemes used or errors in the experimental data. An important source of error which is often overlooked is the specification of the experimental boundary conditions in the CFD codes.
- The Baldwin-Lomax algebraic turbulence model is used in a number of CFD codes. Its main advantages are simplicity and robustness. However, this model has several limitations and behaves poorly in regions of separated flow. Turbulence models based on ordinary or partial differential equations can be used to better simulate turbulent flow properties. However, all turbulence models have limitations and in most cases some fine tuning is required to improve their performance. Occasionally the application of turbulence models based on differential equations can cause the solution to diverge. In some cases this problem can be rectified by starting the solution with the Baldwin-Lomax turbulence model and then switching to the differential model after a specified number of iterations. The one-equation turbulence model of Baldwin and Barth was tested with several transonic airfoil configurations and was found to perform well.

Computation times for a single element airfoil on the IBM ES 9000/400 mainframe computer are of the order of 7.00×10^{-5} CPU seconds per iteration per grid point. Thus for a grid of 300×90 points and for 10,000 iterations a total of approximately 5 hours of CPU time is required to obtain a converged solution. The times given are for the RTVD code with non-linear dissipation and with the one-equation model of Baldwin and Barth. The computer memory for loading and executing RTVD is in the range of 10 to 16 Megabytes depending on the grid size. For most CFD codes the grid, flow and plot files must be saved for future use. This typically requires 6-8 Megabytes of disk storage per test run for a grid of 300×90 points.

Multi Element Airfoils

Subsonic flows around 3 and 4 element airfoils have been analyzed using the NS72 code. Slat and flap deflections for the 3 element configuration were set to 20° and 10° respectively which correspond to a typical take-off configuration. Both viscous and inviscid flowfield calculations were made at a Mach number of .2 and a Reynolds number of 9,000,000.

A series of 4 unstructured triangular grids with different numbers of grid points were generated for each airfoil. For the 3 element configuration, the coarsest grid had 600 nodes while the finest grid had 42,000 nodes. All four grids were used by the multi-grid solution algorithm of NS72. A close-up view of the fine grid used with the 3 element airfoil is shown in Fig. 8. Generation of all four grids required about 2 hours of CPU time on a Convex computer and a Silicon Graphics Iris workstation.

Computed and experimental pressure distributions for the three element airfoil at $\alpha = 12.145$ deg are shown in Fig. 9. The computed solutions include an inviscid analysis, a viscous analysis with a laminar boundary layer, and a viscous analysis with a turbulent boundary layer. All three solutions were obtained using the same grid. Lower surface pressures are in good agreement with experimental results for all three computational solutions, even in the separated cove regions of the slat and main element. Upper surface pressures show a slight discrepancy between experiment and the viscous solutions. The difference is larger for the turbulent analysis which is surprising since experiment showed that the boundary layers on each

element were either fully turbulent or transitioned very near the leading edge. Interestingly, the inviscid (Euler) solution matched the experimental data quite closely. Generally, minimum pressures obtained from inviscid solutions are lower than the minimum pressure obtained experimentally.

The discrepancy between experiment and the turbulent solution may have been caused by a combination of factors. First, the computed results were produced using free-stream boundary conditions while the experimental results were obtained in a wind tunnel and may have been influenced by interference from the upper and lower tunnel walls. Had the upper and lower walls been modelled in the computations, the results may have matched more closely. Second, it is difficult to get 2 dimensional flow in a wind tunnel, and 3 dimensional flow patterns may have effected experimental pressure distributions. Third, the turbulence model used in this code was not designed to handle the complex interactions of merging boundary layers found in most multi-element airfoil flows and may be incorrectly predicting shear layer mixing.

Experimental and computed lift curves are shown in Fig. 10. The computed values were obtained using the viscous analysis with a turbulent boundary layer. From the numerical results, stall occurred at an angle of attack between 19.0° and 19.9° . Experiments indicated stall around 20.2° . The discrepancy between experiment and computed lift values range from 4 to 8%.

A very large difference between computed and experimental drag was found as seen in Fig. 10. Computed pressure drag was obtained by integrating pressure around the airfoil. Skin friction drag is the difference between total drag and pressure drag. The large discrepancy between computed pressure drag and experiment seems odd since the pressure distributions match fairly closely. Further investigations on the drag differences are being conducted.

Distance from the airfoil to outer boundary was varied from 12 to 20 chords with a negligible effect on the flowfield. Also, the effects increasing and decreasing numerical damping were investigated. Large changes in damping had little effect on the flowfield.

The program typically converged in 300 multi-grid cycles. Four grids were used in each cycle for the three element airfoil. The number of nodes in these four grids were 600, 2400, 9600 and 42000. For the 3 element airfoil, approximately 3200 seconds of CPU time on a CRAY 2 computer were required for convergence. For the 4 element airfoil, 4300 seconds were required to complete 300 multi-grid cycles. The fine grid in this case had a total of 52000 nodes.

Missile Body

In this section preliminary results for a 3-caliber ogive-cylinder missile body are presented. The body was 270 mm long and the diameter (D) of the cylindrical portion was 30mm. Inviscid and laminar viscous computations for $\alpha = 20^\circ$ and for a Mach number of 2 were performed using the ARC3D computer code. The Reynolds number based on the diameter of the missile was 0.16×10^6 . Computational results are compared with the experimental data of Ref. 24 in Fig. 11. In this figure circumferential static pressure distributions at various axial (X/D) locations are given for laminar flow. The circumferential angle is zero at the leeward side of the missile and 180 at the windward side. Overall, agreement between experiment and computations is very good. The location of laminar separation predicted by the computations, however, is closer to the leeward side than the corresponding location given by the experimental data. This discrepancy is due to the uniform grid spacing along the circumferential direction. Grid points should be clustered near the separation point. The grid used had 55 points in the axial direction, 70 points in the circumferential direction, and 65 points in the normal direction. Points were uniformly spaced axially and circumferentially. Exponential stretching was used in the normal direction. The outer boundary of the computational domain was set 8 diameters from the missile body. Only half of the missile body was modeled in these computations due to flow symmetry. The grid was constructed with a simple algebraic grid generator. Results from the inviscid computations show similar trends as the laminar computations but do not correlate as well with the experimental data. It is not clear what mechanism causes separation in the inviscid computations.

Upwind TVD dissipation was used in all computations. The time step was 0.5 times the time step based on the CFL condition. Approximately 2500 iterations were required for the laminar solution to converge. The corresponding CPU time on the IBM ES 9000/400 mainframe was 50 hours or 2.9×10^{-4} seconds per grid point per iteration. Inviscid computations conducted on the $55 \times 70 \times 65$ grid converged in approximately 1200 iterations. The CPU time for the inviscid computations was 24 hours on the IBM ES 9000/400 mainframe. Typically inviscid computations can be performed with coarser grids. In this study the same grid was used so that CPU times can be compared on a per grid point basis for the inviscid and viscous computations. Approximately 60 Megabytes of computer memory were necessary to load and run

this test case. Approximately 18 Megabytes of disk storage were required to store the grid and output files for each test run.

Summary

Several aerodynamic configurations have been studied with a number of CFD codes on a variety of computer platforms. Descriptions of the computer codes used in this study have been presented. The significance of various code parameters and their influence on the numerical solution and guidelines regarding the application of the computer codes described to single and multi-element airfoils were discussed. Results from a simple three dimensional ogive-cylinder configuration were also presented. In summary the CFD codes used in this investigation can accurately predict detailed flow properties for a range of aerodynamic configurations. Users, however, must have a good understanding of how to set the various code parameters which control the solution process and how to define conditions at flow boundaries. Future efforts should be directed toward validation of existing codes and in making CFD codes more robust and user friendly. Efforts should also be devoted to automating the grid generation process and in providing criteria for assessing the quality of computational grids.

References

1. Sorenson, R.L., "A Computer Program to Generate Two-Dimensional Grids About Airfoils and Other Shapes by the Use of Poisson's Equation," NASA Technical Memorandum 81198, May 9180.
2. Sorenson, R.L., "The 3DGRAPE Book: theory, User's Manual, Examples," NASA TM-10224, July 1989.
3. Lijewski, L.E., et al., "Program Eagle User's Manual," AFATL-TR-88-117, Air Force Armament Laboratory, Air Force Systems Command, Eglin Air Force Base, Florida, September 1988.
4. "The GRIDGEN 3D Multiple Block Grid Generation System, Volume I: Final Report," WRDC-TR-90-3022, DTIC AD # B148 627 L, Defense Logistic Agency, Defense Technical Information Center, Building 5, Cameron Station, Alexandria, VA 22304-6145.
5. "PLUTO : 3D Grid Generator User's Manual," WL-TM-91-312, Defense Logistic Agency, Defense Technical Information Center, Building 5, Cameron Station, Alexandria, VA 22304-6145.
6. "RAMBO-4G: An Interactive General 3-D Multi-block Grid Generation And Graphics Package For Complex Multi-body CFD Applications," ATR-91(9990)-1, Defense Logistic Agency, Defense Technical Information Center, Building 5, Cameron Station, Alexandria, VA 22304-6145.
7. Baldwin, B. S. and Lomax, H. , "Thin Layer Approximation and Algebraic Model for Separated Turbulent Flows," AIAA Paper 78-275, 1978.
8. Mavriplis, D., "Algebraic Turbulence Modelling for Unstructured and Adaptive Meshes," AIAA 90-1653, 1990.
9. Baldwin, B. S. and Barth, T. J., "One-Equation Turbulence Transport Model for High Reynolds Number Wall-Bounded Flows," AIAA Paper 91-0610, 1991, Reno.
10. Mitcheltree, R.A., Salas, M.D. and Hassan, H.A., " One-Equation Model for Transonic Airfoil Flows," AIAA Journal, Vol. 28, pp. 1625-1632, September 1990.
11. Narayan, J.R., " A Two-Equation Turbulence Model for Compressible Reacting Flows," Paper AIAA-91-0755, January 1991.
12. Hoffmann, K.H., "Computational Fluid Dynamics for Engineers," A Publication of Engineering Education System, Austin, Texas 78713.
13. Reddy, S., Klausmeyer, S., Liu, X. and Papadakis, M., " TVD Formulations of the 2D Navier-Stokes Equations for Airfoil Analysis," SAE Technical Paper 910992, 1991 SAE General, Corporate, and regional Aviation Meeting, Wichita, Kansas, April 9-11, 1991.

14. Reddy, S., Papadakis, M., and Liu, X., "Transonic Airfoil Analysis by Explicit TVD Formulations of the Navier-Stokes Equations," AIAA 91-3334, AIAA 9th Applied Aerodynamics Conference, Baltimore, Maryland, September 23-25, 1991.
15. Pulliam, T.H., "Solution Methods In Computational Fluid Dynamics," NASA Ames Research Center, January 1986
16. Mavriplis, D. , Jameson, A., Martinelli, L., "Multigrid Solution of the Navier-Stokes Equations on Triangular Meshes," AIAA 89-0120, 1989.
17. "FIELDVIEW," Intelligent Light, P.O. Box 65, Fair Lawn, N.J. 07410
18. Walatka P.P., Buning, P.G., Pierce, L., and Elson, P.A., "PLOT3D User's Manual," NASA Technical Memorandum 101067, March 1990.
19. Wattson, V., Merritt, F., Plessel, T., Bancroft, G. and Walatka, P., "Visualisation of Fluid Dynamics at NASA Ames," The Numerical Aerodynamics Simulation Program Newsletter, Vol. 5, No.10, October 1990, Ames Research Center, MS 258-6, Moffett Field, California 94035.
20. "COSMIC," Customer Support Department, 382 East Broad St., Athens, GA 30602.
21. Papadakis, M. and Miller, L.S., "Experimental and Computational Investigation of Wind Tunnel Effects on Airfoil Flow Fields," Paper AIAA 92-0672, 30th Aerospace Sciences Meeting, Reno, Nevada, January 6-9, 1992.
22. "Experimental Data base for Computer Program Assessment," AGARD-AR-138, May 1979.
23. Zingg, D.W., "Grid studies for Thin-Layer Navier-Stokes Computations of Airfoil Flow-fields," Paper AIAA 92-0184, 30th Aerospace Sciences Meeting, Reno, Nevada, January 6-9, 1992.
24. Pagan, D. and Molton, P., "Basic Experiment on a Supersonic Vortex Flow Around a Missile Body," Paper AIAA-91-0287, January 1991.

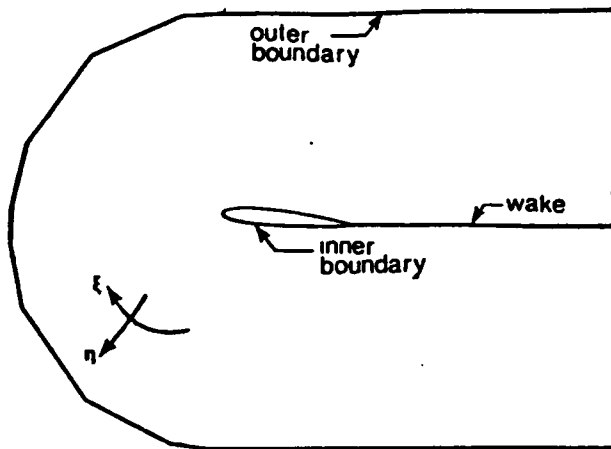


Fig. 1 C-Grid Topology

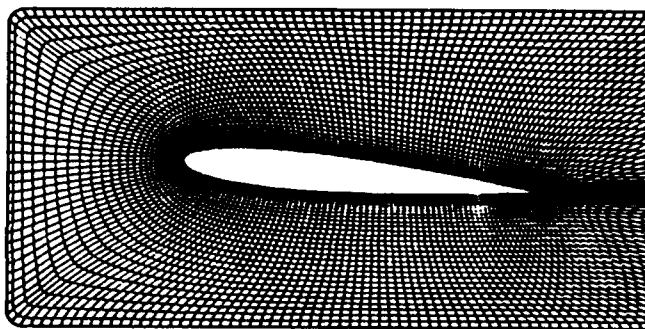


Fig. 2 Elliptic C-Grid about NACA 0011 Airfoil (Close-Up)

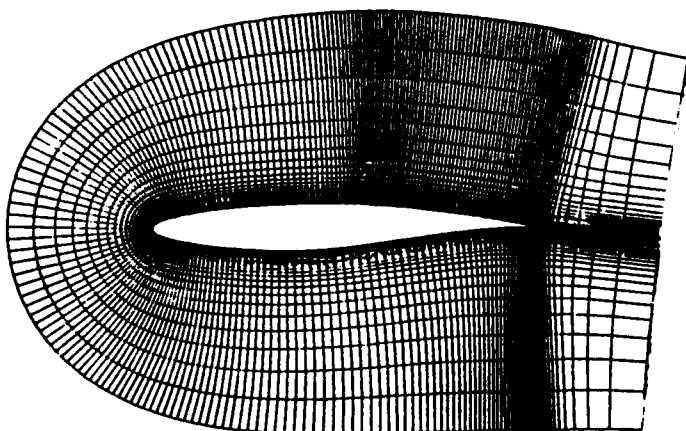
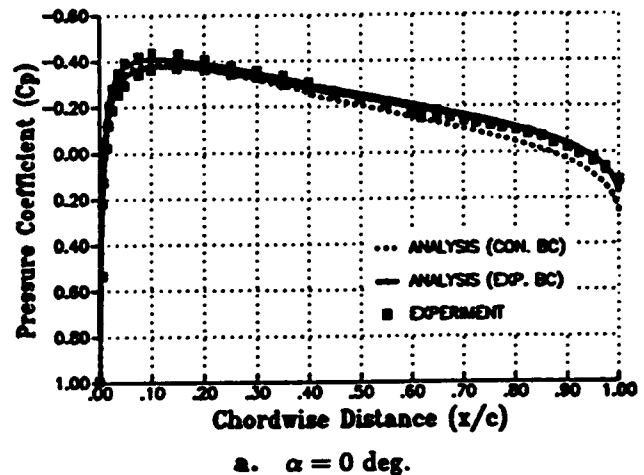
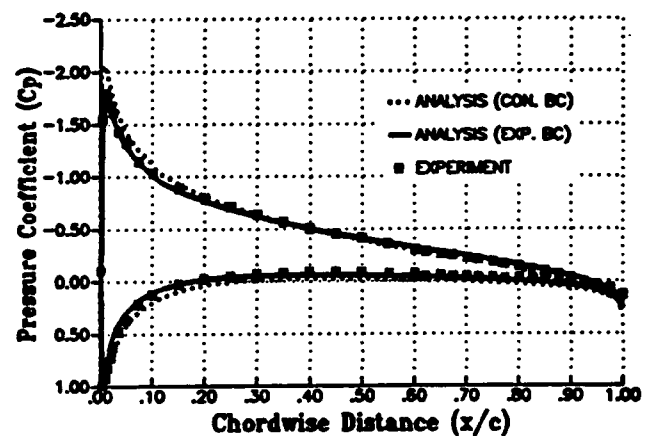


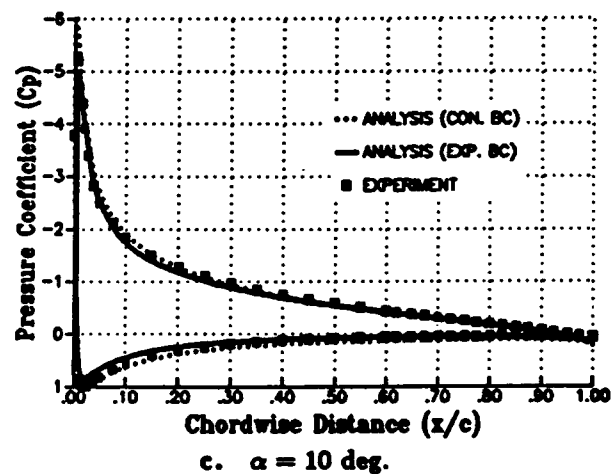
Fig. 3 Hyperbolic C-Grid about RAE 2822 Airfoil (Close-Up)



a. $\alpha = 0$ deg.



b. $\alpha = 5$ deg.



c. $\alpha = 10$ deg.

Fig. 4 Comparison of Experimental and Computational Pressure Coefficients for NACA 0011 Airfoil $M=0.13$, $Re = 2.2 \times 10^6$.

(Experiment - $C_L=0.743$, $C_D=0.0242$, from Ref. 22)

Run ID	C_L	C_D	Integration Scheme	TVD Scheme	Turbulence Model	CFL	Iteration Number
TARU	0.8879	0.0502	Runge-Kutta	Upwind	Algebraic	0.20	12500
TARU ¹	0.8618	0.0458	Runge-Kutta	Upwind	Algebraic	0.20	22500
TORU	0.8351	0.0407	Runge-Kutta	Upwind	One Equation	0.50	10500
TARS	0.9096	0.0587	Runge-Kutta	Symmetric	Algebraic	0.20	12600
TORS	0.8636	0.0439	Runge-Kutta	Symmetric	One Equation	0.50	12500
TAMU	0.8435	0.0436	MacCormack	Upwind	Algebraic	0.35	12000
TAMS	0.8590	0.0470	MacCormack	Symmetric	Algebraic	0.35	12000

1 - Results from this run are not presented in any of the figures.

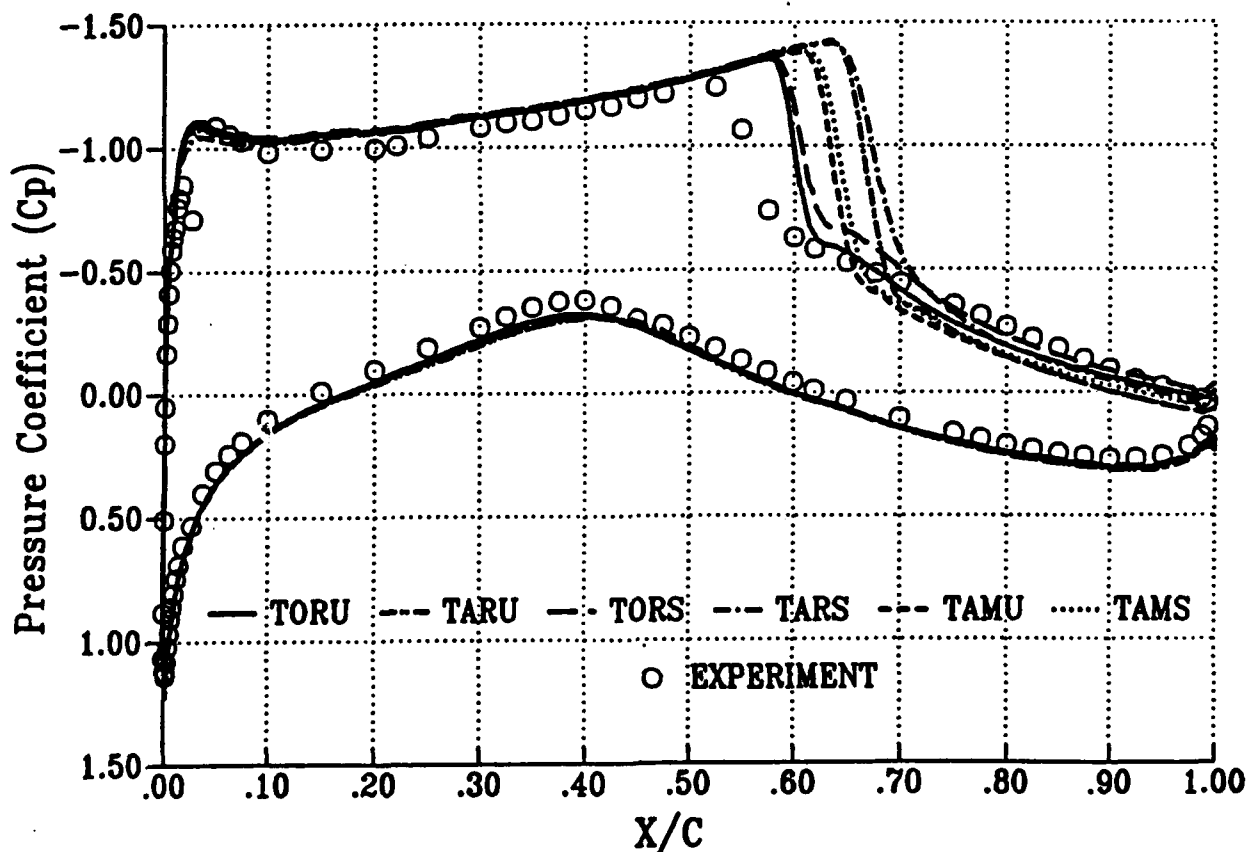


Fig. 5 Comparison of Experimental and Computational Pressure Distributions for RAE 2822 Airfoil Section ($\alpha = 2.8^\circ$, $M = 0.750$, $Re = 6.2 \times 10^6$).

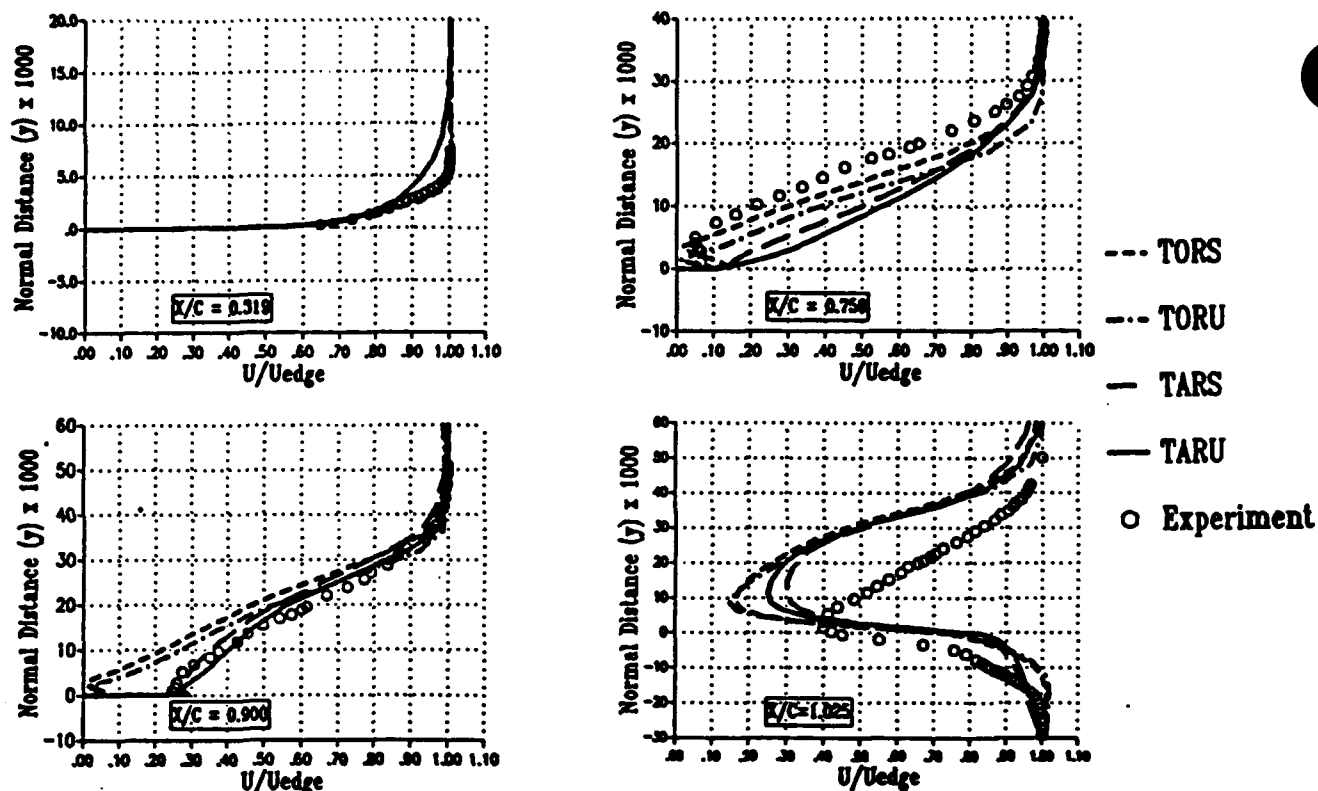


Fig. 6 Comparison of Experimental and Computational Boundary Layer Profiles for RAE 2822 Airfoil Section, $\alpha = 2.8^\circ$, $M = 0.750$, $Re = 6.2 \times 10^6$, (TORS, TORU, TARS and TARU are defined in Fig. 5)

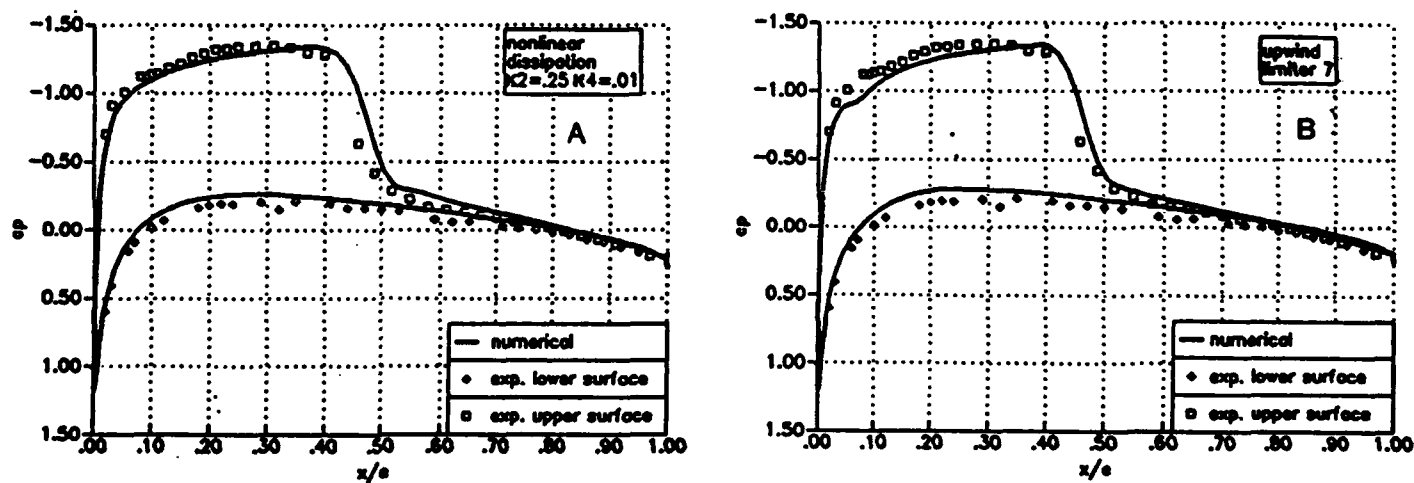


Fig. 7 Comparison of Experimental and Computational Pressure Distributions for NACA 0012 Airfoil Section, $\alpha = 3.02^\circ$, $M = 0.752$, $Re = 9.0 \times 10^6$,
A. Explicit MacCormack Scheme with Non-linear Dissipation
B. Explicit MacCormack Scheme with Upwind TVD Dissipation

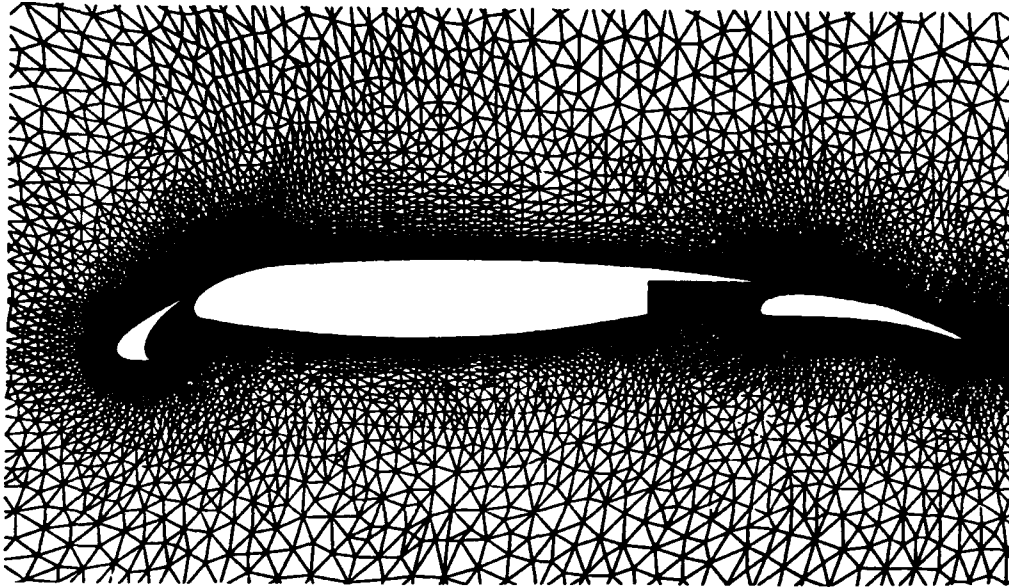


Fig. 8 Unstructured Triangular Grid for Three Element Airfoil (Close-Up)

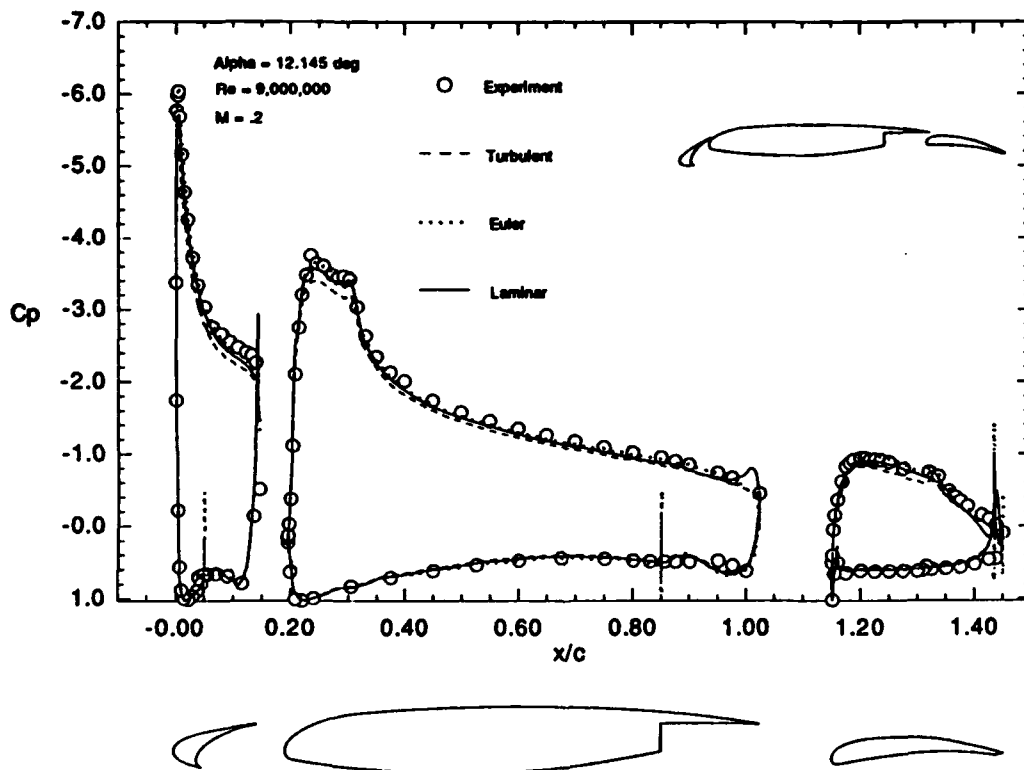


Fig. 9 Comparison of Experimental and Computational Pressure Distributions for Three Element Airfoil, $\alpha = 12.145^\circ$, $M = 0.20$, $Re = 9.0 \times 10^6$.

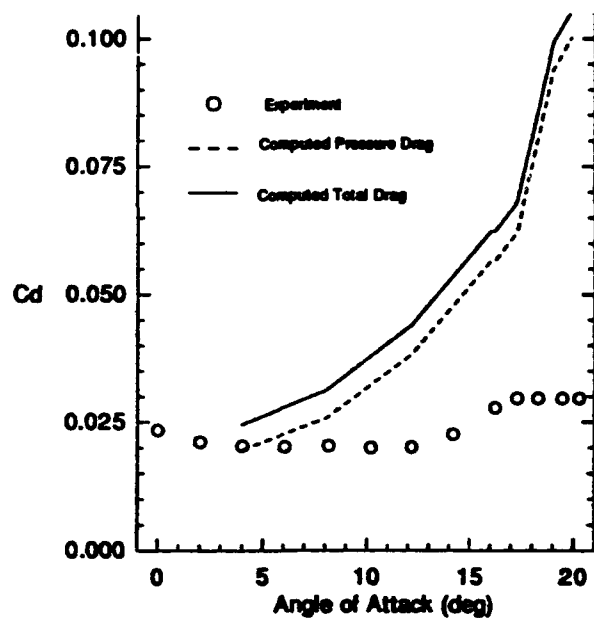
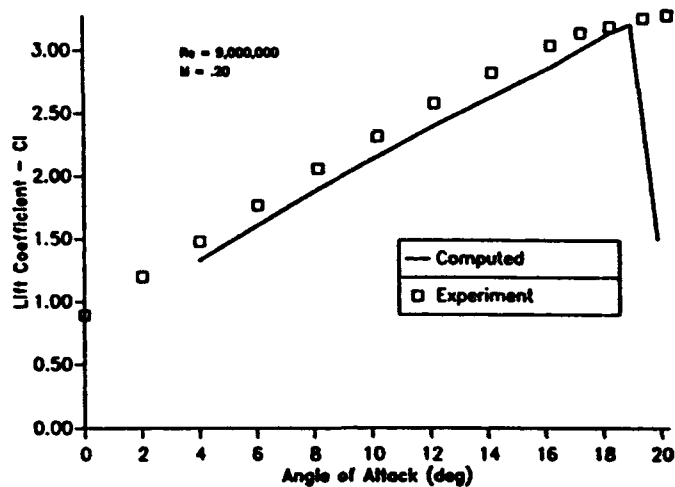


Fig. 10 Lift and Drag Coefficients for Three Element Airfoil, $M = 0.2$, $Re = 9 \times 10^6$.

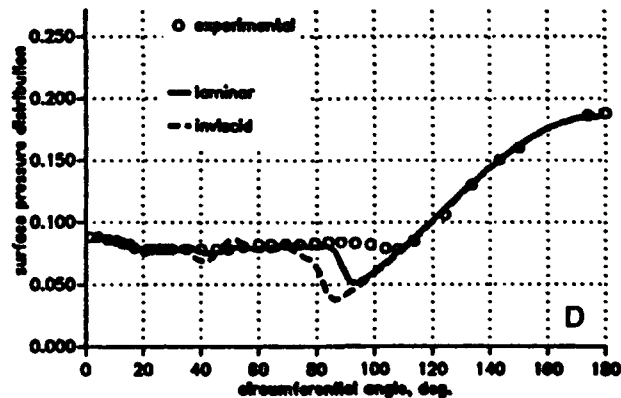
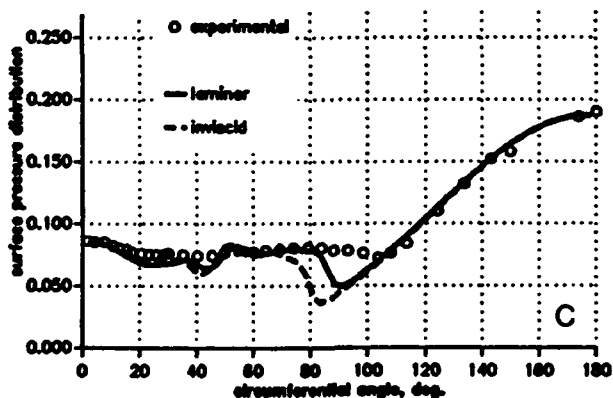
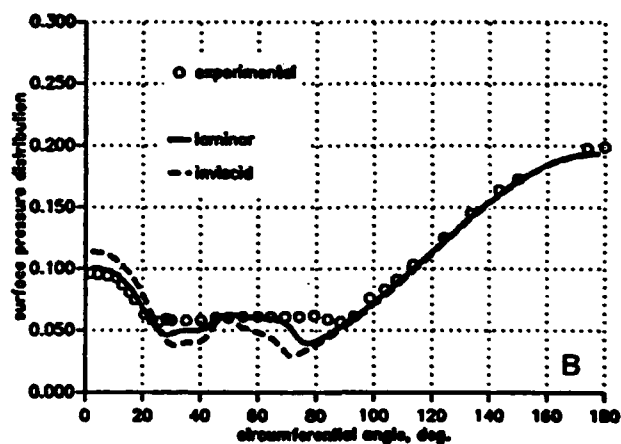
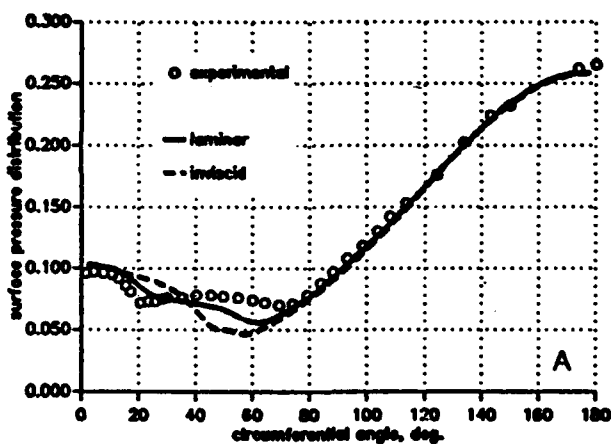


Fig. 11 Comparison of Experimental and Computational Pressure Distributions for 3-Caliber Ogive, $\alpha = 20^\circ$, $M = 2$, $Re_D = 0.16 \times 10^6$,
A. $X/D = 2$, B. $X/D = 4$, C. $X/D = 6$, D. $X/D = 7$.

**AN AERODYNAMIC COMPARISON OF G A FACTORY &
AMATUER BUILT AIRCRAFT**

by

**Shadid Siddiqi
Jeffery Viken
Analytical Services and Materials**

NO COPIES AVAILABLE

**For Presentation to the AIAA/FAA Joint Symposium on General
Aviation Systems at the Hilton Inn-East, Wichita, KS
on March 16-17, 1992**

EVALUATION OF FIVE DISPLAYS FOR AIRCRAFT GUIDANCE

by

**Saeid Mirsafian
M.G. Nagati
Aerospace Engineering Department
Wichita State University
Wichita, Kansas 67208**

**For Presentation to the AIAA/FAA Joint Symposium on General
Aviation Systems at the Hilton Inn-East, Wichita, KS
on March 16-17, 1992**

EVALUATION OF FIVE DISPLAYS FOR AIRCRAFT GUIDANCE

by

Saeid Mirsafian and M.G. Nagati
Aerospace Engineering Department
Wichita State University

Abstract

The intensity of pilot workload in the cockpit has been a major factor in the cause of air traffic accidents. The occurrence of pilot error is greatly increased when considering normal to severe IFR conditions with the absence of a co-pilot. The pilot has to process the incoming information from the instruments and the control tower. Then, he has to make a decision based on his judgement of the situation and perform the appropriate response based on judgement. The increase in workload effects the pilot's judgement thus increasing the probable occurrence of pilot error. Therefore, it is necessary to give the pilot the information needed in an efficient form so as to reduce the workload in the cockpit.

Five advanced displays were evaluated in the National Institute for Aviation Research flight simulator. The displays include 3 head up displays and two displays that could be implemented as either head up or head down displays. The latter two displays depend on the auto-pilot for operation and are similar to a flight director in which they guide the pilot by presenting him with the control surface deflection necessary to stay on course. The other three displays are independent of the autopilot and present an image of the path the pilot must follow or simply show the pilot a visual representation of the airport.

Several subject pilots with extensive to low IFR experience were used to evaluate the displays. For each display, the pilots flew a simulated IFR approach to runway 12L at St. Louis Lambert International Airport. The trajectory of the approach was plotted and the exceedance errors were recorded for each pilot. A questionnaire was designed to rate the displays using the Cooper/Harper scale for display characteristics. The feedback from the pilots and the experimental data collected during each approach were used to determine the most effective of the five displays for single pilot IFR operation.

INTRODUCTION

Single pilot flight is a demanding task specifically in IFR conditions, which require the pilot's divided attention on controls, reception and processing of data from the instruments, and communication with the control tower. The intensity of these activities can influence the pilot's judgement and decision; in addition, other factors such as severity of the weather elements or disorientation of the pilot highly contribute to the workload in the cockpit. Flights near or around thunderstorms and in gusty conditions certainly increase the workload on the pilot by requiring him to process the incoming information and make decision at a faster rate. Also, the judgement of the pilot is affected by false visual or sensing of the inputs from the instruments and the outside view. Vestibular sensations contribute to this effect. A classic example of such is vertigo, in which, the pilot falsely senses that the aircraft is in a turn while the instruments indicate a level flight. The heavy workload in a single pilot IFR flight is one of the chief causes of most general aviation accidents as noted in reference (1).

To increase the safety of IFR and VFR flight, it is desirable to supply information to the pilot in a better and more useful way than what the current cockpit instruments offer. Advanced visual instruments are needed to cope with this problem. Most of today's cockpit instruments offer the pilot only one type of information. Due to the lack of outside visual queues in an IFR approach, the pilot must conduct constant visual scans of the instruments to ensure that the proper attitude, airspeed, and altitude are reached and maintained. Regarding other tasks in the cockpit, the instrument scan is a rigorous effort for the pilot because he must process the information available. An advanced visual instrument should reduce or eliminate the pilot's task of scanning the other instruments. The display must present the pilot with all of the necessary information for the approach to be carried out effectively. This information must be arranged and organized in such a way that the pilot can determine deviations in attitude, airspeed, altitude, and perhaps other necessary data by a glance at the display. Furthermore, these displays should be able to reduce the workload in the cockpit when flying under VFR conditions. The success of these displays is highly dependent on their interface with the pilot. With the current electronic technologies, it is possible to create such a display in which it presents the good interface with the pilot.

The purpose of this work is to evaluate several such displays for single pilot flight and to investigate the displays' effectiveness in simulated IFR flights. The experiments consisted of flight tests conducted by several subject pilots with extensive to no IFR experience. The trajectory of each flight was recorded and plotted in order to determine the effectiveness of the displays for each pilot and to provide qualitative evaluation to be correlated with the pilot opinion rating. The Cooper-Harper scale from reference (2) was adopted to conduct pilot opinion rating. Also, pilot comments and suggestions were used for comparison with the experimental data to measure the effectiveness of the display and to consider improvements and further developments.

FLIGHT SIMULATION

The aircraft modeled in this experiment was a twin engine turboprop commuter described in reference (3) and (4). The non-linear Euler equations of motion with linear aerodynamics were used for the simulation. The autopilot was

designed using full state feedback without a Kalman Filter. The feedback gains were determined by solving the algebraic Riccati equation.

For the longitudinal and lateral axes, random gust was generated using the computer's random number generator, considered to be white noise, then filtered to produce the Dryden gust spectrum.

The purpose of the Head Up Displays (HUD) is to replace or supplement the conventional VOR instrument by indicating the localizer-glideslope offset to the pilot in a way as to eliminate the high workload associated with an landing approach, to reduce the sensitivity when approaching the runway, and to effectively combine the output of several instruments and display that information to the pilot.

The display consisted of a minimal instrument panel with the following components: An airspeed indicator, a vertical speed indicator, an altimeter, thrust indication, a compass, and a VOR or a localizer-glideslope instrument. These instruments were projected on the screen as a HUD to complement the head up displays which were evaluated. Five head up displays (HUD) were evaluated by several subject pilots. Two of the displays require the autopilot output for operation, while the other HUDs require only navigation data. The Control-box display could be implemented both as a HUD or a head down display and requires the aid of the autopilot. The other displays are 3 dimensional images which, with the aid of a head up display system similar to the units used in fighter aircraft or a visor worn by the pilot, superimposed on the outside view.

Control-box

This display consists of two rectangles or boxes on the screen. The red box is stationary at all times and serves as a reference for the control surface deflections of the aircraft. The simulator autopilot calculates the necessary control inputs to eliminate the course deviation. These control inputs required by the autopilot are translated into the position and orientation of the blue box.

Tunnel

This display, uses a series of equally sized rectangles projected from the touch down point of the runway at an angle equal to the glideslope angle of the ILS system. These rectangles are viewed as a tunnel and should line up when the aircraft is on the glideslope.

Airport Image

This display consists of an outline of the runway, two parallel lines, runway width apart, extending from the runway up to the outer marker beacon, and the marker beacons.

EXPERIMENT PROCEDURE

The approach flown by all pilots is described in reference (5). When the approach was completed, each pilot was asked to fill out a questionnaire given in reference (5). The questionnaire included questions concerning the approach and the display. Furthermore, the pilots were asked to write their comments about the advantages and disadvantages of the display in IFR flight, give general comments about the display, and to use an adaptation of the Cooper-Harper rating scale to give an overall evaluation of the display. For each pilot, information concerning the

approach were recorded. This information included: The x, y, and z position of the aircraft at 2.5 second time steps and the path error from the localizer and glideslope line. The x, y, and z position and the deviation from the localizer-glideslope line were used to plot the approach trajectories for each pilot and flight.

RESULTS

Control-box

The Control-box display was determined to be one of the best displays among the five HUDs. Figure (1) shows the descend trajectory plot for all pilots performing an approach with the Control-box display. The largest course deviation occurred when transitioning from cruise to approach configuration. Once the aircraft had transitioned, the pilots spent a few seconds to establish on the localizer and glideslope using the Control-box.

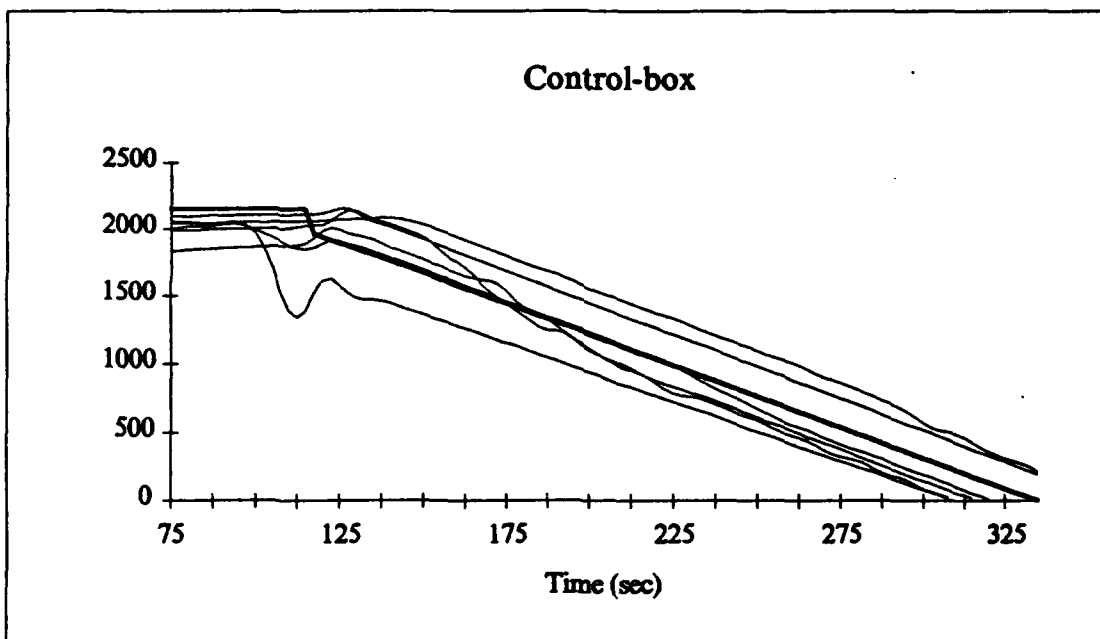


Figure (1)

Pilot comments on the Control-box display were as follows:

The attitude and bank angle are difficult to determine with this display.

The display is very effective in localizer and glideslope interception.

The display is highly effective in reducing instrument scans and performing an approach with this display requires fewer instruments.

Very precise approaches can be performed using this display.

Lower workload than the conventional two needle localizer-glideslope instrument.

Easier transition to a visual approach near the runway.

Once established on the approach, continuous course correction is required.

Requires other supporting information to complete such as heading, attitude, and airspeed information..

It requires too much attention and the other instruments tend to be ignored.

Requires DME information.

All pilots indicated that performing an instrument approach with the Control-box is easier than the conventional localizer-glideslope instrument, but very small course corrections are needed continuously to stay on the precise track. All subject pilots expressed uncertainty in aircraft position relative to the airport when concentrating on flying a precise approach with the Control-box. They also commented that the box does not indicate any information about attitude and bank angle and since it requires continuous attention, they tend to ignore the other essential instruments such as the airspeed indicator. Most pilots performed the approaches very efficiently using the Control-box display with minimal training when compared to the Tunnel or the Airport Image display.

Tunnel

The Tunnel display was one of the most difficult displays to follow according to almost all of the subject pilots. The descend trajectory plot in figure (2) shows this approach performed using this display by all of the test pilots. The descend line is never smooth, showing that the pilots' workload was high. They were continuously compensating to keep the aircraft on the right track. At several points in the trajectory, the flight line crosses the localizer-glideslope line showing the overshoot experienced by the pilots when trying to establish the aircraft on a descend inside the tunnels. The trajectory plot shows high oscillations during the last few seconds of the approach when the aircraft is very close to the runway. As the aircraft approached the touch down point, the pilots over compensated to achieve the correct course. This reaction was common among most of the pilots, which is due to the high visibility of the runway and its markings.

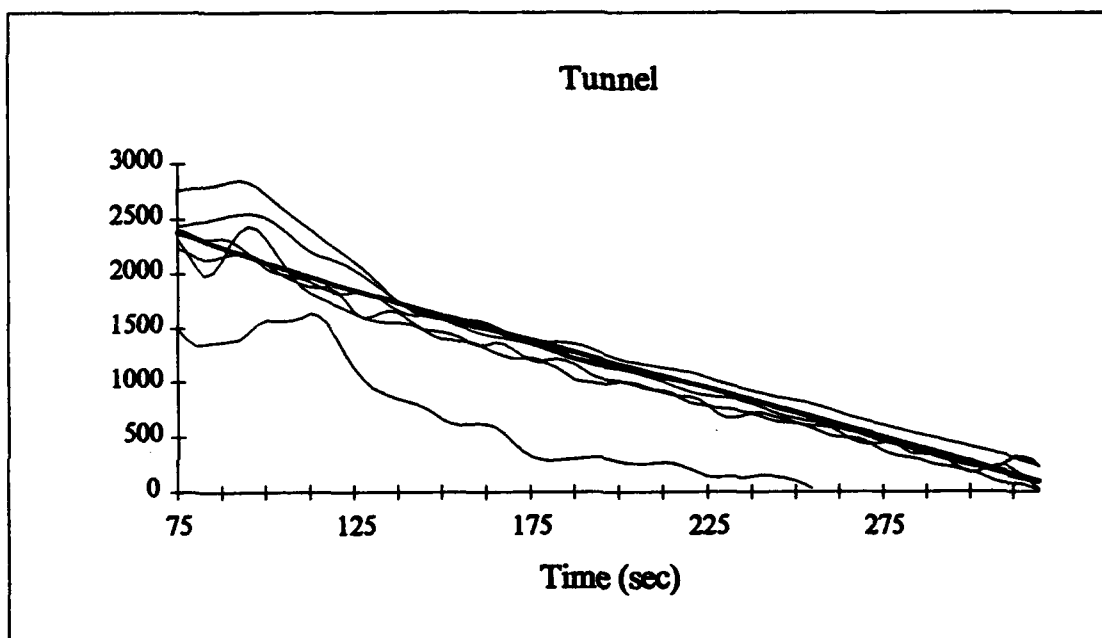


Figure (2)

Pilot comments on the Tunnel display were as follows:

Deficiencies in bank angle and attitude determination. More effective than the

Control-box display.

Very effective in localizer-glideslope interception.

Reduced workload when tracking the localizer-glideslope, but difficult to stay on course or to fly through the tunnel.

Good visual representation of the runway location and heading with respect to the aircraft.

Good visual representation of the airport location and runway heading.

Good visual representation of the course offset or deviation.

Difficult to establish on the approach. Always chasing the next box.

Leads to overcorrection and constant oscillations.

Very difficult to track localizer. Glideslope tracking is easier.

The pilot comments correlate with the results obtained from the trajectory and exceedance plots. This display was very difficult to fly for most of the pilots. The difficulty was higher in tracking the localizer (lateral direction) than tracking of the glideslope. When the aircraft had initiated on the approach, the thrust was set at the thrust value required for a 3 degree descend. This feature of the simulator made the glideslope tracking easier. Furthermore, the small size of the rectangles added to

the difficulty of the tracking. Several pilots mentioned that the glideslope-localizer tolerance of the Tunnel display is very small, so they were actually attempting to fly a very high precision approach with no course deviation. This is a very difficult task for any pilot. The display was praised for its visual representation of the airport location and runway heading. There is no position uncertainty when flying with this display, since the display can to a high degree of accuracy feedback to the pilot his distance from the airport, his location relative the landing runway, and the path he needs to follow to intercept the runway.

Airport Image

All subject pilots considered this display to be the most difficult to use as an essential instrument for an approach or a replacement for the localizer instrument. The pilots flew the approach with this display, but they heavily relied on the localizer-glideslope instrument. Figure (3) shows the descend trajectory performed by all of the subject pilots using this display.

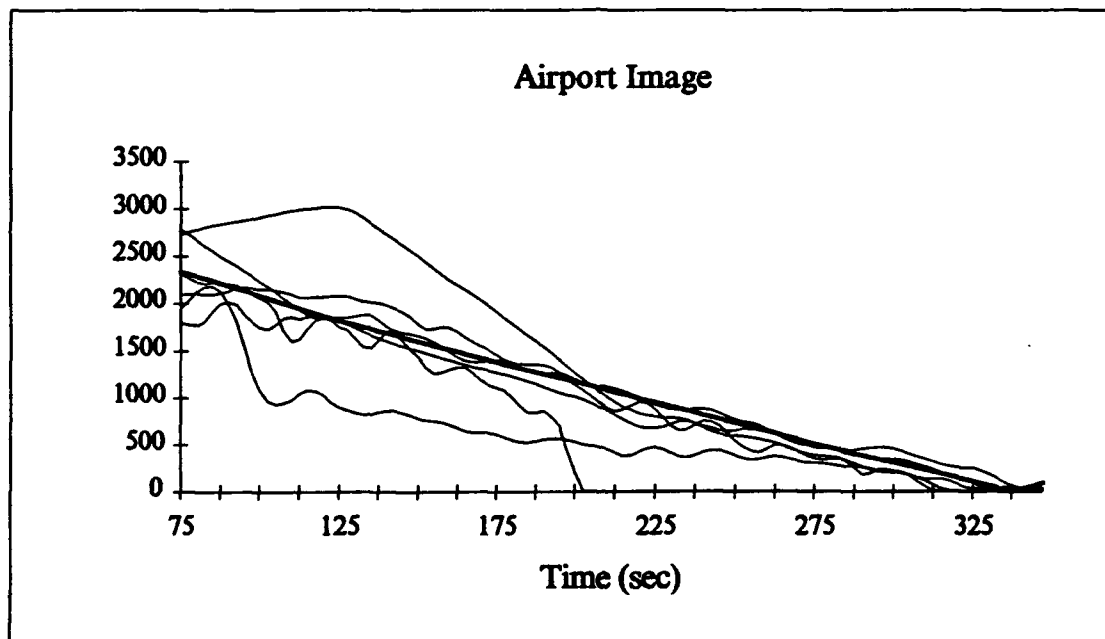


Figure (3)

The Airport Image and the line extending from it served only as a reference in which it informed the pilots of the location of the airport, the aircraft's approximate distance from the runway, and the localizer offset distance. Some of the other subject pilots relied on this display extensively during their approach procedure. The airport image only gives a visual representation of the airport. Also, approximate distance from the runway can be estimated. However, other instruments including a localizer-glideslope guidance instrument is required for a precision approach.

Pilot comments on the Airport Image display were as follows:

Poor indication of bank angle and attitude of aircraft.

Good visual representation of the localizer-glideslope interception point and the marker beacons but will not yield accurate localizer-glideslope capture.

Good visual representation of the airport and runway heading. Minor deficiencies in determining distance from the airport and the deviation from the localizer line.

The pilot would be able to visually track the runway presentation when the aircraft is close to touchdown.

Good position determination with respect the airport and the marker beacons.

Poor visual cues of the intercept angle.

Difficult to align the aircraft with the line due to the small line width.

Difficult to align for localizer interception.

The difficulty to align the aircraft with the line as mentioned by the pilots is due to the perspective view of the simulator image. This problem can be corrected by widening the line. Runway orientation, airport location, and marker beacon locations are the only information given by this display. Thus, it can only be used in conjunction with all other instruments necessary for an IFR approach. If used as a reference display, all subject pilots commented that they would like to have such a display available.

Control-box plus Airport Image

The best display of the five HUDs. The descend performance for all pilots performing with this display is shown in figure (4).

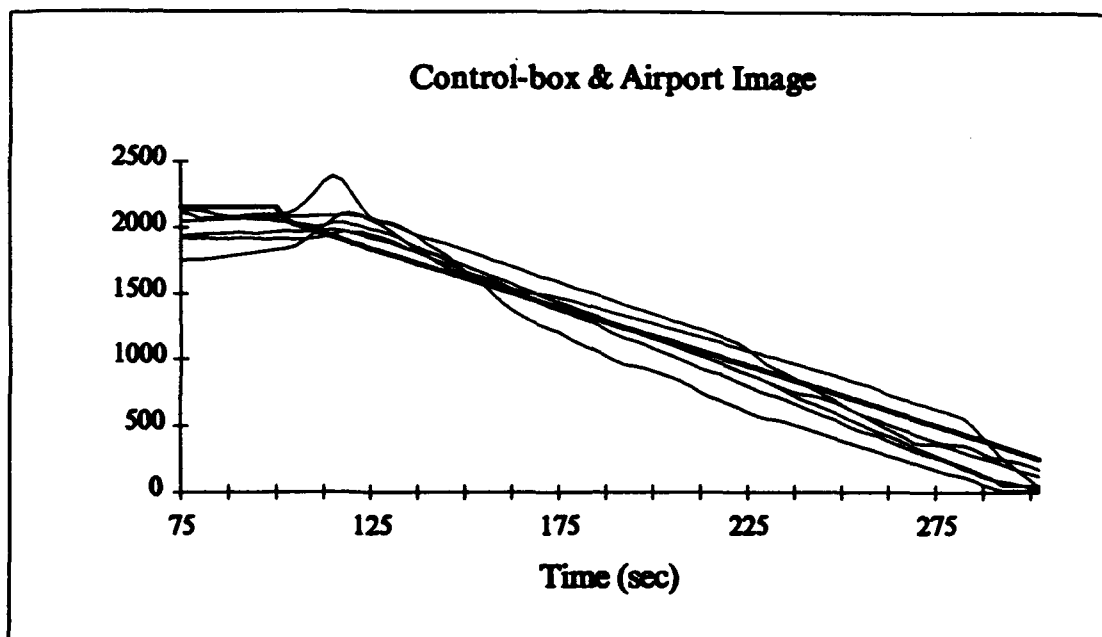


Figure (4)

As seen in the plot of the glideslope trajectory above, the pilots performed extremely well during the approach. The first several seconds of the flight, where transition from cruise conditions to approach conditions were made, shows the stable behavior of this display. Unlike the Control-box display alone, the transition is not oscillatory. The aircraft was slowly established on the approach with no course deviation or oscillation. When course was intercepted, most of the pilots flew the remaining part of the descend with very high precision.

Pilot comments on the Control-box and the Airport Image display are as follows:

Better attitude and bank angle determination than the Control-box.

Localizer-glideslope interception is easier than all other displays.

Good reduction in instrument scans.

Good visual representation of the airport location and distance.

No uncertainty about airport location or orientation compared to the Control-box display.

Constant course correction required after established on the approach.

This display was rated as the best display by all subject pilots. The Control-box display had several deficiencies. The most important one being position uncertainty. The addition of the Airport Image display to the Control-box eliminated this problem. It was difficult to determine an approximate bank angle and attitude from the Control-box alone. The Airport Image being attached to the ground eliminates this problem by acting as a reference line for the pilot. The transition from cruise configuration to descend configuration cause high course deviation and oscillation in the flights with the Control-box. The pilot can view the

outmarker on the line extended from the airport image before he reaches it. Being certain of the transition time and location (outer marker), the pilot can initiate the transition well ahead of the transition point and establish a smooth transition with no oscillatory behavior.

Tunnel plus Airport Image

The subject pilots performed better with this display than the tunnel and the Airport Image displays alone. Figure (5) shows all of the descend performances plotted vs. time for this display.

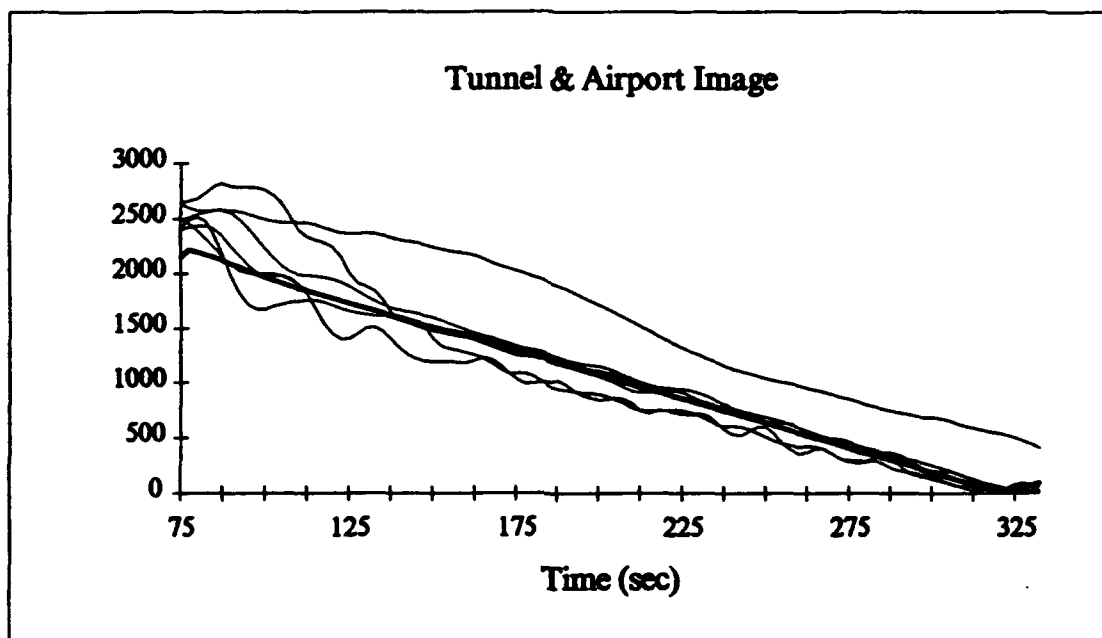


Figure (5)

The approaches performed with the Tunnel display tended to be very oscillatory. When the pilots were outside of the tunnel or off course and course correction was required, the pilots usually overshoot the tunnels. This oscillation was caused by the uncertainty in the rate or heading the pilot needed to achieve to return inside the tunnel. The Airport Image and the Tunnel superimposed to give most of the pilots intercept angle information. The Airport Image being on the ground and the Tunnel in front of the airplane, created a vertical offset angle with the slightest course deviation. This angle was interpreted by several of the subject pilots as an intercept angle and yielded positive results. After a few flights with this display, the offset between the Tunnel and the Airport Image helped the pilots get back on course more efficiently thus reducing the oscillations associated with the Tunnel display. Small oscillations were still present when this display was used. The oscillations exist when the approach was performed with this display, however, the course deviations are fewer and less frequent than the Tunnel or the Airport Image displays alone.

Pilot comments on the Tunnel-Airport Image display were as follows:

Exact attitude and bank angle determination is difficult.

Localizer and Glideslope interception is easy.

Difficult to follow the Tunnels on descend.

Instrument scans reduced but needed with this display.

Excellent visual representation of the airport and runway heading.

Tunnel and the airport extension line represent a good intercept angle for getting back on course.

Very difficult to stabilize or establish on the approach as mentioned before with the Tunnel display alone.

The presentation of the Airport Image and the extension line from the runway make this display slightly better than the Tunnel display alone and much better than the Airport Image display alone. The presentation of the intercept angle which helped the pilots get back on course more efficiently with reduced oscillations, is the only better feature of this display. The Tunnels are very difficult to fly through. The pilots as before, tended to chase each box. This caused overshooting of the tunnel rectangles and the pilot was constantly making large corrections to stay on course.

The Cooper-Harper rating for all five displays is shown in figure (6).

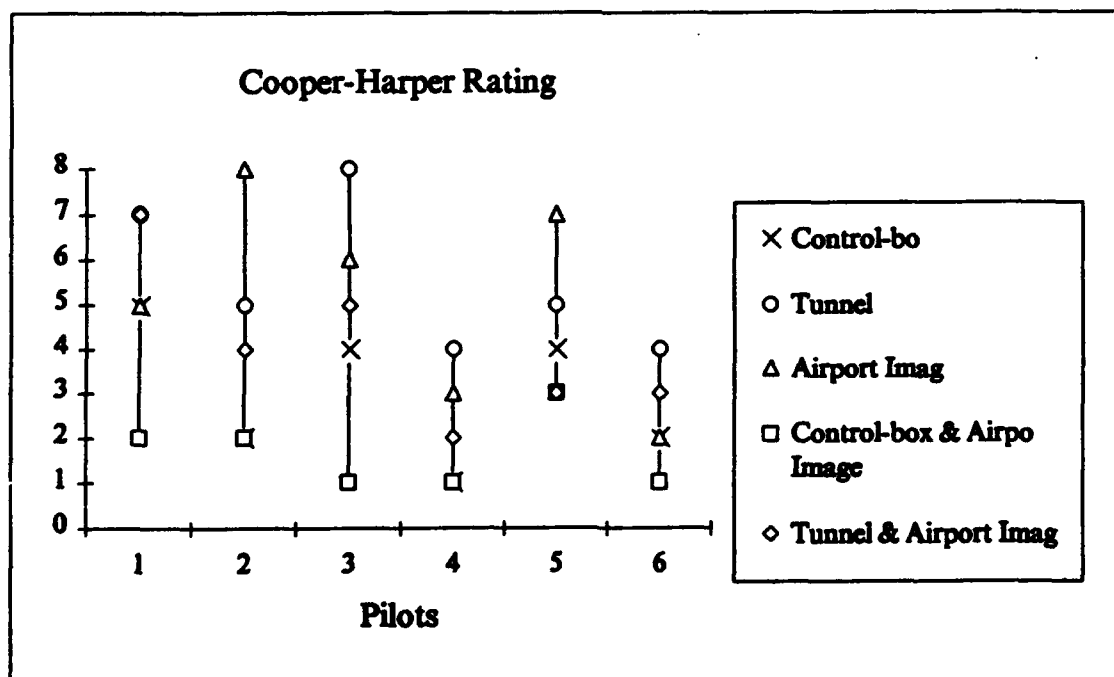


Figure (6)

CONCLUSION

The Control-box was rated as the second best display. Several pilots indicated that the Control-box display should be coupled with a DME for higher efficiency. Also, according to several of the pilots, if heading was displayed close to the red box, the orientation and attitude uncertainty would be eliminated and the approach could be flown efficiently.

The Tunnel display received one the worst ratings among the five displays. Most subject pilots found the Tunnel display very difficult to track. They all overshot the rectangles and had difficulty making course corrections. The size of the rectangles and the distance between them are the most important factors in the efficiency of the Tunnel display. To improve this display, an optimum size for the rectangles is needed for better approach performance, the size of the rectangles should be a function of distance from the airport, an optimum distance between each rectangle should be determined. Also, this display can be used for curved approaches such as the MLS (Microwave Landing System) approach system.

The Airport Image display provides very little information to the pilot, except an approximate airport location, and orientation. It is very difficult to solely rely on this instrument for an instrument approach. This display received the worst ratings of the five displays. Some of the pilots mentioned that this display would be very valuable in a non-precision approach. Example of such an approach would be a VOR or an ADF approach. For a precision instrument approach, this display only would serve as a reference to the pilot for position check. Several improvements in the display could improve approach performance. First, the line can be widened as a function of the distance from the airport. Second, tick marks could be placed on the line to serve as a distance scale for the pilot. Also, strobe lights could be placed on the line to serve as direction pointers.

The Control-box plus Airport Image was the best rated display. The Control-box display was rated very high, but suffered minor deficiencies. One of these deficiencies was the lack of the Control-box display to give the pilot information concerning his position relative to the airport and the distance from the airport. The combination of the Control-box display and the Airport Image display eliminated this problem. The other problems with the Control-box display also exist for this display which include the continuous course correction required to track the localizer-glideslope line and the absence of a trend in the blue box movement. Again, the suggestions and improvements for this display are similar to the improvements proposed for the displays' two separate components, the Control-box, and the airport Image.

The Tunnel plus Airport Image Display has Slight improvement over the Tunnel display and major improvement over the Airport Image display. The most important feature of this display combination was the intercept angle information. The angle between the Tunnel and the line extension of the Airport Image display was interpreted by pilots as an intercept angle. This angle gave the pilot a rate feedback of how much control input is needed to return to the correct course. The Airport Image also helped in better determining an approximate distance from the airport compared to the Tunnel display alone.

REFERENCES

- ¹ Adams, John J. "Simulator Study of Conventional General Aviation Instrument Displays in Path-Following Tasks With Emphasis on Pilot-Induced Oscillations.", NASA Technical Paper 1776, December 1980.
- ² Hoh, Roger H., Smith, James C., Hinton, David H. "The effects of Display and Autopilot Functions on Pilot Workload for Single Pilot Instrument Flight Rule (SPIFR) Operations." NASA Contractor Report 4073, June 1987.
- ³ Roskam, Jan. *Airplane Flight Dynamics and Automatic Flight Controls*, Part 1. Roskam Aviation and Engineering Corporation, 1982.
- ⁴ *Jane's All the World Aircraft 1981/82*, Jane's Publishing Company Limited, 1981
- ⁵ Mirsafian, Saeid. "Evaluation of Five Displays for Aircraft Guidance". M.S. Thesis, The Wichita State University. 1991.

EFFECTIVENESS OF COCKPIT DISPLAY FOR GUIDANCE

by

**Cheryl L. Fulton
M.G. Nagati
Aerospace Engineering Department
Wichita State University
Wichita, Kansas 67208**

**For Presentation to the AIAA/FAA Joint Symposium on General
Aviation Systems at the Hilton Inn-East, Wichita, KS
on March 16-17, 1992**

EFFECTIVENESS OF COCKPIT DISPLAY FOR GUIDANCE

by

Cheryl L. Fulton and M. G. Nagati
Aerospace Engineering Department
The Wichita State University

The feasibility of a pilot using an electronic flight guidance display under various simulated workloads, during an IFR approach, using a small single pilot twin engine airplane was evaluated in a simulator. A pilot model is used for this purpose by modifying an autopilot and varying its feedback gains to simulate periods of distraction by other tasks. The pilot model was monitored during 5 minute segments of flight tracking a localizer in turbulent conditions. Variables were chosen to model a pilot based on the assumption that a pilot able to give total attention to controlling the flight path will fly approximately the same as the autopilot, and if the pilot is alternating his full attention between the task of flying and other tasks, he will generally give full attention to flying a percentage of the time and then decrease his attention down to some minimum level. Pilot inattention is therefore simulated by greatly decreasing the feedback and effectively decreasing the control input periodically over time intervals.

A comparison of path deviations was made for the "simulated pilot" giving attention to following the flight guidance display various percentages of the time. Although some of the aspects of the pilot model were inconclusive, results showed that under turbulent conditions a pilot able to devote 70% attention to controlling the flight as directed, can generally perform as well as an autopilot. Of course, this is only if an acceptable flight guidance method is used. Such a method is intended to save the pilot the trouble of interpreting the readings of various navigation instruments. Then, if a pilot devotes no more than 30% of the time to side tasks, a path as good as flown by this particular autopilot will generally be maintained.

INTRODUCTION

Background

Various autopilot and electronic guidance systems are in use today on large jets and military aircraft. However, for various reasons, these systems are not yet widely used on general aviation aircraft. Although general aviation demand for such systems has not been great, the number of incidents and accidents demonstrates the need for additional pilot assistance, especially when the pilot workload is as high as it is in the terminal area during approach and landing. Studies have supported the use of some type of pilot assistance. For example, one study used a simulator to compare a pilot using an autopilot, a flight director instrument and basic flight instruments. Simulated flights made with autopilot and the flight director showed much less deviation from the glideslope and localizer than the flight without the flight director (Adams).

Studies also lead to the conclusion that the form of pilot assistance may be more important than the amount of workload reduction. For example, although the autopilot-aircraft and pilot-aircraft-flight director flights were similar because the same control laws controlled each, the pilots were able to perform slightly better than the autopilot when following the flight director because they were able to use additional information to limit overshoot. In another study conducted on a simulator at Langley Research Center, various levels of automation of autopilot systems for IFR approaches were compared. In this study, the pilots rated each added automation to be at least somewhat easier to fly, however, the most blunders were experienced in the most fully automated mode (Bergeron). Pilots suggested several reasons for their increased blundering including that the advanced autopilot gave such a false sense of security that the pilot would treat it like a copilot who could think for itself. The pilots often become so involved in other tasks that they forgot to reset functions or controls (Bergeron). The problem of increased blunders also appeared at Langley in a later experiment which compared three levels of autopilot control. Although workload was decreased with the more advanced autopilot, this result was somewhat negated by the degraded "blunder avoidance" (Hoh). Typical blunders that occurred without the autopilot were erroneously copying clearances, inability to interpreting information from the navigation equipment quickly and lack of time to make necessary calculations, and path deviations during unattended operation. Using the autopilot prevented many of these errors, but nearly as many errors were made by pilots incorrectly operating the autopilot. Another problem which appeared with more sophisticated systems was that the complexity of operating the system actually increased the total workload instead of decreasing the pilots work (Hoh). Several solutions to these problems have been offered, including improvements in aircraft handling, displays, training and air traffic control procedures (Hinton). Goals are to develop a system which assists the pilot enough to help reduce pilot error, while not allowing the pilot to become so complacent that he is no longer aware of the actual aircraft position or maneuvers.

Scope

This paper discusses the feasibility of a pilot using an electronic flight guidance display under various simulated workloads. It accomplishes this by creating a pilot model based on an autopilot system.

The research consisted of simulating numerous flights using a pilot model developed with the help of the autopilot software. The purpose was to analytically test the feasibility of using a form of computer generated graphical display to assist a pilot following a particular course under various workload conditions. The pilot model is based partly on conclusions of a recent NASA contract report (Hoh). The report discusses an analytical representation of a divided attention pilot model. The two points found were: (1) a highly stressed human operator can only tend to one item at a time in a divided attention task environment; and (2) Short term memory tends to be wiped out by an important piece of information (Hoh). These two basic ideas were used to model a pilot during short test periods of flights under various simulated workloads. The simulated pilot's ability to follow a graphical guidance display was evaluated for 5 minute segments of a flight tracking a localizer in turbulent conditions.

EVALUATION

Tests were done on a flight simulator developed at the National Institute for Aviation Research. The aircraft modeled was a twin engine aircraft during power approach. Control laws were developed for total aircraft control by linear feedback of aircraft variables and control values. The option was added to allow the control laws to act as an autopilot and control the flight or control values calculated by the control laws to be presented in some form to assist the pilot.

Turbulence was incorporated into the simulation by including random vertical and lateral wind gusts. These gusts were developed using the Dryden filter model with mean gust being preset before each simulated flight.

All of the simulated test flights were started at the same position under the same conditions. Vertical gusting was not included and the longitudinal autopilot system was used throughout the flights. The longitudinal autopilot flew the aircraft at constant altitude with no glideslope. These simplifications were made to reduce data collection to more specific instances for more specific comparisons. Only the lateral component of the of flight was evaluated and only for the case of following a localizer.

Description of Procedures

The research consisted of a comparison of path deviations for a "simulated pilot" where the pilot was modeled assuming he accomplishes various side tasks while tracking the localizer as recommended by the graphical display's guidance in turbulent conditions. The simulated pilot was created by using the autopilot intermittently. This method is

supported by a previous study which showed similar system period and damping for an autopilot controlled flight and a pilot flight using a guidance system created with the same control laws as the autopilot system (Adams). For this evaluation, the amount of feedback was decreased by various percentages to represent a pilot not operating controls exactly as recommended. The system with 100% feedback was assumed to be comparative to a pilot giving complete attention to controlling the flight path of the plane and imputing exact controls as recommended by the display. Pilot inattention was modelled by decreasing the feedback by methods explained later to effectively decrease the control input periodically over time intervals. The greater the percentage of time the full feedback was used, the closer the simulated pilot was to following the path recommended by the graphical display.

Four different variables were considered to estimate the required pilot tracking accuracy. These variables were determined based on the assumption that a pilot able to give full attention to controlling the flight path will fly approximately the same as the autopilot and if the pilot is unable to give complete attention to flying he will generally give his full attention to flying a percentage of the time and then gradually or quickly decrease his attention down to some minimum level. Although at first, the suggestion of a minimum level of feedback control may not seem to fit the pilot model described earlier (Hoh). The model of a pilot only giving attention to one task at a time does allow for more important tasks to interrupt. It is reasonable to assume a pilot would respond to drastic changes such as a sharp dive. Thus, with the minimum feedback model, drastic changes will cause some amount of feedback. Although it will not completely correct path deviation, it will slow down the deviation until full attention is again given to the controls.

The four variables used in the analysis are

- (1) percent of time flight is controlled by 100% attention
- (2) cycle length, time interval which consisted of 100% attention, degradation of attention, and minimum attention flight
- (3) percentage of degradation of control input each time step during the second half of each cycle; ie. control degradation rate
- (4) minimum control input, the lowest percentage of the recommended control input of the system

Numerous five minute flights were simulated by varying the above four variables. For each flight, 3 sets of data were taken.

- (1) maximum deviation (in feet) from the desired flight path
- (2) number of times each predetermined deviation distance is exceeded
- (3) duration of time spent in each deviation range

All distances were measured horizontally perpendicular to the desired flight path. Since no vertical gusting was introduced and the vertical autopilot was allowed to control the flight, no significant deviations were expected. The vertical perturbations were viewed during one initial flight simulation and the deviations were negligible.

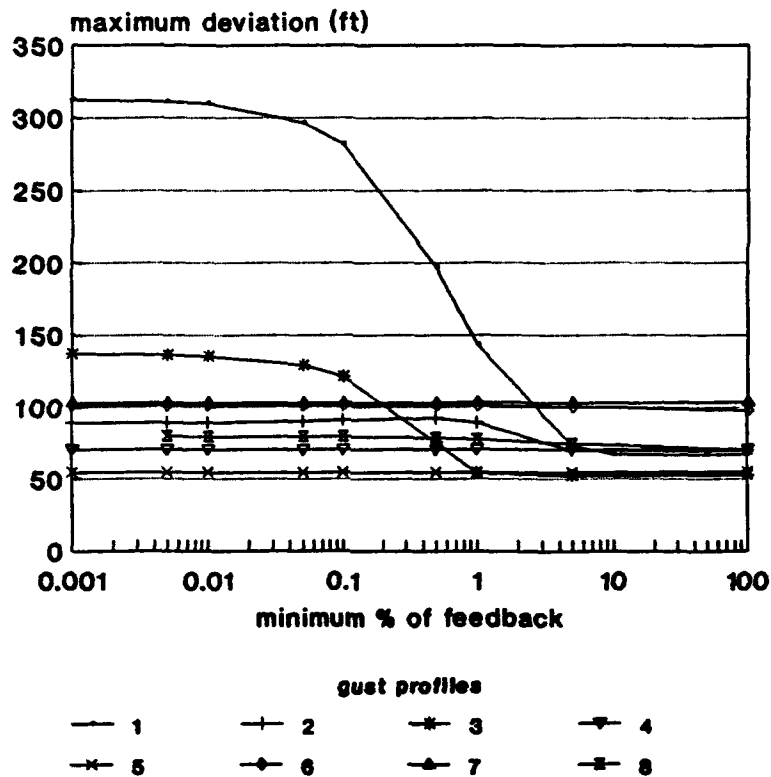
Two different root mean square gust values were used in the model for the various tests. The majority of flights simulated used gusts modelled with the rms gust equal 1.8 feet/second. The rest of the gusts were modelled with the rms gust equal 5.5 feet/second. For most of the simulated flights, a set of 8 random gust patterns were used. By using the same 8 patterns to generate the turbulence, an easier comparison was created. The same ensemble was used to generate a higher turbulence level set. This set was compared to another large sampling set with the only difference in results being that all of the values examined with the stronger gust profile sets were approximately 3 times greater the gust profile sets created with the models rms gust of 1.8 feet/second.

Results of Evaluation

The various results were plotted on graphs shown throughout this section. These include comparisons the four variables listed previously, the gust profile model used and any other variations. The graphs are titled according to the particular type of data used to create them. Six graphs show varied maximum deviation and eight have varied durations of time spent in certain deviation ranges. Exceedance counts were taken for all flights but trends were much more difficult to see with this information. The first graphs in this discussion are comparisons of various gust profiles. The maximum deviations are compared to different minimums feedback values. The next sets of graphs discussed show various cycles lengths on graphs which have average maximum deviation from the localizer path versus either the degradation rate or the percentage of time the pilot guided the aircraft with full attention. Graphs also compare the average duration in ranges and average exceedance counts versus the distance or range with the three cycle lengths. For discussion of degradation rates and percentages of time pilot gave attention to guidance, average maximum deviations are plotted against percentages of cycle attention time for various degradation rates. A graph of average duration in ranges versus the range was plotted for various degradation rates and attention time percentages. Most of the charts were made with the rms gust of the model at 1.8. However, an average duration chart with various degradation rates, an average duration chart with various percentages of pilot attention and a graph with average maximum deviation versus percentage of cycle with full attention for various degradation rates all show the higher rms gust of 5.5.

Figures 1 and 2 show the result of varying the minimum percentage of control input used. The two graphs show comparison of various winds gust pattern. For each gust, the minimum percentage of control input was the only value varied on each graph. On the first graph, the percentage of full attention was held at 50% with a degradation rate of 40%/ tenth second. On the other graph, full attention was 20% and the degradation rate was 50%. Both used 60 second cycle times. The graphs show that maximum deviation during the simulated flights was nearly always the same when the controls actually fed back were at least 5% of the original feedback value. For the pilot model, the pilot gives full attention to one task at a time, so a small minimum feedback is more likely to be an accurate approximation. The small minimum will assure that only large perturbations will cause feedback from the simulated pilot. For over half of the runs which showed change in path deviation, the change occurred when the chosen minimum value was .1% or less. In the first case where total autopilot feedback was 50% of the cycle, the highest

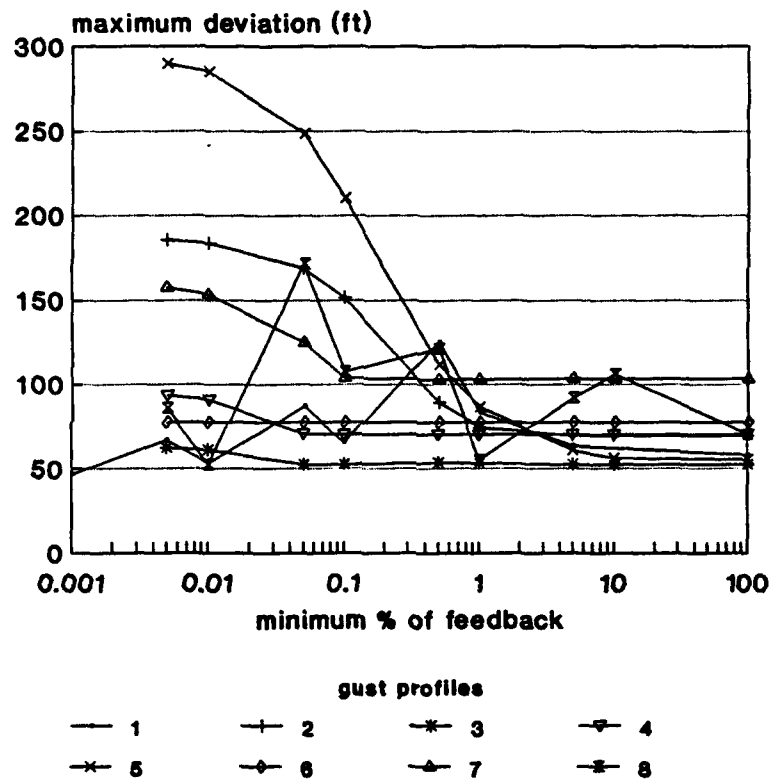
maximum deviation varied minimum feedback



50% cycle full attention, rms gust: 1.8
40%/tenth sec degrade, 60 sec cycle

Figure 1. Maximum Deviation for Gust Profiles (A)

maximum deviation varied minimum feedback



20% cycle full attention, rms gust: 1.8
50%/tenth sec degrade, 60 sec cycle

Figure 2. Maximum Deviation for Gust Profiles (B)

minimum percentage which allowed the largest maximum deviation to be reached was approximately .1%. For these reasons, .1% was selected as the minimum value to be used throughout the remainder of the simulations.

Another variable, the cycle length, was compared using lengths of 10, 30, and 60 seconds. Figures 3 and 4 show a comparison of the average maximum deviations for various wind gust patterns. Figure 3 shows the cycles with various degradation rates and figure 4 shows various percentages of attention being given to flying the aircraft. These graphs show the longer cycle having more deviation overall. This was not a surprise since a factor expected to cause most of the variation in flight path was the length of time the aircraft was flown continuously at minimum control input.

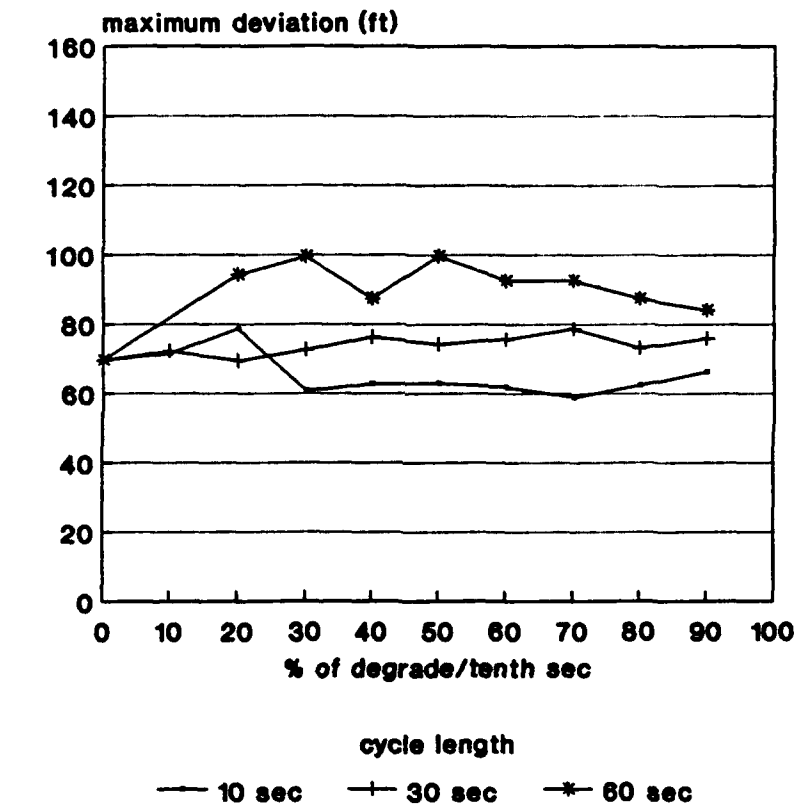
The plots of duration in each range also showed the similar trend. Figures 5 through 9 are comparisons of the 3 cycle lengths with varying degradation rates and full attention percentages. The longest cycles are again more likely to show more time spent farther from the desired location. The further the distance of the range, the less likely the flights with the shortest cycle will have spent time in that range. The averaged times definitely support the expected trend. The individual simulated flights had very random results. Comparison of any two flights with different cycle lengths were not likely to show a trend, however a trend appeared when the average of the values were compared.

The results of varying the degradation rate was not as predicable as varying the cycle length. In figure 3, the longest cycle length had not only the most deviation, but also the maximum deviation varied randomly with variation of degradation rate. Figures 10 and 11 illustrate that the degradation rate has very little influence on the amount of deviation until the percentage of the cycle with full autopilot is less than 70%. However, from 60% to 10%, the faster degradation rate seems to give much less deviation than a slower degradation rate. It appears that the method of reducing feedback each time step, result in feedback that causes deviations to increase. This is very different from the desired and expected result of degraded feedback guiding the aircraft back to the desired path, only slower and less efficiently than 100% feedback. For the cases where pilot full attention is less than 70%, there appears to be benefit in reducing the feedback as quickly as possible when the autopilot is being allowed to degrade.

The durations graphs do not to show very specific trends when results of varying degradation rates are compared. Figure 12 compares various degradation rates with the full attention 50% of each cycle. The amount of time each flight exceeded 300 feet from the correct path show that the 90% degradation rate may be slightly better than other cases. If the average amount of time spent between 240 feet and 300 feet is compared, then 70% and 80% degradation rates also appeared to have somewhat better performance. These results are consistent with the other data.

Unlike the results of varying the degradation rate, the results of varying the amount of pilot attention were very predictable. The percentage of time the "pilot" was able to spend following the path directed by the display appeared to have much influence on how well the aircraft tracked the localizer. This was very apparent on the maximum deviation

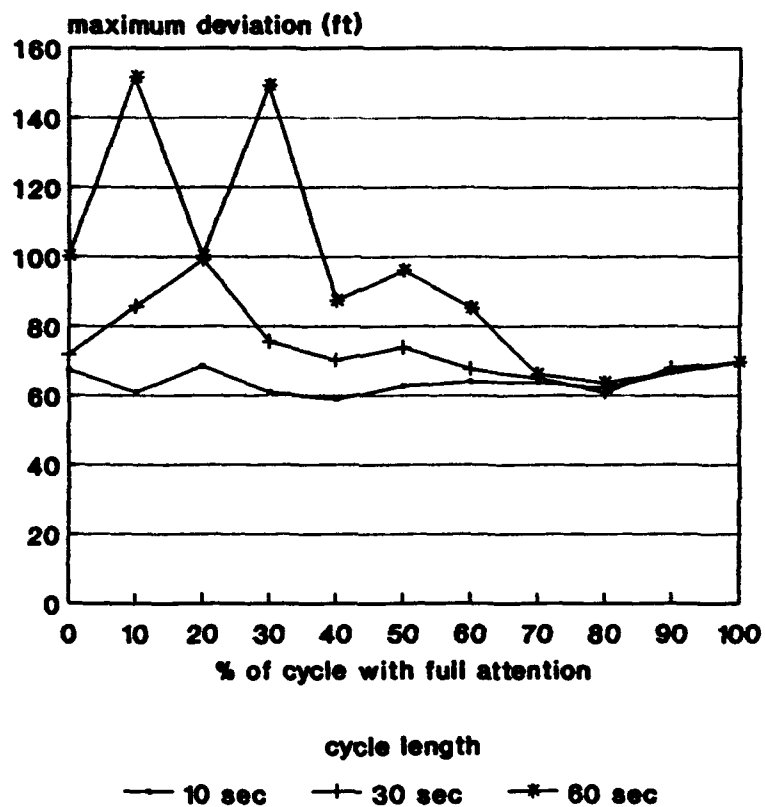
maximum deviations(avg) varied cycle lengths



50% of cycle full attention
rms gust: 1.8

Figure 3. Maximum Deviation for Different Cycle Lengths (A)

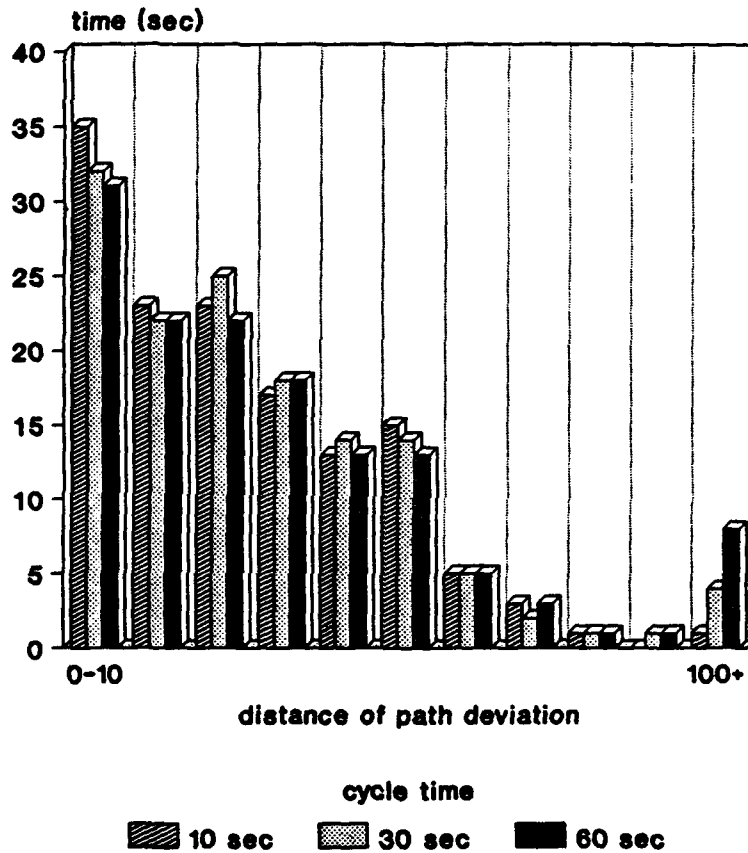
maximum deviations(avg) varied cycle lenth



40%/1 sec degrade
rms gust: 1.8

Figure 4. Maximum Deviation for Different Cycle Lengths (B)

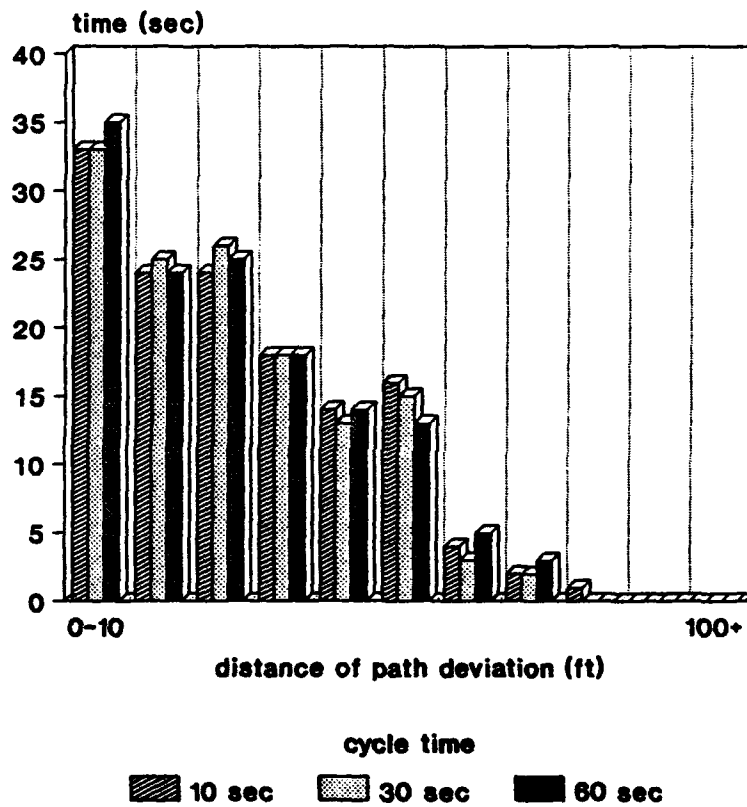
duration in ranges (avg)



40%/1 sec degrade, rms gust: 1.8
 20% of cycle full attention

Figure 5. Duration in Ranges for Different Cycle Lengths (A)

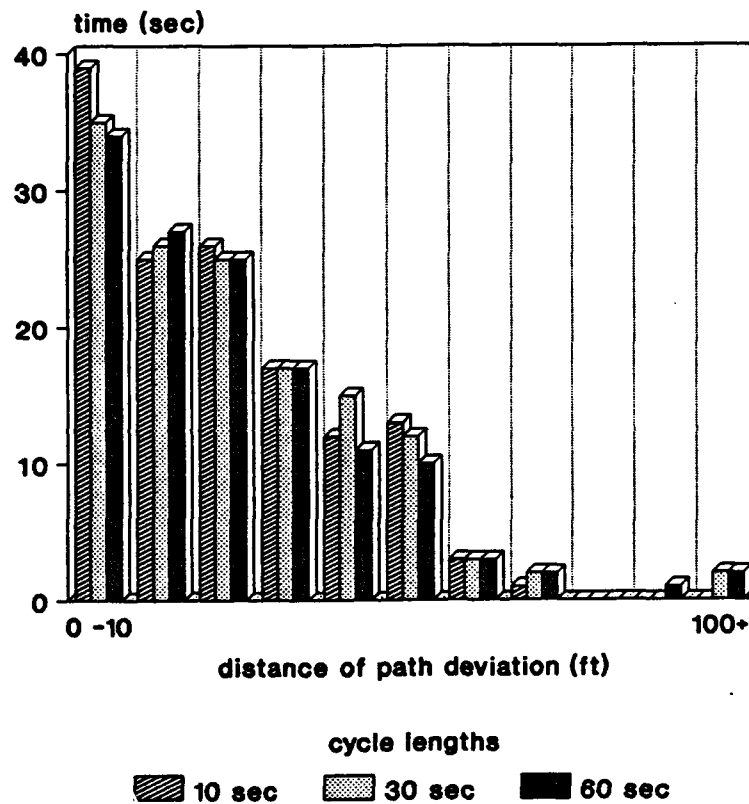
duration in ranges (avg) varied cycle lengths



40%/1 sec degrade, rms gust: 1.8
70% of cycle full attention

Figure 6. Duration in Ranges for Different Cycle Lengths (B)

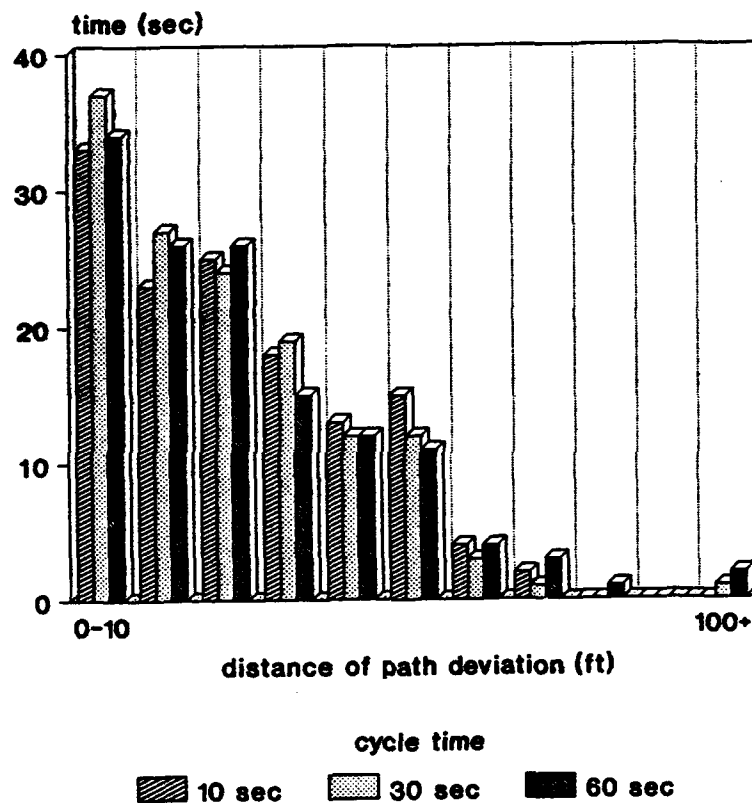
duration in ranges (avg) varied cycle lengths



70%/.1 sec degrade, rms gust: 1.8
50% of cycle full attention

Figure 7. Duration in Ranges for Different Cycle Lengths (C)

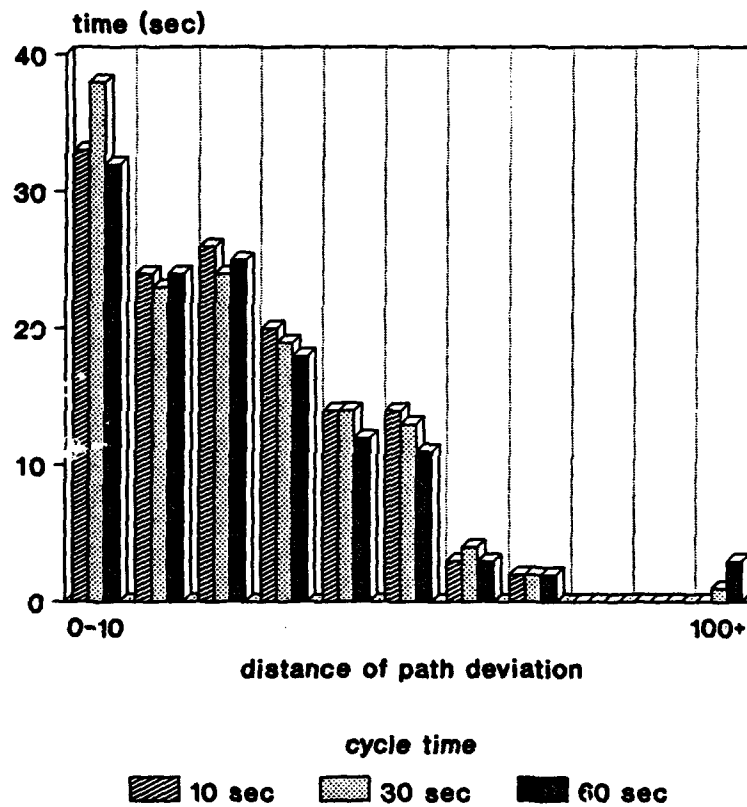
duration in ranges (avg) varied cycle lengths



20%/1 sec degrade, rms gust: 1.8
50% of cycle full attention

Figure 8. Duration in Ranges for Different Cycle Lengths
(D)

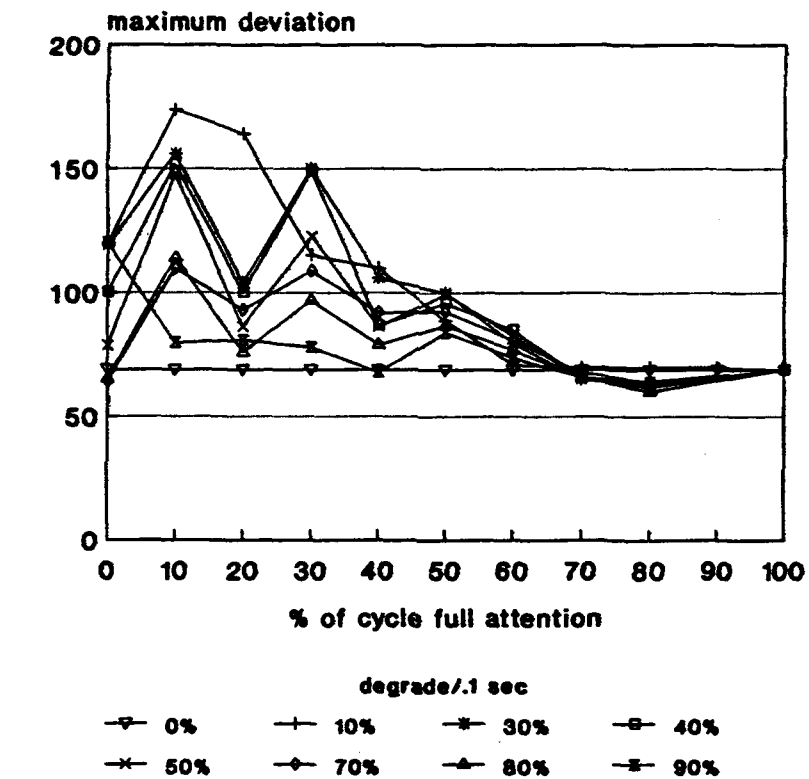
duration in ranges (avg) varied cycle lengths



40%/1 sec degrade, rms gust: 1.8
50% of cycle full attention

Figure 9. Duration in Ranges for Different Cycle Lengths (E)

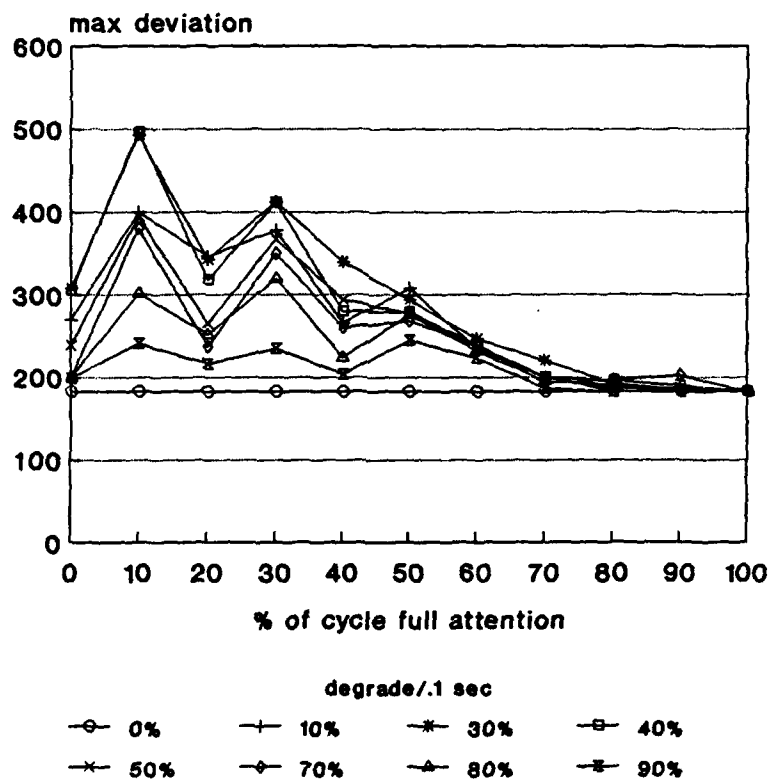
maximum deviation (avg) various degrades



60 sec cycle
rms gust: 1.8

Figure 10. Maximum Deviation for Various Degradation Rates
(A)

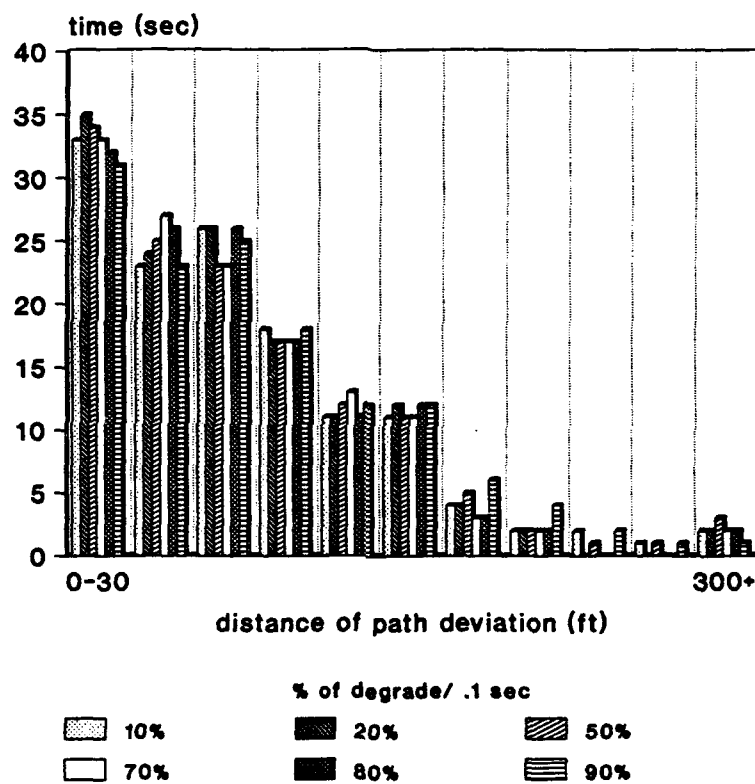
maximum deviation (avg) various degrades



60 sec cycle
rms gust: 5.5

Figure 11. Maximum Deviation for Various Degradation Rates
(B)

duration in ranges (avg) varied degradation rate



50% of cycle full attention
gust rms: 5.5

Figure 12. Duration in Ranges for Various Degradation Rates

graphs. Figure 4 shows 3 different cycle lengths not having much effect on the maximum deviation when the pilot is able to give full attention to flying at least 70% of the cycle. Figures 10 and 11 show various degradation rates having little effect when the pilot's attention is 70% or more.

The duration charts also show best results when pilot attention is 70% or more. In figures 5 through 9 and 13, the same root mean square gust model was used. Only in one instance was 70 feet exceeded when the amount of full attention 70% or more. This instance occurred in the case shown on figure 6, where the aircraft averaged 1 second spent further than 70 feet from the flight path. Most simulated flight with full attention less than 70% generally resulted in time spent further than 100 feet from the correct path.

With the higher wind gust rms, 5.5, the results were clear on the duration plots. Figure 14 shows results with a 20% degradation rate. All average maximum deviations were greater than they had been with the weaker gusts. But again, simulated flights using full attention at least 70% of the time showed much more desirable results than in the cases where full attention was less than 70%. Only in cases where the pilot gave 50% or less attention, was time spent further than 500 feet from the desired path.

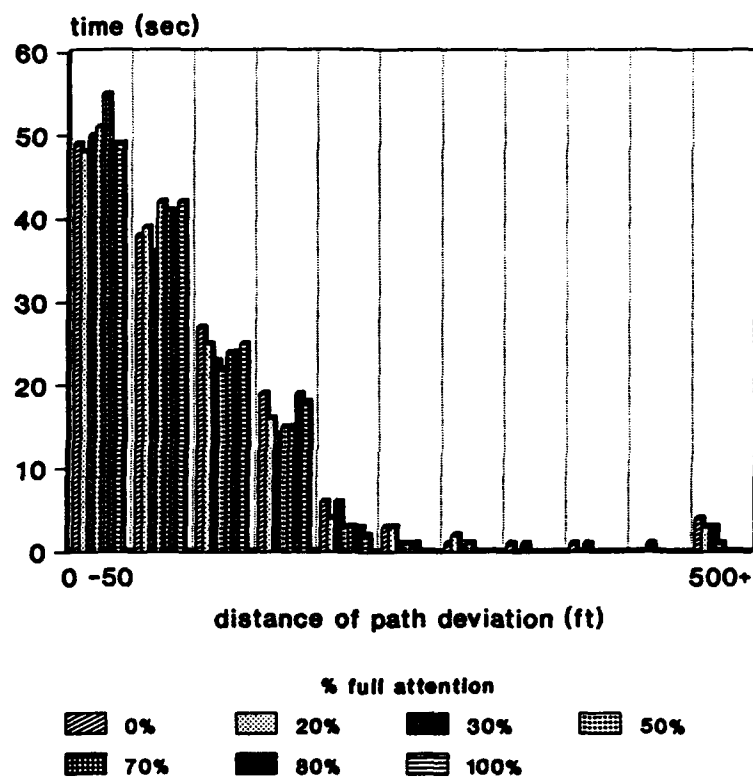
The exceedance charts do not seem to show any clear results. Figure 15 shows various percentages of pilot attention with the differences between best and worst cases being small. Figure 16 shows both 100% attention and no attention and yet the average differences appear to be small.

Possible Explanations for Discrepancies

Two somewhat unusual results occurred in the data. The most unexpected result was the effect of the degradation rate on the path deviation. This appeared to be almost opposite of what was expected. Before the simulations were run, it was assumed that the slower degradation rates would allow more feedback during the transition and thus improve performance. However, the opposite appeared to be true. The slower degradation rates actually appeared to make the performance much worse. This may be because the frequency of the response is changed when the amount of control input is decrease. Also, the result of the feedback is no longer a solution to the original problem. The original gains were a solution to the Riccati equation with a certain set of constraints. The new gains are not likely to be solutions to the Riccati with any reasonable set of constraints.

The other apparent discrepancy, the ability of the "pilot" to perform best when the feedback is maximum only 80% or 90% of the time, may be explained by looking at the system response. For all feedback variables, the initial response is the greatest, then the system gradually goes to steady state slowing converging more and more slowly as it gets close to the goal state. When the system is brought down to almost no feedback and then brought back to the original feedback, the initial quick response may be repeated at the new closer point thus allowing the overall response to become quicker. It is not known if this is similar to a real pilots response.

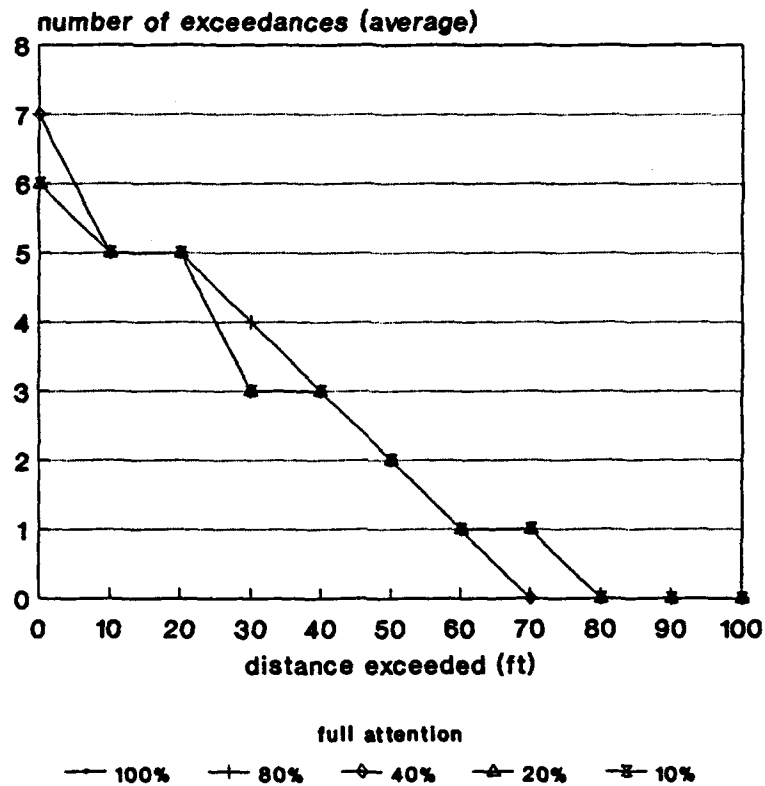
duration in ranges (avg)
varied % of cycle full attention



20%/1 sec degrade
quat rms: 5.5

Figure 14. Duration in Ranges for Different Attention Percentages (B)

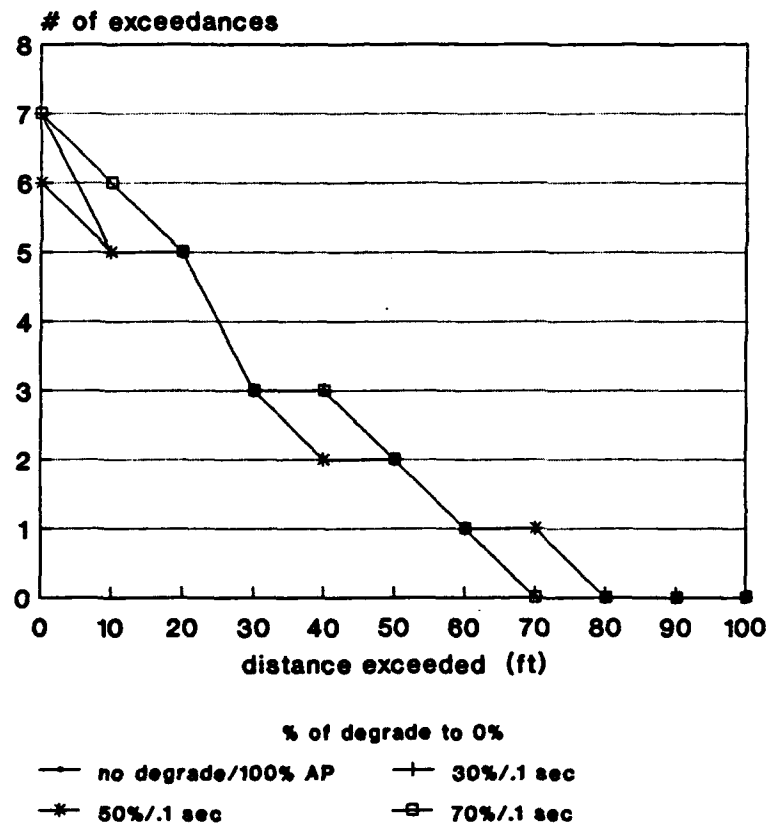
of exceedances (avg) varied % of cycle with full attention



10%/1 sec degrade
60 sec cycle, rms gust: 1.8

Figure 15. Number of Exceedances for Different Attention Percentages

of exceedances (avg)



no cycles,
rms gust: 1.8

Figure 16. Number of Exceedances for Various Degradation Rates

CONCLUSIONS

The results of this evaluation seem to support the use of some sort of interactive pilot assist such as graphical display. Since the simulated pilot was able to follow a path similar to an autopilot while only giving 70% attention to guiding the aircraft, it is reasonable to assume the pilot may spend 30% of the time doing other tasks and not decrease flight performance. It appears feasible for a pilot to do nearly as well as an autopilot while still performing a side task, i.e. the tracking error is only slightly increased when the distraction occurs less than 30% of the time. For cases where distractions occupy more than 30% of a pilots time, the tracking results may still be acceptable for many instances. The magnitude of the deviations general increases as the amount of attention decreases so as more deviation is allowed a lower the percentage of attention can be allowed.

Since the pilot model assumes a pilot under high stress conditions is only able to perform one task at a time, the unusual result of the best flights occurring when the feedback degradation rate is fast is acceptable. However, reasoning behind this occurrence as explained above make the comparison of these results unrealistic for an actual pilot. Therefore no valid conclusions can actually be made about varying degradation rates. For any simulation, there must still be a degradation rate to keep the numerical solutions acceptable within the simulation. Unfortunately, the feedback generally can not be decreased to a low value (in the extreme, zero) when the aircraft is not steady state, without increasing the possibility of strange results with the current calculation methods used.

Assuming the information used by the autopilot could be given to the pilot in an easily interpreted form, the results of this evaluation show that a pilot able to devote 70% attention to controlling the flight as directed, will be able to perform as well as an autopilot. If pilot can accomplish side tasks using no more than 30% of the time, a flight path similar to one flown by an autopilot will be maintained.

REFERENCES

Adams, James J., "Simulator Study of a Flight Director Display", Langley Research Center, NASA TM-84581, 1983.

Bergeron, Hugh P., "General Aviation Single Pilot IFR Autopilot Study", Presented at the 1980 Aircraft Safety and Operating Problems Conference, Hampton, VA, November 5-7, 1980. NASA CP-2170, 1981.

Hoh, Roger H., Smith, James C., Hinton, David A., "The Effects of Display and Autopilot Functions on Pilot Workload for Single Pilot Instrument Flight Rule (SPIFR) Operations", NASA CR-4073, 1987.

Hinton, David A. and Shaughnessy, John D., "Conceptual Design and Simulator Implementation of an Automatic Terminal Approach System", Langley Research Center, NASA TM-85667, 1984.

Roskam, Jan, Airplane Flight Dynamics and Automatic Flight Controls, Roskam Aviation and Engineering Corporation, Ottawa, KS, 1979.

Hoblit, Frederic M., Gust Loads on Aircraft: Concepts and Applications, American Institute of Aeronautics and Astronautics, Inc., S.W., Washington, D.C. 20024

**TECHNOLOGICAL OPPORTUNITIES FOR ADVANCEMENT OF HUMAN
FACTORS BY THE YEAR 2000**

by

**Charles W. Howard
Raytheon**

COPIES NOT AVAILABLE

**For Presentation to the AIAA/FAA Joint Symposium on General
Aviation Systems at the Hilton Inn-East, Wichita, KS
on March 16-17, 1992**

ALL WEATHER LANDING--MAN OVER AUTOMATION

by

Norris J. Krone
Maryland Advanced Development Lab.
University of Maryland

NO COPIES AVAILABLE

For Presentation to the AIAA/FAA Joint Symposium on General
Aviation Systems at the Hilton Inn-East, Wichita, KS
on March 16-17, 1992

**AN INVESTIGATION INTO THE CUMULATIVE AND INTERACTIVE
EFFECTS OF STRESSORS ON PILOT PERFORMANCE**

by

**Susan M. Murray
Central Missouri State University**

***The Appendices were not reproduced with this paper.**

**For Presentation to the AIAA/FAA Joint Symposium on General
Aviation Systems at the Hilton Inn-East, Wichita, KS
on March 16-17, 1992**

An Investigation Into the Cumulative and Interactive Effects of Stressors on Pilot Performance

Abstract

by
Susan M. Murray

The purpose of the present study is to examine the cumulative and interactive effects of combined stressors on the performance of aircraft pilots during the conduct of complex flight operations demanding a high degree of both skill and vigilance. It was hypothesized that an interaction would occur between the two independent variables of noise exposure and sleep deprivation such that the deleterious effects of these two combined stressors would be significantly more pronounced than performance decrements resulting from exposure to either stressor separately. This expected pattern of results would support the proposed concept that, as the number of stressors acting on a human operator increase, performance of a complex task will be decreased correspondingly.

A two-by-two factorial design was implemented to examine the performance of 16 instrument-rated pilots during the conduct of ILS approaches in a flight simulator under four various stress conditions. Mean Pilot Performance Scores (MPPS) were employed to numerically evaluate subject performance of the ILS approaches. The noise exposure condition consisted of 90 decibels of a continuous, steady, simulated engine noise, and the sleep deprivation condition consisted of approximately 24 hours of sleep deprivation. In order to evenly distribute the possible confounding effects of pilot experience level, each group was assigned 2 instrument pilots with relatively low experience and 2 with relatively high experience.

A Two-Way Analysis of Variance revealed no significant cumulative or interactive effects of the stressors of noise exposure and sleep deprivation on pilot performance. These unexpected results were largely due to the extreme variability of the MPPS of three subjects. The effects of experience level on performance approached, but fell short of, statistical significance ($p=0.085$). Apparently, individual differences in instrument pilot skill may be substantial enough to overcome the potentially deleterious effects of the stressors of noise and sleep deprivation, whether experienced separately or in combination, in the levels used in the present study. Skill may be a factor that can also supersede the effects of experience level. It appears that lack of familiarity with flight equipment and negative transfer were extraneous factors which affected performance in this study. Another possible explanation is that the amounts of the stressors to which the subjects were exposed, and the differences in pilot experience level, were not large enough to significantly affect performance.

Because the working environment of aircraft pilots is one requiring precision and vigilance in the face of numerous combinations of stressors, the potential for cumulative and interactive effects of stressors which may degrade aircraft pilot performance, and therefore aviation safety, warrants further investigation. Effective methods of better controlling or compensating for these variables should also be the goal of future research and regulatory measures.

Table of Contents

	Page
List of Tables & Figures	v
Chapter	
I. Introduction	1
II. The Problem and Its Setting	2
The Statement of the Problem	2
The Null Hypothesis	2
The Delimitations	2
Basic Assumptions	3
The Definitions of the Terms	4
The Value of the Study	8
III. The Review of the Related Literature	12
Introduction	12
Related Studies	13
Noise as a stressor	13
Combined stressors of noise and fatigue	13
VI. Methodology	16
The Data	16
Criteria for the Admissability of the Data	16
The Research Methodology	17
Subjects	17
Apparatus	21
Procedure	21

	Statistical Analysis	24
VII.	Results	25
VIII.	Discussion	29
	Summary	29
	Conclusions	30
	Recommendations	32
	References	44

List of Tables and Figures

Table	Page
1. Permissible Noise Exposures	10
2. Subject Experience Characteristics: Low Time Subjects (Instrument Time < 100 hrs)	19
3. Subject Experience Characteristics: High Time Subjects (Instrument Time > 100 hrs)	20
4. Mean Pilot Performance Scores for Individual Subjects by Groups	26
5. Group Performance Means and Standard Deviations	27
6. Summary of Two-Way Analysis of Variance of Mean Pilot Performance Scores	27
7. Effects of Instrument Flight Experience Level: Summary of One-Way Analysis of Variance	28
Figure	
1. Effects of the Magnitude and Amplitude of Sound on Human Hearing	9

An Investigation Into the Cumulative and Interactive Effects of Stressors on Pilot Performance

Presently, much of the relevant research on stress has been limited to single stressors and does not provide an adequate picture of how combinations of stressors may act on the human performance of complex tasks such as those required in the operation of aircraft. Since human factors knowledge is critical to safety in aviation, it is vital to establish a greater understanding of the effects of combined stressors on human performance.

The purpose of the present study is to examine the cumulative and interactive effects of an environmental stressor (noise) and a physiological stressor (fatigue induced by sleep deprivation) on flight performance during instrument approaches. For the purposes of this study, the instrument approaches were conducted in a flight simulator. It was hypothesized that the results would demonstrate a significant interaction between the two stressors such that, when the stressors were combined, the resulting performance decrements would be measurably greater than those occurring from exposure to either stressor separately. Such a pattern of results would support the proposed concept that, as the number of stressors acting on a human operator increase, performance of a complex task will be degraded. The independent variables in this study are stressors which aircraft pilots frequently encounter. The levels of noise intensity (90 dbs) and duration of sleep deprivation (approximately 24 hours) used in this study have been demonstrated by previous research to have significant effects on human performance, but were not great enough to cause any damage or long-term harm to humans.

THE PROBLEM AND ITS SETTING

The Statement of the Problem

This research attempts to determine whether an interaction exists between the two stressors of noise exposure and sleep deprivation, such that the deleterious effects on pilot performance of these two stressors combined is significantly more pronounced than any performance decrements resulting from exposure to either stressor separately. The aim of this study is to develop a better understanding of how combinations of stressors may interact to affect pilot performance, particularly during flight operations which require a high degree of vigilance and precision. The stressors used as independent variables in the present study include continuous exposure to 90 decibels of noise and fatigue induced by 24 hours of sleep deprivation. The complex task serving as the dependent variable in this study is the performance of precision instrument approaches by qualified instrument pilots, as measured by a Mean Pilot Performance Score which imposes penalties for deviations from published instrument approach procedures.

The Null Hypothesis

The null hypothesis states that no significant interaction will occur between the two stressors of noise exposure and fatigue induced by sleep deprivation. Subsequently, the null hypothesis supposes that a combination of these two stressors will not produce performance decrements measurably greater than those which might result from exposure to either stressor singularly.

The Delimitations

In order to select appropriately qualified participants for this study, subjects were required to meet the following stipulations:

- possession of an airplane instrument rating;
- must have logged a minimum of 6 hours of instrument time in the past 6 months, and 3 of these hours were flown in an airplane in either simulated or actual instrument conditions; and
- must have performed a minimum of 6 instrument approaches in either a simulator or aircraft within the previous 6 months.

Because of these requirements for the selection of subjects, and because the subjects for this study were selected primarily from instrument pilots in the Warrensburg area, randomized selection of subjects, and therefore the validity of generalizations made from the results of this study, will be limited.

The results of this study may be task specific, and while they may be representative of the cumulative and interactive effects of similar stressors on complex tasks imposing similar demands on the operator, such generalizations do not necessarily apply to tasks which are simple, monotonous, or require low levels of operator skill or low mental workload. This study is limited to the examination of the effects of stressors during the conduct of a precision instrument approach during simulated night instrument flight conditions.

The noise exposure variable manipulated during this study involved a sound intensity of 90 decibels of a continuous, steady-state noise simulating that of an aircraft engine, with duration of exposure not exceeding 30 minutes. Therefore, the results of this study are limited in scope and may not be construed to present a realistic representation of the effects of noise intensities other than 90 dbA, noise exposure of extended duration, or intermittent or variable noise.

Basic Assumptions

The first assumption. The first assumption is that all statements made by the subjects on the Personal Data Sheet are true and accurate.

The second assumption. The second assumption is that all subjects complied with the criteria and stipulations set forth by the researcher; including no alcohol consumption within 48 hours prior to the experimental simulator session, and for the sleep deprivation subjects, no sleep within the 24 hours prior to being tested in the flight simulator.

The third assumption. The third assumption is that the process of subject selection, assignment to groups, and matching on the subject variable of instrument flight experience was adequate to ensure equivalent groups.

The Definitions of Terms

Actual Instrument Time. Flight conducted by sole reference to aircraft instruments in actual Instrument Meteorological Conditions.

Air Traffic Control (ATC). Any federal facility engaged in the direction and control of aircraft in controlled airspace.

Audiometer. An instrument which measures noise levels in decibels.

CAMI. The Federal Aviation Administration Civil Aeromedical Institute, located in Oklahoma City, Oklahoma. CAMI conducts research on aviation-related topics pertaining to the flight of aircraft and air traffic control operations.

Circadian Rhythm. The "biological clock" of the human body, which regulates sleep/wake cycles, and is prone to temporary disruptions of normal sleep/wake cycles when habitual sleep/wake patterns are disrupted by changes in sleeping habits, sleep deprivation, or travel through time zones.

Complex Task. A task, the performance of which demands a high degree of vigilance and precision, and requires the operator of the task to draw upon specialized knowledge, skill, and experience to integrate and coordinate several simpler tasks in the performance of the complex task.

Cumulative Effects of Stress. For the purpose of this study, the hypothesized cumulative effects of stress refers to an accumulation of effects caused by various forms of stress in such a manner that exposure to more than one stressor at a given time will result in performance decrements greater than those observed under exposure to a single stressor.

Decibel. (db). A unit used in the measurement of noise intensity (loudness).

Decision Height (DH). The altitude, as designated on the appropriate instrument approach chart, at which an aircraft pilot conducting a precision instrument approach to a runway must decide whether or not to continue the approach. This decision is made based on whether any component of the runway environment is visible to the pilot upon reaching the designated mean sea level height on the glide slope as determined by the altimeter reading.

Glide Slope. An electronically emitted radio navigation signal which provides vertical guidance to an aircraft during a precision instrument approach. The horizontal needle on the ILS instrument display in the cockpit of an aircraft conducting an ILS approach is activated by the glide slope signal, giving the

pilot a visual indication of the aircraft's position in reference to the desired glide path to the runway.

Instrument. In regards to aircraft, refers to a device using an internal mechanism to show visually or aurally the attitude, altitude, or operation of an aircraft or aircraft part.

Instrument Approach. A system of electronically transmitted signals which are received by instruments in the cockpit of an aircraft and which provide a means of guidance for aircraft operating under Instrument Flight Rules to approach a runway and assume a position from which a landing can be made visually. Instrument Approach Procedures are prescribed and approved for a specific airport by a competent authority.

Instrument Flight Rules (IFR). Flight conducted under Instrument Meteorological Conditions (IMC), during which pilots must operate aircraft completely by reference to flight instruments, since visual reference to outside cues is not available.

Instrument Landing System (ILS). A type of precision instrument approach which provides both localizer (horizontal) and glide slope (vertical) guidance to a runway via a combination of electronic components which provide signals that are received and displayed by the appropriate instruments in aircraft.

Instrument Meteorological Conditions (IMC). Weather conditions which do not permit flight by visual reference to objects or landmarks on the ground, or which are below the minimum conditions legally required for flight under visual flight rules (VFR). Also referred to as instrument flight rules or IFR conditions.

Interaction. An interaction is said to occur between two or more independent variables if dependent variable values obtained under levels of one independent variable behave differently under different levels of the other independent variable. Dependent variable values related to one independent variable in a factorial design thus depend on, or vary systematically with, the values of another independent variable in that design.

Interactive Effects of Stressors. For the purposes of this study, refers to the theoretical relationship that exists between combinations of stressors and measures of aircraft pilot performance. Theoretically, measures of pilot performance obtained under a single stressor will differ, or vary systematically with, measures of pilot performance obtained under exposure to a combination of stressors.

Localizer. An electronic extension of the runway center line which provides horizontal guidance to an aircraft during an ILS approach.

Main Effects. Average treatment effects; which are manifested by a superior difference in the dependent variable which is maintained under all conditions of the independent variable.

Mean Pilot Performance Score. The mathematical average of scores designed for the purpose of evaluating pilot performance during the conduct of instrument approaches in the present study. These scores will be determined according to specific penalties incurred by deviations from the desired altitude/glide path, heading/localizer track, airspeed, or operating procedures; or by failure to initiate appropriate missed approach procedures when the runway is not visible or the aircraft (flight simulator) is not in a position to make a normal, safe landing. Such penalties will be subtracted from the highest achievable score of zero, which would reflect zero errors.

Missed Approach. A maneuver conducted by a pilot when an instrument approach cannot be completed to a landing.

Missed Approach Point (MAP). The point at which a missed approach must be executed, expressed as an altitude on the glide slope for a precision instrument approach, or in terms of time or distance from the final approach fix for a non-precision instrument approach.

Nonspecific Responses to Stress. Changes that occur indirectly as a result of a particular stressor. The nonspecific reaction to a physical injury would be the endocrine changes that occur in response to the injury - the increased output of the adrenal cortical steroids, and a variety of other endocrine changes that precede and react to the increased adrenal output.

OSHA. The Occupational Safety and Health Administration.

Personal Data Sheet. An information sheet which each potential subject volunteering to participate in the proposed study will be required to fill out prior to being selected for the study. It will be used to obtain information from the subjects relevant to the study, and will also serve as a screening device to target qualified subjects for the study.

Precision Instrument Approach. A standard instrument approach procedure in which an electronic glide slope is provided, of which the most common in civilian use is the Instrument Landing System (ILS).

Runway Environment. The runway threshold, approved lighting aids, or other markings identifiable with the runway. A pilot must have the runway environment in sight in order to descend below the Decision Height (DH) on an ILS approach.

Simulated Instrument Time. Flight conducted solely by reference to aircraft instruments in which outside visual references are blocked out by a "hood" or other device in order to simulate instrument flight in Instrument Meteorological Conditions. Also, a flight simulator may be used for training purposes to simulate instrument flight in an aircraft.

Sleep Deprivation. An independent variable used in research to study the behavior and performance of human subjects after exposure to extended periods of time without sleep.

Specific Responses to Stress. Local reactions that occur as the direct consequence of a stressor; that are specific to that stressor. For example, if a person were to break a leg, the specific responses to the leg breaking would be the fracture of the bone, the tissue damage in that area, the disruption of the blood supply, the edema, and all other consequences brought about precisely by the breaking of the leg.

The Value of the Study

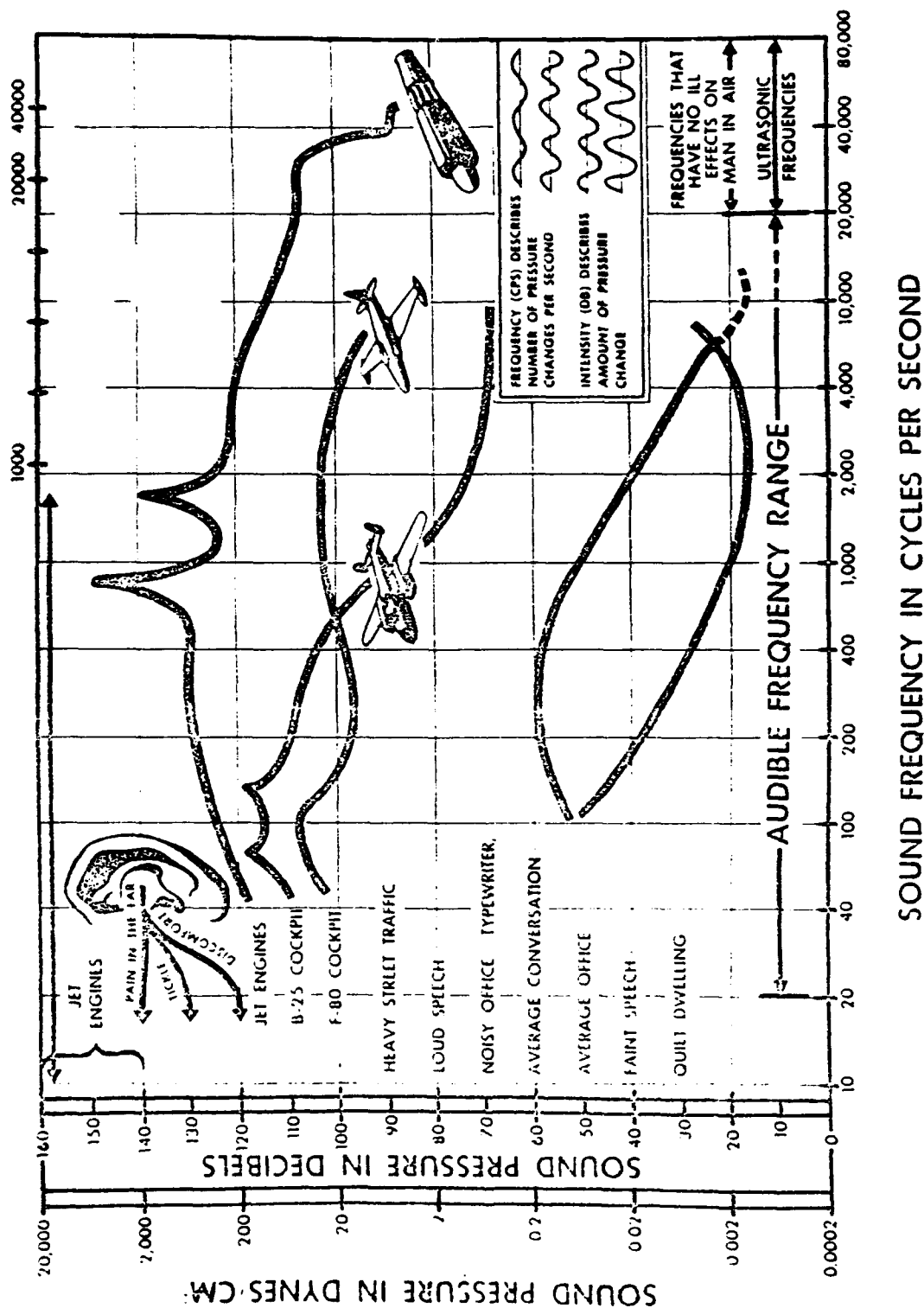
Presently, much of the relevant research on stress has been limited to single stressors and does not provide an adequate picture of how combinations of stressors may act on the human performance of complex tasks (Hancock & Warm, 1989). Since human factors knowledge is critical to safety in aviation, it is vital to establish a greater understanding of the effects of various forms of stress on human performance. The present study will attempt to examine the cumulative and interactive effects of an environmental stressor (noise) and a physiological stressor (fatigue induced by sleep deprivation) on flight performance during instrument approaches.

For the purpose of this study, the hypothesized cumulative effects of stress refers to an accumulation of effects caused by various forms of stress in such a manner that exposure to more than one stressor at a given time will result in performance decrements greater than those observed under exposure to a single stressor. The interactive effects of stressors examined in this study refers to the theoretical relationship that exists between combinations of stressors and measures of aircraft pilot performance. Hypothetically, measures of pilot performance obtained under a single stressor will differ, or vary systematically with, measures of pilot performance obtained under exposure to a combination of stressors.

Exposure to noise is a relevant variable for this study, since many aircraft in commercial aviation produce a substantial level of engine noise, which represents a potential source of stress and distraction in the cockpit. This is especially true when a high intensity of cockpit noise or prolonged exposure is a factor. Noise is a generally recognized source of stress which contributes to physiological and mental fatigue, and also presents the risk of permanent or temporary damage to hearing. Figure 1 illustrates common sources of noise and the magnitude and amplitude at which sound causes physical discomfort to humans. As a measure to prevent hearing loss, OSHA has established regulations limiting exposure of American workers to noise levels that have been demonstrated as potentially damaging (Table 1). These regulations apply to flight crews as well as industrial workers. The adequacy of these regulations to protect commercial pilots from the potentially deleterious effects of excessive mental and physical fatigue resulting from the stress of noise exposure is currently indeterminate, due to the lack of data concerning the effects of noise exposure on these variables effecting aircraft pilot performance. There have, however, been reports of pilots experiencing excessive fatigue after flights in particularly noisy aircraft (CAMI, 1980). There is also evidence in a study conducted by the Federal Aviation's Civil Aeromedical Institute (Thackray & Touchstone, 1979) that the fatiguing effects of noise appear to be more

Figure 1

The Effects of the Magnitude and Amplitude of Sound on Human Hearing



Note. From Physiological Aspects of Flight. (p. 92) by R. J. Del Vecchio, 1977, Oakdale, NY: Dowling College Press.

Table 1

Permissible Noise Exposures¹

<i>Duration per Day (Hours)</i>	<i>Sound Level, dbA* Slow Response</i>
8	90
6	92
4	95
3	97
2	100
1 1/2	102
1	105
1/2	110
1/4 or less	115

*Measured on the A weighting scale of a standard sound level meter as slow response. When the daily noise exposure is composed of two or more periods of noise exposure of different levels, their combined effect should be considered, rather than the individual effect of each. If the sum of the following fractions

$$\frac{C_1}{T_1} + \frac{C_2}{T_2} + \frac{C_3}{T_3} + \dots = \frac{C_n}{T_n}$$

exceeds unity, then the mixed exposure is considered to exceed the limit value. C_n indicates the total time of exposure at a specified noise level and T_n indicates the total time of exposure at that level. Exposure to impulsive or impact noise should not exceed 140db peak sound pressure level.

¹U.S. Department of Labor, chapter 18, Part 1910. "Occupational Safety and Health Standards," subpart G., section 1910.95, Occupational Safety and Health Administration (Washington, D.C. revised March 11, 1983), pp. 105-6.

Note. From Safety Management. (5th ed.). (p. 386) by J.V. Grimaldi and R. H. Simonds, 1989, Homewood, IL: Richard D. Irwin, Inc.

pronounced if the exposed individual is mentally active rather than relaxed. In their 1979 study, Thackray and Touchstone produced evidence that effort expenditure is actually increased by noise exposure, which may help explain the increased fatigue encountered by pilots of noisy aircraft.

Public service pilots normally fly 40-80 hours per month. Commuter pilots operating under FAR Part 135 may legally fly up to 120 hours in a single month, and air carrier pilots operating under FAR Part 121 may legally fly up to a maximum of 100 hours a month (FAR/AIM, 1991). Such prolonged exposure to the high levels of noise present in many aircraft cockpits is a source of environmental stress which may have adverse effects on performance and therefore deserves thorough investigation. Also, the forms of continuous noise experienced by many aircraft pilots and the complexity of various flight duties is apt to result in very different effects on performance than those observed in studies examining the effects of intermittent noise on vigilance during the conduct of relatively simple tasks, as has been the focus of many previous studies concerning the effects of noise on human performance (Koelega & Brinkman, 1986).

The sleep deprivation conditions to be studied in this experiment represent a realistic simulation of the fatigue which may be experienced after a long work day, particularly if the work day has not been preceded by a good night's sleep. Legally, a commercial pilot in domestic U.S. operations may be required to work a 16 hour duty day, which may also legally be extended if adverse weather conditions and traffic congestion delay flights. Other factors which may contribute to pilot fatigue are flight schedules which require swing shifts, or travel through time zones, both of which disrupt circadian rhythm and may be further aggravated by temporary occurrences of insomnia which often occur during a pilot's physiological adjustment to changes in sleep/wake cycles.

THE REVIEW OF THE RELATED LITERATURE

Introduction

In aviation, there are complex relationships which occur between human operators of aircraft, the machine, and various aspects of the external environment. Within this complex interface, many sources of stress are also present, and it is important to gain insight into how these stressors may interact to affect the performance of the human operator in order that he/she may learn to perform at optimal efficiency within the constraints of human strengths and limitations. Stress has been broadly defined as the sum of all the specific and nonspecific responses to a sudden or chronic demand for extra physiological, mental, or psychological functions (Berdanier, 1987). In the present study, stressors may be considered as any form of stimuli which require a response, and therefore increase demands on the human operator to channel energy into a stress response.

Stressors may occur in several forms, which may present themselves in any possible combination. The effects of these stressors may be perceived by the person responding to them as "stress," however, individual perceptions of stress vary widely. For the purposes of the present study, four broad categories of stress are identified here and defined as follows:

- 1.) Physiological stress - that which results in an increased physical demand on the human body, such as injury, exercise, changes in diet or eating habits, and changes in sleeping habits;
- 2.) Psychological stress - that which results in an increased emotional demand on the individual;
- 3.) Mental stress - that which results in an increased mental or cognitive demand on the individual;
- 4.) Environmental stress - that occurring when stimuli external to the human organism produce the demand for physiological, mental, or psychological responses, such as temperature changes, or exposure to noise or vibration.

The relatively novel discipline of human factors research is directed towards the development, understanding, and optimization of the relationships between people and their activities through the systematic application and integration of the human and engineering sciences (Wiener & Nagel, 1988). The nature of human factors studies necessitates that work in this domain be directed towards operations in the face of multifaceted and multi-originating forms of stress. It has been generally concluded that a theoretical account capable of satisfactorily predicting the effects of the discrete and interactive stresses acting

on human operators in real-world settings has not yet been established (Hancock & Warm, 1989; Hockey, Gaillard, & Coles, 1986).

Related Studies

Noise as a stressor. This lack of a common theoretical model is especially apparent in the many previous studies concerning the effects of noise on the performance of a task, which have revealed many conflicting results with no parsimonious explanation as to the inconsistency of these findings. Previous studies have reported widely differing results, with noise sometimes facilitating performance, sometimes degrading performance, and at other times having no affect at all (Broadbent, 1979; Coates, Adkins, & Alluisi, 1975; Hancock, 1984; Kryter, 1970; Loeb, 1980). Presently, no psychological effects of noise have been established (Grimaldi & Simonds, 1989).

Several studies have attempted to provide some introspection as to why such controversy exists. The findings of one study performed by Koelega, et. al. (1986) indicate that noise does affect performance, but suggests that this can only be observed when taking into account the conditions underlying the response, and also that the statistical analyses used in many noise studies were inadequate to accurately reflect variations in performance. Other investigators (Sanders, 1961; Woukon, 1969) had previously observed that noise sometimes has profound effects on performance variability that "can far overshadow or mask mean differences" and this may, in itself, be a significant finding. Another factor which may contribute to the inconsistency in results of noise studies is the type of experimental design which is used (Koelega & Brinkman, 1986). Apparently, within-subjects designs must be used with caution for this type of study, since they are vulnerable to asymmetrical transfer of training, which unnecessarily complicates their interpretation (Poulton, 1977). It must also be considered that most of the previous studies on noise have been limited in that they only applied to varieties of intermittent noise, which may have profoundly different effects on performance than various intensities of a sustained noise, as that of an aircraft engine or other machinery. Also, many of these studies focused on vigilance in the performance of a relatively simple task, in contrast to the performance of a highly complex task placing not only a high demand on vigilance, but on cognitive, mental, and other psychological aspects as well, such as would be the case in the conduct of a precision instrument approach in an aircraft under Instrument Meteorological Conditions.

Combined stressors of noise and fatigue. According to Hancock & Warm (1989), much of the previous research efforts have been limited to singular sources of stress rather than various combinations of stressors. Furthermore, previous studies have indicated that current knowledge of the effects of exposure to differing variables of noise on task performance in humans is

incomplete (Koelega & Brinkman, 1986). Presently, no clear pattern of physiological and behavioral reactions to noise by humans have been positively identified. This is in part due to the difficulty of directly analyzing the effects of noise-induced stress on the human organism in terms of a measurable physiological or psychological response. It has generally been assumed, however, that noise has deleterious effects on sustained mental concentration and cognitive functions (Hancock & Warm, 1989; Jerison, 1959), and that the mental effort required to block out or ignore constant noise during the performance of complex tasks by humans is mentally taxing (Cohen, 1978). Theoretically, then, the increased effort to sustain attention in the face of various stressors increases perceived workload since it requires mental energy which otherwise could have been directed to cognitive activities associated with performance of the task at hand. With this being the case, it seems only logical to propose that under conditions of high mental workload that the deleterious effects of noise on sustained attention would increase as a function of increases in noise intensity, or loudness, and time exposed to the noise stressor. Subsequently, task performance could be observed to suffer correspondingly to noise-induced decrements in attention. Increased susceptibility to fatigue would also be expected to result from the additional energy required to maintain a high degree of attention during task performance under the constant stress induced by noise.

High levels of an environmental stressor such as noise, under conditions of high mental workload during the performance of a complex task requiring a high degree of vigilance may result in an increased susceptibility to fatigue (CAMI, 1980; Thackray & Touchstone, 1979). This effect, when coupled with existing fatigue, such as that resulting from temporary sleep deprivation or sudden changes in sleeping habits, may cause an individual to exceed his or her tolerance limits for the attentional capacity and psychological adaptability necessary to sustain performance of a complex task to acceptable levels of competency, particularly under the added stress of high workload conditions (Hancock & Warm, 1989).

In his studies of human performance conducted at Cambridge University in 1939, Bartlett observed that when fatigued, pilots exhibited a disintegration of skilled performance which resulted in a loss in the overall management of a complex task (Wiener & Nagel, 1988). Peripheral activities (secondary activities), for example, checking fuel gauges, were overlooked by the participants, and there was a tendency to fixate on one or two instruments to the neglect of others. As a result of his studies of commercial airline pilots, McFarland (1953) concluded that it is reasonable to assume that if a pilot is unduly fatigued, an increased frequency of errors caused by forgetfulness, improper adjustment of controls, and similar operational errors will occur. The

role of fatigue as a causative factor in aviation incidents is further substantiated by reports submitted to NASA's Aviation Safety Reporting System (Billings & Reynard, 1984; Lyman & Orlady, 1981). Also, relationships have been shown to exist between injury experience and conditions that are believed to contribute to the cause of fatigue, such as long work shifts, insufficient rest, etc. (Grimaldi & Simonds, 1989). These studies demonstrated that fatigue leads to the breakdown of more complex skills during the performance of a complex task. Such a failure of a human operator under the driving influences of stress in a complex scenario demanding vigilance and precision could, even if momentarily debilitating, have profound consequences on safety. Therefore, it is important to develop a better understanding of the stress-related dynamics which subsume human performance limitations.

The present study purposes to gain insight into the cumulative and interactive effects that the stressors of noise exposure and fatigue induced by sleep deprivation have on aircraft pilot performance when these stressors are combined. It was expected that a significant interaction would occur between the two independent variables such that mean pilot performance scores would reflect a significantly greater number of operational errors under these variables when in combination than when either stressor was introduced separately. Therefore, the greatest performance decrements were expected to be seen in the group exposed to both the noise exposure and sleep deprivation variables. Also, the subjects in groups exposed to a singular stressor were expected to demonstrate poorer performance than the subjects in the control group. Such a pattern of results would lend support to the proposed concept that, as the number of stressors acting on a human operator mount, performance of a complex task requiring both skill and precision will deteriorate.

METHODOLOGY

The Data

In this study, two types of data were examined: the primary data and the secondary data. The nature and distinction of these two types of data is summarized below.

The primary data. The Mean Pilot Performance Scores (MPPS's) to be obtained in the study constitute the primary source of data to be analyzed. The MPPS's represent the dependent variable in this study, which will be examined in regards to the effects of noise exposure and/or sleep deprivation variables on subject performance.

The secondary data. The effects of pilot instrument experience level on Mean Pilot Performance Scores was examined separate from the primary data pertaining to the independent variables. MPPS's related to pilot experience level were subjected to appropriate statistical analysis in order to determine whether the results of this study supported those of previous research (Hancock, 1986) that have shown that more skilled pilots perform better than their less experienced counterparts when exposed to an environmental stressor.

The Criteria for the Admissibility of the Data

Clearance for the use of human subjects in this study was obtained from the Human Subjects Committee at Central Missouri State University. The signed clearance forms are included in Appendix A.

Only pilots who possessed a current airplane instrument rating were included in this study. For the purposes of this study, those pilots with less than 100 hours of total instrument experience, whether actual or simulated, were considered to be representative of a low level of instrument pilot experience. Pilots with over 100 hours of instrument experience, whether actual or simulated, were considered to be representative of high instrument pilot experience. These groupings of "low" and "high" instrument pilot experience are necessarily arbitrary, and were established relative to the population of pilots from which the participants for this study were selected. These relative measures of pilot instrument experience were employed in order to distribute the effects of pilot experience level on performance as evenly as possible across all four groups in the present study. This was accomplished by assigning to each group an equal number of "low experience" and "high experience" instrument pilots.

Only the last three ILS approaches executed by each subject under the experimental conditions appropriate to the subjects's assigned group were evaluated and scored for the purposes of this study. The first three approaches conducted by each subject were provided for subject familiarization of the flight simulator and also to control for practice effects, which could be a confounding variable, especially for those subjects who are not familiar with the flight simulator.

The Research Methodology

Subjects. The subjects for this study were voluntarily recruited from instrument rated airplane pilots in the Warrensburg, Missouri area who met the instrument flight experience requirements specified for this study. These requirements were that each participant must be able to meet applicable knowledge, skill, and proficiency standards as set forth in FAR 61.57(e) and FAR 61.65 for airplane instrument rated pilots, since it was necessary for the participants of this study to be able to conduct ILS approaches competently without assistance. It was assumed that pilots who had successfully acquired an airplane instrument pilot rating met the knowledge and skill criteria. Students and flight instructors at Central Missouri State University (CMSU), as well as one local commuter airline captain, were targeted for this study because of their availability and proximity. Screening of volunteers for the study on the basis of experience and proficiency qualifications was accomplished via a Subject Personal Data Sheet (Appendix B), which was completed by prospective subjects.

Sixteen male subjects between the ages of 21 and 31 years of age (mean age, 25 years) were originally selected to participate in the study. However, two of the subjects assigned to sleep deprivation groups were dropped from the study when they failed to show up as scheduled for their respective all-night sleep deprivation session on the evening prior to their flight simulator session. The study was conducted with the fourteen remaining subjects (N=14).

Tables 2 and 3 provide a summary of pilot experience characteristics, including the amount of total flight time and instrument time that each subject possessed immediately prior to the study. Instrument time is further broken down into the amount of actual instrument flight time, hood (simulated instrument flight) time, and simulator experience possessed by each subject. The pilot licenses and ratings held by each subject are also indicated on Tables 2 and 3.

The fourteen subjects included ten flight instructors (CFI's), six of whom were instrument flight instructors (CFII's) as well. Seven of the subjects held multi engine airplane ratings. Of the seven multi engine rated pilots, two were airline

transport pilots (ATP's), and one of the ATP's also held a multi engine flight instructor rating (MEI). All of the seven multi engine rated pilots were licensed commercial pilots; six of these were also certificated flight instructors (four CFII's and two CFI's). Of the four subjects who were not flight instructors, one was an instrument rated private pilot (not multi engine rated), and the other three possessed commercial pilot licenses with instrument airplane ratings. Of the three commercial/instrument pilots who were not flight instructors, only one possessed a multi engine airplane rating.

The four subjects who were not flight instructors were all students enrolled in the baccalaureate program in Aviation Technology at Central Missouri State University. Eight of the flight instructors were currently employed by CMSU; the other two flight instructors were formerly employed by CMSU, and one of these was currently employed as a captain at a commuter airline.

The participants of this study were selected from volunteers who filled out a Subject Personal Data Sheet (SPDS-see Appendix 1). The SPDS served as a screening device to select instrument pilots with experience qualifications appropriate for the study. It was necessary to select an equal number of pilots with "high" and "low" instrument pilot experience in order to evenly distribute the effects of varying pilot experience levels across all four experimental groups. Also, subjects were selected according to their times of availability for participation in the study so that subject availability could be matched with research and flight simulator schedules. Because of the measures necessary for screening, scheduling, and matching of subjects on experience level, generally accepted procedures of randomization in subject selection and assignment to groups was not possible. However, in order to obtain a segment of the pilot population appropriate for this study, screening and matching on instrument experience level was necessary, and for the purposes of this study, the advantages of such a selection process outweighed the obstacles presented by a purely random procedure of selection and assignment.

The 16 subjects initially selected for this study were divided into two pools according to relative instrument pilot experience level. The two subject pools were classified as "High" (instrument rated pilots with more than 100 hours of total instrument time), and "Low" (instrument rated pilots with less than 100 hours of total instrument time). For the purposes of this study, any combination of the following was considered to meet the instrument time requirements previously stipulated: simulated (hood) instrument flight time, actual instrument flight time, or instrument time obtained in a flight simulator.

Two subjects representing each of the two different flight experience levels ("High" and "Low") were arbitrarily assigned to each of the four experimental

Table 2

Subject Experience Characteristics: Low Time Subjects (Instrument Time < 100 hours)

Subject	Group	Total Flight Time	Instrument Time Logged	Instrument Time:		Pilot Ratings*	AST 300 Time
				Actual	Hood Sim		
S2	N-N	445	76	5	55	6	C/I, ME, CFII yes
S4	N-N	285	83	0	51	32	C/I yes
S7	H-N	550	72	3	65	9	ATP, CFII, CG yes
S8	H-N	245	44	10	30	4	P/I no
S11	N-H	380	58	3	55	0	C/I no
S12	H-H	340	57	10	45	2	C/I, ME yes
<u>S14</u>	<u>H-H</u>	<u>950</u>	<u>66</u>	<u>6</u>	<u>50</u>	<u>10</u>	<u>C/I, ME, CFII</u> <u>yes</u>
Means:		456	65	5	50	10	

* C/I = Licensed Commercial Pilot, Airplane/Instrument Rated
P/I = Licensed Private Pilot, Airplane/Instrument Rated
ME = Multi Engine Airplane Rating
ATP = Licensed Airline Transport Pilot
CG = Commercial Glider Pilot
CFI = Certificated Flight Instructor
CFII = Certificated Instrument Flight Instructor

Table 3

Subject Experience Characteristics: High Time Subjects (Instrument Time > 100 hours)

Subject	Group	Total Flight Time	Instrument Time Logged	Instrument Time:		Pilot Ratings*	AST 300 Time
				Actual	Hood Sim		
S1	N-N	900	104	22	73	9	C/I, ME, CFII no
S3	N-N	5180	340	166	174	50	ATP, ME, CFII, yes MEI
S5	H-N	2000	105	0	75	20	ATP, ME, CFI yes
S6	H-N	750	200	8	56	136	C/I, CFII yes
S9	N-H	1100	104	4	60	40	C/I, CFI yes
S10	N-H	600	104	3	101	0	C/I, CFI yes
S13	H-H	1400	155	50	90	15	C/I, ME, CFI yes
Means:		1704	159	36	90	39	

* C/I = Licensed Commercial Pilot, Airplane/Instrument Rated CFI = Certificated Flight Instructor
 ME = Multi Engine Airplane Rated CFII = Certificated Instrument Flight Instructor
 ATP = Licensed Airline Transport Pilot MEI = Multi Engine Flight Instructor

groups ($n=4$ for each group) in order to balance out the potentially confounding effects of varying levels of instrument pilot experience on performance. The four groups represented in the two-by-two factorial design of the present study are as follows: no (or ambient) noise/no sleep deprivation (N-N); no noise/24 hour sleep deprivation (N-H); high noise/no sleep deprivation (H-N); and high noise/24 hour sleep deprivation (H-H).

Apparatus. The apparatus required for the performance of the present study included a fully instrument equipped flight simulator model AST-300. Other necessary equipment included: a video camera, tripod, appropriate video film for the camera, a Subject Personal Data Sheet for each subject (see Appendix B), letters of agreement (see Appendix C) signed by each subject to provide written consent to the conditions of the study, a Quest sound meter, and National Oceanic Survey (NOS) instrument approach charts applicable to the approaches used. Housing, snacks, and entertainment in the form of movies was provided for those subjects who were exposed to the sleep deprivation condition. A television, VCR equipment with remote control, a stop watch, and Pilot Performance Scoring Forms (see Appendix D) were necessary for data evaluation. Engine noise simulation was provided by the AST-300 flight simulator, which has an engine noise feature with a volume control knob located on the simulator instrument panel.

The ILS Runway 19 Approach for Kansas City Downtown Airport (MKC) was used for the three practice instrument approaches conducted by the subjects in the AST-300 flight simulator (see Appendix E). The ILS Runway 1 Approach into Kansas City International Airport (MCI) was used for the three experimental instrument approaches conducted by each subject (see Appendix F).

Mean Pilot Performance Scores (MPPS's) were used as the dependent variable to provide a numerical measurement of pilot performance. The MPPS for each subject was the average (mean) of the three pilot performance scores obtained from the three scored experimental approaches conducted by each subject. An individual pilot performance score of zero represented a theoretical baseline measurement of perfect performance on the ILS approach with zero errors. Penalty scores were subtracted from this baseline value for each deviation from the published instrument approach procedure.

Procedure. Each pilot was given a brief flight simulator orientation prior to conducting instrument approaches in order to ensure that the subjects were reasonably familiar with the flight simulator. The time required for the orientation varied somewhat with each subject according to his previous knowledge and familiarity with the flight simulator operating procedures. The orientation process consisted of making sure each subject was acquainted with

the simulator V-speeds and power settings, which were posted on a plaque above the instrument panel for easy reference. The subjects that were not familiar with the flight simulator were permitted to go through the appropriate simulator checklists at their own pace and to "takeoff" and "fly" the simulator until familiar with the controls, power settings, and instrument panel.

Each pilot was allowed three practice ILS approaches before being tested in order to compensate for practice or warm-up effects, or a lack of familiarity with the flight simulator. The three practice approaches were followed by three experimental approaches, during which the subjects were exposed to the experimental conditions appropriate to their assigned groups. The ILS Runway 19 Instrument Approach Procedure (IAP) for Kansas City Downtown Airport (MKC) (see Appendix E) was used for the three practice approaches. A simulated no-wind condition was used for the first two practice ILS approaches, and a simulated wind condition of 150 degrees (a quartering headwind) at 20 knots was used during final practice ILS approach. Each subject performed the three experimental approaches using the ILS Runway 1 Instrument Approach Procedure for Kansas City International Airport (MCI) (see Appendix F) under various simulated wind conditions for each approach. Different approach procedures were used for the practice and experimental approaches in order to prevent a practice effect. Varying wind conditions were simulated during the experimental approaches in order to avoid a practice effect resulting from the use of a single wind condition. Also, the simulated wind conditions provided a more realistic situation requiring the pilots to compensate for wind drift. The same sequence of wind conditions were used for each subject, and were as follows: experimental approach #1: no wind; experimental approach #2: wind from 030 at 15 knots; experimental approach #3: wind from 340 at 20 knots. For each instrument approach, the subject was instructed to position the flight simulator at the proper altitude, heading, airspeed, and power configuration appropriate for crossing the published final approach fix, and then to indicate that he was ready, at which time he was automatically positioned over the final approach fix to begin the approach. Each subject was instructed to conduct a missed approach upon reaching the published decision height, but rather than following the published missed approach procedure, to maintain the localizer heading during the missed approach and to climb and maintain 2600 feet MSL.

Each subject was exposed to the stressor(s) appropriate to his assigned group. The subjects in the N-N, or control, group conducted approaches with ambient noise only, and were instructed to get a normal amount of sleep the night before the study. The subjects in the H-N group were exposed to 90 decibels of the simulated engine noise while conducting instrument approaches and were instructed to get a normal amount of sleep the night prior to being tested. The subjects in the N-H group were exposed to ambient noise only in the flight

simulator and were deprived sleep for approximately 24 hours prior to the study. The subjects in the H-H group were exposed to 90 decibels of simulated engine noise while conducting instrument approaches in addition to being sleep deprived for approximately 24 hours prior to the study. The decibel level of the noise exposure condition was adjusted to 90 decibels and monitored using a Quest sound meter.

The three experimental approaches conducted by each subject were videotaped and later reviewed and scored by the researcher. For each deviation from desired performance on one of the experimental approaches, penalty scores were subtracted from a theoretical "perfect" performance baseline of zero for each of nine separate components. The error components for which penalty scores were assigned include the following: deviations from localizer course; glideslope deviations; deviations from the recommended approach speed of 120 knots; failure to intercept the glide slope at the published glide slope intercept altitude; failure to extend the landing gear over the final approach fix; failure to execute a timely and proper missed approach procedure at the appropriate decision height; any ensuing descent below decision height; and overshoot or undershoot of the assigned level-off altitude for the missed approach procedure. Glideslope and localizer performance deviation scores, or "penalties," were computed by multiplying the magnitude of the deviation (in number of "dots" on the ILS indicator) by the duration of the deviation in seconds. A double penalty was assigned any full scale needle deflections on either the localizer course or glideslope by multiplying by two the product of the magnitude of the deviation (four "dots" for full scale needle deflection) and the duration of the full scale needle deflection in number of seconds. The airspeed component of the penalty score was the difference between the assigned approach speed of 120 knots and the average airspeed that the subject maintained during the approach. The penalty score assigned for the glideslope intercept altitude (GSIA) component of the approach was equal to the difference between the subject's altitude when crossing the localizer outer marker (LOM) and the published glideslope intercept altitude over the localizer outer marker of 2503 feet MSL on the ILS Runway 1 Approach at MCI. Failure or delay to extend the landing gear over the final approach fix within three seconds was assigned a penalty equal to the excessive delay in seconds. Descent below decision height was assigned a penalty score equal to the number of feet descended below decision height before taking corrective action (application of climb power) multiplied by the number of seconds delay before climb power was applied. Failure or delay to execute a proper and timely missed approach procedure (MAP) was assigned a penalty score equal to the sum of the following: delay in seconds to apply climb power, and/or delay in seconds to retract landing gear. Overshoot or undershoot of the assigned altitude of 2600 feet MSL during the missed approach procedure was assigned a penalty score

equal to the number of feet of deviation from the assigned altitude.

Statistical Analysis. The Mean Pilot Performance Scores obtained in this study were analyzed by Two-Way Analysis of Variance to evaluate the performance of the four separate groups in response to the four respective stress exposure conditions. A One-Way Analysis of Variance was conducted on the MPPS by experience level in order to examine the effects of instrument pilot experience on pilot performance under the various stress conditions used in this study.

RESULTS

The Mean Pilot Performance Scores (MPPS) for each individual subject in each of the four experimental groups are shown on Table 4. The MPPS are all negative scores which reflect deviations from a "perfect" performance baseline of zero. The MPPS for each subject is the mean of three scored ILS instrument approaches.

The group performance means and standard deviations for each of the four experimental groups are shown on Table 5. The lowest group performance mean was seen in the H-H group (Mean = -988.6). However, this group mean does not accurately reflect the performance of the H-H group as a whole due to the extreme variability between the scores of the individual subjects in this group. This was largely the result of the extremely low MPPS of a single individual, as can be seen by the individual subject MPPS for the H-H group presented on Table 4. The second greatest performance decrements were seen in the N-N group (Mean = -759.54). The low performance score average in the N-N group was also due to the extremely low MPPS of a single individual. The next highest group performance mean was produced by the H-N group (Mean = -507.81). The highest group performance mean, reflecting the lowest incidence of performance decrements, was produced by the N-H group (Mean = -340.0).

The data for the four experimental groups was submitted to a Two-Way Analysis of Variance, the results of which are depicted on Table 6. There were no statistically significant differences between the four groups. No significant main effects of noise exposure on aircraft pilot performance were seen ($p = 0.7335$), nor did this study yield any statistically significant main effects of sleep deprivation on performance measures ($p = 0.9368$). No significant interaction was seen to occur between the two stressors of noise exposure and sleep deprivation ($p = 0.2740$).

Apparently, no substantial cumulative stress effects occurred when the two stressors of noise exposure and sleep deprivation were combined at the levels used in this study, as was originally hypothesized. The fact that the poorest group performance mean occurred in the H-H group may at first glance seem to warrant a cumulative stress effect; however, a closer examination of the Mean Pilot Performance Scores of the individual subjects in this group reveals that the low mean score for the group may be attributed solely to the extremely low score of Subject 12. The other two H-H subjects' scores were substantially better than the average MPPS for all the subjects in the study, which was -646.8. Ironically, the best MPPS for the entire study (S13: -198.4) and the worst (S12: -2439.33) both occurred within the H-H group, resulting in a tremendous

Table 4

Mean Pilot Performance Scores for Individual Subjects by Groups

<u>Subject</u>	<u>Group</u>	<u>Experience Level</u>	<u>Total MPPS</u>
S1	N-N	High	-606.3
S2	N-N	Low	-405.6
S3	N-N	High	-253.3
S4	N-N	Low	-1772.97
S5	H-N	High	-408.27
S6	H-N	High	-256.6
S7	H-N	Low	-210.67
S8	H-N	Low	-1155.7
S9	N-H	High	-242.1
S10	N-H	High	-407.0
S11	N-H	Low	-370.9
S12	H-H	Low	-2439.33
S13	H-H	High	-198.37
S14	H-H	Low	-328.2

Table 5

Group Performance Means and Standard Deviations

<u>Group</u>	<u>n</u>	<u>Mean</u>	<u>Standard Deviation</u>
N-N	4	-759.5425	690.9113
H-N	4	-507.8100	440.1016
N-H	3	-340.0000	86.6840
H-H	3	-988.6333	1258.0161

Table 6

Summary of Two-Way Analysis of Variance of Mean Pilot Performance Scores

<u>Source</u>	<u>Means</u>	<u>df</u>	<u>MS</u>	<u>F</u>	<u>p</u>
Between Groups		3			
Noise Level (NL)		1	62976.05	0.12	0.7335
Ambient (N)	-579.7386				
90 dbs (H)	-713.8771				
Sleep Deprivation (SD)		1	3218.86	0.01	0.9368
Normal (N)	-633.6763				
Deprived (H)	-664.3167				
NL x SD		1	694850.25	1.34	0.2740
Within Groups		10	519338.10		

error variance. In fact, it is the extremely high error variance which occurred within each of three of the four experimental groups which precludes any significant differences between the groups. The N-H group was the only experimental group that did not demonstrate notably large differences in the MPPS's of its subjects. However, performance of the subjects within the N-N, H-N, and H-H groups was marked by considerable inconsistencies.

The effect of instrument pilot experience on performance was examined separately by treating the MPPS's of the two experience level groups (Low and High) to a One-Way Analysis of Variance, the results of which are presented on Table 7. The effects of instrument pilot experience approached, but fell short of, statistical significance ($p = 0.0854$).

Table 7

Effects of Instrument Flight Experience Level:
Summary of One-Way Analysis of Variance

Source	df	MS	F	p
Between	1	1327744.9062	3.4437	0.0854
Within	12	385556.7714		
Total	13			

DISCUSSION

Summary

The lack of significant findings in this study failed to support the hypothesis that a significant interaction would occur between the two stressors of 90 db of continuous noise exposure and fatigue induced by 24 hours of sleep deprivation. The hypothesized cumulative effects of stressors predicted that these two stressors, when combined, would produce performance decrements measurably greater than those which might result from exposure to either stressor singularly. No cumulative effects of stressors were observed in the present study. In order for the results of this study to lend support to the proposed concept of the cumulative and interactive effects of stressors on pilot performance, the pattern of results would have to demonstrate the lowest incidence of performance decrements in the N-N group, and the highest incidence of performance decrements in the H-H group, with the performance measures for the H-N and N-H groups falling somewhere in between those of the N-N and H-H groups. This pattern of results did not occur. Instead, there was no consistent pattern in the results indicative of cumulative stress effects; nor did the MPPS's obtained under the different stress conditions vary with each other in a systematic manner characteristic of an interactive stress effect. No main effects of either noise exposure or sleep deprivation were observed.

At first glance, the fact that the H-H group had the lowest group performance mean score would seem to support the proposed concept that the effects of multiple stressors would accumulate to degrade performance to a greater degree than would a single stressor. However, the low mean of the H-H group was the result of the extremely low MPPS of a single subject. The N-H group showed the lowest incidence of performance decrements, with a Group Performance Mean Score of -340.0, followed by the H-N group with a Group Performance Mean Score of -507.81. The N-N group had the second largest measure of deviation from desired performance with a Group Mean Performance Score of -759.54. The H-H group demonstrated the largest measure of performance decrements with a Group Performance Mean Score of -988.63. The unexpected findings of this study were in large part due to the extreme variability of the MPPS of three subjects (Subjects 4, 8, and 12), all of whom had relatively low instrument pilot experience (< 100 hours).

The effect of instrument pilot experience on performance was expected to be significant, however, the results of a One-Way Analysis of Variance fell short of statistical significance.

Conclusions

The large error variance demonstrated in the results of this study precludes any conclusive determinations concerning the cumulative and interactive effects of combined stressors on aircraft pilot performance. There are several possible explanations to account for the source of the error variance. One is that the sample size was too small to ensure generalizability. Another is that the individuals participating in the present study varied so greatly in their overall pilot experience in terms of total flight time, pilot training, and ratings earned that instrument pilot flight time did not accurately reflect experience level or individual piloting skill. This could also explain the lack of a significant main effect of pilot experience.

It appears that negative transfer and/or lack of familiarity with the AST 300 flight simulator used in the study may have contributed to the low MPPS's of some of the subjects. Two of the subjects who scored excessively below the average MPPS of -646.8 for all four groups combined had little or no experience in the AST 300 flight simulator. Subject 12, who scored the lowest MPPS of -2439.33, had only two hours of previous experience in the simulator; and Subject 8, who scored the third lowest score of -1155.7, had neither previous experience in the AST 300 simulator or a multi engine rating. Both Subjects 8 and 12 had less than 100 hours of total instrument flight experience. Of the pilots with over 100 hours of instrument flight time, Subject 1, who had no previous experience in the AST 300 simulator, scored the lowest MPPS of -606.3, well below the average MPPS of -338.9 for the "high" experience pilots.

Possibly, the 24 hours of sleep deprivation was not sufficient to cause substantial performance decrements during the short length of time that the subjects spent in the flight simulator conducting instrument approaches. In addition, the nature of the task of conducting instrument approaches may have produced ample mental stimulation to temporarily offset or delay the effects of fatigue. Pilot performance may also have been influenced by the fact that the subjects knew that they were being observed and video-taped, and this resulted in increased alertness. The short length of time (20-30 minutes) that the subjects spent in the simulator conducting approaches may not have been of sufficient duration for the deleterious effects of either of the stressors of noise exposure or sleep deprivation to manifest themselves in terms of significant performance decrements. It is likely that these stressors become more pernicious in their effects on the performance of a complex, high-vigilance task over a more extended period of time. These stressors may also vary in their effects over an extended length of time depending on whether the nature of the task is monotonous (such as extended straight-and-level cross-country flight operations) or requires a high degree of vigilance, which provides more mental

stimulation (as does an instrument approach).

Although the predicted pattern of results was not obtained in this study, there is still strong evidence that high stress loads do contribute to performance deficits in the operation of flight skills, particularly during high work load conditions requiring a high degree of attentiveness and precision, such as in the conduct of instrument approach procedures. Subsequently, the safety of aircraft operations could be seriously compromised as performance-degrading stressors mount. Professional pilots are subject to a myriad of stressors-psychological, physiological, mental, and environmental-which may occur in any combination at any time.

Pilot accounts submitted to NASA's Aviation Safety Reporting System provide documentation of the potential safety hazards presented by excessive stressors, particularly fatigue, in the cockpit (Billings & Reynard, 1984; Lyman & Orlady, 1981; Food Fatigue, 1991). Del Vecchio (1977) anticipated such consequences when he commented that "fatigue in flying should be considered with respect to performance decrements resulting from prolonged application at a skilled task in the presence of exposure to stress of many kinds." It is therefore essential that a serious effort be made to minimize or eliminate all controllable forms of stress which could combine with unavoidable stressors to impair pilot performance. These same implications could be expanded apply to other workers, such as air traffic controllers, whose jobs demand a high degree of vigilance and precision in the face of a variety of stressors.

Since substantial evidence exists supporting the pernicious effects of fatigue and noise in the cockpit (CAMI, 1980; Mac Farland, 1953) the sources of fatigue and excessive noise should be controlled to the greatest extent possible. Such an effort to control safety-critical forms of stress requires cooperation and coordination between pilots, management, scheduling personnel, and regulatory authorities. The individual pilot is normally aware of the amount of sleep necessary for his or her optimal performance capacity, and therefore must assume responsibility to assure that an adequate amount of sleep is obtained prior to scheduled duty periods. It is the responsibility of company management and crew scheduling to allow adequate rest periods for flight crews on overnight assignments, taking into account time that is needed for transportation to and from lodging facilities, meals, and possible flight delays. It is also necessary that regulatory authorities evaluate current legislation defining duty time and rest period requirements to determine whether they are sufficient. There is evidence which indicates that, currently, pilots are not protected against the potentially hazardous effects of fatiguing duty schedules (Mark, 1991).

Concerning noise exposure, pilots have the responsibility to wear hearing

protection devices, which help to alleviate the psychological and physiological effects of noise stress, but may also serve to impair communications between pilots in a noisy cockpit. Quieter aircraft engines are currently being manufactured to meet more stringent noise control regulations. However, many aircraft with the older, noisier engines are still in commercial operation, and may produce noise levels in the cockpit which may not only impair pilot performance and communications and contribute to fatigue, but are also capable of inflicting permanent hearing damage.

In conclusion, aircraft pilots are exposed to many stressors which may interact in such a manner, or accumulate to such an extent, that performance of safety-critical tasks may be adversely affected. The extent to which various stressors effect pilot performance, the potential threats to safety, and methods by which potential sources of stress may be controlled, therefore deserve continuing research and consideration.

Recommendations

To ensure greater homogeneity among subjects, it is recommended that future studies select a population that is better matched not only on instrument pilot experience, but on the subject variables of total flight experience and level of previous flight training as well. To prevent the confounding effects of negative transfer or lack of familiarity with flight simulator equipment, future studies should ensure that subjects are more equivalent in their experience with the type of equipment to be used. Larger sample sizes would allow for greater generalizability of results, and would also decrease the chance for large error variance.

It is likely that the detrimental effects of noise exposure and sleep deprivation on complex task performance may be a function of the duration of time that the task is performed. From the results of the present study, it appears that the levels of noise exposure and sleep deprivation used in this study may not substantially affect pilot performance during the conduct of instrument approaches during the initial 20-30 minutes of flight. Since each pilot spent only 20-30 minutes in the flight simulator during this study, the results of this study cannot necessarily predict the cumulative and interactive effects of the stress conditions examined here on the long-term performance of pilots exposed to similar conditions. Future studies should examine the effects of these variables over a more extended period of time. Pilot performance after longer periods of sleep deprivation, or the more realistic conditions of minimum legal rest periods in combination with extended duty periods, should also be the focus of continuing research.

No attempt was made in this study to control for the extraneous variables of diet and caffeine intake. In light of the evidence that poor dietary habits, especially in combination with existing fatigue, may have profound effects on performance ("Food Fatigue," 1991), efforts should be made to further study and control for these variables. The results of the present study indicate that negative transfer, and the extent to which it is a threat to aviation safety, is another variable which should be studied and controlled.

References

- Berdanier, C. A. (1987, March/April). The many faces of stress. Nutrition Today, pp. 12-17.
- Billings, C. E., & Reynard, W. D. (1984). Human factors in aircraft incidents: Results of a seven-year study. Aviation, Space, and Environmental Medicine, 55, 960-965.
- Broadbent, D. E. (1979). Human performance and noise. In C. M. Harris (Ed.), Handbook of noise control (pp. 17-1 to 17-20). New York: McGraw-Hill.
- Coates, G. D., Adkins, C. J., Jr., & Alluisi, E. A. (1975). Human performance and aircraft-type noise interactions. The Journal of Auditory Research, 15, 197-207.
- Cohen, S. (1978). Environmental load and the allocation of attention. In A. Baum, J. E. Singer, & S. Valins (Eds.), Advances in environmental psychology (Vol. 1), (pp. 1-29). Hillsdale, NJ: Erlbaum.
- Del Vecchio, R. J. (1977). Physiological aspects of flight. Oakdale, N. Y.: Dowling College Press.
- Federal Aviation Administration, Civil Aeromedical Institute. (1980). Physiological Training. Oklahoma City, OK: Mike Monroney Aeronautical Center.
- Federal Aviation Regulations/Airman's Information Manual. (1991). Renton, WA: Aviation Supplies and Academics, Inc.
- Food Fatigue. (1991, November). Air Line Pilot, 60, p. 15.
- Grimaldi, J. V., & Simonds, R. H. (1989). Safety management. (5th ed.). Homewood, Illinois: Richard D. Irwin, Inc
- Hancock, P. A. (1984). Environmental stressors. In J. S. Warm, (Ed.), Sustained attention in human performance (pp. 103-142). Chichester, U. K.: Wiley.
- Hancock, P. A. (1986). The effect of skill on performance under an environmental stressor. Aviation, Space, and Environmental Medicine, 57, 59-64.

- Hancock, P. A., & Warm, J. S. (1989). A dynamic model of stress and sustained attention. Human Factors, 31, 519-537.
- Hockey, G. R. J., Gaillard, A. W. K., & Coles, M. G. H. (Eds.). (1986). Energetics and human information processing. Dordrecht, the Netherlands: Martinus Nijhoff.
- Koelega, H. S., & Brinkman, J. A. (1986). Noise and vigilance: An evaluative review. Human Factors, 28, 465-481.
- Koelega, H. S., Brinkman, J. A., & Bergman, H. (1986). No effect of noise on vigilance performance? Human Factors, 28, 581-593.
- Kryter, K. D. (1985). (2nd ed.). The effects of noise on man. New York: Academic Press.
- Loeb, M. (1980). Noise and performance: Do we know more now? In J. V. Tobias, G. Jansen, & W. D. Ward (Eds.), Proceedings of the Third International Congress on Noise as a Public Health Problem (pp. 303-321), Rockville, MD: The American SLH Assn.
- Mark, R. (1991, September). Continuous duty overnight. Air Line Pilot, pp. 22-25.
- McFarland, R. A. (1953). Human factors in air transportation. New York: Mc Graw-Hill.
- Mertens, H. W., & Collins, W. E. (1985). The effects of age, sleep deprivation, and altitude on complex performance. (Report No. FAA-AM-85-3). Oklahoma City, OK: FAA Civil Aeromedical Institute.
- Poulton, E. C. (1977). Arousing stress increases vigilance. In R. R. Mackie (Ed.), Vigilance: Theory, operation performance, and physiological correlates (pp. 423-459). New York: Plenum.
- Reinhart, R. O. (1988, December). The fatigued pilot. Business and Commercial Aviation, pp. 126.
- Sanders, A. F. (1961). The influence of noise on two discrimination tasks. Ergonomics, 4, 253-259.
- Taylor, L. (1988). Air travel: How safe is it? (pp. 40-46) Oxford: BSP Professional Books.

Thackray, R. I., & Touchstone, R. M. (1979). Effects of noise exposure on performance of a simulated radar task. (Report No. FAA-AM-79-24). Oklahoma City, OK: Civil Aeromedical Institute.

Wiener, E. L., & Nagel, D. C. (Eds.). (1988). Human factors in aviation. San Diego: Academic Press, Inc.

Wokoun, W. (1969). Music for working. Science Journal, 5A, 54-59.

AGING COMMERCIAL AIRFRAMES

by

**Howard W. Smith, Ph.D.
University of Kansas**

**For Presentation to the AIAA/FAA Joint Symposium on General
Aviation Systems at the Hilton Inn-East, Wichita, KS
on March 16-17, 1992**

AGING COMMERCIAL AIRFRAMES

Howard W. Smith, Ph.D.

Abstract

This paper contains a discussion of important factors which contribute to the aging of airframes, a brief historical background of the present focus on "aging aircraft fleets", and a plan to ensure structural safety is presented. The new plan is a proposed modification of an existing military plan, called ASIP (Aircraft Structural Integrity Program). The proposed commercial version, like its military predecessor has five phased tasks. The primary difference between military and commercial airplanes stems from the multiplicity of commercial operations. The plan utilizes a feedback system which connects and loops all structural damage, such as corrosion and crack growth, from individual airplane tracking data back through the original design process.

INTRODUCTION

After the Aloha Airline Flight 242 accident on April 28, 1988, aviation magazines and popular media were replete with "aging aircraft" articles (Ref. 1). The U.S. Congress responded by passing a 1990 amendment to the 1958 Federal Aviation Regulations act, authorizing "suspension of airworthiness certificates" (grounding of a fleet) (Ref. 2). The following year, the Senate and House passed H.R. 172,

the "Aging Aircraft Safety Act of 1991" (Ref 3)

This important piece of legislation delegated responsibility to the FAA to ensure safe operations of aging aircraft.

DISCUSSION

Scope In this paper, aircraft are defined as airplanes, rotorcraft, and similar vehicles that operate within the earth's atmosphere. Airframes are portions of the aircraft that carry the structural loads. The structural elements are skins, stringers, spars, ribs, longerons, bulkheads, fittings, and fasteners; decks and floors are also important elements. An aircraft's life is the time between its original conception, to the time the airplane is crashed or removed from service. The three most important factors of aging evidenced in airframes are fatigue, crack growth, and corrosion. The two mechanical factors, fatigue and crack growth, are discussed in this paper.

Aging airframes and airplane systems age simultaneously, but at different rates. This paper is focused on deterioration of the airframe structure. The earliest concepts of airplane deterioration were based on observations of structures that existed long before fleets of airplanes populated the skies. Buildings, bridges, and machines were observed to "fail" for diverse reasons. They would rupture, collapse, break, and buckle. Post-examination of the broken parts revealed that the faults were often near a scratch, a hole, or a small radius; welds and casting imperfections were also cited as contributing causes. It was also noted that many parts were corroded or discolored, and that some fracture faces had "crystallized" and exhibited "beach marks". A whole set of terminology emerged to classify the failures and their causes. "Durability and damage tolerance," used extensively in the airframe industry, has almost replaced the older terminology of "fatigue and fracture mechanics;" even the old "rust" has been

expanded to include corrosion and its many species, fretting, flaking, exfoliation, and galvanic action. The causes of the airframe aging have not changed, but the jargon has. Some people and events that furthered the study of structural failure are listed in Fig. (1)

Life People concerned with the "aging fleet" usually infer the question, "How many safe years of operation remain?"- in other words "How much life is left". The roll-out date of an airplane like the chronological age of a human, is only an indication of health. Some would measure an airplane's age instead by the number of flight hours it has accumulated, but this measure is also insufficient as a measure of age. Gerontologists use terms such as "frail elderly" to differentiate people who are younger and in poor health from those who are perhaps older and in better health. Similarly, there are airplanes that may have several landings with relatively few flight hours. There are many factors that contribute to the aging, and thus the true "age" of an airplane. If all of those causes of death could be eliminated, then immortality could be achieved. Since this is a simplistic idea, a second best plan would be to carefully monitor the aging process and postpone the inevitable as long as possible. We now do this by priming, painting, plating and similar delaying actions. When these methods are inadequate, imperiled structures are replaced by project "Re-skin" or SEPs (Service Life Extension Programs). A total life cycle can be depicted with a wheel of life, Fig. 2.

Durability (Fatigue) The fatigue phenomenon was studied in laboratories with rotating beam specimens. Repeated stresses were applied at a constant mean stress and a sinusoidal alternating stress. The effects of variation in specimen alloy, heat treat, surface roughness, and

induced notches were methodically studied. Hostile environments (such as elevated temperatures, salt and mist), and coatings to defend against them were superimposed upon the variables mentioned above. Great labor was expended to prepare the specimens and to simulate the environmental conditions which deteriorate airframes. Catalogs of data were collected and assembled for use in cumulative damage formulas; the formulas were then used to predict the "life" of a structure. It was discovered that the number of variables was so large that the effects could mask one another. There are numerous reports which remind us that the number of operational environment variables require a probability approach to design for prevention of fatigue failure. In aircraft structures, engineers originally applied conservative "scatter factors" to ensure that a catastrophic failure would not occur during the useful lifetime of the aircraft. This philosophy is still used, and has been dubbed "the safe life approach". The difficulties encountered with this fatigue method provide incentive for improving methods of design, construction and analysis.

Damage Tolerance (crack growth) This new terminology has replaced older phrases such as "tear-resistance" and "fracture mechanics". After the Comet crashes, tear-stoppers and multiple load path structures received increased attention. Structural analysis and construction became more complicated, but reliability rose. The famous FAR-25.571 emerged and structural engineers were afforded another option, "fail-safe" design. With multiple load path design, structures could tolerate damage and cracks and still make it safely to base. It was planned that cracks could be found by inspection and then repaired. To eliminate repeated inspection of the entire airframe, critical locations on each craft were predetermined by crack growth analysis and tests.

Additional "critical locations" were found after the aircraft entered service. Engineers employed in DADTA groups, (Durability And Damage Tolerance Analysis) became sensitive to many factors that adversely affect the airframe, and found ways to extend an aircraft's utility. They informed their colleagues about subtle weaknesses that appear as a result of seemingly unrelated but combined loads. Methods were then sought to restore the life of the aircraft. For example, a wing-mounted landing gear may impose a heavy stress spectrum due to the GAG (ground-air-ground) cycle. The same wing spar location may accumulate significant damage and crack growth due to gust and maneuver loads. Likewise, a fuselage longeron may wear out due to the combined actions of flight, landing, and multiple pressurizations. Crack growth methods are more formidable than fatigue methods because many airframe materials exhibit retardation characteristics. Unlike fatigue methods, the growth methods require the sequence of loads be specified as well as their magnitudes. In addition the environmental factors that affect fatigue are ever-present during crack growth. When a crack grows to a critical length, and safety is compromised, the aircraft has lost its residual strength, as shown in Fig. 4.

Feedback

"When is your airplane too old to trust?"

This title and variations of it appear periodically in aviation literature. Decades ago, the Guggenheim safety foundation published technical notes and accounts of serious accidents and incidents. It was expected that designers would read them and take preventative action in order to avoid repeating old blunders on new models. Later, the Federal Aviation Administration published Advisory Circulars called AIDS for the same purpose. Now "Alerts" and Service Difficulty Reports serve the same

purpose as the old Guggenheim papers. A clinical method that engineers call feedback is a powerful tool for design and maintenance. By observing prolific cracking and corrosion in the field, and retracing the design steps with the new data in hand, engineers can make educated decisions which result in higher levels of reliability. This procedure has been shown to be quite successful on military aircraft fleets.

ASIP

The Aircraft Structural Integrity Program is a current military standard, (Ref. 4). Each aircraft's prime manufacturer must submit an ASIP master plan to obtain approval for use in service. An outline of the plan appears in Fig. 3. It shows the five main tasks which comprise ASIP; Task I is the early design phase, and Task V extends through the flight operational phase until actual retirement of the aircraft from service. Roughly speaking, the aircraft belongs to the manufacturer during the first three Tasks, is delivered to the customer at Task IV and belongs to the customer thereafter. Two examples of the use of an ASIP feedback plan are given below. Example No. 1. A maintenance inspector discovers a crack in the primary structure of one airplane. He writes the discrepancy up according to the specified reporting requirements, and submits the written report to his immediate supervisor. The supervisor suggests inspection on the opposite side of the airplane and all similar locations on other airplanes under the purview of the supervisor. The supervisor is then required to share his findings with the next level of management and headquarters. They will then check the fleet records (Task IV) to see if similar airplanes based at other geographical locations have experienced similar difficulties. At this time, it can be determined whether this is an isolated case, or the possible onset of an epidemic. That decision may result in grounding of the fleet. A subsequent decision to return the fleet to flying

status will undoubtedly require a re-review of the full scale tests (Task III), the analysis and component tests (Task II) and the basic requirements (Task I).

Example No. 2. An airplane has crashed.

Preliminary crash investigation reveals that the airplane broke up in flight. Several scenarios are possible: there was an undetected flaw, the airplane exceeded critical flutter speed, the airplane encountered severe turbulence, there was a control system failure (Task V). As in the first example, the crash investigator reports his findings to his supervisor. The supervisor relays the preliminary findings to the cognizant group at headquarters; management then reviews previous reports of flight tests and full scale ground tests. As in example No. 1, the feedback should be applied to all relevant analysis reports and technical reports and drawings. If individual airplane tracking reveals that the original design assumptions are inaccurate, then new analyses can be undertaken using the corrected specifications.

CASIP. The appropriate acronym for "Commercial Aircraft Structural Integrity Program," first appeared as an element of "The National Aging Aircraft Research Program" in 1990, Ref. 5. Although it has the same objectives as its military analog, it would, out of necessity, be managed differently. In contrast to the small number of military branches, there are multitudes of commercial owners and operators. Additionally, two airplanes of the same model can experience vastly different loading conditions under different use and ownership. For these reasons, individual airplane tracking will be difficult and burdensome. Task IV in CASIP will have to revert to the manufacturer, or to another independent agency. Owners and operators would have to be trained to perform the duties required by Task V. The actual management of CASIP could best be specified after all 35 elements of

CASIP are detailed. The detailed descriptions should be formulated with "DIDs," (Data Item Descriptions) currently in use by military branches to control and certify structural integrity.

Other Feedback Systems ASIP is a large and comprehensive system, but not the only possibility. The Boeing Company initiated a closed loop comprehensive system in 1968. It was reported informally in 1972 (Ref. 6) and presented formally in 1976 (Ref. 7), Figure 5 was originally published in Ref. 7. Each rectangle in the figure represents a computer module for performing a task. Only the weights, structures and cost modules are shown.

During the early 1970's NASA Langley and several companies were also synthesizing large systems. An interesting program reported in 1990 is contained in (Ref. 8); an update of (Ref. 5) is reported in (Ref. 9).

CONCLUSIONS

1. A growth of specific structural index (number of reliability "nines" per life cycle cost dollar), is achievable in all classes of commercial aviation aircraft and rotorcraft.
2. Many independent engineering monitoring procedures are currently practiced. More benefits can be gained by formal feedback loops.
3. Information reported in "Alerts", and in Accident Investigation reports is the substance of aircraft geriatrics.
4. Aircraft gerontology can benefit young aircraft as well as the aging aircraft suffering the consequences of prolonged and severe operational usage.
5. Many of the same failure modes occur in seemingly different classes of aircraft. A well conceived structural integrity program master plan for new aircraft will

make maximum use of all knowledge gained from previous programs. Maximum usefulness is achieved by rigorous feedback analysis and corresponding engineering and operational use changes.

6. An ideal cross-feed structural integrity program for any aircraft would accept new information from any branch of military service, any flag, and any commercial aircraft, regardless of its certification classification.

7. Smith, Howard W., "Computer Interactive Graphics in Aerospace Engineering Design Education," AIAA No. 76-900, Dallas, TX, September 27, 1976.
8. Pemberton, Stephen L., "Field Failure Return Program," Reliability Analysis Center, July 1990.
9. ACD-200, "National Aging Aircraft Research Program", DOT/FAA/CT-88/32-1, September 1991.

REFERENCES

1. NTSB, "Aircraft Accident Report: Aloha Airlines, Flight 243." NTSB/AAR-89/03, 28 April 1988.
2. Hon. Mr. Anderson, "Aging Aircraft Safety Act of 1990." 101st Congress, H.R. 3774, 16 July 1990.
3. Hon. Mr. Oberstar, "To Assure the Continuing Airworthiness of Aging Aircraft." 102nd Congress, H.R. 172, 3 January 1991.
4. "Airplane Structural Integrity Program." MIL-STD-1530A, 11 December 1975.
5. ACD-200/210 AAM-500, "National Aging Aircraft Research Program." DOT/FAA/CT-88/32, August 1989.
6. Smith, Howard W., "Airplane Geriatric Engineering", speech to Society of Manufacturing Engineers, student branch, University of Kansas. 27 September 1972.

J. Bauschinger	1886	Cyclic Stresses
B.A. Griffith	1920	Rupture of Solid
J. Doolittle	1925	"Bumpy Air"
Bland and Sandorf	1943	Tear Resistance
M. Miner	1945	Cumulative Damage
K. Lenzen	1949	Bolted Joint Fatigue
A. Freudenthal	1951	Statistical Distribution
H.L. Cox	1952	Fuselage Fracture
H. Hardrath	1953	Plasticity Near Notches
R. Peterson	1953	Stress Concentration
-- --	1954	Comet Crashes
H. Grover	1954	Fatigue of Metals
W. Weibull	1954	Non-Gaussian Statistical Theory
H.W. Smith	1956	Military Crash Investigation
A. Sorensen	1956	Tear Resistance
W. Illg	1956	Stress Risers
G. Irwin	1957	Crack Tip Focus
P. Paris	1957	Fracture Mechanics Approach
A. Fuchs	1959	"Dos & Don'ts"
W. Walker	1959	VGH Data (Piston ASRPs)
S. Manson	1960	Thermal Stress, Low Cycle Fatigue
J. Shive	1961	Programmed Testing
R. Gatts	1961	Rigorous Statistical Theory
G. Barenblatt	1962	Wedge Testing
FAA	1989	Inception of CASIP

Fig. 1 Study of Structural Failure --- History

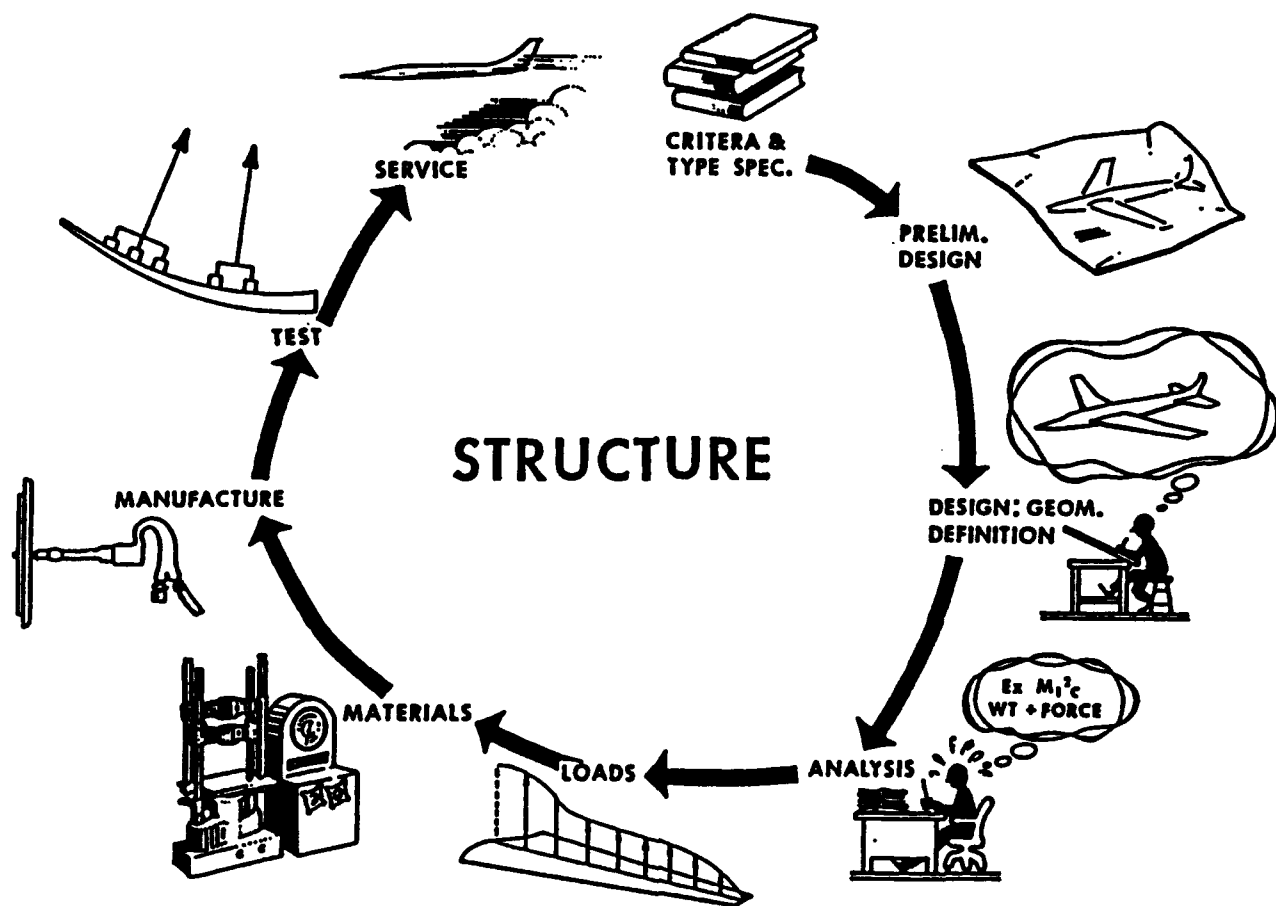


Fig. 2 Wheel of Life

TASK I	TASK II	TASK III	TASK IV	TASK V
DESIGN INFORMATION	DESIGN ANALYSES AND DEVELOPMENT TESTS	FULL SCALE TESTING	FORCE MANAGEMENT DATA PACKAGE	FORCE MANAGEMENT
ASIP MASTER PLAN STRUCTURAL DESIGN CRITERIA DAMAGE TOLERANCE & DURABILITY CONTROL PLANS SELECTION OF MAT'L'S, PROCESSES, & JOINING METHODS DESIGN SERVICE LIFE AND DESIGN USAGE	MATERIALS AND JOINT ALLOWABLES LOAD ANALYSIS DESIGN SERVICE LOADS SPECTRA DESIGN CHEMICAL/ THERMAL ENVIRONMENT SPECTRA STRESS ANALYSIS DAMAGE TOLERANCE ANALYSIS DURABILITY ANALYSIS SONIC ANALYSIS VIBRATION ANALYSIS FLUTTER ANALYSIS NUCLEAR WEAPONS EFFECTS ANALYSIS NON-NUCLEAR WEAPONS EFFECTS ANALYSIS DESIGN DEVELOPMENT TESTS	STATIC TESTS DURABILITY TESTS DAMAGE TOLERANCE TESTS FLIGHT & GROUND OPERATIONS TESTS SONIC TESTS FLIGHT VIBRATION TESTS FLUTTER TESTS INTERPRETATION & EVALUATION OF TEST RESULTS	FINAL ANALYSES STRENGTH SUMMARY FORCE STRUCTURAL MAINTENANCE PLAN LOADS/ENVIRONMENT SPECTRA SURVEY INDIVIDUAL AIRPLANE TRACKING PROGRAM	LOADS/ENVIRONMENT SPECTRA SURVEY INDIVIDUAL AIRPLANE TRACKING DATA INDIVIDUAL AIRPLANE MAINTENANCE TIMES STRUCTURAL MAINTENANCE RECORDS

MIL-STD-1530A

Fig. 3 ASIP: Five Tasks

STRENGTH VS CRACK LENGTH

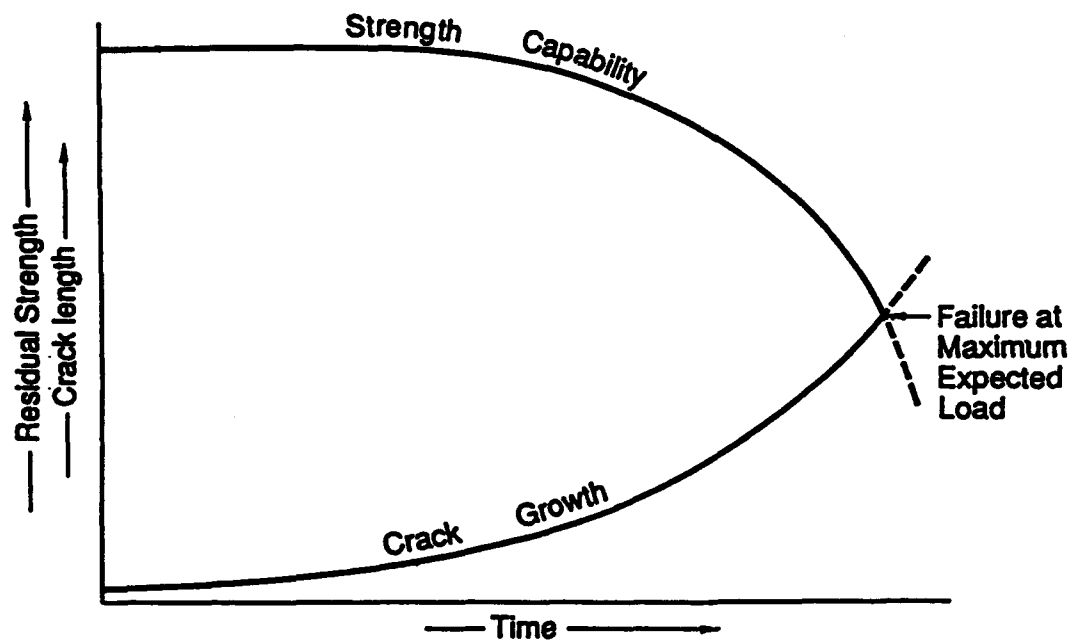


Fig. 4 Residual Strength

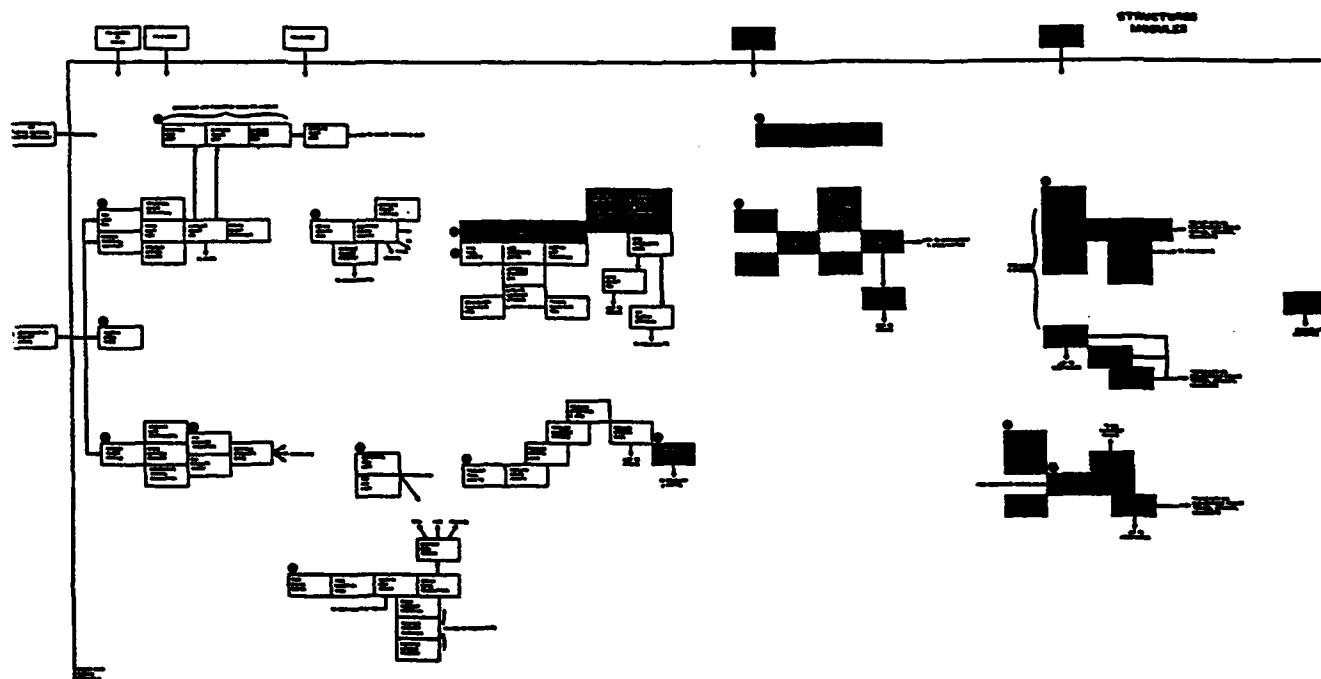


Fig. 5 Large Feedback System

**A COPARISON OF THE V-G METHOD AND THE
ROOT LOCUS METHOS FOR FLUTTER**

by

**Brian Sibbit
McDonnell Aircraft Company
and
Walter Eversman
University of Missouri-Rolla**

**For Presentation to the AIAA/FAA Joint Symposium on General
Aviation Systems at the Hilton Inn-East, Wichita, KS
on March 16-17, 1992**

A COMPARISON OF THE V-G METHOD AND THE ROOT LOCUS METHOD FOR FLUTTER

Brian Sibbitt
McDonnell Aircraft Company

and

Walter Eversman
University of Missouri-Rolla

ABSTRACT

The root locus method using transient aerodynamics is applied to a flutter analysis of a T-Tail to demonstrate its capabilities and advantages in predicting the flutter point. The standard V-G method is used as a basis against which the results are compared. The essential features of the root locus method are discussed, including the generation of the transient airforce model. It is shown that the root locus method produces the same flutter point as the V-G method, but has the added advantage of providing valid results for damping and frequency of the response of the structure at speeds below flutter.

INTRODUCTION

Flutter analysis has traditionally been carried out using methods based on the assumption of harmonic motion of the aeroelastic system. The conditions on velocity and Mach number, oscillation frequency, and structural damping which permit the harmonic motion are determined by the use of an iterative scheme based on a sequence of eigensolutions. The flutter point found in this way constitutes the boundary between stable response (convergent oscillations) and unstable response (divergent oscillations). No fully valid information can be obtained about the stable response or about the rate of onset of the unstable behavior as Mach number is increased.

The V-G method is the best known of the harmonic response formulations. In this approach the altitude is specified and the Mach number is varied. For each Mach number the reduced frequency is varied, permitting the evaluation of the airforces from one of a number harmonic airforce theories which require that density, Mach number and reduced frequency be specified. For each reduced frequency an eigensolution yields the velocity (V), structural damping (g), and frequency at which harmonic motions can exist. The reduced frequency is varied until the lowest velocity is found at which oscillations can occur with a specified positive (or zero) value of the structural damping coefficient g . This defines a flutter velocity for the current value of Mach number. This process is continued for a range of Mach numbers. For the fixed altitude there is unique relation between Mach number and velocity. The point at which the Mach number and flutter velocity are consistent can be determined and is noted as the matched flutter point. The flutter Mach number and corresponding frequency are thus determined for the specified altitude.

The root locus method is based on a model of the aeroelastic system in the time domain, as opposed to a frequency domain model in the V-G method. The aeroelastic system is modeled with aerodynamic forces which are derived from a set of aerodynamic state equations appended to the structural equations of motion. The aerodynamic forces are functions of density and Mach number. The model for the aeroelastic system is put in the form of a linear time invariant system, the standard form of modern control theory. At a specified altitude the Mach number can be considered as a "gain" which is varied to produce a locus of the roots which determine the character of the transient response of the system to perturbations in the initial state. If a suitable transient aerodynamic representation is available, this method will yield valid results for the flutter point, as well as subcritical and supercritical response. The results obtained provide essentially the same type of information available from flight test and can serve as a valuable supplement to aid in an efficient and safe flutter clearance program.

The intent of this study is to show how a root locus formulation is structured, and particularly that only a modest change in the traditional V-G method is required. This is demonstrated by considering a relatively complicated aeroelastic system consisting of an aft fuselage and T-Tail empennage. A brief discussion is given of the formulation followed by a comparison of results for the flutter point obtained by the root locus and the V-G methods. Questions regarding the relative cost of the two types of analysis will also be addressed.

THE AEROELASTIC MODEL

The aeroelastic model is that of a linearly elastic system with aerodynamic loads which are dependent on the structural deformations. In terms of generalized coordinates based on the coupled free vibration modes the equations of motion can be written in matrix form as

$$[M]\ddot{\mathbf{x}} + [C]\dot{\mathbf{x}} + [K]\mathbf{x} = \{Q(t)\} \quad (1)$$

where $[M]$ and $[K]$ are diagonal generalized mass and stiffness matrices and $[C]$ is the generalized damping matrix which may be diagonal if viscous modal damping is assumed. \mathbf{x} is the vector of generalized coordinates, which in this case are the modal amplitudes. If structural damping is assumed the viscous damping matrix is not used and the energy dissipation is accounted for by out of phase components in the stiffness matrix. The generalized force vector $\{Q(t)\}$ represents the aerodynamic loading. For harmonic motion at frequency ω it can be written as

$$\{Q(t)\} = \omega^2 \frac{\rho}{\rho_0} [C_h(k, M)] \mathbf{x} e^{i\omega t} \quad (2)$$

ρ_0 is the sea level density and ρ is the density at the specified altitude. The generalized aerodynamic matrix $[C_h(k, M)]$ has coefficients which are functions of reduced frequency k and Mach number M . The reduced frequency is defined by $k = \omega b/U$, where ω is the

frequency of oscillation, b is a suitable reference length, and U is the flight velocity. In the V-G method the aerodynamic model of equation (2) is used, as is the out of phase component in the stiffness matrix, and harmonic motion is assumed to yield

$$\{(1 + ig)[K] - \omega^2[M]\} \mathbf{x}(\omega) = \omega^2 \frac{\rho}{\rho_0} [C_h(k, M)] \mathbf{x}(\omega) \quad (3)$$

g is the structural damping coefficient. This form can be interpreted in the frequency domain with the vector $\mathbf{x}(\omega)$ identified as the Fourier Transform of the generalized coordinates and the matrix $\omega^2 \rho / \rho_0 [C_h(k, m)]$ as an aerodynamic transfer matrix. The familiar V-G method proceeds to seek the conditions on V , g and ω for which the assumed harmonic motions can exist. Aerodynamic generalized forces of the form of equation (3) for general aerodynamic configurations can be derived from a number of methods including the Doublet Lattice Method [1], the Doublet Point Method [2], and the Hybrid Doublet Lattice-Doublet Point Method [3].

In the present study the aerodynamic generalized forces are not restricted to harmonic motion. There does not exist a systematic method of modeling the time dependent airforces in an exact form, however, the harmonic airforces of equation (3) can be used as a basis for arriving at an approximate form which allows for the evaluation of $\{Q(t)\}$ as the solution of a subsidiary set of linear time invariant differential equations.

TRANSIENT AIRFORCES

In the time domain method the equations of motion are represented in the Laplace domain in a form similar to equation (3),

$$([M]p^2 + [C]p + [K]) \mathbf{x}(p) = q[A(p, M)] \mathbf{x}(p) \quad (4)$$

$\mathbf{X}(p)$ is the Laplace Transform of the vector of generalized coordinates and $q[A(p, M)]$ is the aerodynamic transfer matrix in the Laplace domain. Here q is the dynamic pressure.

Under the assumption that the aerodynamic impulse responses are stable and causal, the transfer matrices in the Laplace domain and in the frequency domain are related by

$$\omega^2 \frac{\rho}{\rho_0} [C_h(k, M)] = q[A(k, M)] = q[A(p, M)]_{p=ik} \quad (5)$$

It is in the frequency domain that information about $[A(k, M)]$ is known, however it is not known in closed form. Instead, it is typically known at a relatively small number of values of reduced frequency. The approach followed is to use interpolation functions of the reduced frequency k to fit each term in the transfer matrix over a suitable range of discrete values of k . Interpolation functions are chosen to provide an approximation to the elements of the transfer matrix which have simple inverse transformations into the time domain.

The specific details of obtaining the curve fit have been the subject of a number of investigations [4-13]. The technique used in this study is based on the work of Roger [7] and Abel [8]. The form of the interpolating function is

$$[A(k,M)] = [A_0] + [A_1](ik) + [A_2](ik)^2 + \sum_{m=3}^{M+2} [A_m] \frac{(ik)}{(ik) + k_m} \quad (6)$$

where the matrices $[A_0]$, $[A_1]$, $[A_2]$, and $[A_m]$ are constant matrices to be determined in the curve fitting procedure, q is the dynamic pressure, k is the reduced frequency, and k_m are constants which may be determined in the curve fitting procedure. This form of the interpolation function is chosen because it yields a simple inversion into the time domain. In the original work of Roger and Abel, the parameters k_m , defined here as lag parameters, were chosen a priori to span the reduced frequency range over which the fit is carried out. A least squares curve fit procedure was used to determine the elements in the $[A]$ matrices. Extensions to the curve fitting procedure which simultaneously allow optimal choices of the lag parameters have been described by Tiffany and Adams [12] and modified by Eversman and Tewari [13].

Once the curve fit is accomplished based on the results of evaluations of the aerodynamic transfer matrix in the frequency domain, the approximate form can be transformed into the Laplace domain by the simple replacements $ik = (b/U)p$ and $k_m = (b/U)p_m$ to yield

$$[A(p,M)] = [A_0] + \left(\frac{b}{U}\right) [A_1]p + \left(\frac{b}{U}\right)^2 [A_2]p^2 + \sum_{m=3}^{M+2} [A_m] \frac{p}{p+p_m} \quad (7)$$

The Laplace Transform of the aerodynamic generalized force is then written

$$\begin{aligned} Q(p) = & q([A_0] + \sum_{m=2}^{M+2} [A_m])\dot{x}(p) + q\left(\frac{U}{b}\right) [A_1]p\dot{x}(p) \\ & + q\left(\frac{U}{b}\right)^2 [A_2]p^2 \dot{x}(p) - q \sum_{m=2}^{M+2} [A_m] \frac{p_m}{p+p_m} \dot{x}(p) \end{aligned} \quad (8)$$

and it is noted that the coefficient matrix $[A_2]$ becomes part of the generalized mass matrix, and can be interpreted as added aerodynamic mass. Similarly, $[A_1]$ contributes as aerodynamic damping and $[A_0]$ plus the sum of the $[A_m]$ matrices contribute as aerodynamic stiffness. Aerodynamic state vectors defined by M sets of state equations

$$(p + p_m)Z_m(p) = p_m \dot{x}(p) \quad (9)$$

plus the structural equations

$$([\bar{M}]p^2 + [\bar{C}]p + [\bar{K}])\mathbf{x}(p) = -q \sum_{m=2}^{M+2} [A_m]z_m \quad (10)$$

with

$$\begin{aligned} [\bar{M}] &= [M] - q \left(\frac{U}{b} \right)^2 [A_2], \quad [\bar{C}] = [C] - q \left(\frac{U}{b} \right) [A_1] \\ [\bar{K}] &= [K] - q([A_0] + \sum_{m=2}^{M+2} [A_m]) \end{aligned}$$

now form the model of the aeroelastic system in the Laplace Transform domain. Equations (9) and (10) form the basis for the root locus flutter analysis. They constitute N structural equations of second order, or equivalently $2N$ first order structural equations, plus M sets of N first order aerodynamic state equations. With suitable rearrangement, a set of $N(2+M)$ linear time invariant equations in the Laplace Transform domain can be set up in the form

$$p\mathbf{Y}(p) = [D]\mathbf{Y}(p) \quad (11)$$

where $\mathbf{Y}(p)$ is an augmented vector of state variables which include the structural generalized coordinates, the corresponding generalized velocities, and the aerodynamic states. The dynamic matrix $[D]$ is constructed from the matrices $[\bar{M}]$, $[\bar{C}]$, $[\bar{K}]$, and $[A_m]$, and is a function of the Mach number and the dynamic pressure. Equation (11) is in the form of a linear algebraic eigenvalue problem which can be solved for the $N(2+M)$ eigenvalues which are the poles of the system transfer function. These poles determine the system stability. If the poles are found as a function of the Mach number, thought of as a "gain" in the context of classical control theory, then the process can be viewed as the familiar root locus analysis.

The $N(2+M)$ eigenvalues of equation (11) correspond to system responses in the time domain of the form

$$\mathbf{Y}(t) = \mathbf{Y}_0 e^{pt} \quad (12)$$

p is in general a complex number $p = \sigma + i\omega$ and stable and unstable responses are identified by the sign of σ . In the language of root locus, poles in the left-half plane correspond to stable transient response, poles on the imaginary axis correspond to undamped oscillatory motion, and poles in the right half plane correspond to unstable transient response. In the terminology of a flutter analysis, poles on the imaginary axis correspond to the flutter condition, while poles in the left half plane represent damped, or subcritical response, and poles in the right half plane correspond to divergent, or supercritical response.

In analogy to the standard single degree of freedom damped oscillator it is common to categorize each mode of transient response by its undamped natural frequency ω_d , damped natural frequency ω_o , and damping ratio ξ . In terms of σ and ω , it is determined that ω is the damped natural frequency. If ω_d is different from zero, the motion is oscillatory, and the damping ratio and undamped natural frequency are defined by

$$\omega_o = \sqrt{\sigma^2 + \omega_d^2}, \quad \xi = -\frac{\sigma}{\omega_o} \quad (13)$$

The most convenient means of displaying the results of a root locus flutter analysis is with plots of damping ratio and damped natural frequency as functions of Mach number for a given altitude. These would be similar to the usual presentation in the V-G method of structural damping and frequency as functions of velocity. Note that in the root locus method Mach number is the "gain" and it is not required to find a matched flutter point where Mach number and velocity are consistent for the given altitude.

In the curve fitting procedure in the frequency domain implied by equation (7) the number of aerodynamic states required is not specified. In the current study the number of aerodynamic lag terms has been limited to a maximum of four. For each lag term NM aerodynamic states are added to the aeroelastic model. It is therefore advantageous to minimize the number of lag terms. It has been found possible to reduce the number of lag states for a given accuracy level by optimizing the choice of the values of the lag parameters pm at the same time that the curve fit procedure is carried out. It would not be unusual to obtain excellent results for flutter calculations using only two lag states.

A PROCEDURE FOR ROOT LOCUS FLUTTER ANALYSIS

A comparison between the procedure required to carry out a conventional V-G flutter analysis and a root locus flutter analysis can be obtained by reference to Figure 1 where each block represents a computational step. For both approaches there are common steps which are discussed first:

1. **STRUCT** is the structural model for the aeroelastic system. A finite element model is used to establish the free vibration equations of motion and to solve the resulting eigenvalue-eigenvector problem for the coupled natural frequencies and mode shapes. The generalized mass, damping, and stiffness matrices and the modal matrix are generated and stored for subsequent use in the flutter analysis.
2. **AERO** is the aerodynamic model for harmonic motion of general aeroelastic configurations. It is based on the Doublet Lattice Method, Doublet Point Method, or the Hybrid Doublet Lattice-Doublet Point Method. The aerodynamic transfer matrix in the pertinent aerodynamic degrees of freedom is established for a range of reduced frequencies and Mach numbers.

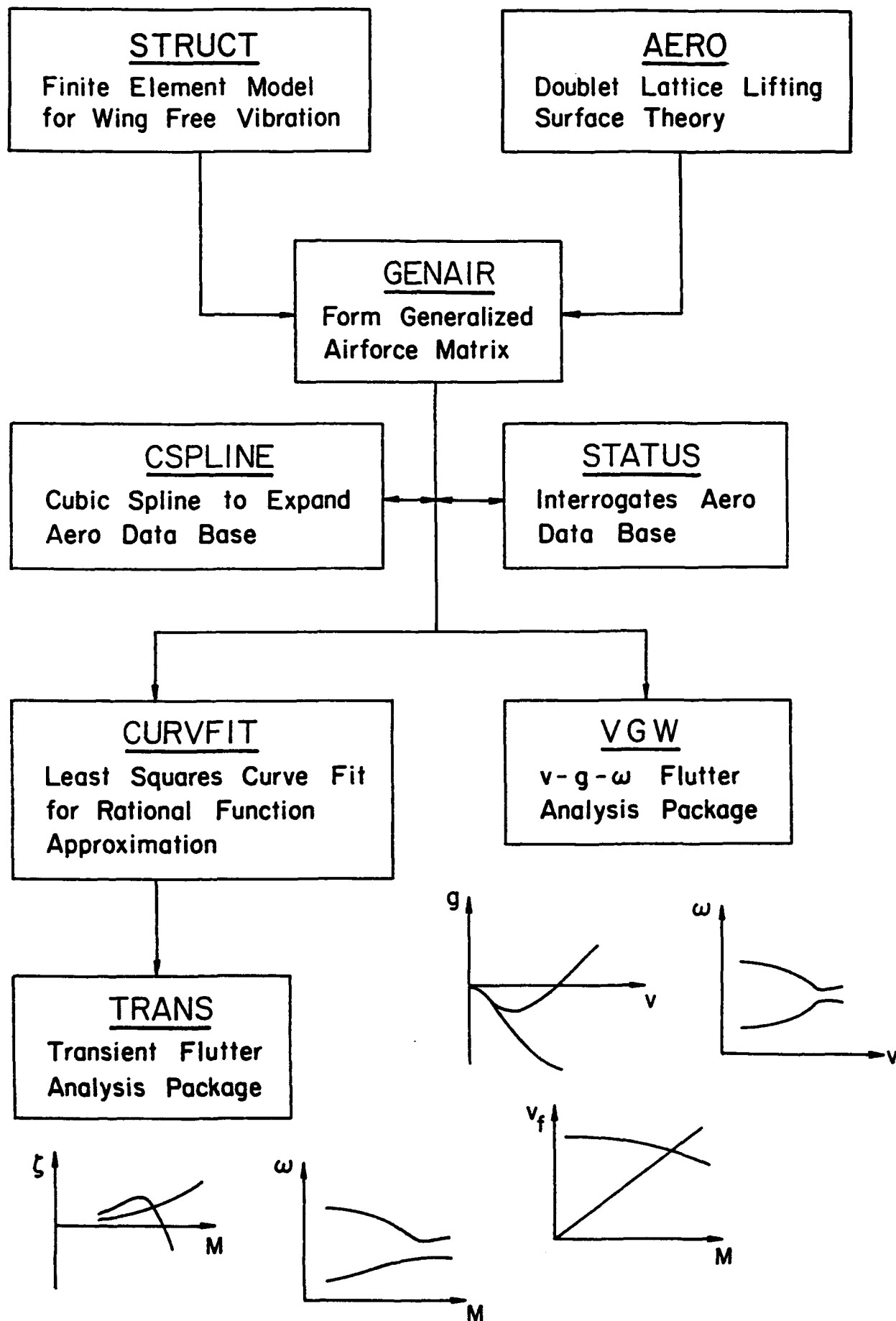


Figure 1. Flow Chart of V-G and Root Locus Flutter Analyses.

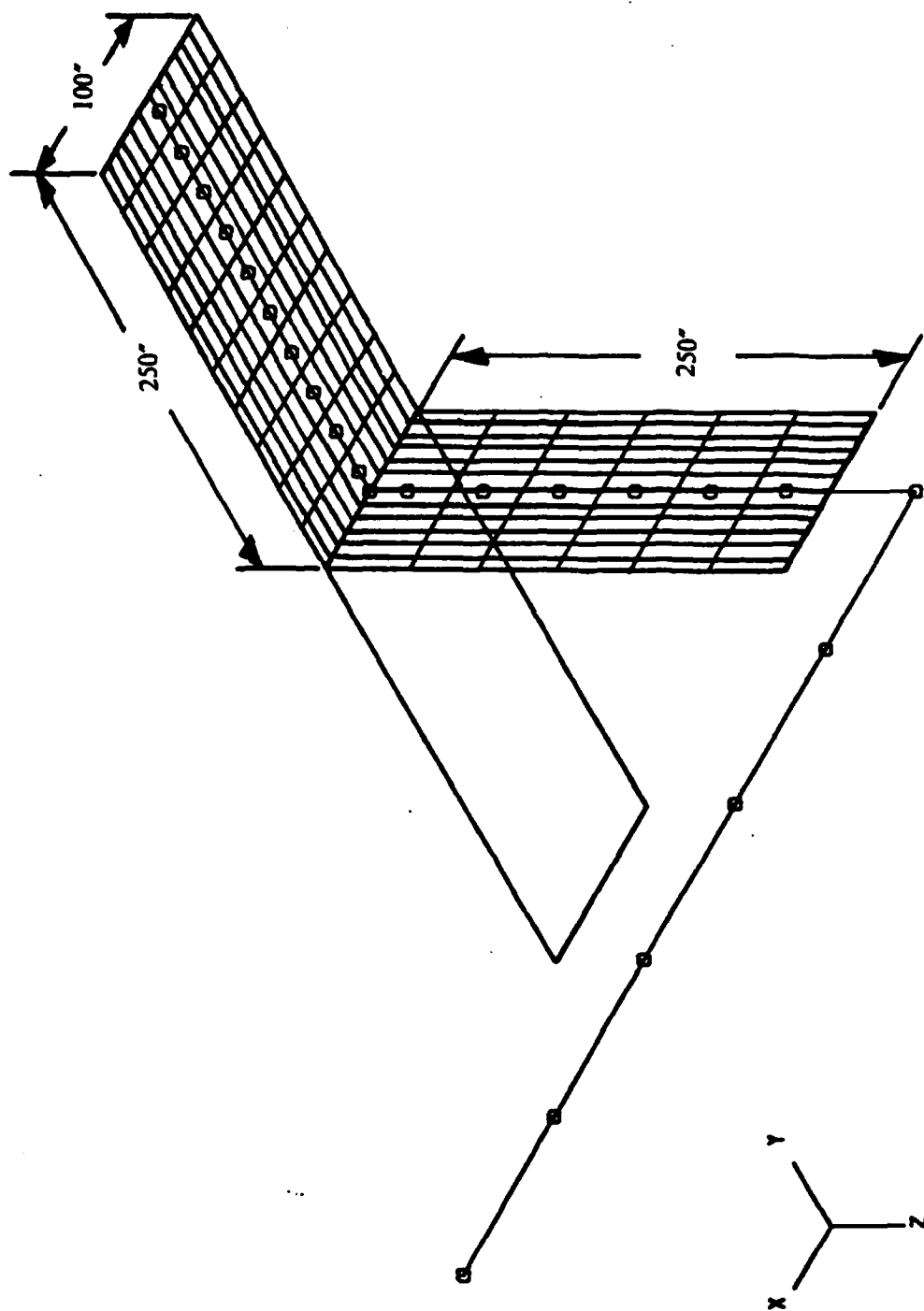


Figure 2. Structural and Aerodynamic Model of the T-Tail.

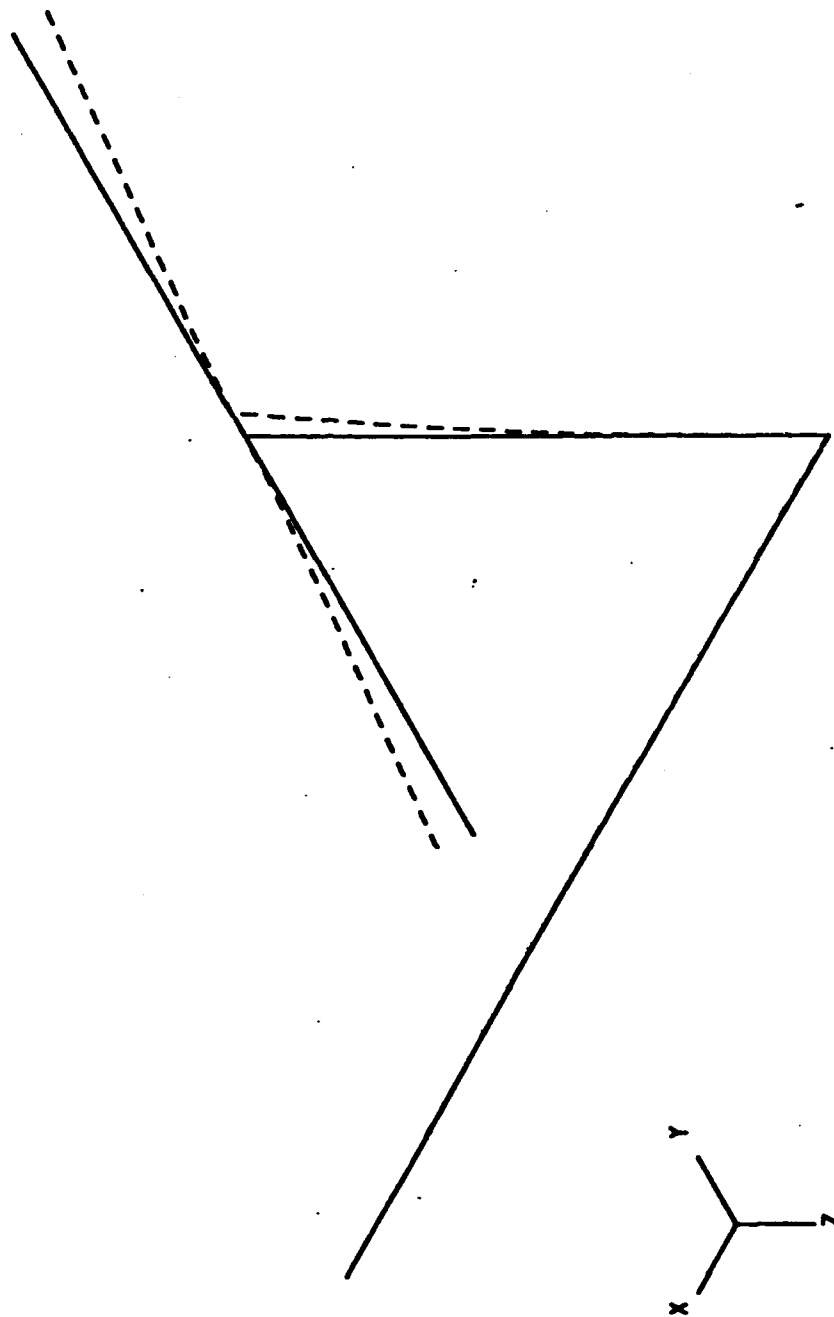


Figure 3. First Mode Shape - Antisymmetric Case.
Vertical Tail Side Bending. Frequency 1.54 Hz.

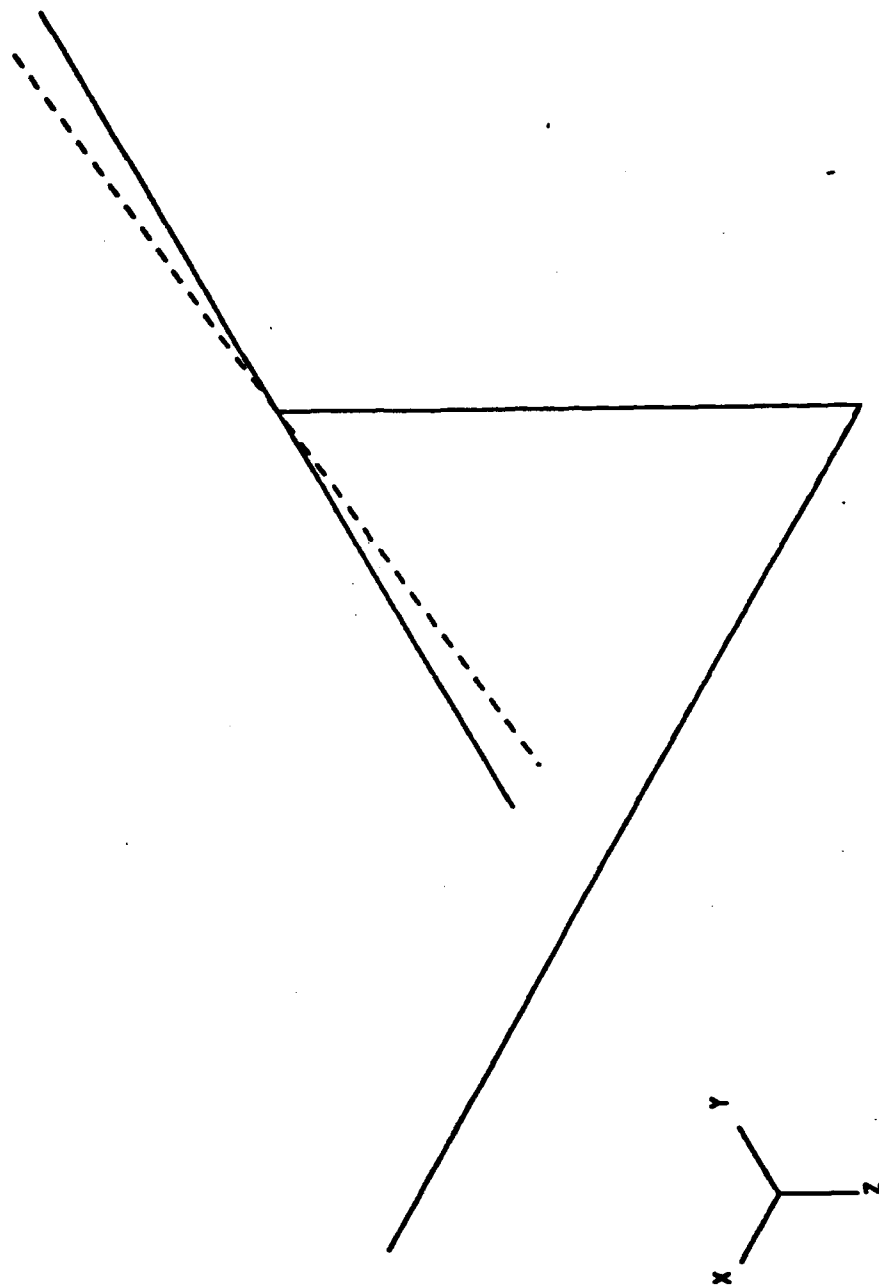


Figure 4. Second Mode Shape - Antisymmetric Case.
Vertical Tail Torsion. Frequency 2.18 Hz.

3. GENAIR transforms the aerodynamic transfer matrices into the generalized coordinate system using the modal matrix generated in the STRUCT program.
4. CSPLINE is a spline curve fitting procedure which is used to expand the generalized aerodynamic transfer matrices in the data base by interpolating between the values of reduced frequency and Mach number which are available.
5. STATUS is a program which will interrogate the aerodynamic data base to determine what generalized aerodynamic transfer matrices are available.

The five programs described are common to either a V-G analysis or to the root locus analysis. If the V-G procedure is chosen the software package VGW is used:

6. VGW takes the structural model from STRUCT and the aerodynamic model from AERO and GENAIR and assembles the flutter problem in the form of equation (3). The resulting eigenvalue problem is solved for a specified altitude by varying the Mach number and reduced frequency until a matched flutter point is found for each required Mach number. Results are presented as structural damping and oscillation frequency as functions of velocity and flutter velocity as a function of Mach number for the determination of the matched flutter point.

If the root locus method is chosen, then two steps are required in the final flutter solution:

7. CURVFIT generates the curve fit of the generalized aerodynamic transfer matrices over a specified range of reduced frequencies for each Mach number. In terms of equation (7) this means generation of the matrices $[A_0]$, $[A_1]$, $[A_2]$, and $[A_m]$ so the interpolation function provides the best fit to the aerodynamic data in a least squares sense. If desired, the lag parameters p_m can be simultaneously optimized using a simplex optimizer in a loop with the least squares procedure. This additional optimization step has the potential of reducing the number of aerodynamic states required for a given accuracy, or of increasing the curve fit accuracy for a given number of states.
8. TRANS is the root locus program. It accepts the structural model from STRUCT and the aerodynamic model from CURVFIT, constructs the dynamic matrix $[D]$ in equation (11), carries out the eigenvalue solution routine, sorts the eigenvalues to distinguish between structural and aerodynamic contributions, and postprocesses the results. TRANS is run for each Mach number. As shown, the results are presented as damping ratio for the important structural modes as a function of Mach number and the corresponding damped natural frequencies as a function of Mach number.

COMPUTATIONAL EXAMPLE

In order to demonstrate the effectiveness of the root locus method for flutter computations a realistic example of complicated geometry is chosen. Figure 2 shows an aft fuselage and T-Tail empennage. The structure is modeled using conventional bending-torsion elements and the aerodynamics are represented by the Doublet Lattice Method. The important feature in this type of configuration is the aerodynamic coupling between the horizontal stabilizer and the vertical fin. This coupling presents a challenge to the curve fitting procedure in the transient analysis. Figure 2 shows a general layout of the configuration with the finite element nodes of the structural model and the paneling of the aerodynamic model. It is found that flutter occurs in an antisymmetric mode so that only an antisymmetric model is discussed here. Figures 3 and 4 show the first two antisymmetric modes for the structure with frequencies 1.54 Hz and 2.18 Hz. The first mode is primarily fin side bending and the second mode is fin torsion. Six antisymmetric modes were included in the model with frequencies up to 22.4 Hz. The aerodynamic curve fit was accomplished using only least squares fitting for the aerodynamic matrices $[A_0]$, $[A_1]$, $[A_2]$, $[A_m]$. No effort was made to optimize the choices of the lag parameters.

RESULTS AND DISCUSSION

A. The V-G Method

Figures 5 through 7 summarize the results of the V-G method for the antisymmetric case. For this case the Mach numbers used were 0.55, 0.6, 0.65, 0.7, 0.73, 0.75, 0.8, and 0.85 and reduced frequencies of 0.05, 0.06, 0.07, 0.08, 0.1, 0.2, 0.3, and 0.5 at each Mach number. At each Mach number a pair of plots is generated. One plot is of structural damping factor vs. flight speed and the other is of frequency vs. flight speed. Only the plots for $M = 0.73$ are presented here.

Figure 5 is the plot of structural damping factor as a function of velocity for Mach number 0.73. This plot is typical of those generated for each Mach number. In these plots it is seen that the structural damping factors are negative for each mode at low flight speeds. As the flight speed increases the structural damping factor of the second mode becomes positive while the others remain negative and decrease. Thus, the second mode is unstable and is the flutter mode. All other modes are stable. To determine the flutter speed of the flutter mode the flight speed is found where the structural damping factor is zero for the second mode (flutter mode) for each Mach number case. Once this point is found for each Mach number it is plotted on a graph of flight speed vs. Mach number. This plot is indicated by the circles in Figure 6. The straight line in this figure indicates the actual variation of flight speed with Mach number at the chosen altitude (sea level). The point where the circles intersect the straight line gives the flutter speed and flutter Mach number. For this case the flutter speed is 815 ft/sec which is equivalent to a Mach number of 0.73.

Figure 7 is the plot of frequency vs. flight speed for Mach number 0.73. It is typical of plots obtained for each Mach number. These plots are useful in illustrating the activity of the aeroelastic modes. At very low flight speeds the frequencies of the aeroelastic modes

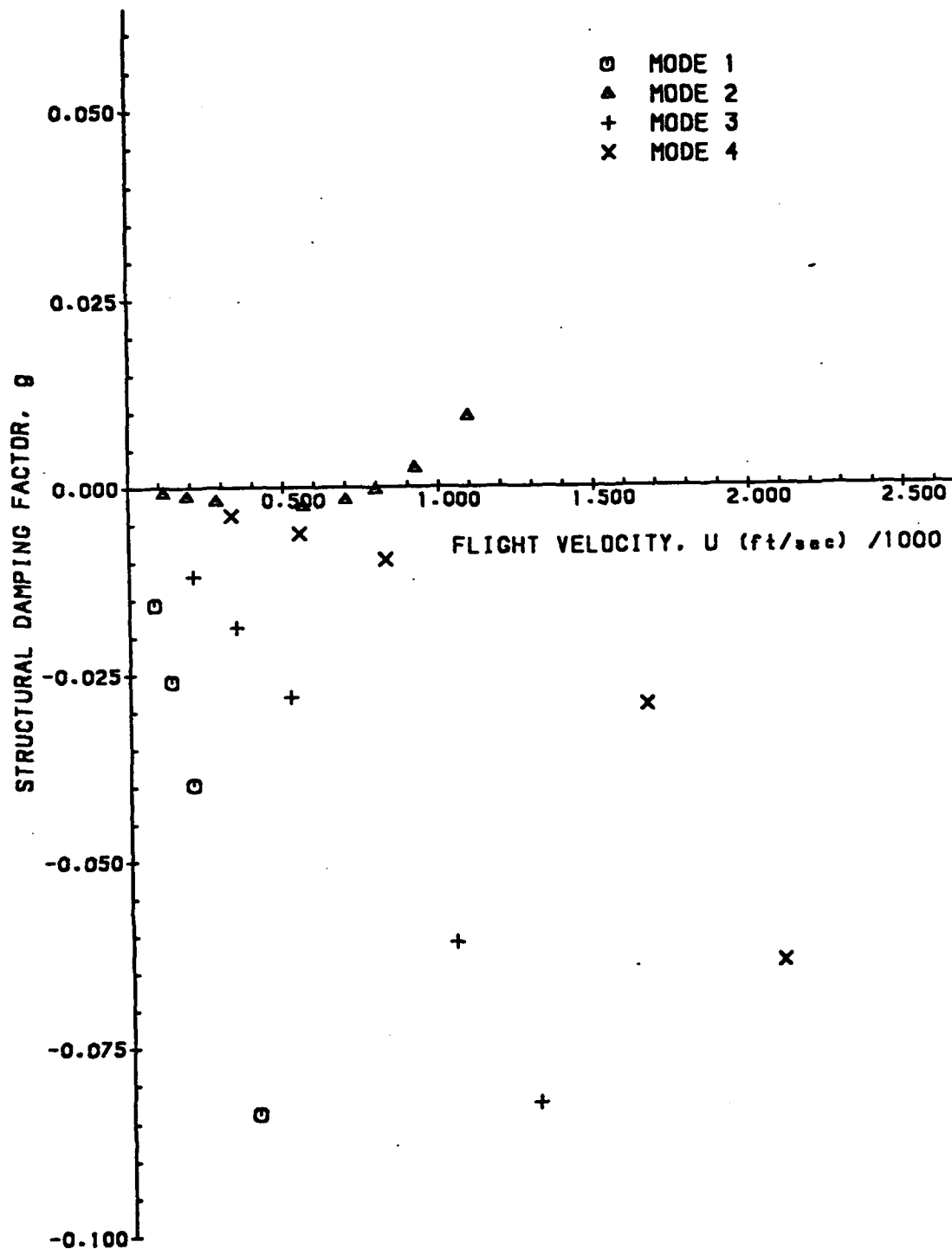


Figure 5. Structural Damping Factor vs. Flight Speed, Mach 0.73, Antisymmetric Case.

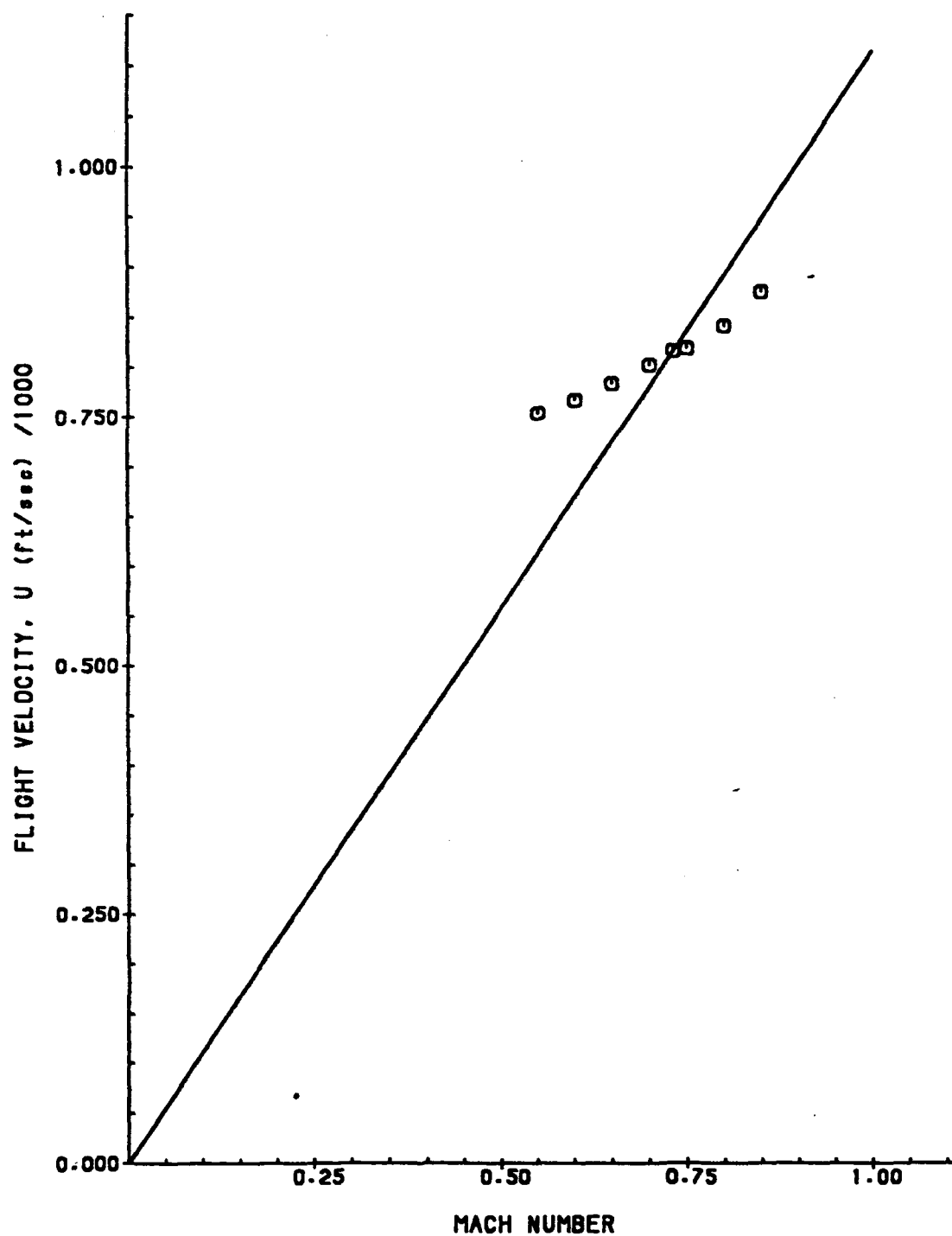


Figure 6. Flight Speed vs. Mach Number.
Antisymmetric Case, Altitude = Sea Level.

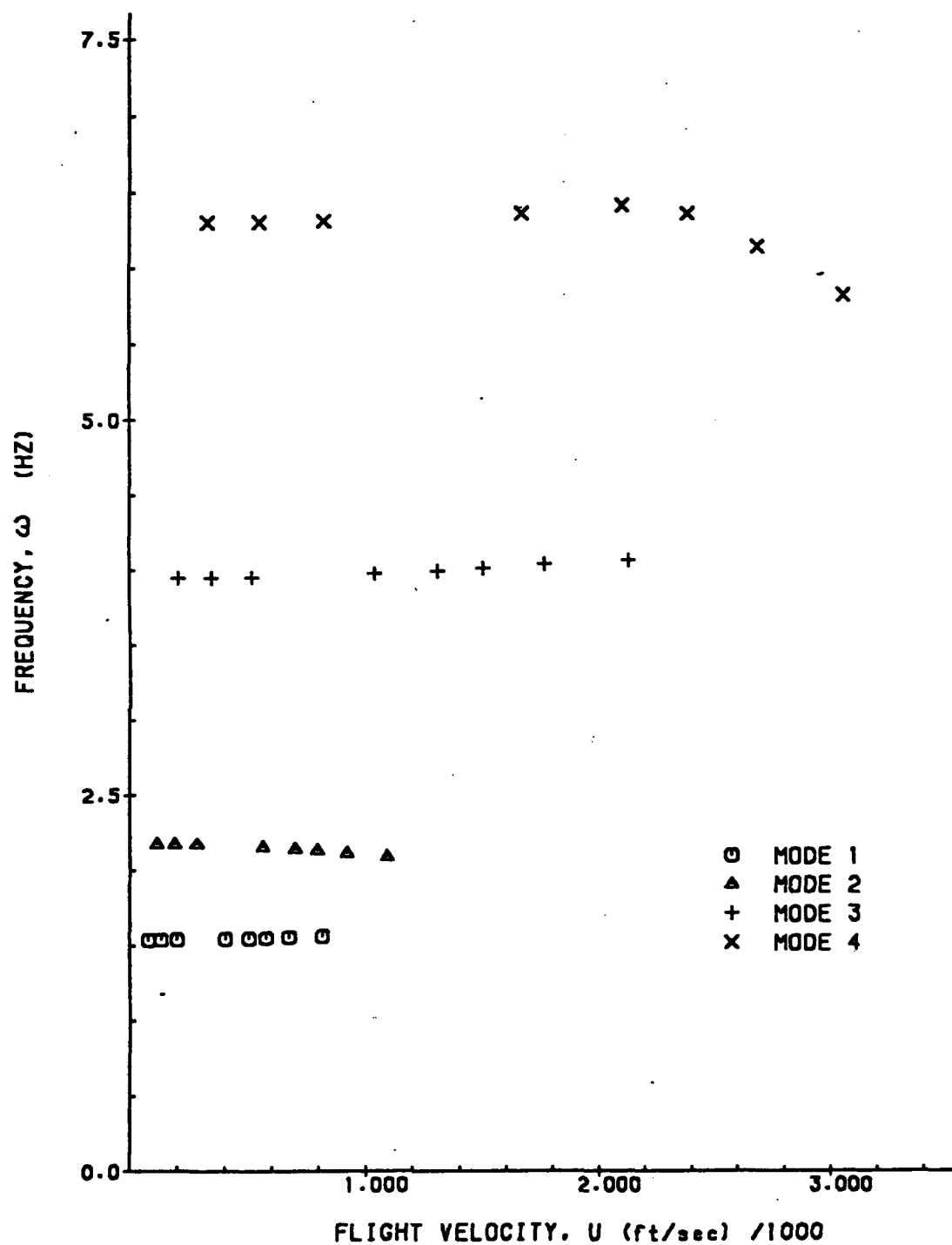


Figure 7. Frequency vs. Flight Speed,
Mach 0.73, Antisymmetric Case.

are very close to the structural natural frequencies, as expected. As the flight speed increases the frequencies of the aeroelastic modes change slightly. This is due to the involvement of more than one natural mode in an aeroelastic mode. It is seen that the frequency of the flutter mode (mode 2) does not vary appreciably with flight speed, however, there is a slight merging of modes 1 and 2. Thus, the flutter mode consists almost entirely of the second natural mode. From Figure 4 it is seen that the second natural mode is mainly torsion or yawing of the fin at a frequency of 2.18 Hz. The first natural vibration mode is seen from Figure 3 to be fin side bending at a frequency of 1.54 Hz. The flutter frequency is 2.13 Hz which is slightly less than that of the second natural mode due to the slight involvement of the first natural mode in the flutter mode.

To summarize the results for the antisymmetric case the flutter mode was found to be mainly torsion of the fin with a flutter frequency of 2.13 Hz occurring at a flight speed of 815 ft/sec (Mach 0.73) at sea level.

B. The Transient Response Method

Results of the approximation of the generalized aerodynamic matrix transfer function are shown in Figures 8 and 9 for Mach 0.73. Four lag terms were used and reduced frequencies of 0.0, 0.05, 0.06, 0.07, 0.08, 0.1, 0.2, 0.3, and 0.5 were used to determine the coefficient matrices of the approximate matrix transfer function. The values of k_m were $k_3 = 0.01$, $k_4 = 0.10$, $k_5 = 0.30$, $k_6 = 1.0$. These figures are polar plots of elements 2,1 and 6,3 of the generalized aerodynamic matrix transfer function as a function of reduced frequency. The crosses represent exact values of the transfer functions while the solid line is the approximate transfer function. The circles on the solid line indicate where the approximate transfer function has been evaluated at the same reduced frequencies as the exact transfer function. These results typify those of every element in the approximate matrix transfer function and thus the exact matrix transfer function has been approximated very well in this example.

Using four lag terms and the reduced frequencies listed above the approximate matrix transfer functions at Mach numbers of 0.55, 0.6, 0.65, 0.7, 0.75, 0.8, and 0.85 were also obtained. These approximate matrix transfer functions exhibited the same accuracy as that for Mach 0.73 discussed above. The results for the transient flutter analysis using these approximate matrix transfer functions are summarized in Figures 10 and 11.

Figure 10 is a plot of damping ratio vs. Mach number for modes 2, 3, and 4. It is seen that the damping ratios of modes 3 and 4 are positive and increase with Mach number. A positive damping ratio indicates stability which is the opposite of the U-g- ω results where a negative structural damping factor indicates stability. The damping ratio of mode 2 is positive up to Mach 0.73 where it is zero and subsequently becomes negative. This indicates that the structure flutters at Mach 0.73 with mode 2 as the flutter mode. Though mode 1 is not shown in this figure it remains stable. These results are in agreement with those of the V-G results for the antisymmetric case.

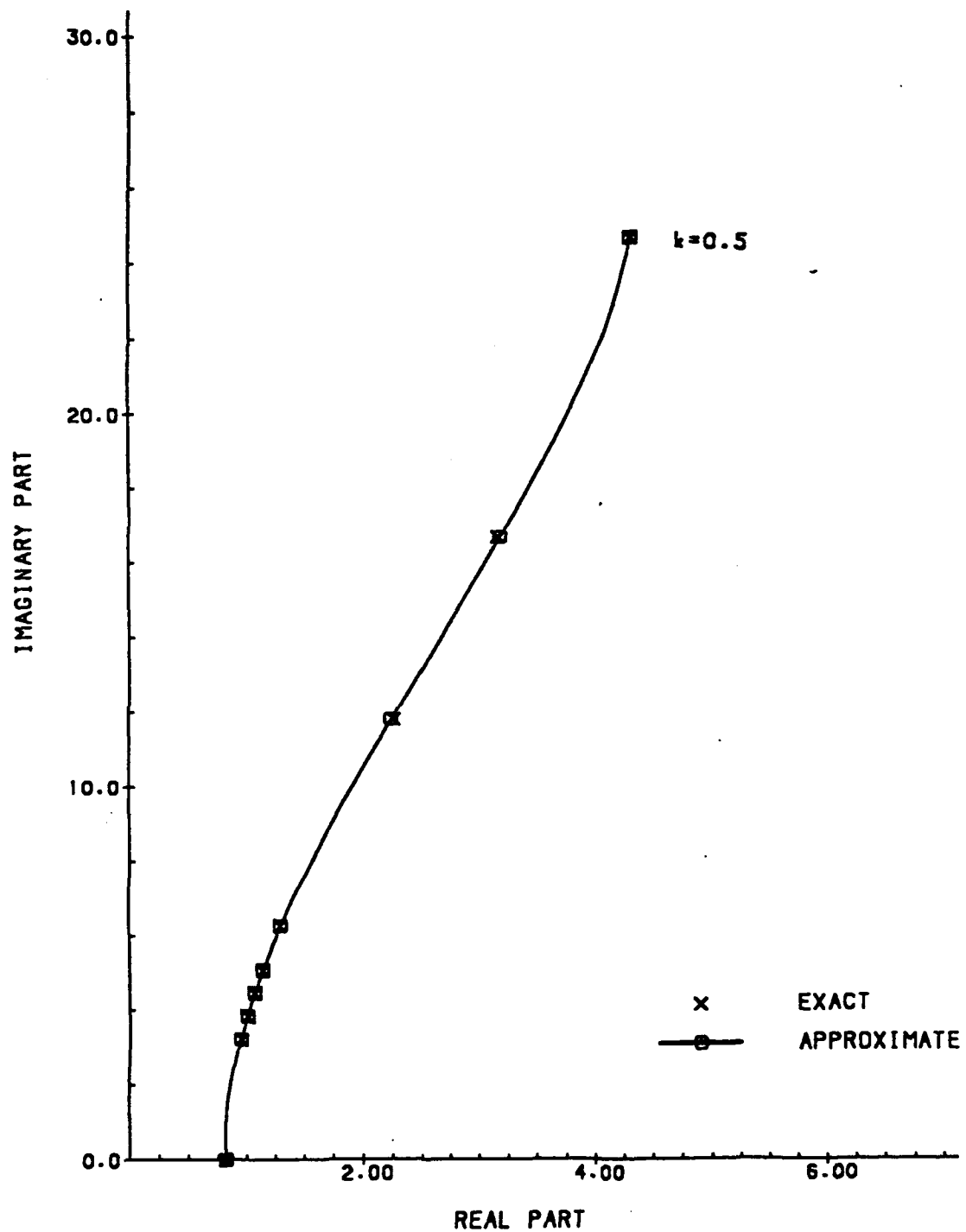


Figure 8. Element 2,1 of Aerodynamic Transfer Function, Mach 0.73, 4 Lag Terms, Antisymmetric Case.

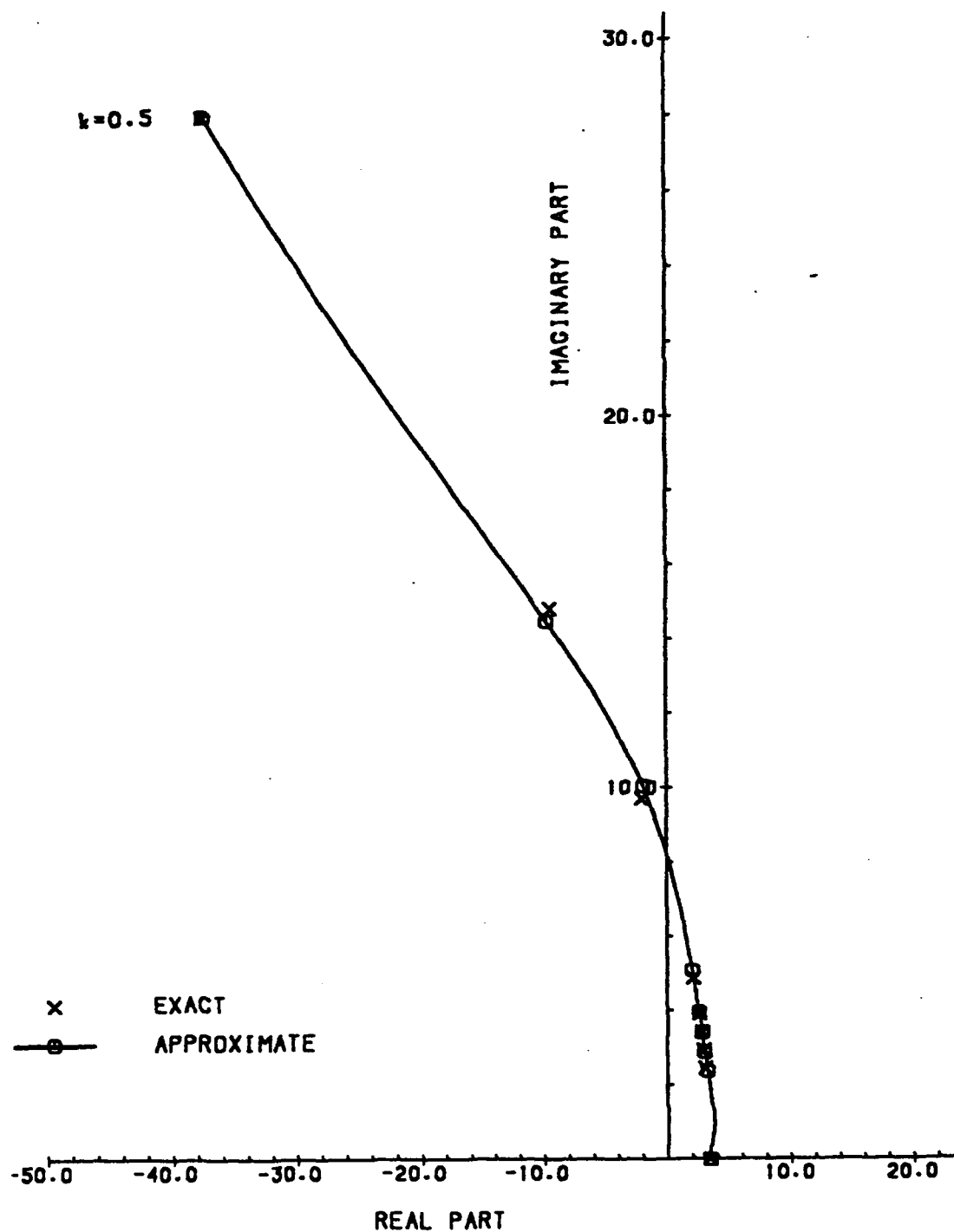


Figure 9. Element 6,3 of Aerodynamic Transfer Function, Mach 0.73, 4 Lag Terms, Antisymmetric Case.

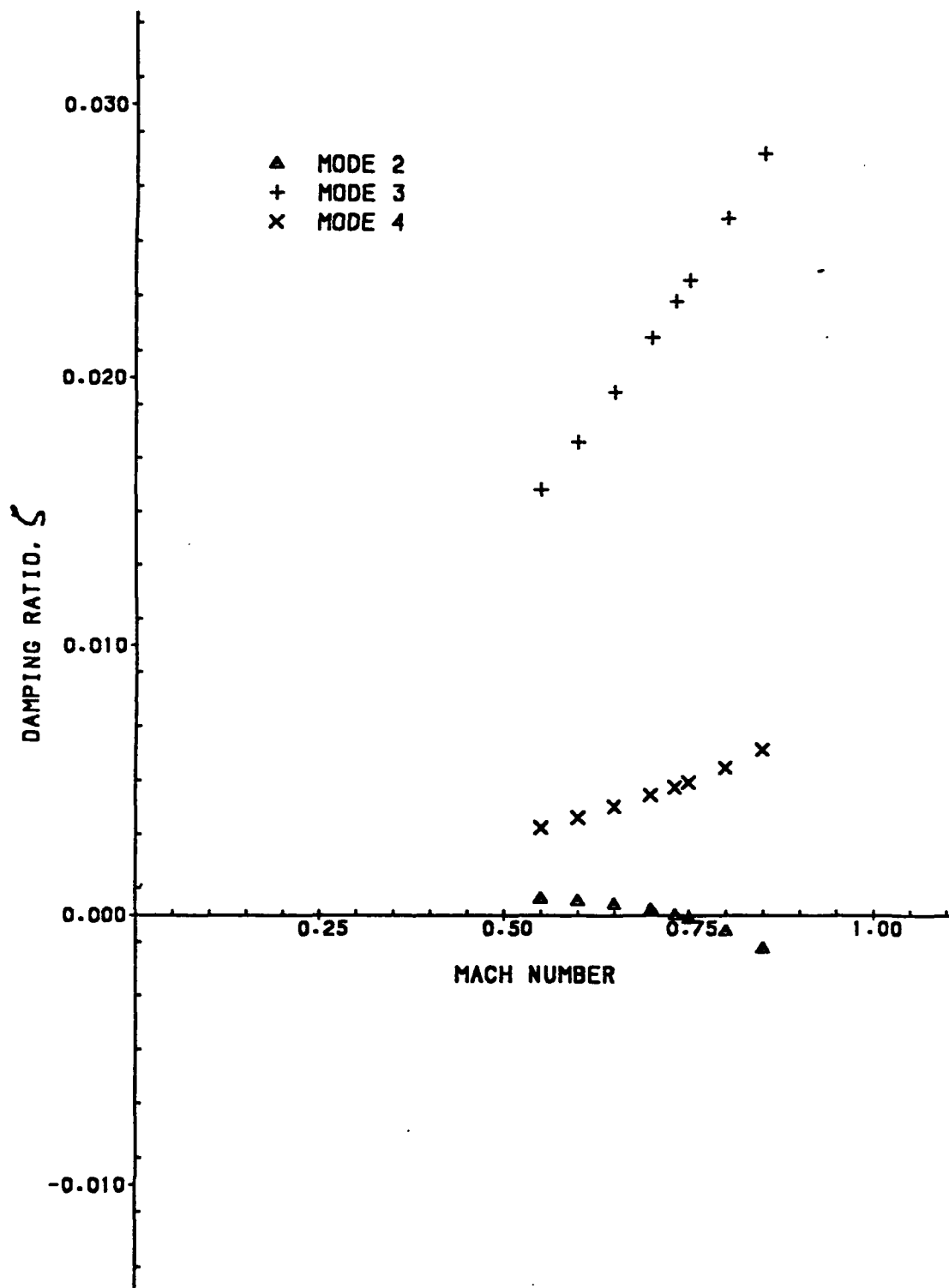


Figure 10. Damping Ratio vs. Mach Number, 4 Lag Terms, Antisymmetric Case.

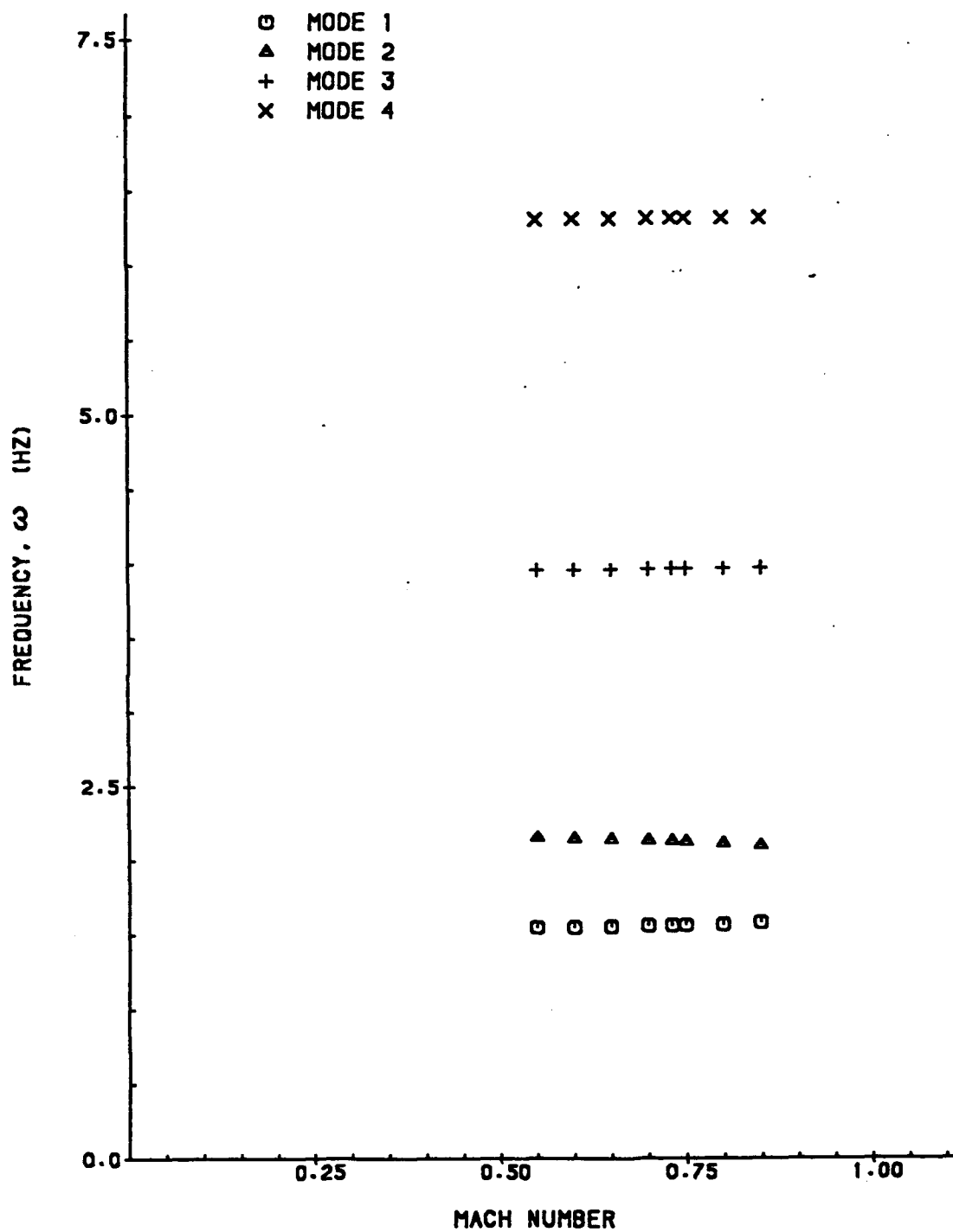


Figure 11. Frequency vs. Mach Number, 4 Lag Terms, Antisymmetric Case.

Figure 11 is a plot of frequency vs. Mach number for modes 1, 2, 3, and 4. It can be seen that the frequency of each mode does not vary appreciably with Mach number and the flutter mode consists mainly of the second natural mode with a slight involvement of the first natural mode. From these results the flutter frequency is determined to be 2.13 Hz. These results are also in agreement with U-g- ω results for the antisymmetric case.

In addition to the results shown here, a study was made of the effect of the range of reduced frequencies over which the curve fit is carried out and of the number of lag terms retained. It was found that without optimization of the lag parameters, the accuracy of the flutter solution is sensitive to the range of the reduced frequencies used for the curve fit. In the case of four lag terms the use of the wider range of reduced frequencies $k = 0.0, 0.05, 0.06, 0.07, 0.08, 0.1, 0.2, 0.3, 0.5, 0.7, 0.9$, and 1.0 resulted in a flutter Mach number of $M = 0.8$. The point to be made here is that an effort to fit the aerodynamics over an excessively wide range of reduced frequencies results in a poor curve fit. The correct procedure is to make the fit over a relatively narrow range of reduced frequencies which is centered on the expected range of flutter reduced frequencies. In the present case the flutter is expected to occur at under $k = 0.5$ so the choice of reduced frequencies was in the range $0.0 < k < 0.5$ and the fit was very good. In fact, good flutter results were obtained with the choice of 1, 2, 3, and 4 lag terms.

An important point to note in the root locus procedure is the direct determination of the frequency and damping of the modes of motion in the transient response as a function of Mach number. The reduced frequency only plays a role in the development of the aerodynamic curve fit. In this respect the root locus analysis more nearly represents the type of results which would be forthcoming from a flight flutter test, that is, frequency and damping as the Mach number is increased. Of particular importance is the fact that damping and frequency calculations are valid over the entire Mach number range. The dangerous possibility that the onset of flutter occurs very quickly over a very narrow Mach number range would be predictable using the root locus method.

The question of the relative efficiency of the V-G method and the root locus method can only be assessed in general terms because of differences in individual cases. The root locus method introduces the additional complications of the curve fit procedure and the increase in the problem size created by the additional aerodynamic states. On the other hand, the necessity in the V-G method of varying both Mach number and reduced frequency is eliminated and the determination of the damping and frequency of the transient response modes of motion is a direct function of Mach number. More useable information is available in the root locus results because there is no restriction of simple harmonic motion. Perhaps the best way to assess efficiency is to look at a specific test case and to compare the time involved for the application of the two methods. Table 1 shows the time taken in each module to produce a flutter analysis using both methods. The root locus method has been applied using up to four aerodynamic lag terms. The total time for the V-G method is the sum of the times through module VGW. The total time for the transient method is found by deleting VGW but including CURVFIT and TRANS. The conditions of the comparison are specified below the table. It is clear that the time is dominated by the aerodynamic calculations which are common to the two methods. However, these calculations produce

Table 1

CPU TIME - IBM 3081D

	N-4	N-3	N-2	N-1
STRUCT	2.5			
AERO	435.5			
GENAIR	43.8			
CSPLINE	16.7			
VGW	21.18			
CURVFIT	14.57	14.76	14.46	14.40
TRANS	12.72	9.0	5.25	2.82

PARAMETERS

- a) 30 DOF STRUCTURE
- b) 6 RETAINED MODES
- c) 11 LIFTING SURFACE REDUCED FREQUENCIES at 8
Mach numbers for a 50 box grid in AERO
- d) 8 Mach numbers, one k value per Mach number
interpolated in CSPLINE
- e) 9 REDUCED FREQUENCIES IN VGW
- f) 8 REDUCED FREQUENCIES IN CURVFIT

a data base which can be used for many flutter analyses and are an unavoidable overhead. The important issue is the tradeoff between VGW and the combination of CURVFIT and TRANS. In this example the cost is comparable for four lag terms in the aerodynamics, but the root locus approach becomes more efficient when the number of aerodynamic states is reduced. The conclusion here is that for this case there is no significant extra cost for the root locus analysis. In this case no optimization of the lag parameters was carried out. The optimization would increase the time in CURVFIT, but would allow the use of fewer aerodynamic states and would reduce the time in TRANS. Not considered here is the tradeoff for an aeroelastic system described by a very large structural model, say 30 elastic modes. With four aerodynamic lag terms the eigenvalue problem in TRANS is of size 180×180 while in VGW it is of size 60×60 . In this case the additional cost of the root locus procedure may be a consideration, and it becomes essential to use a curve fit procedure which optimizes the lag parameters and reduces the number of aerodynamic states required [12,13].

CONCLUSIONS

The root locus method is an alternative to the conventional frequency domain flutter analysis techniques. Recent developments in the representation of the unsteady aerodynamics for general configurations in the time domain have made it possible to develop a systematic transient response prediction procedure which has many steps in common with the frequency domain techniques. In this study it was shown that the flutter analysis of the aerodynamically complex configuration of a T-Tail could be carried out using the V-G method and the root locus method with equivalent results for the flutter Mach number. The root locus method has the advantage of providing physically meaningful results for the damped response at Mach numbers below the flutter point. For most cases the added complication in the root locus method introduced by the curve fit is offset by the elimination of the need to vary both reduced frequency and Mach number to find the matched flutter point in the V-G method.

REFERENCES

1. Albano, E. and Rodden, W. P., "A Doublet Lattice Method for Calculating Lift Distributions on Oscillating Surfaces in Subsonic Flows," AIAA Journal, Vol. 7, No. 2, 1969, pp. 279-285.
2. Ueda, T. and Dowell, E. H., "A New Solution Method for Lifting Surfaces in Subsonic Flow," AIAA Journal, Vol. 20, No. 3, 1982, pp. 348-355.
3. Eversman, W. and Pitt, D. M., "Hybrid Doublet Lattice-Doublet Point Method for Lifting Surfaces in Subsonic Flow," Journal of Aircraft, Vol. 28, No. 9, 1991, pp. 572-578.
4. Burkhart, T. H., "Subsonic Transient Lifting Surface Aerodynamics," Journal of Aircraft, Vol. 14, No. 1, January 1977, 44-50.

5. Vepa, R., "Finite State Modeling of Aeroelastic Systems," NASA Contractor Report CR-2779, February 1977.
6. Dowell, E. H., "A Simple Method for Converting Frequency Domain Aerodynamics to the Time Domain," NASA TM 81844, 1980.
7. Roger, K., "Airplane Math Modeling Methods for Active Control Design," AGARD CP-228, August 1977.
8. Abel, I., "An Analytical Technique for Predicting the Characteristics of a Flexible Wing Equipped with an Active Flutter Suppression System and Comparison with Wind-Tunnel Data," NASA Technical Paper 1367, 1979.
9. Edwards, J. W., Ashley, H., and Breakwell, J. V., "Unsteady Aerodynamic Modeling for Arbitrary Motions," AIAA Journal, Vol. 17, No. 4, 1979, pp. 365-374.
10. Dunn, H. J., "An Analytical Technique for Approximating Unsteady Aerodynamics in the Time Domain," NASA Technical Paper 1738, 1980.
11. Karpel, M., "Design for Active and Passive Flutter Suppression and Gust Alleviation," NASA Contractor Report 3482, November 1981.
12. Tiffany, S. H. and Adams, W. M., Jr., "Nonlinear Programming Extensions to Rational Function Approximations of Unsteady Aerodynamics," AIAA Paper 87-0854, April 1987, 406-420.
13. Eversman, W. and Tewari, A., "Consistent Rational Function Approximation for Unsteady Aerodynamics," Vol. 28, No. 9, 1991, pp. 545-552.

ROTOR CONTAINMENT ISSUES IN GENERAL AVIATION

by

**J.A. Mathis
Assistant Professor, Mechanical Engineering
Wichita State University
Wichita, Kansas**

**For Presentation to the AIAA/FAA Joint Symposium on General
Aviation Systems at the Hilton Inn-East, Wichita, KS
on March 16-17, 1992**

ROTOR CONTAINMENT ISSUES IN GENERAL AVIATION

J.A. MATHIS
ASSISTANT PROFESSOR, MECHANICAL ENGINEERING
WICHITA STATE UNIVERSITY

INTRODUCTION

Among the causes of aviation accidents, those related to noncontainment of turbine engine rotor components continue to be an identifiable area for improvement. Some statistics on the continuing occurrence of these accidents are presented as motivation for continued research in improving design for rotor containment methods. Elements of a research project at WSU's Institute for Aviation Research aimed at standardizing design methods for rotor containment are discussed. Special concerns of the general aviation manufacturer are identified.

MOTIVATION FOR CONTINUED EFFORTS AT IMPROVING ROTOR CONTAINMENT

Incidents of turbine engine rotor failure persist in occurrence. In commercial aviation, propulsion system related accidents account are 12% of all accidents, and 47.5% of these are uncontained failures [1]. In 1987, data on U.S. commercial aviation, collected and published by the FAA Technical Center [2], 332 rotor failures occurred. Of these failures, rotor fragments were generated in 170 occurrences and 12 of these were not contained. An uncontained rotor failure, according to FAA definition, is a rotor failure that produces fragments which penetrate and escape the confines of the engine casing. The twenty five year average, from 1963 to 1987 for rotor noncontainment incidents was 18.4 occurrences per year; from 1977 to 1987 the rate dropped slightly to an average of 14.9 incidents per year (see Figure 1).

The numbers can also be cast in terms of engine non-containment rate per million engine operating hours. Data from U.S. commercial aviation shown in Figure 2 with the seven year average from 1981 to 1987 of 0.59 incidents per one million engine operating hours per year (see Figure 2). Compare this with data gathered worldwide in the years 1964 to 1975, where an average yearly non-containment rate is 1.07

per million engine operating hours per year [3] (see Figure 2). Fortunately, these statistics indicate some improvement.

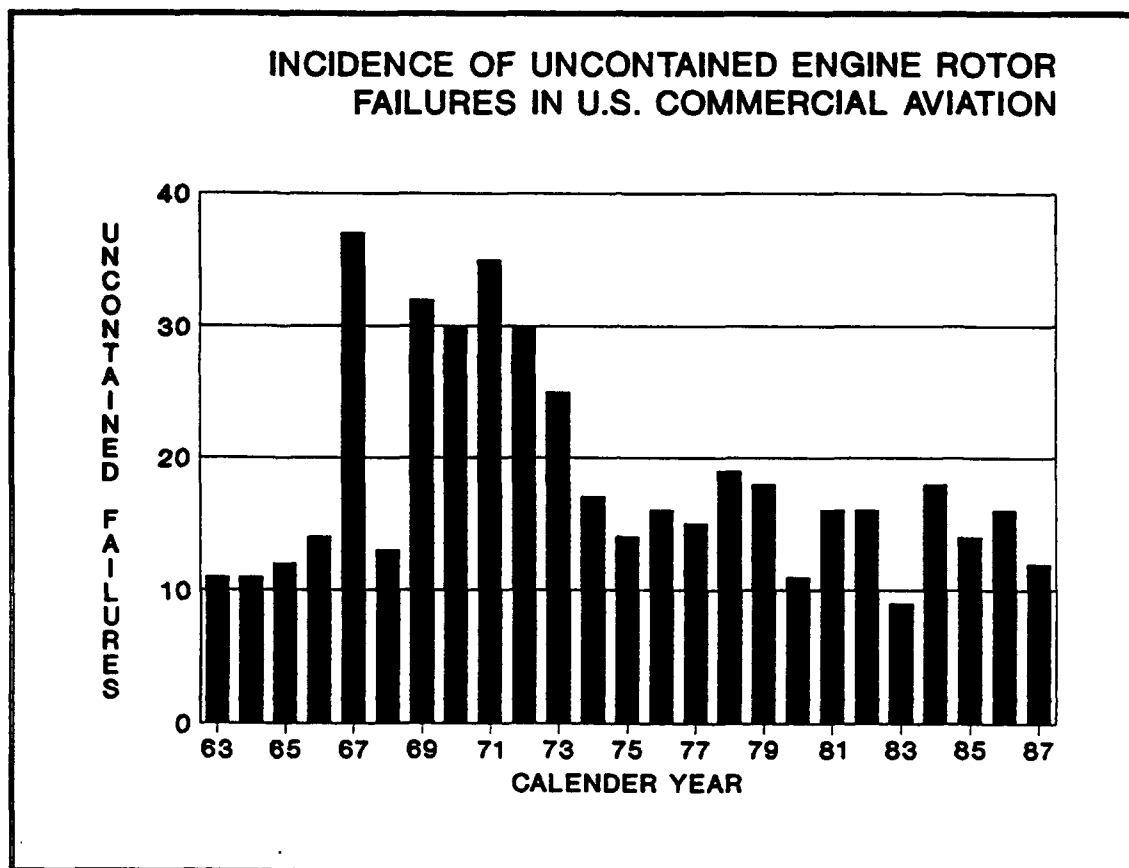


Figure 1.

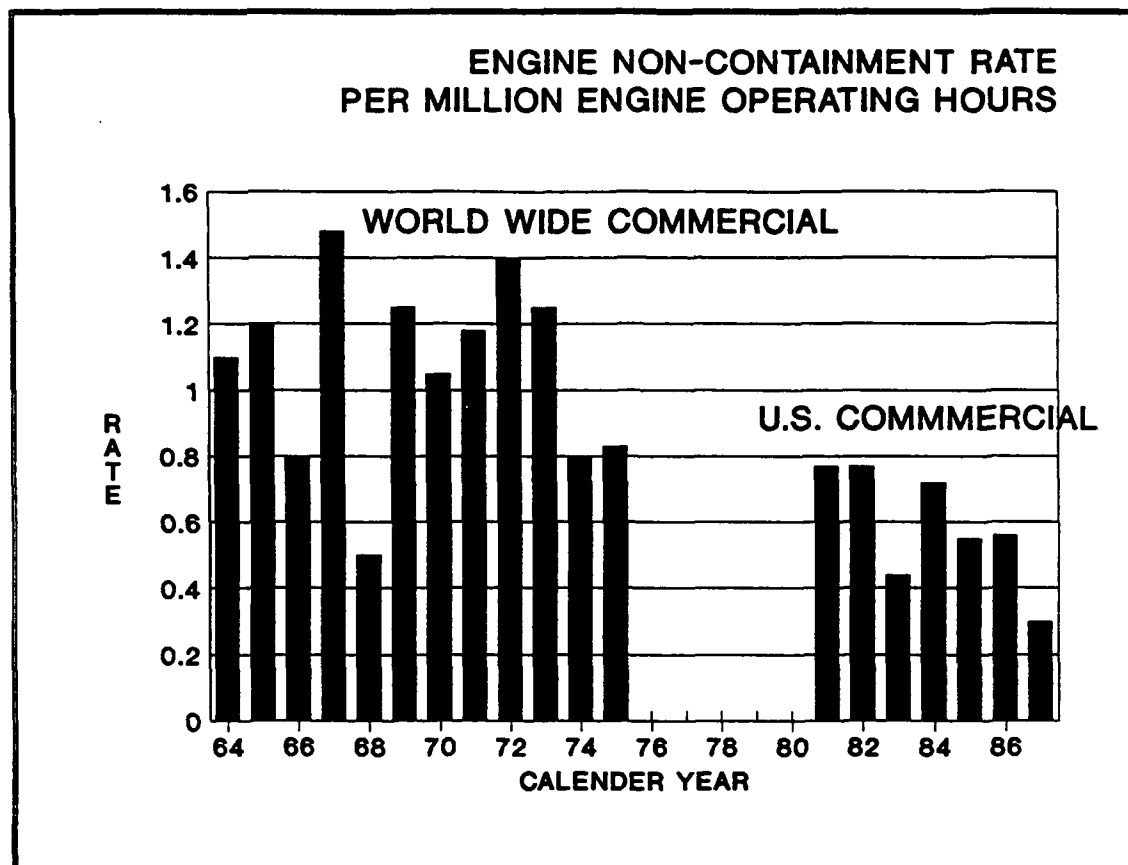


Figure 2.

Which rotor component failures result in noncontainment? The FAA published statistics have also tracked this data. Of rotor failures occurring between 1976 and 1987, Table 1 shows the breakdown between disks, rims, blades and seals.

Component	Percentage of Total Uncontained Failures
Disks	22.7%
Rims	4.4%
Blades	66.3%
Seals	6.6%
Total	100.0%

Table 1: Uncontained Engine Rotor Failures, 1976–1987

While blade failures account for 66.3% of uncontainment incidents, it is also interesting to note that disk failures, when they occur, are rarely contained (Table 2). Hence, containment of and shielding from disk fragments poses one of the most difficult challenges in design.

Year	No. of Disk Failures	No. of Disk Failures Uncontained
1987	3	3
1986	4	4
1985	2	2
1984	6	6
1983	7	7
1982	5	4
1981	7	7
Total	34	33

Table 2: Containment of Disk Failures

The consequences of uncontained failures vary from minor damage to severe damage with fatalities, severe injuries and hull loss. The SAE Committee on Engine Containment groups noncontainment incidents into four categories of varying severity [4]. A Boeing Study [1] analyzing failures from 1984 through 1989 reports the following events sorted according to SAE category (see Table 3).

No. of Events Type of Damage

74	Engine debris exited the engine cases and/or nacelle but no other damage
50	Engine debris exited the engine, nacelle, minor airframe damage not impacting safety, and controlled fires
8	Engine debris exited engine, nacelle, significant aircraft damage, damage to systems or other engines, uncontrolled fires and/or minor injuries
6	Engine debris exited engine nacelle, crash landing, hull loss, fatalities or critical injuries

Table 3: Non-contained Rotor Failures, 1984 through 1989

DESIGN FOR ROTOR CONTAINMENT

The FAA is currently engaged in preparing an Advisory Circular "Design Precautions for Minimizing Hazards to Aircraft From Uncontained Turbine Engine and Auxiliary Power Unit Rotor Failures" [5].

Some fundamental assumptions here are that engine rotor failures cannot be completely eliminated and complete containment by the engine case for all failures is not feasible. Hence, attention must be focused on two areas (1) to not locate an engine where a rotor noncontainment will impact critical components and (2) design the aircraft so that if primary structures or critical systems are damaged by rotor debris, critical aircraft functions are not lost.

The Advisory Circular suggests a disk mass--spread angle distribution as shown in Table 4.

Mass of Disk Fragment, as a Percentage of Total Disk Mass	Spread Angle from Plane of Rotation (+/- Degrees)
33% and greater	3
10%	5
3%	10
1%	15

Table 4: Disk Mass--Spread Angle Distribution
from Draft AC 20-128X

Another portion of the Advisory Circular provides suggestions for proving the effectiveness of shields and deflectors intended to protect systems or components. Testing, or analysis supported by testing is suggested.

ELEMENTS OF RESEARCH AT WSU

Research at WSU is focused toward standardizing the design process for rotor containment. This research, support by the FAA Technical Center contains the following elements:

1. Review of existing literature on design for containment, test data, accident reports, current FAA regulations and standards, and foreign airworthiness authorities' regulations and standards.
2. Contact engine manufacturers and propulsion departments of airframe manufacturers (general aviation as well as commercial) and determine

what design methods are currently employed for analyzing containment problems.

3. Assess the effectiveness of commercially available computational codes for realistically predicting containment capabilities.
4. Develop a table of parameters that would support design selections for hazardous fragment containment or barrier isolation. These parameters would include such things as material properties, geometry for containment or shielding, fragment energy/geometry/trajectory.
5. Assess and determine the minimum analysis and testing necessary for containment design.
6. Present results of this study for the public domain in a format designed to guide the development of certification standards.

GENERAL AVIATION CONCERNS

1. The FAA's draft advisory circular suggests that noncontainment hazards must be minimized. How is this to be interpreted? Does a "degree of safety" analysis have no place in regulatory standards?
2. How will the finalized versions of FAA regulations compare to the JAR's?
3. Should statistics and service history of general aviation aircraft engines play any role in the degree to which containment/shielding must be provided?
4. Maintenance and monitoring methods for General Aviation aircraft can be very different than for commercial aviation (customized trend monitoring, for example). Should maintenance play any role in design requirements?

SUMMARY

The rotor containment research project at WSU has, as a primary goal, the presentation of useful design guidelines for rotor containment and shielding. It is hoped that the product of this research will be especially useful to the general aviation community, and the input of the GA community is being actively solicited and sincerely appreciated.

REFERENCES

1. Boeing Commercial Airplane Company, "An Overview of Propulsion System Risks 1959 through 1989", Document No. D6-55456, November, 1990.
2. DeLucia, R.A., Fenton, B.C., and Blake, Janine, "Statistics on Aircraft Gas Turbine Engine Rotor Failures that Occurred in U.S. Commercial Aviation During 1987", FAA Technical Center, DOT/FAA/CT-90/19, January 1991.
3. Gunstone, G.L., "Engine Non-Containment--The UK CAA View", proc. An Assessment of Technology for Turbojet Engine Rotor Failures, NASA CP-2017, March 1977.
4. Society of Automotive Engineers, "Report on Aircraft Engine Containment", AIR 1537, October 1977.

**WIND TUNNEL AND FLIGHT TESTING OF A NOVEL
AIRCRAFT DESIGN**

by

**Hugh Schmittle, President
Freewing Aircraft Corporation
Technology Advancement Program
University of Maryland
College Park, Maryland 20742**

**For Presentation to the AIAA/FAA Joint Symposium on General
Aviation Systems at the Hilton Inn-East, Wichita, KS
on March 16-17, 1992**

Wind Tunnel and Flight Testing of a Novel Aircraft Design

**Hugh Schmittle, President
Freewing Aircraft Corporation
Technology Advancement Program
University of Maryland
College Park, Maryland 20742**

In two weeks, at the Experimental Aircraft Association's Sun 'N' Fun Airshow in Lakeland, Florida, there will be something new on the flightline. Generically it's called a freewing. The trade name of this prototype is the Freebird MK-IV. This airplane is being put on the market by my company, Freewing Aircraft Corporation.

Since 1989 Freewing Aircraft has been a member of the University of Maryland's Technology Advancement Program, a business incubator for high-tech companies. As resident members of TAP we have a kind of quasi-faculty status, with access to many of the university's facilities on a not-to-interfere basis. Freewing's co-founder, Odile Legeay, and I have gradually expanded the firm, winning a series of grants from the Maryland Industrial Partnerships program, the state's Office of Technology Development, and other sources. We have been joined by Didier Esteyne and others, Didier being the chief designer on the project.

Dr. Jewel Barlow, director of the university's Glenn L. Martin Wind Tunnel, has been our faculty sponsor and PI within the university system on all of our wind tunnel work. Dr. Barlow will be publishing a report of this work in the AIAA literature. And at least one graduate thesis, by Wei Ping Chen, will be finished this year on the wind tunnel program.

That describes who we are. My purpose in being here today is threefold. First I will describe the freewing and how it works. Second, I will recite my ten favorite reasons why freewings will never work. Ten good reasons why they are a terrible idea. Then I will show you some video tape footage of our wind tunnel and full-size models in action.

In order to make it clear to you why the freewing -- and therefore the Freebird MK-IV -- is such a bad idea, I need first to tell you why I used to think it was such a good idea that I have spent 15 years, off and on, developing the Freebird. Just so that you can know what it is that will never work.

A freewing is a revolutionary aircraft masquerading as a fixed-wing. At least that's the case with the Freebird MK-IV. It's rather typical for its market -- that of the light plane. It's a high wing, has two seats arranged in tandem, a pusher propeller, tricycle gear, and an open-framework cockpit. A 32' wingspan of D-tube construction brings us to its distinguishing characteristic: the wing is not rigidly attached to the fuselage with bolts, but is allowed to pivot freely in pitch. Hence the name freewing.

The spanwise hingeline is located forward of the center of aerodynamic action of the wing, and the airfoil itself is reflexed at the trailing edge. Stability is created by a balancing of forces. The weight of the fuselage, being ahead of the wing's aerodynamic center, tries to pitch the wing down, while the characteristics of the airfoil try to nose the wing up. These pitching moments resolve to zero at a certain angle of attack, and you have stable flight.

Now, why go to all this trouble? Why the freewing? One benefit is that the airplane is effectively stall-free, which is implied by its tendency to maintain a constant angle of attack. I should add here that with the Freebird we have complicated matters by coupling the wing's

ailerons to serve also as elevators. These elevons mean that the pilot controls the angle of attack within a certain range as he moves the stick. But for each stick setting, or elevon setting, the wing is still setting itself at an essentially constant angle of attack.

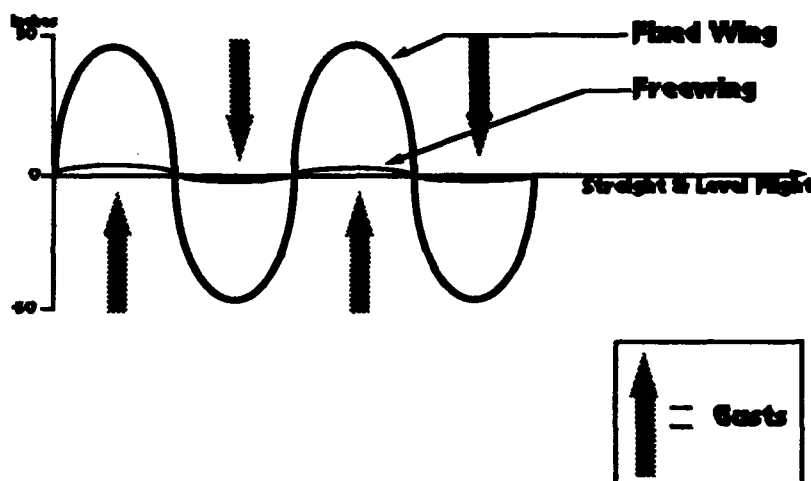
So the first benefit is that the wing is stall-free.

The second benefit is that the sensitivity of freewings to turbulence is reduced quite substantially -- from 50 to 75 percent, depending on the specifics of the aircraft and the frequency range of the gusts. This should mean less stress on the airframe, a longer service life for the airplane, and the ability to fly in conditions that might otherwise ground the aircraft.

I'll close this section of my talk with one final advantage of the freewing. Reduced G-loading and increased comfort can also be expressed geometrically, in terms of deviation from the nominal flight path. From this point of view, a freewing acts as if it suddenly had been given a higher wing loading -- and by no small measure. As can be seen in this chart, perturbation from flight path is roughly an order or magnitude less than an otherwise identical aircraft.

Imagine the implications for UAVs, or unmanned aerial vehicles. These carry video cameras and other sensors which must stay locked on a target. However, UAVs tend to be very lightly wing loaded, and their typical mission is in the altitudes where turbulence is strongest. A platform that rocks and rolls is hard on delicate avionics and requires an expensive gimbaling system to stabilize cameras and the like. So the UAV that is a freewing presents possibilities for strong competitive advantage in what is a growing market. At Freewing, by the way, we are now developing for testing in the wind tunnel a proof-of-concept prototype that is also designed to be capable of free flight. This should make for an interesting demonstrator, and the earlier-mentioned advantage of being able to fly when similar vehicles are grounded also applies here.

Relative displacement from flight path:



Now, with all these advantages, we come to the question that we freewingers hear most often: if this freewing is so good, why ain't everybody doing it? There is a suspicion embedded in that question, which is that there must therefore be something wrong with it -- or else everyone would be using it. QED. And speaking at a wide variety of forums over the years, I have learned a lot of reasons why the freewing just won't work.

Here are my ten favorites.

1. You can't develop a high enough C_L -max to slow the airplane down for takeoff and landing, since you can't use flaps on freewings.
2. You have no place to put the fuel.

3. You can't have multi-engine configuration since you can't put the engines in the wings.
4. You have no way to react out the torsional loads in the wing since it is hinged to the fuselage.
5. You have too much weight penalty by having to beef up the hard points where the hinge attaches.
6. You have too much weight penalty because you have to mass balance the wing about the hingeline.
7. You have too much drag penalty from the hinging mechanism.
8. The FAA would never approve it.
9. Pilots and/or passengers would never accept it.
10. You can't do aerobatics.

I don't want to minimize the fact that some of these negatives hold some truth, nor that there are many engineering problems to be solved between the Freebird MK-IV and the first 50-passenger freewing. However, we in Freewing Aircraft Corporation have become convinced that all of them except number 10 either have or can be overcome. And aerobatics are frankly one liability-inducing behavior we are willing to sacrifice, leaving that to the airplanes designed for the task.

What I do want to say by coming here today is this. As word about the freewing concept spreads, you will hear many people instantly dismiss it as something that couldn't possibly work. Please ask them to work to keep that magical frame of mind that accompanies suspended disbelief.

Ask them not to rush to judgment and say, it's obvious that it won't work for this reason or that, or that it probably couldn't be scaled up to large flying vehicles.

Instead, what if they ask themselves, what would it be like to fly in a freewing? What if we really could devise airplanes that were effectively immune to vertical turbulence, and that couldn't stall? Sure there are weight accretion possibilities associated with hinging and mass balancing wings, but what if that could be solved? Might the reverse be true? Could we get away with lighter wings and fuselages because we don't have to design for such heavy loads, and therefore use smaller engines and less fuel for the same payload/range mission?

In any event, this is what we at Freewing have done; we have focused on the tantalizing potential of this novel technology, and are thus less easily sidetracked by the negatives that are always at hand, in any aspect of life, waiting to short-circuit the desire for exploration.

[Videos of the Freebird in flight, and of wind tunnel runs.]

Test results:

- Basic stability is strong.
- Take off and landing speeds are satisfactory.

- Controllability about three axes is satisfactory; important since Freebird is first attempt in a freewing to use only aerodynamic controls.

As of March 1, 1992, we are only weeks into flight testing, with only qualitative results for the moment. After the Lakeland EAA Airshow in April, we plan to begin instrumented flight tests, and should begin to have more quantitative data.

Conclusion:

The engineering and flight test hours on fixed wing aircraft number in the millions. For the freewing concept we're looking at mere thousands. If this freewing technology is ever going to permeate aviation -- as we in Freewing believe it one day may -- then we have to resist being overcome by all the obvious reasons why the freewing won't work, so that we can concentrate on finding out what is possible.

This is a potentially life-saving technology. For that reason if for no other, it deserves a chance to be explored.